NOVEL MOLECULAR IMAGING OF CARDIOVASCULAR DISEASE IN MAN

NIKHIL VILAS JOSHI
MB BS, MRCP (UK), PgC Med Ed.

Thesis presented for the degree of Doctor of Philosophy at

The University of Edinburgh

2016

To Alka and Vihaan

Table of Contents

Table of Tables

Table of Figures

DECLARATION

This thesis represents research undertaken at the Centre for Cardiovascular Sciences, University of Edinburgh, and the Edinburgh Heart Centre. The studies described in this thesis were funded by Chief Scientist Office, Scotland (ETM/160), the British Heart Foundation (PG/12/8/29371, PG/09/083) and the Evelyn Trust (09/22). I was personally involved in the conception, initiation, conduct and data analysis of all the studies. In keeping with collaborative nature of research, data from patients with carotid atherosclerosis was provided by Dr Alex Vesey (chapter 3), data from the GRACE study was provided by Professor Keith Fox (chapter 4), data from patients with aortic aneurysms from the Addenbrook's Hospital was provided by Dr James Rudd and Dr Maysoon Elkhawad from the Cambridge group (Chapter 5). Dr Olivia McBride helped with data analysis of patients with aortic aneurysms (chapter 6).

Chapters 1, 3, 4, and 6 have been either published in peer-reviewed journals or currently under review. The thesis has not been accepted in any previous applications for a degree and all sources of information have been acknowledged. All studies were undertaken in accordance with the regulations of the local Ethics Board within NHS Lothian and with the Declaration of Helsinki of the World Medical Association.

NIKHIL VILAS JOSHI **10th April 2016**

ACKNOWLEDGEMENTS

I would like to express my sincere gratitude to my supervisor and mentor Professor David Newby at the University of Edinburgh for his continuous support, guidance and motivation. This body of work would not have been possible without his vision and personal dedication. I would also like to thank Professor Nicholas Mills and Dr Marc Dweck at the University of Edinburgh for their supervision of this thesis. I am extremely grateful for their guidance and inspiration over the last few years, and I look forward to working with them in the future. Over the course of my research I have had the opportunity to work closely as part of an international collaboration, and would like to acknowledge the help, support and friendship offered from these collaborators, especially Dr James Rudd at the University of Cambridge, Professor Daniel Berman and Dr Poitr Smolka at the Cedars Sinai Medical Centre.

I would like to acknowledge the Chief Scientist Office, Scotland (ETM/160), the BMA Josephine Lansdell Award (2011) and the British Heart Foundation (PG/12/8/29371) for supporting the studies through research grants. Without their generosity this thesis and the research material presented would not have been possible. I am also grateful to the staff members at the Clinical Research Facility and the Clinical Research Imaging Centre at the University of Edinburgh.

In particular I would like to acknowledge the help of my friend and colleague Dr Marc Dweck. Marc has become a close and dear friend and throughout my research period provided valuable guidance and support. He has continued to help me whilst

he was senior registrar and now a consultant cardiologist at the Royal Infirmary of Edinburgh.

Professor Newby ‘s vision, aspiration and mentorship has been invaluable and has played a major role in both my academic and clinical achievements. He has created a fantastic academic unit that strives to achieve excellence in cardiovascular research. He has created an environment where fellows are encouraged to discuss, debate and develop hypothesis that I am sure will be the driver of future research excellence.

I would like to acknowledge help of my colleagues while conducting research studies. In particular my debates and arguments about research and data with Anoop, Shirjel, Alex and Marc in the *‘barn’* have been instrumental in shaping my thinking about cardiology. In particular, I would like to thank my close friend Dr Anoop Shah, for his help with the studies as well as his great banter!

I would like to thank my family for invaluable support and guidance. I appreciate the share of the burden they have taken during the preparation of this thesis especially, my parents and in-laws. My parents have been extremely influential in shaping my thinking as well as my career, and words simply cannot express my gratitude towards them. Finally I would like to thank my wife Alka and my son Vihaan for their unconditional love, support and continuous encouragement, without them this accomplishment would have been impossible.

ABSTRACT

Cardiovascular disease remains the commonest cause of death worldwide. The majority of deaths are caused by atherosclerotic plaque rupture with resultant myocardial infarction or stroke, or rupture of abdominal aortic aneurysms. Conventional imaging modalities have consistently failed to identify atherosclerotic plaques or aneurysms with high-risk pathological features that are at highest risk of rupture or progression. The development of modern molecular imaging techniques targeted at these features could lead to the identification of such high-risk plaques and aneurysms *in vivo* and guide the development of novel treatment strategies. The aim of this thesis was to evaluate whether novel molecular modalities have a role in providing new insights into biological disease processes, and identify high-risk plaques and aneurysms. Using positron emission tomography-computed tomography (PET-CT), 18F-fluorodeoxyglucose and 18F-fluoride were utilised as markers of metabolic inflammation and active calcification. Cellular inflammation was assessed using ultrasmall superparamagnetic particles of iron oxide (USPIO) enhanced magnetic resonance imaging (MRI).

In a prospective trial, 80 patients with myocardial infarction (n=40) and stable angina (n=40) underwent 18F-fluoride and 18F-fluorodeoxyglucose PET-CT, and invasive coronary angiography (Chapter 3). Intense 18F-fluoride uptake localised to recently ruptured plaque in patients with acute myocardial infarction. In patients with stable coronary artery disease, 18F-fluoride uptake identified coronary plaques with high-

risk features on intravascular ultrasound. 18F-fluoride PET-CT is the first non-invasive imaging method to identify and localise ruptured and high-risk coronary plaques.

Aortic vascular uptake of 18F- fluorodeoxyglucose was studied in patients with myocardial infarction and stable angina (Chapter 4). In a separate outcome of 1,003 patients enrolled in the Global Registry of Acute Coronary Events, we further evaluated whether infarct size predicted recurrent coronary events. Patients with myocardial infarction had higher remote atherosclerotic tracer uptake that correlated with the degree of myocardial necrosis, and exceeded that observed in patients with stable coronary disease. The outcome cohort demonstrated that patients with higher degree of myocardial necrosis had the highest risk of early recurrent myocardial infarction. This supports the hypothesis that acute myocardial infarction exacerbates systemic atherosclerotic inflammation and remote plaque destabilization: myocardial infarction begets myocardial infarction.

In a prospective imaging cohort, the role inflammation and calcification was assessed in 63 patients with abdominal aortic aneurysms and 19 age and sex matched patients with atherosclerosis (Chapter 5). Compared to non-aneurysmal segments, enhanced inflammation and calcification was observed within the wall of aortic aneurysmal segments. In comparison to matched controls with atherosclerosis, the entire aorta in those with aortic aneurysm appears more highly inflamed, suggesting presence of a

global aortopathy rather than a disease confined only to the abdominal region of the aorta. Aortic aneurysms have greater active inflammation and calcification than atherosclerotic controls suggesting a more intense, destructive and transmural pathological process. A subgroup of fifteen patients with aortic aneurysms underwent imaging with both PET-CT with 18F-fluorodeoxyglucose, and T2*-weighted MRI before and 24 h after administration of USPIO (Chapter 6). Whilst there was a moderate correlation between the two tracers, there were distinct differences in the pattern and distribution of uptake suggesting a differential detection of macrophage glycolytic and phagocytic activity respectively.

These studies provide novel insights into vascular biological processes involved in the initiation, progression and rupture of atherosclerotic plaques and aortic aneurysms. Future longitudinal studies are needed to establish whether these techniques have a role in improving the clinical management and treatment of patients with coronary artery disease and aortic aneurysms.

ABBREVIATIONS

18F-FDG = 18F-flurodeoxyglucose

18F-NaF = 18F-sodium fluoride

AAA = abdominal aortic aneurysm

CAC = coronary artery calcium

CAD = coronary artery disease

CHD = coronary heart disease

CI = confidence interval

CT = computed tomography

CTA = computed tomography aortogram

CVA = cerebrovascular accident

CVD = cardiovascular disease

HASTE = Half Fourier Acquisition Single Shot Turbo Spin Echo

MACE = major adverse cardiovascular events

MI = myocardial infarction

MRI = magnetic resonance imaging

PET = positron emission tomography

PET-CT = positron emission tomography-computed tomography

ROI = region of interest

SI = signal intensity

SUV = standardised uptake value

T2*W = T2* weighted

T2W = T2 weighted

TBR = tissue-to-background ratio

TE = Echo time

TR = repetition time

USPIO = ultrasmall superparamagnetic particles of iron oxide

ΔR2* = change in R2* (1/T2*)

ΔT2* = change in T2*

Chapter 1. IMAGING OF ATHEROSCLEROSIS AND ANEURYSMAL DISEASE

Extracts of this chapter have been published in following review articles and book chapters:

1. JOSHI, N. V., VESEY, A., NEWBY, D. E. & DWECK, M. R. 2014. Will 18F-sodium fluoride PET-CT imaging be the magic bullet for identifying vulnerable coronary atherosclerotic plaques? *Curr Cardiol Rep,* 16**,** 521.

2. JOSHI, N. V., NEWBY, D. E. & DWECK, M. R. 2014. Identifying high risk plaques prior to heart attack using PET-CT. *Future Cardiol,* 10**,** 307-10.

3. JOSHI, N. V., NEWBY, D. E. & DWECK, M. R. 2015. Role of Multimodality Imaging in Atherosclerotic Plaque Burden and Metabolism. *In:* SCHINDLER, H. T., GEORGE, T. R. & LIMA, A. C. J. *Molecular and Multimodality Imaging in Cardiovascular Disease*: Springer International Publishing.

1.1. OVERVIEW

Cardiovascular diseases are the leading cause of death and illness worldwide (Lozano et al., 2012, Mozaffarian et al., 2014). Atherosclerosis — a progressive disease characterized by the accumulation of lipids and fibrous elements in the large arteries — constitutes the single most important contributor to this burden, and has been intensely studied over the past century. Our understanding of the pathophysiology underlying this important disease has evolved substantively over this period. Previously it was considered to be a bland lipid storage disorder, with passive deposition of lipid encapsulated within the intima and separated from the vessel lumen by a capsule of smooth muscle cells. More recently substantial advances in basic and translational science have highlighted the role of inflammation, lipid oxidization, cell death, matrix metalloproteinase activity, calcification and angiogenesis (Tahara et al., 2014, Otsuka et al., 2014, Golestani and Sadeghi, 2014, Thompson et al., 2013). In particular compelling evidence has emerged with respect to the importance of inflammation at both the basic and clinical level, indicating that better understanding the link between inflammation and atherosclerosis might yield predictive and prognostic information of considerable clinical utility (Falk et al., 2013b, Budoff et al., 2013, Palombo et al., 2012a, Kataoka et al., 2012).

Atherosclerosis has origins in childhood and by middle age subclinical atheroma is almost ubiquitous (Libby et al., 2010, Jaffer et al., 2009, Jaffer et al., 2007, Naghavi et al., 2003). Indeed, atherosclerosis has one of the longest incubation periods among

human disease, offering the tantalizing opportunity to prevent clinical events via timely detection and treatment of subclinical disease. Whilst anti-atherosclerotic agents of increasing efficacy are evolving constantly, identification of those in need of preventive therapy remains a real challenge.

Atherosclerosis is a true systemic disease characterised by widespread development of its localized manifestation: the atherosclerotic plaque. Atherosclerosis has a particular predilection for medium and large sized arteries, with the coronary arteries, carotid arteries, ilio-femoral arteries, and aorta being particularly susceptible. The location of the plaque and its stability largely determines the clinical manifestation of the disease process. These manifestations can be diverse. At one end of the spectrum fixed obstructive stenoses results in demand ischemia leading to classical symptoms of exertional angina and leg claudication (Falk et al., 1995, Hackett et al., 1988, Falk et al., 1995, Ambrose et al., 1988). However, the most dreaded consequences of atherosclerotic disease – stroke and myocardial infarction- instead occur as a result of abrupt atherosclerotic plaque rupture and subsequent thrombosis. Whilst angiographic techniques can identify lesions likely to cause angina, we lack the ability to identify high-risk atherosclerotic plaques at risk of rupture and causing myocardial infarction. This is seen as a major goal in cardiology because if these plaques could be identified and subsequent rupture and thrombosis averted, then atherosclerosis would be rendered a much more benign disease.

1.2. PATHOLOGY OF ATHEROSCLEROTIC DISEASE: INITIATION AND PROGRESSION

Atherosclerotic lesions are focal thickenings of the innermost arterial layer, the intima. The content of these lesions typically consists of connective tissue, lipids and inflammatory and smooth muscle cells (Stary et al., 1995). This chronic inflammatory process preferentially occurs at sites of disturbed laminar flow, such as branch points and bifurcations, most likely due to the effects of reduced shear stress (Moore and Tabas, 2011). Endothelial cells in these regions appear to be more permeable due to their polygonal shape, allowing large molecules such as low-density lipoproteins (LDL) to accumulate beneath the endothelium (Gimbrone, 1999). This accumulation appears to be greatest in cases of hypercholesterolemia as a result of excess levels of circulating LDL. Indeed, the earliest stages of lesion development are characterised by subendothelial accumulation and retention of apolipoprotein B-containing lipoproteins (Williams and Tabas, 1995). LDL retained within the vessel wall undergoes a series of modifications including oxidation, lipolysis, proteolysis and aggregation (Skalen et al., 2002, Goldstein et al., 1979). Initially this results in the formation of minimally oxidised LDL which has a stimulatory effect on the endothelial cells to produce a variety of growth factors, chemotactic proteins and adhesion molecules. These pro-inflammatory molecules allow leukocytes entry into the arterial wall.

Adhesion, the 'rolling' of leukocytes along the endothelial surface, is mediated by selectins, which bind to carbohydrate ligands on leukocytes. Studies of mice deficient in P- and E-selectins or the cell adhesion molecule ICAM, has revealed the role of these adhesion molecules in atherosclerosis (Dong et al., 1998, Collins et al.,

2000). In particular, adhesion of monocytes and T cells has been shown to be controlled by the interaction of the integrin VLA-4 with VCAM-1 on the endothelial surface (Shih et al., 1999). Following the passage of these monocytes in to the vessel wall the growth factor M-CSF promotes their proliferation and differentiation to macrophages. Normally, LDL is not taken up by macrophages quickly enough to produce heavily lipid-laden foam cells. Further modification of LDL is first required by reactive oxygen species and the enzymes myeloperoxidase, sphingomyelinase and secretory phospholipase 2. This modification process produces a highly oxidised form of LDL, which is rapidly taken up by macrophages, resulting in the generation of foam cells (Falk, 2006, Hansson, 2005). This process appears to be mediated by a group of receptors which recognise a wide array of ligands. Two such "scavenger receptors", SR-A and CD-36, are thought to be of particular importance (Suzuki et al., 1997, Febbraio et al., 2000). As the lesion progresses there is formation of a fibrous cap mainly consisting of smooth muscle cells (SMC) and a proteoglycan-collagen matrix which covers an underlying lipid pool (Virmani et al., 2000b). In time the cells present within this lipid pool undergo apoptosis or necrosis, ultimately leading to the formation of a necrotic core consisting primarily of cellular debris (Littlewood and Bennett, 2003).

1.2.1. STAGES OF PLAQUE PROGRESSION

Atherosclerosis is a dynamic process with multiple stages: intimal thickening, fibrous cap atheroma (fibroatheroma) formation, thin-cap fibroatheroma, and plaque rupture (Virmani et al., 2000b). To understand the process of plaque rupture better, it is useful to review these different stages of plaque development.

Intimal thickening and intimal xanthomas

The flow mediated adaptive, intimal thickening is observed at bifurcation points soon after birth. While some plaques may begin as fatty-streaks, evidence suggests that the intimal thickening is the likely precursor to symptomatic atherosclerotic disease since these lesions occur in children at similar locations as advanced plaques in adults, although fatty streaks are known to regress (Velican, 1981). However considerable debate exists as to whether these lesions should be classified as atherosclerosis per se (Getz, 2000). Intimal thickening primarily consists of smooth muscle cells and proteoglycan-collagen matrix without significant infiltrating inflammatory cells. Fatty streaks, which are predominantly observed at branch points, correspond to the accumulation of macrophages within the intima and regress with age (McGill et al., 2000).

Pathologic intimal thickening

The stage in between intimal thickening and fatty streaks and more advanced lesions known as fibroatheromas is referred to as pathologic intimal thickening and is

characterized by presence of lipid pools containing proteoglycans typically without necrosis (Virmani et al., 2000b). The lipid pools are located in the deeper intimal layers near the arterial media but in contrast the macrophage infiltrates are present in the luminal surface away from the area of accumulated lipid. Early calcification may be seen and likely results from the death of smooth muscle cells and as a healing response to early inflammation (Kolodgie et al., 2007). Pathologic intimal thickening can be associated with plaque erosion and subsequent acute coronary syndromes.

Fibrous cap atheroma

Fibrous cap atheroma or fibroatheromas represents the earliest of the advanced coronary lesions (Virmani et al., 2000b). Typically, the fibroatheromas consist of lipid-rich necrotic core consisting of macrophage infiltration within lipid pool and encapsulated by fibrous tissue. There is loss of proteoglycans and collagen without much free cholesterol in the early phases. The later phases of fibroatheromas are characterized by increased free cholesterol, cellular debris and an expanding necrotic core. Such plaques may expand outwardly (positive remodeling) or inwards often due to progressive fibrosis and calcification (negative remodeling). The latter may lead to significant luminal stenosis and the development of anginal symptoms.

The thin-cap fibroatheroma is a subtype of fibroatheromas characterised by a large necrotic core (typically > 25% of total plaque volume) that is separated from the lumen by a thin fibrous cap (typically < 65 μm). Usually, the fibrous cap tends to be heavily infiltrated with macrophages (Virmani et al., 2000b). This well-characterized

lesion is considered to be the plaque sub-type most likely to result in plaque rupture and is therefore a key imaging target for both invasive and non-invasive approaches (Virmani et al., 2000b) (Figure 1-1).

Figure 1-1 Photomicrographic cross-section of human coronary artery with varying degree of luminal stenosis.

(A to C) Plaque rupture with mild, moderate, and severe luminal stenosis, respectively. Non-occlusive thrombus (Thr) is observed in the microphotograph A whereas occlusive thrombus is occupying the lumen in the image B and C. (D to F) Thin Fibrous Cap Atheroma (TCFA) with mild, moderate, and severe luminal stenosis. Necrotic Core (NC) is covered by a thin fibrous cap, and thrombus is not present in the lumen. (G to I) Stable plaque or FA with mild, moderate, and severe luminal stenosis, respectively. The size of necrotic core is relatively small when present, and calcification (Ca++) is frequently seen. Reprinted from (Narula et al., 2013)

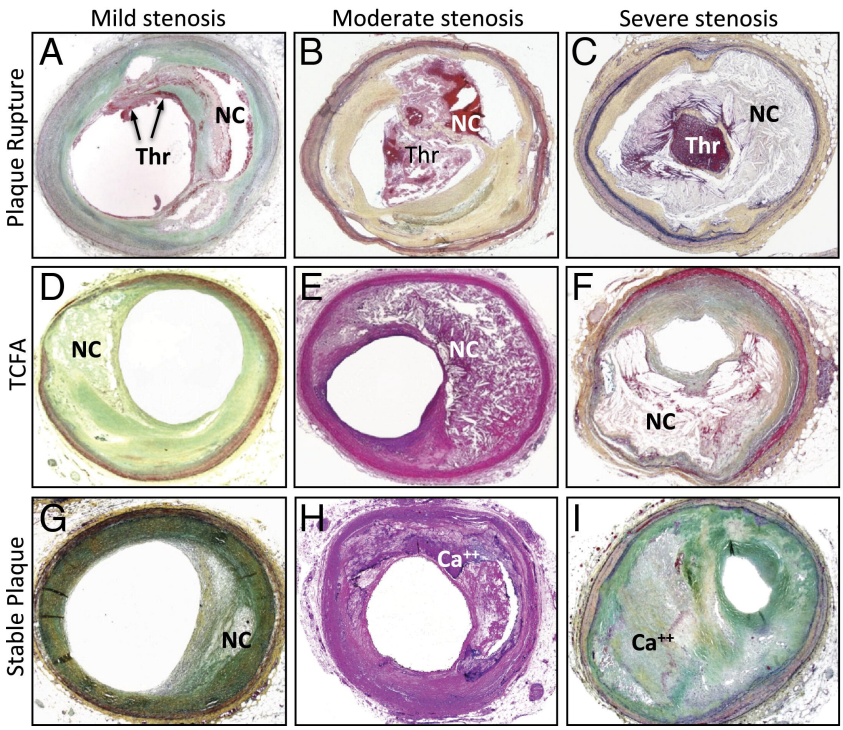

1.2.2. THE LINK BETWEEN INFLAMMATION AND CALCIFICATION IN ATHEROSCLEROSIS: INFLAMMATION DEPENDENT CALCIFICATION PARADIGM

Inflammation plays a critical role in the formation, progression and rupture of atherosclerotic plaques and is typically characterised by the presence of macrophages within the plaque lipid core (Figure 1-2) (Burke et al., 1997a, Burke et al., 2001, Falk et al., 2013a, Finn et al., 2010, Virmani et al., 2006b, Virmani et al., 2000a). In an attempt to clear lipid from the vessel intima, these macrophages set up an inflammatory cycle that ultimately proves difficult to contain, leading to progressive matrix degradation and plaque destabilization. Indeed ongoing macrophage infiltration and cell death along with accelerated lipid accumulation contribute to an enlarging necrotic core that becomes progressively more inflamed and hypoxic. Moreover these cells secrete pro-inflammatory cytokines (including interleukin-1, monocyte chemotactic protein-1 and tumour necrosis factor-alpha) and matrix metalloproteinases, which actively weaken the fibrous cap: the only barrier between this highly thrombogenic lipid core and the vessel lumen. Fortunately this is where body defence mechanisms are believed to respond, triggering a calcific healing response that attempts to subdue and wall off this inflamed necrotic environment, thereby reducing the risk of plaque rupture.

Calcification occurs widely in the body and frequently occurring as a healing response to intense necrotic inflammation. This is perhaps best exemplified by tuberculosis where the body attempts to wall off the intense necrotic inflammation associated with caseating granulomata using calcification. Similar mechanisms are

believed to occur within coronary atheroma, with calcification occurring as a healing response to intense inflammation within the necrotic core. However within the atheroma, calcification appears to have a bi-phasic response, with each stage associated with markedly different plaque characteristics and clinical consequences. The latter phase of macroscopic calcification is readily imaged using standard x-ray angiography and CT, and is widely believed to impart stability to the plaque. Indeed by this stage the healing process has often successfully subdued inflammation within the vessel wall and separated it from the contents of the vascular lumen. By contrast the earlier phase of micro-calcification is not visible using standard non-invasive imaging techniques and is associated with plaque instability and an increased risk of rupture (Aikawa et al., 2007, Otsuka et al., 2013). The likely explanation is that at this early time-point the healing process has not yet been effective and that the inflamed necrotic environment triggering calcification still exists within the plaque. This risk of plaque rupture related to inflammation therefore persists. However recent data have indicated that micro-calcification might itself increase the propensity to rupture, acting as a focal point that intensifies mechanical stresses on the surface of the cap (Vengrenyuk et al., 2006a).

Although there have been significant advances in our understanding as to why atherosclerotic plaques calcify, the exact molecular mechanisms underpinning this observation still remain unclear. Multiple potential pathways have been proposed although often these have been established using models of vascular medial calcification. Calcification in the coronary arteries is almost uniquely intimal, with

medial and adventitial involvement occurring only rarely in conditions such as renal failure. Calcification activity in the intima appears to be closely related to inflammation and cell death within the necrotic core. Several putative pathways have been proposed linking these entities (New and Aikawa, 2011, Tintut et al., 2000, Radcliff et al., 2005, Demer and Tintut, 2008, Proudfoot et al., 2000, Shanahan, 2007). First and most obviously, necrosis of foam cells, vascular smooth muscle cells and other cells in the inflammatory plaque milieu leads to the release of large quantities of phosphate and calcium which may lead to spontaneous dystrophic calcification (as observed in infarctions, haematomas and scars). Second, inflammation may trigger osteogenic metaplasia in a variety of cell types (VSMC, endothelial cells, etc.) which make a phenotypic switch to osteoblast like cells under the influence of RUNX-2 transcription and become capable of roughly recapitulating skeletal osteogenesis in the plaque matrix. Third, circulating osteoprogenitors may be recruited to the plaque before undergoing maturation to classical osteoblasts. Fourth, cells undergoing programmed cell death within the plaque may provide calcifying substrate through the release of apoptotic bodies. Fifth and finally, macrophages may, themselves, provide the substrate for calcification by directly releasing matrix vesicles (the key and final executors of ordered tissue mineralization) into the extracellular matrix. Aikawa *et al.* have published the key and highly elegant longitudinal experiments in a mouse model that have demonstrated the link between inflammation and calcification (Aikawa et al., 2007). They showed that macrophage infiltration is closely associated with osteogenic activity (as assayed by accumulation of Osteosense; a bisphosphonate-conjugated to a fluorescent reporter). They have also shown that apoptotic bodies and matrix vesicles that contain calcium

orthophosphate nanocrystals execute this early calcific process (Bobryshev et al., 2007, Golub, 2011, Proudfoot et al., 2000).

1.2.3. THE VULNERABLE ATHEROSCLEROTIC PLAQUE: WHAT EXACTLY DEFINES A HIGH-RISK PLAQUE?

The concept of the vulnerable plaque was first introduced by James Muller in 1989 when he described 'hemodynamically insignificant, albeit dangerous lesions'(Muller et al., 1989), that he believed were at high risk of rupturing and causing myocardial infarction. Since then multiple observational studies have confirmed that most of the plaques causing myocardial infarction are non-flow limiting at the time of antecedent coronary arteriography or myocardial stress testing. However pioneering work over the last two decades has now established that ruptured plaques do have certain key histopathological features including: the presence of a large necrotic core, a thin fibrous cap (<65 μm), a positively remodelled vessel, macrophage infiltration resulting in plaque inflammation, hypoxia leading to neovascularization and finally early stage microcalcification (Figure 1-2) (Burke et al., 1997a, Burke et al., 2001, Falk et al., 2013a, Finn et al., 2010, Virmani et al., 2006b, Virmani et al., 2000a). Moreover it is widely postulated that intact high-risk plaques are likely to demonstrate the same pathophysiological features immediately before a clinical plaque rupture event, so that identification of these characteristics may be of use prospectively. Recent technological advances, coupled with the failure of percutaneous coronary intervention to reduce myocardial infarction in patients with stable angina (Boden et al., 2007) has renewed interest in detecting these plaques *in vivo*. Indeed, this has been described by many as the 'holy grail' of clinical cardiology (Calvert et al., 2011, Naghavi et al., 2003, Stone et al., 2011a, Kato et al., 2012a).

Two distinct plaque morphologies have been implicated in majority of acute coronary events: plaque rupture and plaque erosion. A few cases (2% to 7%) are attributable to a third plaque morphology called calcified nodule (Virmani et al., 2006a). It is believed that 60-75% of acute coronary syndromes are initiated by plaque rupture (Davies, 1992). Plaque erosion or denudation of the coronary arterial endothelium with an intact fibrous cap is responsible for acute coronary syndromes in most of the remainder cases, and is typically observed in young, female smokers (Virmani et al., 2000b).

Traditionally, the term vulnerable plaque has been used for all plaque types that have been associated with luminal thrombosis (Virmani et al., 2006a). However recently attention has focused on the thin fibrous cap atheroma as the most common precursor of plaque rupture. In particular virtual histology intravascular ultrasound (VH-IVUS) has been used to identify such plaque in the recent Providing Regional Observations to Study Predictors of Events in the Coronary Tree (PROSPECT) and the VH-IVUS in Vulnerable Atherosclerosis (VIVA) studies (Calvert et al., 2011, Stone et al., 2011b). Whilst most of the clinical events in these studies were attributable to TCFAs, what was also clear is the vast majority of these lesions are clinically silent.

Pioneering work over the last two decades has established that plaques that go on to rupture demonstrate several histological features that differentiate them above and beyond the classical infact TCFA. These include a large necrotic core, high

macrophage infiltration of the fibrous cap and plaque micro-calcification (Virmani et al., 2006a, Kolodgie et al., 2001). This would suggest that there is an intermediate stage between a thin-capped fibrous atheroma and a ruptured plaque, which appears characterised by advanced plaque metabolism.

Figure 1-2 Pathological characteristics of the vulnerable plaques

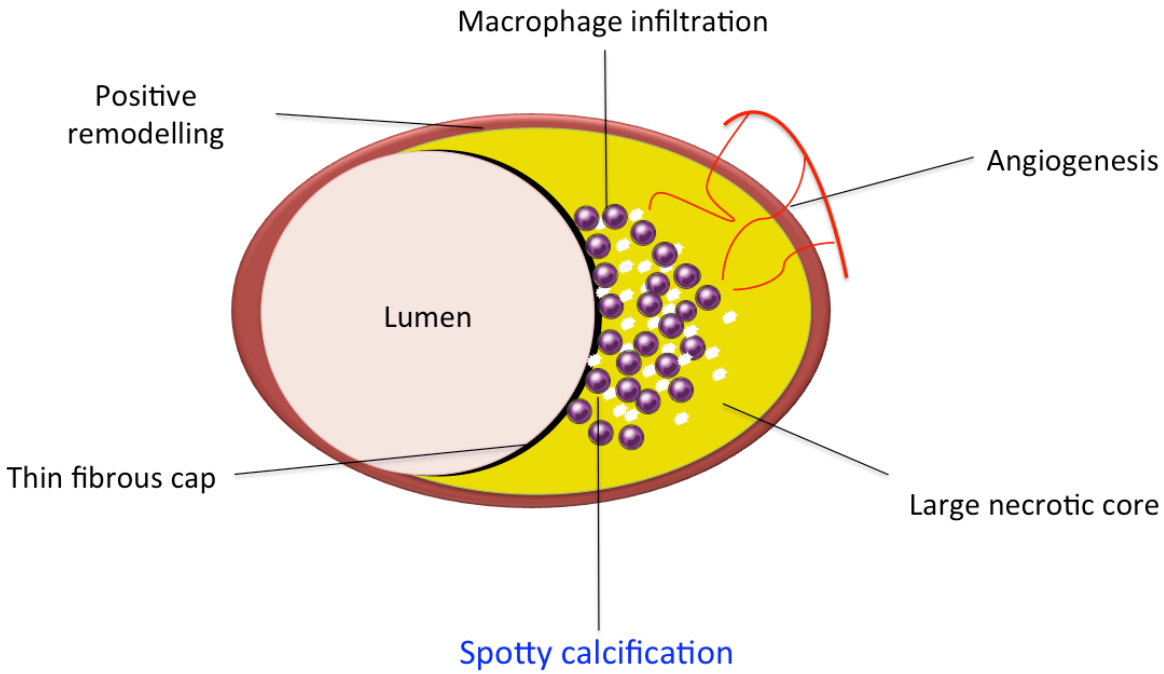

1.3. ABDOMINAL AORTIC ANEURYSMS

Abdominal aortic aneurysms (AAA) have a prevalence of 5% in adults 65-74 years and when ruptured, are associated with a mortality of up to 90% (Scott, 2002). Ruptured aortic aneurysms are a common cause of death in the United Kingdom, being the thirteenth commonest cause of death and accounting for 6,800 deaths each year in England and Wales (Scott, 2002). Open surgical or endovascular intervention to prevent rupture is considered when the diameter exceeds 55 mm or expansion rates are greater than 10 mm/year (Lederle et al., 2002, UKSAT 1998, Powell et al., 2007). Population screening has been shown to halve the mortality associated with abdominal aortic aneurysms (Scott, 2002) and has led to the establishment of a national screening and surveillance programme (Lederle et al., 2002, UKSAT 1998). Currently, abdominal aortic aneurysm surveillance is complex because of the non-linearity and unpredictability of expansion rates (Brady et al., 2004), although the best predictor of aneurysm expansion is the baseline aneurysm diameter (Golledge et al., 2006a). However, up to one fifth of ruptured abdominal aortic aneurysm are less than 55 mm in diameter (Darling et al., 1977), and many patients present with diameters considerably greater than 55 mm without prior symptoms or rupture (Powell et al., 2008). Apart from the simple measurement of aneurysm diameter, there are currently no methods of predicting which patients are at risk of further aneurysm growth and rupture.

1.3.1. ANEURYSMAL DISEASE AND ATHEROSCLEROSIS

Aortic aneurysms and atherosclerosis have traditionally been regarded to have a common background. This is because AAA is invariably associated with atherosclerotic wall damage, supported by the presence of risk factors such as age, male gender, smoking, hypercholesterolemia, hypertension and a positive family history (Reed et al., 1992). However, during the last decade, evidence has emerged highlighting the differences between AAA and atherosclerosis (Golledge and Norman, 2010). Atherosclerotic lesions are pre-dominantly intimal in location, whereas the media and adventitia are primarily involved in aneurysms (Weintraub, 2009). Aneurysmal disease is also much more closely associated with smoking and hypertension, and has a particular predilection for the abdominal aorta. Furthermore, whilst diabetes mellitus is positively associated with atherosclerosis, it is negatively associated with AAA (Golledge et al., 2006b). Although aggressive management of hypertension and hyperlipidemia is recommended in patients with AAA, therapies for these conditions have little effect on aneurysmal growth and rupture (Weintraub, 2009). Whether this association between AAA and atherosclerosis is causal or simply due to common risk factors is unknown.

One possibility is that AAA develops as a pathological response to aortic atherosclerosis. This theory was first suggested more than half a century ago (Eiseman and Hughes, 1956), when the term “atherosclerotic aneurysms” was commonly used (Kaschina et al., 2009). Arterial remodelling is thought to be central to this theory. It has been proposed that arterial luminal stenosis leads to

compensatory changes in media in response to shear stress alterations (Ward et al., 2000). The subsequent remodeling of the extracellular matrix compensates for the shear stresses (Ward et al., 2000). Although this theory explains severe medial thinning observed in AAA, it fails to explain the inflammation observed in the biopsies of the walls of advanced AAA. Elastin breaks, stimulated by medial proteolysis and the diffusion of pro-inflammatory cytokines from inflammatory cells present within atheroma or associated thrombosis could, however, provide the stimulation for the chronic inflammatory response seen (Golledge et al., 2006b, Golledge and Norman, 2009, Ward et al., 2000). A unique feature of the arterial wall in aneurysmal disease is degradation of the connective tissue (Sakalihasan et al., 2005). Moreover, an increased proteolytic activity has been demonstrated in the wall of abdominal aortic aneurysm (AAA) (Sakalihasan et al., 1996, Thompson and Parks, 1996).

An alternative theory suggests that the development of AAA and atherosclerosis are independent. Shared environmental and genetic risk factors may promote the development of both atherosclerosis and AAA in some patients, but the mechanisms involved are distinct (Golledge and Norman, 2010). Perhaps, it is obvious that the inflammation either due to atheroma or the thrombus holds the vital clue to the underlying pathological processes.

The AAA wall usually becomes laminated with thrombus and its intraluminal

diameter often appears relatively normal by angiography (Shimizu et al., 2006). There is now increasing evidence that this intraluminal non-occlusive thrombus plays a key role in AAA evolution (Kazi et al., 2003). Recent studies demonstrate that inhibition of thrombus formation via the prevention of platelet aggregation limit AAA enlargement in a model of experimental aneurysm in rats (Touat et al., 2006). These findings suggest that thrombus formation compromises the structural integrity and stability of the arterial wall (Houard et al., 2006). The thrombus mass itself is biologically active (Adolph et al., 1997, Fontaine et al., 2002a) with fibrin generation demonstrable at the luminal interface (Touat et al., 2006, Houard et al., 2007).

The formation, growth and rupture of aneurysms is now recognised to be the result of a complex interplay between biological and mechanical factors.

1.3.2. INFLAMMATION AND ANEURYSMAL DISEASE

Aneurysmal tissue is characterised by excessive medial neovascularisation, infiltration of inflammatory cells (principally macrophages and B-lymphocytes) and irreversible remodelling of the extracellular matrix. These pathological processes are focal and do not affect the aorta uniformly. Shear wall stress varies spatially within the aneurysm (Raghavan et al., 2000) and tensile strength varies in different parts of the aneurysm sac (Vallabhaneni et al., 2004). Focal neovascularisation is present at the site of rupture only (Choke et al., 2006) and its presence corresponds to the degree of inflammation (Thompson et al., 1996). These biological 'hotspots' represent sites of potential rupture and are targets of developing imaging strategies to assess the aneurysm expansion and the risk of rupture.

In contrast to the thoracic aorta, the tunica media of the abdominal aorta is not normally supplied by vasa vasorum and the presence of microvasculature in the abdominal aortic wall is a pathological finding (Wolinsky and Glagov, 1969). Hypoxia of the inner layer of the media, resulting from the presence of intraluminal thrombus, is thought to attract inflammatory cells and induce the secretion of angiogenic factors promoting neovascularisation (Vorp et al., 2001). These new vessels not only supply oxygen and nutrients to the arterial wall but also amplify the pathological process by promoting further inflammatory infiltration. The inflammatory infiltrate in aneurysm disease is characterised by macrophages and B lymphocytes that may be attracted, in part, by the products of extra-cellular matrix degradation. Inflammatory cells secrete matrix metalloproteinases that leads to

degradation of elastin and then collagen, thus disrupting the structural integrity of the aortic wall and rendering it vulnerable to aneurysm formation and rupture.

1.4. NOVEL IMAGING MODALITIES TO IDENTIFY HIGH RISK ATHEROSCLEROTIC AND ANEURYSMAL DISEASE

Over the last few years, advances in basic cardiovascular research coupled with improvement in novel imaging technology has resulted in improved understanding of biological processes underlying formation, progression, and complications of atherosclerosis that in turn has renewed interest in detecting the high-risk plaques and aneurysms *in vivo* prior to rupture. (Calvert et al., 2011, Naghavi et al., 2003, Stone et al., 2011a, Kato et al., 2012a).

Traditionally the assessment of cardiovascular diseases is evaluated using anatomical and physiological modalities. Undoubtedly, these techniques have a significant role in assessing the severity of coronary stenosis and are indeed routinely used in diagnosis of coronary disease in patients with stable and unstable symptoms. Modalities such as stress perfusion and X-ray contrast angiography help identify high risk patients by identifying disease severity by assessment of plaque stenosis, burden and ischaemia, and guide the need to revascularisation in a certain subset of patients. Similarly, routine ultrasound assessment of AAAs is undertaken to assess progression of aneurysmal size. However, these modalities primarily focus on anatomical and structural element of the disease and give very little insight into the molecular or biological processes within the vasculature. In contrast to approaches, molecular and cellular imaging target specific biochemical and cellular processes to provide unique insights into the etiology, biology and pathogenesis of the disease. Indeed by harnessing recent imaging advances, many believe that it is possible to

develop imaging approaches beyond traditional domains and move towards a more refined technique that allow identification of more complex molecular, cellular and metabolic components of atherosclerotic and aneurysmal disease (Jaffer et al., 2009, Jaffer et al., 2007, Choudhury and Fisher, 2009, Tawakol et al., 2006, Rudd et al., 2002, Tahara et al., 2006b, Nahrendorf et al., 2011).

The common aims of novel molecular imaging are to inform molecular and biological processes within a tissue, help refine the diagnosis and risk-stratification, and assess responses to specific therapeutic interventions (Jaffer et al., 2009, Jaffer et al., 2007, Choudhury and Fisher, 2009, Nahrendorf et al., 2011). Indeed, the molecular imaging modailities could act as surrogate end points to study and monitor the response of specific interventions. A number of invasive and non-invasive modalities have been developed across various platforms and have shown considerable promise to fulfil these goals. The novel imaging modalities can be broadly divided into non-invasive modalities such as PET-CT, CT coronary angiography, MRI and catheter based invasive modalities such as IVUS and OCT. Each of these modalities will be briefly discussed in the following sections, with primary focus on metabolic and cellular imaging with PET-CT and ultrasmall superparamagnetic particles of iron oxide (USPIO) - enhanced MRI.

1.5. POSITRON EMISSION TOMOGRAPHY IMAGING

Combined positron emission and computed tomography (PET/CT) is a modern non-invasive imaging technique that combines molecular information from PET with the fine anatomical detail provided by CT, allowing study of biochemical processes within small structures. This technique has been widely used in the clinical assessment of patients with cancer for many years, resulting in the widespread availability of PET/CT scanners (Lardinois et al., 2003). Recent technological advances including ECG-gating alongside improved PET resolution has allowed translation of this technology in cardiovascular imaging. Theoretically, a limitless number of pathological processes can be studied subject to appropriate radiotracer being developed, and therefore in principle any high-risk plaque characteristics can be potentially targeted.

Using a cyclotron, a positron emitting atom is generated using an isotope with a relatively short life such as 11C, 13N, 15O and 18F (Zanzonico, 2012). Other less commonly used radioisotopes include 64Cu, 76Br, 82Rb, 68Ga and 124I. The positron emitting atom is bound to a specific protein or sugar that can be translocated into the tissue of interest within the body where the isotope decays releasing a positron that interact with surrounding electrons, resulting in complete annihilation of particles and resulting in two diametrically opposite photons that can be detected by the PET detector. The photons detected by the PET scanner are processed and the tomographic images define the tracer distribution within the body using a specialized algorithm. Corrections for attenuation, dead time, scatter, and random coincidences

are applied. This information is then superimposed upon anatomical CT images and regions of interest are drawn to determine standardized uptake values (SUV) and tissue-to-background ratio (TBR) (Dweck et al., 2012a, Dweck et al., 2012b, Fayad et al., 2011a, Rudd et al., 2002, Tawakol et al., 2006). Typically, radioisotopes with short half-lives are used for PET tracers, because they decay at a predictable rate after intravenous administration, and keep patient radiation dose low. Furthermore, many of these isotopes can be incorporated into biological substrates (glucose, H2O, NH3, CO2, O2, etc.) and pharmaceuticals, without altering their biological activity. One of the major challenges and expenses is reliable and efficient production of novel and complex PET tracers to a Good Manufacturing Practices standard.

Within the atherosclerotic tissue, specific pathological processes can be targeted to assess inflammation, calcification and other related processes such as macrophage activity, hypoxia and neoangiogenesis. To date the most promising studies investigating atherosclerosis have utilised the tracers 18F-fluorodeoxyglucose (18F-FDG) as a marker of inflammation and 18F-fluoride as a marker of micro-calcification.

1.5.1. 18F- FLUORODEOXYGLUCOSE

18-Fluorine-labelled 2-deoxy-2-fluoro-D-glucose (18F-FDG) is used extensively to image metabolically active cells with PET-CT. Indeed it has been employed very successfully to identify metastases in patients with high-grade poorly differentiated tumours (Lardinois et al., 2003). The first study to evaluate 18F-FDG in human was undertaken at the University of Pennsylvania, Philadelphia in 1976 with the aim of demonstrating cerebral and total body glucose utilisation (Reivich et al., 1977). 18F-FDG identifies metabolically active tissue by directly competing with glucose for transportation by GLUT receptors and then undergoes phosphorylation to 18F-FDG-6-phosphate by hexokinase. However, once bound to phosphoglucose isomerase, 18F-FDG-phosphate is unable to progress down the glycolytic pathway and is effectively trapped within the cell and can be targeted with PET imaging. By this virtue, 18F-FDG is able to identify cells with high glucose requirements, and not specific to one cell type it be taken by the cells with high energy and metabolic demand e.g. neurons, active muscle cells, neoplastic cells and activated inflammatory cells.

Vascular imaging with 18F-FDG PET was pioneered by Rudd at Cambridge University in 2002 (Rudd et al., 2002). Within the vascular bed, it is thought that macrophages have the highest metabolic requirement and therefore its uptake has become synonymous with macrophage activity (Rudd et al., 2002, Tawakol et al., 2006). Indeed, several studies have demonstrated a close association between 18F-FDG and tissue macrophage burden in the carotid arteries (Satomi et al., 2013b).

Furthermore, 18F-FDG uptake is associated with traditional cardiovascular risk factors including age, male gender and metabolic syndrome as well as inflammatory biomarkers (Yun et al., 2002, Tahara et al., 2007). Moreover, vascular 18F-FDG uptake is elevated in patients infected with human immunodeficiency virus (Subramanian et al., 2012) and with rheumatoid arthritis (Maki-Petaja et al., 2012), perhaps accounting for the increased cardiovascular events in these patient populations. Indeed, 18F-FDG has become a widely used measure of vascular inflammation, and employed to demonstrate the anti-inflammatory effects of statins and other lipid lowering agents (Tahara et al., 2006b, Fayad et al., 2011a). However, recent data have suggested that the mechanisms underlying vascular 18F-FDG activity may be more complex, implicating hypoxia as an important driver of 18F-FDG uptake by both macrophages and vascular smooth-muscle cells (Folco et al., 2011). Recent data have also suggested that 18F-FDG preferentially labels M1 type proinflammatory macrophages rather than the anti-inflammatory M2 type (Satomi et al., 2013b).

Whilst 18F-FDG uptake has been validated in large vessels such as the aorta, carotid, iliac and femoral arteries, attempts to utilise this tracer in the coronary arteries have been less successful. Increased 18F-fluorodeoxyglucose in the coronary arteries has been described in patients with coexisting malignancy (Dunphy et al., 2005, Wykrzykowska et al., 2009). Since then, three prospective studies have examined the feasibility and reproducibility of assessing uptake of this tracer in the coronary vasculature (Rogers et al., 2010, Dweck et al., 2012a, Cheng et al., 2012). Whilst two

early studies (Cheng et al., 2012, Rogers et al., 2010) suggested that 18F-fluorodeoxyglucose might identify some inflamed coronary plaques in patients with recent myocardial infarction, others have more recently demonstrated that in 50% of patients with acute myocardial infarction, there was no uptake of 18F-fluorodeoxyglucose in the culprit plaque (Cheng et al., 2012).

18F-FDG Imaging in aneurysmal disease

The feasibility of assessing 18F-FDG uptake within the AAA has been assessed in several studies with variable results (Morel et al., 2015, Palombo et al., 2012b) (Tegler et al., 2012, Kotze et al., 2011a, Barwick et al., 2014, Nchimi et al., 2014). Uptake of 18F-FDG has been shown to be higher in the aneurysmal region of the aorta as compared to controls (Truijers et al., 2008, Kotze et al., 2009), and is associated with inflammation, aortic wall instability and symptomatic disease (Reeps et al., 2008). However, others have reported low and variable 18F FDG uptake in aneurysms below the cut off for surgical intervention (Palombo et al., 2012b, Marini et al., 2012, Tegler et al., 2012). Indeed it has been suggested that there is waxing and waning of inflammation within the aneurysmal tissue due to cyclical metabolic pattern of aneurysmal growth (Morel et al., 2015). Important limitation of these studies was small sample size and variable parameters to define tracer activity. Larger prospective studies are required to understanding the relationship between 18F-FDG uptake and different stages of aneurysms.

1.5.2. 18F-FLUORIDE

18F-Fluoride is a PET tracer with favourable pharmacokinetic properties, first introduced by Blau and coworkers in 1962 for the study of bone disease (Blau et al., 1962, Blau et al., 1972, Hawkins et al., 1992). After an intravenous injection, approximately 70% of 18F-fluoride is plasma based with the remaining 30% found in erythrocytes. Because of its small size and negligible protein binding, 18F-fluoride demonstrates almost complete clearance from the blood stream on first pass, (Blake et al., 2001, Wootton and Dore, 1986, Hoh et al., 1993) resulting in low blood-pool activity. This coupled with its specificity for bone and vascular calcification ensures that it provides excellent signal to noise in these tissues with little contamination from adjacent structures.

The mechanism of 18F-fluoride uptake in bone is well established. First it diffuses via the capillary network into the bone extracellular fluid. Then it exchanges with hydroxyl groups on exposed regions of hydroxyapatite crystal on the bone surface, forming fluoroapatite. The intensity of the signal depends both on the bone blood flow but also upon the surface area of exposed hydroxyapatite, which is increased in regions of new bone formation and remodelling (Blau et al., 1962, Blau et al., 1972, Hawkins et al., 1992). As a consequence 18F-fluoride has been extensively utilized as a marker of bone turnover and used to study various bone related clinical conditions such as Paget's disease (Cook et al., 2002, Installe et al., 2005) osteoporosis (Frost et al., 2004, Messa et al., 1993) renal osteodystrophy (Messa et al., 1993), fracture healing (Hsu et al., 2007) and osteonecrosis . Moreover, 18F-

fluoride PET has become widely established as the most sensitive imaging modality for the detection of malignant bone involvement, leading to its widespread and commercial availability (Petren-Mallmin et al., 1998, Schirrmeister et al., 1999, Hetzel et al., 2003, Even-Sapir et al., 2006, Beheshti et al., 2008).

The mechanism underlying 18F-fluoride in the vascular tissue is similar to bone uptake. Hydroxyapatite is also the key structural component of vascular calcium, so that arterial 18F-fluoride uptake is likely to relate closely to the available surface area of this crystal. Transmission electron microscopy studies have demonstrated that during the early stages of calcification hydroxyapitate crystals are nanosized, very thin and long (Rey et al., 2009). This results in a much larger surface area of hydroxyapatite for 18F-fluoride binding in the early stages of microcalcification compared to macroscopic calcification in which much of the hydroxyapatite is internalised and not accessible to the tracer. Indeed recent pre-clinical work performed by our collaborators at Cambridge University has confirmed that 18F-fluoride adsorbs to calcified deposits within plaque with high affinity and is selective and specific and distinguishes between areas of macro- and microcalcification (Agnese Irkle, 2013, Irkle et al., 2015) (Figure 1-3)

Derlin *et al.* first described the vascular uptake of 18F-fluoride in 2010 in a retrospective analysis of patients with malignancy (Derlin et al., 2010). The authors noted increased 18F-fluoride uptake in large vessels such as the aorta, carotids and

femoral vessels in about three quarters of the patients studied. Interestingly, only a fifth of all calcified plaques on CT demonstrated increased 18F-fluoride uptake, highlighting even at this early stage that 18F-fluoride provides different information to the presence of calcium on CT. Subsequent work by the same group retrospectively compared the distribution of 18F-fluoride and 18F-FDG uptake in oncology patients (Derlin et al., 2011a) and suggested that 18F-fluoride signal in the femoral vessels correlated with the calcified plaque burden and cardiovascular risk factors (Janssen et al., 2013). Beheshti and colleagues first described 18F-fluoride activity localizing to the heart (Beheshti et al., 2011) whilst we and other groups have confirmed increased 18F-fluoride activity in the aorta and importantly in the valves of patients with aortic stenosis, (Dweck et al., 2011, Dweck et al., 2013b) where it acts as a marker of calcification activity and predicts disease progression (Dweck et al., 2014).

We first described 18F-fluoride uptake in the coronary arteries as a novel marker of plaque biology in subjects with and without aortic valve disease (Dweck et al., 2012a). This demonstrated the feasibility and excellent reproducibility of this tracer in the coronary vasculature. Moreover increased uptake of this tracer localised to individual coronary plaques and importantly identified patients at increased cardiovascular risk, with those subjects having increased Framingham risk scores and prior MACE event rates. This study also confirmed that, as in the aorta, 18F-fluoride provided different information to the presence of coronary calcium on CT. Indeed we observed that >40% of patients with coronary artery calcium scores >1000 Agatston

Units did not have 18F-fluoride uptake, suggesting the ability of 18F- fluoride to distinguish between dormant pacified calcific disease and metabolically active ongoing micro-calcification (Table 1-1).

Figure 1-3 The relationship between inflammation, biphasic calcific response and adverse cardiovascular events

(A) Typical features of a vulnerable plaque: The initial stages of plaque inflammation and vulnerability are associated with macrophage influx into a large lipid core. By this stage, other features of plaque vulnerability such as positive remodelling, thinning of the fibrous cap, are observed. (B) Microcalcification within the necrotic core: Cell death occurring within the lipid core as a consequence of necrosis and apoptosis triggers microcalcification. This is a high risk plaque type that is ripe to rupture. This can have two consequences: successful plaque calcification by walling off the inflamed area, or initiation of plaque rupture with subsequent thrombotic occlusion. This is the plaque type that is believed to be have avid 18F-fluoride uptake on PET/CT. (C) Plaque stabilization with successful healing of the necrotic core with obvious macrocalcification that can be detected with conventional imaging modalities such as computed tomography and X-ray angiography. (D) Plaque rupture with thrombotic occlusion of the lumen resulting in myocardial infarction

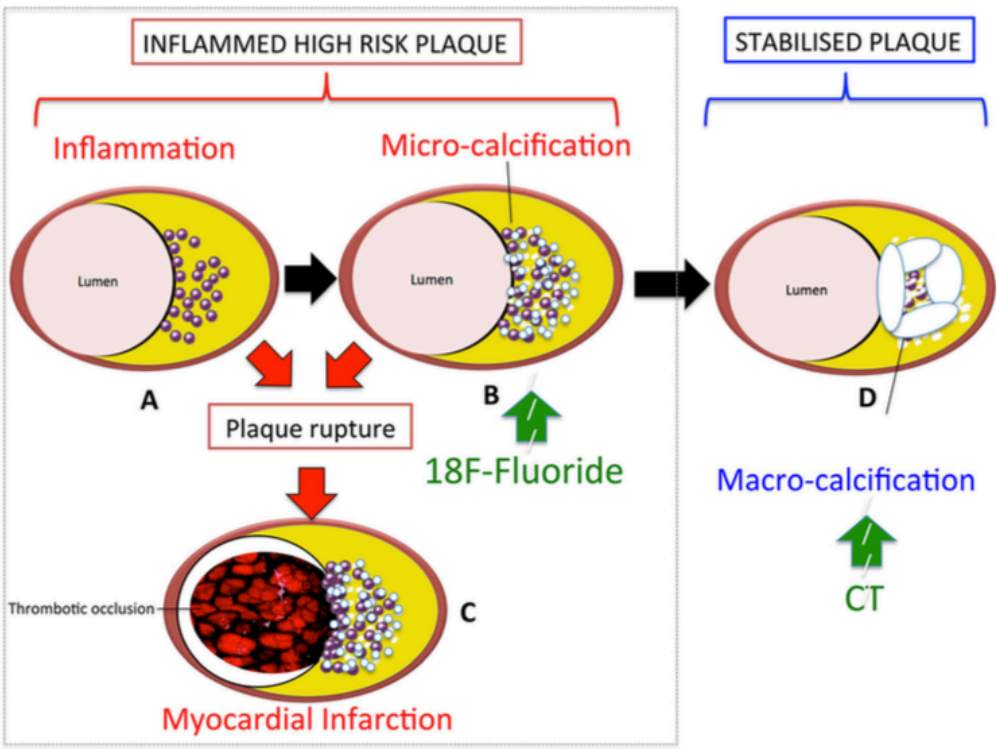

Table 1-1 Key differences between micro and macrocalcification

	Microcalcification	***Macrocalcification***
Size	<5μm	>5μm
Stage of calcification	Early	Late
Inflammation	Persistent	Healed
Surface area	High	Low
Exposed hydroxyapatite	High	Low
Risk of rupture	High risk of rupture	Low risk of rupture
Computed Tomography/ X-ray angiography	Undetectable	Detectable
18F-fluoride binding on Positron Emission Tomography	Avid binding	Low binding

1.5.3. ALTERNATIVE NOVEL TRACERS

The great strength of PET imaging is that tracers can ultimately be developed to target any pathological process of interest and can therefore be directed to any of the features that characterise high-risk plaques. Whilst this is an expensive process, the studies using 18F-fluoride have clearly demonstrated that metabolic plaque imaging in the coronary arteries is now feasible, making an expansion of activity in this area likely.

Given its pathophysiological importance, inflammation would appear to be the prime potential target. As discussed 18F-FDG, whilst an excellent tracer for measuring inflammation in the aorta and carotids arteries, is of limited use in the coronary arteries, the metabolic activity of which governs the majority of clinical events. There is therefore an urgent need to develop more macrophage-specific tracers that crucially do not demonstrate increased activity in adjacent structures as the myocardium.

There has been significant interest in inflammation imaging with 68Ga-DOTATATE, a novel tracer with receptor binding specificity to somatostatin 2. Although primarily overexpressed in malignancies, in particular neuro-endocrine tumors, somatostatin receptors are thought to be preferentially expressed in damaged and proliferating endothelium and by activated macrophages (Armani et al., 2007, Adams et al., 2005, Dalm et al., 2003). Indeed murine data has shown good

correlation between tracer activity and macrophage density in atherosclerotic lesions (Li et al., 2013). Observational data from oncology patients has reported uptake for this tracer in large vessels, again demonstrating a good correlation with calcific plaque burden. Interestingly, in this study, 18F-FDG uptake did not colocalise with 68Ga-DOTATATE suggesting labeling of distinct process within vascular inflammation. (Li et al., 2012a) Furthermore, uptake has been described in the coronaries with modest correlation with calcific plaque burden and previous cardiovascular events. (Rominger et al., 2010, Mojtahedi et al., 2015).

Other tracers that have shown early promise in atherosclerotic inflammation imaging include *11C-PK11195, 18F-FMCH and 11C-choline* (Laitinen et al., 2009, Gaemperli et al., 2012, Pugliese et al., 2010). Furthermore, tracers aimed at other important features of plaque vulnerability such as hypoxia (*18F-Fluoromisonadazole)* (Mateo et al., 2014) and neoangiogenesis (*18F-Galacto and 18F-fluciclatide)* (Brooks et al., 1994, Beer et al., 2006) have also shown promise and studies to assess their role in patients with atherosclerosis are underway.

1.6. MAGNETIC RESONANCE IMAGING

Magnetic resonance imaging (MRI) has emerged as a powerful investigation for cardiovascular disease offering high-resolution images without radiation, thus allowing serial imaging to monitor disease progression and regression. Similar to PET-CT, various processes within plaque biology remain legitimate targets for development of specific MRI contrast agents (Winter et al., 2003, Burtea et al., 2008, Nahrendorf et al., 2006, Briley-Saebo et al., 2008). MRI evaluates response of a tissue subjected to transient electromagnetic radiofrequency pulses when placed in a strong static magnetic field. It uses different contrast weightings — T1, T2, proton-density, and time-of-flight providing insights into biophysical and biochemical properties including physical state, chemical composition and concentration, water content, molecular motion, or diffusion. In atherosclerotic disease, MRI can distinguish different plaque components including the fibrous cap, the lipid core and areas of calcification (Cai et al., 2005, Yuan et al., 2001). For instance, on the T1-weighted images, plaque fibrous tissue and lipid core appears iso to hypointense where as on T2-weighted images, fibrous tissue has a high intensity signal intensity while the lipid content may appears hypointense. In contrast, calcific areas appears hypointense on both T1- and T2-weighted images. Furthermore, MRI provides a high degree of spatial resolution and soft tissue contrast yielding excellent anatomic detail. However, it is of inherently low sensitivity for molecular imaging applications. Given low temporal resolution, MR imaging is best suited for the study of large or relatively “static” arteries, such as the carotid arteries and the aorta. Because of their small dimensions and their continuous motion during data

acquisition, coronary arteries remain a particular challenge (Vancraeynest et al., 2011).

MRI has been shown to identify plaque ruptures (Yuan et al., 2002) and hemorrhages (Chu et al., 2004) in carotid atherosclerosis with a good correlation between the plaque components with histopathology (Yuan et al., 2001). However, one of the main limitations with MRI in identification of high-risk vulnerable plaques is poor reproducibility, especially in context of necrotic core and fibrous cap (Touze et al., 2007). Alternative imaging strategies have therefore been developed to overcome this limitation with use of contrast media that enables signal enhancement of the tissues and this expands the overall assessment of the plaque. Indeed novel MR contrasts allows targeted imaging of the cellular mediators of plaque components in atherosclerosis. In comparision to the picomolar range of the tracers for PET imaging, MRI contrast requires relatively large quantities of contrast agents to the site of interest at micromolar range. These could be gadolinium-based ions chelated to small molecules leading to bright appearance or positive contrast on T1-weighted images or iron oxides based contrast, causing signal drop out and an intense negative contrast on T2*-weighted images.

1.6.1. ULTRASMALL SUPERPARAMAGNETIC PARTICLES OF IRON OXIDE ENHANCED MRI

Recently a novel class of MRI contrast agents containing superparamagnetic particles of iron oxide (SPIO) has been developed that provides additional biological and functional information through the detection of cellular inflammation within tissues. The initial focus of SPIO development was imaging of the reticuloendothelial system and oncology imaging. Subsequent studies have demonstrated incorporation of SPIOs into aortic atherosclerotic plaques in rabbits (Schmitz et al., 2000). In comparison to SPIOs, the smaller ultrasmall SPIOs (USPIO) have additional property to extravasate via tight capillary pores that makes them an attractive option for cellular MR imaging. With a particle size in the range 10-30 nm, USPIOs escape immediate recognition by the reticulo-endothelial system and persist for longer in the bloodstream allowing them to be used to assess the accumulation of macrophages within vascular and lymphatic tissues (Harisinghani et al., 2003, Heesakkers et al., 2008, Kooi et al., 2003a, Trivedi et al., 2006a, Tang et al., 2009a). Capitalising on these effects, USPIOs have been used in the diagnosis of diseases of the liver, spleen and lymph nodes in oncology imaging. Current preparations are biodegradable and safe for clinical administration (Bernd et al., 2009, Bourrinet et al., 2006, Muller et al., 2007). The safety of USPIOs as a contrast agent in humans is well established (Ersoy et al., 2004, Li et al., 2007, Li et al., 2005, Prince et al., 2003, Neuwelt et al., 2007). Most of these studies have examined and confirmed its utility as a blood-pool contrast agent. However, it has also been assessed for its use in lymph node imaging for cancer staging. In a study of patients with prostate cancer, USPIOs were administered after baseline scan and further was performed at 5, 8 and 24 hours using a 1.5 T scanner. Maximum signal to noise ratio

was observed in lymph nodes at 24 hours on T2*-weighted MR imaging (Harisinghani et al., 2007).

USPIO have also been shown to accumulate in the aortae of hypercholesterolemic rabbits (Ruehm et al., 2001, Herborn et al., 2006) and in murine models of AAAs (Turner et al., 2009). Susceptibility artefacts were detected in the aortic wall at day 2 to 3 post administration of contrast and signal voids were observed as a result of T2/T2* effects. Histology confirmed the accumulation of iron particles under the endothelium and into the medial layer of diseased vessels (Herborn et al., 2006). USPIOs have been shown to reduce T2*-weighted MRI signal within the carotid plaques in patients undergoing carotid endarterectomy, and it is suggested that USPIO signal effect correlates with the propensity for plaque rupture. Indeed, the presence of intracellular USPIO in plaque macrophages has been demonstrated in the carotid plaque (Kooi et al., 2003b, Trivedi et al., 2006b). The ATHEROMA (Atorvastatin Therapy: Effects on Reduction of Macrophage Activity) study evaluated the effects of low and high-dose statin therapy on carotid plaque inflammation as determined by ultrasmall superparamagnetic iron oxide (USPIO)-enhanced carotid magnetic resonance imaging (MRI). Using serial USPIO-enhanced MR imaging over a 3-month period, a significant reduction in carotid plaque inflammation with high-dose statin-lowering therapy was reported (Tang et al., 2009a).

1.6.2. USPIO IN ANEURYSMAL DISEASE

The cellular uptake of USPIO in aneurysms was first reported in 2009 in patients with malignancies (Truijers et al., 2009). Since then prospective studies have demonstrated the feasibility of this technique using T2* qualitative and quantitative analysis (Sadat et al., 2011a, Richards et al., 2011b). Richards et al. conducted a series of MRI studies in patients with AAA and shown that uptake of USPIO in AAA correlates with macrophage activity and identifies cellular inflammation. Using 3T MRI scanner, asymptomatic AAA patients (n=29; aneurysm diameter 4.0-6.6 cm) from surveillance program were imaged before and 24-36 h after administration of USPIO. Histological examination of aneurysm tissue has confirmed co-localization and uptake of USPIO in areas with macrophage infiltration (Richards et al., 2010). Furthermore, patients with deep-seated mural uptake had 3-fold higher aneurysm growth rate as compared to patients with peri-luminar or diffuse patchy uptake. Uptake of USPIOs therefore, may identify rapidly expanding AAA and possible rupture. If future studies confirm these findings, this technique holds major promise in risk-stratifying patients with abdominal aortic aneurysms.

1.7. CORONARY CALCIUM AND COMPUTED TOMOGRAPHY CORONARY ANGIOGRAPHY

Ever since Agatston et al. described the calculation of the total calcific burden using coronary artery calcium (CAC) scoring in 1990, this method has become a reliable and reproducible non-invasive technique to quantify coronary atherosclerosis (Agatston et al., 1990). Total CAC score is derived by multiplying individual areas of calcified plaque by a factor derived from the maximal plaque density (CT attenuation) in Hounsfield Units, and then adding the values obtained for all coronary plaques identified. Subsequent studies have established CT calcium scoring to be one of the most powerful predictors of future cardiovascular events in asymptomatic individuals irrespective of ethnicity (Detrano et al., 2008, Greenland et al., 2004), (Budoff et al., 2007, Arad et al., 2005, Taylor et al., 2005). Moreover risk prediction can be further refined by examining the progression of coronary calcification (Raggi et al., 2004b).

CT calcium scoring quantifies macroscopic calcification in the coronary arteries. These plaques are believed to be stable, healed and unlikely to rupture. Indeed, it is well established that calcific fibroatheromas and calcified nodules are very rarely responsible for coronary thrombosis (Virmani et al., 2006b). Why then does calcium scoring predict cardiovascular risk related to rupture? The likely explanation is that is provides a surrogate of plaque burden. The more calcified stable plaques you have the more unstable non-calcified plaques you are also likely to have in addition (Otsuka et al., 2013, Mauriello et al., 2013).

Due to its wide availability and adoption, one of the most important noninvasive techniques for the evaluation of the coronary vasculature is CTCA. Indeed, recent studies and guidelines support the utility of this modality for assessment of patients with new onset anginal chest pain for evaluation of coronary stenosis (SCOT-HEART investigators, 2015, Douglas et al., 2015, Skinner et al., 2010).

Assessment of plaque morphology with CT allows identification of several high-risk features on CTCA primarily because of its ability to assess not only the lumen but also the vessel wall. Indeed, several studies have reported on the correlation between CTCA plaque features with invasive coronary imaging modalities, such as IVUS, IVUS-VH, and OCT. Identification of spotty calcification using CTCA has been associated with high-risk plaque type (Motoyama et al., 2007). Furthermore, Motoyama et al reported that positive remodeling and low attenuation plaque on CTCA predict a higher likelihood of future plaque rupture (Motoyama et al., 2009b). Others have described features such as the "Napkin ring" or the "Signet ring" sign for identification of plaque vulnerability (Maurovich-Horvat et al., 2010). However, interpretation of such features on CTCA comes with significant limitations. Suboptimal resolution does not allow precise definition of the vascular boundary, and the extent of positive remodelling may be over or underestimated. Similarly, low attenuation plaque is defined based on specific thresholds in the Hounsfield unit measurements which may be influenced by various imaging and technical parameters in regions of non-calcified plaque.

1.8. INTRAVASCULAR ULTRASOUND IMAGING

Intravascular ultrasound (IVUS) was one of the earliest invasive techniques to allow imaging of the lumen and vessel wall and despite the development of novel techniques, IVUS still remains the standard method for assessing plaque burden. This technique also allows us to assess many other structural features within the plaques, including positive remodelling, thrombi, plaque length, lumen narrowing, spotty and macroscopic calcification and the presence of a lipid-rich core (Yamagishi et al., 2000, Kotani et al., 2003, Fujii et al., 2003, Ehara et al., 2004, Garcia-Garcia et al., 2014). Moreover recent advances make the use of ultrasound backscatter (VH-IVUS) thus providing even more information with respect to plaque morphology and characteristics (Garcia-Garcia et al., 2009a). Various plaque contents such as calcium, fibrous tissue, fibrofatty tissue and necrotic core can be resolved. Moreover as discussed VH-IVUS can classify plaque types such as pathological intimal thickening, thick and thin capped fibroatheromas with a high degree of accuracy (Garcia-Garcia et al., 2009a).

VH-IVUS has become widely available and has been the subject of intense investigation, having to date been tested in 3 major prospective clinical studies: Providing Regional Observations to Study Predictors of Events in the Coronary Tree (PROSPECT)(Stone et al., 2011b) VH-IVUS in Vulnerable Atherosclerosis (VIVA)(Calvert et al., 2011) and the European Collaborative Project on Inflammation and Vascular Wall Remodeling in Atherosclerosis (ATHEROREMO-IVUS) study (Cheng et al., 2014). However, the prospects of identifying patients or

indeed plaques that will cause future cardiovascular events, using radiofrequency IVUS, have been rather disappointing. Indeed amongst 697 patients enrolled in the PROSPECT study, 595 thin- cap fibroatheromas were identified by IVUS across the cohort, only 26 of these plaques were sites of subsequent events at 3 years, and the majority of events were related to rehospitalization for angina rather than myocardial infarction. Plaque burden greater than 70%, minimal luminal area less than 4 mm2 and presence of thin capped fibroatheromas were thought to be the primary drivers. However when all these three factors were present in the same lesion, the positive predictive value of an event was only 18 %. Consistent with these findings, the VIVA and ATHEROREMO- IVUS studies suggested that whilst identification of thin fibrous cap athermas identified subsequent MACE, it did not predict future MI per se, and once again the vast majority of these lesions did not result in clinical sequelae (Calvert et al., 2011, Cheng et al., 2014).

One of the important limitations of VH-IVUS is its limited axial resolution of 100 to 150 microns (Rodriguez-Granillo et al., 2005), which means that it will tend to overestimate the number of plaques with a thin fibrous cap (traditionally defined by a thickness of < 60μm). This may account for the low event rate associated with VH-IVUS defined TCFAs.

1.9. AIMS AND HYPOTHESIS

The overall aims of these studies are to assess the role of novel molecular imaging techniques in human atherosclerotic and aneurysmal disease. A multimodality approach for assessment of atherosclerotic plaques and aneurysms will be undertaken with 18F-FDG and 18F-fluoride PET-CT as markers of inflammation and active calcification. We will gain complementary information regarding plaque inflammation, vulnerability and rupture in patients with stable and unstable coronary artery disease in the culprit and remote atherosclerotic plaques. Role of inflammation and calcification will be assessed in patients with AAA and compared with patients with atherosclerosis.

In Chapter 3, utilising cardiac gated PET-CT imaging, we will develop the methodology for assessing coronary uptake of PET tracers. The tracer activity will be assessed in patients with acute myocardial infarction and patients with stable angina. The plaque characteristics will be assessed using multi-modality imaging with CTCA and VH-IVUS in patients with stable angina and histopathological analysis of atheromatous tissue from endartectomy specimens will be analysed to assess 18F-Fluoride uptake in patients with symptomatic carotid disease.

In Chapter 4, systemic atherosclerotic plaque inflammation will be assessed in patients with acute myocardial infarction and will be compared to those with stable

angina. The clinical relevance of infarct size, remote plaque inflammation and the risk of recurrent myocardial infarction will also be evaluated.

In Chapter 5, the relationship between the size of aneurysm and inflammation will be studied. Using 18F-FDG as a marker of metabolic inflammation, uptake will be quantified in patients will smaller aneurysms and compared to patients with atherosclerosis.

In Chapter 6, the relationship between metabolic imaging of inflammation will be assessed against the cellular inflammation with USPIO, using AAA as a model of inflammation. Multimodality hybrid imaging will be used to register the PET and R2* color maps to derive the similarities and differences on PET and MR platforms.

The following hypothesis will be addressed:

i) Plaque inflammation and calcification with 18F-FDG and 18F-fluoride will be higher in patients with ruptured and unstable coronary atherosclerotic plaques as compared to those with stable plaques. (Chapter 3).

ii) Patients with recent myocardial infarction will have higher remote atherosclerotic plaque inflammation as compared to patients with stable coronary disease. (Chapter 4).

iii) Patients with abdominal aortic aneurysms will have higher inflammation in the aneurysmal part of the aorta as compared to the non-aneurysmal part of the aorta and patients with atherosclerosis (Chapter 5).

iv) Using AAA as a model of vascular inflammation, cellular inflammation as assessed by USPIO enhanced MRI will concur with metabolic activity using 18F-FDG PET. (Chapter 6).

Chapter 2. METHODS

2.1. OVERVIEW

The specific study designs and methodology for each of the cohorts are described in detail in relevant chapters. The following sections will provide the overview of the patient populations and the novel imaging modalities utilised in these studies.

2.2. PATIENT POPULATION

2.2.1. PATIENTS WITH CORONARY AND CAROTID ATHEROSCLEROSIS

Patients were recruited from the Edinburgh Heart Centre, Royal Infirmary of Edinburgh in three cohorts: patients with acute ST- or non-ST-segment elevation myocardial infarction, patients with stable angina pectoris undergoing elective invasive coronary angiography, and patients undergoing carotid endartectomy for symptomatic carotid artery disease.

Consecutive patients with myocardial infarction were approached and recruited if they fulfilled the criteria for type 1 myocardial infarction according to the Universal Definition of Myocardial Infarction (Thygesen et al., 2012). ST segment elevation myocardial infarction was defined as new ST segment elevation at the J point in two contiguous leads with the cut-points: ≥0.1 mV in all leads except V_2-V_3 where the thresholds were ≥0.2 mV for men ≥40 years and ≥0.25 mV for women (Thygesen et al., 2012).

Consecutive patients with stable angina pectoris were recruited if they had typical symptoms of exertional anginal chest pain, previously documented coronary artery disease (>70% stenosis of at least one major epicardial coronary artery), and had been scheduled for invasive coronary angiography. Patients were excluded if they had suffered an acute coronary syndrome within the last 3 months.

Patients with typical symptoms and signs of an acute transient ischemic attack, amaurosis fugax or stroke were recruited within 1-14 days of symptom onset. All patients underwent clinical evaluation and carotid Doppler assessment. Inclusion criteria were carotid stenosis >50% (North American Symptomatic Carotid Endarterectomy Trial, 1991) consistent with clinical presentation, and planned carotid endarterectomy.

Exclusion Criteria

Exclusion criteria were age <50 years, insulin-dependent diabetes mellitus, women of childbearing age not taking contraception, severe renal failure (serum creatinine >250 μmol/L), known contrast allergy and inability to provide informed consent. Only patients older than 50 years were recruited in the study to reduce any long-term risks associated with radiation exposure. Uncontrolled diabetes and high blood glucose concentrations (>11 mmol/L) interfere with image quality of 18F-FDG PET imaging due to competition between glucose and 18F-fluorodeoxyglucose for cellular entry. It has therefore been a convention to exclude such patients from vascular 18F-fluorodeoxyglucose positron emission tomography studies (Dweck et al., 2012a, Dweck et al., 2011, Rudd et al., 2002, Tawakol et al., 2013, Elkhawad et al., 2012, Maki-Petaja et al., 2012). Studies were performed with the approval of the local research ethics committee, in accordance with the Declaration of Helsinki, and with the written informed consent of each participant.

2.2.2. PATIENTS WITH ATHEROSCLEROSIS AND ANEURYSMAL DISEASE

Patients were recruited from Addenbrooke's Hospital, Cambridge and the Royal Infirmary of Edinburgh in two cohorts: (i) A study cohort consisting of patients with abdominal aortic aneurysm and (ii) a control cohort of age- and sex- matched atherosclerotic patients. All control subjects were recruited in Cambridge, and the study patients were recruited across both sites. Consecutive patients presenting at both institutions were considered for enrolment. The inclusion criteria for the study cohort were age >50 years and presence of an aneurysm between 3.0 and 5.5 cm. The inclusion criteria for the control cohort were clinically stable (>6 months) cardiovascular disease (defined as previous myocardial infarction, stroke, or peripheral vascular disease). Exclusion criteria for both cohorts were insulin dependent diabetes, type 2 diabetes with a fasting glucose of >11 mmol/L, illness/condition that may result in a life expectancy <2 years, women of childbearing age not taking contraception, severe renal failure (serum creatinine >250 μmol/L), hepatic cirrhosis (Child Pugh score B or C), planned AAA surgery within 6 months of screening or a contra-indication to magnetic resonance imaging, known contrast allergy or the inability to provide informed consent. Baseline clinical characteristics and cardiovascular risk factors were recorded. Full blood count, renal and lipid profiles were measured. The study was performed in accordance to the protocol approved by the local research ethics committee and the Declaration of Helsinki. All subjects provided written informed consent.

2.3. POSITRON EMISSION TOMOGRAPHY - COMPUTED TOMOGRAPHY IMAGING

Patients underwent combined PET-CT scanning using validated PET-CT imaging protocols (Dweck et al., 2012a, Dweck et al., 2011, Rudd et al., 2002, Tawakol et al., 2013, Elkhawad et al., 2012, Maki-Petaja et al., 2012). In Edinburgh, Siemens PET CT scanner (Biograph mCT, Siemens Medical Systems, Erlangen, Germany) was used while in Cambridge, an equivalent GE Discovery 690 PET/CT scanner was utilized for scanning. The detailed scanning protocol has been described in relevant sections. Briefly, after consenting to participate in the study, patients were invited to undergo a PET-CT scan. Patients were asked to follow a low-carbohydrate, high-protein and high-fat diet for at least 24 h prior to undergoing 18F-FDG PET-CT (Elkhawad et al., 2012, Maki-Petaja et al., 2012) and refrain from alcohol and caffeine on the day of the scan prior to 18F-FDG scan to minimise myocardial uptake. There were no restrictions for 18F-fluoride scan. A 20 G cannula was inserted in a large peripheral vein and blood was drawn for analysis. Patients were then administrated radioactive tracer and rested in a quiet environment. Based on previous studies (Rudd et al., 2002, Dweck et al., 2012a, Dweck et al., 2011), the tracer uptake times were 90 minutes for 18F-FDG and 60 minutes for 18F-fluoride scan to produce optimal contrast between the tissue of interest and the blood pool.

Image Acquisition and reconstruction

Patients were transferred onto the PET-CT scanner and a non-contrast-enhanced attenuation correction CT scan was performed followed by a PET scan. The PET

data were reconstructed using standard time of flight reconstruction algorithms. Corrections were applied for attenuation, dead time, scatter and random coincidences.

Image Analysis

Anonymized PET-CT datasets were analyzed using OsiriX workstation (64 bit; version 5.5.1 OsiriX Imaging Software, Geneva, Switzerland) (Joshi et al., 2013, Maki-Petaja et al., 2012). Readers were blinded to the patients' clinical status and presented images in a random order. PET images were fused with the CT, and regions of interest (ROIs) drawn around the tissue of interest. The general principles of coronary and aortic PET image analysis have been illustrated in the examples below (Figure 2-1 and Figure 2-2). Within these regions, tracer activity was measured using standard uptake values (SUV; the decay corrected tissue concentration of the tracer divided by the injected dose per body weight) and corrected for blood pool activity in the superior vena cava to provide tissue-to-background ratios (TBRs).

Figure 2-1 Tracer uptake in coronary arteries.

The tracer uptake within the tissue of interest was analysed by fusing the CT image (A) with PET image (C). Region of interests were then drawn on the CT (B) and fused PET-CT (D) image to calculate standardised uptake values.

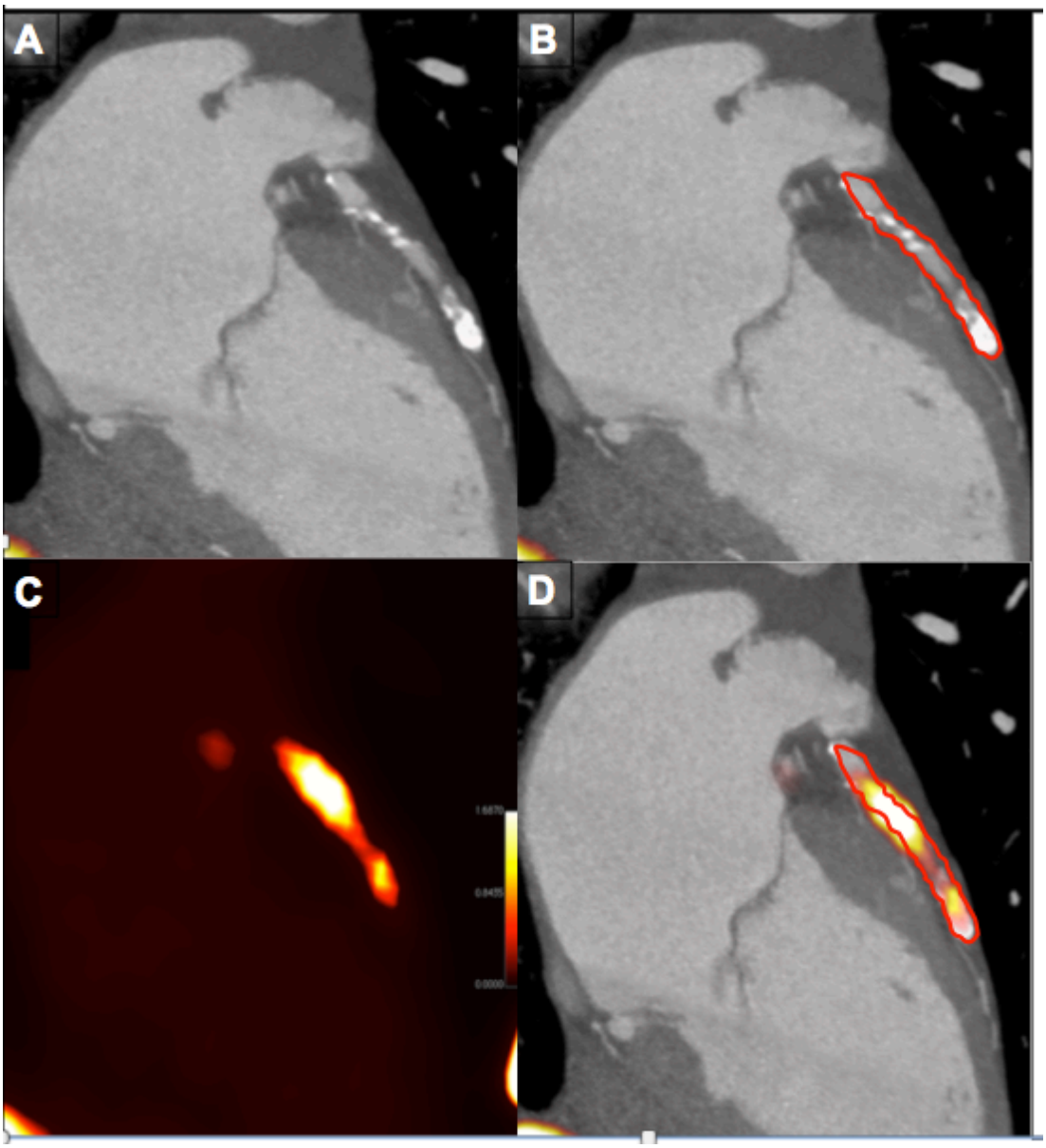

Figure 2-2 Tracer uptake in the aneurysmal tissue

In this illustration, tracer uptake is visualised within the shoulder region of the aortic aneurysm on fused sagittal PET-CT scan (A). The uptake within the aneurysmal tissue was analysed by drawing regions of interest along the aneurysmal adventitial border (B). These were then applied to the PET image to derive the standardised uptake values (C). Panel D represents fused PET-CT image.

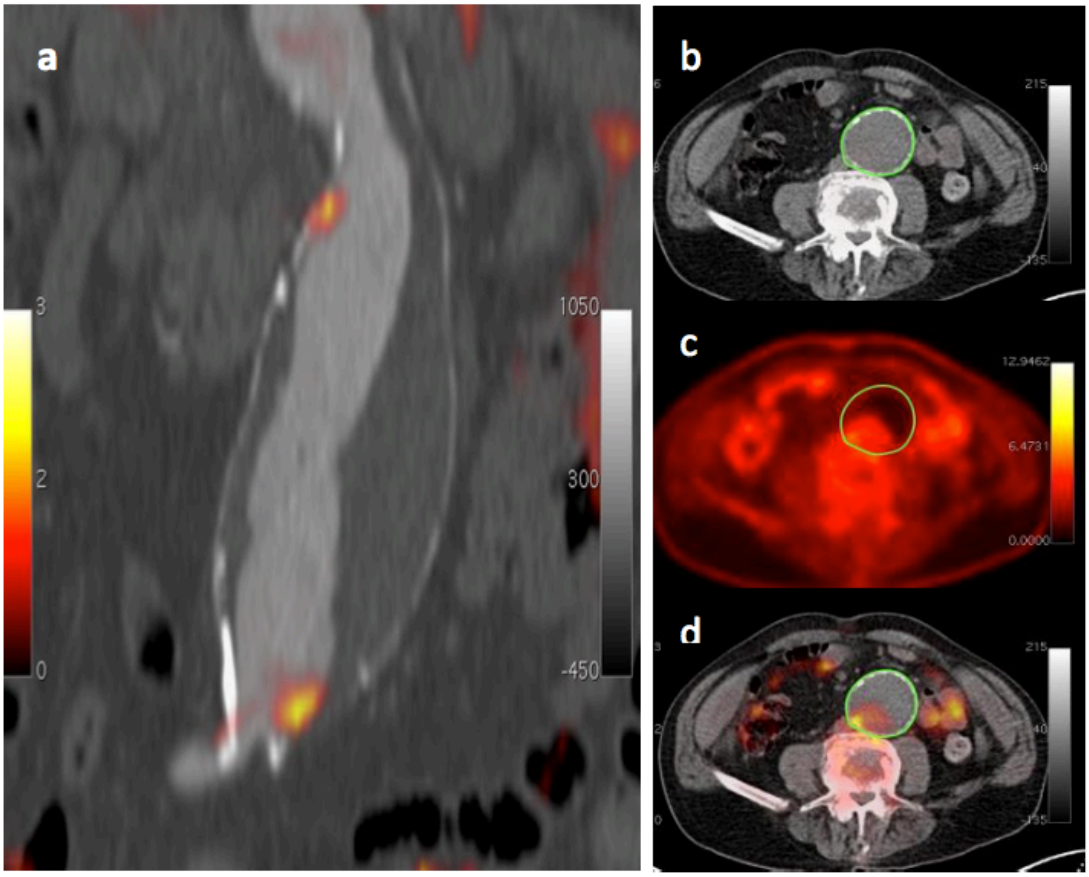

2.3.1. REPRODUCIBILITY OF PET-CT IMAGING

Several studies have assessed the reproducibility of PET CT imaging in multiple vascular beds (Rudd et al., 2007, Rudd et al., 2008). The scan re-scan reproducibility of PET imaging within the aorta and carotids over a 2-week period is excellent (Rudd et al., 2007, Rudd et al., 2008). Furthermore, the intra-observer agreement is very high with intra-class correlation coefficients values ranging between 0.93 and 0.98. Similarly, the results from our previously reported studies have shown an excellent intra-observer agreement of PET-CT imaging in the coronary vasculature (Dweck et al., 2012a).

The reproducibility of vascular PET signal is comparable to more established imaging modalities (Rudd et al., 2007, Rudd et al., 2008) that includes the magnetic resonance imaging (MRI)(Varghese et al., 2005), intra-vascular ultrasound (Hagenaars et al., 2000), and computed tomography (Budoff et al., 2006) Additionally, the high sensitivity of FDG-PET might allow detection of small metabolic changes within plaque that occur before structural alterations can be detected by other modalities (Rudd et al., 2007, Rudd et al., 2008).

2.4. COMPUTED TOMOGRAPHY

Patients underwent coronary artery calcium and CT angiography or aortography following acquisition of PET/CT images. In patients undergoing CT coronary angiography, oral metoprolol 50 mg was administered in patients with a heart rate of greater than 60 beats/min. If necessary, patients were given further intravenous metoprolol. Patients with a contraindication to beta-blockade were considered for oral verapamil 80 mg followed by intravenous verapamil 2.5 mg. For the acquisition of CTCA, following setting were used: 330 ms rotation time, 100 (body mass index [BMI] <25 kg/m^2) or 120 (body mass index >25 kg/m^2) kV tube voltage, 160-245 mAs tube current, 3.8 mm/rotation table feed, prospective (heart rate regular and <60/min), or retrospective (heart rate >60 / min) electrocardiogram-gated. Depending on the BMI, a bolus of 80-100 mL of contrast (400 mgI/mL; Iomeron, Bracco, Milan, Italy) was injected intravenously at 5 mL/s, after determining the appropriate trigger delay with a test bolus of 20 mL contrast material.

Off-line analyses using automated computerised software programmes that employ the Agatston scoring method using 130 HU thresholds was used to determine degree of coronary calcification. Computed tomography scans were reported by two trained observers (radiologist and cardiologist). Vitrea software (Vital Images Inc, Minnetonka) was be used to visualise computed tomography coronary angiography data and perform region of interest measurements on particular slices and objects.

2.5. INTRA-VASCULAR ULTRASOUND

Intravascular ultrasound analysis was performed as described previously (Calvert et al., 2011) using dedicated VIAS software (Volcano Corp, USA) by operators blinded to the positron emission tomography data (Figure 2-3). Briefly, in patients undergoing coronary angiography, grey-scale and radiofrequency intravascular ultrasound was acquired with a dedicated IVUS catheter (20 MHz Eagle Eye Platinum Catheters [Volcano Corp, San Diago, CA, USA]), passed over coronary guidewire after injecting intracoronary nitrates with a motorized catheter pullback. The analysis was performed offline and was not used for procedural guidance. Regions of interest were drawn around the external elastic membrane and luminal borders, and plaque area and composition (dense calcium, necrotic core, fibro-fatty tissue and fibrous tissue) calculated (Calvert et al., 2011), (Mintz et al., 2001). The presence of microcalcification (spotty calcification in the absence of acoustic shadowing on ≥3 consecutive frames) and the maximum frame necrotic core (the highest percentage of necrotic core on a single frame) were recorded. The remodeling index was defined as the ratio between the external elastic membrane cross-sectional area of the lesion and a proximal reference region in the same vessel. Plaques were classified as thin-cap fibroatheroma, thick-cap fibroatheroma, pathologic intimal thickening or fibrocalcific plaque as defined previously (Garcia-Garcia et al., 2009b).

Figure 2-3: Grey-scale and radiofrequency intravascular ultrasound analysis

The grey-scale intravascular ultrasound (A) was used to identify the lumen (B) and the external elastic lamina (C). This allowed assessment of plaque dimensions such as plaque burden (D). Radiofrequency ultrasound was then used to assess plaque characteristics (E). Finally the composition of the plaque elements such as fibrous, fibro-fatty tissue, necrotic core and calcium were calculated.

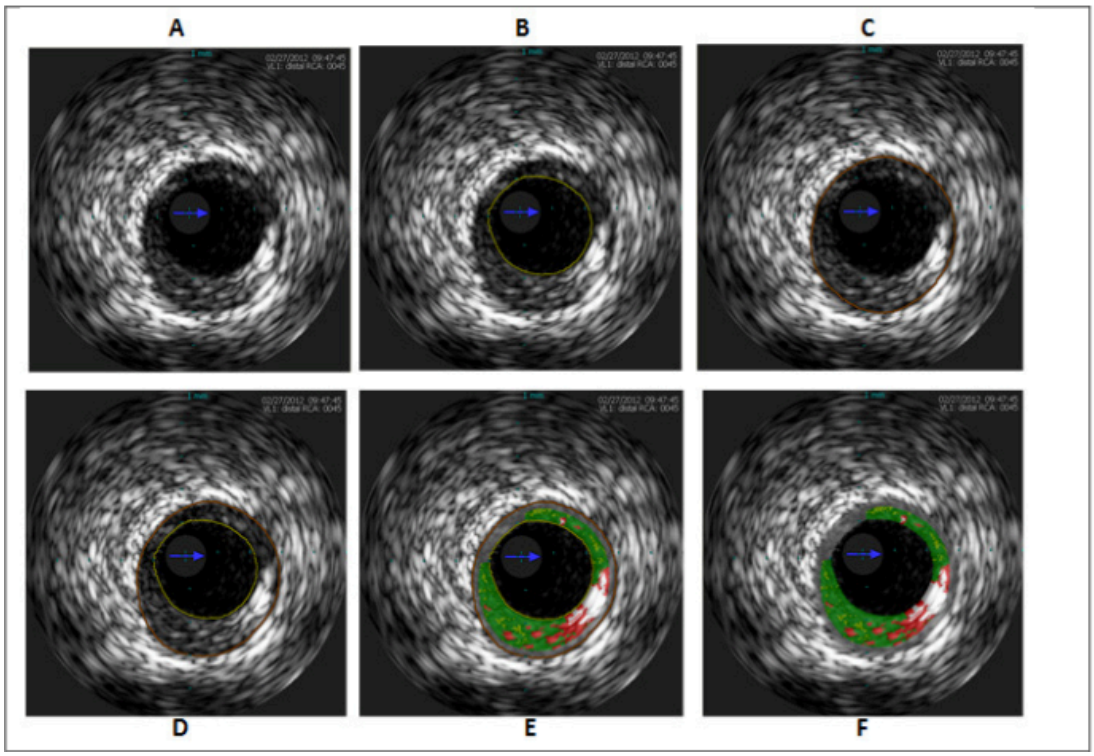

2.6. HISTOLOGICAL ANALYSIS

2.6.1. RATIONALE FOR IMMUNOHISTOCHEMISTRY OF CAROTID ATHEROMA

We used immunohistochemistry to investigate macrophage infiltration (CD68), calcification activity (tissue non-specific alkaline phosphatase and osteocalcin), and cell death (apoptosis, cleaved caspase 3; presence of necrotic core).

Inflammation is a key feature of human atherosclerosis and is thought to precede the early stages of calcification (Aikawa et al., 2007). CD68 is expressed by macrophages and has been closely correlated with the 18F-FDG signal in the carotid arteries. Apoptotic cell death is a recognized phenomenon in atherosclerotic plaque and is thought to be detrimental to plaque stability (Kockx and Herman, 2000). Cleaved caspase 3 is a critical executioner of apoptosis, being responsible for the proteolytic cleavage of many key proteins, such as the nuclear enzyme poly (ADP-ribose) polymerase (PARP). Its expression has been previously demonstrated in atherosclerotic plaque (Fernandes-Alnemri et al., 1994).

During propagation of atherosclerosis, vascular smooth muscle cells undergo osteogenic differentiation (New and Aikawa, 2011). Additionally, matrix vesicles released from living cells and apoptotic bodies from dying macrophages and smooth muscle cells are thought to provide a nidus for microcalcification(Proudfoot et al., 2000, Shanahan, 2007). Tissue non-specific alkaline phosphatase (TNAP) is an

enzyme that plays a key role in atherosclerotic calcification by increasing availability of inorganic phosphate levels through the hydrolyzing pyrophosphate, a key inhibitor of mineralization (Demer and Tintut, 2008). Unlike dyes such as alizarin red that directly stains tissue calcium, TNAP provides information about calcification activity and gives information distinct from mere anatomical calcium.

Osteocalcin, or bone Gla protein, is a small protein secreted by osteoblasts that can undergo γ-carboxylation (Kapustin and Shanahan, 2011). The γ-carboxylated form binds hydroxyapatite and is abundant in bone extracellular matrix. Osteocalcin is thought to be a regulator of osteochondrogenic differentiation of pathologically mineralizing vascular smooth muscle cells (Kapustin and Shanahan, 2011). The presence of osteocalcin is therefore suggestive of up regulated vascular mineralization (Idelevich et al., 2011).

2.6.2. CAROTID ATHEROMA

Intact atherosclerotic plaques were retrieved at the time of carotid endarterectomy and scanned using *ex-vivo* PET-CT to allow precise anatomical co-localisation of 18F-fluoride activity with pathological evidence of plaque rupture. Plaques were divided into 18F- fluoride positive and negative areas, and histological sections were assessed using Movat's pentachrome and immunohistochemistry to investigate both calcification activity (tissue non-specific alkaline phosphatase and osteocalcin), macrophage infiltration (CD68) and cell death (apoptosis, cleaved caspase 3; presence of necrotic core).

2.6.3. *EX-VIVO* 18F-FLUORIDE PET

Carotid plaques were retrieved intact at the time of carotid endarterectomy, and photographed before being wrapped in foil and frozen at -80 °C. Subsequently, they were thawed in a batch and immersed in 18F- fluoride solution diluted with phosphate buffered saline (PBS) to a total activity of 10 MBq/mL. After 60 min, plaques were rinsed 3 times in PBS before being oriented and placed in a PET-CT hybrid scanner (64-multidetector Biograph mCT, Siemens Medical Systems, Erlangen, Germany). After an attenuation correction CT scan, PET imaging was undertaken over a single bed for 15 min.

Histology and Immunohistochemistry

Immediately following scanning, plaques were fixed in 4% paraformaldehyde for 24 hours before transfer to 70% ethanol. Plaques were decalcified in ethylenediaminetetraacetic acid before being divided into segments with or without 18F-Fluoride uptake that were paraffin-embedded, and 5-μm sections were prepared and stained with Movat's pentachrome. Immunohistochemical staining for CD68 expression (mouse anti-human CD68 mAb, M087601-2, Dako), cleaved caspase 3 (anti-human rabbit mAb #9664, Cell Signalling Technology) and tissue non-specific alkaline phosphatase (anti-human rabbit pAb CAT#LF PA50004, Abfrontier) was then undertaken following heat induced epitope retrieval (HIER) using 0.01 M citrate buffer at pH 6.0 in a decloaking chamber. Osteocalcin staining (anti-human mouse mAb ab13418, Abcam) required no HIER. Sections were stained using a Leica

Vision Biosystems Bond x immunostaining robot. Optimization of antibody dilution was undertaken by determining positive and negative controls. Positive controls for CD68 were generated using human kidney, cleaved caspase 3 using sections of normal human tonsil and spleen, and for tissue non-specific alkaline phosphatase and osteocalcin using decalcified human bone to determine optimal antibody dilutions. Negative controls were generated by omitting the primary antibody. After blocking in peroxide for 10 min, sections were incubated with the specific anti-human antibodies for 2 hours at room temperature at the following dilutions: CD68 1:100, osteocalcin 1:200, cleaved caspase 3 1:150, and tissue non-specific alkaline phosphatase 1:100. All incubation steps were followed by washing in TBS/Tween. Sections for osteocalcin were incubated for 15 min with pre-polymer/post primary followed by 15 min with polymer (HRP) for all antibodies prior to DAB (3,3'-Diaminobenzidine) visualization and haematoxylin counterstaining. Sections were dehydrated in graded ethanol, cleared in xylene before cover slipping in Pertex.

Images were taken on a Zeiss Axioskop2 fitted with an Axiocam MRc digital camera using Axiovision software. Total vessel and plaque cross-sectional area was calculated using Image Pro Plus 5 (Rockville, MD, USA). Staining was quantified by automated colour-coded segmentation. Immunohistochemical markers were expressed as number of cells per mm^2 or percentage staining of total cross-sectional area.

2.7. MAGNETIC RESONANCE IMAGING

Patients with aneurysmal disease (Chapter 6) underwent MRI in a whole body 3T scanner (Magnetom Verio, Siemens, Erlangen, Germany) before and 24 h after intravenous administration of USPIO contrast agent (Ferumoxytol; Advanced Magnetics Inc., Cambridge, MA, USA; dose 4 mg/kg at a rate of 1 mL/s) as described previously (Richards et al., 2011b, Alam et al., 2012). Briefly, coronal and sagittal breath-held T2-weighted multi-slice HASTE localizer sequences were used to identify the position and extent of the aneurysm following which a respiratory-gated, electrocardiographically-triggered T2 weighted (T2W) turbo-spin echo sequence was used to acquire detailed anatomical data. (TR/TE 2R-R intervals/72 ms; flip angle 180°; matrix 192 × 256; field of view 400 × 400 mm; slice width 5 mm, zero slice-gap). A multi-echo, gradient-echo T2*W sequence (TE 4.9, 7.7, 10.5, 13.3 ms; TR 133 ms; flip angle 15°; matrix 192 × 256; field of view 400 × 400 mm; slice width 5 mm, zero slice-gap) was used to acquire axial images of the entire aneurysm with slice positions corresponding to those of the T2W images. When performing the post-contrast scans, axial acquisitions were positioned to match those of the pre-contrast scan by reference to the vertebral bodies. Pre- and post- contrast T2*W images were utilized to generate R2* color maps (Matlab, Maths works) for quantification of USPIO uptake (Alam et al., 2012, Richards et al., 2011b).

2.7.1. IMAGE REGISTRATION AND ANALYSIS

The MRI dataset was registered to the PET dataset using a semi-automatic rigid 3D voxel registration protocol (Analyze 11.0, Mayo Clinic). The accuracy of PET-CT to CTA registration was confirmed by visual assessment and minor intra-scan patient movement was corrected. Registration of the MRI data allowed both the excellent anatomical detail on the T2W images and the high sensitivity of T2*W images for iron to be utilized. All the images were registered to the pre-contrast T2W image using the same semi-automatic 3D voxel registration protocol (Analyze 11.0, Mayo Clinic). The CTA and T2W MRI datasets were co-registered. At the end of the registration process, the pre-USPIO T2*W MRI, the post-USPIO T2*W MRI, the CTA and the PET-CT were all co-registered to enable direct comparison.

USPIO quantification

Using validated in-house software (Matlab, Mathworks, USA), four echoes in the multi-echo T2*W sequence were combined to generate a T2* map in which the magnitude of each voxel represented the T2*value ($S(t)=S(0)exp-(t/T2^*)$. The T2* value is the decay constant for the exponential decay of signal intensity with time. In the presence of USPIO, the signal decays more rapidly because of local magnetic field inhomogeneities and the T2* value is reduced. A 3×3 voxel Gaussian filter was applied to the individual echoes to reduce noise. An experimentally determined threshold for the coefficient of determination ($r^2>0.85$) was used to exclude data that did not have an acceptable exponential decay when signal intensity (SI) was plotted against echo time. USPIO uptake was detected using the change in T2* (or R2*; R2*=1/T2*) following USPIO administration. A previously defined threshold of

significance (59% increase in T2*) was used to distinguish USPIO accumulation from artefactual changes in T2* (Richards et al., 2012, Richards et al., 2011c). To enable the spatial distribution of USPIO uptake within the aneurysm to be assessed, colour maps were generated in which each voxel represented the change in T2* (ΔT2*) or R2* (ΔR2*) following USPIO administration.

2.8. STATISTICAL ANALYSIS

Specific statistical analysis has been described in each chapter separately. Statistical analysis was performed with Graph Pad Prism version 6 (GraphPad Software Inc., California USA) or SPSS 19.0 (SPSS Inc., Chicago, Illinois) where appropriate. Continuous data were checked for normality using the D'Agostino-Pearson omnibus test. Parametric variables were expressed as mean ± standard deviation and compared using Student's t-tests or repeat measure one-way ANOVA with Tukey's multiple comparison test when appropriate. Non-parametric data were presented as median [interquartile range] and compared with Mann-Whitney test, Wilcox matched-pairs signed rank, or Friedman test as appropriate. Inter-observer reproducibility was estimated using the Bland Altman method and presented as mean bias ± 2 standard deviation, and intra-class correlation coefficients with 95% confidence intervals were also calculated. A two-sided $P<0.05$ was taken as statistically significant. Inter-observer reproducibility was calculated by the Bland Altman method and presented as mean bias ± 2 standard deviation, and intra-class correlation coefficients with 95% confidence intervals were calculated.

The primary end-point of the study in patients with atherosclerosis (Chapter 3) was the comparison of 18F-fluoride tissue-to-background ratios of culprit and non-culprit coronary plaques of patients with acute myocardial infarction. The main secondary endpoints were comparative imaging and histological characterisation of 18F-fluoride positive and negative atherosclerotic plaques in patients with carotid and coronary artery disease. Based on our previous data (Dweck et al., 2012a), we

required 36 patients with myocardial infarction to detect a difference of 0.23 in the tissue-to-background ratio between culprit and non-culprit plaques at 90% power and two-sided $p<0.05$. We recruited 40 patients to account for incomplete data and recruited a similar sized (n=40) comparator group of patients with stable angina. As a pre-specified end-point (ClinicalTrials.gov: NCT01749254), we explored 18F-FDG uptake in remote aortic atheroma of patients with recent myocardial infarction or stable coronary heart disease.

Patients in the registry cohort were divided into tertiles according to their peak troponin concentration (Chapter 4). Kaplan Meier curves were used to estimate the distribution of early recurrent myocardial infarction across the tertiles. Univariate analysis was undertaken to identify associations with early (≤30 days) and late (>30 days) recurrent myocardial infarction that were then entered into the multivariate logistic regression model based on univariate association of $p<0{\cdot}1$. In addition, age and sex were included in the model. Statistical analysis was performed with Graph Pad Prism version 6 (GraphPad Software Inc., California USA) and SPSS 19.0 (SPSS Inc., Chicago, Illinois) where appropriate. Unless stated, a two-sided $P<0.05$ was taken as statistically significant.

Chapter 3. 18F-FLUORIDE POSITRON EMISSION TOMOGRAPHY IDENTIFIES RUPTURED AND HIGH-RISK CORONARY ATHEROSCLEROTIC PLAQUES

Published by JOSHI, N. V., VESEY, A. T., WILLIAMS, M. C., SHAH, A. S., CALVERT, P. A., CRAIGHEAD, F. H., YEOH, S. E., WALLACE, W., SALTER, D., FLETCHER, A. M., VAN BEEK, E. J., FLAPAN, A. D., UREN, N. G., BEHAN, M. W., CRUDEN, N. L., MILLS, N. L., FOX, K. A., RUDD, J. H., DWECK, M. R. & NEWBY, D. E. 2013. F-fluoride positron emission tomography for identification of ruptured and high-risk coronary atherosclerotic plaques: a prospective clinical trial. *Lancet,* 383**,** 705-13.

3.1. SUMMARY

Non-invasive imaging to identify ruptured or high-risk coronary atherosclerotic plaque would represent a major clinical advance. Using combined positron emission tomography (PET) and computed tomography (CT), we investigated the identification of ruptured and high-risk atherosclerotic plaque using 18F-fluoride and 18F-fluorodeoxyglucose (18F-FDG).

In this prospective clinical trial, patients with myocardial infarction (n=40) and stable angina (n=40) underwent 18F-fluoride and 18F-FDG PET-CT, and invasive coronary angiography. 18F- fluoride uptake was compared with histology in carotid endarterectomy specimens from patients with symptomatic carotid disease, and with intravascular ultrasound in patients with stable angina.

In 37 (93%) of the patients with myocardial infarction, the highest coronary 18F-fluoride activity was observed in the culprit plaque (maximum tissue-to-background ratio: culprit 1.66 [1.40-2.25] *versus* highest non-culprit 1.24 [1.06-1.38], $p<0.001$). In contrast, coronary 18F-FDG uptake was commonly obscured by myocardial uptake and where discernible, there were no differences between culprit and non-culprit plaques (1.71 [1.40-2.13] *versus* 1.58 [1.28-2.01], $p=0.34$). Marked 18F-fluoride uptake occurred at the site of all carotid plaque ruptures and was associated with histological evidence of active calcification, macrophage infiltration, apoptosis

and necrosis. Eighteen (45%) patients with stable angina had plaques with focal 18F-Fluoride uptake (maximum tissue-to-background ratio: 1.90 [1.61-2.17]) that were associated with more high-risk features on intravascular ultrasound than those without uptake: positive remodeling (remodeling index: 1.12 [1.09-1.19] *versus* 1.01 [0.94-1.06]; $p<0.001$), microcalcification (73 *versus* 21%, $p=0.002$) and necrotic core (25 [21-29] *versus* 18 [14-22] %, $p=0.001$).

18F- fluoride PET-CT is the first non-invasive imaging method to identify and localise ruptured and high-risk coronary plaque. Future studies are needed to determine whether this can improve the management and treatment of patients with coronary artery disease.

3.2. INTRODUCTION

Coronary atherosclerotic plaque rupture is the principal aetiological precipitant of acute myocardial infarction and an important cause of sudden cardiac death. It is challenging to predict because most plaques that subsequently rupture are non-obstructive and are not identified by stress testing or coronary angiography (Naghavi et al., 2003, Virmani et al., 2000a). Atherosclerotic lesions at risk of rupture have certain histopathological characteristics that include positive remodeling, microcalcification and a large necrotic core (Naghavi et al., 2003, Virmani et al., 2000a, Virmani et al., 2006b). The development of modern molecular imaging techniques targeted at these features could lead to the identification of such high-risk plaques *in vivo* and guide the development of novel treatment strategies (Rogers and Tawakol, 2011).

Combined positron emission tomography (PET) and computed tomography (CT) is a non-invasive imaging technique that brings functional molecular imaging together with precise anatomical information. We have recently reported preliminary PET-CT data using the tracer 18F-fluoride (18F-Fluoride) as a marker of valvular and vascular calcification activity in patients with aortic stenosis (Dweck et al., 2013b, Dweck et al., 2013a, Dweck et al., 2012a). Other studies have demonstrated the utility of 18F-flurodeoxyglucose (18F-FDG) as a surrogate of vascular inflammation and macrophage burden (Rogers et al., 2010, Tawakol et al., 2006, Rudd et al., 2002, Wykrzykowska et al., 2009, Cheng et al., 2012). We therefore sought to investigate whether, in comparison to the current non-invasive gold-standard of 18F-FDG, 18F-

Fluoride uptake could identify ruptured and high-risk atherosclerotic plaques in patients with symptomatic coronary and carotid artery disease.

3.3. METHODS

3.3.1. STUDY POPULATION

Patients were recruited from the Royal Infirmary of Edinburgh between February 2012 to January 2013 in three cohorts : 40 patients with acute ST- or non-ST-segment elevation myocardial infarction (Thygesen et al., 2012) 40 patients with stable angina pectoris undergoing elective invasive coronary angiography, and 12 patients undergoing carotid endartectomy for symptomatic carotid artery disease. Studies were performed with the approval of the local research ethics committee, in accordance with the Declaration of Helsinki, and with the written informed consent of each participant.

Consecutive patients with myocardial infarction were approached and recruited if they fulfilled the criteria for type 1 myocardial infarction according to the Universal Definition of Myocardial Infarction (Thygesen et al., 2012), ST segment elevation myocardial infarction was defined as new ST segment elevation at the J point in two contiguous leads with the cut-points: ≥0.1 mV in all leads except V_2-V_3 where the thresholds were ≥0.2 mV for men ≥40 years and ≥0.25 mV for women.

Consecutive patients with stable angina pectoris were recruited if they had typical symptoms of exertional anginal chest pain, previously documented coronary artery disease (>70% stenosis of at least one major epicardial coronary artery), and had been scheduled for invasive coronary angiography. Patients were excluded if they had suffered an acute coronary syndrome within the last 3 months.

Patients with typical symptoms and signs of an acute transient ischemic attack, amaurosis fugax or stroke were recruited within 1-14 days of symptom onset. All patients underwent clinical evaluation and carotid Doppler assessment. Inclusion criteria were carotid stenosis >50% (NASCENT Criteria, 1991) consistent with clinical presentation, and planned carotid endarterectomy.

Exclusion Criteria

Exclusion criteria were age <50 years, insulin-dependent diabetes mellitus, women of childbearing age not taking contraception, severe renal failure (serum creatinine >250 μmol/L), known contrast allergy and inability to provide informed consent. Only patients older than 50 years were recruited in the study to reduce any long-term risks associated with radiation exposure. Uncontrolled diabetes and high blood glucose concentrations (>11 mmol/L) interfere with image quality of 18F-FDG PET imaging due to competition between glucose and 18F-fluorodeoxyglucose for cellular entry. It has therefore been the convention to exclude such patients from vascular 18F-fluorodeoxyglucose positron emission tomography studies (Tawakol et al., 2006, Wykrzykowska et al., 2009, Williams and Kolodny, 2008, Cheng et al., 2012).

All patients underwent a comprehensive baseline clinical assessment including evaluation of their cardiovascular risk factor profile. Plasma troponin I concentrations were measured in patients with stable angina using the ARCHITECT *STAT* high-sensitivity troponin I assay (Abbott Laboratories, Abbott Park, Illinois;

lower limit of detection, 1.2 ng/L; 99th percentile diagnostic threshold, 26 ng/L).

3.3.2. PET-CT IMAGING AND ANALYSIS

Patients with a heart rate exceeding 65 beats/min received oral beta-blockade (50 or 100 mg metoprolol orally) 1 h before the computed tomography (CT) examination. All patients received sublingual glyceryl trinitrate (300 μg) just prior to the CT coronary angiography (CTCA). Patients were asked to refrain from alcohol and caffeine on the day of the scan.

Visit 1: 18F-Fluoride

All patients underwent dual cardiac and respiratory-gated positron emission tomography (PET)-CT imaging of the coronary arteries with a hybrid scanner (64-multidetector Biograph mCT, Siemens Medical Systems, Erlangen, Germany). Study subjects were administered a target dose of 125 MBq 18F-fluoride (18F-Fluoride) intravenously and subsequently rested in a quiet environment for 60 min. An attenuation correction CT scan (non-enhanced 120 kV and 50 mA) was then performed, followed by PET imaging of the thorax in list-mode for 20 min.

Coronary artery calcium and CTCA were undertaken in the same visit as the 18F-Fluoride scan. With the patient lying still on the scanner after acquisition of the PET, an electrocardiogram-gated breath-hold CT scan (non-contrast-enhanced, 40 mAs/rotation, 120 kV; CareDose, Siemens Medical Systems) of the coronary arteries was performed. CTCA was performed using the following settings: 330 ms rotation time, 100 (body mass index [BMI] <25 kg/m^2) or 120 (body mass index >25 kg/m^2) kV tube voltage, 160-245 mAs tube current, 3.8 mm/rotation table feed, prospective

(heart rate regular and <60/min), or retrospective (heart rate >60 /min) electrocardiogram-gated. Depending on the BMI, a bolus of 80-100 mL of contrast (400 mgI/mL; Iomeron, Bracco, Milan, Italy) was injected intravenously at 5 mL/s, after determining the appropriate trigger delay with a test bolus of 20 mL contrast material.

Although the PET scans were acquired with the potential for dual motion correction, inclusion of respiratory gating led to significant loss of signal with increased noise. Therefore, only electrocardiogram-gated cardiac motion correction was undertaken. The PET scans were reconstructed in multiple phases of the cardiac cycle, with the diastolic phase (50-75%) used for analysis. The CTCA scans were reconstructed at 0.75 x 0.7 mm and 0.6 x 0.3 mm for retrospective and prospective acquisitions respectively at 60%, 65% and 70% of the cardiac cycle. Additional reconstructions were undertaken if necessary. Although the PET scans were acquired with the potential for dual motion correction, inclusion of respiratory gating led to significant loss of signal with increased noise. Therefore, only electrocardiogram-gated cardiac motion correction was undertaken.

Visit 2: 18F-Fluorodeoxyglucose

Intense uptake of 18F-fluorodeoxyglucose (18F-FDG) by the left ventricle leads to difficulties in discriminating between activity in the coronary arteries and the myocardium. All patients in our cohort were asked to observe a low-carbohydrate, high-protein and high-fat diet for 24 hours before their 18F-FDG scan because this suppresses myocardial uptake as the heart switches from glucose to free fatty acid metabolism (Tawakol et al., 2006, Wykrzykowska et al., 2009, Cheng et al., 2012, Williams and Kolodny, 2008).Patients were provided with a list of food and drink to avoid and reminded of these restrictions the day before their scan. Dietary diaries were recorded for all patients.

Subjects were administered a target dose of 200 MBq 18F-FDG intravenously and subsequently rested in a quiet environment for 90 min. Combined PET-CT imaging was then performed as described for the 18F-Fluoride scan.

Patients with myocardial infarction and stable angina underwent 18F- fluoride and 18F-FDG PET-CT, CT coronary angiography and CT calcium scoring (Dweck et al., 2012a). To minimize myocardial uptake, patients were instructed to adhere to a low-carbohydrate, high-protein and high-fat diet for at least 24 h prior to undergoing 18F-FDG PET-CT.

Electrocardiogram-gated PET images were reconstructed in diastole (50-75% of the R-R interval, Ultra-HD, time of flight x True X), fused with the CT coronary angiogram, and analysed by experienced observers blinded to the clinical diagnosis (NJ, MD, FC) using an OsiriX workstation (OsiriX version 5.5.1 64-bit; OsiriX Imaging Software, Geneva, Switzerland). Two-dimensional regions of interest (ROIs) were drawn around all major (diameter >2 mm) epicardial vessels on 3-mm axial slices just beyond the discernible adventitial border. The maximum standard uptake value (SUV; the decay corrected tissue concentration of the tracer divided by the injected dose per body weight) was measured and corrected for blood pool activity in the superior vena cava to provide tissue-to-background ratios (TBRs) measurements. Using this methodology, we have previously demonstrated excellent reproducibility for 18F-Fluoride TBR measurements in the coronary arteries with an intraclass correlation coefficient of 0.99 (Dweck et al., 2012a).

We used a previously established 95% lower reference limit to categorise coronary plaques into 18F-Fluoride positive lesions (focal uptake with a TBR >25 % higher than a proximal reference lesion) and negative plaques if these criteria were not achieved. This was based on our previous study, where plaques with high 18F-Fluoride uptake had maximum TBRs that were 44% (95% confidence intervals, 26-62%) higher than a proximal quiescent reference lesion (Dweck et al., 2012a). In patients with acute myocardial infarction, 18F- fluoride uptake in the culprit plaque was compared with the highest value in any of the non-culprit vessels.

Quantification of 18F-FDG uptake was performed as for 18F- fluoride uptake but restricted to the proximal and mid-portions of the coronary arteries, and to regions where myocardial uptake and spillover could be confidently excluded (Dweck et al., 2012a). Again 18F-FDG positive plaques were defined using the >25% threshold as described for 18F-Fluoride. Effective myocardial suppression of 18F-FDG was predefined as SUV ≤5.0 in the basal ventricular septum as per published data (Wykrzykowska et al., 2009).

Image Analysis Repeatability

Thirty patients were selected randomly to test the repeatability of image analysis in between two trained readers (NVJ, MRD). Fifteen patients from each of the 18F-FDG and 18F-Fluoride cohorts were selected and each reader repeated the analysis of these patients independently in random order to avoid recall bias.

3.3.3. GRAY-SCALE AND RADIOFREQUENCY INTRAVASCULAR ULTRASOUND AND COMPUTED TOMOGRAPHY

In patients with stable angina, PET-CT imaging was prospectively used to direct gray-scale and radiofrequency intravascular ultrasound (20 MHz Eagle Eye Platinum Catheters [Volcano Corp, USA], motorized pull-back 0.5 mm/s) to the 18F-Fluoride positive and negative plaques. The interventional cardiologist acquiring the intravascular ultrasound data was blinded to the PET-CT status of the plaque.

Intravascular ultrasound analysis was performed as described previously using dedicated VIAS software (Volcano Corp, USA) by operators blinded to the positron emission tomography data (Calvert et al., 2011). Regions of interest were drawn around the external elastic membrane and luminal borders, and plaque area and composition (dense calcium, necrotic core, fibro-fatty tissue and fibrous tissue) calculated (Calvert et al., 2011, Stone et al., 2011a, Murray et al., 2013). The presence of microcalcification (spotty calcification in the absence of acoustic shadowing on ≥3 consecutive frames) and the maximum frame necrotic core (the highest percentage of necrotic core on a single frame) were recorded (Ehara et al., 2004). The remodeling index was defined as the ratio between the external elastic membrane cross-sectional area of the lesion and a proximal reference region in the same vessel (Mintz et al., 2001). Plaques were classified as thin-cap fibroatheroma, thick-cap fibroatheroma, pathologic intimal thickening or fibrocalcific plaque as defined previously (Stone et al., 2011a, Garcia-Garcia et al., 2009b).

CT analysis was performed on a dedicated cardiovascular workstation (Vital Images, Minnetonka, Minnesota, USA). Vessel-specific and total Agatston calcium scores were calculated as described previously (Dweck et al., 2012a). An independent experienced and blinded observer determined stenosis severity, plaque composition (calcified, non-calcified, mixed plaque) and the presence of high-risk CT features (positive remodeling, microcalcification, necrotic core) according to standard definitions in plaques with and without increased 18F-fluoride activity (Motoyama et al., 2009a).

3.3.4. CAROTID ATHEROMA

Intact atherosclerotic plaques were retrieved at the time of carotid endarterectomy and scanned using *ex-vivo* PET-CT to allow precise anatomical co-localisation of 18F-fluoride activity with pathological evidence of plaque rupture. Plaques were divided into 18F- fluoride positive and negative areas, and histological sections were assessed using Movat's pentachrome and immunohistochemistry to investigate both calcification activity (tissue non-specific alkaline phosphatase and osteocalcin), macrophage infiltration (CD68) and cell death (apoptosis, cleaved caspase 3; presence of necrotic core).

Rationale for Immunohistochemistry of Carotid Atheroma

We used immunohistochemistry to investigate macrophage infiltration (CD68), calcification activity (tissue non-specific alkaline phosphatase and osteocalcin), and cell death (apoptosis, cleaved caspase 3; presence of necrotic core).

Inflammation is a key feature of human atherosclerosis and is thought to precede the early stages of calcification (Aikawa et al., 2007). CD68 is expressed by macrophages and has been closely correlated with the 18F-FDG signal in the carotid arteries. Apoptotic cell death is a recognized phenomenon in atherosclerotic plaque and is thought to be detrimental to plaque stability (Kockx and Herman, 2000). Cleaved caspase 3 is a critical executioner of apoptosis, being responsible for the

proteolytic cleavage of many key proteins, such as the nuclear enzyme poly (ADP-ribose) polymerase (PARP). Its expression has been previously demonstrated in atherosclerotic plaque (Fernandes-Alnemri et al., 1994).

During propagation of atherosclerosis, vascular smooth muscle cells undergo osteogenic differentiation (New and Aikawa, 2011). Additionally, matrix vesicles released from living cells and apoptotic bodies from dying macrophages and smooth muscle cells are thought to provide a nidus for microcalcification(Proudfoot et al., 2000, Shanahan, 2007). Tissue non-specific alkaline phosphatase (TNAP) is an enzyme that plays a key role in atherosclerotic calcification by increasing availability of inorganic phosphate levels through the hydrolyzing pyrophosphate, a key inhibitor of mineralization (Demer and Tintut, 2008). Unlike dyes such as alizarin red that directly stains tissue calcium, TNAP provides information about calcification activity and gives information distinct from mere anatomical calcium.

Osteocalcin, or bone Gla protein, is a small protein secreted by osteoblasts that can undergo γ-carboxylation (Kapustin and Shanahan, 2011). The γ-carboxylated form binds hydroxyapatite and is abundant in bone extracellular matrix. Osteocalcin is thought to be a regulator of osteochondrogenic differentiation of pathologically mineralizing vascular smooth muscle cells (Kapustin and Shanahan, 2011). The presence of osteocalcin is therefore suggestive of up regulated vascular mineralization (Idelevich et al., 2011).

Ex-vivo 18F-Fluoride Positron Emission Tomography

Carotid plaques were retrieved intact at the time of carotid endarterectomy, and photographed before being wrapped in foil and frozen at -80 °C. Subsequently, they were thawed in a batch and immersed in 18F- fluoride solution diluted with phosphate buffered saline (PBS) to a total activity of 10 MBq/mL. After 60 min, plaques were rinsed 3 times in PBS before being oriented and placed in a PET-CT hybrid scanner (64-multidetector Biograph mCT, Siemens Medical Systems, Erlangen, Germany). After an attenuation correction CT scan, PET imaging was undertaken over a single bed for 15 min.

Histology and Immunohistochemistry

Immediately following scanning, plaques were fixed in 4% paraformaldehyde for 24 hours before transfer to 70% ethanol. Plaques were decalcified in ethylenediaminetetraacetic acid before being divided into segments with or without 18F-Fluoride uptake that were paraffin-embedded, and 5-μm sections were prepared and stained with Movat's pentachrome. Immunohistochemical staining for CD68 expression (mouse anti-human CD68 mAb, M087601-2, Dako), cleaved caspase 3 (anti-human rabbit mAb #9664, Cell Signalling Technology) and tissue non-specific alkaline phosphatase (anti-human rabbit pAb CAT#LF PA50004, Abfrontier) was then undertaken following heat induced epitope retrieval (HIER) using 0.01 M citrate buffer at pH 6.0 in a decloaking chamber. Osteocalcin staining (anti-human mouse mAb ab13418, Abcam) required no HIER. Sections were stained using a Leica

Vision Biosystems Bond x immunostaining robot. Optimization of antibody dilution was undertaken by determining positive and negative controls. Positive controls for CD68 were generated using human kidney, cleaved caspase 3 using sections of normal human tonsil and spleen, and for tissue non-specific alkaline phosphatase and osteocalcin using decalcified human bone to determine optimal antibody dilutions. Negative controls were generated by omitting the primary antibody. After blocking in peroxide for 10 min, sections were incubated with the specific anti-human antibodies for 2 hours at room temperature at the following dilutions: CD68 1:100, osteocalcin 1:200, cleaved caspase 3 1:150, and tissue non-specific alkaline phosphatase 1:100. All incubation steps were followed by washing in TBS/Tween. Sections for osteocalcin were incubated for 15 min with pre-polymer/post primary followed by 15 min with polymer (HRP) for all antibodies prior to DAB (3,3'-Diaminobenzidine) visualization and haematoxylin counterstaining. Sections were dehydrated in graded ethanol, cleared in xylene before cover slipping in Pertex.

Images were taken on a Zeiss Axioskop2 fitted with an Axiocam MRc digital camera using Axiovision software. Total vessel and plaque cross-sectional area was calculated using Image Pro Plus 5 (Rockville, MD, USA). Staining was quantified by automated colour-coded segmentation. Immunohistochemical markers were expressed as number of cells per mm^2 or percentage staining of total cross-sectional area.

3.3.5. STATISTICAL ANALYSIS

The primary end-point of the study was the comparison of 18F-fluoride tissue-to-background ratios of culprit and non-culprit coronary plaques of patients with acute myocardial infarction. The main secondary endpoints were comparative imaging and histological characterisation of 18F-fluoride positive and negative atherosclerotic plaques in patients with carotid and coronary artery disease. Based on our previous data (Dweck et al., 2012a), we required 36 patients with myocardial infarction to detect a difference of 0.23 in the tissue-to-background ratio between culprit and non-culprit plaques at 90% power and two-sided $p<0.05$. We recruited 40 patients to account for incomplete data and recruited a similar sized (n=40) comparator group of patients with stable angina.

Continuous data were tested for normality with the D'Agostino and Pearson Omnibus test. Continuous parametric variables were expressed as mean ± standard deviation and compared using Student's *t*-tests. Non-parametric data were presented as median [interquartile range] and compared using Mann-Whitney U test or Wilcoxon signed-rank test as appropriate. Fisher's exact test or Chi-Squared test was used for analysis of categorical variables. Statistical analysis was performed with Graph Pad Prism version 5 (GraphPad Software Inc., California USA). A two-sided $p<0.05$ was taken as statistically significant.

The study was registered with ClinicalTrials.gov number NCT01749254.

3.4. RESULTS

Patients were predominantly middle-aged men and had multiple cardiovascular risk factors (Table 3-1). They underwent both 18F-fluoride (60±9 min after 123±5 MBq) and 18F-FDG (90±7 min after 192±11 MBq) PET-CT scanning within a median of 6 [3-9] days. The median duration between PET-CT scanning and coronary angiography was 7 [1-12] days. The total effective radiation dose from study participation was 13.7±3.0 mSv (conversion factor of 0.014 mSv/mGy.cm): 18F-Fluoride (3.8±0.3 mSv) and 18F-FDG (4.9±0.5 mSv) PET-CT, CT coronary angiogram (3.7±2.1 mSv) and calcium score (1.3±0.5 mSv).

The total time spent in the imaging centre for each patient was ~100 min for visit 1 (18F-Fluoride PET-CT scans) and ~120 min for visit 2 (18F-FDG PET-CT scans).

3.4.1. REPEATABILITY OF IMAGE ANALYSIS

The repeatability for measurements of coronary 18F-FDG and 18F- fluoride activity in the present study were excellent, with no fixed or proportional biases for measurements of the maximum tissue-to-background ratios for either tracer. The limits of agreement for maximum coronary 18F-FDG tissue to background ratios were 0.04±0.23 (mean bias±2SD) with intraclass correlation coefficient values of 0.97 after exclusion of uninterpretable segments [95% CI 0.90-0.99]. For 18F-fluoride limits of agreement were 0.01±0.11 with intraclass correlation coefficient values of 0.99 [95% CI 0.99-1.00].

3.4.2. PATIENTS WITH MYOCARDIAL INFARCTION

The culprit vessel was the left anterior descending artery in 17 (42%) patients, the left circumflex artery in seven (18%) and the right coronary artery in 16 (40%). Patients underwent 18F-Fluoride scans 6 [3-10] days following hospitalization for myocardial infarction (symptoms to 18F- fluoride scan, 8 [3-10] days). 18F- fluoride activity in the culprit plaque was 34% higher than the maximum activity recorded anywhere else in the coronary vasculature (maximum TBR, 1.66 [1.40-2.25] *versus* 1.24 [1.06-1.38] respectively, $p<0.001$; Figures 3-1, 3-2 and 3-3). In 37 of the 40 patients (93%), increased 18F-Fluoride uptake was observed in the culprit plaque (Figure 3-1). In the three patients without uptake, two were younger smokers and, in the third, the culprit lesion was adjudicated as the right coronary artery although focal increased activity was observed in the left circumflex artery. In five patients, increased 18F-fluoride activity was observed at multiple sites within the coronary circulation.

Table 3-1: Baseline characteristics of patients with coronary artery disease

		Myocardial Infarction		Stable Angina
	All (n=40)	STEMI (n=26)	NSTEMI (n=14)	All (n=40)
Age (years)	62±8	63±9	60±8	67±8
Male sex	37 (93%)	24 (92%)	13 (93%)	36 (90%)
BMI (kg/m^2)	28±5	27±5	30±4	30±5
Antecedent angina (active)	9 (23%)	5 (19%)	4 (29%)	40 (100%)
Heart rate (per min)	56±7	56±7	56±7	59±9
Systolic blood pressure (mmHg)	132±21	131±20	121±21	134±14
Diastolic blood pressure (mmHg)	76±9	76±9	76±8	77±10
Cardiovascular History				
Previous MI	5 (13%)	1 (4%)	4 (29%)	15 (38%)
Previous CVA/TIA	2 (5%)	1 (4%)	1 (7%)	4 (10%)
Previous PCI	5 (13%)	2 (8%)	3 (21%)	19 (48%)
Previous CABG	2 (5%)	2 (8%)	0	11 (28%)
Risk Factors				
Smoking Habit (ex or current)	25 (63%)	19 (73%)	6 (43%)	24 (60%)
Non-insulin dependent diabetes	8 (20%)	7 (27%)	1 (7%)	13 (33%)
Hypertension	17 (43%)	11 (42%)	6 (43%)	36 (90%)
Hypercholesterolemia	19 (48%)	11 (42%)	8 (57%)	39 (98%)
Medications				
Aspirin	40 (100%)	26 (100%)	14 (100%)	33 (83%)
Clopidogrel	39 (98%)	25 (96%)	14 (100%)	5 (13%)
Statin	39 (98%)	26 (100%)	13 (93%)	36 (90%)
β-Blocker	32 (80%)	20 (77%)	12 (86%)	28 (70%)
ACEI/ARB	35 (88%)	25 (96%)	10 (71%)	20 (50%)
Calcium channel blockers	2 (5%)	2 (8%)	0	16 (40%)
Other Anti-hypertensive	3 (8%)	1 (4%)	2 (14%)	6 (15%)
Oral Nitrates	1 (3%)	0	1 (7%)	15 (38%)
Serum Biochemistry				
Cholesterol (mmol/L)	4.7±1.2	4.7±1.3	4.8±1.1	3.9±0.8
HDL Cholesterol (mmol/L)	1.1±0.3	1.1±0.3	1.0±0.3	1.1±0.3

LDL Cholesterol (mmol/L)	2.9±1.1	2.8±1.1	3.1±1.0	2.1±0.7
Triglycerides (mmol/L)	1.6±0.8	1.7±0.7	1.5±0.7	1.6±0.7
Creatinine (μmol/L)	84±27	86±29	82±24	85±23
Coronary Artery Calcium Score (AU)	159 [42-456]	176 [45-474]	122 [26-442]	599 [60-1302]
Peak Troponin Concentration (ng/L)	32,300 [10,200-50,000]	11,200 [3,300-50,000]	3,800 [1,000-9,200]	

[*]Heart rate at the time of CTCA; [†] Medications at the time of scan

STEMI ST elevation myocardial infarction, NSTEMI non-ST elevation myocardial infarction, BMI body mass index, MI myocardial infarction, CVA cerebrovascular accident, TIA transient ischemic attack, PCI percutaneous coronary intervention, ACEI angiotensin converting enzyme inhibitor, ARB angiotensin receptor blocker, CABG coronary artery bypass graft, HDL high-density lipoprotein, LDL low-density lipoprotein, TG Triglycerides. AU Agatston Units

Figure 3-1: Focal 18F-fluoride and 18F-fluorodeoxyglucose uptake in patients with myocardial infarction and stable angina

Patient with acute ST-segment elevation myocardial infarction with (A) proximal occlusion (red arrow) of the left anterior descending artery on invasive coronary angiography and (B) intense focal 18F-fluoride (18F-Fluoride; tissue-to-background ratios, culprit 2.27 versus reference segment 1.09 [108% increase]) uptake (yellow-red) at the site of the culprit plaque (red arrow) on the combined positron emission and computed tomogram (PET-CT). Corresponding 18F-fluorodeoxyglucose PET-CT image (C) showing no uptake at the site of the culprit plaque (18F-FDG tissue-to-background ratios; 1.63; versus 1.91 reference segment; 15% decrease). Note the significant myocardial uptake overlapping with the coronary artery (yellow arrow) and uptake within the oesophagus (blue arrow).

Patient with anterior non-ST-segment elevation myocardial infarction with (D) culprit (red arrow; left anterior descending artery) and bystander non-culprit (white arrow; circumflex artery) lesions on invasive coronary angiography that were both stented during the index admission. Only the culprit lesion had increased 18F- fluoride uptake (18F-Fluoride, tissue-to-background ratios; culprit 2.03 versus reference segment 1.08 [88% increase]) on PET-CT (E) following percutaneous coronary intervention. Corresponding 18F-fluorodeoxyglucose PET-CT showing no uptake either at the culprit (18F-FDG, tissue-to-background ratios; culprit 1.62 versus reference segment 1.49 [9% increase]) or the bystander stented lesion. Note intense uptake within the ascending aorta.

In a patient with stable angina with previous coronary artery bypass grafting, invasive coronary angiography (G) demonstrated non-obstructive disease in the right coronary artery. Corresponding PET-CT scan (H) showed a region of increased 18F- fluoride activity (positive lesion, red line) in the mid-right coronary artery (tissue-to-background ratio, 3.13) and a region without increased uptake in the proximal vessel (negative lesion, yellow line). Radiofrequency intravascular ultrasound shows that the 18F-Fluoride negative plaque (I) is principally composed of fibrous and fibrofatty tissue (green) with confluent calcium (white with acoustic shadow) but little evidence of necrosis. On the contrary, the 18F- fluoride positive plaque (J) demonstrates high risk features such as a large necrotic core (red) and microcalcification (white).

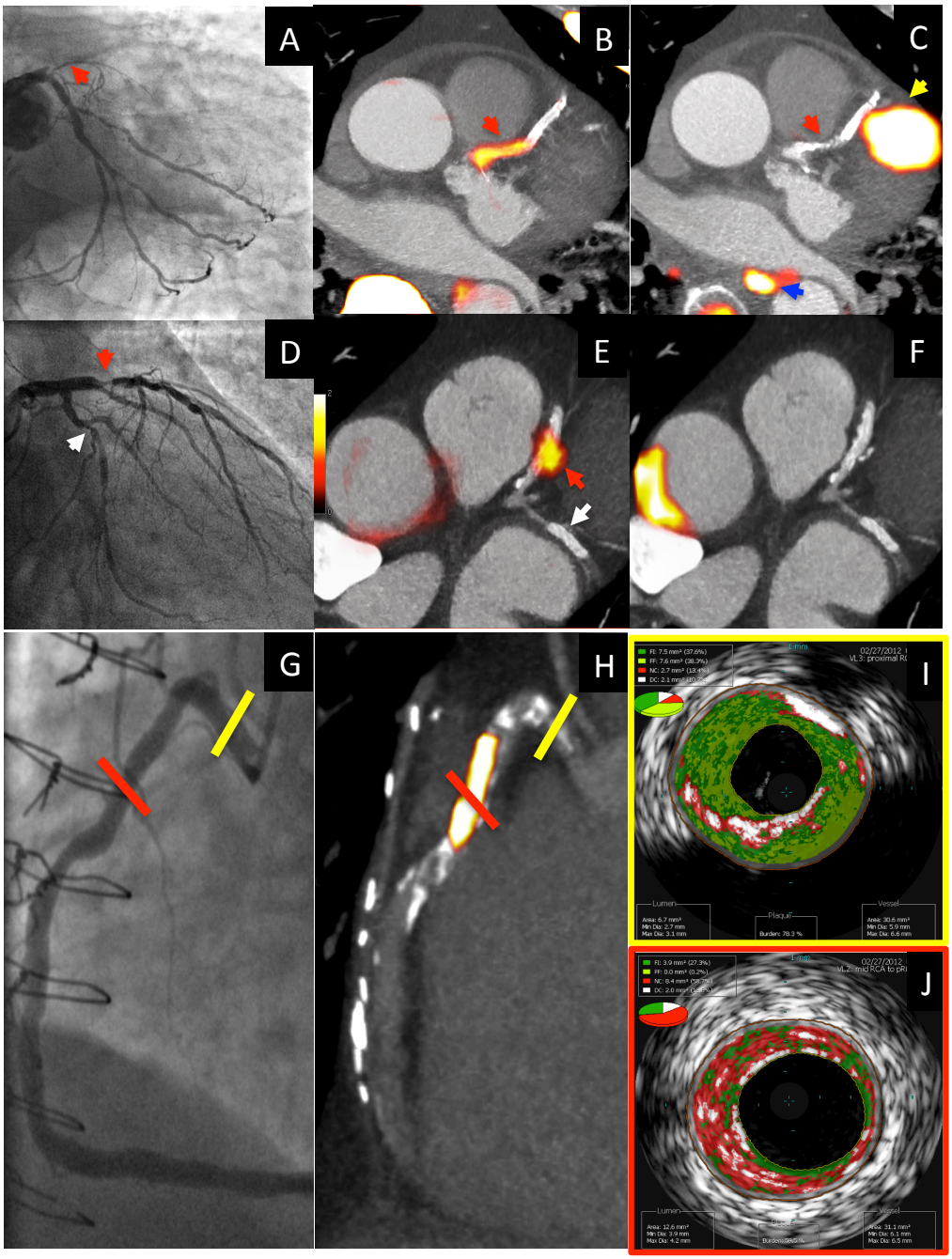
A
B
C
D
E
F
G
H
I
J

Figure 3-2: 18F-fluoride and 18F-fluorodeoxyglucose uptake in patients with myocardial infarction

18F-fluoride activity (maximum tissue-to-background ratio, TBR) was increased in the culprit plaque (red) compared to the maximum uptake in any of the non-culprit plaques (blue). By contrast there was no difference in the activity of 18F-fluorodeoxyglucose between these regions.

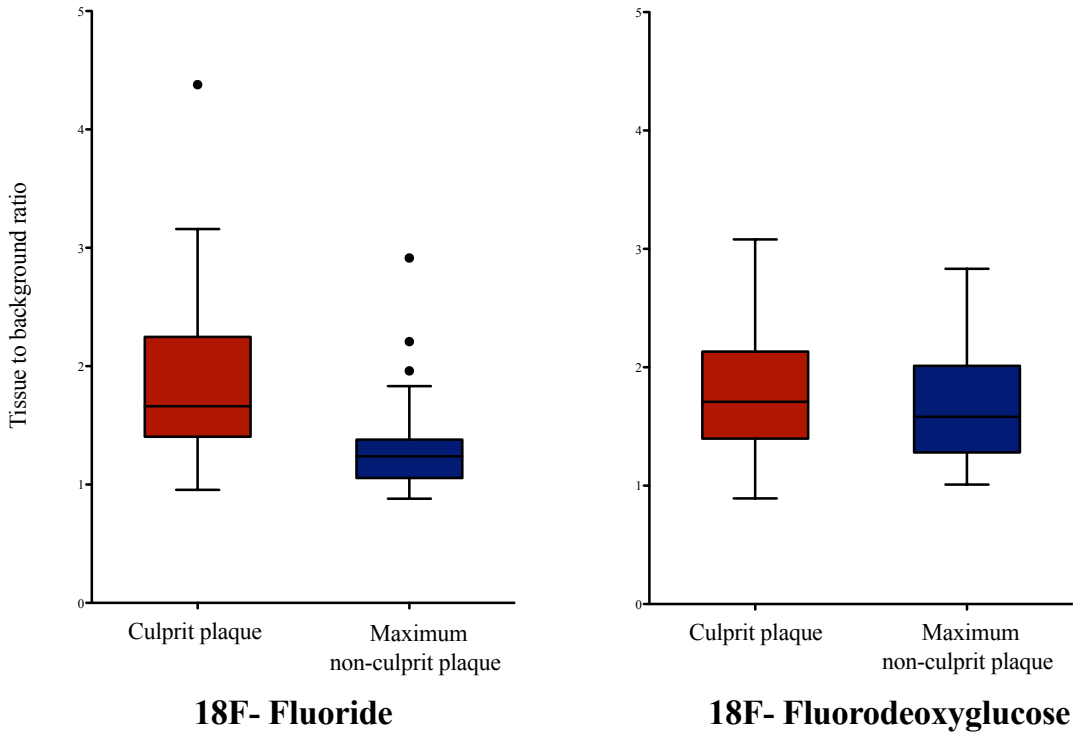

Pre-defined myocardial suppression of 18F-FDG uptake was achieved in 28 (70%) patients (median myocardial SUV=3.92 [2.71-5.55]). However, coronary 18F-FDG uptake could not be distinguished from patchy myocardial uptake in 22 patients affecting 52% of vessel territories. Increased uptake of 18F-FDG was observed in the culprit vessels of 6 (33%) of the remaining 18 patients. Overall, no significant differences could be demonstrated between the maximum TBRs in the culprit plaques and those recorded elsewhere in the coronary vasculature (1.71 [1.40-2.13] *versus* 1.58 [1.28-2.01], p=0.34: Figure 2) with a mean difference of 0.09 (95% confidence interval, -0.07 to 0.24).

Figure 3-3: Patients with myocardial infarction and 18F- fluoride uptake.

Panels A-D, invasive coronary angiograms of patients admitted with myocardial infarction with red arrows highlighting the culprit stenosis. Panels E-H, corresponding fused positron emission tomograms and computed tomography coronary angiograms showing intense coronary 18F-fluoride uptake in the culprit plaque (tissue-to-background ratios 1.55, 3.15, 2.91 and 1.75 respectively).

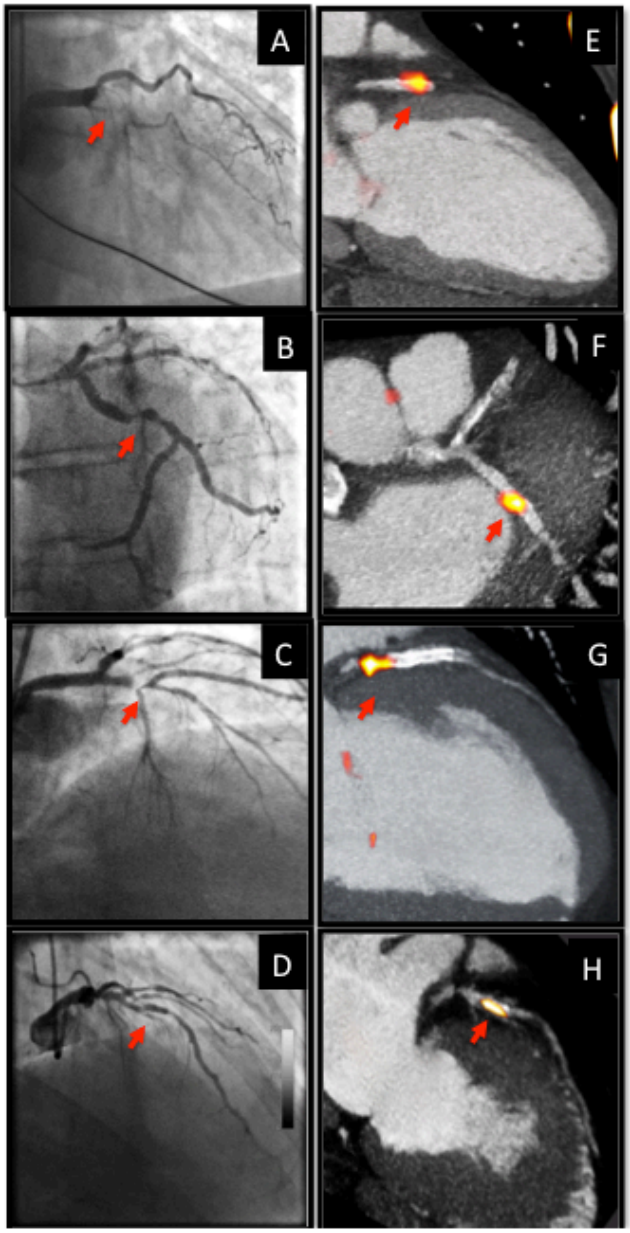

3.4.3. PATIENTS UNDERGOING CAROTID ENDARTERECTOMY

The median duration between clinical symptoms to carotid endarterectomy was 17 [10-27] days (Table 3-2). Carotid endarterectomy specimens (Figure 3-4 and 3-5) were collected in 12 patients although three specimens could not be excised intact and were discarded. *Ex vivo* 18F- fluoride PET-CT was undertaken in nine specimens and uptake was localized to the site of macroscopic plaque rupture in all patients (Figure 3-4). In comparison to sections of tissue without uptake (n=15), those with increased 18F- fluoride uptake (n=24) had increased calcification activity (tissue non-specific alkaline phosphatase, 4.07±3.42 *versus* 0.76 ±0.51 %, $p<0.001$; osteocalcin, 1.88 [0.58-4.10] *versus* 0.25 [0.11-0.58] %, $p<0.001$), macrophage infiltration (CD68, 350 [172-840] *versus* 145 [24-362] cells/mm^2, $p=0.013$) and cell death (apoptosis, cleaved-caspase-3, 1.23 [0.69-1.91] *versus* 0.09 [0.04-1.38] %, $p=0.005$; necrotic core, 22/24 *versus* 4/15; $p<0.0001$).

Figure 3-4: Carotid 18F-fluoride uptake and carotid plaque rupture

In-vivo (A and B) and ex vivo (C and D) positron emission and computed tomograms showing co-localization of 18F-fluoride (18F-Fluoride) uptake (yellow-orange) to the site of plaque rupture with adherent thrombus on excised carotid endarterectomy tissue (E and F). Histology of the 18F- fluoride -positive region demonstrates a large necrotic core (Movat's pentachrome, magnification 4x, G), within which increased staining for tissue non-specific alkaline phosphatase can be observed as a marker of calcification activity on immunohistochemistry (magnification 4x, H; magnification 10x, I).

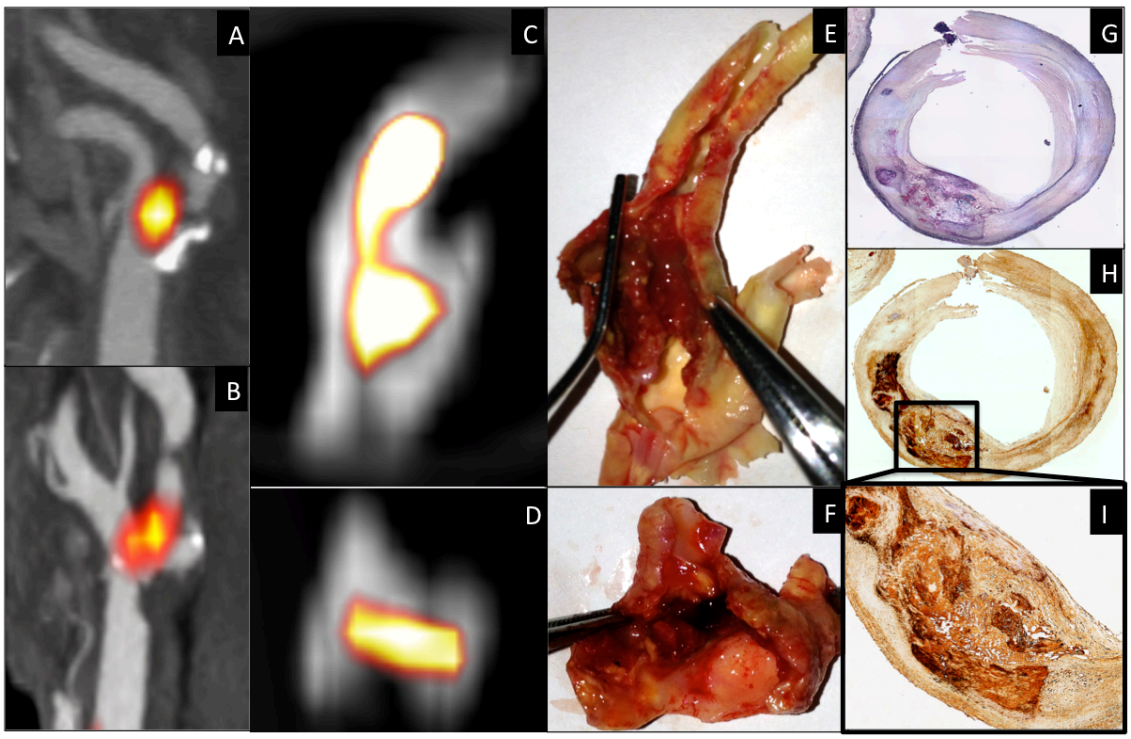

Figure 3-5:Histological comparison of 18F-fluoride positive and negative regions of carotid endarterectomy specimens

Histological sections of carotid endarterectomy specimens in regions with (A-C) and without (D-F) 18F-fluoride (18F-Fluoride) uptake. Movat's pentachrome (A and D) showing a large necrotic core in a plaque with increased 18F- fluoride uptake (A; arrows). Calcification activity (non-specific alkaline phosphatase) and apoptosis (cleaved caspase-3) are increased in the necrotic core and its shoulder region of 18F-Fluoride positive plaque (B and C respectively; brown staining) compared to the 18F-Fluoride negative plaque (E and F respectively).

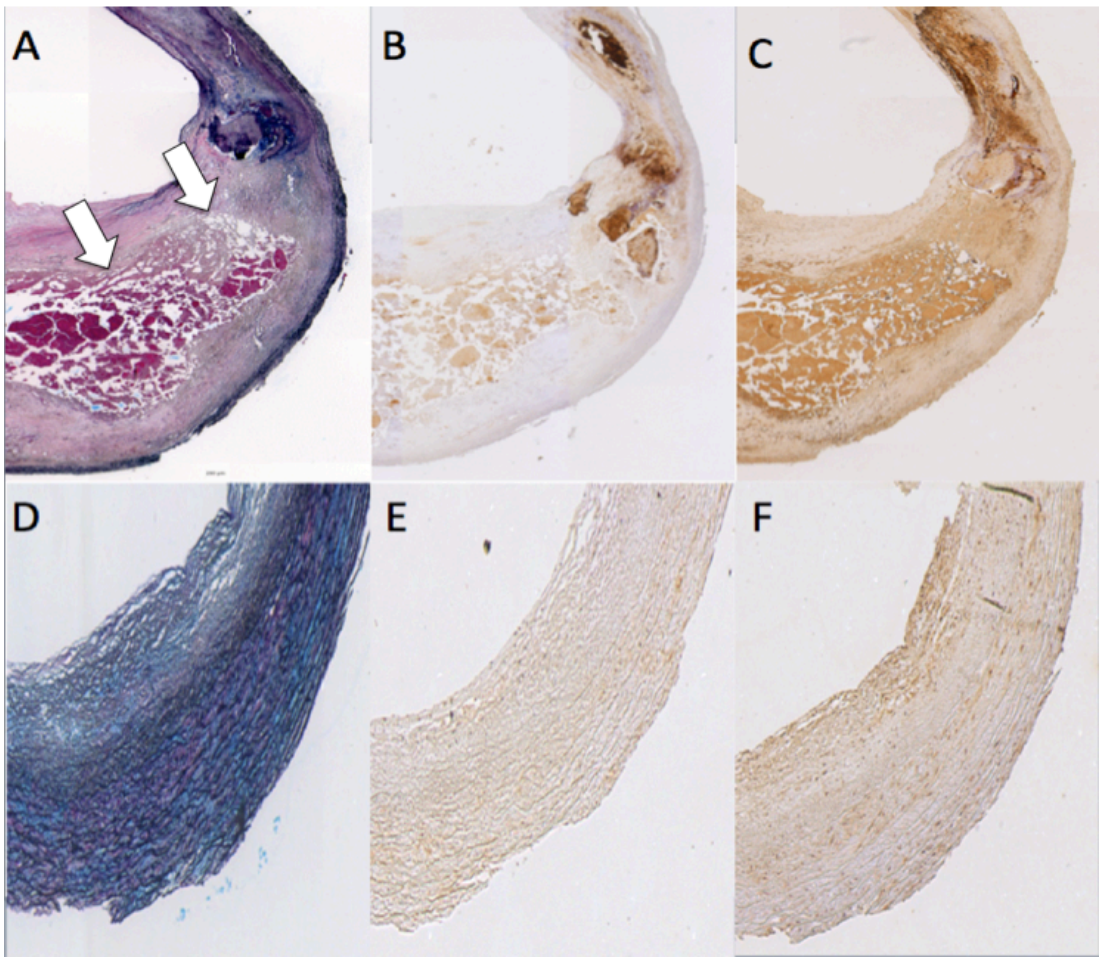

Table 3-2 Baseline characteristics of patients with symptomatic carotid disease (n=12) undergoing carotid endarterectomy.

Male sex	**8 (67%)**
BMI (kg/m^2)	27±3
Antecedent angina (active)	0 (0%)
Heart rate (per min)	67±13
Systolic blood pressure (mmHg)	141±25
Diastolic blood pressure (mmHg)	75±11
Clinical Presentation	
Ischaemic Stroke	6 (50%)
Transient Ischaemic Attack	3 (25%)
Amaurosis Fugax	3 (25%)
Cardiovascular History	
Previous MI	3 (25%)
Previous CVA/TIA	3 (25%)
Previous PCI	1 (8%)
Previous CABG	2 (16%)
Risk Factors	
Smoking Habit (ex or current)	9 (75%)
Non-insulin dependent diabetes	1 (8%)
Hypertension	8 (66%)
Hypercholesterolemia	7 (58%)
Medications	
Aspirin	3 (25%)
Clopidogrel	9 (75%)
Statin	12 (100%)
β-Blocker	1 (8%)
ACEI/ARB	5 (42%)
Calcium channel blockers	3 (25%)
Other Anti-hypertensive	5 (41%)
Oral Nitrates	0 (0%)
Serum Biochemistry	

Cholesterol (mmol/L)	4.2±0.9
HDL-Cholesterol (mmol/L)	1.1±0.4
LDL-Cholesterol (mmol/L)	1.9±0.6
Triglycerides (mmol/L)	1.4±0.5
Creatinine (µmol/L)	80±17

BMI body mass index, MI myocardial infarction, CVA cerebrovascular accident, TIA transient ischemic attack, PCI percutaneous coronary intervention, ACEI angiotensin converting enzyme inhibitor, ARB angiotensin receptor blocker, CABG coronary artery bypass graft, HDL high-density lipoprotein, LDL low-density lipoprotein.

3.4.4. PATIENTS WITH STABLE ANGINA

Patients with stable angina were older (67±8 versus 62±8 years, p=0.006) and had more severe coronary artery disease (coronary artery calcium score 599 [60-1302] versus 159 [42-456] Agatston Units, p=0.006) than those with myocardial infarction (Table 3-1). Focal 18F- fluoride uptake was noted in 18 patients (45%) that did not appear related to percutaneous coronary intervention and stent deployment. The maximum TBR for 18F- fluoride positive plaques was 1.90 [1.61-2.17] and for 18F-fluoride positive plaques was 1.02 [0.82-1.17]. 18F-fluoride positive plaques were predominantly (72% of patients) non-obstructive (<70% luminal stenosis) on coronary angiography and demonstrated multiple high-risk features on radiofrequency intravascular ultrasound (positive remodeling [remodeling index: 1.12 [1.09-1.19] *versus* 1.01 [0.94-1.06]; p<0.001, microcalcification (73 *versus* 21%, p=0.002) and necrotic core (24.6 [20.5-28.8] *versus* 18.0 [14.0-22.4]) %, p=0.001), with similar observations for CT (Figure 3-1, 3-6 and 3-7; Table 3-3 and 3-4). Multi-vessel uptake was commonly observed: 2-vessel uptake in six (15%) and 3-vessel uptake in five (13%) patients. Patients with 18F- fluoride positive lesions had higher baseline plasma troponin concentrations (3.35 [2.35-10.20] *versus* 2.45 [1.85-4.02] ng/L; p=0.047) with one individual having a concentration (35 ng/L) above the 99th percentile diagnostic threshold.

Although pre-defined myocardial suppression of 18F-FDG uptake was achieved in 34 (85%) patients (median myocardial SUV=2.60 [1.83-3.83]), coronary 18F-FDG uptake could not be confidently interpreted in 45% of vessel territories. Increased

focal 18F-FDG uptake was noted in just four patients: three at the site of recent coronary stenting and one at the ostium of a saphenous vein graft.

Percutaneous Coronary Intervention With Stent Implantation

Seven patients with myocardial infarction underwent 18F- fluoride scanning prior to percutaneous coronary intervention with stent implantation (6 non-ST elevation myocardial infarction and 1 late presentation ST elevation myocardial infarction). Focal 18F- fluoride uptake was observed at the site of culprit plaque in all 7 patients (culprit lesion tissue to background ratios 1.74 [1.40-1.95] *versus* maximum non-culprit lesion 1.25 [1.07-1.29], p=0.007). Furthermore at the time of their PCI, two patients with myocardial infarction underwent additional coronary stenting to a bystander non-culprit stenosis (Figure 3-1). Although intense 18F- fluoride uptake was observed at the site of culprit lesion, none was observed at the site of the bystander lesions. Amongst patients with stable angina, 5 patients underwent 18F-Fluoride PET imaging shortly after elective coronary stenting (24 [12-29] days). There was no uptake noted at the site of the percutaneous coronary intervention in these patients (TBR stented lesion 1.07 [0.78-1.16] *versus* reference lesion 0.98 [0.81-0.98], p=0.92). Taken together, these data indicate that 18F-Fluoride uptake does not appear to occur as a response to stent implantation.

Figure 3-6: Lesions with and without 18F-fluoride uptake, and gray-scale and radiofrequency intravascular ultrasound in patients with stable angina.

Panels A and B: Proximal left anterior descending artery lesion showing intense 18F-fluoride uptake (tissue-to-background ratio 2.81; arrows) on combined positron emission tomography and computed tomography images (A). The radiofrequency and grey-scale intravascular ultrasound of this lesion (B) shows significant necrotic core (red arrow) and microcalcification (white arrow).

Panels C and D: Proximal left anterior descending artery lesion with no 18F-fluoride uptake. The radiofrequency and grey-scale intravascular ultrasound shows that this lesion is principally composed of fibrous and fibro-fatty tissue (green arrow) with minimal necrotic core.

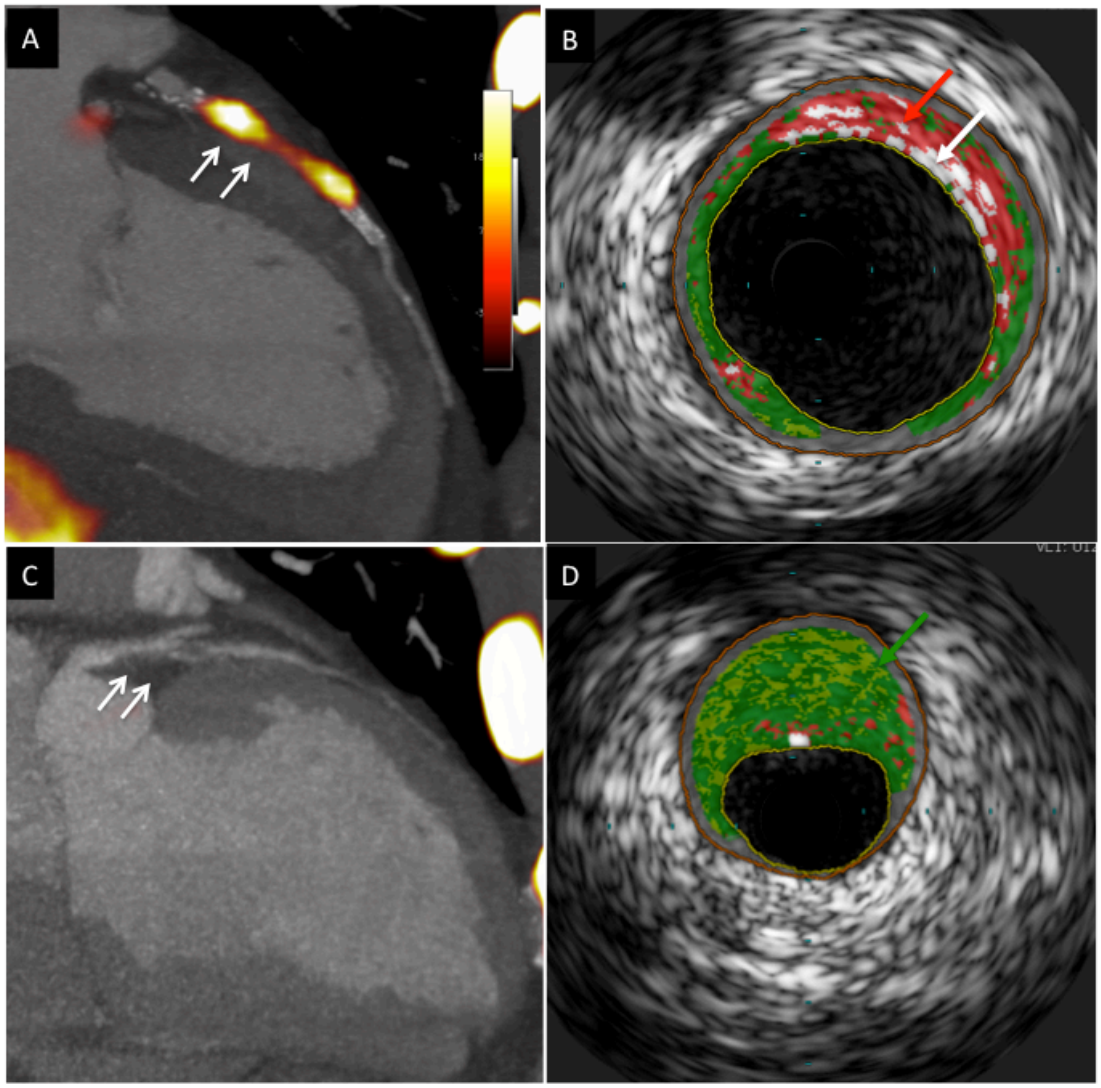

Table 3-3 Gray-scale and radiofrequency intravascular ultrasound characteristics in 18F-fluoride positive and negative plaques of patients with stable angina.

	18F-fluoride Positive Plaques (n=15)	18F-fluoride Negative Plaques (n=24)	P value
Lumen			
Area (mm^2)	9.0 [5.7-13.5]	6.7 [4.7-9.7]	0.078
Minimal Diameter (mm)	2.6 [1.7-3.1]	1.9 [1.7-2.6]	0.165
Maximum Diameter (mm)	4.9 [4.1-5.3]	3.6 [3.1-4.6]	0.006
Vessel			
Area (mm^2)	24.1 [17.2-27.1]	14.5 [11.9-18.1]	0.002
Minimal Diameter (mm)	4.4 [3.4-5.2]	3.6 [3.0-4.1]	0.057
Maximum Diameter (mm)	6.5 [6.0-7.1]	5.2 [4.7-5.9]	<0.001
Plaque			
Length (mm)	14.2 [6.2-23.5]	15.2 [6.7-25.0]	0.941
Volume (mm^3)	152.9 [99.6-289.7]	91.0 [45.8-158.2]	0.032
Burden (%)*	55.6 [48.6-64.4]	54.2 [46.3-57.3]	0.174
Remodeling Index	1.12 [1.09-1.19]	1.01 [0.94-1.06]	<0.001
Plaque Composition			
Fibrous Tissue (%)	51.0 [46.3-56.6]	58.1 [51.6-65.5]	0.015
Fibro-Fatty (%)	10.9 [6.0-13.8]	12.6 [9.3-17.8]	0.092
Necrotic Core (%)	24.6 [20.5-28.8]	18.0 [14.0-22.4]	0.001
Max Frame Necrotic Core (%)	35.5 [34.2-40.5]	29.2 [23.9-42.1]	0.009
Dense Calcium (%)	12.6 [9.1-18.1]	10.2 [4.0-14.9]	0.092
Microcalcification	11 (73%)	5 (21%)	0.002
Plaque Classification			
Thin-cap fibroatheroma	7 (47%)	4 (16%)	0.068
Thick-cap fibroatheroma	5 (33%)	9 (38%)	1.0
Pathological intimal thickening	0	7 (29%)	0.003
Fibrocalcific plaque	3 (20%)	4 (16%)	1.0

Median [IQR] maximum frame necrotic core: refers to maximum necrotic core in any single frame in the plaque.*Plaque burden calculation: (average vessel area-average lumen area) /average vessel area. IQR Interquartile Range.

Table 3-4 Plaque characteristics on invasive and computed tomography coronary angiography in patients with stable angina.

	18F-Fluoride positive plaques (n=32)	18F-Fluoride negative plaques (n=53)	p value
Lesion stenosis*			
>70%	9 (28%)	8 (15%)	0.99
50% to 70%	11 (39%)	23 (43%)	0.67
10% to 50%	6 (19%)	10 (19%)	1.00
<10%	6 (19%)	12 (23%)	1.00
Type of Plaque†			
Non-calcified	2 (6 %)	11 (21%)	0.97
Mixed	23 (72%)	28 (53%)	0.98
Calcified	7 (22%)	14 (26%)	1.00
Plaque Analysis			
Positive remodeling‡	16 (50%)	30 (57%)	0.650
Necrotic core§	10 (31%)	9 (17%)	0.179
Microcalcification¶	20 (63%)	15 (28%)	<0.001
Dense calcification	21 (66%)	34 (64%)	1.000

*On invasive coronary angiogram. †On CT Coronary Angiogram. ‡Positive Remodeling: diameter at the plaque site was at least 10% larger than the proximal reference segment. §Necrotic core: Based on Hounsfield Units of less than 30 within the plaque.¶Microcalcification: Defined <3 mm in size on curved multi-planar reformation images and occupying <180° on crosssectional images.

Figure 3-7: Patients with stable angina and 18F-fluoride uptake

Representative examples for 18F-fluoride uptake in patients with stable angina. Panels A-D, computed tomography coronary angiograms; panels E-H, 18F-fluoride positron emission tomograms; and panels I-L, fused positron emission tomograms and computed tomography coronary angiograms (tissue-to-background ratios 2.80, 3.84, 1.80 and 2.38 respectively).

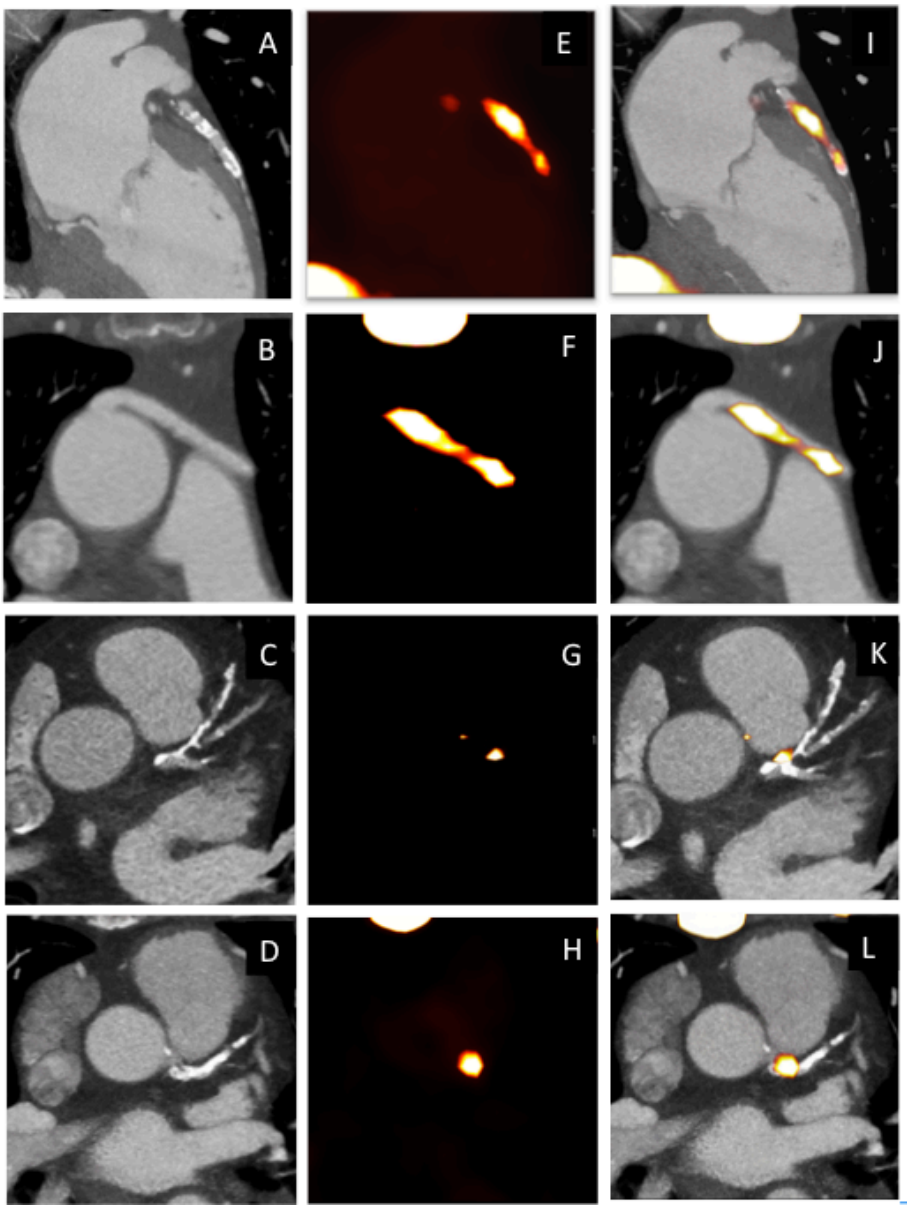

3.5. DISCUSSION

We report the first non-invasive imaging technique to identify ruptured and high-risk coronary atherosclerotic plaque. We have demonstrated that intense 18F- fluoride uptake localises to recent plaque rupture in patients with acute myocardial infarction and those with symptomatic carotid disease. Moreover, in patients with stable coronary artery disease, 18F- fluoride uptake appears to identify coronary plaques with high-risk features on intravascular ultrasound. This technique holds major promise as a means of identifying high-risk and ruptured plaque, and potentially informing the future management and treatment of patients with stable and unstable coronary artery disease.

Over 90% of our patients with myocardial infarction had increased 18F- fluoride uptake at the site of their culprit ruptured plaque with TBR values that were a third higher than the maximum activity anywhere else in the coronary vasculature. These findings were not unique to the coronary circulation since we also observed increased focal 18F- fluoride uptake at the site of plaque rupture in all excised carotid endarterectomy specimens from patients with symptomatic carotid disease. However, we do acknowledge that this was not a universal finding. Of the three patients with myocardial infarction who had no uptake, two were younger smokers with only mild underlying irregularities on coronary angiography, implicating plaque erosion and thrombosis as the mechanism of their infarction rather than plaque rupture (Burke et al., 1997b). The third patient sustained an infero-lateral non-ST segment elevation myocardial infarction and had a lesion in the right coronary artery

stented. Increased 18F- fluoride activity was observed in the co-dominant circumflex artery that could have equally explained the clinical presentation, raising the intriguing possibility that 18F- fluoride may have a clinical role for patients in whom the culprit lesion is not readily apparent.

Focal regions of increased 18F- fluoride activity were observed in almost one half of our patients with stable coronary artery disease. In order to understand the mechanism of uptake in these patients, we sought to compare plaque characteristics of lesions with and without increased 18F- fluoride uptake. Because histology of the coronary arteries in this population is not feasible, we undertook gray-scale and radiofrequency intravascular ultrasound; a widely used and validated tool that provides detailed characterization of plaque composition (Garcia-Garcia et al., 2009b). This demonstrated that lesions with increased 18F- fluoride uptake were associated with greater positive remodeling, more microcalcification and a larger necrotic core. These findings were corroborated by, and consistent with, the findings of plaque analysis performed using CT coronary angiography. Intriguingly, plasma troponin concentrations measured by a novel high-sensitivity assay were also higher in those patients with 18F- fluoride positive plaques: perhaps implicating sub-clinical plaque rupture with embolization and micro-infarction.

Why does 18F- fluoride bind to ruptured or high-risk plaque? Similar to the caseating granulomata of tuberculosis, atherosclerotic vascular calcification is a controlled

cellular response to an intense, necrotic and chronic inflammatory stimulus. Indeed, direct links between inflammatory cells and osteoblastic metaplasia in the vasculature are well described (Aikawa et al., 2007, New et al., 2013a). Hydroxyapatite is the central structural component of vascular calcification and is laid down during the very earliest and active stages of mineralization (Aikawa et al., 2007): hydroxyapatite nanocrystals nucleate, propagate and mineralize the extracellular matrix. Fluoride ions are incorporated into the hydroxyapatite by ion exchange with hydroxyl groups at the crystal surface. This is critically dependent on the crystal surface area that will be greatest in the earliest and most active nanocrystalline stages of mineralization associated with plaque inflammation and necrosis. We believe that this is responsible for the observed 18F- fluoride uptake and is consistent with our data demonstrating 18F- fluoride uptake in regions of necrosis, macrophage infiltration, apoptosis, microcalcification and alkaline phosphatase and osteocalcin staining. Moreover, mathematical modeling indicates that microcalcification at the surface of thin-capped atheroma can intensify and double incident stresses (Vengrenyuk et al., 2006b). Microcalcification is therefore not only a marker of acute plaque rupture but is implicated in its precipitation.

Coronary arterial calcification is considered pathognomonic of atherosclerosis and is a powerful independent risk predictor for cardiovascular events that can be further refined by the rapidity of its progression (Raggi et al., 2004a, McEvoy et al., 2010). Why then not rely on CT coronary calcium scoring alone as a biomarker? Microcalcification cannot be detected on CT and confluent coronary

macrocalcification develops slowly taking many months or years to become apparent on CT and can become dormant once inflammation in the plaque has subsided. By identifying areas of nascent and ongoing calcification activity, 18F- fluoride uptake allows us to detect regions of metabolically active plaque, thus providing complementary information to CT (Derlin et al., 2010, Li et al., 2012b, Beheshti et al., 2008). Indeed, we observed large areas of coronary CT calcium in the absence of increased 18F-Fluoride uptake whereas other regions with minimal or no CT calcium had intense 18F-Fluoride uptake in keeping with previous observations by Derlin *et al.* in the aorta (Derlin et al., 2010, Derlin et al., 2011b). Moreover given that 18F-Fluoride appears more closely aligned with the process of necrotic inflammation and plaque metabolic activity, we believe that it potentially offers major improvements to the prediction of cardiovascular risk compared to calcium scoring.

Our data have already established that 18F- fluoride identifies plaque with multiple high-risk features but prospective studies are now required in a broad range of patients to assess whether increased coronary 18F- fluoride activity will ultimately translate into future adverse events. If the results prove confirmatory then this technique has the potential to alter fundamentally the way we treat coronary artery disease: moving us away from the current paradigm based on lesion severity and ischemia to one focused on plaque metabolism and inflammation. It could, for example, permit the identification of the "vulnerable patient" with single or multiple high-risk or silently ruptured plaques, providing an opportunity to treat and modify their risk to prevent future adverse cardiovascular events.

In contrast to 18F- fluoride, 18F-FDG imaging was hampered by problems related to tracer uptake in the myocardium. Our stringent dietary recommendations resulted in suppression of myocardial activity in 70-85% of patients: a rate that compares favorably with previous studies (57-84%) (Rogers and Tawakol, 2011, Cheng et al., 2012, Wykrzykowska et al., 2009). However, this suppression resulted in a patchy distribution of myocardial uptake that frequently obscured activity in one or more coronary vessels. It remains a possibility that 18F-FDG uptake is increased in the culprit plaque and we failed to demonstrate this because of incomplete data or the delay in scanning. However, given its limitations, we believe that 18F-FDG is unlikely to become sufficiently robust to permit its clinical application to the coronary circulation. In contrast, 18F-FDG uptake remains an important measure of more general vascular inflammation in the aorta and carotid arteries, providing complementary and distinct metabolic information to that of 18F- fluoride uptake.

We do acknowledge that there are limitations of our study that include a lack of respiratory gating, potential partial volume artifacts and the use of surrogate measures for coronary histology (Garcia-Garcia et al., 2009b). However, we believe that the totality of our comprehensive evidence using multiple approaches and imaging modalities, provides a robust and cogent argument to support our contention that 18F-fluoride uptake identifies vulnerable and high-risk plaques in patients with stable and unstable coronary heart disease. Further work is now needed to establish whether 18F- fluoride PET-CT will provide a clinically useful technique capable of

improving risk stratification, monitoring disease progression, guiding therapeutic interventions and assessing novel anti-atherosclerotic therapies.

Chapter 4. SYSTEMIC ATHEROSCLEROTIC INFLAMMATION FOLLOWING ACUTE MYOCARDIAL INFARCTION

Published by JOSHI, N. V., TOOR, I., SHAH, A. S., CARRUTHERS, K., VESEY, A. T., ALAM, S. R., SILLS, A., HOO, T. Y., MELVILLE, A. J., LANGLANDS, S. P., JENKINS, W. S., UREN, N. G., MILLS, N. L., FLETCHER, A. M., VAN BEEK, E. J., RUDD, J. H., FOX, K. A., DWECK, M. R. & NEWBY, D. E. 2015. Systemic Atherosclerotic Inflammation Following Acute Myocardial Infarction: Myocardial Infarction Begets Myocardial Infarction. *J Am Heart Assoc,* 4**,** e001956.

4.1. SUMMARY

In murine models, acute myocardial infarction exacerbates atherosclerotic inflammation and progression. Using combined positron emission and computed tomography (PET-CT), we investigated whether this phenomenon occurs in humans.

Forty patients with recent myocardial infarction and 40 with stable angina pectoris underwent thoracic 18F-fluorodeoxyglucose (18F-FDG). Radiotracer uptake was measured in aortic atheroma and non-vascular tissue (para-spinal muscle). In 1,003 patients enrolled in the Global Registry of Acute Coronary Events, we assessed whether infarct size predicted early (≤30 days) and late (>30 days) recurrent coronary atherothombotic events.

Compared to patients with stable angina, patients with myocardial infarction had higher aortic 18F-FDG uptake (mean TBR_{max} 2·15±0·30 *versus* 1·84±0·18, P<0·0001) and plasma C-reactive protein concentrations (6·50 [2·00-12·75] *versus* 2·00 [0·50-4·00] mg/dL, P=0·0005), despite having similar aortic (aortic Agatston score: 135 [0-805] *versus* 538 [4-1870] AU, P=0·12) and less coronary (coronary Agatston score: 599 [60-1302] *versus* 159 [42-456] AU, P=0·006) atherosclerotic burden, and similar para-spinal muscular 18F-FDG uptake (0·79±0·25 *versus* 0·75±0·21, P=0·52). Patients with ST-segment elevation myocardial infarction had larger infarcts (peak plasma troponin concentration 32,300 [10,200->50,000] *versus* 3,800 [1,000-9,200]

ng/L, P<0·0001) and greater aortic 18F-FDG uptake (2·24±0·32 *versus* 2·02±0·21, P=0·03) than those with non-ST elevation myocardial infarction. Peak plasma troponin concentration correlated with aortic 18F-FDG uptake (r=0·43, P=0·01) in patients with myocardial infarction. On multivariate analysis, peak troponin I concentrations were an independent predictor of early recurrent myocardial infarction (tertile-3 *versus* tertile-1: relative risk 4·30 [95% CI, 1·85-9·96], p=0·001) but did not predict late re-infarction.

The presence and extent of myocardial infarction is associated with increased aortic atherosclerotic inflammation and early recurrent myocardial infarction. This supports the hypothesis that acute myocardial infarction exacerbates and promotes systemic atherosclerotic inflammation and remote plaque destabilisation.

4.2. INTRODUCTION

Despite recent advances, prognosis following acute myocardial infarction remains poor (Roger et al., 2011, Naghavi et al., 2003, Virmani et al., 2000a) because of a considerable risk of recurrent infarction (Milonas et al., 2010) and ischemia (Goldstein et al., 2000). Such recurrent events are as likely to occur at the site of non-culprit plaques as the original culprit lesion (Stone et al., 2011a). Indeed, in post-mortem studies of patients dying after acute myocardial infarction, there is evidence of multiple plaque-related thrombotic events: on average 2.4 per patient (Mann and Davies, 1999). Moreover, there is an increased incidence of ischemic stroke following myocardial infarction (not exclusively as a consequence of embolic events) suggesting systemic as well as localized destabilization of remote atherosclerotic plaque (Witt et al., 2006, Mooe et al., 1997).

Myocardial infarction occurs predominantly as a consequence of acute atherosclerotic plaque rupture (Virmani et al.,2000, Burke et al. 1997), with inflammation believed to be a key precipitant (Libby, 2013, Swirski and Nahrendorf, 2013). Macrophages infiltrate high-risk plaque and secrete matrix metalloproteinases that weaken the fibrous cap and predispose the plaque to rupture (Libby, 2013, Swirski and Nahrendorf, 2013). Recent pre-clinical murine data have indicated that myocardial infarction induced by coronary artery ligation causes a systemic inflammatory response that involves macrophage mobilization, a generalized

increase in atherosclerotic inflammation and accelerated plaque progression (Dutta et al., 2012). However, this phenomenon has not been directly observed in humans.

Positron emission tomography (PET) combined with computed tomography (CT) allows the *in vivo* assessment of atherosclerotic disease in humans. 18F-fluorine-2-deoxy-D-glucose (18F-FDG) is a glucose analogue that is taken up by cells with high metabolic requirements. It has become a widely used as a measure of acute vascular inflammation, correlating with atherosclerotic macrophage burden, response to drug therapy and symptomatic status (Rogers et al., 2010, Tawakol et al., 2006, Rudd et al., 2002, Satomi et al., 2013b). Indeed, its generalized uptake within large arteries is a powerful predictor of subsequent adverse cardiovascular events (Rominger et al., 2009).

In this prospective clinical trial, we determined whether systemic atherosclerotic plaque metabolism is increased in patients with myocardial infarction compared to those with stable coronary disease, and whether this is more marked in those with larger infarctions. Furthermore, we explored whether this might be of clinical relevance and whether infarct size could predict recurrent early myocardial infarction.

4.3. METHODS

The study comprised two cohorts of patients: an imaging cohort consisting of subjects with stable angina and myocardial infarction, and an outcome cohort comprising patients enrolled in the Global Registry of Acute Coronary Events (GRACE)(Fox et al., 2006).

4.3.1. IMAGING COHORT

Consecutive patients with acute ST- or non-ST-segment elevation myocardial infarction (Thygesen et al., 2012) and stable angina pectoris scheduled for invasive coronary angiography were recruited from the Royal Infirmary of Edinburgh. Patients with myocardial infarction fulfilled the criteria for type 1 myocardial infarction according to the Universal Definition of Myocardial Infarction (Thygesen et al., 2012). ST segment elevation myocardial infarction was defined as new ST segment elevation at the J point in two contiguous leads with the cut-points: ≥0.1 mV in all leads except V_2-V_3 where the thresholds were ≥0.2 mV for men ≥40 years and ≥0.25 mV for women. Consecutive patients with stable angina pectoris were recruited if they had typical symptoms of exertional anginal chest pain, previously documented coronary artery disease (>70% stenosis of at least one major epicardial coronary artery), and had been scheduled for invasive coronary angiography. Patients were excluded if they had suffered an acute coronary syndrome within the last 3 months.

Other exclusion criteria were age <50 years, insulin-dependent diabetes mellitus, women of childbearing age not taking contraception, severe renal failure (serum creatinine >250 μmol/L), known contrast allergy and inability to provide informed consent. Studies were performed with the approval of the local research ethics committee, in accordance with the Declaration of Helsinki, and with the written informed consent of each participant. All patients underwent a comprehensive baseline clinical assessment including evaluation of their cardiovascular risk factor profile. Blood was drawn from all participants for evaluation of plasma C-reactive protein (CRP) concentrations that were measured using the MULTIGENT CRP Vario assay (ARCHITECH cSystems Assay, Abbott Laboratories, Abbott Park, Illinois, USA).

PET-CT Imaging

All patients underwent PET-CT imaging of the thorax with a hybrid scanner (Biograph mCT, Siemens Medical Systems, Erlangen, Germany) using 18F-FDG as well as coronary calcium scoring and CT angiography of the aorta and coronary arteries (Joshi et al., 2013, Dweck et al., 2012a, Dweck et al., 2011).

Image Analysis

Anonymized PET-CT datasets were presented in a random order on an OsiriX workstation (64 bit; version 5.5.1 OsiriX Imaging Software, Geneva, Switzerland) to trained observers blinded to the patient's clinical status. To aid image analysis, PET

images were fused with the CT angiograms, and regions of interest (ROIs) drawn around the thoracic aorta on serial 3-mm axial slices. Within these regions, mean and maximum tracer activities were measured using standard uptake values (SUV) and corrected for blood pool activity in the superior vena cava to provide tissue-to-background ratios (TBRs) (Joshi et al., 2013, Dweck et al., 2012a, Dweck et al., 2011, Wong et al., 2009, Dweck et al., 2013c). The ascending aorta was defined as the segment of the aorta from the lower level of the right pulmonary artery up to the last slice where the aorta maintained its circular cross-sectional appearance. The descending aorta was defined similarly as the region extending up from the tip of the diaphragm to the last circular slice. The aortic arch was defined as the region of aorta connecting the ascending and descending aorta (Figure 4-1). Aortic radiotracer uptake was quantified using the method of Fayad *et al*. (Fayad et al., 2011a). In brief, the following measures of uptake were measured on axial slices across the aorta as a whole and within each region: TBR_{max}, the average of the maximum TBR values measured on each axial slice; TBR_{mean}, the average of the mean TBR values measured on each slice; max TBR, the maximum uptake TBR value in any axial section and TBR_{MDS}, the most diseased segment, defined as the highest maximal TBR value averaged over 3 consecutive slice (Fayad et al., 2011a) . Thirty patients were selected randomly to test the repeatability of 18F-FDG measurements in the aorta. Fifteen patients from each cohort were selected and two trained readers (NVJ, SPL) quantified aortic activity independently. Activity within non-vascular tissue was assessed using oval-shaped ROIs drawn within paraspinal muscle (area ~7 cm^2) on 5 consecutive axial slices.

CT analysis was performed on a dedicated cardiovascular workstation (Vitrea,Vital Images, Minnetonka, Minnesota, USA). Vessel-specific and total Agatston calcium scores were calculated as described previously (Dweck et al., 2012a) for the coronary arteries, the aorta and its different regions using a threshold of 130 Hounsfield units (Santos et al., 2010).

Figure 4-1: Measurement of radiotracer uptake in the aorta

The aorta was divided into ascending (A), arch (B) and descending aorta (C) as shown. Regions of interest were drawn around the aorta on axial slices to provide measures of radiotracer uptake.

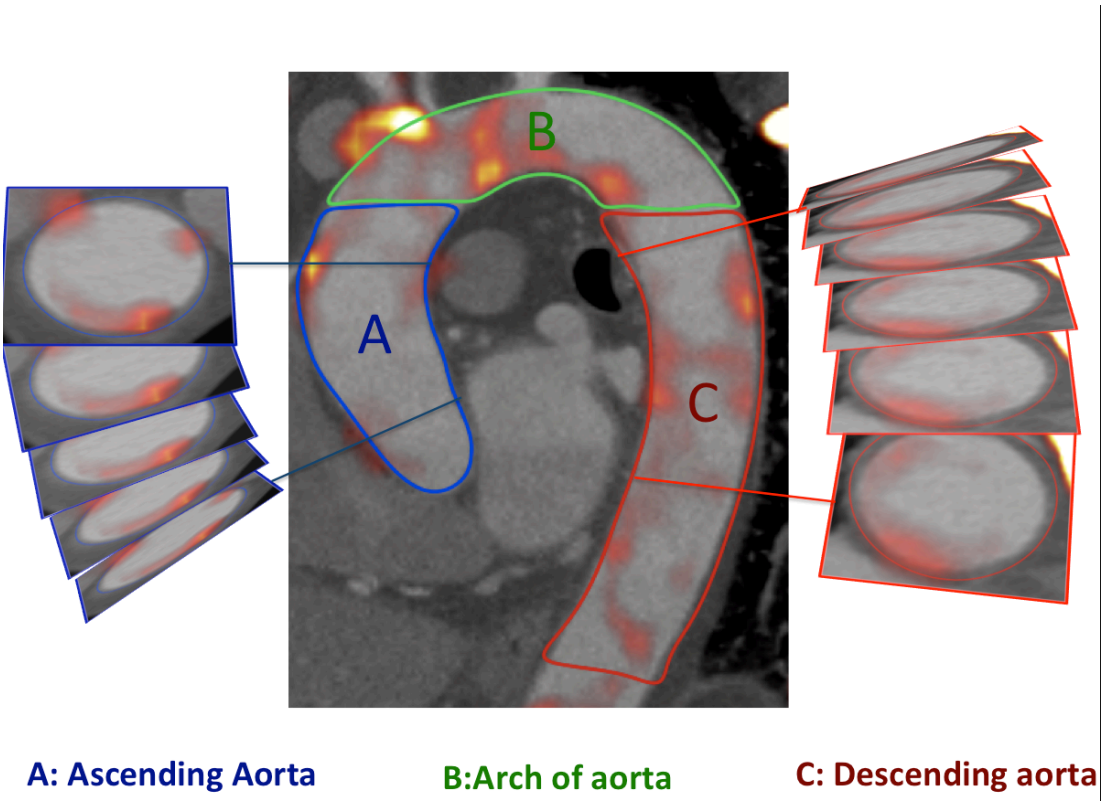

4.3.2. OUTCOME COHORT

Full details of the GRACE methods have been published previously (Fox et al., 2007, Steg et al., 2002). The Edinburgh cohort of the prospectively maintained GRACE database was used to identify 1,003 patients admitted with an acute coronary syndrome between 20th January 2003 to 9th June 2009 (Fox et al., 2010). To be eligible, patients (>18 years) had to be admitted with an acute coronary syndrome as a presumptive diagnosis and have at least 1 of the following: electrocardiographic changes consistent with acute coronary syndrome, serial increases in biomarkers of cardiac necrosis or documented coronary artery disease. For consistency, only patients who had plasma troponin I concentrations quantified (Abbott Laboratories, Abbott Park, IL, USA) in a standardized accredited laboratory were included. Exclusion criteria were secondary myocardial injury precipitated or accompanied by a significant comorbidity, trauma, or surgery. Information regarding patient demographic characteristics, medical history, timing and occurrence of acute coronary symptoms, clinical characteristics, electrocardiographic findings, treatment approaches, and in-hospital outcomes is collected through completion of a standardized proforma (Fox et al., 2007, Steg et al., 2002). The baseline and peak troponin I concentrations during admission were recorded and patients divided into tertiles based on their peak troponin I to reflect the degree of myocardial injury and the size of their infarct (Younger et al., 2007).

The primary endpoint of the analysis was early recurrent myocardial infarction following the index admission, defined as recurrent type 1 myocardial infarction

within 30 days of index admission (Fox et al., 2006). To avoid confounding with the index presentation, only those patients having recurrent myocardial infarction beyond the first 24 hours after presentation were analyzed as described previously (Fox et al., 2006). We also examined the factors associated with late recurrent myocardial infarction as an exploratory end-point, defined as a recurrent type 1 myocardial infarct >30 days following index admission.

4.3.3. STATISTICAL ANALYSIS

As a pre-specified end-point of our previously reported trial (ClinicalTrials.gov: NCT01749254), we explored 18F-FDG uptake in remote aortic atheroma of patients with recent myocardial infarction or stable coronary heart disease. Continuous data were tested for normality with the D'Agostino and Pearson Omnibus test. Continuous parametric variables were expressed as mean±standard deviation and compared using Student's *t*-tests. Non-parametric data were presented as median [interquartile range] and compared using Mann-Whitney U test or Wilcoxon signed-rank test as appropriate. Interobserver reproducibility was calculated by Bland Altman method and intraclass correlation coefficients with 95% confidence intervals. Fisher's exact test or chi-squared test was used for analysis of categorical variables. Corelations were performed using Pearson's and Spearman's rank correlation coefficient for parametric and non-parametric data respectively.

Patients in the registry cohort were divided into tertiles according to their peak troponin concentration. Kaplan Meier curves were used to estimate the distribution of early recurrent myocardial infarction across the tertiles. Univariate analysis was undertaken to identify associations with early (≤30 days) and late (>30 days) recurrent myocardial infarction that were then entered into the multivariate logistic regression model based on univariate association of $p<0{\cdot}1$. In addition, age and sex were included in the model. Statistical analysis was performed with Graph Pad Prism version 6 (GraphPad Software Inc., California USA) and SPSS 19.0 (SPSS

Inc., Chicago, Illinois) where appropriate. Unless stated, a two-sided $P<0.05$ was taken as statistically significant.

4.4. RESULTS

4.4.1. IMAGING COHORT

A total of 40 patients with stable angina and 40 with myocardial infarction underwent 18F-FDG PET imaging. The median time between hospitalization and 18F-FDG PET imaging was 11 [8-17] days in patients with myocardial infarction. As compared to patients with stable angina, patients with myocardial infarction were younger and had less extensive coronary artery disease (Table 4-1), and lower coronary artery calcium scores (coronary artery calcium score: stable angina 599 [60-1302] *versus* myocardial infarction 159 [42-456] Agatston Units, P=0.006; Tables 4-1 and 4-2). Although apparently higher aortic calcium scores were noted in patients with stable angina, this did not reach statistical significance (aortic calcium scores; stable angina 538 [4-1870] *versus* myocardial infarction 135 [0-805] Agatston Units; P=0.12; Table 4-2).

Table 4-1 Baseline characteristics of patients with coronary artery disease

	Stable angina	**Myocardial infarction**		
	All (n=40)	All (n=40)	STEMI (n=26)	NSTEMI (n=14)
Age (years)	67±8	62±8	63±9	60±8
Male sex	36 (90%)	37 (93%)	24 (92%)	13 (93%)
BMI (kg/m^2)	30±5	28±5	27±5	30±4
Antecedent angina (active)	40 (100%)	9 (23%)	5 (19%)	4 (29%)
Heart rate (/min)	59±9	56±7	56±7	56±7
Systolic BP (mmHg)	134±14	132±21	131±20	121±21
Diastolic BP (mmHg)	77±10	76±9	76±9	76±8
Cardiovascular History				
Previous MI	15 (38%)	5 (13%)	1 (4%)	4 (29%)
Previous CVA/TIA	4 (10%)	2 (5%)	1 (4%)	1 (7%)
Previous PCI	19 (48%)	5 (13%)	2 (8%)	3 (21%)
Previous CABG	11 (28%)	2 (5%)	2 (8%)	0
Risk Factors				
Smoking Habit	24 (60%)	25 (63%)	19 (73%)	6 (43%)
Diabetes Mellitus	13 (33%)	8 (20%)	7 (27%)	1 (7%)
Hypertension	36 (90%)	17 (43%)	11 (42%)	6 (43%)
Hypercholesterolaemia	39 (98%)	19 (48%)	11 (42%)	8 (57%)
Medications				
Aspirin	33 (83%)	40 (100%)	26 (100%)	14 (100%)
Clopidogrel	5 (13%)	39 (98%)	25 (96%)	14 (100%)
Statin	36 (90%)	39 (98%)	26 (100%)	13 (93%)
β-Blocker	28 (70%)	32 (80%)	20 (77%)	12 (86%)
ACEI/ARB	20 (50%)	35 (88%)	25 (96%)	10 (71%)
Calcium channel blockers	16 (40%)	2 (5%)	2 (8%)	0
Other Anti-hypertensive	6 (15%)	3 (8%)	1 (4%)	2 (14%)
Oral Nitrates	15 (38%)	1 (3%)	0	1 (7%)
Serum Biochemistry				
Cholesterol (mg/dL)	151±31	181±46	181±50	185±43
HDL-Cholesterol (mg/dL)	43±12	43±12	43±12	39±12

LDL-Cholesterol (mg/dL)	81±27	112±43	108±43	120±39
Triglycerides (mg/dL)	62±27	62±31	66±27	58±27
Creatinine (mg/dL)	0.96±0.26	0.96±0.30	0.97±0.33	0.93±0.27
Peak Troponin Concentration (ng/L)	-	11,200 [3,300 – 50,000]	32,300 [10,200->50,000]	3,800 [1,000-9,200]

Heart rate at the time of CTCA; ‡ Medications at the time of scan

STEMI ST elevation myocardial infarction, NSTEMI non-ST elevation myocardial infarction, BMI body mass index, MI myocardial infarction, CVA cerebrovascular accident, TIA transient ischemic attack, PCI percutaneous coronary intervention, ACEI angiotensin converting enzyme inhibitor, ARB angiotensin receptor blocker, CABG coronary artery bypass graft, HDL high-density lipoprotein, LDL low-density lipoprotein, TG Triglycerides.

Table 4-2 Aortic calcium scores and 18F-FDG tissue-to-background ratios in patients with stable angina and myocardial infarction

	Patients with Stable Angina (n=40)	Patients with Myocardial Infarction (n=40)	P value	Patients with STEMI (n=26)	Patients with NSTEMI (n=14)	P value
Aortic Calcium						
tston Units (AU)	538 [4-1870]	135 [0-805]	0.12	183 [0-377]	55 [0-2523]	0.91
ume (mm^3)	532 [7-1718]	149 [0-717]	0.12	192 [0-387]	94 [0-2263]	0.85
s (mg)	131 [2-517]	31 [31-1415]	0.07	131 [2-517]	43 [0-86]	0.9
- FDG						
racic aorta n TBR_{max}	1.84±0.18	2.15±0.30	<0.0001	2.24±0.32	2.02±0.21	0.03
racic aorta n TBR_{mean}	1.41±0.14	1.60±0.17	<0.0001	1.51±0.16	1.66±0.17	0.01
racic aorta max	2.22±0.31	2.64±0.52	<0.0001	2.78±0.57	2.40±0.35	0.02
racic aorta $_{MDS}$*	2.11±0.23	2.54±0.49	<0.0001	2.66±0.53	2.34±0.33	0.04
tic sub-regions						
ending aorta n TBR_{max}	1.84±0.20	2.21±0.35	<0.0001	2.35±0.35	2.03±0.26	0.01
n of aorta mean $_{max}$	1.88±0.22	2.26±0.34	<0.0001	2.35±0.35	2.11±0.26	0.03
cending aorta n TBR_{max}	1.82±0.18	2.10±0.30	<0.0001	2.17±0.32	1.98±0.21	0.08

I: ST elevation myocardial infarction, NSTEMI: non ST elevation myocardial infarction, mean TBR_{max} average of the maximum tissue to ound ratios across all slices in the segment, mean TBR_{mean} average of the mean tissue to background ratios all slices in the segment, max TBR : value tissue to background ratios in any axial slice , TBR_{MDS} Tissue to background ratio in the Most Diseased Segment.

Positron Emission Tomography

The reproducibility of TBR measurements in the aorta for tracer activity was excellent, with no fixed or proportional biases and narrow limits of agreement. In contrast to the calcium scores, 18F-FDG uptake was 20% higher in the aortae of patients with recent myocardial infarction than those with stable coronary artery disease (Table 4-2, Figure 4-2). This was a consistent finding in all regions of the aorta assessed (entire thoracic aorta, ascending aorta, aortic arch, descending aorta; all $P<0.0001$) and with all measures of tracer activity (mean TBR_{max}, mean TBR_{mean}, max TBR, TBR_{MDS}, all $P<0.001$). Furthermore 18F-FDG activity was higher in patients with ST-segment elevation compared to those with non-ST-segment elevation myocardial infarction (TBR_{max} 2.24±0.32 *versus* 2.02±0.21 respectively, P=0.03; Table 4-2) consistent with the former having sustained larger myocardial infarctions (peak plasma troponin concentration 32,300 [10,200-50,000] *versus* 3,800 [1,000-9,200] ng/L; $P<0.0001$). Indeed, aortic 18F-FDG activity correlated with peak plasma troponin I concentrations (r=0.43, P=0.01).

In patients with stable angina and those with myocardial infarction, paraspinal uptake of 18F-FDG (mean TBR_{max} 0.79±0.25 *versus* 0.75±0.21 respectively, P=0.52) was similar.

Figure 4-2: **Uptake of 18F-fluorodeoxyglucose by aortic atherosclerosis in patients with stable and unstable coronary heart disease**

Aortic mean of the maximum tissue-to-background ratios (mean TBR_{max}) for 18F-flurodeoxyglucose uptake in patients with stable angina, ST elevation myocardial infarction (STEMI) and non-ST elevation myocardial infarction (NSTEMI). Mean with 95% confidence intervals.

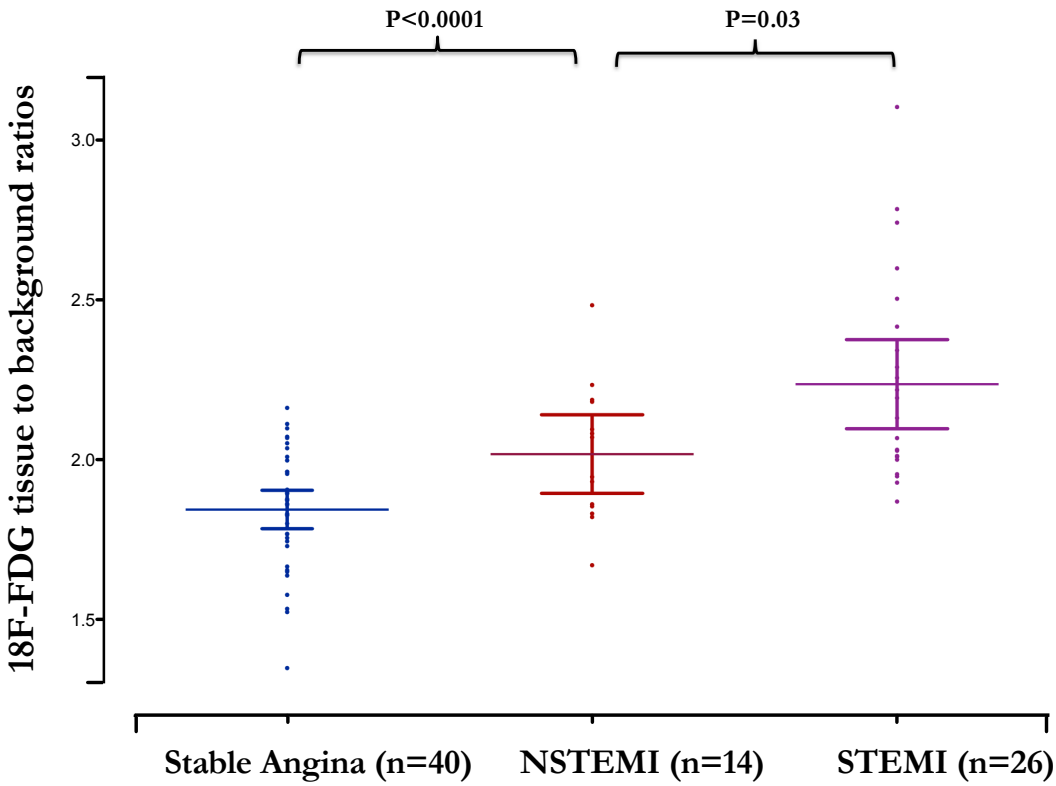

C-reactive Protein

Compared to patients with stable angina, patients with myocardial infarction had higher plasma C-reactive protein concentrations (6.50 [2.00-12.75] *versus* 2.00 [0.50-4.00]) mg/dL, P=0.0005). Amongst patients with myocardial infarction, patients with ST-segment elevation myocardial infarction appeared to have higher plasma C-reactive protein concentrations (7.50 [2.00-13.75] *versus* 2.50 [1.75-9.50] mg/dL) but this did not reach statistical significance (P=0.22). There was a modest correlation between peak troponin I concentrations and C-reactive protein (r=0.35, P=0.03).

4.4.2. OUTCOME COHORT

One thousand and three patients enrolled in the GRACE database were followed up for a median follow up period of 34 [18-50] months. Early recurrent myocardial infarction occurred in 54 patients following index admission, whilst late recurrent myocardial infarction occurred in 89 patients.

Patients were classified into tertiles according to their peak plasma troponin I concentrations measured during the index admission (tertile 1, ≤ 220; tertile 2, 230-6,130; and tertile 3, ≥6,140 ng/L; Table 4-3). On univariate analysis, the risk of early recurrent infarction (≤30 days) was more than four-fold higher amongst patients in the highest troponin tertile compared to the lowest, whilst it was double in the middle tertile compared to the lowest (Table 4-4 and Figure 4-3). The variables with univariate association of p<0·1 were Killip score ≥2, ST segment deviation, multivessel disease and troponin I concentrations. On multivariate analysis, troponin emerged as an independent predictor of early myocardial infarction on multivariate analyses after adjustment for other relevant variables (tertile 3 *versus* tertile 1: relative risk 4.30 [95% CI, 1.85-9.96], P=0.001; tertile 2 *versus* tertile 1: relative risk 2.48 [95% CI 1.02-6.05], P=0.05). The only other independent predictor being Killip class 2 (1.79 [95% CI, 1.02 - 3.15], P=0.04).

By contrast, recurrent late myocardial infarction was not associated with troponin tertiles on univariate analysis (tertile 1 *versus* tertile 2: relative risk 1·07 [95%CI

(0·64 –1·79)], P=0·79; tertile 1 *versus* tertile 3: relative risk 0·80 [95%CI, (0·46–1·39)], P=0·43), instead being more closely related to traditional predictors of myocardial infarction (Table 4-4).

Table 4-3 Baseline Characteristics of Patients From the GRACE Cohort

	Tertile 1	Tertile 2	Tertile 3	P value
	(n=332)	(n=336)	(n=335)	
Peak Troponin I (range)	≤220	230 – 6130	≥6140	-
Age (years)	65 ± 12	66 ± 12	63 ± 13	0.02
GRACE score	124 ± 47	197 ± 49	218 ± 41	<0.0001
Male sex	212 (63.9%)	226 (67.3%)	254 (75.8%)	0.003
Smoking Habit	214 (64.5%)	243 (72.3%)	235 (70.1%)	0.08
Previous MI	149 (44.9%)	91 (27.1%)	51 (15.2%)	<0.0001
Killip score ≥2	82 (24.7%)	114 (33.9%)	98 (29.3%)	0.03
Previous CABG	61 (18.4%)	25 (7.4%)	12 (3.6%)	<0.0001
Previous heart failure	26 (7.8%)	25 (7.4%)	13 (3.9%)	0.07
Diabetes	53 (16.0%)	47 (14.0%)	47 (14.0%)	0.71
ST deviation	77 (23.2%)	142 (42.3%)	275 (82.1%)	<0.0001
Multi-vessel disease	92 (27.7%)	141 (42.0%)	125 (37.3%)	<0.0001
Recurrent MI ≤30 days	7 (2.1%)	18 (5.4%)	29 (8.7%)	0.001

Table 4-4: Univariate predictors of early (≤30 day) and late (>30 day) recurrent myocardial infarction (MI)

	Early (≤30 day) recurrent MI	P value	Late (>30 day) recurrent MI	P valve
Age (yrs)	1.02 (0.99 – 1.04)	0.14	1.04 (1.02 – 1.06)	<0.0001
Male gender	1.30 (0.70 – 2.43)	0.45	0.89 (0.56 – 1.41)	0.63
Smoker	0.82 (0.46 – 1.46)	0.55	1.04 (0.65 – 1.67)	0.91
Previous MI	0.69 (0.36 – 1.32)	0.28	3.81 (2.43 – 5.95)	<0.0001
Killip score ≥2	1.86 (1.06 – 3.24)	0.03	1.79 (1.14 – 2.82)	0.01
Previous CABG	0.94 (0.37 – 2.42)	0.99	2.91 (1.66 – 5.10)	<0.0001
Previous heart failure	0.86 (0.26 – 2.82)	0.99	2.77 (1.40 – 5.45)	0.008
Diabetes	0.72 (0.30 – 1.71)	0.56	1.41 (0.80 – 2.48)	0.27
ST deviation	1.81 (1.03 – 3.19)	0.05	1.18 (0.76 – 1.82)	0.5
Multi-vessel disease	1.73 (0.99 – 2.99)	0.06	1.57 (1.01 – 2.44)	0.05
Troponin Tertiles				
Tertile 2 *versus* Tertile 1	2.63 (1.08–6.38)	0.03	1.07 (0.64 – 1.79)	0.79
Tertile 3 *versus* Tertile 1	4.40 (1.90–10.19)	0.001	0.80 (0.46 – 1.39)	0.43
Linear trend across tertiles	-	<0.0001	-	0.57

Risk Ratios (95% Confidence Interval), CABG: coronary artery bypass surgery, MI: myocardial infarction.

Figure 4-3: **Kaplan–Meier curves demonstrating survival free from early recurrent myocardial infarction at 30 days**

Patients were divided into tertiles according to their peak plasma troponin I concentrations (tertile 1, ≤ 220; tertile 2, 230-6,130; and tertile 3, ≥6,140 ng/L).

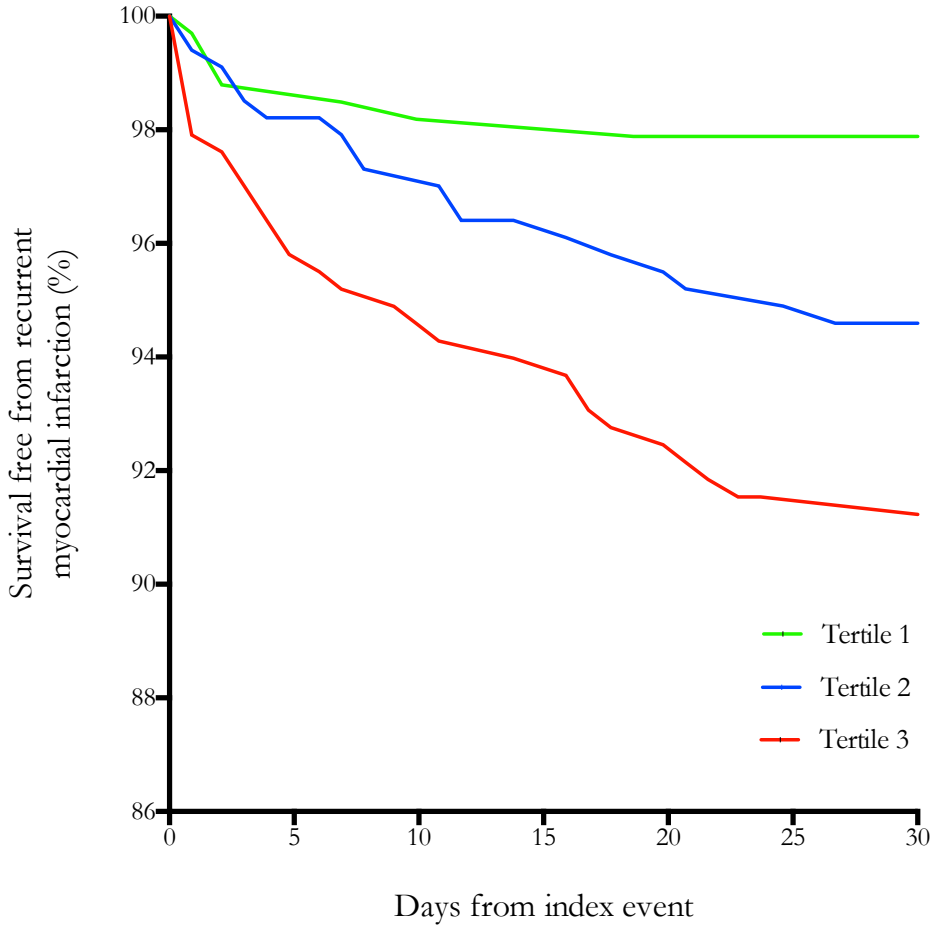

	Days			
	0	**10**	**20**	**30**
Tertile 1	**332**	**326**	**324**	**323**
Tertile 2	**336**	**325**	**317**	**313**
Tertile 3	**335**	**312**	**304**	**298**

4.5. DISCUSSION

Using 18F-FDG PET imaging, we have demonstrated increased metabolic activity in remote aortic atherosclerotic plaques in patients with recent myocardial infarction that correlated with the degree of myocardial necrosis, and exceeded that observed in patients with stable coronary disease who had a greater atherosclerotic burden. Using the GRACE registry, we explored the clinical relevance of these findings to assess whether infarct size and the associated increase in atherosclerotic inflammation could predict recurrent coronary atherothombotic events in every day clinical practice. Intriguingly, patients with the largest infarcts had more than a four-fold increase in the risk of early recurrent myocardial infarction, with baseline tertiles of plasma troponin concentration emerging as an independent predictor of these events. We therefore provide clinical data to support the hypothesis that myocardial infarction exacerbates systemic atherosclerotic inflammation, destabilizes remote atheromatous plaque, and causes an increase in early recurrent atherothrombotic events.

Pre-clinical data have indicated that myocardial infarction induces a macrophage-driven pro-inflammatory state (Ono et al., 1998), that directly increases inflammation in remote atheroma and induces further atherosclerosis (Dutta et al., 2012, Takaoka et al., 2006, Wright et al., 2010).In a mouse model, myocardial infarction induced by coronary artery ligation increased splenic monocyte motility (Dutta et al., 2012), with these cells exiting the spleen *en masse* and migrating both to the injured myocardium and crucially to remote atherosclerotic plaque (Swirski et al., 2009). In addition sympathetic stimulation following infarction increased the production and liberation

of hematopoietic stem and progenitor cells from the bone marrow, resulting in further increases in circulating monocytes and the accumulation of macrophages within regions of remote atheroma. The net result was a marked accumulation of macrophages in remote atherosclerotic plaque following myocardial infarction that resulted in acceleration of the disease process in these areas. The first aim of the current study was to test whether this pro-inflammatory phenomenon also occurs in humans using 18F-FDG as a marker of vascular macrophage inflammatory activity. Because we cannot measure 18F-FDG uptake before and after myocardial infarction, we prospectively compared uptake between patients with stable coronary heart disease and those with recent myocardial infarction. Despite a comparable or lower overall aortic and coronary plaque burden, aortic 18F-FDG uptake was 20% higher in patients who had sustained a recent myocardial infarction. Indeed, the aortic 18F-FDG uptake was consistently increased across all regions of the thoracic aorta. In contrast, para-spinal muscle uptake was similar between the cohorts indicating a specific vascular and atherosclerotic response rather than a generalized non-specific inflammation across all tissues. Based on clinical factors and the peak plasma troponin concentration, patients with ST-segment elevation myocardial infarction had larger infarcts and demonstrated greater increases in aortic 18F-FDG uptake than those with non-ST elevation myocardial infarction. Indeed we observed a good correlation between peak plasma troponin I concentrations and aortic 18F-FDG activity suggesting that the association may be causal.

Next we investigated whether the observed increases in vascular inflammatory activity were of clinical importance in real life practice. Our imaging cohort was not large enough to address this question so we turned to data from the well-established GRACE registry. In more than 1,000 patients, we demonstrated that the size of the initial myocardial infarction emerged as an independent predictor of early recurrent myocardial infarction over and above traditional risk factors, with a four-fold increase in these events amongst those with the biggest infarcts. This would indicate that the increased vascular inflammation associated with myocardial infarction translates into adverse clinical events, perhaps due plaque destabilization and the associated increased risk of rupture. Interestingly our data also suggest that the clinical effects of this systemic inflammatory response are only transitory, with no association between infarct size and later recurrent events after 30 days, by which time the inflammation will have subsided and plaques begun to stabilise once more. Our data are also consistent with those of the smaller (n=378) EValuation Of MCC-135 for Left VEntricular Salvage in Acute Myocardial Infarction (EVOLVE) randomised controlled trial (Chia et al., 2008) that also observed an increased early event rate in patients with the highest tertile of troponin concentration with a trend for an increase in recurrent myocardial infarction. Moreover our findings are supported by recently reported studies (Kim et al., 2014, Han et al., 2014, Wald et al., 2014, Kato et al., 2012b). Patients with acute coronary syndromes have increased plaque vulnerability in non-culprit lesions with increased incidence of thin-capped fibroatheromas and adherent thrombus (Kato et al., 2012b). Furthermore, patients with ST elevation myocardial infarction have accelerated plaque progression in non-culprit lesions, on follow up angiography (Han et al., 2014), whilst stenting of

such lesions at the same time as culprit lesions reduces adverse cardiovascular events (Wald et al., 2014). Moreover, patients with unstable coronary disease have higher metabolic carotid plaque activity as compared to patients with stable disease thereby suggesting a pan-vascular inflammatory process as indicated by our study (Kim et al., 2014).

Figure 4-4: Schematic representation showing remote atherosclerotic inflammation following myocardial infarction

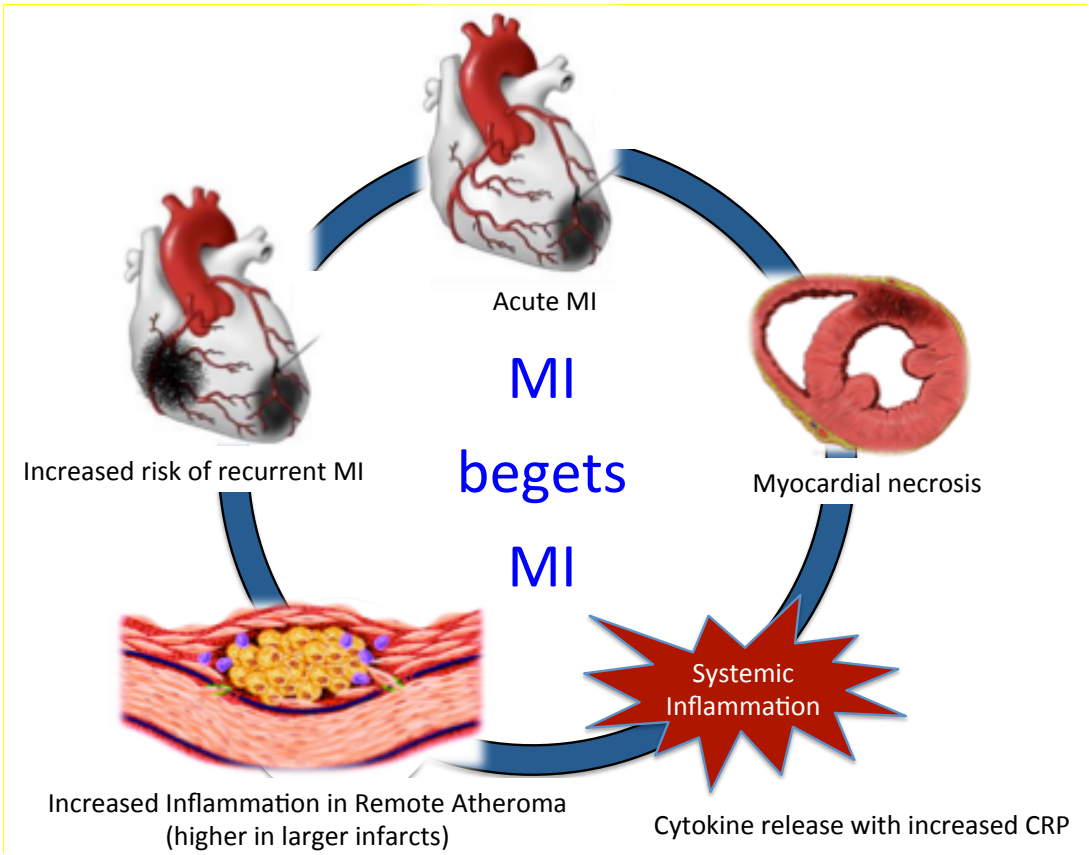

Taken together, our data offer clear support for the hypothesis that myocardial infarction begets early recurrent myocardial infarction due to up regulated macrophage-mediated inflammation in remote atherosclerotic plaque (Figure 4-4). It would also offer an explanation for the increased incidence of ischemic stroke following myocardial infarction and explain why immediate reperfusion for ST-segment elevation myocardial infarction and the resultant limitation in myocardial injury, confers a greater reduction in the risk of recurrent events, than revascularisation after infarct completion (Ioannidis and Katritsis, 2007, Libby, 2013).

Although our data support the hypothesis that myocardial infarction results in remote arterial inflammation, it could also be argued that more widespread and intense atherosclerotic inflammation occurs prior to the precipitation of myocardial infarction and this is the explanation for the association. The correlation between infarct size and the inflammatory signal would support the former explanation, however to resolve this issue, 18F-FDG imaging would be required both before and after myocardial infarction, which given the unpredictable nature of these events is extremely challenging in the clinical context. We also acknowledge that we did not directly measure myocardial infarct size and have used peak plasma troponin concentration as a surrogate measure. However, peak plasma troponin concentration has a strong correlation with infarct size ($r=0.740$, $p<0.001$)(Younger et al., 2007, Chia et al., 2008) and is a valid surrogate marker especially when applied to large datasets such as the registry cohort used here. Finally, we were unable to measure

systemic markers of inflammation such as C-reactive protein in our outcome cohort. However, C-reactive protein is well known to correlate with troponin release after myocardial infarction (Anzai et al., 1997, Orn et al., 2009, Brunetti et al., 2006) and indeed this was observed in our imaging cohort.

In summary we have demonstrated that the presence and extent of myocardial infarction is associated with increased aortic atherosclerotic inflammation and early recurrent myocardial infarction supporting the hypothesis that myocardial infarction begets myocardial infarction in humans.

Chapter 5. DIFFERENTIAL AORTIC INFLAMMATION AND CALCIFICATION IN ABDOMINAL AORTIC ANEURYSMS AND ATHEROSCLEROSIS

Presented by *NIKHIL V JOSHI, *MAYSOON ELKHAWAD, NIKIL K RAJANI, ADAM J MELVILLE, JASON M TARKIN, MOHAMMED CHOWDHURY, EMMA DONOGHUE, ALISON FLETCHER, EDWIN JR VAN BEEK, OLIVIA MCBRIDE, JENNIFER RICHARDS, JONATHAN BOYLE, JOHN BUSCOMBE, TIMOTHY D FRYER, MARC R DWECK, AHMED A TAWAKOL, JONATHAN H GILLARD, IAN B WILKINSON, DAVID E NEWBY, JAMES HF RUDD. Inflammation and calcification are greater in abdominal aortic aneurysm disease than atherosclerosis - a prospective 18F-FDG PET-CT study. **(Manuscript in preparation).**

5.1. SUMMARY

The vascular biology of both abdominal aortic aneurysms (AAAs) and atherosclerosis remains incompletely understood. We aimed to investigate the role of inflammation and calcification in AAAs, and to test the hypothesis that these processes contribute differently in AAAs compared to atherosclerosis.

In 63 patients (mean age 76.12±6.75 years; 89% male) with asymptomatic aneurysms (mean size 4.33±0.73 cm) and 19 age- and sex-matched patients with atherosclerosis, we measured inflammation and calcification using 18F-fluorodeoxyglucose (18F-FDG) positron emission tomography and computed tomography (PET-CT). Inflammation and calcification were quantified using 18F-FDG tissue-to-background ratios (TBR) and Agatston scores respectively.

18F-FDG uptake was higher within aneurysms than in non-aneurysmal aorta (mean TBR_{max} 2.23±0.46 *vs.* 2.12±0.46, p=0.02). Compared to controls with atherosclerosis only, both aneurysmal and non-aneurysmal aorta in patients with AAA showed higher 18F-FDG uptake (total aorta mean TBR_{max} 2.16±0.51 *vs.* 1.70±0.22, p=0.001; abdominal aortic mean TBR_{max} 2.23±0.45 *vs.* 1.68±0.21, p<0.0001). There was no correlation between aneurysm size and 18F-FDG uptake (Pearson's r=0.12, p=0.36), although smaller aneurysms (≤4.33 cm, n=32) trended to higher 18F-FDG uptake than larger ones (≥4.34 cm, n=30), mean TBR_{max} 2.36±0.45 *vs.* 2.14±0.45, p=0.065). Patients without aneurysmal thrombus has higher tracer activity within the

aneurysmal wall compared to those with thrombus (mean TBR_{max} aneurysm wall 2.43±0.45 *versus* 2.14±0.43, p=0.018) with the thrombus itself demonstrating very low levels of uptake (mean TBR_{max} within thrombus 1.30±0.48 *vs.* aneurysm wall 2.23±0.46, p<0.0001). Calcification in the aneurysmal segment of the aorta was higher than in non-aneurysmal segments in patients with AAA (Agatston 4918 [2901-8008] *vs.* 1017 [139-2226], p<0.0001) and equivalent regions in patients with atherosclerosis (442 [304-920] *vs.* 166 [80-374] Agatston units per cm, p=0.0042).

This prospective imaging study has demonstrated enhanced active inflammation and calcification within the wall of aortic aneurysms suggesting an intense, destructive and transmural pathological process. As compared to atherosclerotic controls, patients with AAA have inflammation involving the entire aorta, supporting a hypothesis of global aortopathy in these subjects.

5.2. INTRODUCTION

Abdominal aortic aneurysm (AAA) is a vascular disorder resulting in localized aortic dilatation (diameter >3cm)(Shimizu et al., 2006). Aneurysms have a prevalence of around 5% in adults aged 65-74 years and are frequently asymptomatic until rupture (Scott, 2002). If rupture occurs, death results in 60-90% of patients(Scott, 2002). National ultrasound screening programs for high-risk patients have significantly reduced deaths from rupture by identifying asymptomatic subjects with large aneurysms for elective repair (Scott, 2002, Lederle et al., 2002, UKSAT, 1998) However, screening also identifies many patients with small aneurysms, below the threshold for intervention, and in this group the rate of future expansion and risk of rupture are difficult to predict.

The treatment of AAA is either open or endovascular repair to prevent aneurysm rupture, recommended when the diameter exceeds 5.5cm (Powell et al., 2007). There are no medical treatments with proven prognostic benefit for AAA (Golledge et al., 2006b, Norman et al., 2004), and therefore continued surveillance is the only option for those who do not fulfil criteria for AAA repair. Repeat ultrasound frequency is currently determined by baseline aneurysm size. The rate of AAA rupture is around 1% per year in smaller aneurysms (3.0-5.5cm), although they still account for about a fifth of all ruptures. Some aneurysms can exceed 5.5cm without rupture, suggesting aneurysm size is not the only determinant of rupture (Darling et al., 1977, Powell et al., 2008). To improve risk stratification in patients with AAA, a better

understanding of the pathology leading to AAA growth and rupture is needed (Golestani and Sadeghi, 2014).

Pathologically, aneurysms are associated with inflammatory infiltration of the aortic wall, smooth muscle cell apoptosis and matrix degradation (Nordon et al., 2011). These changes lead to weakening of the wall, allowing expansion and rupture to occur. Although aneurysms are most common in the abdominal aorta, it has been suggested that the entire arterial system is abnormal in susceptible subjects (Ward, 1992), with dilatation of the carotid arteries being a common finding in these patients (Makita et al., 2000, Vorp et al., 2001).

18-fluorine-labelled 2-deoxy-2-fluoro-D-glucose (18F-FDG) positron emission tomography - computed tomography (PET-CT) is commonly used to image metabolically active cells in patients with cancer as a means of diagnosis and risk-stratification. This technique has been adapted to measure vascular metabolic activity and provides a reproducible, non-invasive measure of arterial inflammation (Tawakol et al., 2006, Rudd et al., 2002), reflecting glucose uptake by macrophages and other plaque cells. Consequently, 18F-FDG PET has been demonstrated to predict future cardiovascular events in several studies and can be used to test the efficacy of anti-inflammatory drugs (Tahara et al., 2006a, Fayad et al., 2011b, Tawakol et al., 2013, Kotze et al., 2009).

This study set out to determine the extent of inflammation and calcification in these two diseases. We hypothesized that both aortic inflammation and calcification would be greater in aneurysm subjects than in matched controls with atherosclerosis. We also sought to investigate the relationship between baseline aneurysm size, calcification and inflammation in the wall and within aneurysmal thrombus.

5.3. METHODS

5.3.1. SUBJECTS

Patients were recruited from the Royal Infirmary of Edinburgh and Addenbrooke's Hospital, Cambridge and in two cohorts: (i) patients with asymptomatic abdominal aortic aneurysm and (ii) age- and sex- matched control patients with atherosclerosis but no aortic aneurysm disease. Control subjects were originally recruited and imaged as part of a drug trial (Elkhawad et al., 2012, Maki-Petaja et al., 2012); only their baseline PET data was used in this study. All control subjects were recruited in Cambridge, whereas study patients were recruited across both sites. Consecutive patients presenting at both institutions were considered for enrolment. The inclusion criteria for the study cohort were age >50 years and presence of an aneurysm between 3.0 and 5.5cm on ultrasound. The inclusion criteria for the control cohort were clinically stable (>6 months) cardiovascular disease (defined as previous myocardial infarction, stroke, or peripheral vascular disease). Exclusion criteria for both cohorts were type 1 diabetes, type 2 diabetes with a fasting glucose of >11mmol/L, renal impairment (serum creatinine >250 μmol/L), known contrast allergy or the inability to provide informed consent. The study was performed in accordance to the protocol approved by the local research ethics committee and the Declaration of Helsinki. All subjects provided written informed consent.

5.3.2. POSITRON EMISSION TOMOGRAPHY AND COMPUTED TOMOGRAPHY IMAGING

All patients underwent 18F-FDG PET-CT imaging of the entire aorta. In addition, patients in the study group underwent contrast-enhanced CT imaging of the abdominal aorta. We used validated, reproducible, previously published PET imaging protocols (Elkhawad et al., 2012, Maki-Petaja et al., 2012).

Patient preparation

Patients were asked to fast for 6 hours prior to PET imaging.

Image Acquisition and reconstruction

In Cambridge, a GE Discovery 690 PET-CT scanner was used. In Edinburgh, an equivalent Siemens machine was used (Biograph mCT, Siemens Medical Systems, Erlangen, Germany). A target dose of 240MBq 18F-FDG was injected intravenously after which patients rested in a quiet environment for 90 min before being transferred to the scanner. A non-contrast-enhanced attenuation correction CT scan (40mAs per rotation [CareDose], 100 kV) was then performed followed by PET scan covering three bed positions from the arch of aorta to the aortic bifurcation over 30 min (10 min per bed position). Tracer circulation times were based on previous studies using 18F-FDG in atherosclerosis (Rudd et al., 2002, Dweck et al., 2012a, Dweck et al., 2011) and aimed to produce optimal contrast between the aortic wall and the blood pool. With the patient in the same position, a CT aortogram from the diaphragm to the aortic bifurcation was performed using 75-100mL of iodinated contrast (400mgI/mL; Iomeron, Bracco, Milan, Italy), followed by 50mL of 0.9% saline flush. The PET data were reconstructed using standard time of flight reconstruction

algorithms. Corrections were applied for attenuation, dead time, scatter and random coincidences.

5.3.3. IMAGE ANALYSIS

PET-CT

Anonymized PET-CT datasets were analysed using the OsiriX workstation (64 bit; version 5.5.1 OsiriX Imaging Software, Geneva, Switzerland) (Joshi et al., 2013, Maki-Petaja et al., 2012). Readers were blinded to the patients' clinical status (study group or control). PET images were fused with corresponding CT datasets, and regions of interest (ROIs) drawn on serial axial slices. Within these regions, mean and maximum tracer activities were measured using standard uptake values (SUV; the decay corrected tissue concentration of the tracer divided by the injected dose per body weight) and corrected for blood pool activity in the superior vena cava to provide tissue-to-background ratios (TBRs) (Joshi et al., 2013, Maki-Petaja et al., 2012). The average of the maximum TBR values within each slice was expressed as the mean TBR_{max}.

The aorta was divided into 5 distinct segments for further comparisons: ascending aorta, descending thoracic aorta, abdominal non-aneurysmal aorta, aneurysm shoulder and aneurysm sac. The ascending aorta was defined as the segment of the aorta from the lower level of the right pulmonary artery up to the last slice where the aorta maintained its circular cross-sectional appearance. The descending thoracic aorta was defined as the region extending down from the circular slice below the arch of aorta to the slice where the diaphragm was first visible. The non-aneurysmal abdominal aorta was defined as the region between the descending aorta and the start

of the aneurysm. The aortic aneurysm was defined as the region of abdominal aorta with all slices having a diameter of at least 3cm. The aneurysm shoulder was defined as that segment of aorta bordering the first slice of aneurysmal aorta (2 slices above and below the first 3 cm diameter slice). The aneurysm sac comprised the region between the aneurysm shoulder and the inferior aspect of the aneurysm.

Thrombus within the aneurysm was identified on the contrast CT aortogram using previously published Hounsfield unit definitions (Golledge et al., 2008) and sequential ROIs were drawn, avoiding over-spill both from the lumen and aneurysm wall.

CT Calcium Scoring

Calcium scoring was performed using a cardiovascular workstation (Vital Images, Minnetonka, Minnesota, USA). Total Agatston scores were recorded for the entire aorta, using a threshold of 130 Hounsfield units for calcium, on the non-contrast attenuation CT scan (Santos et al., 2010). In addition, arterial calcium scores corrected for length of artery evaluated (in Agatston units per centimeter) (Criqui et al., 2014) were generated to allow comparison of aneurysmal segments in the study group and equivalent length segments of non-aneurysmal aorta in control subjects.

5.3.4. REPRODUCIBILITY STUDIES

PET-CT data from 10 patients were selected at random to test the reproducibility of the 18F-FDG PET analyses. Two trained readers analysed the scans independently to provide a measure of the inter-observer bias and variation for 18F-FDG uptake in each region of the aorta.

5.3.5. STATISTICAL ANALYSIS

Statistical analysis was performed with Graph Pad Prism version 6 (GraphPad Software Inc., California USA) or SPSS 19.0 (SPSS Inc., Chicago, Illinois) where appropriate. Continuous data were checked for normality using the D'Agostino-Pearson omnibus test. Parametric variables were expressed as mean ± standard deviation and compared using Student's t-tests or repeat measure one-way ANOVA with Tukey's multiple comparison test when appropriate. Non-parametric data were presented as median [interquartile range] and compared with Mann-Whitney test, Wilcox matched-pairs signed rank, or Friedman test as appropriate. Inter-observer reproducibility was estimated using the Bland Altman method and presented as mean bias ± 2 standard deviation, and intra-class correlation coefficients with 95% confidence intervals were also calculated. A two-sided $P<0.05$ was taken as statistically significant.

5.4. RESULTS

Sixty-three patients with abdominal aortic aneurysms and 19 age-and sex matched subjects with atherosclerosis were recruited (Table 5-1). In one patient, PET-CT data were acquired only for the abdominal aorta and was excluded from final analysis. The mean age was 76.1±6.8 years, and 89% of the study group was male. The mean baseline AAA size was 4.33±0.73cm.

Table 5-1: Baseline characteristics of patients with AAA

	Total (n=63)	Cambridge (n=33)	Edinburgh (n=30)
Average Age (years)	76.1±6.8	77.6±7.2	74.5±5.9
Male sex	56 (89%)	31 (94%)	25 (83%)
BMI (kg/m^2)	25.7±3.4	26.2±2.5	25.2±4.1
Systolic blood pressure (mmHg)	137±19	137±20	138±18
Diastolic Blood Pressure (mmHg)	79±12	80±12	76±12
Average Size of AAA Baseline	4.33±0.72	4.07±0.65	4.62±0.70
Risk Factors			
Current Smoker	14 (22.2%)	3 (9.1%)	11 (36.7%)
Ex-Smoker	33 (52.3%)	16 (48.4%)	17 (56.7%)
Hypertension	26 (41.6%)	9 (27.3%)	17 (56.7%)
Past Medical History			
Diabetes Mellitus	5 (7.9%)	3 (9.1%)	2 (6.7%)
Previous Myocardial Infarction	14 (22.2%)	6 (18.2%)	8 (26.7%)
Stroke	8 (12.7%)	2 (6.1%)	6 (20%)
Peripheral Vascular Disease	9 (14.3%)	6 (18.2%)	3 (10%)
Medications Prior to Admission			
Aspirin	48 (76.2%)	25 (75.8%)	23 (76.7%)
Statin	53 (84.1%)	28 (84.8%)	25 (83.3%)
β-Blocker	21 (33.3%)	11 (33.3%)	10 (33.3%)
ACEI/ARB	30 (47.62%)	14 (42.4%)	16 (53.3%)
Thiazide Diuretic	6 (9.5%)	3 (9.1%)	3 (10%)

5.4.1. INFLAMMATION IN ABDOMINAL AORTIC ANEURYSM

Average 18F-FDG accumulation was higher within aortic aneurysms than non-aneurysmal aortae (mean TBR_{max} 2.23±0.46 *vs.* 2.12±0.46, p=0.024, Figures 5-1 and 5-2 and Table 5-2). Exploring further, 18F-FDG uptake was consistently higher in both the sac and shoulder regions of the aneurysm than any non-aneurysmal segment of the aorta (p=0.0004, Table 5-2). Within the aneurysm itself, there were no significant differences in 18F-FDG uptake between the sac and the shoulder (p=0.89).

Comparison between aneurysm and control groups

The two groups were well matched for age and sex. Most subjects were taking statins. Compared to age- and sex-matched patients with atherosclerosis (n=19, mean age 69.4±5.8 years, 89.5% males), patients with AAA (n=19, mean AAA diameter 4.3±0.7cm) had higher aortic 18F-FDG uptake (mean TBR_{max} 2.16±0.51 *vs.* 1.70±0.22, p=0.001). This higher FDG uptake was not confined to the aneurysm, but noted in all non-aneurysmal aortic segments (Table 5-2).

Association between 18F-FDG uptake and clinical parameters in aneurysms

There was no correlation between aneurysm size and 18F-FDG uptake within it (r=0.12, p=0.36). However, when divided into two groups by size, the 32 smaller aneurysms (below the mean cohort size of 4.33cm) trended towards 18F-FDG

accumulation than the 30 larger aneurysms above the mean cohort size (mean TBR_{max} 2.36±0.45 *vs.* 2.14±0.45, p=0.065).

18F-FDG uptake within aneurysm thrombus

Aneurysmal thrombus was present in 43 of the 63 aneurysm patients. Patients without aneurysmal thrombus has higher 18F-FDG uptake within the aneurysmal wall as compared to those with thrombus (mean TBR_{max} aneurysm 2.43±0.45 *versus* 2.14±0.43, p=0.018). 18F-FDG uptake within the thrombus itself was consistently lower than in any region of the aortic wall in these subjects (mean TBR_{max} within thrombus 1.30±0.48 *vs.* aneurysm wall 2.23±0.46, p<0.0001).

Table 5-2 Inflammation and calcification in aortic aneurysm

Inflammation (mean TBRmax) and calcification (Agatston score) data for all aneurysm subjects.

Table 5-2a compares aneurysmal and non-aneurysmal aortic regions.

	Aneurysmal aorta	Non-aneurysmal aorta	p value
Mean TBR_{max}	2.23±0.46	2.12±0.46	0.024
Agatston score (median [IQR])	4918 [2901-8008]	1017 [139-2226]	<0.0001

Table 5-2b displays the values for each individual region of the aorta.

	Shoulder	Sac	Ascending	Descending	Abdominal	p value
Mean TBR_{max}	2.26±0.46	2.25±0.46	2.12±0.41	2.15±0.38	2.13±0.38	0.0004
Agatston score	342 [109-727]	4436 [2554-7441]	50 [0-674]	549 [118-1606]	1575 [717-3275]	<0.0001

Figure 5-1: Aneurysmal 18F-FDG uptake.

Coronal and transaxial fused PET and contrast CT images demonstrating focal 18F-FDG uptake within the aneurysmal wall (white arrowheads). Note also the calcified lateral aspect of the aneurysm.

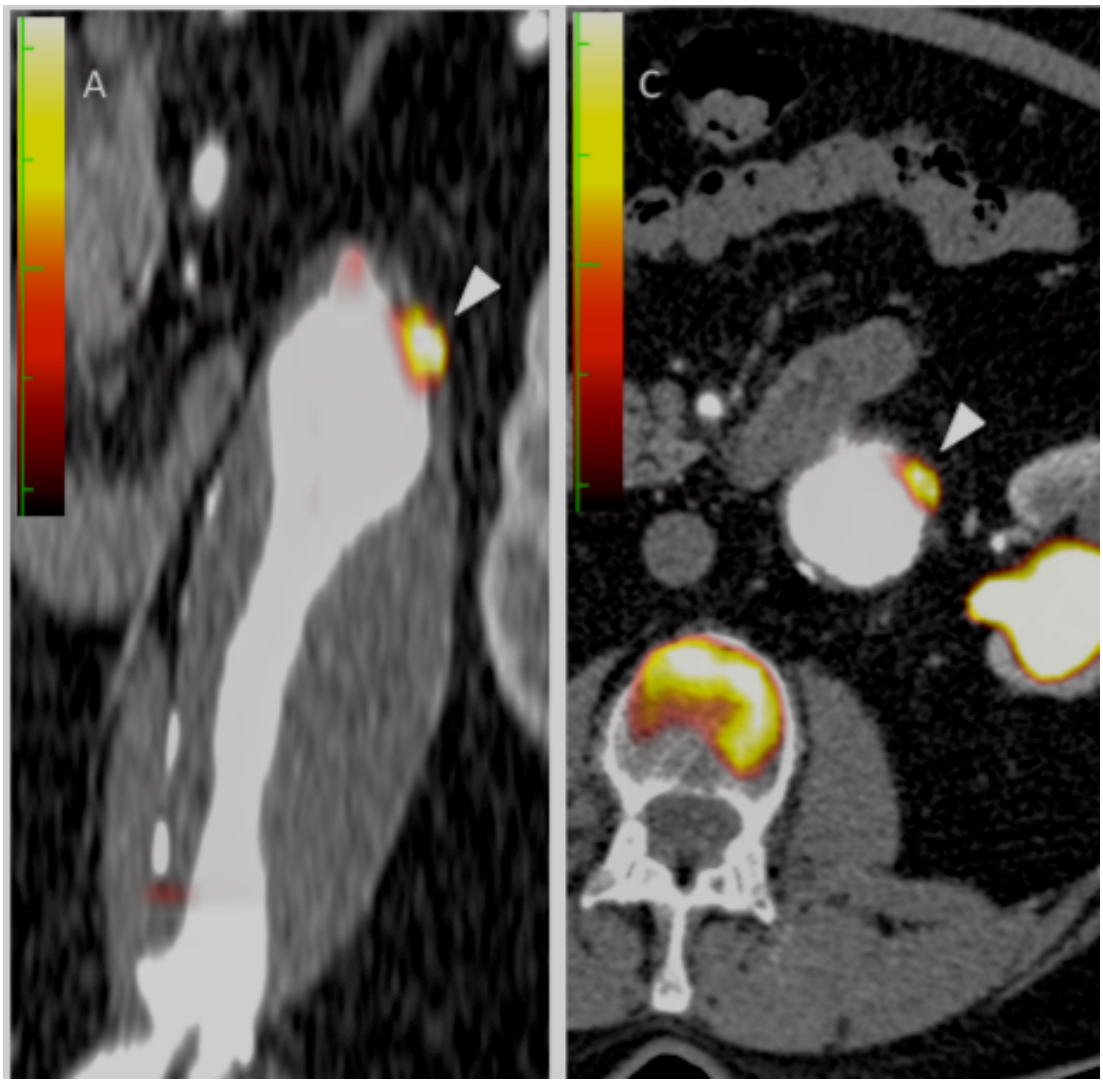

5.4.2. CALCIFICATION IN ABDOMINAL AORTIC ANEURYSM

In the aneurysm group, calcification was greater within the aneurysmal aortic wall than in the non-aneurysmal segments of aorta (4918 Agatston units [2901-8008] *vs.* 1017 [139-2226], p<0.0001). This calcification was highest within the aneurysm sac compared to the other aortic regions (p<0.0001, Table 5-2b). Consistent with these findings, aortic aneurysms were more calcified than the corresponding regions of abdominal aorta in atherosclerotic controls (442 Agatston units per cm [304-920] *vs.* 166 [80-374], p=0.0042). Of note, no differences in calcification were detected between aneurysm subjects and controls in any other aortic region. No significant relationships were observed between aneurysm diameter and extent of calcification (r=0.08, p=0.53). No differences were observed in the calcification in patients without or with intraluminal thrombus within the aneurysm (5310 [2748-9165] *versus* 4903 [2952-7856], p=0.574).

Relationship between inflammation and calcification in AAA and atherosclerosis

There was no relationship between inflammation and calcification within aneurysms (r=-0.153, p=0.235). Similarly, in the control group, there was no correlation between aortic inflammation and calcification (total aorta: r=-0.19, p=0.45; abdominal aorta: r=-0.13, p=0.6).

Figure 5-2: 18F-FDG uptake in AAA

Coronal contrast CT, 18F-FDG PET and fused images of a subject with a large (4.5cm) aneurysm demonstrating focal 18F-FDG uptake within the aneurysmal wall (golden color on PET images). Note also the presence of intra-luminal thrombus and calcification.

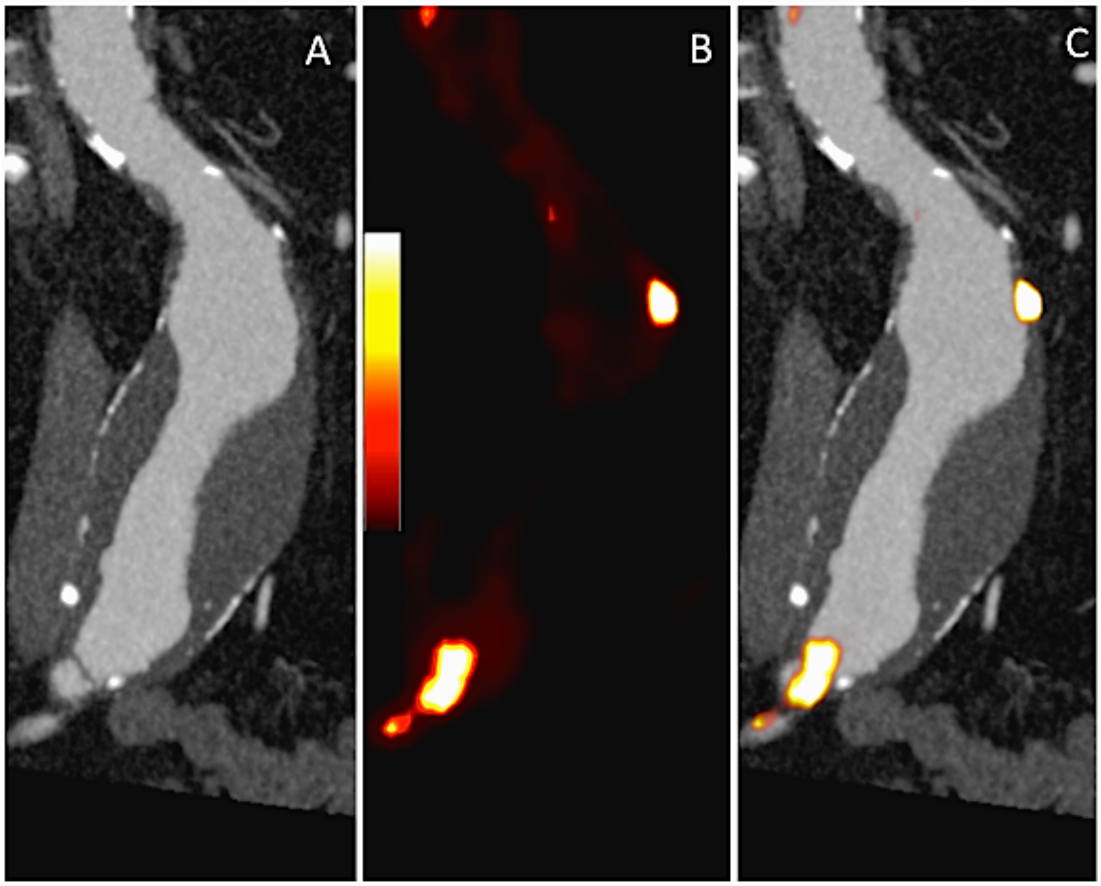

5.4.3. REPRODUCIBILITY OF 18F-FDG MEASUREMENTS

The inter-observer reproducibility for 18F-FDG measurements was excellent across all regions of the aorta, including aneurysmal regions, and consistent with previous studies in atherosclerosis. Across the aorta as a whole, the limits of agreement for mean TBR_{max} were 0.04±0.07. All intra-class correlation values were >0.90, with the shoulder and sac of the aneurysm having the lowest ICC values at 0.91 and 0.96, respectively.

5.5. DISCUSSION

18F-FDG PET imaging of aortic aneurysm was first reported in 2002 (Sakalihasan et al., 2002). This present work is the largest series to measure both 18F-FDG uptake and calcification, and to compare these with well-characterised controls with atherosclerosis.

We have presented evidence that subjects with asymptomatic aortic aneurysms have excessive inflammation within the aneurysmal segment of the aorta. In comparison to matched controls with atherosclerosis, the entire aorta in those with abdominal aortic aneurysm appears more highly inflamed. This suggests the presence of a global aortopathy rather than a disease confined only to the abdominal region of the aorta. We also noted that the intra-luminal thrombus, frequently seen in conjunction with aneurysms, was metabolically inert with low 18F-FDG uptake in most of our cases.

There was no linear relationship between baseline aneurysm size and 18F-FDG uptake, but, consistent with a previous report (Kotze et al., 2011a), small aneurysms appeared more 18F-FDG-avid than larger examples. This might be explained in a scenario where intense early inflammation causes mechanical weakening of the aortic wall, allowing expansion to occur. Inflammation then reduces as the wall becomes more calcified.

In terms of calcification, as with inflammation, this appeared greatest within the aortic aneurysm itself in the study group. Compared with atherosclerotic controls, calcification was more prevalent in the aneurysms than in control abdominal aortas. But, in contrast to the pattern of inflammation described above, aneurysm patients did not exhibit more calcification than controls in other regions of their aortae.

Aortic aneurysms frequently occur in patients with atherosclerosis. The two disease processes share several common risk factors, notably cigarette smoking (Brady et al., 2004). The underlying pathologies of the two conditions overlap to an extent, with inflammation and calcification being common to both. Nevertheless, there are important differences. While aneurysms are characterised by weakening of the media of the aorta by chronic inflammation and degradation of the extracellular matrix (Hellenthal et al., 2009), in atherosclerosis the main insult is to the intima of the artery, at least initially. In atherosclerosis, a fibrous cap is typical over the necrotic core of the lesion, whereas in aneurysm, there is very often a large adherent thrombus, variously described as protective against expansion in some studies (Thubrikar et al., 2003) and encouraging destabilization in others (Hinnen et al., 2005, Fontaine et al., 2002b). Our results lend more support to the former hypothesis, thrombus being metabolically inactive with respect to glucose usage. The role of calcification is also debated in both conditions (Buijs et al., 2013). In atherosclerosis, macro-calcification is thought to be a healing response conferring plaque stability (Joshi et al., 2013, Aikawa et al., 2007, New et al., 2013b), but micro-calcification appears to be associated with a risk of plaque rupture (Libby and Aikawa, 2002). On

a patient level, a non-zero calcium score, derived from CT imaging of the coronary arteries, is strongly associated with future vascular events and overall mortality (Budoff et al., 2013). In aneurysms, the role of calcification is less understood than in atherosclerosis with fewer large prospective studies. One recent paper (Buijs et al., 2013) showed that more calcium was present within the walls of aneurysms that had ruptured compared to those repaired electively, although numbers in both groups were small with several confounding factors. In another publication (Lindholt, 2008) the authors reported the opposite, namely that calcification within the aneurysm (this time measured by ultrasound) was protective and associated with slower annual mean growth rates (1.72mm *vs.* 2.97mm, p=0.001).

Our study group consisted of patients with aneurysms below the size limit for surgery, and therefore tissue harvesting for testing of the relationship between 18F-FDG uptake and inflammation was not possible. Nevertheless, the degree of 18F-FDG uptake in the aortic wall, measured by PET, has correlated strongly with histologically-proven inflammation in tissue removed during aneurysm repair surgery in several prior studies (Reeps et al., 2008, Courtois et al., 2013, Sakalihasan et al., 2002, Truijers et al., 2008). We therefore believe that our 18F-FDG data are at least partly reflective of underlying inflammation. It may be that imaging agents more specific for inflammation, such as 68Ga-DOTATATE PET, 11C-PK11195 PET or USPIO-MRI might provide differing insights into the pathology of the disease.

No partial volume correction methods were applied to the PET data presented here, which might have affected quantification of the 18F-FDG signal. However, a recent publication by Reeps and colleagues addressed this question, concluding that such corrections were not needed when imaging vascular structures as relatively large as aortic aneurysms (Reeps et al., 2013).

In terms of whether 18F-FDG uptake predicts future aneurysm behavior, published work presents a mixed picture. There is evidence to suggest that 18F-FDG can discriminate between asymptomatic and symptomatic aneurysms, but its potential as a marker of aneurysm expansion and rupture has yet to be established (Reeps et al., 2008, Truijers et al., 2008, Reeps et al., 2013, Nchimi et al., 2010, Kotze et al., 2011a, Sakalihasan et al., 2004). There also appear to be positive correlations between 18F-FDG uptake and the degree of mechanical wall stress within an aneurysm (Xu et al., 2010). Considerably more work is needed to determine whether data derived from advanced imaging, such as inflammation and calcification, can improve clinical decision-making and our understanding of this common, deadly condition.

Chapter 6. POSITRON EMISSION TOMOGRAPHY AND MAGNETIC RESONANCE IMAGING OF CELLULAR INFLAMMATION IN PATIENTS WITH ABDOMINAL AORTIC ANEURYSMS

Published by *MCBRIDE, O. M., *JOSHI, N. V.*, ROBSON, J. M., MACGILLIVRAY, T. J., GRAY, C. D., FLETCHER, A. M., DWECK, M. R., VAN BEEK, E. J., RUDD, J. H., NEWBY, D. E. & SEMPLE, S. I. 2016. Positron Emission Tomography and Magnetic Resonance Imaging of Cellular Inflammation in Patients with Abdominal Aortic Aneurysms. *Eur J Vasc Endovasc Surg,* 51**,** 518-26.

6.1. SUMMARY

Inflammation is critical in the pathogenesis of abdominal aortic aneurysm (AAA). Combined positron emission tomography and computed tomography (PET-CT) with 18F-flurodeoxyglucose (18F-FDG) and ultrasmall superparamagnetic particles of iron oxide (USPIO)-enhanced magnetic resonance imaging (MRI) are non-invasive methods of assessing tissue inflammation. The aim of this study was to compare 18F-FDG PET-CT with USPIO-enhanced MRI in patients with AAA.

Fifteen patients with asymptomatic AAA with diameter 46±7 mm underwent PET-CT with 18F-FDG and T2*-weighted MRI before and 24 h after administration of USPIO. The PET-CT and MRI data were co-registered. Standardized uptake values (SUV) were calculated to measure 18F-FDG uptake, and USPIO uptake was determined using change in R2*. Comparisons between the techniques were made using a quadrant analysis and on a voxel-by-voxel evaluation.

Maximum SUV was lower in patients with mural USPIO uptake. When all areas of the aneurysm were evaluated, there was a modest correlation between the SUV on PET-CT and the change in R2* on USPIO-enhanced MRI (n=70,345 voxels; r=0.30; $p<0.0001$). Co-localization of 18F-FDG and USPIO uptake was poor (kappa statistic 0.074; 95% CI, 0.026 - 0.122).

Both 18F-FDG PET-CT and USPIO-MRI uptake identify vascular inflammation associated with AAA. Whilst they demonstrate a weak correlation, there are distinct differences in the pattern and distribution of uptake suggesting a differential detection of macrophage glycolytic and phagocytic activity respectively.

6.2. INTRODUCTION

Recent advances in imaging modalities have generated considerable interest in novel molecular and cellular techniques. In contrast to anatomical and structural approaches, molecular and cellular imaging targets the activity of specific biochemical and cellular processes to provide insight into the etiology, biology and pathogenesis of diseased states. Moreover, this has the potential to refine the diagnosis and risk-stratification of cardiovascular disease as well as to assess responses to specific therapeutic interventions (Jaffer et al., 2009, Jaffer et al., 2007, Choudhury and Fisher, 2009, Tawakol et al., 2006, Rudd et al., 2002, Tahara et al., 2006b).

18F-Fluorodeoxyglucose (18F-FDG) is used extensively to image metabolically active cells with positron emission tomography (PET) combined with computed tomography (CT). It accumulates in cells and tissues with increased metabolic activity, and in vascular tissue, 18F-FDG uptake correlates with the degree of inflammation (Lardinois et al., 2003). Indeed, 18F-FDG uptake correlates with acute plaque events and cardiovascular risk factors, and has being used as a biomarker to demonstrate the anti-inflammatory effects of statins (Tawakol et al., 2006, Rudd et al., 2002, Tahara et al., 2006b, Fayad et al., 2011a). 18F-FDG also accumulates in the wall of abdominal aortic aneurysms (AAA) and appears to identify active aortic inflammation. However, its potential use as a marker of aneurysm expansion, progression and rupture has yet to be established.

Magnetic resonance imaging (MRI) with ultrasmall superparamagnetic particles of iron oxide (USPIOs) is an alternative approach for detecting cellular inflammation. (Ruehm et al., 2001) (Alam et al., 2012, Richards et al., 2012). Due to their small particle size (diameter 10-30 nm), USPIOs escape immediate recognition by the reticulo-endothelial system, persist in the bloodstream and accumulate at sites of vascular inflammation. Here they are phagocytosed by tissue-resident macrophages within which they accumulate and are detectable on T2- and T2*-weighted MRI sequences. Within atheromatous plaques, USPIO uptake correlates with macrophage density, distinguishes stable from unstable carotid plaques, and is reduced following high-dose atorvastatin therapy (Trivedi et al., 2006a, Tang et al., 2009b, Morishige et al., 2010). We have previously demonstrated USPIO uptake in the wall of AAAs where it co-localizes with macrophages and is associated with a three-fold higher AAA growth rate (Richards et al., 2012).

Given that both 18F-FDG PET and USPIO-enhanced MRI have been used to assess vascular inflammation in patients with AAA, the aim of this study was to compare 18F-FDG PET and USPIO-enhanced MRI in patients with AAAs. Specifically, we assessed the spatial distribution and intensity of the inflammatory process using both techniques to determine whether they provide unique or common insights into the pathogenesis and disease progression of AAAs.

6.3. METHODS

6.3.1. SUBJECTS

Patients with asymptomatic AAA (diameter 30-55 mm on duplex ultrasound examination) were recruited from the outpatient aneurysm surveillance clinic at the Royal Infirmary of Edinburgh. Exclusion criteria were age <50 years, active systemic inflammatory or malignant disease, insulin-dependent diabetes mellitus, renal dysfunction (estimated glomerular filtration rate <30 mL/min), hepatic cirrhosis (Child Pugh score B or C), planned AAA surgery within 6 months of screening and a contra-indication to MRI. Studies were performed with the approval of the local research ethics committee, in accordance with the Declaration of Helsinki, and with the written informed consent of each participant. All patients underwent a comprehensive baseline clinical assessment including evaluation of their cardiovascular risk factor profile and recording of an abdominal ultrasound scan.

6.3.2. POSITRON EMISSION TOMOGRAPHY AND COMPUTED TOMOGRAPHY AORTOGRAM

PET-CT scans were performed followed by a CT aortogram (CTA) using a hybrid scanner (Biograph mCT, Siemens Medical Systems, Erlangen, Germany). Patients were asked to fast for 6 h prior to the scan. A target dose of 240 MBq 18F-FDG was injected intravenously after which patients rested in a quiet environment for 90 min before scanning. An attenuation correction CT scan (non-enhanced, 40 mAs per rotation [CareDose], 100 kV) was then performed followed by a PET scan covering three bed positions from the arch of aorta to the aortic bifurcation over 30 min. Tracer circulation times were based on previous studies using 18F-FDG in atherosclerosis (Dweck et al., 2012a, Dweck et al., 2011, Rudd et al., 2002, Tawakol et al., 2013) and aimed to allow for optimal contrast between the aortic wall and the blood pool. With the patient lying in the same position, a CT aortogram from the diaphragm to the aortic bifurcation was performed using 75 mL of iodine contrast, followed by 50 mL of 0.9% saline flush. The PET data were reconstructed using the Siemens Ultra-HD (time of flight +True X) reconstruction algorithm. Corrections were applied for attenuation, dead time, scatter and random coincidences. Image acquisition and reconstructions for CTA were undertaken as per pre-specified protocol (voltage 120kV, ref mAs 145, slice thicknesses 1 and 3 mm, field of view 300 x 400 mm).

6.3.3. USPIO ENHANCED MAGNETIC RESONANCE IMAGING

Participants underwent MRI in a whole body 3T scanner (Magnetom Verio, Siemens, Erlangen, Germany) before and 24-36 h after intravenous administration of the USPIO contrast agent (ferumoxytol; Feraheme, Advanced Magnetics Inc., Cambridge, MA, USA; dose 4 mg/kg at a rate of 1 mL/s). Routine clinical coronal and sagittal breath-held T2-weighted multi-slice HASTE localizer sequences were used to identify the position and extent of the aneurysm following which a respiratory-gated, electrocardiographically-triggered T2 weighted (T2W) turbo-spin echo sequence was used to acquire detailed anatomical data (TR/TE 2R-R intervals/72 ms; flip angle 180°; matrix 192 × 256; field of view 400 × 400 mm; slice width 5 mm). A multi-echo, gradient-echo T2*W sequence (TE 4.9, 7.7, 10.5, 13.3 ms; TR 133 ms; flip angle 15°; matrix 192 × 256; field of view 400 × 400 mm; slice width 5 mm) was used to acquire axial images of the entire aneurysm with slice positions corresponding to those of the T2W images. When performing the post-contrast scans, axial acquisitions were positioned to match those of the pre-contrast scan by reference to the vertebral bodies (Richards et al., 2012, Richards et al., 2011c).

6.3.4. IMAGE ANALYSIS

Registration of PET and MRI images

The accuracy of PET-CT to CTA registration was confirmed by visual assessment and minor intra-scan patient movement was corrected using a semi-automatic rigid 3D voxel registration protocol (Analyze 11.0, Mayo Clinic).

Registration of the MRI data allowed both the excellent anatomical detail on the T2W images and the high sensitivity of T2*W images for iron to be utilized. All the images were registered to the pre-contrast T2W image using the same semi-automatic 3D voxel registration protocol (Analyze 11.0, Mayo Clinic). The CTA and T2W MRI datasets were co-registered. At the end of the registration process, the pre-USPIO T2*W MRI, the post-USPIO T2*W MRI, the CTA and the PET-CT were all co-registered to enable direct comparison.

18F-FDG quantification

The maximum standardized uptake value (SUV) was used to assess 18F-FDG activity in the aneurysm. The SUV is the decay corrected tissue uptake divided by the injected dose per unit body weight and is a semi-quantitative dimensionless unit that has been previously validated and is commonly used measure of tissue 18F-FDG activity (Dweck et al., 2012a, Dweck et al., 2011, Rudd et al., 2002, Tawakol et al., 2013). The SUV in vascular structures can be heavily influenced by variability of 18F-FDG activity in the blood pool. Therefore, the tissue-to-background ratio (TBR)

was also calculated by dividing the tissue maximum SUV by the mean SUV in the blood pool (average of five randomly selected regions in the descending thoracic aorta). An area of 18F-FDG uptake was defined as significant if the maximum SUV or TBR was >125% of the value obtained from non-aneurysmal descending thoracic aorta (average of five randomly selected areas).

USPIO quantification

Using validated in-house software (Matlab, Mathworks, USA), four echoes in the multi-echo T2*W sequence were combined to generate a T2* map in which the magnitude of each voxel represented the T2*value ($S(t)=S(0)exp-(t/T2^*)$. The T2* value is the decay constant for the exponential decay of signal intensity with time. In the presence of USPIO, the signal decays more rapidly because of local magnetic field inhomogeneities and the T2* value is reduced. A 3×3 voxel Gaussian filter was applied to the individual echoes to reduce noise. An experimentally determined threshold for the coefficient of determination ($r^2>0.85$) was used to exclude data that did not have an acceptable exponential decay when signal intensity (SI) was plotted against echo time. USPIO uptake was detected using the change in T2* (or R2*; R2*=1/T2*) following USPIO administration. A previously defined threshold of significance (59% increase in T2*) was used to distinguish USPIO accumulation from artefactual changes in T2* (Richards et al., 2012, Richards et al., 2011c). To enable the spatial distribution of USPIO uptake within the aneurysm to be assessed, colour maps were generated in which each voxel represented the change in T2* (ΔT2*) or R2* (ΔR2*) following USPIO administration.

We chose to analyze the correlation between 18F-FDG uptake and USPIO distribution using three methods: first we compared these signals in different regions of the aneurysm by drawing regions of interests around the wall and thrombus, and second we studied co-localization across the whole aneurysm using a voxel-by-voxel analysis. Finally, a previously defined aneurysm classification system based on USPIO uptake on MRI (Richards et al., 2011c) was compared to the SUV and TBR for each aneurysm.

Colour maps

Two independent observers, blinded to patient demographics and aneurysm size reviewed the ΔT2* colour maps and the fused PET-CT data. Each axial slice was divided into quadrants and each quadrant was defined as positive if it included at least one region of increased USPIO or 18F-FDG uptake, or negative if it did not. On the ΔT2* colour maps, regions were defined as consisting of at least ten contiguous voxels with ΔT2* above the threshold of 59%.[16] On the PET-CT scans, regions of interest were drawn around areas of maximum uptake in the wall and thrombus of the aneurysm and defined as positive if the maximum SUV was >125% of the mean SUV.

In order to define the area of the aneurysm where there was increased uptake of either USPIO or 18F-FDG, the aneurysm was divided in the axial plane into three distinct regions; on MRI the shoulder region extended 1 slice (5 mm) above and

below the point at which the aorta dilated to 30 mm and on PET-CT, 2 slices (6 mm) were considered. The bifurcation region was defined in an identical way but from the point where the aneurysm reduced in diameter to 30 mm. The area between these two points was defined as the main body of the aneurysm.

Voxel-by-voxel analysis

The MRI images were reconstructed by down-sampling to achieve equivalent voxel sizes on MR and PET images. A region of interest (ROI) encompassing the entire aortic wall and thrombus was drawn on each slice of the pre-contrast T2W image. These ROI were then applied to the PET images and to the ΔR2* colour maps. This enabled a quantitative voxel-by-voxel analysis of USPIO uptake and 18F-FDG activity.

Aneurysm Classification

We have previously shown that mural USPIO uptake predicts expansion therefore aneurysms were classified into three pre-defined groups by two independent blinded observers: Group 1, no mural or thrombus USPIO uptake, except for isolated periluminal enhancement; Group 2, diffuse USPIO uptake, distinct from the periluminal thrombus and aortic wall; and Group 3, focal areas (with at least 10 contiguous voxels) of USPIO uptake within the aortic wall of the aneurysm, distinct from the periluminal area and thrombus (Richards et al., 2011c). The classification of

each aneurysm was then compared to the maximum SUV and TBR of each aneurysm.

6.3.5. STATISTICAL ANALYSIS

Normally distributed continuous variables were expressed as mean ± standard deviation. Non-parametric data were presented as median with interquartile ranges. Correlations between normally distributed data were performed using Pearson's correlation. Comparisons were undertaken with paired or unpaired Student's *t*-tests as appropriate. A two-sided $P<0.05$ was regarded as statistically significant. Statistical analysis was performed with the use of Graph Pad Prism version 5 (GraphPad Software Inc., California USA).

6.4. RESULTS

Fifteen predominantly elderly men with multiple cardiovascular risk factors and a mean AAA diameter of 46 mm (range 36-54 mm) participated in the study (Table 6-1). All patients were asymptomatic and had fusiform aneurysms confined to the abdominal aorta. 18F-FDG PET-CT and USPIO-enhanced MRI scans were performed a median of 7 days apart. PET imaging of the abdomen was undertaken a median of 92 min (IQR, 89-97 min) after injection of 237±16 MBq of 18F-FDG. The effective radiation from participation in the study was 10.8 mSv using a conversion factor of 0.014 mSv/mGy.cm. The administration of 18F-FDG and USPIO was well tolerated with no adverse events.

Table 6-1: Baseline characteristics of patients with Abdominal Aortic Aneurysm (n=15)

Age (years)	73±4
Maximum AP diameter (cm)	4.6 (range 34 – 55)
Cardiovascular History	
Coronary artery disease	5 (33%)
Stroke or transient ischemic attack	2 (13%)
Peripheral vascular disease	2 (13%)
Risk Factors	
Current smoking habit	6 (40%)
Previous smoking habit	8 (60%)
Diabetes mellitus	1 (7%)
Hypertension	10 (67%)
Hypercholesterolemia	15 (100%)
Medications	
Antiplatelet agent	1 (80%)
Statin	13 (87%)
β-Blocker	6 (40%)
ACE inhibitor/ARB*	8 (53%)
Other Anti-hypertensive	2 (13%)

*Angiotensin converting enzyme (ACE) inhibitor or angiotensin II receptor blocker (ARB)

6.4.1. 18F-FDG UPTAKE

There was demonstrable 18F-FDG activity within the wall of the AAA and increased activity was present in 13 of the 15 aneurysms. All areas of increased activity of 18F-FDG were diffuse and involved the wall (Table 6-2). There was increased activity in the peri-luminal zone around the thrombus but the thrombus itself was metabolically inert. The majority of areas of increased 18F-FDG uptake occurred in the shoulder region of the aneurysm (25/42, 60%), with a third (14/42) occurring within the main body of the aneurysm and the remainder in close proximity to the bifurcation (3/42).

6.4.2. USPIO UPTAKE

All aneurysms had focal areas of USPIO uptake involving the wall of the aneurysm and most of these areas were confined to the main body of the aneurysm (146/271, 54%), with 28% (75/271) located in the shoulder region and 19% (50/271) adjacent to the bifurcation (Table 2). In keeping with the peri-luminal effect seen in previous studies, all patients had USPIO uptake in the periluminal area, representing a movement of particles directly into the thrombus from the blood pool.

Figure 6-1: A. Comparison of standard uptake value (SUV) and absolute change in R2* in the wall of the abdominal aortic aneurysm (AAA).

When the thrombus and wall of the aneurysm are considered there is a modest correlation between the SUV and the absolute change in R2 (r^2 value = 0.09). B. MRI group classification compared to maximum absolute change in R2*, maximum SUV and tissue-to-background ratio (TBR) in the wall of the AAA. There was no significant difference between the absolute change in R2* (p=0.4123, 95% CI -86.99 – 37.98), maximum SUV (p=0.4696, 95% CI -1.682 – 0.8194) or TBR (p=0.7884, 95% CI -2.181 – 1.690) of patients in group 1 and 2 and those in group 3.*

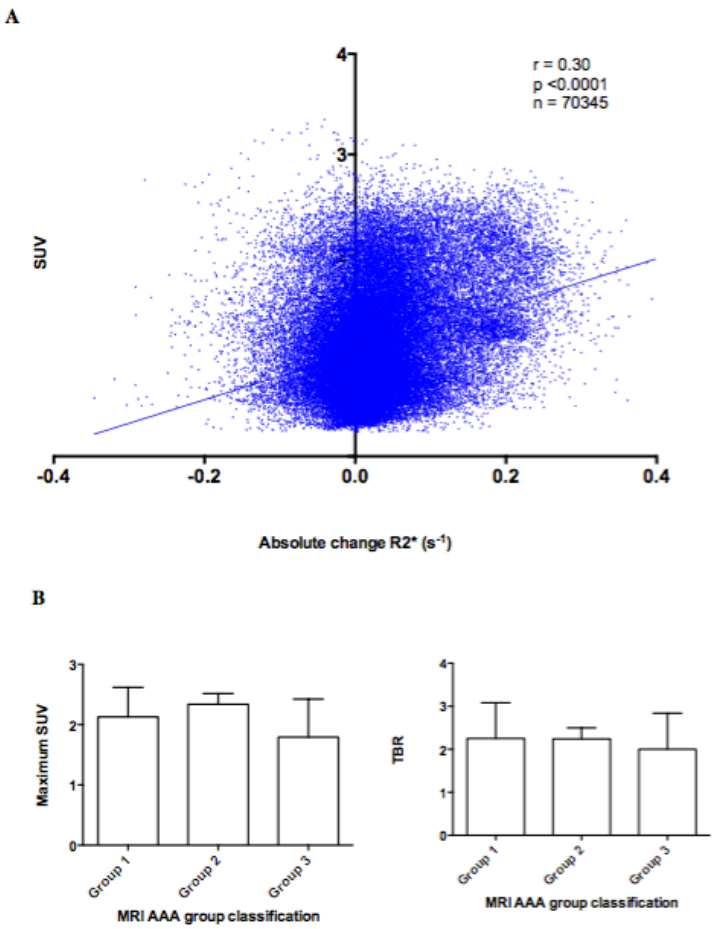

6.4.3. COMPARISON BETWEEN 18F-FDG AND USPIO UPTAKE

Based on USPIO uptake, 4 patients were classified into Group 3 and 11 into Groups 1 and 2. Maximum SUV and TBR appeared to be lower in those classified as Group 3 than in those in Groups 1 and 2, but this did not reach statistical significance (p=0.7884, 95% CI -2.181–1.690; Figure 6-1). There was no correlation between the grouping classification and the maximum absolute change in R2* (p=0.4123, 95% CI -86.99 – 37.98). When all areas of the aneurysm were considered, there was a modest correlation between the SUV on PET-CT and the absolute change in R2* on MRI (r=0.30; 95% CI 0.29–0.31, p<0.0001; Figure 6-1).

On occasion, MRI and fused PET-CT scans co-localized to the same area of increased USPIO and 18F-FDG uptake in the aortic wall, although regions of USPIO uptake without corresponding 18F-FDG activity were also commonly seen (Figure 6-2). Focal and discrete uptake of USPIO can be readily discerned on MRI, whereas there was more diffuse and ill-defined uptake of 18F-FDG involving both the wall and the thrombus on PET-CT. Co-localization of areas of increased uptake of USPIO on MRI and 18F-FDG activity on PET-CT was poor (kappa statistic 0.074; 95% CI, 0.026-0.122) and there were more areas of increased uptake identified on MRI, than on PET-CT (Table 6-3).

Table 6-2: Quadrant analysis of USPIO enhanced MRI and 18F-FDG PET-CT uptake

Regions of uptake identified in the MRI wall versus PET-CT wall. Kappa statistic = 0.074 (95% C.I. 0.026 – 0.122), representing a poor strength of agreement.

		18F-FDG PET-CT		
MRI-USPIO		Regions of uptake	No regions of uptake	Total
	Regions of uptake	70	353	423
	No regions of uptake	69	613	682
	Total	139	966	1015

Classification of AAA according to 18F-FDG activity or USPIO uptake using the quadrant technique was consistent and reproducible with excellent inter-observer agreement and a kappa statistic of 0.87 for 18F-FDG and 0.85 for USPIO.

Figure 6-2: A & B: Representative MRI (A) and fused PET-CT (B) scans from the same patient with an abdominal aortic aneurysm (AAA).

USPIO uptake, defined by percentage change in T2 is demonstrated using a color scale. Changes in T2* value over the threshold (59%) are presented on a graduated (yellow-red) color scale and data below the threshold appears blue. Corresponding 18F-FDG activity (red arrow) can be seen in image B. Differences in the location of regions of uptake between the techniques are apparent, as marked by the white arrow. Image C & D are corresponding MRI and fused PET-CT slices from the same patient who has no USPIO or 18F-FDG uptake in the wall of the AAA, with uptake limited to the peri-luminal area.*

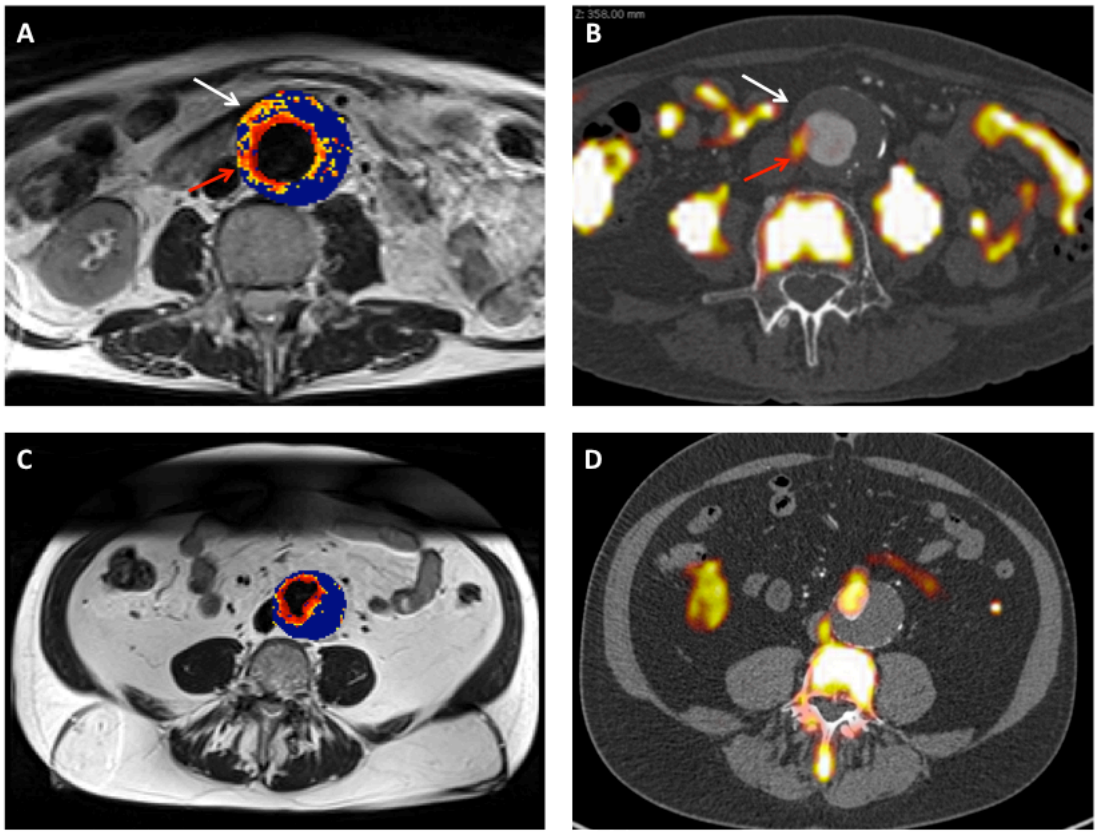

Table 6-3: Qualitative evaluation of 18F-FDG uptake on PET-CT versus USPIO uptake on MRI

	18F-FDG PET-CT	**USPIO MRI**
Spatial resolution	5-6mm	3-4mm
Periluminal enhancement	Present	Present
Region of uptake	Predilection for shoulder region	Predilection for sac of aneurysm
Definition of uptake	>125% mean SUV (5 randomly selected regions of descending thoracic aorta)	10 contiguous voxels with % change in T2* ≥59%
Functional assessment	Glycolytic activity	Phagocytic activity
Ionising radiation	Yes	No

6.5. DISCUSSION

In comparing 18F-FDG PET-CT with USPIO-enhanced MRI in patients with AAA, we have identified a modest correlation between these two imaging modalities, yet a number of key differences. In particular activity detected with these two techniques appears to be concentrated in different regions of the aneurysm: largely in the shoulder region with 18F- FDG and in the body of the aneurysm using USPIOs. We believe that this reflects the different elements of inflammatory activity detected by these two approaches, with PET-CT providing information related to glycolysis and USPIO information on phagocytosis. Further studies are now required to assess which modality will have the greatest predictive power to determine aneurysm growth and clinical outcome.

Inflammatory cells have a key role in the development and progression of abdominal aortic aneurysms (Courtois et al., 2013). Histopathologically, the aneurysmal aortic wall is characterised by focal medial neovascularisation, infiltration of inflammatory cells (principally macrophages and lymphocytes) and fragmentation of elastin and collagen fibres within the extracellular matrix. Both 18F-FDG and USPIO imaging aim to detect and quantify the inflammatory cellular component and it is therefore encouraging that a modest correlation between these two measures was observed in this study, confirming that ultimately both identify vascular inflammation, albeit through differing pathways.

Vascular inflammatory cells are metabolically active and take up 18F-FDG in an insulin- insensitive manner. Therefore, 18F-FDG uptake in the fasted state has been proposed as a marker of risk for aneurysm progression and rupture with higher uptake associated with inflammation, aortic wall instability, and clinical symptoms (Reeps et al., 2008). However, recent data have suggested that vascular 18F-FDG activity may relate to more than simply macrophage burden, implicating hypoxia as an important driver to 18F-FDG uptake (Folco et al., 2011). Furthermore, although several small studies have demonstrated the ability of 18F-FDG to discriminate between symptomatic and asymptomatic AAA (Reeps et al., 2012, Reeps et al., 2013, Reeps et al., 2008, Courtois et al., 2013, Sakalihasan et al., 2002, Truijers et al., 2008), one report showed an inverse relationship between 18F-FDG uptake and future aneurysm growth rates (Kotze et al., 2011b). USPIO-enhanced MRI has been used to explore a number of inflammatory conditions, including atherosclerotic plaques and abdominal aortic aneurysms (Sadat et al., 2011b, Richards et al., 2011b, Trivedi et al., 2006a, Morishige et al., 2010). USPIOs are taken up by inflammatory phagocytic cells, particularly macrophages, and accumulate at sites of cellular inflammation at sufficient concentrations to cause signal changes on MRI. In addition, histological examination of excised tissue, including aneurysm tissue, has confirmed the co-localisation and uptake of USPIO in areas of macrophage infiltration (Richards et al., 2011b, Trivedi et al., 2006a, Kooi et al., 2003a, Schmitz et al., 2001). We speculate that USPIO and 18F-FDG uptake represent distinct markers of vascular inflammation that correspond to differing inflammatory and macrophage activities. Clearly, USPIO uptake is a measure of ongoing phagocytic activity of tissue-resident macrophages and potentially neutrophils, whereas 18F-

FDG reflects glucose utilisation by cells with high metabolic requirements including the cells implicated in vascular inflammation (Millon et al., 2013). Moreover there is evidence that the two techniques target different macrophage subsets. Macrophages exist in varying polarised states and have different roles in vascular tissue. M1 macrophages are considered more destructive, promoting the destabilisation and rupture of atherosclerotic plaques, whereas phagocytosis is more important in the role of M2 macrophages stimulating reparative processes, mediated by the production of anti-inflammatory cytokines and the suppression of pro-inflammatory signaling (Mosser and Edwards, 2008). It has been suggested that 18F-FDG and USPIO uptake may be able to differentiate these two distinct M1 and M2 macrophage sub- populations respectively (Satomi et al., 2013a). In our study the majority of 18F-FDG uptake was identified in the shoulder region of the aneurysm, an area of high biomechanical stress (Nchimi et al., 2014, Xu et al., 2010), with a particular tendency to rupture: perhaps related to a destructive macrophage phenotype in this area. Even though it has been demonstrated that our USPIO aneurysm classification identifies aneurysms likely to progress and dilate (Group 3; distinct mural USPIO uptake) we found no correlation between this classification and 18F-FDG uptake nor the maximum absolute change in R2*. This supports the suggestion that it is the location of USPIO uptake that is crucial, rather than the degree of USPIO uptake. However, the modest correlation that was demonstrated between maximum absolute change in R2* and SUV on a voxel-by-voxel basis supports the contention that these imaging modalities are both detecting elements of macrophage activity, namely phagocytosis and glucose metabolism.

There are important study limitations and technical considerations when interpreting our findings. We acknowledge that co-registration of the MRI and PET-CT datasets was challenging and cannot exclude partial or incomplete co-registration. Moreover the limited in-plane resolution of PET-CT makes definition of the wall more difficult and therefore challenging to locate the exact site of activity. Indeed this may also explain the increased 18F-FDG uptake observed in the shoulder region, which is more prone to partial volume effects due to its angulation through the slice. Additionally, there is no consensus or validated definition of quantitative significance values for 18F-FDG or USPIO uptake and despite the excellent interobserver reproducibility demonstrated in this study, this may contribute to the differences observed. This is also a small study population that will require prospective evaluation in larger patient cohorts. Given this limited sample size, we were unable to assess the relationship between uptake of either 18F-FDG or USPIOs with AAA growth rates or clinical outcome. A number of small studies have demonstrated the ability of 18F-FDG's ability to differentiate between symptomatic and asymptomatic AAA (Reeps et al., 2012, Reeps et al., 2013, Courtois et al., 2013, Sakalihasan et al., 2002, Truijers et al., 2008) and a recent study has suggested an association between 18F-FDG activity and future clinical events (Nchimi et al., 2014). We have previously demonstrated in a pilot study of 29 patients that USPIO uptake in the wall of AAA is associated with accelerated expansion rates (Richards et al., 2011c). Further datasets are therefore required to undertake more complete evaluation of these promising imaging approaches.

In conclusion, the correlation between 18F-FDG PET-CT and USPIO-enhanced MRI to detect vascular inflammation in AAAs is modest and reflects the differing elements of macrophage activity that they detect: glycolysis and phagocytosis respectively. Whether the identification of this varying activity will impact on aneurysm growth rates or risk of aneurysm rupture will require larger longitudinal study.

Chapter 7. CONCLUSIONS AND FUTURE DIRECTIONS

7.1. SUMMARY OF FINDINGS

Despite significant advances in our understanding, cardiovascular diseases still remain the commonest cause of death worldwide (Lozano et al., 2012, Mozaffarian et al., 2014). Majority of these deaths are sudden and are caused by atherosclerotic plaque rupture with resultant myocardial infarction or cerebrovascular accident and ruptured aortic aneurysms. Conventional imaging modalities such coronary angiography and stress echocardiography have consistently failed to identify plaques at risk of rupture (Stone et al., 2011a, Libby, 2013, Boden et al., 2007) and an ever-expanding repertoire of cardiovascular imaging techniques are currently being investigated in detecting the so-called vulnerable plaques. Similarly, AAA growth and rupture are highly unpredictable and current imaging modalities are unable to guide early interventions (Scott, 2002, Lederle et al., 2002, Golledge et al., 2006b, Norman et al., 2004). Recent advances in imaging modalities that target biochemical and cellular processes have generated considerable interest in novel molecular and cellular techniques (Jaffer et al., 2009, Jaffer et al., 2007, Choudhury and Fisher, 2009, Tawakol et al., 2006, Rudd et al., 2002, Tahara et al., 2006b). These techniques have a potential to provide novel biological insights, risk-stratify patients, and allow assessment of responses to specific therapeutic interventions (Jaffer et al., 2009, Jaffer et al., 2007, Choudhury and Fisher, 2009, Nahrendorf et al., 2011)

The aims of the studies presented in this thesis were to develop and evaluate the role of novel molecular imaging techniques in human atherosclerotic and aneurysmal disease. A multimodality approach for assessment of atherosclerotic plaques and

aneurysms was utilised, with 18F-FDG PET and USPIO enhanced MRI as markers metabolic and cellular inflammation and 18F-fluoride PET as a marker of active calcification. From the series of studies presented in this thesis, we can conclude that the molecular imaging techniques hold major promise in identifying patients with high-risk vulnerable atherosclerotic plaques (chapter 3), provide novel insights into atherosclerotic disease process and risk of future recurrent cardiovascular events (chapter 4), and aid our understanding of pathobiological processes in vascular disease (chapter 5 and 6).

7.1.1. FLUORIDE PET IMAGING CAN IDENTIFY HIGH RISK AND VULNERABLE CORONARY ATHEROSCLEROSIS

We assessed the potential of 18F-fluoride positron emission tomography to become the first practical non-invasive method of identifying ruptured or high-risk coronary atherosclerotic plaque in patients with symptomatic stable and unstable coronary artery disease. The study provides a robust and cogent argument to support the contention that 18F-fluoride uptake identifies vulnerable and high-risk plaques in patients with stable and unstable coronary heart disease.

18F-fluoride identified the culprit plaque in patients with acute ST-segment and non ST-segment elevation myocardial infarction. Histologic evaluation of patients with symptomatic carotid disease undergoing carotid endarterectomy confirmed 18F-fluoride uptake at the site of plaque rupture and correlates with histologically confirmed areas of active calcification, apoptosis and necrosis. We extended our findings to patients with stable symptomatic coronary artery disease and compared 18F-fluoride uptake with plaque characteristics defined by gray-scale and radiofrequency intravascular ultrasound, and computed tomography coronary angiography. 18F-fluoride uptake is associated with coronary plaques that have high-risk features including positive remodeling, microcalcification and necrosis.

18F-fluoride PET-CT holds major promise as a means of identifying high-risk and ruptured plaque, and potentially informing the future management and treatment of

patients with stable and unstable coronary artery disease. Further work is now needed to establish whether 18F- fluoride PET-CT will provide a clinically useful technique capable of improving risk stratification, monitoring disease progression, guiding therapeutic interventions and assessing novel anti-atherosclerotic therapies.

7.1.2. MYOCARDIAL INFARCTION BEGETS MYOCARDIAL INFARCTION.

Pre-clinical data suggest an acute inflammatory response following myocardial infarction accelerates systemic atherosclerosis (Dutta et al., 2012). Using combined positron emission and computed tomography (PET-CT), we investigated whether this phenomenon occurs in humans.

Using an imaging cohort, we have demonstrated increased metabolic activity in remote aortic atherosclerotic plaques in patients with recent myocardial infarction that correlated with the degree of myocardial necrosis. Using the well-validated prospective GRACE registry (Fox KA at al., 2007), we showed that the patients with the largest infarcts had more than a four-fold increase in the risk of early recurrent myocardial infarction.

We therefore provide clinical data to support the hypothesis that myocardial infarction exacerbates systemic atherosclerotic inflammation, destabilizes remote atheromatous plaque, and causes an increase in early recurrent atherothrombotic events. The presence and extent of myocardial infarction is associated with increased aortic atherosclerotic inflammation and early recurrent myocardial infarction supporting the hypothesis that myocardial infarction begets myocardial infarction in humans.

7.1.3. *IN-VIVO* ASSESSMENT OF INFLAMMATION AND CALCIFICATION IN ABDOMINAL AORTIC ANEURYSMS AND ATHEROSCLEROSIS

Despite recent advances, the pathobiological processes underlying aneurysmal expansion remain poorly understood. Using 18F –FDG as a marker of vascular inflammation, we sought to evaluate the extent of inflammation and calcification in patients with AAA and atherosclerosis. We hypothesized that both aortic inflammation and calcification would be greater in aneurysmal subjects than in matched controls with atherosclerosis.

We showed that there was increased aortic and aneurysmal inflammation in patients with AAA as compared to patients with atherosclerosis. Furthermore the aneurysms displayed higher degree of calcification as compared to atherosclerotic controls, suggesting an intense, destructive and trans-mural pathological process involving the aneurysmal aorta.

We conclude that patients with AAA have enhanced active inflammation and calcification within the aortic aneurysmal wall. As compared to atherosclerotic controls, patients with AAA have inflammation involving the entire aorta, supporting a hypothesis of global aortopathy in these subjects. Prospective studies are now underway to evaluate whether the degree of aneurysmal inflammation is associated with rate of progression of aneurysmal size, growth and rupture.

7.1.4. IN VIVO ASSESSMENT OF CELLULAR AND METABOLIC INFLAMMATION IN AAA

Using two contemporary molecular imaging techniques: USPIO enhanced MRI and 18F-FDG PET, we assessed cellular and metabolic inflammation in patients with aneurysmal disease.

We showed that there was modest correlation between the 18-FDG and USPIO uptake, although there were importance differences in distribution of molecular agents, suggesting a differential detection of macrophage glycolytic and phagocytic activity respectively. In particular activity detected with these two techniques appears to be concentrated in different regions of the aneurysm: largely in the shoulder region with 18F- FDG and in the body of the aneurysm using USPIOs.

Further studies are now underway to assess which modality will have the greatest predictive power to determine aneurysm growth and clinical outcome.

7.2. FUTURE DIRECTIONS

The conclusions of this thesis raises questions on whether cardiovascular molecular imaging techniques will aid risk stratification, monitoring of disease progression, guide therapeutic interventions, and assess novel anti-atherosclerotic therapies in patients with stable and unstable atherosclerotic and aneurysmal diseases.

A number of studies are now ongoing to evaluate:

i) whether 18F- fluoride PET will aid in identifying patients with coronary disease at high risk of future cardiovascular events.

ii) the role of 18F-fluoride in identifying patients who benefit from potent anti-thrombotic therapy.

iii) the role of molecular imaging in predicting AAA progression and rupture.

7.2.1. PREDICTION OF RECURRENT EVENTS WITH 18F-FLUORIDE TO IDENTIFY RUPTURED AND HIGH-RISK CORONARY ARTERY PLAQUES IN PATIENTS WITH MYOCARDIAL INFARCTION (THE PRE18FFIR STUDY)

In patients with myocardial infarction, will coronary 18F-fluoride uptake predict future disease progression and clinical outcomes? The PRE18FFIR study (ClinicalTrials.gov number: NCT02278211) is a multicentric outcome based study that aims to confirm our preliminary findings (chapter 3) in a larger cohort of patients with recent myocardial infarction. A total of 700 patients with recent myocardial infarction and multi-vessel coronary heart disease will be recruited from four UK centres. The primary end point is cardiovascular death or non-fatal recurrent myocardial infarction at two years. Additional sub-studies will assess the reproducibility, natural history and further *in vivo* plaque characterization techniques with 18F-fluoride PET (Appendix).

These series of studies will evaluate the role of a surrogate non-invasive marker of high-risk vulnerable plaque in patients with acute myocardial infarction, over and above standard prognostic markers for future cardiovascular events.

7.2.2. DUAL ANTIPLATELET THERAPY TO INHIBIT CORONARY ATHEROSCLEROSIS AND MYOCARDIAL INJURY IN PATIENTS WITH NECROTIC HIGH-RISK CORONARY PLAQUE DISEASE (THE DIAMOND STUDY)

Myocardial infarction is initiated by coronary atherosclerotic plaque rupture and subsequent thrombosis (Burke et al., 1997a, Burke et al., 2001, Falk et al., 2013a, Finn et al., 2010, Virmani et al., 2006b, Virmani et al., 2000a). Given the central role of thrombosis in progression of atherosclerosis, anti-thrombotic interventions have major potential to impact on the consequences and progression of atherosclerotic disease (Williams et al., 1997, Rioufol et al., 2004). With the advent of more potent platelet inhibition with newer P2Y12 receptor antagonist such as ticagrelor (Wallentin et al., 2009), there is now the opportunity to assess whether dual anti-platelet therapy can improve markers of myocardial injury and disease progression.

Will aggressive secondary treatment with potent P2Y12 inhibitor ticagrelor reduce biomarkers of myocardial injury and inhibit disease progression in patients with stable coronary heart disease and evidence of high-risk coronary plaque defined by 18F-fluoride uptake on positron emission tomography? The DIAMOND study is a randomised double blind placebo-controlled trial in patients with angiographically proven multivessel disease that will aim address this question. The primary end point of the study is to determine whether ticagrelor will influence the degree of myocardial injury in patients with stable coronary heart disease and high-risk coronary atheroma as compared to placebo (Appendix).

7.2.3. USPIO-ENHANCED MRI AND 18F-FLUORIDE PET CT IN AAA

The imaging modalities used in our studies (chapters 5 and 6) provide important pathobiological insights into vascular inflammation and calcification. Specifically, the aneurysmal wall had more pronounced calcification as compared to other areas thereby suggesting an intense, destructive and transmural pathological process involving AAA (chapter 5). Furthermore, a distinct distribution of cellular vascular inflammation was noted with USPIO enhanced MRI in AAA patients (chapter 6). Whether uptake of these tracers using novel imaging techniques translates to important clinical events or progression of disease remains unknown. We have designed two prospective observational studies to evaluate the role of these tracers in AAA.

The MRI Abdominal Aortic Aneurysms to predict Rupture or Surgery (The MA3RS trial) is a prospective multicentre observational cohort study across 350 patients evaluating the role of USPIO enhanced MRI in patients with AAA. The study aims to assess whether mural uptake of USPIO provides incremental risk prediction in addition to standard risk markers such as aneurysm diameter, smoking and blood pressure. The primary end-point of the study will be the composite of aneurysm rupture or aortic aneurysm repair, with the rates of surgical repair and aneurysmal growth as secondary endpoints.

18F-Sodium Fluoride PET-CT in Abdominal Aortic Aneurysms (The SoFIA3 Study) is a prospective study to evaluate the role of 18F-fluoride PET-CT in patients with abdominal aortic aneurysms. The aim of the study is to explore whether 18F-fluoride uptake in the aortic wall correlates with aneurysm expansion.

These studies will provide insights into how molecular imaging relate to both adverse clinical events and progression of disease in patients with aortic aneurysmal disease.

7.3. PERSPECTIVE

The ability to identify high-risk vulnerable atherosclerotic plaques has been described as the 'holy grail' of clinical cardiology (Naghavi et al., 2003). Similarly, an ability to identify high-risk aneurysmal disease at highest risk of progression and rupture will transform the way we manage patients with aneurysmal disease (Shimizu et al., 2007). Novel molecular imaging techniques by targeting the biological processes driving disease progression have shown a great potential to fundamentally in identifying the diseases *in vivo*. The studies described in this thesis represent a major step in achieving the aim of identifying high-risk coronary and aneurysmal disease. Further studies are now needed to assess if these techniques can identify vulnerable patients at highest risk of having future coronary events and aneurysmal progression and rupture.

The discovery of 18F-fluoride in assessment of coronary heart disease represents a new frontier in cardiovascular imaging (Thomas and Haraszti, 2014, van der Wall, 2014, Mearns, 2014). It represents a step change in our scientific understanding of atherosclerosis, in particular the mechanisms underlying calcification (George, 2012). We already know that CT coronary calcium scoring is one of the most powerful predictors for cardiovascular events (Budoff et al., 2007). However, unlike established macrocalcification visible on CT, 18F-fluoride uptake identifies actively calcifying atherosclerotic plaques that, similar to the caseating granulomata of tuberculosis, occurs as a healing response to intense inflammation either within the necrotic core or related to the plaque rupture event itself. Given that such inflamed

lesions are at the highest risk of rupture, there is therefore a clear rationale for why 18F-fluoride uptake should predict myocardial infarction and why this technique also has important potential clinical applications.

The discovery of fluoride PET as a marker of high-risk plaques has many potential and wide reaching applications. It might prove a useful tool to test the effectiveness of new treatments. In the clinical setting, this technique holds hope as a means of defining and selecting the best treatments for our patients with coronary heart disease. Future studies aimed to assess which patient group will derive the most benefit from this technique are now needed. If this is established then 18F-fluoride PET is likely to fundamentally alter the way we assess and treat coronary artery disease – moving us away from the current paradigm based on lesion severity and ischemia to one based on plaque metabolism and vulnerability.

The concept of systemic inflammation following myocardial infarction provides fascinating insight into remote plaque inflammation and destabilization following myocardial infarction, thus explaining the clinical observations of early recurrent infarction and ischaemia in patients post myocardial infarction. This supports the concept of "myocardial infarction begets myocardial infarction".

The studies on abdominal aortic aneurysms provide unique perspective on this common and deadly condition. The current clinical practice involves patients with AAA participating in national screening and surveillance programs designed to detect and monitor aneurysmal progression. However, the AAA expansion rates are non-linear and unpredictable, and more refined techniques are necessary to predict AAA growth and rupture. The molecular imaging studies on AAA provide novel insights into plaque biology of atherosclerosis and aneurysmal disease. This is the first step in adapting novel molecular imaging techniques in refining the approach taken to evaluate the progression of disease and identifying patients at risk of future adverse events.

In undertaking these studies, we have developed robust methodologies to ultimately study large cohorts of patients with coronary atherosclerotic and aneurysmal disease. Prospective outcome based studies with these molecular imaging techniques are now required in a range of cardiovascular disease with an aim to identify the vulnerable patients who are at highest risk of plaque and aneurysmal rupture.

REFERENCES

ADAMS, R. L., ADAMS, I. P., LINDOW, S. W., ZHONG, W. & ATKIN, S. L. 2005. Somatostatin receptors 2 and 5 are preferentially expressed in proliferating endothelium. *Br J Cancer,* 92**,** 1493-8.

ADOLPH, R., VORP, D. A., STEED, D. L., WEBSTER, M. W., KAMENEVA, M. V. & WATKINS, S. C. 1997. Cellular content and permeability of intraluminal thrombus in abdominal aortic aneurysm. *Journal of Vascular Surgery,* 25**,** 916-926.

AGATSTON, A. S., JANOWITZ, W. R., HILDNER, F. J., ZUSMER, N. R., VIAMONTE, M., JR. & DETRANO, R. 1990. Quantification of coronary artery calcium using ultrafast computed tomography. *J Am Coll Cardiol,* 15**,** 827-32.

AGNESE IRKLE, J. L. B., JEREMY N SKEPPER, MARC R DWECK, FRANCIS R JOSHI, ALEX T VESEY, MARTIN BENNETT, DAVID E NEWBY, ELIZABETH A WARBURTON, JAMES H RUDD, ANTHONY P DAVENPORT 2013. 18F-NaF - a Specific Marker for Vascular Calcification in Atherosclerosis *Circulation,* 128: A17385.

AIKAWA, E., NAHRENDORF, M., FIGUEIREDO, J. L., SWIRSKI, F. K., SHTATLAND, T., KOHLER, R. H., JAFFER, F. A., AIKAWA, M. & WEISSLEDER, R. 2007. Osteogenesis associates with inflammation in early-stage atherosclerosis evaluated by molecular imaging in vivo. *Circulation,* 116**,** 2841-50.

ALAM, S. R., SHAH, A. S., RICHARDS, J., LANG, N. N., BARNES, G., JOSHI, N., MACGILLIVRAY, T., MCKILLOP, G., MIRSADRAEE, S., PAYNE, J., FOX, K. A., HENRIKSEN, P., NEWBY, D. E. & SEMPLE, S. I. 2012. Ultrasmall superparamagnetic particles of iron oxide in patients with acute myocardial infarction: early clinical experience. *Circulation. Cardiovascular imaging,* 5**,** 559-65.

AMBROSE, J. A., TANNENBAUM, M. A., ALEXOPOULOS, D., HJEMDAHL-MONSEN, C. E., LEAVY, J., WEISS, M., BORRICO, S., GORLIN, R. & FUSTER, V. 1988. Angiographic progression of coronary artery disease and the development of myocardial infarction. *J Am Coll Cardiol,* 12**,** 56-62.

ANZAI, T., YOSHIKAWA, T., SHIRAKI, H., ASAKURA, Y., AKAISHI, M., MITAMURA, H. & OGAWA, S. 1997. C-reactive protein as a predictor of infarct expansion and cardiac rupture after a first Q-wave acute myocardial infarction. *Circulation,* 96**,** 778-84.

ARAD, Y., GOODMAN, K. J., ROTH, M., NEWSTEIN, D. & GUERCI, A. D. 2005. Coronary calcification, coronary disease risk factors, C-reactive protein, and atherosclerotic cardiovascular disease events: the St. Francis Heart Study. *J Am Coll Cardiol,* 46**,** 158-65.

ARMANI, C., CATALANI, E., BALBARINI, A., BAGNOLI, P. & CERVIA, D. 2007. Expression, pharmacology, and functional role of somatostatin receptor subtypes 1 and 2 in human macrophages. *J Leukoc Biol,* 81**,** 845-55.

BARWICK, T. D., LYONS, O. T., MIKHAEEL, N. G., WALTHAM, M. & O'DOHERTY, M. J. 2014. 18F-FDG PET-CT uptake is a feature of both normal diameter and aneurysmal aortic wall and is not related to aneurysm size. *Eur J Nucl Med Mol Imaging,* 41**,** 2310-8.

BEER, A. J., HAUBNER, R., SARBIA, M., GOEBEL, M., LUDERSCHMIDT, S., GROSU, A. L., SCHNELL, O., NIEMEYER, M., KESSLER, H., WESTER, H. J., WEBER, W. A. & SCHWAIGER, M. 2006. Positron emission tomography using [18F]Galacto-RGD identifies the level of integrin alpha(v)beta3 expression in man. *Clin Cancer Res,* 12**,** 3942-9.

BEHESHTI, M., SABOURY, B., MEHTA, N. N., TORIGIAN, D. A., WERNER, T., MOHLER, E., WILENSKY, R., NEWBERG, A. B., BASU, S., LANGSTEGER, W. & ALAVI, A. 2011. Detection and global quantification of cardiovascular molecular calcification by fluoro18-fluoride positron emission tomography/computed tomography--a novel concept. *Hellenic journal of nuclear medicine,* 14**,** 114-20.

BEHESHTI, M., VALI, R., WALDENBERGER, P., FITZ, F., NADER, M., LOIDL, W., BROINGER, G., STOIBER, F., FOGLMAN, I. & LANGSTEGER, W. 2008. Detection of bone metastases in patients with prostate cancer by 18F fluorocholine and 18F fluoride PET-CT: a comparative study. *European journal of nuclear medicine and molecular imaging,* 35**,** 1766-74.

BERND, H., DE KERVILER, E., GAILLARD, S. & BONNEMAIN, B. 2009. Safety and tolerability of ultrasmall superparamagnetic iron oxide contrast agent: comprehensive analysis of a clinical development program. *Invest Radiol,* 44**,** 336-42.

BLAKE, G. M., PARK-HOLOHAN, S. J., COOK, G. J. & FOGELMAN, I. 2001. Quantitative studies of bone with the use of 18F-fluoride and 99mTc-methylene diphosphonate. *Seminars in nuclear medicine,* 31**,** 28-49.

BLAU, M., GANATRA, R. & BENDER, M. A. 1972. 18 F-fluoride for bone imaging. *Seminars in nuclear medicine,* 2**,** 31-7.

BLAU, M., NAGLER, W. & BENDER, M. A. 1962. Fluorine-18: a new isotope for bone scanning. *Journal of nuclear medicine : official publication, Society of Nuclear Medicine,* 3**,** 332-4.

BOBRYSHEV, Y. V., KILLINGSWORTH, M. C., HUYNH, T. G., LORD, R. S., GRABS, A. J. & VALENZUELA, S. M. 2007. Are calcifying matrix vesicles in atherosclerotic lesions of cellular origin? *Basic research in cardiology,* 102**,** 133-43.

BODEN, W. E., O'ROURKE, R. A., TEO, K. K., HARTIGAN, P. M., MARON, D. J., KOSTUK, W. J., KNUDTSON, M., DADA, M., CASPERSON, P., HARRIS, C. L., CHAITMAN, B. R., SHAW, L., GOSSELIN, G., NAWAZ, S., TITLE, L. M., GAU, G., BLAUSTEIN, A. S., BOOTH, D. C., BATES, E. R., SPERTUS, J. A., BERMAN, D. S., MANCINI, G. B. & WEINTRAUB, W. S. 2007. Optimal medical

therapy with or without PCI for stable coronary disease. *The New England journal of medicine,* 356**,** 1503-16.

BOURRINET, P., BENGELE, H. H., BONNEMAIN, B., DENCAUSSE, A., IDEE, J. M., JACOBS, P. M. & LEWIS, J. M. 2006. Preclinical safety and pharmacokinetic profile of ferumoxtran-10, an ultrasmall superparamagnetic iron oxide magnetic resonance contrast agent. *Invest Radiol,* 41**,** 313-24.

BRADY, A. R., THOMPSON, S. G., FOWKES, F. G., GREENHALGH, R. M., POWELL, J. T. & PARTICIPANTS, U. K. S. A. T. 2004. Abdominal aortic aneurysm expansion: risk factors and time intervals for surveillance. *Circulation,* 110**,** 16-21.

BRILEY-SAEBO, K. C., SHAW, P. X., MULDER, W. J., CHOI, S. H., VUCIC, E., AGUINALDO, J. G., WITZTUM, J. L., FUSTER, V., TSIMIKAS, S. & FAYAD, Z. A. 2008. Targeted molecular probes for imaging atherosclerotic lesions with magnetic resonance using antibodies that recognize oxidation-specific epitopes. *Circulation,* 117**,** 3206-15.

BROOKS, P. C., CLARK, R. A. & CHERESH, D. A. 1994. Requirement of vascular integrin alpha v beta 3 for angiogenesis. *Science,* 264**,** 569-71.

BRUNETTI, N. D., TROCCOLI, R., CORREALE, M., PELLEGRINO, P. L. & DI BIASE, M. 2006. C-reactive protein in patients with acute coronary syndrome: correlation with diagnosis, myocardial damage, ejection fraction and angiographic findings. *International journal of cardiology,* 109**,** 248-56.

BUDOFF, M. J., ACHENBACH, S., BLUMENTHAL, R. S., CARR, J. J., GOLDIN, J. G., GREENLAND, P., GUERCI, A. D., LIMA, J. A., RADER, D. J., RUBIN, G. D., SHAW, L. J., WIEGERS, S. E., AMERICAN HEART ASSOCIATION COMMITTEE ON CARDIOVASCULAR, I., INTERVENTION, AMERICAN HEART ASSOCIATION COUNCIL ON CARDIOVASCULAR, R., INTERVENTION & AMERICAN HEART ASSOCIATION COMMITTEE ON CARDIAC IMAGING, C. O. C. C. 2006. Assessment of coronary artery disease by cardiac computed tomography: a scientific statement from the American Heart Association Committee on Cardiovascular Imaging and Intervention, Council on Cardiovascular Radiology and Intervention, and Committee on Cardiac Imaging, Council on Clinical Cardiology. *Circulation,* 114**,** 1761-91.

BUDOFF, M. J., SHAW, L. J., LIU, S. T., WEINSTEIN, S. R., MOSLER, T. P., TSENG, P. H., FLORES, F. R., CALLISTER, T. Q., RAGGI, P. & BERMAN, D. S. 2007. Long-term prognosis associated with coronary calcification: observations from a registry of 25,253 patients. *J Am Coll Cardiol,* 49**,** 1860-70.

BUDOFF, M. J., YOUNG, R., LOPEZ, V. A., KRONMAL, R. A., NASIR, K., BLUMENTHAL, R. S., DETRANO, R. C., BILD, D. E., GUERCI, A. D., LIU, K., SHEA, S., SZKLO, M., POST, W., LIMA, J., BERTONI, A. & WONG, N. D. 2013. Progression of coronary calcium and incident coronary heart disease events: MESA (Multi-Ethnic Study of Atherosclerosis). *J Am Coll Cardiol,* 61**,** 1231-9.

BUIJS, R. V., WILLEMS, T. P., TIO, R. A., BOERSMA, H. H., TIELLIU, I. F., SLART, R. H. & ZEEBREGTS, C. J. 2013. Calcification as a risk factor for rupture of abdominal aortic aneurysm. *Eur J Vasc Endovasc Surg,* 46**,** 542-8.

BURKE, A. P., FARB, A., MALCOM, G. T., LIANG, Y. H., SMIALEK, J. & VIRMANI, R. 1997b. Coronary risk factors and plaque morphology in men with coronary disease who died suddenly. *The New England journal of medicine,* 336**,** 1276-82.

BURKE, A. P., KOLODGIE, F. D., FARB, A., WEBER, D. K., MALCOM, G. T., SMIALEK, J. & VIRMANI, R. 2001. Healed plaque ruptures and sudden coronary death: evidence that subclinical rupture has a role in plaque progression. *Circulation,* 103**,** 934-40.

BURTEA, C., LAURENT, S., MURARIU, O., RATTAT, D., TOUBEAU, G., VERBRUGGEN, A., VANSTHERTEM, D., VANDER ELST, L. & MULLER, R. N. 2008. Molecular imaging of alpha v beta3 integrin expression in atherosclerotic plaques with a mimetic of RGD peptide grafted to Gd-DTPA. *Cardiovasc Res,* 78**,** 148-57.

CAI, J., HATSUKAMI, T. S., FERGUSON, M. S., KERWIN, W. S., SAAM, T., CHU, B., TAKAYA, N., POLISSAR, N. L. & YUAN, C. 2005. In vivo quantitative measurement of intact fibrous cap and lipid-rich necrotic core size in atherosclerotic carotid plaque: comparison of high-resolution, contrast-enhanced magnetic resonance imaging and histology. *Circulation,* 112**,** 3437-44.

CALVERT, P. A., OBAID, D. R., O'SULLIVAN, M., SHAPIRO, L. M., MCNAB, D., DENSEM, C. G., SCHOFIELD, P. M., BRAGANZA, D., CLARKE, S. C., RAY, K. K., WEST, N. E. & BENNETT, M. R. 2011. Association between IVUS findings and adverse outcomes in patients with coronary artery disease: the VIVA (VH-IVUS in Vulnerable Atherosclerosis) Study. *JACC. Cardiovascular imaging,* 4**,** 894-901.

CHENG, J. M., GARCIA-GARCIA, H. M., DE BOER, S. P., KARDYS, I., HEO, J. H., AKKERHUIS, K. M., OEMRAWSINGH, R. M., VAN DOMBURG, R. T., LIGTHART, J., WITBERG, K. T., REGAR, E., SERRUYS, P. W., VAN GEUNS, R. J. & BOERSMA, E. 2014. In vivo detection of high-risk coronary plaques by radiofrequency intravascular ultrasound and cardiovascular outcome: results of the ATHEROREMO-IVUS study. *Eur Heart J,* 35**,** 639-47.

CHENG, V. Y., SLOMKA, P. J., LE MEUNIER, L., TAMARAPPOO, B. K., NAKAZATO, R., DEY, D. & BERMAN, D. S. 2012. Coronary arterial 18F-FDG uptake by fusion of PET and coronary CT angiography at sites of percutaneous stenting for acute myocardial infarction and stable coronary artery disease. *Journal of nuclear medicine : official publication, Society of Nuclear Medicine,* 53**,** 575-83.

CHIA, S., SENATORE, F., RAFFEL, O. C., LEE, H., WACKERS, F. J. & JANG, I. K. 2008. Utility of cardiac biomarkers in predicting infarct size, left ventricular function, and clinical outcome after primary percutaneous coronary intervention for ST-segment elevation myocardial infarction. *JACC. Cardiovascular interventions,* 1**,** 415-23.

CHOKE, E., THOMPSON, M. M., DAWSON, J., WILSON, W. R., SAYED, S., LOFTUS, I. M. & COCKERILL, G. W. 2006. Abdominal aortic aneurysm rupture is associated with increased medial neovascularization and overexpression of proangiogenic cytokines. *Arterioscler Thromb Vasc Biol,* 26**,** 2077-82.

CHOUDHURY, R. P. & FISHER, E. A. 2009. Molecular imaging in atherosclerosis, thrombosis, and vascular inflammation. *Arteriosclerosis, thrombosis, and vascular biology,* 29**,** 983-91.

CHU, B., KAMPSCHULTE, A., FERGUSON, M. S., KERWIN, W. S., YARNYKH, V. L., O'BRIEN, K. D., POLISSAR, N. L., HATSUKAMI, T. S. & YUAN, C. 2004. Hemorrhage in the atherosclerotic carotid plaque: a high-resolution MRI study. *Stroke,* 35**,** 1079-84.

COLLINS, R. G., VELJI, R., GUEVARA, N. V., HICKS, M. J., CHAN, L. & BEAUDET, A. L. 2000. P-Selectin or intercellular adhesion molecule (ICAM)-1 deficiency substantially protects against atherosclerosis in apolipoprotein E-deficient mice. *J Exp Med,* 191**,** 189-94.

COOK, G. J., BLAKE, G. M., MARSDEN, P. K., CRONIN, B. & FOGELMAN, I. 2002. Quantification of skeletal kinetic indices in Paget's disease using dynamic 18F-fluoride positron emission tomography. *Journal of bone and mineral research : the official journal of the American Society for Bone and Mineral Research,* 17**,** 854-9.

COURTOIS, A., NUSGENS, B. V., HUSTINX, R., NAMUR, G., GOMEZ, P., SOMJA, J., DEFRAIGNE, J. O., DELVENNE, P., MICHEL, J. B., COLIGE, A. C. & SAKALIHASAN, N. 2013. 18F-FDG uptake assessed by PET/CT in abdominal aortic aneurysms is associated with cellular and molecular alterations prefacing wall deterioration and rupture. *J Nucl Med,* 54**,** 1740-7.

CRIQUI, M. H., DENENBERG, J. O., MCCLELLAND, R., ALLISON, M. A., IX, J. H., GUERCI, A., COHOON, K. P., SRIKANTHAN, P., WATSON, K. E. & WONG, N. D. 2014. Abdominal Aortic Calcium, Coronary Artery Calcium, and Cardiovascular Morbidity and Mortality in the Multi-Ethnic Study of Atherosclerosis. *Arterioscler Thromb Vasc Biol*.

DALM, V. A., VAN HAGEN, P. M., VAN KOETSVELD, P. M., ACHILEFU, S., HOUTSMULLER, A. B., POLS, D. H., VAN DER LELY, A. J., LAMBERTS, S. W. & HOFLAND, L. J. 2003. Expression of somatostatin, cortistatin, and somatostatin receptors in human monocytes, macrophages, and dendritic cells. *Am J Physiol Endocrinol Metab,* 285**,** E344-53.

DARLING, R. C., MESSINA, C. R., BREWSTER, D. C. & OTTINGER, L. W. 1977. Autopsy study of unoperated abdominal aortic aneurysms. The case for early resection. *Circulation,* 56**,** II161-4.

DAVIES, M. J. 1992. Anatomic features in victims of sudden coronary death. Coronary artery pathology. *Circulation,* 85**,** I19-24.

DEMER, L. L. & TINTUT, Y. 2008. Vascular calcification: pathobiology of a multifaceted disease. *Circulation,* 117**,** 2938-48.

DERLIN, T., RICHTER, U., BANNAS, P., BEGEMANN, P., BUCHERT, R., MESTER, J. & KLUTMANN, S. 2010. Feasibility of 18F-sodium fluoride PET/CT for imaging of atherosclerotic plaque. *Journal of nuclear medicine : official publication, Society of Nuclear Medicine,* 51**,** 862-5.

DERLIN, T., TOTH, Z., PAPP, L., WISOTZKI, C., APOSTOLOVA, I., HABERMANN, C. R., MESTER, J. & KLUTMANN, S. 2011a. Correlation of inflammation assessed by 18F-FDG PET, active mineral deposition assessed by 18F-fluoride PET, and vascular calcification in atherosclerotic plaque: a dual-tracer PET/CT study. *Journal of nuclear medicine : official publication, Society of Nuclear Medicine,* 52**,** 1020-7.

DERLIN, T., WISOTZKI, C., RICHTER, U., APOSTOLOVA, I., BANNAS, P., WEBER, C., MESTER, J. & KLUTMANN, S. 2011b. In vivo imaging of mineral deposition in carotid plaque using 18F-sodium fluoride PET/CT: correlation with atherogenic risk factors. *Journal of nuclear medicine : official publication, Society of Nuclear Medicine,* 52**,** 362-8.

DETRANO, R., GUERCI, A. D., CARR, J. J., BILD, D. E., BURKE, G., FOLSOM, A. R., LIU, K., SHEA, S., SZKLO, M., BLUEMKE, D. A., O'LEARY, D. H., TRACY, R., WATSON, K., WONG, N. D. & KRONMAL, R. A. 2008. Coronary calcium as a predictor of coronary events in four racial or ethnic groups. *N Engl J Med,* 358**,** 1336-45.

DONG, Z. M., CHAPMAN, S. M., BROWN, A. A., FRENETTE, P. S., HYNES, R. O. & WAGNER, D. D. 1998. The combined role of P- and E-selectins in atherosclerosis. *J Clin Invest,* 102**,** 145-52.

DOUGLAS, P. S., HOFFMANN, U., PATEL, M. R., MARK, D. B., AL-KHALIDI, H. R., CAVANAUGH, B., COLE, J., DOLOR, R. J., FORDYCE, C. B., HUANG, M., KHAN, M. A., KOSINSKI, A. S., KRUCOFF, M. W., MALHOTRA, V., PICARD, M. H., UDELSON, J. E., VELAZQUEZ, E. J., YOW, E., COOPER, L. S., LEE, K. L. & INVESTIGATORS, P. 2015. Outcomes of anatomical versus functional testing for coronary artery disease. *N Engl J Med,* 372**,** 1291-300.

DUNPHY, M. P., FREIMAN, A., LARSON, S. M. & STRAUSS, H. W. 2005. Association of vascular 18F-FDG uptake with vascular calcification. *Journal of nuclear medicine : official publication, Society of Nuclear Medicine,* 46**,** 1278-84.

DUTTA, P., COURTIES, G., WEI, Y., LEUSCHNER, F., GORBATOV, R., ROBBINS, C. S., IWAMOTO, Y., THOMPSON, B., CARLSON, A. L., HEIDT, T., MAJMUDAR, M. D., LASITSCHKA, F., ETZRODT, M., WATERMAN, P., WARING, M. T., CHICOINE, A. T., VAN DER LAAN, A. M., NIESSEN, H. W., PIEK, J. J., RUBIN, B. B., BUTANY, J., STONE, J. R., KATUS, H. A., MURPHY, S. A., MORROW, D. A., SABATINE, M. S., VINEGONI, C., MOSKOWITZ, M. A., PITTET, M. J., LIBBY, P., LIN, C. P., SWIRSKI, F. K., WEISSLEDER, R. & NAHRENDORF, M. 2012. Myocardial infarction accelerates atherosclerosis. *Nature,* 487**,** 325-9.

DWECK, M. R., CHOW, M. W., JOSHI, N. V., WILLIAMS, M. C., JONES, C., FLETCHER, A. M., RICHARDSON, H., WHITE, A., MCKILLOP, G., VAN BEEK, E. J., BOON, N. A., RUDD, J. H. & NEWBY, D. E. 2012a. Coronary arterial 18F-sodium fluoride uptake: a novel marker of plaque biology. *Journal of the American College of Cardiology,* 59**,** 1539-48.

DWECK, M. R., JENKINS, W. S., VESEY, A. T., PRINGLE, M. A., CHIN, C. W., MALLEY, T. S., COWIE, W. J., TSAMPASIAN, V., RICHARDSON, H., FLETCHER, A., WALLACE, W. A., PESSOTTO, R., VAN BEEK, E. J., BOON,

N. A., RUDD, J. H. & NEWBY, D. E. 2014. 18F-Sodium Fluoride Uptake Is a Marker of Active Calcification and Disease Progression in Patients With Aortic Stenosis. *Circulation. Cardiovascular imaging,* 7**,** 371-8.

DWECK, M. R., JONES, C., JOSHI, N. V., FLETCHER, A. M., RICHARDSON, H., WHITE, A., MARSDEN, M., PESSOTTO, R., CLARK, J. C., WALLACE, W. A., SALTER, D. M., MCKILLOP, G., VAN BEEK, E. J., BOON, N. A., RUDD, J. H. & NEWBY, D. E. 2012b. Assessment of valvular calcification and inflammation by positron emission tomography in patients with aortic stenosis. *Circulation,* 125**,** 76-86.

DWECK, M. R., JOSHI, N. V., RUDD, J. H. & NEWBY, D. E. 2013a. Imaging of inflammation and calcification in aortic stenosis. *Current cardiology reports,* 15**,** 320.

DWECK, M. R., KHAW, H. J., SNG, G. K., LUO, E. L., BAIRD, A., WILLIAMS, M. C., MAKIELLO, P., MIRSADRAEE, S., JOSHI, N. V., VAN BEEK, E. J., BOON, N. A., RUDD, J. H. & NEWBY, D. E. 2013b. Aortic stenosis, atherosclerosis, and skeletal bone: is there a common link with calcification and inflammation? *European Heart Journal,* 34**,** 1567-74.

EHARA, S., KOBAYASHI, Y., YOSHIYAMA, M., SHIMADA, K., SHIMADA, Y., FUKUDA, D., NAKAMURA, Y., YAMASHITA, H., YAMAGISHI, H., TAKEUCHI, K., NARUKO, T., HAZE, K., BECKER, A. E., YOSHIKAWA, J. & UEDA, M. 2004. Spotty calcification typifies the culprit plaque in patients with acute myocardial infarction: an intravascular ultrasound study. *Circulation,* 110**,** 3424-9.

EISEMAN, B. & HUGHES, R. 1956. Repair of an abdominal aortic vena caval fistula caused by rupture of an atherosclerotic aneurysm. *Surgery,* 39**,** 498.

ELKHAWAD, M., RUDD, J. H., SAROV-BLAT, L., CAI, G., WELLS, R., DAVIES, L. C., COLLIER, D. J., MARBER, M. S., CHOUDHURY, R. P., FAYAD, Z. A., TAWAKOL, A., GLEESON, F. V., LEPORE, J. J., DAVIS, B., WILLETTE, R. N., WILKINSON, I. B., SPRECHER, D. L. & CHERIYAN, J. 2012. Effects of p38 mitogen-activated protein kinase inhibition on vascular and systemic inflammation in patients with atherosclerosis. *JACC Cardiovasc Imaging,* 5**,** 911-22.

ERSOY, H., JACOBS, P., KENT, C. K. & PRINCE, M. R. 2004. Blood pool MR angiography of aortic stent-graft endoleak. *AJR Am J Roentgenol,* 182**,** 1181-6.

EVEN-SAPIR, E., METSER, U., MISHANI, E., LIEVSHITZ, G., LERMAN, H. & LEIBOVITCH, I. 2006. The detection of bone metastases in patients with high-risk prostate cancer: 99mTc-MDP Planar bone scintigraphy, single- and multi-field-of-view SPECT, 18F-fluoride PET, and 18F-fluoride PET/CT. *Journal of nuclear medicine : official publication, Society of Nuclear Medicine,* 47**,** 287-97.

FALK, E. 2006. Pathogenesis of atherosclerosis. *J Am Coll Cardiol,* 47**,** C7-12.

FALK, E., NAKANO, M., BENTZON, J. F., FINN, A. V. & VIRMANI, R. 2013b. Update on acute coronary syndromes: the pathologists' view. *Eur Heart J,* 34**,** 719-28.

FALK, E., SHAH, P. K. & FUSTER, V. 1995. Coronary plaque disruption. *Circulation,* 92**,** 657-71.

FAYAD, Z. A., MANI, V., WOODWARD, M., KALLEND, D., ABT, M., BURGESS, T., FUSTER, V., BALLANTYNE, C. M., STEIN, E. A., TARDIF, J. C., RUDD, J. H., FARKOUH, M. E. & TAWAKOL, A. 2011a. Safety and efficacy of dalcetrapib on atherosclerotic disease using novel non-invasive multimodality imaging (dal-PLAQUE): a randomised clinical trial. *Lancet,* 378**,** 1547-59.

FEBBRAIO, M., PODREZ, E. A., SMITH, J. D., HAJJAR, D. P., HAZEN, S. L., HOFF, H. F., SHARMA, K. & SILVERSTEIN, R. L. 2000. Targeted disruption of the class B scavenger receptor CD36 protects against atherosclerotic lesion development in mice. *J Clin Invest,* 105**,** 1049-56.

FERNANDES-ALNEMRI, T., LITWACK, G. & ALNEMRI, E. S. 1994. CPP32, a novel human apoptotic protein with homology to Caenorhabditis elegans cell death protein Ced-3 and mammalian interleukin-1 beta-converting enzyme. *The Journal of biological chemistry,* 269**,** 30761-4.

FINN, A. V., NAKANO, M., NARULA, J., KOLODGIE, F. D. & VIRMANI, R. 2010. Concept of vulnerable/unstable plaque. *Arteriosclerosis, thrombosis, and vascular biology,* 30**,** 1282-92.

FOLCO, E. J., SHEIKINE, Y., ROCHA, V. Z., CHRISTEN, T., SHVARTZ, E., SUKHOVA, G. K., DI CARLI, M. F. & LIBBY, P. 2011. Hypoxia but not inflammation augments glucose uptake in human macrophages: Implications for imaging atherosclerosis with 18fluorine-labeled 2-deoxy-D-glucose positron emission tomography. *Journal of the American College of Cardiology,* 58**,** 603-14.

FONTAINE, V., JACOB, M. P., HOUARD, X., ROSSIGNOL, P., PLISSONNIER, D., ANGLES-CANO, E. & MICHEL, J. B. 2002a. Involvement of the mural thrombus as a site of protease release and activation in human aortic aneurysms. *American Journal of Pathology,* 161**,** 1701.

FONTAINE, V., JACOB, M. P., HOUARD, X., ROSSIGNOL, P., PLISSONNIER, D., ANGLES-CANO, E. & MICHEL, J. B. 2002b. Involvement of the mural thrombus as a site of protease release and activation in human aortic aneurysms. *Am J Pathol,* 161**,** 1701-10.

FOX, K. A., CARRUTHERS, K. F., DUNBAR, D. R., GRAHAM, C., MANNING, J. R., DE RAEDT, H., BUYSSCHAERT, I., LAMBRECHTS, D. & VAN DE WERF, F. 2010. Underestimated and under-recognized: the late consequences of acute coronary syndrome (GRACE UK-Belgian Study). *European Heart Journal,* 31**,** 2755-64.

FOX, K. A., DABBOUS, O. H., GOLDBERG, R. J., PIEPER, K. S., EAGLE, K. A., VAN DE WERF, F., AVEZUM, A., GOODMAN, S. G., FLATHER, M. D., ANDERSON, F. A., JR. & GRANGER, C. B. 2006. Prediction of risk of death and myocardial infarction in the six months after presentation with acute coronary syndrome: prospective multinational observational study (GRACE). *Bmj,* 333**,** 1091.

FOX, K. A., STEG, P., EAGLE, K. A. & ET AL. 2007. DEcline in rates of death and heart failure in acute coronary syndromes, 1999-2006. *JAMA : the journal of the American Medical Association,* 297**,** 1892-1900.

FROST, M. L., FOGELMAN, I., BLAKE, G. M., MARSDEN, P. K. & COOK, G., JR. 2004. Dissociation between global markers of bone formation and direct measurement of spinal bone formation in osteoporosis. *Journal of bone and mineral research : the official journal of the American Society for Bone and Mineral Research,* 19**,** 1797-804.

FUJII, K., KOBAYASHI, Y., MINTZ, G. S., TAKEBAYASHI, H., DANGAS, G., MOUSSA, I., MEHRAN, R., LANSKY, A. J., KREPS, E., COLLINS, M., COLOMBO, A., STONE, G. W., LEON, M. B. & MOSES, J. W. 2003. Intravascular ultrasound assessment of ulcerated ruptured plaques: a comparison of culprit and nonculprit lesions of patients with acute coronary syndromes and lesions in patients without acute coronary syndromes. *Circulation,* 108**,** 2473-8.

GAEMPERLI, O., SHALHOUB, J., OWEN, D. R., LAMARE, F., JOHANSSON, S., FOULADI, N., DAVIES, A. H., RIMOLDI, O. E. & CAMICI, P. G. 2012. Imaging intraplaque inflammation in carotid atherosclerosis with 11C-PK11195 positron emission tomography/computed tomography. *Eur Heart J,* 33**,** 1902-10.

GARCIA-GARCIA, H. M., JANG, I. K., SERRUYS, P. W., KOVACIC, J. C., NARULA, J. & FAYAD, Z. A. 2014. Imaging plaques to predict and better manage patients with acute coronary events. *Circ Res,* 114**,** 1904-17.

GARCIA-GARCIA, H. M., MINTZ, G. S., LERMAN, A., VINCE, D. G., MARGOLIS, M. P., VAN ES, G. A., MOREL, M. A., NAIR, A., VIRMANI, R., BURKE, A. P., STONE, G. W. & SERRUYS, P. W. 2009b. Tissue characterisation using intravascular radiofrequency data analysis: recommendations for acquisition, analysis, interpretation and reporting. *EuroIntervention,* 5**,** 177-89.

GEORGE, R. T. 2012. 18F-sodium fluoride positron emission tomography: an in vivo window into coronary atherosclerotic plaque biology. *J Am Coll Cardiol,* 59**,** 1549-50.

GETZ, G. S. 2000. When is atherosclerosis not atherosclerosis? *Arterioscler Thromb Vasc Biol,* 20**,** 1694.

GIMBRONE, M. A., JR. 1999. Vascular endothelium, hemodynamic forces, and atherogenesis. *Am J Pathol,* 155**,** 1-5.

GOLDSTEIN, J. A., DEMETRIOU, D., GRINES, C. L., PICA, M., SHOUKFEH, M. & O'NEILL, W. W. 2000. Multiple complex coronary plaques in patients with acute myocardial infarction. *The New England journal of medicine,* 343**,** 915-22.

GOLDSTEIN, J. L., HO, Y. K., BASU, S. K. & BROWN, M. S. 1979. Binding site on macrophages that mediates uptake and degradation of acetylated low density lipoprotein, producing massive cholesterol deposition. *Proc Natl Acad Sci U S A,* 76**,** 333-7.

GOLESTANI, R. & SADEGHI, M. M. 2014. Emergence of molecular imaging of aortic aneurysm: implications for risk stratification and management. *J Nucl Cardiol,* 21**,** 251-67; quiz 268-70.

GOLLEDGE, J., MULLER, J., DAUGHERTY, A. & NORMAN, P. 2006a. Abdominal aortic aneurysm: pathogenesis and implications for management. *Arteriosclerosis, Thrombosis, and Vascular Biology,* 26**,** 2605-13.

GOLLEDGE, J., MULLER, J., DAUGHERTY, A. & NORMAN, P. 2006b. Abdominal aortic aneurysm: pathogenesis and implications for management. *Arteriosclerosis, thrombosis, and vascular biology,* 26**,** 2605.

GOLLEDGE, J. & NORMAN, P. E. 2009. Pathophysiology of abdominal aortic aneurysm relevant to improvements in patients' management. *Current Opinion in Cardiology,* 24**,** 532.

GOLLEDGE, J. & NORMAN, P. E. 2010. Atherosclerosis and Abdominal Aortic Aneurysm: Cause, Response, or Common Risk Factors? *Arteriosclerosis, thrombosis, and vascular biology,* 30**,** 1075.

GOLLEDGE, J., WOLANSKI, P., PARR, A. & BUTTNER, P. 2008. Measurement and determinants of infrarenal aortic thrombus volume. *Eur Radiol,* 18**,** 1987-94.

GOLUB, E. E. 2011. Biomineralization and matrix vesicles in biology and pathology. *Seminars in immunopathology,* 33**,** 409-17.

GREENLAND, P., LABREE, L., AZEN, S. P., DOHERTY, T. M. & DETRANO, R. C. 2004. Coronary artery calcium score combined with Framingham score for risk prediction in asymptomatic individuals. *JAMA,* 291**,** 210-5.

HACKETT, D., DAVIES, G. & MASERI, A. 1988. Pre-existing coronary stenoses in patients with first myocardial infarction are not necessarily severe. *Eur Heart J,* 9**,** 1317-23.

HAGENAARS, T., GUSSENHOVEN, E. J., VAN ESSEN, J. A., SEELEN, J., HONKOOP, J. & VAN DER LUGT, A. 2000. Reproducibility of volumetric quantification in intravascular ultrasound images. *Ultrasound Med Biol,* 26**,** 367-74.

HAN, Y., JING, J., TU, S., TIAN, F., XUE, H., CHEN, W., CHEN, J., REIBER, J. H. & CHEN, Y. 2014. ST elevation acute myocardial infarction accelerates non-culprit coronary lesion atherosclerosis. *Int J Cardiovasc Imaging,* 30**,** 253-61.

HANSSON, G. K. 2005. Inflammation, atherosclerosis, and coronary artery disease. *N Engl J Med,* 352**,** 1685-95.

HARISINGHANI, M., ROSS, R. W., GUIMARAES, A. R. & WEISSLEDER, R. 2007. Utility of a new bolus-injectable nanoparticle for clinical cancer staging. *Neoplasia,* 9**,** 1160-5.

HARISINGHANI, M. G., BARENTSZ, J., HAHN, P. F., DESERNO, W. M., TABATABAEI, S., VAN DE KAA, C. H., DE LA ROSETTE, J. & WEISSLEDER, R. 2003. Noninvasive detection of clinically occult lymph-node metastases in prostate cancer. *N Engl J Med,* 348**,** 2491-9.

HAWKINS, R. A., CHOI, Y., HUANG, S. C., HOH, C. K., DAHLBOM, M., SCHIEPERS, C., SATYAMURTHY, N., BARRIO, J. R. & PHELPS, M. E. 1992. Evaluation of the skeletal kinetics of fluorine-18-fluoride ion with PET. *Journal of nuclear medicine : official publication, Society of Nuclear Medicine,* 33**,** 633-42.

HEESAKKERS, R. A., HOVELS, A. M., JAGER, G. J., VAN DEN BOSCH, H. C., WITJES, J. A., RAAT, H. P., SEVERENS, J. L., ADANG, E. M., VAN DER KAA, C. H., FUTTERER, J. J. & BARENTSZ, J. 2008. MRI with a lymph-node-specific contrast agent as an alternative to CT scan and lymph-node dissection in patients with prostate cancer: a prospective multicohort study. *Lancet Oncol,* 9**,** 850-6.

HELLENTHAL, F. A., BUURMAN, W. A., WODZIG, W. K. & SCHURINK, G. W. 2009. Biomarkers of AAA progression. Part 1: extracellular matrix degeneration. *Nat Rev Cardiol,* 6**,** 464-74.

HERBORN, C. U., VOGT, F. M., LAUENSTEIN, T. C., DIRSCH, O., COROT, C., ROBERT, P. & RUEHM, S. G. 2006. Magnetic resonance imaging of experimental atherosclerotic plaque: comparison of two ultrasmall superparamagnetic particles of iron oxide. *J Magn Reson Imaging,* 24**,** 388-93.

HETZEL, M., ARSLANDEMIR, C., KONIG, H. H., BUCK, A. K., NUSSLE, K., GLATTING, G., GABELMANN, A., HETZEL, J., HOMBACH, V. & SCHIRRMEISTER, H. 2003. F-18 NaF PET for detection of bone metastases in lung cancer: accuracy, cost-effectiveness, and impact on patient management. *Journal of bone and mineral research : the official journal of the American Society for Bone and Mineral Research,* 18**,** 2206-14.

HINNEN, J. W., KONING, O. H., VISSER, M. J. & VAN BOCKEL, H. J. 2005. Effect of intraluminal thrombus on pressure transmission in the abdominal aortic aneurysm. *J Vasc Surg,* 42**,** 1176-82.

HOH, C. K., HAWKINS, R. A., DAHLBOM, M., GLASPY, J. A., SEEGER, L. L., CHOI, Y., SCHIEPERS, C. W., HUANG, S. C., SATYAMURTHY, N., BARRIO, J. R. & ET AL. 1993. Whole body skeletal imaging with [18F]fluoride ion and PET. *Journal of computer assisted tomography,* 17**,** 34-41.

HOUARD, X., LECLERCQ, A., FONTAINE, V., COUTARD, M., MARTIN-VENTURA, J. L., HO-TIN-NOÈ, B., TOUAT, Z., MEILHAC, O. & MICHEL, J. B. 2006. Retention and Activation of Blood-Borne Proteases in the Arterial Wall:: Implications for Atherothrombosis. *Journal of the American College of Cardiology,* 48**,** A3-A9.

HOUARD, X., ROUZET, F., TOUAT, Z., PHILIPPE, M., DOMINGUEZ, M., FONTAINE, V., SARDA MANTEL, L., MEULEMANS, A., LE GULUDEC, D. & MEILHAC, O. 2007. Topology of the fibrinolytic system within the mural thrombus of human abdominal aortic aneurysms. *The Journal of Pathology,* 212**,** 20-28.

HSU, W. K., FEELEY, B. T., KRENEK, L., STOUT, D. B., CHATZIIOANNOU, A. F. & LIEBERMAN, J. R. 2007. The use of 18F-fluoride and 18F-FDG PET scans to assess fracture healing in a rat femur model. *European journal of nuclear medicine and molecular imaging,* 34**,** 1291-301.

IDELEVICH, A., RAIS, Y. & MONSONEGO-ORNAN, E. 2011. Bone Gla protein increases HIF-1alpha-dependent glucose metabolism and induces cartilage and vascular calcification. *Arteriosclerosis, thrombosis, and vascular biology,* 31**,** e55-71.

INSTALLE, J., NZEUSSEU, A., BOL, A., DEPRESSEUX, G., DEVOGELAER, J. P. & LONNEUX, M. 2005. (18)F-fluoride PET for monitoring therapeutic response in Paget's disease of bone. *Journal of nuclear medicine : official publication, Society of Nuclear Medicine,* 46**,** 1650-8.

INVESTIGATORS, S.-H. 2015. CT coronary angiography in patients with suspected angina due to coronary heart disease (SCOT-HEART): an open-label, parallel-group, multicentre trial. *Lancet*.

IOANNIDIS, J. P. & KATRITSIS, D. G. 2007. Percutaneous coronary intervention for late reperfusion after myocardial infarction in stable patients. *American heart journal,* 154**,** 1065-71.

IRKLE, A., VESEY, A. T., LEWIS, D. Y., SKEPPER, J. N., BIRD, J. L., DWECK, M. R., JOSHI, F. R., GALLAGHER, F. A., WARBURTON, E. A., BENNETT, M. R., BRINDLE, K. M., NEWBY, D. E., RUDD, J. H. & DAVENPORT, A. P. 2015. Identifying active vascular microcalcification by (18)F-sodium fluoride positron emission tomography. *Nat Commun,* 6**,** 7495.

JAFFER, F. A., LIBBY, P. & WEISSLEDER, R. 2007. Molecular imaging of cardiovascular disease. *Circulation,* 116**,** 1052-61.

JAFFER, F. A., LIBBY, P. & WEISSLEDER, R. 2009. Optical and multimodality molecular imaging: insights into atherosclerosis. *Arteriosclerosis, thrombosis, and vascular biology,* 29**,** 1017-24.

JANSSEN, T., BANNAS, P., HERRMANN, J., VELDHOEN, S., BUSCH, J. D., TRESZL, A., MUNSTER, S., MESTER, J. & DERLIN, T. 2013. Association of linear (18)F-sodium fluoride accumulation in femoral arteries as a measure of diffuse calcification with cardiovascular risk factors: A PET/CT study. *Journal of nuclear cardiology : official publication of the American Society of Nuclear Cardiology,* 20**,** 569-77.

JOSHI, N. V., VESEY, A. T., WILLIAMS, M. C., SHAH, A. S., CALVERT, P. A., CRAIGHEAD, F. H., YEOH, S. E., WALLACE, W., SALTER, D., FLETCHER, A. M., VAN BEEK, E. J., FLAPAN, A. D., UREN, N. G., BEHAN, M. W., CRUDEN, N. L., MILLS, N. L., FOX, K. A., RUDD, J. H., DWECK, M. R. & NEWBY, D. E. 2013. F-fluoride positron emission tomography for identification of ruptured and high-risk coronary atherosclerotic plaques: a prospective clinical trial. *Lancet*. 383, 705-13.

KAPUSTIN, A. N. & SHANAHAN, C. M. 2011. Osteocalcin: a novel vascular metabolic and osteoinductive factor? *Arteriosclerosis, thrombosis, and vascular biology,* 31**,** 2169-71.

KASCHINA, E., SCHOLZ, H., STECKELINGS, U. M., SOMMERFELD, M., KEMNITZ, U. R., ARTUC, M., SCHMIDT, S. & UNGER, T. 2009. Transition from

atherosclerosis to aortic aneurysm in humans coincides with an increased expression of RAS components. *Atherosclerosis,* 205**,** 396-403.

KATAOKA, Y., WOLSKI, K., UNO, K., PURI, R., TUZCU, E. M., NISSEN, S. E. & NICHOLLS, S. J. 2012. Spotty calcification as a marker of accelerated progression of coronary atherosclerosis: insights from serial intravascular ultrasound. *Journal of the American College of Cardiology,* 59**,** 1592-7.

KATO, K., YONETSU, T., KIM, S. J., XING, L., LEE, H., MCNULTY, I., YEH, R. W., SAKHUJA, R., ZHANG, S., UEMURA, S., YU, B., MIZUNO, K. & JANG, I. K. 2012a. Nonculprit plaques in patients with acute coronary syndromes have more vulnerable features compared with those with non-acute coronary syndromes: a 3-vessel optical coherence tomography study. *Circ Cardiovasc Imaging,* 5**,** 433-40.

KAZI, M., THYBERG, J., RELIGA, P., ROY, J., ERIKSSON, P., HEDIN, U. & SWEDENBORG, J. 2003. Influence of intraluminal thrombus on structural and cellular composition of abdominal aortic aneurysm wall. *Journal of Vascular Surgery,* 38**,** 1283-1292.

KIM, E. J., KIM, S., KANG, D. O. & SEO, H. S. 2014. Metabolic activity of the spleen and bone marrow in patients with acute myocardial infarction evaluated by 18f-fluorodeoxyglucose positron emission tomograpic imaging. *Circ Cardiovasc Imaging,* 7**,** 454-60.

KOCKX, M. M. & HERMAN, A. G. 2000. Apoptosis in atherosclerosis: beneficial or detrimental? *Cardiovascular research,* 45**,** 736-46.

KOLODGIE, F. D., BURKE, A. P., FARB, A., GOLD, H. K., YUAN, J., NARULA, J., FINN, A. V. & VIRMANI, R. 2001. The thin-cap fibroatheroma: a type of vulnerable plaque: the major precursor lesion to acute coronary syndromes. *Curr Opin Cardiol,* 16**,** 285-92.

KOLODGIE, F. D., BURKE, A. P., NAKAZAWA, G. & VIRMANI, R. 2007. Is pathologic intimal thickening the key to understanding early plaque progression in human atherosclerotic disease? *Arterioscler Thromb Vasc Biol,* 27**,** 986-9.

KOOI, M. E., CAPPENDIJK, V. C., CLEUTJENS, K. B., KESSELS, A. G., KITSLAAR, P. J., BORGERS, M., FREDERIK, P. M., DAEMEN, M. J. & VAN ENGELSHOVEN, J. M. 2003a. Accumulation of ultrasmall superparamagnetic particles of iron oxide in human atherosclerotic plaques can be detected by in vivo magnetic resonance imaging. *Circulation,* 107**,** 2453-8.

KOOI, M. E., CAPPENDIJK, V. C., CLEUTJENS, K. B. J. M., KESSELS, A. G. H., KITSLAAR, P. J. E. H. M., BORGERS, M., FREDERIK, P. M., DAEMEN, M. J. A. P. & VAN ENGELSHOVEN, J. M. A. 2003b. Accumulation of ultrasmall superparamagnetic particles of iron oxide in human atherosclerotic plaques can be detected by in vivo magnetic resonance imaging. *Circulation,* 107**,** 2453-8.

KOTANI, J., MINTZ, G. S., CASTAGNA, M. T., PINNOW, E., BERZINGI, C. O., BUI, A. B., PICHARD, A. D., SATLER, L. F., SUDDATH, W. O., WAKSMAN, R., LAIRD, J. R., JR., KENT, K. M. & WEISSMAN, N. J. 2003. Intravascular

ultrasound analysis of infarct-related and non-infarct-related arteries in patients who presented with an acute myocardial infarction. *Circulation,* 107**,** 2889-93.

KOTZE, C. W., GROVES, A. M., MENEZES, L. J., HARVEY, R., ENDOZO, R., KAYANI, I. A., ELL, P. J. & YUSUF, S. W. 2011a. What is the relationship between (1)(8)F-FDG aortic aneurysm uptake on PET/CT and future growth rate? *Eur J Nucl Med Mol Imaging,* 38**,** 1493-9.

LAITINEN, I., MARJAMAKI, P., NAGREN, K., LAINE, V. J., WILSON, I., LEPPANEN, P., YLA-HERTTUALA, S., ROIVAINEN, A. & KNUUTI, J. 2009. Uptake of inflammatory cell marker [11C]PK11195 into mouse atherosclerotic plaques. *Eur J Nucl Med Mol Imaging,* 36**,** 73-80.

LARDINOIS, D., WEDER, W., HANY, T. F., KAMEL, E. M., KOROM, S., SEIFERT, B., VON SCHULTHESS, G. K. & STEINERT, H. C. 2003. Staging of non-small-cell lung cancer with integrated positron-emission tomography and computed tomography. *The New England journal of medicine,* 348**,** 2500-7.

LEDERLE, F. A., WILSON, S. E., JOHNSON, G. R., REINKE, D. B., LITTOOY, F. N., ACHER, C. W., BALLARD, D. J., MESSINA, L. M., GORDON, I. L., CHUTE, E. P., KRUPSKI, W. C., BUSUTTIL, S. J., BARONE, G. W., SPARKS, S., GRAHAM, L. M., RAPP, J. H., MAKAROUN, M. S., MONETA, G. L., CAMBRIA, R. A., MAKHOUL, R. G., ETON, D., ANSEL, H. J., FREISCHLAG, J. A. & BANDYK, D. 2002. Immediate repair compared with surveillance of small abdominal aortic aneurysms. *N Engl J Med,* 346**,** 1437-44.

LI, W., SALANITRI, J., TUTTON, S., DUNKLE, E. E., SCHNEIDER, J. R., CAPRINI, J. A., PIERCHALA, L. N., JACOBS, P. M. & EDELMAN, R. R. 2007. Lower extremity deep venous thrombosis: evaluation with ferumoxytol-enhanced MR imaging and dual-contrast mechanism--preliminary experience. *Radiology,* 242**,** 873-81.

LI, W., TUTTON, S., VU, A. T., PIERCHALA, L., LI, B. S. Y., LEWIS, J. M., PRASAD, P. V. & EDELMAN, R. R. 2005. First-pass contrast-enhanced magnetic resonance angiography in humans using ferumoxytol, a novel ultrasmall superparamagnetic iron oxide (USPIO)-based blood pool agent. *J Magn Reson Imaging,* 21**,** 46-52.

LI, X., BAUER, W., KREISSL, M. C., WEIRATHER, J., BAUER, E., ISRAEL, I., RICHTER, D., RIEHL, G., BUCK, A. & SAMNICK, S. 2013. Specific somatostatin receptor II expression in arterial plaque: (68)Ga-DOTATATE autoradiographic, immunohistochemical and flow cytometric studies in apoE-deficient mice. *Atherosclerosis,* 230**,** 33-9.

LI, X., SAMNICK, S., LAPA, C., ISRAEL, I., BUCK, A. K., KREISSL, M. C. & BAUER, W. 2012a. 68Ga-DOTATATE PET/CT for the detection of inflammation of large arteries: correlation with18F-FDG, calcium burden and risk factors. *EJNMMI Res,* 2**,** 52.

LI, Y., BERENJI, G. R., SHABA, W. F., TAFTI, B., YEVDAYEV, E. & DADPARVAR, S. 2012b. Association of vascular fluoride uptake with vascular calcification and coronary artery disease. *Nuclear medicine communications,* 33**,** 14-20.

LIBBY, P. 2013. Mechanisms of acute coronary syndromes and their implications for therapy. *The New England journal of medicine,* 368**,** 2004-13.

LIBBY, P. & AIKAWA, M. 2002. Stabilization of atherosclerotic plaques: new mechanisms and clinical targets. *Nat Med,* 8**,** 1257-62.

LIBBY, P., DICARLI, M. & WEISSLEDER, R. 2010. The vascular biology of atherosclerosis and imaging targets. *Journal of nuclear medicine : official publication, Society of Nuclear Medicine,* 51 Suppl 1**,** 33S-37S.

LINDHOLT, J. S. 2008. Aneurysmal wall calcification predicts natural history of small abdominal aortic aneurysms. *Atherosclerosis,* 197**,** 673-8.

LITTLEWOOD, T. D. & BENNETT, M. R. 2003. Apoptotic cell death in atherosclerosis. *Curr Opin Lipidol,* 14**,** 469-75.

LOZANO, R., NAGHAVI, M., FOREMAN, K., LIM, S., SHIBUYA, K., ABOYANS, V., ABRAHAM, J., ADAIR, T., AGGARWAL, R., AHN, S. Y., ALVARADO, M., ANDERSON, H. R., ANDERSON, L. M., ANDREWS, K. G., ATKINSON, C., BADDOUR, L. M., BARKER-COLLO, S., BARTELS, D. H., BELL, M. L., BENJAMIN, E. J., BENNETT, D., BHALLA, K., BIKBOV, B., BIN ABDULHAK, A., BIRBECK, G., BLYTH, F., BOLLIGER, I., BOUFOUS, S., BUCELLO, C., BURCH, M., BURNEY, P., CARAPETIS, J., CHEN, H., CHOU, D., CHUGH, S. S., COFFENG, L. E., COLAN, S. D., COLQUHOUN, S., COLSON, K. E., CONDON, J., CONNOR, M. D., COOPER, L. T., CORRIERE, M., CORTINOVIS, M., DE VACCARO, K. C., COUSER, W., COWIE, B. C., CRIQUI, M. H., CROSS, M., DABHADKAR, K. C., DAHODWALA, N., DE LEO, D., DEGENHARDT, L., DELOSSANTOS, A., DENENBERG, J., DES JARLAIS, D. C., DHARMARATNE, S. D., DORSEY, E. R., DRISCOLL, T., DUBER, H., EBEL, B., ERWIN, P. J., ESPINDOLA, P., EZZATI, M., FEIGIN, V., FLAXMAN, A. D., FOROUZANFAR, M. H., FOWKES, F. G., FRANKLIN, R., FRANSEN, M., FREEMAN, M. K., GABRIEL, S. E., GAKIDOU, E., GASPARI, F., GILLUM, R. F., GONZALEZ-MEDINA, D., HALASA, Y. A., HARING, D., HARRISON, J. E., HAVMOELLER, R., HAY, R. J., HOEN, B., HOTEZ, P. J., HOY, D., JACOBSEN, K. H., JAMES, S. L., JASRASARIA, R., JAYARAMAN, S., JOHNS, N., KARTHIKEYAN, G., KASSEBAUM, N., KEREN, A., KHOO, J. P., KNOWLTON, L. M., KOBUSINGYE, O., KORANTENG, A., KRISHNAMURTHI, R., LIPNICK, M., LIPSHULTZ, S. E., OHNO, S. L., et al. 2012. Global and regional mortality from 235 causes of death for 20 age groups in 1990 and 2010: a systematic analysis for the Global Burden of Disease Study 2010. *Lancet,* 380**,** 2095-128.

MAKI-PETAJA, K. M., ELKHAWAD, M., CHERIYAN, J., JOSHI, F. R., OSTOR, A. J., HALL, F. C., RUDD, J. H. & WILKINSON, I. B. 2012. Anti-tumor necrosis factor-alpha therapy reduces aortic inflammation and stiffness in patients with rheumatoid arthritis. *Circulation,* 126**,** 2473-80.

MAKITA, S., OHIRA, A., TACHIEDA, R., ITOH, S., MORIAI, Y., NIINUMA, H., NAKAMURA, M. & HIRAMORI, K. 2000. Dilation and reduced distensibility of carotid artery in patients with abdominal aortic aneurysms. *Am Heart J,* 140**,** 297-302.

MANN, J. & DAVIES, M. J. 1999. Mechanisms of progression in native coronary artery disease: role of healed plaque disruption. *Heart,* 82**,** 265-8.

MARINI, C., MORBELLI, S., ARMONINO, R., SPINELLA, G., RIONDATO, M., MASSOLLO, M., SAROCCHI, F., PANE, B., AUGERI, C., ABETE, L., GHIGLIOTTI, G., PALMIERI, D., FIZ, F., CITTADINI, G., FULCHERI, E., PALOMBO, D. & SAMBUCETI, G. 2012. Direct relationship between cell density and FDG uptake in asymptomatic aortic aneurysm close to surgical threshold: an in vivo and in vitro study. *Eur J Nucl Med Mol Imaging,* 39**,** 91-101.

MATEO, J., IZQUIERDO-GARCIA, D., BADIMON, J. J., FAYAD, Z. A. & FUSTER, V. 2014. Noninvasive assessment of hypoxia in rabbit advanced atherosclerosis using (1)(8)F-fluoromisonidazole positron emission tomographic imaging. *Circ Cardiovasc Imaging,* 7**,** 312-20.

MAURIELLO, A., SERVADEI, F., ZOCCAI, G. B., GIACOBBI, E., ANEMONA, L., BONANNO, E. & CASELLA, S. 2013. Coronary calcification identifies the vulnerable patient rather than the vulnerable Plaque. *Atherosclerosis,* 229**,** 124-9.

MAUROVICH-HORVAT, P., HOFFMANN, U., VORPAHL, M., NAKANO, M., VIRMANI, R. & ALKADHI, H. 2010. The napkin-ring sign: CT signature of high-risk coronary plaques? *JACC Cardiovasc Imaging,* 3**,** 440-4.

MCEVOY, J. W., BLAHA, M. J., DEFILIPPIS, A. P., BUDOFF, M. J., NASIR, K., BLUMENTHAL, R. S. & JONES, S. R. 2010. Coronary artery calcium progression: an important clinical measurement? A review of published reports. *Journal of the American College of Cardiology,* 56**,** 1613-22.

MCGILL, H. C., JR., MCMAHAN, C. A., ZIESKE, A. W., SLOOP, G. D., WALCOTT, J. V., TROXCLAIR, D. A., MALCOM, G. T., TRACY, R. E., OALMANN, M. C. & STRONG, J. P. 2000. Associations of coronary heart disease risk factors with the intermediate lesion of atherosclerosis in youth. The Pathobiological Determinants of Atherosclerosis in Youth (PDAY) Research Group. *Arterioscler Thromb Vasc Biol,* 20**,** 1998-2004.

MEARNS, B. M. 2014. Coronary artery disease: noninvasive imaging technique can identify high-risk coronary plaques. *Nat Rev Cardiol,* 11**,** 2.

MESSA, C., GOODMAN, W. G., HOH, C. K., CHOI, Y., NISSENSON, A. R., SALUSKY, I. B., PHELPS, M. E. & HAWKINS, R. A. 1993. Bone metabolic activity measured with positron emission tomography and [18F]fluoride ion in renal osteodystrophy: correlation with bone histomorphometry. *The Journal of clinical endocrinology and metabolism,* 77**,** 949-55.

MILLON, A., DICKSON, S. D., KLINK, A., IZQUIERDO-GARCIA, D., BINI, J., LANCELOT, E., BALLET, S., ROBERT, P., MATEO DE CASTRO, J., COROT, C. & FAYAD, Z. A. 2013. Monitoring plaque inflammation in atherosclerotic rabbits with an iron oxide (P904) and (18)F-FDG using a combined PET/MR scanner. *Atherosclerosis,* 228**,** 339-45.

MILONAS, C., JERNBERG, T., LINDBACK, J., AGEWALL, S., WALLENTIN, L. & STENESTRAND, U. 2010. Effect of Angiotensin-converting enzyme inhibition on

one-year mortality and frequency of repeat acute myocardial infarction in patients with acute myocardial infarction. *The American journal of cardiology,* 105**,** 1229-34.

MINTZ, G. S., NISSEN, S. E., ANDERSON, W. D., BAILEY, S. R., ERBEL, R., FITZGERALD, P. J., PINTO, F. J., ROSENFIELD, K., SIEGEL, R. J., TUZCU, E. M. & YOCK, P. G. 2001. American College of Cardiology Clinical Expert Consensus Document on Standards for Acquisition, Measurement and Reporting of Intravascular Ultrasound Studies (IVUS). A report of the American College of Cardiology Task Force on Clinical Expert Consensus Documents. *Journal of the American College of Cardiology,* 37**,** 1478-92.

MOJTAHEDI, A., ALAVI, A., THAMAKE, S., AMERINIA, R., RANGANATHAN, D., TWOROWSKA, I. & DELPASSAND, E. S. 2015. Assessment of vulnerable atherosclerotic and fibrotic plaques in coronary arteries using (68)Ga-DOTATATE PET/CT. *Am J Nucl Med Mol Imaging,* 5**,** 65-71.

MOOE, T., ERIKSSON, P. & STEGMAYR, B. 1997. Ischemic stroke after acute myocardial infarction. A population-based study. *Stroke; a journal of cerebral circulation,* 28**,** 762-7.

MOORE, K. J. & TABAS, I. 2011. Macrophages in the pathogenesis of atherosclerosis. *Cell,* 145**,** 341-55.

MOREL, O., MANDRY, D., MICARD, E., KAUFFMANN, C., LAMIRAL, Z., VERGER, A., CHEVALIER-MATHIAS, E., MATHIAS, J., KARCHER, G., MENEROUX, B., ROSSIGNOL, P. & MARIE, P. Y. 2015. Evidence of Cyclic Changes in the Metabolism of Abdominal Aortic Aneurysms During Growth Phases: 18F-FDG PET Sequential Observational Study. *J Nucl Med,* 56**,** 1030-5.

MORISHIGE, K., KACHER, D. F., LIBBY, P., JOSEPHSON, L., GANZ, P., WEISSLEDER, R. & AIKAWA, M. 2010. High-resolution magnetic resonance imaging enhanced with superparamagnetic nanoparticles measures macrophage burden in atherosclerosis. *Circulation,* 122**,** 1707-15.

MOSSER, D. M. & EDWARDS, J. P. 2008. Exploring the full spectrum of macrophage activation. *Nat Rev Immunol,* 8**,** 958-69.

MOTOYAMA, S., KONDO, T., SARAI, M., SUGIURA, A., HARIGAYA, H., SATO, T., INOUE, K., OKUMURA, M., ISHII, J., ANNO, H., VIRMANI, R., OZAKI, Y., HISHIDA, H. & NARULA, J. 2007. Multislice computed tomographic characteristics of coronary lesions in acute coronary syndromes. *Journal of the American College of Cardiology,* 50**,** 319-26.

MOTOYAMA, S., SARAI, M., HARIGAYA, H., ANNO, H., INOUE, K., HARA, T., NARUSE, H., ISHII, J., HISHIDA, H., WONG, N. D., VIRMANI, R., KONDO, T., OZAKI, Y. & NARULA, J. 2009a. Computed tomographic angiography characteristics of atherosclerotic plaques subsequently resulting in acute coronary syndrome. *J Am Coll Cardiol,* 54**,** 49-57.

MOZAFFARIAN, D., BENJAMIN, E. J., GO, A. S., ARNETT, D. K., BLAHA, M. J., CUSHMAN, M., DE FERRANTI, S., DESPRES, J., FULLERTON, H. J., HOWARD, V. J., HUFFMAN, M. D., JUDD, S. E., KISSELA, B. M.,

LACKLAND, D. T., LICHTMAN, J. H., LISABETH, L. D., LIU, S., MACKEY, R. H., MATCHAR, D. B., MCGUIRE, D. K., MOHLER, E. R., 3RD, MOY, C. S., MUNTNER, P., MUSSOLINO, M. E., NASIR, K., NEUMAR, R. W., NICHOL, G., PALANIAPPAN, L., PANDEY, D. K., REEVES, M. J., RODRIGUEZ, C. J., SORLIE, P. D., STEIN, J., TOWFIGHI, A., TURAN, T. N., VIRANI, S. S., WILLEY, J. Z., WOO, D., YEH, R. W. & TURNER, M. B. 2014. Heart Disease and Stroke Statistics-2015 Update: A Report From the American Heart Association. *Circulation*.

MULLER, J. E., TOFLER, G. H. & STONE, P. H. 1989. Circadian variation and triggers of onset of acute cardiovascular disease. *Circulation,* 79**,** 733-43.

MULLER, K., SKEPPER, J. N., POSFAI, M., TRIVEDI, R., HOWARTH, S., COROT, C., LANCELOT, E., THOMPSON, P. W., BROWN, A. P. & GILLARD, J. H. 2007. Effect of ultrasmall superparamagnetic iron oxide nanoparticles (Ferumoxtran-10) on human monocyte-macrophages in vitro. *Biomaterials,* 28**,** 1629-42.

MURRAY, S. W., STABLES, R. H., HART, G. & PALMER, N. D. 2013. Defining the magnitude of measurement variability in the virtual histology analysis of acute coronary syndrome plaques. *European heart journal cardiovascular Imaging,* 14**,** 167-74.

NAGHAVI, M., LIBBY, P., FALK, E., CASSCELLS, S. W., LITOVSKY, S., RUMBERGER, J., BADIMON, J. J., STEFANADIS, C., MORENO, P., PASTERKAMP, G., FAYAD, Z., STONE, P. H., WAXMAN, S., RAGGI, P., MADJID, M., ZARRABI, A., BURKE, A., YUAN, C., FITZGERALD, P. J., SISCOVICK, D. S., DE KORTE, C. L., AIKAWA, M., JUHANI AIRAKSINEN, K. E., ASSMANN, G., BECKER, C. R., CHESEBRO, J. H., FARB, A., GALIS, Z. S., JACKSON, C., JANG, I. K., KOENIG, W., LODDER, R. A., MARCH, K., DEMIROVIC, J., NAVAB, M., PRIORI, S. G., REKHTER, M. D., BAHR, R., GRUNDY, S. M., MEHRAN, R., COLOMBO, A., BOERWINKLE, E., BALLANTYNE, C., INSULL, W., JR., SCHWARTZ, R. S., VOGEL, R., SERRUYS, P. W., HANSSON, G. K., FAXON, D. P., KAUL, S., DREXLER, H., GREENLAND, P., MULLER, J. E., VIRMANI, R., RIDKER, P. M., ZIPES, D. P., SHAH, P. K. & WILLERSON, J. T. 2003. From vulnerable plaque to vulnerable patient: a call for new definitions and risk assessment strategies: Part I. *Circulation,* 108**,** 1664-72.

NAHRENDORF, M., JAFFER, F. A., KELLY, K. A., SOSNOVIK, D. E., AIKAWA, E., LIBBY, P. & WEISSLEDER, R. 2006. Noninvasive vascular cell adhesion molecule-1 imaging identifies inflammatory activation of cells in atherosclerosis. *Circulation,* 114**,** 1504-11.

NAHRENDORF, M., KELIHER, E., MARINELLI, B., LEUSCHNER, F., ROBBINS, C. S., GERSZTEN, R. E., PITTET, M. J., SWIRSKI, F. K. & WEISSLEDER, R. 2011. Detection of macrophages in aortic aneurysms by nanoparticle positron emission tomography-computed tomography. *Arteriosclerosis, thrombosis, and vascular biology,* 31**,** 750-7.

NARULA, J., NAKANO, M., VIRMANI, R., KOLODGIE, F. D., PETERSEN, R., NEWCOMB, R., MALIK, S., FUSTER, V. & FINN, A. V. 2013. Histopathologic characteristics of atherosclerotic coronary disease and implications of the findings

for the invasive and noninvasive detection of vulnerable plaques. *J Am Coll Cardiol,* 61**,** 1041-51.

NCHIMI, A., CHERAMY-BIEN, J. P., GASSER, T. C., NAMUR, G., GOMEZ, P., SEIDEL, L., ALBERT, A., DEFRAIGNE, J. O., LABROPOULOS, N. & SAKALIHASAN, N. 2014. Multifactorial relationship between 18F-fluoro-deoxy-glucose positron emission tomography signaling and biomechanical properties in unruptured aortic aneurysms. *Circ Cardiovasc Imaging,* 7**,** 82-91.

NCHIMI, A., DEFAWE, O., BRISBOIS, D., BROUSSAUD, T. K., DEFRAIGNE, J. O., MAGOTTEAUX, P., MASSART, B., SERFATY, J. M., HOUARD, X., MICHEL, J. B. & SAKALIHASAN, N. 2010. MR imaging of iron phagocytosis in intraluminal thrombi of abdominal aortic aneurysms in humans. *Radiology,* 254**,** 973-81.

NEUWELT, E. A., VÁRALLYAY, C. G., MANNINGER, S., SOLYMOSI, D., HALUSKA, M., HUNT, M. A., NESBIT, G., STEVENS, A., JEROSCH-HEROLD, M., JACOBS, P. M. & HOFFMAN, J. M. 2007. The potential of ferumoxytol nanoparticle magnetic resonance imaging, perfusion, and angiography in central nervous system malignancy: a pilot study. *Neurosurgery,* 60**,** 601-11; discussion 611-2.

NEW, S. E. & AIKAWA, E. 2011. Molecular imaging insights into early inflammatory stages of arterial and aortic valve calcification. *Circulation research,* 108**,** 1381-91.

NEW, S. E., GOETTSCH, C., AIKAWA, M., MARCHINI, J. F., SHIBASAKI, M., YABUSAKI, K., LIBBY, P., SHANAHAN, C. M., CROCE, K. & AIKAWA, E. 2013a. Macrophage-derived matrix vesicles: an alternative novel mechanism for microcalcification in atherosclerotic plaques. *Circulation research,* 113**,** 72-7.

NORDON, I. M., HINCHLIFFE, R. J., LOFTUS, I. M. & THOMPSON, M. M. 2011. Pathophysiology and epidemiology of abdominal aortic aneurysms. *Nat Rev Cardiol,* 8**,** 92-102.

NORMAN, P. E., JAMROZIK, K., LAWRENCE-BROWN, M. M., LE, M. T. Q., SPENCER, C. A., TUOHY, R. J., PARSONS, R. W. & DICKINSON, J. A. 2004. Population based randomised controlled trial on impact of screening on mortality from abdominal aortic aneurysm. *Bmj,* 329**,** 1259.

NORTH AMERICAN SYMPTOMATIC CAROTID ENDARTERECTOMY TRIAL, C. 1991. Beneficial effect of carotid endarterectomy in symptomatic patients with high-grade carotid stenosis. *N Engl J Med,* 325**,** 445-53.

ONO, K., MATSUMORI, A., SHIOI, T., FURUKAWA, Y. & SASAYAMA, S. 1998. Cytokine gene expression after myocardial infarction in rat hearts: possible implication in left ventricular remodeling. *Circulation,* 98**,** 149-56.

ORN, S., MANHENKE, C., UELAND, T., DAMAS, J. K., MOLLNES, T. E., EDVARDSEN, T., AUKRUST, P. & DICKSTEIN, K. 2009. C-reactive protein, infarct size, microvascular obstruction, and left-ventricular remodelling following acute myocardial infarction. *European Heart Journal,* 30**,** 1180-6.

OTSUKA, F., FINN, A. V. & VIRMANI, R. 2013. Do vulnerable and ruptured plaques hide in heavily calcified arteries? *Atherosclerosis,* 229**,** 34-7.

OTSUKA, F., SAKAKURA, K., YAHAGI, K., JONER, M. & VIRMANI, R. 2014. Has our understanding of calcification in human coronary atherosclerosis progressed? *Arteriosclerosis, thrombosis, and vascular biology,* 34**,** 724-36.

PALOMBO, D., MORBELLI, S., SPINELLA, G., PANE, B., MARINI, C., ROUSAS, N., MASSOLLO, M., CITTADINI, G., CAMELLINO, D. & SAMBUCETI, G. 2012a. A positron emission tomography/computed tomography (PET/CT) evaluation of asymptomatic abdominal aortic aneurysms: another point of view. *Ann Vasc Surg,* 26**,** 491-9.

PALOMBO, D., MORBELLI, S., SPINELLA, G., PANE, B., MARINI, C., ROUSAS, N., MASSOLLO, M., CITTADINI, G., CAMELLINO, D. & SAMBUCETI, G. 2012b. A positron emission tomography/computed tomography (PET/CT) evaluation of asymptomatic abdominal aortic aneurysms: another point of view. *Annals of vascular surgery,* 26**,** 491-9.

PETREN-MALLMIN, M., ANDREASSON, I., LJUNGGREN, O., AHLSTROM, H., BERGH, J., ANTONI, G., LANGSTROM, B. & BERGSTROM, M. 1998. Skeletal metastases from breast cancer: uptake of 18F-fluoride measured with positron emission tomography in correlation with CT. *Skeletal radiology,* 27**,** 72-6.

POWELL, J. T., BROWN, L. C., FORBES, J. F., FOWKES, F. G., GREENHALGH, R. M., RUCKLEY, C. V. & THOMPSON, S. G. 2007. Final 12-year follow-up of surgery versus surveillance in the UK Small Aneurysm Trial. *Br J Surg,* 94**,** 702-8.

POWELL, J. T., BROWN, L. C., GREENHALGH, R. M. & THOMPSON, S. G. 2008. The rupture rate of large abdominal aortic aneurysms: is this modified by anatomical suitability for endovascular repair? *Ann Surg,* 247**,** 173-9.

PRINCE, M. R., ZHANG, H. L., CHABRA, S. G., JACOBS, P. & WANG, Y. 2003. A pilot investigation of new superparamagnetic iron oxide as a contrast agent for cardiovascular MRI. *Journal of X-Ray Science and Technology,* 11**,** 231-240.

PROUDFOOT, D., SKEPPER, J. N., HEGYI, L., BENNETT, M. R., SHANAHAN, C. M. & WEISSBERG, P. L. 2000. Apoptosis regulates human vascular calcification in vitro: evidence for initiation of vascular calcification by apoptotic bodies. *Circulation research,* 87**,** 1055-62.

PUGLIESE, F., GAEMPERLI, O., KINDERLERER, A. R., LAMARE, F., SHALHOUB, J., DAVIES, A. H., RIMOLDI, O. E., MASON, J. C. & CAMICI, P. G. 2010. Imaging of vascular inflammation with [11C]-PK11195 and positron emission tomography/computed tomography angiography. *J Am Coll Cardiol,* 56**,** 653-61.

RADCLIFF, K., TANG, T. B., LIM, J., ZHANG, Z., ABEDIN, M., DEMER, L. L. & TINTUT, Y. 2005. Insulin-like growth factor-I regulates proliferation and osteoblastic differentiation of calcifying vascular cells via extracellular signal-regulated protein kinase and phosphatidylinositol 3-kinase pathways. *Circulation research,* 96**,** 398-400.

RAGGI, P., CALLISTER, T. Q. & SHAW, L. J. 2004a. Progression of coronary artery calcium and risk of first myocardial infarction in patients receiving cholesterol-lowering therapy. *Arterioscler Thromb Vasc Biol,* 24**,** 1272-7.

RAGHAVAN, M. L., VORP, D. A., FEDERLE, M. P., MAKAROUN, M. S. & WEBSTER, M. W. 2000. Wall stress distribution on three-dimensionally reconstructed models of human abdominal aortic aneurysm. *J Vasc Surg,* 31**,** 760-9.

REED, D., REED, C., STEMMERMANN, G. & HAYASHI, T. 1992. Are aortic aneurysms caused by atherosclerosis? *Circulation,* 85**,** 205.

REEPS, C., BUNDSCHUH, R. A., PELLISEK, J., HERZ, M., VAN MARWICK, S., SCHWAIGER, M., ECKSTEIN, H. H., NEKOLLA, S. G. & ESSLER, M. 2013. Quantitative assessment of glucose metabolism in the vessel wall of abdominal aortic aneurysms: correlation with histology and role of partial volume correction. *Int J Cardiovasc Imaging,* 29**,** 505-12.

REEPS, C., ESSLER, M., PELISEK, J., SEIDL, S., ECKSTEIN, H. H. & KRAUSE, B. J. 2008. Increased 18F-fluorodeoxyglucose uptake in abdominal aortic aneurysms in positron emission/computed tomography is associated with inflammation, aortic wall instability, and acute symptoms. *J Vasc Surg,* 48**,** 417-23; discussion 424.

REIVICH, M., KUHL, D., WOLF, A., GREENBERG, J., PHELPS, M., IDO, T., CASELLA, V., FOWLER, J., GALLAGHER, B., HOFFMAN, E., ALAVI, A. & SOKOLOFF, L. 1977. Measurement of local cerebral glucose metabolism in man with 18F-2-fluoro-2-deoxy-d-glucose. *Acta Neurol Scand Suppl,* 64**,** 190-1.

REY, C., COMBES, C., DROUET, C. & GLIMCHER, M. J. 2009. Bone mineral: update on chemical composition and structure. *Osteoporosis international : a journal established as result of cooperation between the European Foundation for Osteoporosis and the National Osteoporosis Foundation of the USA,* 20**,** 1013-21.

RICHARDS, J., SEMPLE, S., GRAY, C., MCKILLOP, G., CHALMERS, R., GARDEN, O. & NEWBY, D. 2010. PS114. Magnetic Resonance Imaging of Abdominal Aortic Aneurysms (AAA) Using Ultrasmall Superparamagnetic Particles of Iron Oxide (USPIO). *Journal of Vascular Surgery,* 51**,** 48S.

.

RICHARDS, J. M., SEMPLE, S. I., MACGILLIVRAY, T. J., GRAY, C., LANGRISH, J. P., WILLIAMS, M., DWECK, M., WALLACE, W., MCKILLOP, G., CHALMERS, R. T., GARDEN, O. J. & NEWBY, D. E. 2011a. Abdominal aortic aneurysm growth predicted by uptake of ultrasmall superparamagnetic particles of iron oxide: a pilot study. *Circ Cardiovasc Imaging,* 4**,** 274-81.

RICHARDS, J. M., SHAW, C. A., LANG, N. N., WILLIAMS, M. C., SEMPLE, S. I., MACGILLIVRAY, T. J., GRAY, C., CRAWFORD, J. H., ALAM, S. R., ATKINSON, A. P., FORREST, E. K., BIENEK, C., MILLS, N. L., BURDESS, A., DHALIWAL, K., SIMPSON, A. J., WALLACE, W. A., HILL, A. T., RODDIE, P. H., MCKILLOP, G., CONNOLLY, T. A., FEUERSTEIN, G. Z., BARCLAY, G. R., TURNER, M. L. & NEWBY, D. E. 2012. In vivo mononuclear cell tracking using

superparamagnetic particles of iron oxide: feasibility and safety in humans. *Circulation. Cardiovascular imaging,* 5**,** 509-17.

RIOUFOL, G., GILARD, M., FINET, G., GINON, I., BOSCHAT, J. & ANDRE-FOUET, X. 2004. Evolution of spontaneous atherosclerotic plaque rupture with medical therapy: long-term follow-up with intravascular ultrasound. *Circulation,* 110**,** 2875-80.

RODRIGUEZ-GRANILLO, G. A., GARCIA-GARCIA, H. M., MC FADDEN, E. P., VALGIMIGLI, M., AOKI, J., DE FEYTER, P. & SERRUYS, P. W. 2005. In vivo intravascular ultrasound-derived thin-cap fibroatheroma detection using ultrasound radiofrequency data analysis. *J Am Coll Cardiol,* 46**,** 2038-42.

ROGER, V. L., GO, A. S., LLOYD-JONES, D. M., ADAMS, R. J., BERRY, J. D., BROWN, T. M., CARNETHON, M. R., DAI, S., DE SIMONE, G., FORD, E. S., FOX, C. S., FULLERTON, H. J., GILLESPIE, C., GREENLUND, K. J., HAILPERN, S. M., HEIT, J. A., HO, P. M., HOWARD, V. J., KISSELA, B. M., KITTNER, S. J., LACKLAND, D. T., LICHTMAN, J. H., LISABETH, L. D., MAKUC, D. M., MARCUS, G. M., MARELLI, A., MATCHAR, D. B., MCDERMOTT, M. M., MEIGS, J. B., MOY, C. S., MOZAFFARIAN, D., MUSSOLINO, M. E., NICHOL, G., PAYNTER, N. P., ROSAMOND, W. D., SORLIE, P. D., STAFFORD, R. S., TURAN, T. N., TURNER, M. B., WONG, N. D. & WYLIE-ROSETT, J. 2011. Heart disease and stroke statistics--2011 update: a report from the American Heart Association. *Circulation,* 123**,** e18-e209.

ROGERS, I. S., NASIR, K., FIGUEROA, A. L., CURY, R. C., HOFFMANN, U., VERMYLEN, D. A., BRADY, T. J. & TAWAKOL, A. 2010. Feasibility of FDG imaging of the coronary arteries: comparison between acute coronary syndrome and stable angina. *JACC. Cardiovascular imaging,* 3**,** 388-97.

ROGERS, I. S. & TAWAKOL, A. 2011. Imaging of coronary inflammation with FDG-PET: feasibility and clinical hurdles. *Current cardiology reports,* 13**,** 138-44.

ROMINGER, A., SAAM, T., VOGL, E., UBLEIS, C., LA FOUGERE, C., FORSTER, S., HAUG, A., CUMMING, P., REISER, M. F., NIKOLAOU, K., BARTENSTEIN, P. & HACKER, M. 2010. In vivo imaging of macrophage activity in the coronary arteries using 68Ga-DOTATATE PET/CT: correlation with coronary calcium burden and risk factors. *J Nucl Med,* 51**,** 193-7.

ROMINGER, A., SAAM, T., WOLPERS, S., CYRAN, C. C., SCHMIDT, M., FOERSTER, S., NIKOLAOU, K., REISER, M. F., BARTENSTEIN, P. & HACKER, M. 2009. 18F-FDG PET/CT identifies patients at risk for future vascular events in an otherwise asymptomatic cohort with neoplastic disease. *Journal of nuclear medicine : official publication, Society of Nuclear Medicine,* 50**,** 1611-20.

RUDD, J. H., MYERS, K. S., BANSILAL, S., MACHAC, J., PINTO, C. A., TONG, C., RAFIQUE, A., HARGEAVES, R., FARKOUH, M., FUSTER, V. & FAYAD, Z. A. 2008. Atherosclerosis inflammation imaging with 18F-FDG PET: carotid, iliac, and femoral uptake reproducibility, quantification methods, and recommendations. *J Nucl Med,* 49**,** 871-8.

RUDD, J. H., MYERS, K. S., BANSILAL, S., MACHAC, J., RAFIQUE, A., FARKOUH, M., FUSTER, V. & FAYAD, Z. A. 2007. (18)Fluorodeoxyglucose positron emission tomography imaging of atherosclerotic plaque inflammation is highly reproducible: implications for atherosclerosis therapy trials. *J Am Coll Cardiol,* 50**,** 892-6.

RUDD, J. H., WARBURTON, E. A., FRYER, T. D., JONES, H. A., CLARK, J. C., ANTOUN, N., JOHNSTROM, P., DAVENPORT, A. P., KIRKPATRICK, P. J., ARCH, B. N., PICKARD, J. D. & WEISSBERG, P. L. 2002. Imaging atherosclerotic plaque inflammation with [18F]-fluorodeoxyglucose positron emission tomography. *Circulation,* 105**,** 2708-11.

RUEHM, S. G., COROT, C., VOGT, P., KOLB, S. & DEBATIN, J. F. 2001. Magnetic resonance imaging of atherosclerotic plaque with ultrasmall superparamagnetic particles of iron oxide in hyperlipidemic rabbits. *Circulation,* 103**,** 415-22.

SADAT, U., TAVIANI, V., PATTERSON, A. J., YOUNG, V. E., GRAVES, M. J., TENG, Z., TANG, T. Y. & GILLARD, J. H. 2011b. Ultrasmall superparamagnetic iron oxide-enhanced magnetic resonance imaging of abdominal aortic aneurysms--a feasibility study. *Eur J Vasc Endovasc Surg,* 41**,** 167-74.

SAKALIHASAN, N., DELVENNE, P., NUSGENS, B. V., LIMET, R. & LAPIËRE, C. M. 1996. Activated forms of MMP2 and MMP9 in abdominal aortic aneurysms. *Journal of Vascular Surgery,* 24**,** 127-133.

SAKALIHASAN, N., HUSTINX, R. & LIMET, R. 2004. Contribution of PET scanning to the evaluation of abdominal aortic aneurysm. *Semin Vasc Surg,* 17**,** 144-53.

SAKALIHASAN, N., LIMET, R. & DEFAWE, O. 2005. Abdominal aortic aneurysm. *The Lancet,* 365**,** 1577-1589.

SAKALIHASAN, N., VAN DAMME, H., GOMEZ, P., RIGO, P., LAPIERE, C. M., NUSGENS, B. & LIMET, R. 2002. Positron emission tomography (PET) evaluation of abdominal aortic aneurysm (AAA). *Eur J Vasc Endovasc Surg,* 23**,** 431-6.

SANTOS, R. D., RUMBERGER, J. A., BUDOFF, M. J., SHAW, L. J., ORAKZAI, S. H., BERMAN, D., RAGGI, P., BLUMENTHAL, R. S. & NASIR, K. 2010. Thoracic aorta calcification detected by electron beam tomography predicts all-cause mortality. *Atherosclerosis,* 209**,** 131-5.

SATOMI, T., OGAWA, M., MORI, I., ISHINO, S., KUBO, K., MAGATA, Y. & NISHIMOTO, T. 2013a. Comparison of contrast agents for atherosclerosis imaging using cultured macrophages: FDG versus ultrasmall superparamagnetic iron oxide. *J Nucl Med,* 54**,** 999-1004.

SATOMI, T., OGAWA, M., MORI, I., ISHINO, S., KUBO, K., MAGATA, Y. & NISHIMOTO, T. 2013b. Comparison of Contrast Agents for Atherosclerosis Imaging Using Cultured Macrophages: FDG Versus Ultrasmall Superparamagnetic Iron Oxide. *Journal of nuclear medicine : official publication, Society of Nuclear Medicine,* 54**,** 999-1004.

SCHIEPERS, C., BROOS, P., MISEREZ, M., BORMANS, G. & DE ROO, M. 1998. Measurement of skeletal flow with positron emission tomography and 18F-fluoride

in femoral head osteonecrosis. *Archives of orthopaedic and trauma surgery,* 118**,** 131-5.

SCHIRRMEISTER, H., GUHLMANN, A., KOTZERKE, J., SANTJOHANSER, C., KUHN, T., KREIENBERG, R., MESSER, P., NUSSLE, K., ELSNER, K., GLATTING, G., TRAGER, H., NEUMAIER, B., DIEDERICHS, C. & RESKE, S. N. 1999. Early detection and accurate description of extent of metastatic bone disease in breast cancer with fluoride ion and positron emission tomography. *Journal of clinical oncology : official journal of the American Society of Clinical Oncology,* 17**,** 2381-9.

SCHMITZ, S. A., COUPLAND, S. E., GUST, R., WINTERHALTER, S., WAGNER, S., KRESSE, M., SEMMLER, W. & WOLF, K. J. 2000. Superparamagnetic iron oxide-enhanced MRI of atherosclerotic plaques in Watanabe hereditable hyperlipidemic rabbits. *Invest Radiol,* 35**,** 460-71.

SCHMITZ, S. A., TAUPITZ, M., WAGNER, S., WOLF, K. J., BEYERSDORFF, D. & HAMM, B. 2001. Magnetic resonance imaging of atherosclerotic plaques using superparamagnetic iron oxide particles. *J Magn Reson Imaging,* 14**,** 355-61.

SCOTT, R. 2002. The Multicentre Aneurysm Screening Study (MASS) into the effect of abdominal aortic aneurysm screening on mortality in men: a randomised controlled trial. *The Lancet,* 360**,** 1531-1539.

SHANAHAN, C. M. 2007. Inflammation ushers in calcification: a cycle of damage and protection? *Circulation,* 116**,** 2782-5.

SHIH, P. T., BRENNAN, M. L., VORA, D. K., TERRITO, M. C., STRAHL, D., ELICES, M. J., LUSIS, A. J. & BERLINER, J. A. 1999. Blocking very late antigen-4 integrin decreases leukocyte entry and fatty streak formation in mice fed an atherogenic diet. *Circ Res,* 84**,** 345-51.

SHIMIZU, K., MITCHELL, R. N. & LIBBY, P. 2006. Inflammation and cellular immune responses in abdominal aortic aneurysms. *Arteriosclerosis, thrombosis, and vascular biology,* 26**,** 987.

SKALEN, K., GUSTAFSSON, M., RYDBERG, E. K., HULTEN, L. M., WIKLUND, O., INNERARITY, T. L. & BOREN, J. 2002. Subendothelial retention of atherogenic lipoproteins in early atherosclerosis. *Nature,* 417**,** 750-4.

SKINNER, J. S., SMEETH, L., KENDALL, J. M., ADAMS, P. C., TIMMIS, A. & CHEST PAIN GUIDELINE DEVELOPMENT, G. 2010. NICE guidance. Chest pain of recent onset: assessment and diagnosis of recent onset chest pain or discomfort of suspected cardiac origin. *Heart,* 96**,** 974-8.

STARY, H. C., CHANDLER, A. B., DINSMORE, R. E., FUSTER, V., GLAGOV, S., INSULL, W., JR., ROSENFELD, M. E., SCHWARTZ, C. J., WAGNER, W. D. & WISSLER, R. W. 1995. A definition of advanced types of atherosclerotic lesions and a histological classification of atherosclerosis. A report from the Committee on Vascular Lesions of the Council on Arteriosclerosis, American Heart Association. *Circulation,* 92**,** 1355-74.

STEG, P. G., GOLDBERG, R. J., GORE, J. M., FOX, K. A. A., EAGLE, K. A., FLATHER, M. D., SADIQ, I., KASPER, R., RUSHTON-MELLOR, S. K. & ANDERSON, F. A. 2002. Baseline characteristics, management practices, and in-hospital outcomes of patients hospitalized with acute coronary syndromes in the Global Registry of Acute Coronary Events (GRACE). *The American journal of cardiology,* 90**,** 358-363.

STONE, G. W., MAEHARA, A., LANSKY, A. J., DE BRUYNE, B., CRISTEA, E., MINTZ, G. S., MEHRAN, R., MCPHERSON, J., FARHAT, N., MARSO, S. P., PARISE, H., TEMPLIN, B., WHITE, R., ZHANG, Z., SERRUYS, P. W. & INVESTIGATORS, P. 2011b. A prospective natural-history study of coronary atherosclerosis. *N Engl J Med,* 364**,** 226-35.

SUBRAMANIAN, S., TAWAKOL, A., BURDO, T. H., ABBARA, S., WEI, J., VIJAYAKUMAR, J., CORSINI, E., ABDELBAKY, A., ZANNI, M. V., HOFFMANN, U., WILLIAMS, K. C., LO, J. & GRINSPOON, S. K. 2012. Arterial inflammation in patients with HIV. *JAMA : the journal of the American Medical Association,* 308**,** 379-86.

SUZUKI, H., KURIHARA, Y., TAKEYA, M., KAMADA, N., KATAOKA, M., JISHAGE, K., UEDA, O., SAKAGUCHI, H., HIGASHI, T., SUZUKI, T., TAKASHIMA, Y., KAWABE, Y., CYNSHI, O., WADA, Y., HONDA, M., KURIHARA, H., ABURATANI, H., DOI, T., MATSUMOTO, A., AZUMA, S., NODA, T., TOYODA, Y., ITAKURA, H., YAZAKI, Y., KODAMA, T. & ET AL. 1997. A role for macrophage scavenger receptors in atherosclerosis and susceptibility to infection. *Nature,* 386**,** 292-6.

SWIRSKI, F. K. & NAHRENDORF, M. 2013. Leukocyte behavior in atherosclerosis, myocardial infarction, and heart failure. *Science,* 339**,** 161-6.

SWIRSKI, F. K., NAHRENDORF, M., ETZRODT, M., WILDGRUBER, M., CORTEZ-RETAMOZO, V., PANIZZI, P., FIGUEIREDO, J. L., KOHLER, R. H., CHUDNOVSKIY, A., WATERMAN, P., AIKAWA, E., MEMPEL, T. R., LIBBY, P., WEISSLEDER, R. & PITTET, M. J. 2009. Identification of splenic reservoir monocytes and their deployment to inflammatory sites. *Science,* 325**,** 612-6.

TAHARA, N., KAI, H., ISHIBASHI, M., NAKAURA, H., KAIDA, H., BABA, K., HAYABUCHI, N. & IMAIZUMI, T. 2006a. Simvastatin attenuates plaque inflammation: evaluation by fluorodeoxyglucose positron emission tomography. *Journal of the American College of Cardiology,* 48**,** 1825-31.

TAHARA, N., KAI, H., YAMAGISHI, S., MIZOGUCHI, M., NAKAURA, H., ISHIBASHI, M., KAIDA, H., BABA, K., HAYABUCHI, N. & IMAIZUMI, T. 2007. Vascular inflammation evaluated by [18F]-fluorodeoxyglucose positron emission tomography is associated with the metabolic syndrome. *Journal of the American College of Cardiology,* 49**,** 1533-9.

TAHARA, N., MUKHERJEE, J., DE HAAS, H. J., PETROV, A. D., TAWAKOL, A., HAIDER, N., TAHARA, A., CONSTANTINESCU, C. C., ZHOU, J., BOERSMA, H. H., IMAIZUMI, T., NAKANO, M., FINN, A., FAYAD, Z., VIRMANI, R., FUSTER, V., BOSCA, L. & NARULA, J. 2014. 2-deoxy-2-[(18)F]fluoro-d-

mannose positron emission tomography imaging in atherosclerosis. *Nature medicine,* 20**,** 215-9.

TAKAOKA, M., UEMURA, S., KAWATA, H., IMAGAWA, K., TAKEDA, Y., NAKATANI, K., NAYA, N., HORII, M., YAMANO, S., MIYAMOTO, Y., YOSHIMASA, Y. & SAITO, Y. 2006. Inflammatory response to acute myocardial infarction augments neointimal hyperplasia after vascular injury in a remote artery. *Arterioscler Thromb Vasc Biol,* 26**,** 2083-9.

TANG, T. Y., HOWARTH, S. P., MILLER, S. R., GRAVES, M. J., PATTERSON, A. J., JM, U. K.-I., LI, Z. Y., WALSH, S. R., BROWN, A. P., KIRKPATRICK, P. J., WARBURTON, E. A., HAYES, P. D., VARTY, K., BOYLE, J. R., GAUNT, M. E., ZALEWSKI, A. & GILLARD, J. H. 2009a. The ATHEROMA (Atorvastatin Therapy: Effects on Reduction of Macrophage Activity) Study. Evaluation using ultrasmall superparamagnetic iron oxide-enhanced magnetic resonance imaging in carotid disease. *J Am Coll Cardiol,* 53**,** 2039-50.

TANG, T. Y., MULLER, K. H., GRAVES, M. J., LI, Z. Y., WALSH, S. R., YOUNG, V., SADAT, U., HOWARTH, S. P. & GILLARD, J. H. 2009b. Iron oxide particles for atheroma imaging. *Arterioscler Thromb Vasc Biol,* 29**,** 1001-8.

TAWAKOL, A., FAYAD, Z. A., MOGG, R., ALON, A., KLIMAS, M. T., DANSKY, H., SUBRAMANIAN, S. S., ABDELBAKY, A., RUDD, J. H., FARKOUH, M. E., NUNES, I. O., BEALS, C. R. & SHANKAR, S. S. 2013. Intensification of statin therapy results in a rapid reduction in atherosclerotic inflammation: results of a multicenter fluorodeoxyglucose-positron emission tomography/computed tomography feasibility study. *J Am Coll Cardiol,* 62**,** 909-17.

TAWAKOL, A., MIGRINO, R. Q., BASHIAN, G. G., BEDRI, S., VERMYLEN, D., CURY, R. C., YATES, D., LAMURAGLIA, G. M., FURIE, K., HOUSER, S., GEWIRTZ, H., MULLER, J. E., BRADY, T. J. & FISCHMAN, A. J. 2006. In vivo 18F-fluorodeoxyglucose positron emission tomography imaging provides a noninvasive measure of carotid plaque inflammation in patients. *Journal of the American College of Cardiology,* 48**,** 1818-24.

TAYLOR, A. J., BINDEMAN, J., FEUERSTEIN, I., CAO, F., BRAZAITIS, M. & O'MALLEY, P. G. 2005. Coronary calcium independently predicts incident premature coronary heart disease over measured cardiovascular risk factors: mean three-year outcomes in the Prospective Army Coronary Calcium (PACC) project. *J Am Coll Cardiol,* 46**,** 807-14.

TEGLER, G., ERICSON, K., SORENSEN, J., BJORCK, M. & WANHAINEN, A. 2012. Inflammation in the walls of asymptomatic abdominal aortic aneurysms is not associated with increased metabolic activity detectable by 18-fluorodeoxglucose positron-emission tomography. *J Vasc Surg,* 56**,** 802-7.

THE UK SMALL ANEURYSM TRIAL PARTICIPANTS. 1998. Mortality results for randomised controlled trial of early elective surgery or ultrasonographic surveillance for small abdominal aortic aneurysms. *Lancet,* 352**,** 1649-55.

THOMAS, G. S. & HARASZTI, R. A. 2014. A new frontier in atherosclerotic coronary imaging. *Lancet,* 383**,** 674-5.

THOMPSON, M. M., JONES, L., NASIM, A., SAYERS, R. D. & BELL, P. R. 1996. Angiogenesis in abdominal aortic aneurysms. *Eur J Vasc Endovasc Surg,* 11**,** 464-9.

THOMPSON, R. C., ALLAM, A. H., LOMBARDI, G. P., WANN, L. S., SUTHERLAND, M. L., SUTHERLAND, J. D., SOLIMAN, M. A., FROHLICH, B., MININBERG, D. T., MONGE, J. M., VALLODOLID, C. M., COX, S. L., ABD EL-MAKSOUD, G., BADR, I., MIYAMOTO, M. I., EL-HALIM NUR EL-DIN, A., NARULA, J., FINCH, C. E. & THOMAS, G. S. 2013. Atherosclerosis across 4000 years of human history: the Horus study of four ancient populations. *Lancet,* 381**,** 1211-22.

THOMPSON, R. W. & PARKS, W. C. 1996. Role of Matrix Metalloproteinases in Abdominal Aortic Aneurysmsa. *Annals of the New York Academy of Sciences,* 800**,** 157-174.

THUBRIKAR, M. J., ROBICSEK, F., LABROSSE, M., CHERVENKOFF, V. & FOWLER, B. L. 2003. Effect of thrombus on abdominal aortic aneurysm wall dilation and stress. *J Cardiovasc Surg (Torino),* 44**,** 67-77.

THYGESEN, K., ALPERT, J. S., JAFFE, A. S., SIMOONS, M. L., CHAITMAN, B. R. & WHITE, H. D. 2012. Third universal definition of myocardial infarction. *European Heart Journal,* 33**,** 2551-67.

TINTUT, Y., PATEL, J., PARHAMI, F. & DEMER, L. L. 2000. Tumor necrosis factor-alpha promotes in vitro calcification of vascular cells via the cAMP pathway. *Circulation,* 102**,** 2636-42.

TOUAT, Z., OLLIVIER, V., DAI, J., HUISSE, M. G., BEZEAUD, A., SEBBAG, U., PALOMBI, T., ROSSIGNOL, P., MEILHAC, O. & GUILLIN, M. C. 2006. Renewal of mural thrombus releases plasma markers and is involved in aortic abdominal aneurysm evolution. *American Journal of Pathology,* 168**,** 1022.

TOUZE, E., TOUSSAINT, J. F., COSTE, J., SCHMITT, E., BONNEVILLE, F., VANDERMARCQ, P., GAUVRIT, J. Y., DOUVRIN, F., MEDER, J. F., MAS, J. L., OPPENHEIM, C. & GROUP, H. I.-R. M. R. I. I. A. S. O. T. C. A. S. 2007. Reproducibility of high-resolution MRI for the identification and the quantification of carotid atherosclerotic plaque components: consequences for prognosis studies and therapeutic trials. *Stroke,* 38**,** 1812-9.

TRIVEDI, R. A., MALLAWARACHI, C., U-KING-IM, J.-M., GRAVES, M. J., HORSLEY, J., GODDARD, M. J., BROWN, A., WANG, L., KIRKPATRICK, P. J., BROWN, J. & GILLARD, J. H. 2006b. Identifying inflamed carotid plaques using in vivo USPIO-enhanced MR imaging to label plaque macrophages. *Arterioscler Thromb Vasc Biol,* 26**,** 1601-6.

TRUIJERS, M., FUTTERER, J. J., TAKAHASHI, S., HEESAKKERS, R. A., BLANKENSTEIJN, J. D. & BARENTSZ, J. O. 2009. In vivo imaging of the aneurysm wall with MRI and a macrophage-specific contrast agent. *AJR Am J Roentgenol,* 193**,** W437-41.

TRUIJERS, M., KURVERS, H. A., BREDIE, S. J., OYEN, W. J. & BLANKENSTEIJN, J. D. 2008. In vivo imaging of abdominal aortic aneurysms: increased FDG uptake suggests inflammation in the aneurysm wall. *J Endovasc Ther,* 15**,** 462-7.

TURNER, G. H., OLZINSKI, A. R., BERNARD, R. E., ARAVINDHAN, K., BOYLE, R. J., NEWMAN, M. J., GARDNER, S. D., WILLETTE, R. N., GOUGH, P. J. & JUCKER, B. M. 2009. Assessment of macrophage infiltration in a murine model of abdominal aortic aneurysm. *J Magn Reson Imaging,* 30**,** 455-60.

VALLABHANENI, S. R., GILLING-SMITH, G. L., HOW, T. V., CARTER, S. D., BRENNAN, J. A. & HARRIS, P. L. 2004. Heterogeneity of tensile strength and matrix metalloproteinase activity in the wall of abdominal aortic aneurysms. *J Endovasc Ther,* 11**,** 494-502.

VAN DER WALL, E. E. 2014. Molecular imaging of coronary atherosclerosis; predictive of an acute myocardial infarction? *Neth Heart J,* 22**,** 1-2.

VANCRAEYNEST, D., PASQUET, A., ROELANTS, V., GERBER, B. L. & VANOVERSCHELDE, J. L. 2011. Imaging the vulnerable plaque. *J Am Coll Cardiol,* 57**,** 1961-79.

VARGHESE, A., CROWE, L. A., MOHIADDIN, R. H., GATEHOUSE, P. D., YANG, G. Z., FIRMIN, D. N. & PENNELL, D. J. 2005. Inter-study reproducibility of 3D volume selective fast spin echo sequence for quantifying carotid artery wall volume in asymptomatic subjects. *Atherosclerosis,* 183**,** 361-6.

VELICAN, C. 1981. A dissecting view on the role of the fatty streak in the pathogenesis of human atherosclerosis: culprit or bystander? *Med Interne,* 19**,** 321-37.

VENGRENYUK, Y., CARLIER, S., XANTHOS, S., CARDOSO, L., GANATOS, P., VIRMANI, R., EINAV, S., GILCHRIST, L. & WEINBAUM, S. 2006a. A hypothesis for vulnerable plaque rupture due to stress-induced debonding around cellular microcalcifications in thin fibrous caps. *Proc Natl Acad Sci U S A,* 103**,** 14678-83.

VIRMANI, R., BURKE, A. P., FARB, A. & KOLODGIE, F. D. 2006a. Pathology of the vulnerable plaque. *J Am Coll Cardiol,* 47**,** C13-8.

VIRMANI, R., BURKE, A. P., FARB, A. & KOLODGIE, F. D. 2006b. Pathology of the vulnerable plaque. *Journal of the American College of Cardiology,* 47**,** C13-8.

VIRMANI, R., KOLODGIE, F. D., BURKE, A. P., FARB, A. & SCHWARTZ, S. M. 2000b. Lessons from sudden coronary death: a comprehensive morphological classification scheme for atherosclerotic lesions. *Arterioscler Thromb Vasc Biol,* 20**,** 1262-75.

VORP, D. A., LEE, P. C., WANG, D. H., MAKAROUN, M. S., NEMOTO, E. M., OGAWA, S. & WEBSTER, M. W. 2001. Association of intraluminal thrombus in abdominal aortic aneurysm with local hypoxia and wall weakening. *J Vasc Surg,* 34**,** 291-9.

WALD, D. S., MORRIS, J. K., WALD, N. J. & INVESTIGATORS, P. 2014. Preventive angioplasty in myocardial infarction. *N Engl J Med,* 370**,** 283.

WALLENTIN, L., BECKER, R. C., BUDAJ, A., CANNON, C. P., EMANUELSSON, H., HELD, C., HORROW, J., HUSTED, S., JAMES, S., KATUS, H., MAHAFFEY, K. W., SCIRICA, B. M., SKENE, A., STEG, P. G., STOREY, R. F., HARRINGTON,

R. A., INVESTIGATORS, P., FREIJ, A. & THORSEN, M. 2009. Ticagrelor versus clopidogrel in patients with acute coronary syndromes. *N Engl J Med,* 361**,** 1045-57.

WARD, A. S. 1992. Aortic aneurysmal disease. A generalized dilating diathesis. *Arch Surg,* 127**,** 990-1.

WARD, M. R., PASTERKAMP, G., YEUNG, A. C. & BORST, C. 2000. Arterial remodeling: mechanisms and clinical implications. *Circulation,* 102**,** 1186.

WEINTRAUB, N. L. 2009. Understanding abdominal aortic aneurysm. *N Engl J Med,* 361**,** 1114-6.

WILLIAMS, G. & KOLODNY, G. M. 2008. Suppression of myocardial 18F-FDG uptake by preparing patients with a high-fat, low-carbohydrate diet. *AJR. American journal of roentgenology,* 190**,** W151-6.

WILLIAMS, K. J. & TABAS, I. 1995. The response-to-retention hypothesis of early atherogenesis. *Arterioscler Thromb Vasc Biol,* 15**,** 551-61.

WILLIAMS, M. J., MORISON, I. M., PARKER, J. H. & STEWART, R. A. 1997. Progression of the culprit lesion in unstable coronary artery disease with warfarin and aspirin versus aspirin alone: preliminary study. *J Am Coll Cardiol,* 30**,** 364-9.

WINTER, P. M., MORAWSKI, A. M., CARUTHERS, S. D., FUHRHOP, R. W., ZHANG, H., WILLIAMS, T. A., ALLEN, J. S., LACY, E. K., ROBERTSON, J. D., LANZA, G. M. & WICKLINE, S. A. 2003. Molecular imaging of angiogenesis in early-stage atherosclerosis with alpha(v)beta3-integrin-targeted nanoparticles. *Circulation,* 108**,** 2270-4.

WITT, B. J., BALLMAN, K. V., BROWN, R. D., JR., MEVERDEN, R. A., JACOBSEN, S. J. & ROGER, V. L. 2006. The incidence of stroke after myocardial infarction: a meta-analysis. *The American journal of medicine,* 119**,** 354 e1-9.

WOLINSKY, H. & GLAGOV, S. 1969. Comparison of abdominal and thoracic aortic medial structure in mammals. Deviation of man from the usual pattern. *Circ Res,* 25**,** 677-86.

WONG, N. D., GRANSAR, H., SHAW, L., POLK, D., MOON, J. H., MIRANDA-PEATS, R., HAYES, S. W., THOMSON, L. E., ROZANSKI, A., FRIEDMAN, J. D. & BERMAN, D. S. 2009. Thoracic aortic calcium versus coronary artery calcium for the prediction of coronary heart disease and cardiovascular disease events. *JACC. Cardiovascular imaging,* 2**,** 319-26.

WOOTTON, R. & DORE, C. 1986. The single-passage extraction of 18F in rabbit bone. *Clinical physics and physiological measurement : an official journal of the Hospital Physicists' Association, Deutsche Gesellschaft fur Medizinische Physik and the European Federation of Organisations for Medical Physics,* 7**,** 333-43.

WRIGHT, A. P., OHMAN, M. K., HAYASAKI, T., LUO, W., RUSSO, H. M., GUO, C. & EITZMAN, D. T. 2010. Atherosclerosis and leukocyte-endothelial adhesive interactions are increased following acute myocardial infarction in apolipoprotein E deficient mice. *Atherosclerosis,* 212**,** 414-7.

WYKRZYKOWSKA, J., LEHMAN, S., WILLIAMS, G., PARKER, J. A., PALMER, M. R., VARKEY, S., KOLODNY, G. & LAHAM, R. 2009. Imaging of inflamed and vulnerable plaque in coronary arteries with 18F-FDG PET/CT in patients with suppression of myocardial uptake using a low-carbohydrate, high-fat preparation. *Journal of nuclear medicine : official publication, Society of Nuclear Medicine,* 50**,** 563-8.

XU, X. Y., BORGHI, A., NCHIMI, A., LEUNG, J., GOMEZ, P., CHENG, Z., DEFRAIGNE, J. O. & SAKALIHASAN, N. 2010. High levels of 18F-FDG uptake in aortic aneurysm wall are associated with high wall stress. *Eur J Vasc Endovasc Surg,* 39**,** 295-301.

YAMAGISHI, M., TERASHIMA, M., AWANO, K., KIJIMA, M., NAKATANI, S., DAIKOKU, S., ITO, K., YASUMURA, Y. & MIYATAKE, K. 2000. Morphology of vulnerable coronary plaque: insights from follow-up of patients examined by intravascular ultrasound before an acute coronary syndrome. *J Am Coll Cardiol,* 35**,** 106-11.

YOUNGER, J. F., PLEIN, S., BARTH, J., RIDGWAY, J. P., BALL, S. G. & GREENWOOD, J. P. 2007. Troponin-I concentration 72 h after myocardial infarction correlates with infarct size and presence of microvascular obstruction. *Heart,* 93**,** 1547-51.

YUAN, C., MITSUMORI, L. M., FERGUSON, M. S., POLISSAR, N. L., ECHELARD, D., ORTIZ, G., SMALL, R., DAVIES, J. W., KERWIN, W. S. & HATSUKAMI, T. S. 2001. In vivo accuracy of multispectral magnetic resonance imaging for identifying lipid-rich necrotic cores and intraplaque hemorrhage in advanced human carotid plaques. *Circulation,* 104**,** 2051-6.

YUAN, C., ZHANG, S. X., POLISSAR, N. L., ECHELARD, D., ORTIZ, G., DAVIS, J. W., ELLINGTON, E., FERGUSON, M. S. & HATSUKAMI, T. S. 2002. Identification of fibrous cap rupture with magnetic resonance imaging is highly associated with recent transient ischemic attack or stroke. *Circulation,* 105**,** 181-5.

YUN, M., JANG, S., CUCCHIARA, A., NEWBERG, A. B. & ALAVI, A. 2002. 18F FDG uptake in the large arteries: a correlation study with the atherogenic risk factors. *Seminars in nuclear medicine,* 32**,** 70-6.

ZANZONICO, P. 2012. Principles of nuclear medicine imaging: planar, SPECT, PET, multi-modality, and autoradiography systems. *Radiat Res,* 177**,** 349-64.

PUBLISHED PAPERS

1. Joshi NV, Toor I, Shah AS, Carruthers K, Vesey AT, Alam SR, Sills A, Hoo TY, Melville AJ, Langlands SP, Jenkins WS, Uren NG, Mills NL, Fletcher AM, van Beek EJ, Rudd JH, Fox KA, Dweck MR, Newby DE. Systemic Atherosclerotic Inflammation Following Acute Myocardial Infarction: Myocardial Infarction Begets Myocardial Infarction. J Am Heart Assoc. 2015 Aug 27;4(9):e001956. doi: 10.1161/JAHA.115.001956. PubMed PMID: 26316523; PubMed Central PMCID: PMC4599491.

2. Joshi, N. V., Newby, D. E. & Sweck, M. R. 2015. Role of Multimodality Imaging in Atherosclerotic Plaque Burden and Metabolism. In: Schindler, H. T., George, T. R. & Lima, A. C. J. (eds.) Molecular and Multimodality Imaging in Cardiovascular Disease: Springer International Publishing.

3. Joshi NV, Vesey A, Newby DE, Dweck MR. Will 18F-sodium fluoride PET-CT imaging be the magic bullet for identifying vulnerable coronary atherosclerotic plaques? Curr Cardiol Rep. 2014 Sep;16(9):521. doi: 10.1007/s11886-014-0521-4. Review. PubMed PMID: 25103772.

4. Joshi NV, Newby DE, Dweck MR. Identifying high risk plaques prior to heart attack using PET-CT. Future Cardiol. 2014 May;10(3):307-10. doi: 10.2217/fca.14.22. PubMed PMID: 24976464.

5. Joshi NV, Vesey AT, Williams MC, Shah AS, Calvert PA, Craighead FH, Yeoh SE, Wallace W, Salter D, Fletcher AM, van Beek EJ, Flapan AD, Uren NG, Behan MW, Cruden NL, Mills NL, Fox KA, Rudd JH, Dweck MR, Newby DE.18F-fluoride positron emission tomography for identification of ruptured and high-risk coronary atherosclerotic plaques: a prospective clinical trial. Lancet. 2014 Feb 22;383(9918):705-13. doi: 10.1016/S0140-6736(13)61754-7. Epub 2013 Nov 11. PubMed PMID: 24224999.

6. Joshi NV, Dweck MR. Is ischemia really bad for you? J Am Coll Cardiol. 2013 Dec 3;62(22):2148-9. doi: 10.1016/j.jacc.2013.06.056. Epub 2013 Aug 28. PubMed PMID: 23994408.

7. Joshi NV, Raftis JB, Lucking AJ, Hunter AH, Millar M, Fitzpatrick M, Feuerstein GZ, Newby DE. Lyophilised reconstituted human platelets increase thrombus formation in a clinical ex vivo model of deep arterial injury. Thromb Haemost. 2012 Jul;108(1):176-82. doi: 10.1160/TH12-02-0059. Epub 2012 May 25. PubMed PMID: 22627761.

8. *McBride OM, *Joshi NV, Robson JM, MacGillivray TJ, Gray CD, Fletcher AM, Dweck MR, van Beek EJ, Rudd JH, Newby DE, Semple SI. Positron Emission Tomography and Magnetic Resonance Imaging of Cellular Inflammation in Patients with Abdominal Aortic Aneurysms. Eur J Vasc Endovasc Surg. 2016 Apr;51(4):518-26. doi: 10.1016/j.ejvs.2015.12.018. Epub 2016 Feb 23. PubMed PMID: 26919936.

9. Rubeaux M, Joshi NV, Dweck MR, Fletcher A, Motwani M, Thomson LE, Germano G, Dey D, Li D, Berman DS, Newby DE, Slomka PJ. Motion Correction of 18F-NaF PET for Imaging Coronary Atherosclerotic Plaques. J Nucl Med. 2016 Jan;57(1):54-9. doi: 10.2967/jnumed.115.162990. Epub 2015 Oct 15. PubMed PMID: 26471691

10. Shah AS, McAllister DA, Mills R, Lee KK, Churchhouse AM, Fleming KM, Layden E, Anand A, Fersia O, Joshi NV, Walker S, Jaffe AS, Fox KA, Newby DE, Mills NL. Sensitive troponin assay and the classification of myocardial infarction. Am J Med. 2015 May;128(5):493-501.e3. doi: 10.1016/j.amjmed.2014.10.056. Epub 2014 Nov 28. PubMed PMID: 25436428; PubMed Central PMCID: PMC4414368.

11. Adamson PD, Vesey AT, Joshi NV, Newby DE, Dweck MR. Salt in the wound: (18)F-fluoride positron emission tomography for identification of vulnerable coronary plaques. Cardiovasc Diagn Ther. 2015 Apr;5(2):150-5. doi: 10.3978/j.issn.2223-3652.2015.03.01. PubMed PMID: 25984456; PubMed Central PMCID: PMC4420673.

12. Venkatasubramanian S, Noh RM, Daga S, Langrish JP, Joshi NV, Mills NL, Hoffmann E, Jacobson EW, Vlasuk GP, Waterhouse BR, Lang NN, Newby DE. Cardiovascular effects of a novel SIRT1 activator, SRT2104, in otherwise healthy cigarette smokers. J Am Heart Assoc. 2013 Jun 14;2(3):e000042. doi: 10.1161/JAHA.113.000042. PubMed PMID: 23770971; PubMed Central PMCID: PMC3698759.

13. Dweck MR, Khaw HJ, Sng GK, Luo EL, Baird A, Williams MC, Makiello P, Mirsadraee S, Joshi NV, van Beek EJ, Boon NA, Rudd JH, Newby DE. Aortic stenosis, atherosclerosis, and skeletal bone: is there a common link with calcification and inflammation? Eur Heart J. 2013 Jun;34(21):1567-74. doi: 10.1093/eurheartj/eht034. Epub 2013 Feb 7. PubMed PMID: 23391586.

14. Dweck MR, Joshi NV, Rudd JH, Newby DE. Imaging of inflammation and calcification in aortic stenosis. Curr Cardiol Rep. 2013 Jan;15(1):320. doi: 10.1007/s11886-012-0320-8. Review. PubMed PMID: 23250657.

15. Alam SR, Shah AS, Richards J, Lang NN, Barnes G, Joshi N, MacGillivray T, McKillop G, Mirsadraee S, Payne J, Fox KA, Henriksen P, Newby DE, Semple SI. Ultrasmall superparamagnetic particles of iron oxide in patients with acute myocardial infarction: early clinical experience. Circ Cardiovasc Imaging. 2012 Sep 1;5(5):559-65. Epub 2012 Aug 8. PubMed PMID: 22875883.

16. Dweck MR, Chow MW, Joshi NV, Williams MC, Jones C, Fletcher AM, Richardson H, White A, McKillop G, van Beek EJ, Boon NA, Rudd JH, Newby DE. Coronary arterial 18F-sodium fluoride uptake: a novel marker of plaque biology. J Am Coll Cardiol. 2012 Apr 24;59(17):1539-48. doi: 10.1016/j.jacc.2011.12.037. PubMed PMID: 22516444.

17. Dweck MR, Jones C, Joshi NV, Fletcher AM, Richardson H, White A, Marsden M, Pessotto R, Clark JC, Wallace WA, Salter DM, McKillop G, van Beek EJ, Boon NA, Rudd JH, Newby DE. Assessment of valvular calcification and inflammation by positron emission tomography in patients with aortic stenosis. Circulation. 2012 Jan 3;125(1):76-86. doi: 10.1161/CIRCULATIONAHA.111.051052. Epub 2011 Nov 16. PubMed PMID: 22090163.

APPENDIX

1. Study protocol: PRE18FFIR study
2. Study protocol: DIAMOND study
3. Study protocol: MA3RS study
4. Study protocol: SoFIA3 study

Academic and Clinical Central Office for Research and Development

Study Protocol

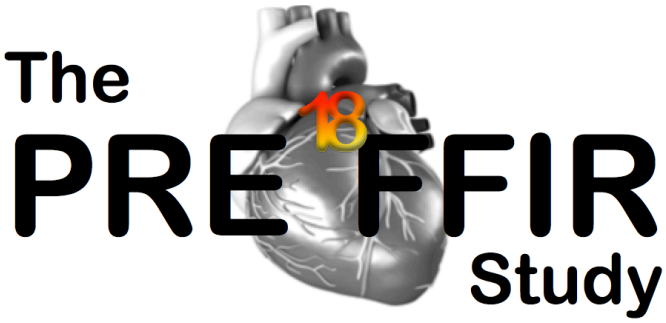

Prediction of Recurrent Events with ^{18}F-Fluoride to Identify Ruptured and High-risk Coronary Artery Plaques in Patients with Myocardial Infarction

Co-sponsors	University of Edinburgh & NHS Lothian ACCORD The Queen's Medical Research Institute 47 Little France Crescent Edinburgh EH16 4TJ
Funder	Wellcome Trust
Funding Reference Number	WT103782AIA - Senior Investigator Award
Chief Investigator	Professor David Newby
REC Number	
EudraCT Number	2014-004021-41
ClinicalTrials.gov ID number	NCT02278211
Number and Date	Version 1.0, 16th March 2015

COORDINATING CENTRE

Chief Investigator Professor David E Newby Centre of Cardiovascular Science Chancellor's Building 51 Little France Crescent Edinburgh EH16 4SB Tel: 0131 242 6515 Fax: 0131 242 6379 Email: d.e.newby@ed.ac.uk	**Co Investigator** Dr Marc Dweck Centre of Cardiovascular Science Chancellor's Building 51 Little France Crescent Edinburgh EH16 4SB Tel: 0131 242 6364 Email: marc.dweck@nhslothian.scot.nhs.uk
Clinical Research Fellow **Dr Alastair Moss** Centre of Cardiovascular Science Chancellor's Building 51 Little France Crescent Edinburgh EH16 4SB Tel: 0131 242 6364 Email: amoss@staffmail.ed.ac.uk	**Clinical Research Fellow** **Dr Philip Adamson** Centre of Cardiovascular Science Chancellor's Building 51 Little France Crescent Edinburgh EH16 4SB Tel: 0131 242 6364 Email: Philip.adamson@ed.ac.uk
Co-sponsor Representative Dr Annya Smyth University of Edinburgh Queen's Medical Research Institute 47 Little France Crescent Edinburgh EH16 4SB Tel: 0131 242 3325 Fax: 0131 242 9447 Email: annya.smyth@ed.ac.uk	**Trial Statisticians** Professor Gordon Murray and Dr Steff Lewis Centre for Population Health Sciences University of Edinburgh Teviot Place, Edinburgh, EH8 9AG Tel: 0131 537 3865 Email: steff.lewis@ed.ac.uk
Trial Manager **Dr Laura Forsyth** Edinburgh Clinical Trials Unit University of Edinburgh Outpatients Building Western General Hospital	

Crewe Road South Edinburgh EH4 2XU Tel: 0131 537 3847 Fax: 0131 537 3851 Email: laura.forsyth@ed.ac.uk	

PARTICIPATING SITES	
NHS Lothian **Principal Investigator** Dr Alastair Moss Royal Infirmary Edinburgh Centre for Cardiovascular Science Chancellor's Building 51 Little France Crescent Edinburgh EH16 4SB Tel: 0131 2426364 Email: amoss@staffmail.ed.ac.uk	**Oxford University Hospitals NHS Trust** **Principal Investigator** Dr Rajesh Kharbanda Division of Cardiovascular Medicine Level 6 West Wing John Radcliffe Hospital Headington Oxford OX3 9DU Tel: 01865 234669 Rajesh.kharbanda@ouh.nhs.uk
NHS Grampian **Principal Investigator** Dr Dana Dawson Royal Infirmary, Aberdeen Foresterhill Road Aberdeen AB25 2ZN Tel: 01224 437965 Dana.dawson@abdn.ac.uk	**Central Manchester University Hospitals Foundation Trust** **Principal Investigator** Dr Parthiban Arumugam Manchester Royal Infirmary Oxford Road Manchester M13 9WL Tel: 044161 2766039 Parthiban.Arumugam@cmft.nhs.uk

CONTENTS

PROTOCOL APPROVAL

PRE^{18}FFIR Study

Signatures

Professor David Newby	_____	_____
Chief Investigator	Signature	Date
Professor Gordon Murray	_____	_____
Study Statistician	Signature	Date
Annya Smyth	_____	_____
Sponsor(s) Representative	Signature	Date
	_____	_____
Principal Investigator	Signature	Date

LIST OF ABBREVIATIONS

ACCORD	Academic and Clinical Central Office for Research & Development - Joint office for University of Edinburgh and NHS Lothian
AE	Adverse Event
AR	Adverse Reaction
CI	Chief Investigator
CT	Computer Tomography
CTA	Clinical Trial Authorisation
CTCA	Computer Tomography Coronary Angiography
CTIMP	Clinical Trial of an Investigational Medicinal Product
CRF	Case Report Form
DNA	Deoxyribose Nucleic Acid
eGFR	Estimated Glomerular Filtration Rate
GCP	Good Clinical Practice
ICH	International Conference on Harmonisation
IMP	Investigational Medicinal Product
ISF	Investigator Site File
IVUS	Intravascular Ultrasound
MHRA	Medicines and Healthcare products Regulatory Authority
NIMP	Non Investigational Medicinal Product
NIRS	Near Infrared Spectroscopy
OCT	Optical Coherence Tomography
PET	Positron Emission Tomography
R&D	Research & Development
REC	Research Ethics Committee
SAE	Serious Adverse Event
SAR	Serious Adverse Reaction
SOP	Standard Operating Procedure
SUSAR	Suspected Unexpected Serious Adverse Reaction
TMF	Trial Master File
UAR	Unexpected Adverse Reaction

1 INTRODUCTION

1.1 BACKGROUND

1.1.1 Pathogenesis of Coronary Artery Disease

Coronary plaque rupture of mildly stenotic coronary atherosclerosis is the commonest cause of acute coronary thrombosis, myocardial infarction and death [Davies, 2000]. It is closely linked to hypercholesterolaemia and has a dominant inflammatory phenotype. Classical histological features include a lipid-rich pool, thin fibrous cap, paucity of vascular smooth muscle cells and an intense inflammatory cell infiltrate [Davies, 2000].

Plaque rupture does not invariably lead to thrombotic occlusion of the coronary artery. Coronary plaque events are very common and the majority of such events do not cause coronary occlusion [Mann & Davies, 1999; Davies, 2000]. Here, plaque rupture and thrombosis is organised, remodelled and incorporated into the atherosclerotic plaque itself. Indeed, 80% of plaques that cause over 50% diameter stenosis have evidence of old healed plaque rupture with incorporation of thrombus into the atheroma [Mann & Davies, 1999]. This process contributes to the progression of coronary atherosclerosis and explains the first appearance, or step change in severity, of angina pectoris.

Coronary plaque events are often not isolated. Plaque rupture can occur throughout the body and is not confined to a single vascular bed. Moreover, in patients with acute coronary syndromes, it is common for multiple plaque events to occur simultaneously and beyond the culprit lesion itself. Post-mortem studies indicate that, on average, 2.4 coronary thrombotic events occur in each patient who presents with fatal coronary heart disease [Mann & Davies, 1999; Davies, 2000]. This suggests that systemic and generalised mechanisms and mediators play an important role in addition to local factors within the coronary artery wall.

In summary, coronary atherosclerosis is characterised by multiple and recurrent plaque rupture events that are often sub-clinical and cause step-wise growth of the plaque as it heals and remodels. Patients undergoing repeated plaque rupture events are likely to be at increased risk of myocardial infarction.

1.1.2 Non-invasive Imaging of the Vulnerable Plaque

In the study of coronary artery disease, many researchers have searched for a non-invasive imaging biomarker of plaque vulnerability and rupture. For the first time, we have demonstrated that 18F-fluoride positron emission tomography can detect high-risk coronary plaque in patients with stable coronary artery disease [Joshi *et al*, 2014].

In the vasculature, 18F-fluoride acts as a marker of novel calcification activity [Dweck *et al*, 2012a; Dweck *et al*, 2013]. Similar to other conditions, calcification in coronary atheroma occurs as a healing response to intense necrotic inflammation, making 18F-fluoride a useful marker of high-risk atherosclerotic plaque. We have previously demonstrated increased uptake of

this tracer in the coronary vasculature localizing to individual coronary lesions and identifying patients with increased cardiovascular risk factor profiles [Dweck *et al*, 2012b]. More recently we have conducted a prospective study of 40 patients with myocardial infarction in whom 18F-fluoride localised to the culprit plaque (Figure 1) in over 90% of patients [Joshi *et al*, 2014]. This finding was confirmed in 12 patients with a recent stroke undergoing carotid endartectomy where 18F-fluoride uptake was observed at the site of plaque rupture in 100% of patients and this uptake correlated with increased calcification activity and areas of necrosis on histology. Finally we studied 40 patients with stable coronary artery disease. Increased uptake was observed in 45% of these patients and this again localized to individual coronary plaques (Figure 2). Interestingly these lesions were associated with multiple high-risk markers on radiofrequency and gray-scale intravascular ultrasound (necrotic core, positive remodeling and microcalcification). Importantly, plasma high-sensitivity troponin concentrations were much higher in patients with 18F-fluoride positive plaques compared to patients without evidence of uptake (7.89±9.34 *versus* 3.10±1.89 ng/L, P=0·047). The latter observation is of particular interest as it supports the hypothesis that 18F-fluoride is detecting subclinical plaque rupture in those with stable disease, similar to its mechanism of activity following myocardial infarction. Moreover plasma troponin concentrations measured by a high-sensitivity assay also predict an adverse outcome amongst patients with stable coronary artery disease [Omland *et al*, 2013] and provide a useful surrogate biomarker of therapeutic efficacy.

1.1.3 Recurrent Events Following Acute Myocardial Infarction

Myocardial infarction and stroke are two of the commonest causes of hospitalisation, major disability and death in the United Kingdom. However, despite many billions of pounds being spent each year on their treatment, recurrent cardiovascular events are common. Indeed, within one year of acute myocardial infarction, one in five patients have recurrent events despite optimal medical therapy [Mills et al, 2011], and one half of these recurrent events occur at sites not felt to have caused their initial presentation [Stone et al, 2011].

Coronary calcification is pathognomonic of atherosclerosis and recent studies in Egyptian mummies have demonstrated that it has been present in humans for millennia [Thompson et al, 2013]. Despite this, the mechanisms of its formation have yet to be precisely defined. Furthermore, the nature and extent of vascular calcification may vary according to the pathophysiological setting and underlying disease process. Given that it is independently associated with a 3 to 4-fold increased risk of death [Detrano et al, 2008], a better understanding of the pathophysiology and mechanisms of vascular calcification will be critical to our understanding of cardiovascular disease. This is particularly important if we are to determine its role in the initiation, progression and consequences of atherosclerosis. This may provide novel insights into the pathophysiology of atherosclerosis as well as identify new and as yet unexplored pathways that could be the target for future life-saving therapeutic interventions. For example, although highly successful in treating

cardiovascular disease, statins only prevent 25% of recurrent cardiovascular events, and have no effect on the progression of vascular calcification. The majority of recurrent events therefore remain unchecked and we urgently need more effective and comprehensive interventions.

Non-invasive imaging techniques to detect early active vascular calcification in atherosclerosis have the potential to identify high-risk and ruptured atherosclerotic plaques, thereby providing a major novel biomarker of plaque vulnerability. This will provide a platform to explore and follow the *in vivo* pathogenesis of atherosclerosis, as well as assess novel anti-atherosclerotic interventions. This will also facilitate the more accurate identification of culprit atherosclerotic plaque in the precipitation of myocardial infarction and stroke, allowing better delivery and targeting of our therapies at both the lesion and patient level. This approach would potentially be a major advance for the treatment of unstable atherosclerotic disease.

1.1.4 Stratified Medicine and Intervention

Current treatment decisions for patients with acute myocardial infarction are based on a large number of major multi-centre international randomised controlled trials. These trials demonstrate major secondary preventative benefits with the use of anti-platelet therapy, statins, angiotensin-converting enzyme inhibition and beta-blockade following acute myocardial infarction. However, all patients are treated with the same combination of medications with little attempt to risk stratify patients and select those who have the most to benefit from such therapies.

Emergency or immediate coronary angiography with a view to coronary revascularisation is now recommended in the vast majority of patients presenting with acute myocardial infarction. Indeed, 80% of patients admitted with non-ST segment elevation myocardial infarction in the United Kingdom undergo coronary angiography with a view to coronary revascularisation during their index hospital admission [MINAP, 2013]. However, coronary revascularisation following myocardial infarction focuses on treating flow-limiting stenoses (≥70% luminal stenosis) with coronary revascularisation strategies such as percutaneous coronary intervention and coronary artery bypass graft surgery. However, we know that the majority of plaque rupture events occur on non-flow limiting stenoses (see section 1.1), and this questions whether we are over treating a large number of patients and indeed coronary artery lesions without actually tackling the future potential culprit lesions. Using 18F-fluoride, we have "the opportunity to better assess the commonly accepted belief that most myocardial infarctions are caused by rupture of previously non-obstructive plaques" [Thomas & Haraszti, 2014].

1.2 RESEARCH HYPOTHESIS

The central hypothesis of the PRE^{18}FFIR study is that coronary 18F-fluoride uptake can identify high-risk and ruptured atherosclerotic plaque in patients with recent myocardial infarction. This has the potential to assist in the diagnosis, risk stratification, investigation, management and treatment of patients with acute myocardial infarction.

1.3 RATIONALE FOR THE STUDY

We have investigated and described the use of 18F-fluoride positron emission tomography and computed tomography coronary angiography to identify high-risk or ruptured coronary atherosclerotic plaque [Joshi et al. Lancet 2014]. This is the first non-invasive imaging technique to achieve this and it has been heralded as a major advance with wide reaching ramifications for the diagnosis, investigation, and treatment of coronary artery disease [Thomas & Haraszti, 2014]. Importantly, it may provide the basis of a new paradigm in the treatment and management of patients with myocardial infarction by tailoring therapy to the presence and extent of plaque inflammation and rupture rather than the anatomical severity of luminal stenoses. More targeted and focused investigations and interventions have the potential to shorten hospital stay, to avoid the indiscriminate application of expensive therapies, and to focus and to maximize the impact of our current successful therapies to reduce recurrent major adverse cardiac events.

The study rationale is therefore to confirm our preliminary findings in a broad range of patients across different centres throughout the United Kingdom. Specifically, the study is intended to confirm whether coronary 18F-fluoride uptake identifies high-risk or ruptured coronary atherosclerotic plaque, and to determine if coronary 18F-fluoride uptake is predictive of disease progression and clinical outcome. We have also planned two sub-studies to assess the reproducibility and natural history of 18F-fluoride uptake and an additional sub-study to provide correlation with in vivo plaque characterization tests. These sub-studies are described in more detail in separate protocols.

2 STUDY OBJECTIVES

2.1 OBJECTIVES

2.1.1 Primary Objective

- To determine whether coronary ^{18}F-fluoride uptake is associated with recurrent coronary thrombotic events in patients with multi-vessel coronary artery disease and recent myocardial infarction.

2.1.2 Secondary Objectives

In patients with multi-vessel coronary artery disease and recent myocardial infarction, to determine whether coronary ^{18}F-fluoride uptake:

- Is associated with secondary clinical outcomes including all-cause death, recurrent major adverse cardiac events defined as cardiac death, recurrent myocardial infarction, and rehospitalization for acute coronary syndrome, unscheduled coronary revascularization, and healthcare resource utilization.
- Can identify areas of high-risk or ruptured atherosclerotic plaque in a large broad population of patients across multiple sites.
- Can predict the territory of subsequent myocardial reinfarction.

- Can identify areas of future progression of coronary atherosclerotic plaque (volume and calcification)
- Is sufficiently repeatable and reproducible for clinical application.
- Changes with time and establish what are the determinants of increasing or decreasing activity.

2.1.3 Safety Objective

- To determine the radiation exposure and effective dose associated with 18F-fluoride positron emission tomography and computed tomography coronary angiography

2.1.4 Exploratory Objectives

We will initially explore whether the identification of 18F-fluoride positive coronary atherosclerotic plaque has the potential to guide patient management. Here positron emission tomography and computed tomography coronary angiography results will be compared with the subsequent application of coronary revascularization and optimal medical therapy. Importantly, we will also explore the feasibility of using the identification of 18F-fluoride positive coronary atherosclerotic plaque to guide coronary revascularisation and intervention. For example, how many stenotic but 18F-fluoride negative lesions undergo intracoronary stenting, and how many 18F-fluoride positive lesions are left untreated and are responsible for recurrent cardiovascular events?

2.2 ENDPOINTS

2.2.1 Primary Endpoints

- Cardiac death or non-fatal recurrent myocardial infarction at 2 years.

2.2.2 Secondary Endpoints

These will include:

- All-cause death
- Recurrent major adverse cardiac events defined as cardiac death, recurrent myocardial infarction, and rehospitalization for acute coronary syndrome and unscheduled coronary revascularization,
- Healthcare resource utilization of patients with and without focal 18F-NaF uptake in coronary plaques unrelated to index myocardial infarction
- Each individual component end-point of the composite end-point of major adverse cardiac event.
- 18F-NaF uptake localisation to culprit plaque causing the index myocardial infarction
- Territory of subsequent myocardial reinfarction.
- Coronary artery plaque progression by computed tomography coronary angiography. Plaque volume, composition and calcification.

3 STUDY DESIGN

This is a multicentre observational cohort study of an investigational medical product with longitudinal follow-up for disease progression and clinical outcomes.

3.1 RATIONALE FOR STUDY DESIGN

We wish to confirm our preliminary single centre findings in a larger multicentre study of patients with recent myocardial infarction. We therefore will undertake an observational study in patients with recent myocardial infarction who will undergo coronary 18F-fluoride positron emission tomography and computed tomography coronary angiography immediately following hospitalisation. However at present, we have no data to determine whether coronary 18F-fluoride can predict disease progression or clinical outcome: a key determinant of its potential clinical utility. The study will therefore have a longitudinal cohort follow-up component where participants will undergo clinical follow-up of at least 2 years duration when repeat computed tomography coronary angiography will be performed.

Before conducting a randomised controlled trial using coronary 18F-fluoride uptake to stratify and guide treatment, it is imperative that we confirm the diagnostic and prognostic importance of coronary 18F-fluoride uptake within a large multicentre observational cohort study.

4 STUDY POPULATION

4.1 Number of Participants

We will recruit 700 patients with recent myocardial infarction and multi-vessel coronary heart disease.

4.2 Inclusion Criteria

For inclusion in the study subjects will fulfil the following criteria:

1. Patients aged ≥50 years with recent (<21 days) type 1 myocardial infarction and angiographically proven multi-vessel coronary artery disease defined as at least two major epicardial vessels with any combination of either (a) >50% luminal stenosis, or (b) previous revascularization (percutaneous coronary intervention or coronary artery bypass graft surgery).
2. Provision of informed consent prior to any study specific procedures

4.3 Exclusion Criteria

Subjects will not enter the study if any of the following exclusion criteria are fulfilled:

1. Inability or unwilling to give informed consent
2. Women who are pregnant, breastfeeding or of child-bearing potential (women who have experienced menarche, are pre-menopausal and have not been sterilised) will not be enrolled into the trial

3. Major intercurrent illness with life expectancy <2 year
4. Renal dysfunction (estimated glomerular filtration rate ≤30 mL/min/1.73 m^2)
5. Contraindication to iodinated contrast agent, positron emission tomography or computed tomography
6. Permanent or persistent atrial fibrillation
7. Previous screening as part of the trial

4.4 Co-enrolment

Co-enrolment with a non-CTIMP or another CTIMP clinical trial may be allowed provided this is not expected to place an undue burden upon participants and their families, and will not compromise the primary end-point of either trial. Consideration will also be given to the total exposure to ionising radiation should additional studies require further exposure.

Co-enrolment with another CTIMP will only be permitted with agreement of the Sponsors, Trial Steering Committees, and Chief Investigators of both studies.

5 PARTICIPANT SELECTION AND ENROLMENT

5.1 IDENTIFYING PARTICIPANTS

Patients presenting with myocardial infarction will be approached for study recruitment by their usual care team. This will normally be undertaken during their index hospital admission. Patients will be provided with a Patient Information Sheet and given an opportunity to ask questions about participation in the trial.

5.2 CONSENTING PARTICIPANTS

After a minimum of 24 hours, patients willing to participate in the study will be asked to consent and undergo screening. Written informed consent will be obtained by a suitably qualified member of the research team before any study related procedures are performed.

5.3 SCREENING FOR ELIGIBILITY

Screening for eligibility based on pre-existing clinical investigations (i.e. standard clinical biochemical and haematological investigations and coronary angiographic findings) will be performed by a member of the research team and will only take place once written consent has been obtained. Once a patient has agreed to participate and is deemed eligible they will be invited to attend the baseline 18F-fluoride positron emission tomography and computed tomography coronary angiogram scan.

5.4 INELIGIBLE AND NON-RECRUITED PARTICIPANTS

Ineligible and non-recruited patients will receive standard medical care. An anonymised log will be kept of patients who were screened for the study and subsequently found to be ineligible or not recruited.

5.5 PROCEDURES FOR HANDLING PARTICIPANTS INCORRECTLY ENROLLED

Patients identified as being incorrectly enrolled prior to their initial CT-PET scan will be excluded from the primary study analysis and replaced. Patients who are identified as incorrectly enrolled but have undergone their initial CT-PET will be included in the primary analysis and we will endeavour to continue to collect study data without involving the participant in any further study related procedures.

5.6 WITHDRAWAL OF STUDY PARTICIPANTS

Participants are free to withdraw from the study at any point or a participant can be withdrawn by the investigator. If withdrawal occurs, the primary reason for withdrawal will be documented in the participant's case record form, if possible. The patient will have the option of withdrawal from (i) all or specific further study procedures but continued collection of routine clinical and safety data, (ii) all further aspects of the study with no further collection of any data, and (iii) all aspects of the trial with removal of all previously collected data.

6 INVESTIGATIONAL MEDICINAL PRODUCT

6.1 STUDY DRUG

Investigational product	Dosage form and strength	Manufacturer
[18F] Sodium Fluoride	250 MBq	See 6.1.2

6.1.1 Study Drug Identification

[18F] Sodium Fluoride (18F-NaF) sterile solution for injection

6.1.2 Study Drug Manufacturers

Manufacturing will be performed by:

Clinical Research Imaging Centre (CRIC)
University of Edinburgh
47 Little France Crescent
Edinburgh
EH16 4TJ
Licence: MIA (IMP) 1384

PETNET Solutions
Lesley Harrison Building

Mount Vernon Hospital
Northwood
Middlesex
HA6 2RN
Licence: MIA (IMP) 21750

6.1.3 Marketing Authorisation Holder

There is currently no Marketing authorisation for [18F] Sodium Fluoride (18F-NaF)

6.1.4 Labelling and Packaging

Labelling and packaging of the [18F] Sodium Fluoride (18F-NaF) will be carried out by:

Clinical Research Imaging Centre (CRIC)
University of Edinburgh
47 Little France Crescent
Edinburgh
EH16 4TJ
Licence: MIA (IMP) 1384

PETNET Solutions
Lesley Harrison Building
Mount Vernon Hospital
Northwood
Middlesex
HA6 2RN
Licence: MIA (IMP) 21750

6.2 DOSING REGIME

Single intravenous injection

6.3 OVERDOSE

Given that the 18F-fluoride will be administered as a single intravenous injection by trained personnel, accidental or unintentional overdose is not anticipated to occur. Moreover the doses and quantities of sodium fluoride are very low (<430 µg) and >1,000-fold below the dose (3-5 mg/kg) where toxicity symptoms may appear and >1,000,000-fold below the anticipated lethal dose

(5-10 g). However, if an overdose of sodium fluoride were to occur then radiation exposure and sodium fluoride toxicity will be the primary considerations. Excretion should be accelerated in order to reduce the dose taken by the patient. For this reason, forced diuresis (furosemide and fluid) should be applied to the patient.

For radiation overexposure, the patient will be contained within a safe environment to allow radioactive decay to occur to acceptable levels. Monitoring for the consequences of excess radiation exposure (such as bone marrow toxicity) will be undertaken as required. Symptoms of sodium fluoride toxicity include abdominal pain, abnormal taste (salty or soapy taste), convulsions, diarrhoea, drooling, headache, arrhythmia, nausea, hypopnea, bradycardia, tremors, vomiting, and weakness. For an intravenous overdose, there are no specific antidotes and supportive measures will be undertaken as clinically indicated, such as hydration and anti-emetic therapy. Consideration will be given to intravenous calcium supplementation to compete with the excess fluoride ions especially in the presence of problematic arrhythmias.

6.4 OTHER MEDICATIONS

6.4.1 Non-Investigational Medicinal Products

At the time of positron emission tomography and computed tomography coronary angiography, patients may receive oral and/or intravenous beta-blockade, such as metoprolol 5-100mg, to slow the heart rate to below 65 beats per minute to maximise image quality and reduce radiation exposure. Glyceryl trintrate spray or tablet will be administered sublingually (200-400 µg) to induce coronary vasodilatation to enhance image quality of the coronary angiogram.

6.4.2 Permitted Medications

As per the standard of care for treatment of myocardial infarction, unless contraindicated, all patients will be encouraged to be maintained on aspirin 75 mg once daily and maximally tolerated doses of statin, angiotensin-converting enzyme inhibition and beta-blocker therapy as clinically indicated and in accordance with local guidelines. Patients will be encouraged to be maintained on a P2Y12 receptor antagonist for at least 1 year.

There are no study specific prohibited medications.

7 STUDY ASSESSMENTS

Trial participants will undergo 3 study visits (Table 1). During their initial hospital admission, medical notes will be screened prior to consent and potentially eligible patients will be approached to take part in the study. Those patients who are potentially eligible and wish to participate will be consented and routine clinical data will be collected following consent (screening visit). The participants will attend a second visit where they will have a baseline 18F-fluoride positron emission tomography, computed tomography (CT) calcium

scan and CT coronary angiography (CTCA) scan performed (baseline visit) before attending for a final clinical review and 2-year computed tomography calcium scan and CT coronary angiogram (2-year visit) when further routine clinical data will be collected. In order to assess for clinical cardiac events and AEs/SAEs participants will contacted by telephone 1 year after their baseline PET and CTCA scans were performed. Following the 2-year visit, data on study outcomes will continue to be collected until study completion (last patient, last visit) via periodic review of the electronic health record and additional annual telephone review as required. This will ensure that late study outcomes can be evaluated over the duration of the study. In order to detect long-term outcome data we will continue to monitor clinical events via annual review of patient electronic clinical records for a period of 5 years following the completion of the participant's final study visit.

Table 1: Study Assessments

	Screening Visit -2 weeks (±1week) (Initial Hospital Admission)	**Baseline Visit** (Day 0)	Additional Visits for Reproducibility and Natural History Sub studies only					**2-Year Visit** (± 2 weeks)
			Week 2 (±1 week)	Week 6 (±1 week)	Week 12 (±2 weeks)	Week 26 (±2 weeks)	Week 52 (±2 weeks)	
Eligibility Criteria and PIS	X							
Consent	X							
Concomitant medications	X							
Clinical Assessment	X							
Haematology, biochemistry and Cardiac Enzymes	X	This data will be collected from the existing patient record and should not require additional procedures						
ECG	X							
GRACE Score Calculation	X							
AE/SAE Reporting		X						X
18F-Fluoride PET		X	X	X	X	X	X	
CT attenuation correction		X	X	X	X	X	X	
CT Calcium Scan		X						X
CT Coronary Angiogram		X	X	X	X	X	X	X
			Additional PET and CT scans will be performed in those patients involved in the sub studies only					
Telephone Review							X	
		Additional annual telephone follow up with review of electronic health records if warranted until study completion (last patient, last visit)						

7.1 SAFETY ASSESSMENTS

The dose-length product and effective radiation dose will be recorded for all study scans: baseline 18F-fluoride positron emission tomography and computed tomography coronary angiography scan, and the final 2-year computed tomography coronary angiogram.

7.2 STUDY ASSESSMENTS

This is a prospective multi-centre observational cohort study. Subjects will attend for clinical assessments at the screening visit (review of clinical records and confirmation of eligibility), baseline visit (18F-fluoride positron emission tomography, computed tomography calcium scan and CT coronary angiography scan), and at 2 years (repeat computed tomography calcium scan and CT coronary angiogram). Clinical outcome data will be obtained from routinely collected clinical data in the electronic health record and, where appropriate, annual telephone calls to the patients or General Practitioners.

7.2.1 Screening Assessment

Screening visit assessments will include clinical history, review of patient records to confirm study eligibility and record clinical profile, standard clinical biochemical and haematological variables, 12-lead electrocardiogram, the Global Registry of Acute Coronary Events (GRACE) score and the invasive coronary angiogram findings and percutaneous coronary interventional procedures.

7.2.2 Baseline Assessment

Baseline visit assessments will include 18F-fluoride positron emission tomography, computed tomography calcium scan and CT coronary angiography scan. AE/SAE's will also be recorded.

7.2.3 Follow Up Assessments

Participants will be contacted by telephone at 12 months and periodically thereafter until the last recruited patient has completed their 2 year follow-up visit. The purpose of the telephone interview is to review any clinical cardiovascular events or AE/SAE that may have occurred in the intervening period. They will attend for a final study visit 2 years after their initial CT-PET scans. At the final study visit, patients will undergo a repeat computed tomography calcium scan and CT coronary angiogram. On-going periodic review of the electronic health records will continue throughout the study and for a period of 5 years after study completion in order to assess long-term outcomes.

7.2.4 Positron Emission and Computed Tomography Coronary Angiography

Patients may receive oral and/or intravenous beta-blockade, such as metoprolol 5-100 mg, to slow the heart rate to below 65 beats per minute to maximise image quality and reduce radiation exposure. Glyceryl trintrate spray or tablet will be administered sublingually (200-400 µg) to induce coronary vasodilatation to enhance image quality of the coronary angiogram.

All patients will undergo dual cardiac and respiratory-gated positron emission and computed tomography imaging of the coronary arteries. Study subjects will be administered a target dose of 250 MBq 18F-fluoride intravenously and subsequently rested in a quiet environment for 60 min. An attenuation correction computed tomography scan will then be performed, followed by positron emission tomography imaging of the thorax in list-mode for 30 min.

Computed tomography coronary calcium scan and angiography will be undertaken in the same visit as the 18F-fluoride scan and again at 2 years. With the patient lying still on the scanner after acquisition of the positron emission tomography scan, an electrocardiogram-gated breath-hold computed tomography scan of the coronary arteries will be performed. A bolus of contrast (BMI adjusted) will be injected intravenously after determining the appropriate trigger delay with a test bolus. Because the use of contrast is required for the CT scan study participants may require pre-procedural check of eGFR according to local study site imaging protocols.

The positron emission tomography scans will be reconstructed in multiple phases of the cardiac cycle, with the diastolic phase (50-75%) used for analysis. Additional reconstructions will be undertaken as necessary. Positron emission tomography scans will correct for cardiac motion correction using electrocardiogram-gated images.

Further technical details of the specific CT-PET scanning procedures and how inter-site imaging standardisation will be achieved will be described in a separate scanning document.

7.3 SUB-STUDY ASSESSMENTS

There will be three main sub-studies in relation to coronary 18F-fluoride uptake that will assess (i) short-term reproducibility, (ii) time course, and (iii) *in vivo* plaque characterisation. These will be performed only at the lead centre in Edinburgh and are described in more detail in separate protocols. Any participant will only be involved in one sub-study that requires a repeat 18F-fluoride positron emission tomography and computed tomography coronary angiogram in addition to the main PRE^{18}FFIR study protocol.

7.3.1 Short-term Reproducibility (PRE^{18}FFIR-REPRO)

Following the baseline assessments, a repeat 18F-fluoride positron emission tomography and computed tomography coronary angiogram will be performed within 21 days of the initial scan. This will allow the assessment of scan-rescan reproducibility. This will be performed in 20 patients.

7.3.2 Time Course (PRE^{18}FFIR-TIME)

Following the baseline assessments, a repeat 18F-fluoride positron emission tomography and computed tomography coronary angiogram will be performed within 6±2, 12±2, 26±2 and 52±2 weeks of the initial scan. This will allow a description of the natural history of 18F-fluoride uptake and positivity. This will be performed in four cohorts of 20 patients each. Any single patient will only undergo a maximum of two 18F-fluoride positron emission tomography and

three computed tomography coronary angiography scans.

7.3.3 *In Vivo* Plaque Characterisation (PRE^{18}FFIR-IMAGE)

In 80 patients, intravascular ultrasound, near infra-red spectroscopy and optical coherence tomography will be performed on the culprit and control non-culprit lesions at the time of invasive coronary angiography. This will permit detailed characterisation of plaque composition and structure with which to compare the 18F-fluoride positron emission tomography and computed tomography coronary angiography scans.

8 DATA COLLECTION

All trial data will be recorded onto paper case record forms (CRF) by a member of the research team and then entered an electronic database designed and developed by the Edinburgh Clinical Trials Unit.

9 STATISTICS AND DATA ANALYSIS

9.1 SAMPLE SIZE CALCULATION

This is based on an event rate of 24% cardiac death or recurrent myocardial infarction at 2 years. This is a conservative estimate since in our recent studies [Mills et al, 2011; Mills et al, 2012], we observed a 1-year event rate of 20% for death or recurrent myocardial infarction in consecutive unselected patients hospitalised with myocardial infarction. In our preliminary data [Joshi et al, 2014], 25-45% of patients had untreated 18F-fluoride positive plaques. Based on the assumption that one third of patients will have multiple 18F-fluoride positive plaques, and that the rate of death or recurrent myocardial infarction is 50% greater in these patients (30% versus 20% 2-year event rate), we will need 700 subjects at 80% power and two-sided $P<0.05$.

This power calculation is conservative as the analysis will be based on survival ('time to event') analysis techniques rather than a simple comparison of proportions.

9.2 PROPOSED ANALYSES

9.2.1 Description of Analysis Sets

The primary analyses will be based on all patients who have undergone the initial CT-PET scan.

9.2.2 Methods of Statistical Analysis

The primary analysis will be performed by calculating Kaplan-Meier estimates of the 'survival' curves for the time to first event (cardiac death or recurrent myocardial infarction) during follow up, and comparing these estimates for patients with and without non-culprit 18F-fluoride positive plaques, using a log-rank test. The results will be expressed as the estimated hazard ratio with the corresponding 95% confidence interval and p value. Patients who die

during follow-up whose deaths are not classified as cardiac deaths will be censored in the above analysis at the time of death.

Since 18F-fluoride uptake is a continuous measure, a potentially more sensitive analysis will explore the relationship between uptake and the risk of suffering an event (cardiac death or recurrent myocardial infarction). This will be performed using the Cox proportional hazards regression model, with (transformed) 18F-fluoride uptake as the only covariate. A range of potential transformations of the 18F-fluoride update will be explored, including fractional polynomials, to find an optimal fit to the data.

Once an appropriate transformation for the 18F-fluoride uptake has been identified (as above), the Global Registry of Acute Coronary Events (GRACE) score will be added into the Cox proportional hazards model, to assess the incremental prognostic value of 18F-fluoride over and above conventional clinical risk markers.

10 ADVERSE EVENTS

The Investigator is responsible for the detection and documentation of events meeting the criteria and definitions detailed below.

Full details of contraindications and side effects that have been reported following administration of the IMP are described in the study Investigator's Brochure.

Participants will be instructed to contact their Investigator at any time after consenting to join the trial if any symptoms develop. All adverse events (AE) as defined in section 10.2 that occur after joining the trial must be reported in detail in the Case Report Form (CRF) or AE form. In the case of an AE, the Investigator should initiate the appropriate treatment according to their medical judgment.

10.1 DEFINITIONS

An **adverse event** (AE) is any untoward medical occurrence in a clinical trial participant which does not necessarily have a causal relationship with an investigational medicinal product (IMP).

An **adverse reaction** (AR) is any untoward and unintended response to an IMP which is related to any dose administered to that participant.

A **serious adverse event** (SAE), **serious adverse reaction** (SAR). Any AE or AR that at any dose:

- results in death of the clinical trial participant
- is life threatening*
- requires in-patient hospitalisation** or prolongation of existing hospitalisation
- results in persistent or significant disability or incapacity
- consists of a congenital anomaly or birth defect

- results in any other significant medical event not meeting the criteria above

*Life-threatening in the definition of an SAE or SAR refers to an event where the participant was at risk of death at the time of the event. It does not refer to an event which hypothetically might have caused death if it were more severe.

**Any hospitalisation that was planned prior to randomisation will not meet SAE criteria. Any hospitalisation that is planned post randomisation will meet the SAE criteria.

A suspected unexpected serious adverse reaction (SUSAR) is any AR that is classified as serious and is suspected to be caused by the IMP, that it is not consistent with the information about the IMP in the Investigator's Brochure.

10.2 IDENTIFYING AEs AND SAEs

There will be a 48 hour time window to collect and record all AEs and SAEs which occur as a result of the 18F-fluoride intravenous injection and which occur during the 18F-fluoride PET and CT angiogram scanning visits including administration of the beta blockade, glyceryl trinitrate, contrast agent and radiation exposure. Patients attending the scanning visits will be asked to contact the research team if they experience any untoward effects within 48 hours of the scans. Only AEs/SAEs experienced during the scan and self-reported within 48 hours of the PET and /or CT scan will be recorded in the AE log and SAE form, respectively. Any AEs or SAEs out with the above definitions will not be recorded during the study although data on hospitalisations and deaths will be collected for long-term outcomes.

All other AEs and SAEs will be recorded from 48 hours until the last study visit in the medical notes.

Participants will be asked about the occurrence of AEs/SAEs at each scanning visit during the study. Open-ended and non-leading verbal questioning of the participant will be used to enquire about AE/SAE occurrence. Participants will also be asked if they have been admitted to hospital, had any accidents, used any new medicines or changed concomitant medication regimens. If there is any doubt as to whether a clinical observation is an AE, the event will be recorded.

AEs and SAEs may also be identified via information from support departments e.g. laboratories.

10.3 RECORDING AEs AND SAEs

Any pre-existing medical conditions (i.e. existed prior to informed consent) are not adverse events but should be recorded as medical history in the CRF. A pre-existing medical condition should only be recorded as an adverse event if

the condition worsens during the study. The event term should clearly document that the condition has worsened from baseline.

When an AE/SAE occurs, it is the responsibility of the Investigator to review all documentation (e.g. hospital notes, laboratory and diagnostic reports) related to the event. The Investigator will then record all relevant information in the CRF and on the SAE form (if the AE meets the criteria of serious). Information to be collected includes dose, type of event, onset date, Investigator assessment of severity and causality, date of resolution as well as treatment required, investigations needed and outcome.

10.4 ASSESSMENT OF AEs AND SAEs

Seriousness, causality, severity and expectedness will be assessed by the Principal Investigator. Cases that are considered serious, possibly, probably or definitely related to IMP and unexpected (i.e. SUSARs) will be unblinded.

The Investigator is responsible for assessing each AE.

The Chief Investigator may not downgrade an event that has been assessed by an Investigator as an SAE or SUSAR, but can upgrade an AE to an SAE, SAR or SUSAR if appropriate.

10.4.1 Assessment of Seriousness

The Investigator will make an assessment of seriousness as defined in Section 10.1.

10.4.2 Assessment of Causality

The Investigator will make an assessment of whether the AE/SAE is likely to be related to the IMP according to the definitions below.

- Unrelated: where an event is not considered to be related to the IMP.
- Possibly Related: The nature of the event, the underlying medical condition, concomitant medication or temporal relationship make it possible that the AE has a causal relationship to the study drug. The assessment of causality will be made against the reference safety information found in the Investigator's Brochure.

Where non Investigational Medicinal Products (NIMPs) e.g. rescue/escape drugs are given: if the AE is considered to be related to an interaction between the IMP and the NIMP, or where the AE might be linked to either the IMP or the NIMP but cannot be clearly attributed to either one of these, the event will be considered as an AR. Alternative causes such as natural history of the underlying disease, other risk factors and the temporal relationship of the event to the treatment should be considered and investigated. The blind should not be broken for the purpose of making this assessment.

10.4.3 Assessment of Expectedness

If an event is judged to be an AR, the evaluation of expectedness will be made based on knowledge of the reaction and the relevant product information documented in the IB.

The event may be classed as either:

Expected: the AR is consistent with the toxicity of the IMP listed in the IB.

Unexpected: the AR is not consistent with the toxicity in the IB.

10.4.4 Assessment of Severity

The Investigator will make an assessment of severity for each AE/SAE and record this on the CRF or SAE form according to one of the following categories:

Mild: an event that is easily tolerated by the participant, causing minimal discomfort and not interfering with every day activities.

Moderate: an event that is sufficiently discomforting to interfere with normal everyday activities.

Severe: an event that prevents normal everyday activities.

Note: the term 'severe', used to describe the intensity, should not be confused with 'serious' which is a regulatory definition based on participant/event outcome or action criteria. For example, a headache may be severe but not serious, while a minor stroke is serious but may not be severe.

10.5 REPORTING OF SAEs/SARs/SUSARs

Once the Investigator becomes aware that an SAE has occurred in a study participant, the information will be reported to the ACCORD Research Governance & QA Office **immediately or within 24 hours**. If the Investigator does not have all information regarding an SAE, they should not wait for this additional information before notifying ACCORD. The SAE report form can be updated when the additional information is received.

The SAE report will provide an assessment of causality and expectedness at the time of the initial report to ACCORD according to Sections 10.4.2, Assessment of Causality and 10.4.3, Assessment of Expectedness.

The SAE form will be transmitted by fax to ACCORD on **+44 (0)131 242 9447** or may be transmitted by hand to the office or submitted via email to Safety.Accord@ed.ac.uk. Only forms in a pdf format will be accepted by ACCORD via email.

Where missing information has not been sent to ACCORD after an initial report, ACCORD will contact the investigator and request the missing information.

All reports faxed to ACCORD and any follow up information will be retained by the Investigator in the Investigator Site File (ISF).

10.6 REGULATORY REPORTING REQUIREMENTS

The ACCORD Research Governance & QA Office is responsible for pharmacovigilance reporting on behalf of the co-sponsors (Edinburgh University and NHS Lothian).

The ACCORD Research Governance & QA Office has a legal responsibility to notify the regulatory competent authority and relevant ethics committee

(Research Ethics Committee (REC) that approved the trial). Fatal or life threatening SUSARs will be reported no later than 7 calendar days and all other SUSARs will be reported no later than 15 calendar days after ACCORD is first aware of the reaction.

ACCORD will inform Investigators at participating sites of all SUSARs and any other arising safety information.

An Annual Safety Report/Development Safety Update Report will be submitted, by ACCORD, to the regulatory authorities and RECs listing all SARs and SUSARs.

10.7 FOLLOW UP PROCEDURES

After initially recording an AE or recording and reporting an SAE, the Investigator should make every effort to follow each event until a final outcome can be recorded or reported as necessary. Follow up information on an SAE will be reported to the ACCORD office.

If, after follow up, resolution of an event cannot be established, an explanation should be recorded on the CRF, AE log or SAE form.

11 PREGNANCY

Women who are pregnant, breastfeeding or of child-bearing potential (women who have experienced menarche, are pre-menopausal and have not been sterilised) will not be enrolled into the trial.

12 TRIAL MANAGEMENT AND OVERSIGHT ARRANGEMENTS

12.1 TRIAL MANAGEMENT GROUP

The trial will be coordinated by a Project Management Group, consisting of the grant holders (Chief Investigator and Principal Investigator in Edinburgh) and site leads.

The Principal Investigator will oversee the study and will be accountable to the Chief Investigator. The Principal Investigator will be responsible for checking the CRFs for completeness, plausibility and consistency. Any queries will be resolved by the Investigator or delegated member of the trial team.

A Delegation Log will be prepared for each site, detailing the responsibilities of each member of staff working on the trial.

12.2 TRIAL STEERING COMMITTEE

A Trial Steering Committee (TSC) will be established to oversee the conduct and progress of the trial. Contact details of the TSC are detailed in a separate TSC charter. The review of SAEs will be added to the TSC agenda to ensure that appropriate action is taken if any safety issues arise.

12.3 DATA MONITORING COMMITTEE

This is an observational open label clinical cohort study involving an established radiotracer with over 40 years of experience. The result of the 18F-fluoride positron emission tomography and computed tomography coronary angiogram will not be fed back to the clinical team responsible for the patients care (except for clinically important incidental findings). For this reason, an independent Data Monitoring Committee (DMC) will not be convened for this study and all study serious adverse events will be reported to the sponsor and will be discussed by the TSC.

12.4 INSPECTION OF RECORDS

Investigators and institutions involved in the study will permit trial related monitoring and audits on behalf of the sponsor, REC review, and regulatory inspection(s). In the event of an audit or monitoring, the Investigator agrees to allow the representatives of the sponsor direct access to all study records and source documentation. In the event of regulatory inspection, the Investigator agrees to allow inspectors direct access to all study records and source documentation.

12.5 RISK ASSESSMENT

A study specific risk assessment has been performed by representatives of the co-sponsors, ACCORD monitors and the QA group, in accordance with ACCORD governance and sponsorship SOPs. Input has been sought from the Chief Investigator or designee. The outcomes of the risk assessment were the basis from which monitoring plans and audit plans were created. The risk assessment outcomes also indicated which risk adaptions (delete if no adaptations were possible) could be incorporated into to trial design.

12.6 BENEFIT/RISK BALANCE

12.6.1 Benefits

Patients may also benefit from additional procedures and investigations that they will undergo as part of the study. This will include closer medical supervision and non-invasive imaging investigations that may identify important incidental findings.

12.6.2 Risks

There are some potential hazards of the non-invasive investigations that we will perform as part of the trial. The main issues relate to exposure to ionising radiation and contrast agent administration. We have a well-developed protocol for cardiac positron emission and computed tomography imaging that minimizes radiation exposure and has clear procedures for managing adverse contrast reactions. We anticipate that the total research protocol dose (TPRD) radiation exposure not exceed 32 mSv. The TRPD includes radiation exposure from both the positron emission tomography and computed tomography scans combined. The estimated associated risk of developing fatal cancer is proportional to dose. Using a risk of 5% per Sv [ARSAC Notes] in a healthy population in this age group the estimated associated risk of

developing fatal cancer as a result of this exposure is in the region 1 in 650. This risk can be classified as moderate. It is likely that in a population of any patients in the age group 50+ the cancer risk is lower than 5% per Sv. For comparison the average annual background radiation dose arising from natural sources of ionising radiation in the environment in the UK is 2.2 mSv. The TRPD of 32 mSv incurred in this study is approximately 14 times annual background radiation from natural sources. This can be compared with other commonly used cardiovascular imaging techniques, such as nucleotide myocardial perfusion imaging (15-20 mSv) and diagnostic coronary angiography (7 mSv) [Einstein *et al*, 2007].

The risks of exposure to the contrast medium include allergic reactions and impairment of kidney function. Amongst patients with moderate-to-severe chronic kidney disease, there is a 2-4% risk of kidney impairment after computed tomography angiography [Barrett *et al*, 2006]. The risk of contrast exposure in this study will be minimised by exclusion of high-risk patients who have significant kidney disease (estimated glomerular filtration rate <30 mL/min/1.73m^2).

12.7 STUDY MONITORING AND AUDIT

ACCORD clinical trial monitors, or designees, will perform monitoring activities in accordance with the study monitoring plan. This will involve on-site visits and central monitoring activities as necessary (delete where not required). ACCORD QA personnel, or designees, will perform study audits in accordance with the study audit plan. This will involve investigator site audits, study management audits and facility (including 3rd parties) audits as necessary (delete where not required).

13 GOOD CLINICAL PRACTICE

13.1 ETHICAL CONDUCT

The study will be conducted in accordance with the principles of the International Conference on Harmonisation Tripartite Guideline for Good Clinical Practice (ICH GCP).

A favorable ethical opinion will be obtained from the appropriate REC and local R&D approval will be obtained prior to commencement of the study.

13.2 REGULATORY COMPLIANCE

The study will not commence until a Clinical Trial Authorisation (CTA) is obtained from the appropriate Regulatory Authority. The protocol and study conduct will comply with the Medicines for Human Use (Clinical Trials) Regulations 2004, as amended.

13.3 INVESTIGATOR RESPONSIBILITIES

The Investigator is responsible for the overall conduct of the study at the site and compliance with the protocol and any protocol amendments. In accordance with the principles of ICH GCP, the following areas listed in this section are also the responsibility of the Investigator. Responsibilities may be delegated to an appropriate member of study site staff.

13.3.1 Informed Consent

The Investigator is responsible for ensuring informed consent is obtained before any protocol specific procedures are carried out. The decision of a participant to participate in clinical research is voluntary and should be based on a clear understanding of what is involved.

Participants must receive adequate oral and written information – appropriate Participant Information and Informed Consent Forms will be provided. The oral explanation to the participant will be performed by the Investigator or qualified delegated person, and must cover all the elements specified in the Participant Information Sheet and Consent Form.

The participant must be given every opportunity to clarify any points they do not understand and, if necessary, ask for more information. The participant must be given sufficient time to consider the information provided. It should be emphasised that the participant may withdraw their consent to participate at any time without loss of benefits to which they otherwise would be entitled.

The participant will be informed and agree to their medical records being inspected by regulatory authorities and representatives of the sponsor(s) but understand that their name will not be disclosed outside the hospital.

The Investigator or delegated member of the trial team and the participant will sign and date the Informed Consent Form(s) to confirm that consent has been obtained. The participant will receive a copy of this document and a copy filed in the Investigator Site File (ISF) and participant's medical notes.

13.3.2 Study Site Staff

The Investigator must be familiar with the IMP, protocol and the study requirements. It is the Investigator's responsibility to ensure that all staff assisting with the study are adequately informed about the IMP, protocol and their trial related duties.

13.3.3 Data Recording

The Principal Investigator is responsible for the quality of the data recorded in the CRF at each Investigator Site. The source data plan identifies which source data correspond to CRF data and states which data are recorded directly into the CRF.

13.3.4 Investigator Documentation

Prior to beginning the study, each Investigator will be asked to provide particular essential documents to the ACCORD Research Governance & QA Office, including but not limited to:

- An original signed Investigator's Declaration (as part of the Clinical Trial Agreement documents);
- Curriculum vitae (CV) signed and dated by the Investigator indicating that it is accurate and current.

The ACCORD Research Governance & QA Office will ensure all other documents required by ICH GCP are retained in a Trial Master File (TMF), where required, and that appropriate documentation is available in local ISFs.

13.3.5 GCP Training

All study staff will hold evidence of GCP training where appropriate.

13.3.6 Confidentiality

All laboratory specimens, evaluation forms, reports, and other records must be identified in a manner designed to maintain participant confidentiality. All records must be kept in a secure storage area with limited access. Clinical information will not be released without the written permission of the participant. The Investigator and study site staff involved with this study may not disclose or use for any purpose other than performance of the study, any data, record, or other unpublished, confidential information disclosed to those individuals for the purpose of the study. Prior written agreement from the sponsor or its designee must be obtained for the disclosure of any said confidential information to other parties.

13.3.7 Data Protection

All Investigators and study site staff involved with this study must comply with the requirements of the Data Protection Act 1998 with regard to the collection, storage, processing and disclosure of personal information and will uphold the Act's core principles. Access to collated participant data will be restricted to those clinicians treating the participants, representatives of the sponsor(s) and representatives of regulatory authorities.

Computers used to collate the data will have limited access measures via user names and passwords.

Published results will not contain any personal data that could allow identification of individual participants.

14 STUDY CONDUCT RESPONSIBILITIES

14.1 PROTOCOL AMENDMENTS

Any changes in research activity, except those necessary to remove an apparent, immediate hazard to the participant in the case of an urgent safety measure, must be reviewed and approved by the Chief Investigator.

Amendments to the protocol must be submitted in writing to the appropriate REC, Regulatory Authority and local R&D for approval prior to participants being enrolled into an amended protocol.

14.2 PROTOCOL VIOLATIONS AND DEVIATIONS

Prospective protocol deviations, i.e. protocol waivers, will not be approved by the sponsors and therefore will not be implemented, except where necessary to eliminate an immediate hazard to study participants. If this necessitates a subsequent protocol amendment, this should be submitted to the REC, Regulatory Authority and local R&D for review and approval if appropriate.

Protocol deviations will be recorded in a protocol deviation log and logs will be submitted to the sponsors every 3 months. Each protocol violation will be reported to the sponsor within 3 days of becoming aware of the violation.

14.3 SERIOUS BREACH REQUIREMENTS

A serious breach is a breach which is likely to effect to a significant degree:

(a) the safety or physical or mental integrity of the participants of the trial; or

(b) the scientific value of the trial.

If a potential serious breach is identified by the Chief investigator, Principal Investigator or delegates, the co-sponsors (accord.seriousbreach@ed.ac.uk) must be notified within 24 hours. It is the responsibility of the co-sponsors to assess the impact of the breach on the scientific value of the trial, to determine whether the incident constitutes a serious breach and report to regulatory authorities and research ethics committees as necessary.

14.4 STUDY RECORD RETENTION

All study documentation will be kept for a minimum of 5 years from the protocol defined end of study point. When the minimum retention period has elapsed, study documentation will not be destroyed without permission from the sponsor.

14.5 END OF STUDY

It is anticipated that the study will last 4 years: two years for recruitment and two years of follow-up. The end of study is defined as the last participant's last visit.

The Investigators and/or the trial steering committee and/or the co-sponsor(s) have the right at any time to terminate the study for clinical or administrative reasons.

The end of the study will be reported to the REC and Regulatory Authority within 90 days, or 15 days if the study is terminated prematurely. The Investigators will inform participants of the premature study closure and ensure that the appropriate follow up is arranged for all participants involved.

A summary report of the study will be provided to the REC and Regulatory Authority within 1 year of the end of the study.

14.6 INSURANCE AND INDEMNITY

The co-sponsors are responsible for ensuring proper provision has been made for insurance or indemnity to cover their liability and the liability of the Chief Investigator and staff.

The following arrangements are in place to fulfil the co-sponsors' responsibilities:

- The Protocol has been designed by the Chief Investigator and researchers employed by the University and collaborators. The University has insurance in place (which includes no-fault compensation) for negligent harm caused by poor protocol design by the Chief Investigator and researchers employed by the University.
- Sites participating in the study will be liable for clinical negligence and other negligent harm to individuals taking part in the study and covered by the duty of care owed to them by the sites concerned. The co-sponsors require individual sites participating in the study to arrange for their own insurance or indemnity in respect of these liabilities.
- Sites which are part of the United Kingdom's Nation Health Service will have the benefit of NHS Indemnity.
- Sites out with the United Kingdom will be responsible for arranging their own indemnity or insurance for their participation in the study, as well as for compliance with local law applicable to their participation in the study.
- The manufacturer supplying IMP has accepted limited liability related to the manufacturing and original packaging of the study drug and to the losses, damages, claims or liabilities incurred by study participants based on known or unknown Adverse Events which arise out of the manufacturing and original packaging of the study drug, but not where there is any modification to the study drug (including without limitation re-packaging and blinding).

15 REPORTING, PUBLICATIONS AND NOTIFICATION OF RESULTS

15.1 AUTHORSHIP POLICY

Ownership of the data arising from this study resides with the study team. On completion of the study, the study data will be analysed and tabulated, and a clinical study report will be prepared in accordance with ICH guidelines.

15.2 PUBLICATION

The clinical study report will be used for publication and presentation at scientific meetings. Investigators have the right to publish orally or in writing the results of the study.

Summaries of results will also be made available to Investigators for dissemination within their clinics (where appropriate and according to their discretion).

15.3 PEER REVIEW

The study has undergone national and international peer review by the Wellcome Trust. There is additional peer review from the Trial Steering Committee and the Edinburgh Clinical Trials Unit as well as the study sponsors.

16 REFERENCES

ARSAC Notes for Guidance on the Clinical Administration of Radiopharmaceuticals and Use of Sealed Radioactive Sources -March 2006 (updated 2014) Appendix VII

Barrett BJ, Katzberg RW, Thomsen HS, Chen N, Sahani D, Soulez G, Heiken JP, Lepanto L, Ni ZH, Ni ZH, Nelson R. Contrast-induced nephropathy in patients with chronic kidney disease undergoing computed tomography: a double-blind comparison of iodixanol and iopamidol. *Invest Radiol*. 2006;41:815-821.

Davies M. The pathophysiology of acute coronary syndromes. Heart. 2000;83:361-6.

Detrano R, Guerci AD, Carr JJ, et al. Coronary calcium as a predictor of coronary events in four racial or ethnic groups. *N Engl J Med* 2008;358:1336-1345.

Dweck MR, Chow MW, Joshi NV, Williams MC, Jones C, Fletcher AM, Richardson H, White A, McKillop G, van Beek EJ, Boon NA, Rudd JH, Newby DE. Coronary arterial 18f-sodium fluoride uptake: A novel marker of plaque biology. *J Am Coll Cardiol*. 2012b;59:1539-1548

Dweck MR, Jones C, Joshi NV, Fletcher AM, Richardson H, White A, Marsden M, Pessotto R, Clark JC, Wallace WA, Salter DM, McKillop G, van Beek EJ, Boon NA, Rudd JH, Newby DE. Assessment of valvular calcification and inflammation by positron emission tomography in patients with aortic stenosis. *Circulation*. 2012a;125:76-86

Dweck MR, Khaw HJ, Sng GK, Luo EL, Baird A, Williams MC, Makiello P, Mirsadraee S, Joshi NV, van Beek EJ, Boon NA, Rudd JH, Newby DE. Aortic stenosis, atherosclerosis, and skeletal bone: Is there a common link with calcification and inflammation? *Eur Heart J*. 2013;34:1567-1574.

Einstein AJ, Moser KW, Thompson RC, Cerqueira MD, Henzlova MJ. Radiation dose to patients from cardiac diagnostic imaging. *Circulation*. 2007;116:1290-1305.

Joshi NV, Vesey AT, Williams MC, Shah ASV, Calvert PA, Craighead FHM, Yeoh SE, Wallace W, Salter D, Fletcher AM, van Beek EJR, Flapan AD, Uren NG, Behan MWH, Cruden NLM, Mills NL, Fox KAA, Rudd JHF, Marc R Dweck MR, Newby DE. 18F-Fluoride positron emission tomography identifies ruptured and high-risk coronary atherosclerotic plaques. *Lancet* 2014;383:705-713.

Mann J, Davies MJ. Mechanisms of progression in native coronary artery disease: role of healed plaque disruption. *Heart*. 1999;82:265-8.

Mills NL, Churchhouse AM, Lee KK, et al. Implementation of a sensitive troponin I assay and risk of recurrent myocardial infarction and death in patients with suspected acute coronary syndrome. *JAMA* 2011;305:1210-16.

Mills NL, Lee KK, McAllister DA, Churchhouse AMD, MacLeod M, Stoddard M, Walker S, Denvir MA, Fox KAA, Newby DE. Implications of lowering the

threshold of plasma troponin in the diagnosis of myocardial infarction: a cohort study. *BMJ* 2012;344:e1533.

Omland T, Pfeffer MA, Solomon SD, de Lemos JA, Rosjo H, Saltyte Benth J, Maggioni A, Domanski MJ, Rouleau JL, Sabatine MS, Braunwald E. Prognostic value of cardiac troponin i measured with a highly sensitive assay in patients with stable coronary artery disease. *J Am Coll Cardiol*. 2013;61:1240-1249

Rioufol G, Gilard M, Finet G, Ginon I, Boschat J, André-Fouët X. Evolution of spontaneous atherosclerotic plaque rupture with medical therapy: long-term follow-up with intravascular ultrasound. *Circulation*. 2004;110:2875-80.

Shah ASV, Griffiths M, Lee KK, McAllister, DA, Hunter AL, Cruikshank A, Alan Reid A, Stoddart M, Strachan F, Walker S, Collinson PO,Apple FS, Gray AJ, Fox KAA, Newby DE, Mills NL. High-sensitivity cardiac troponin and the under diagnosis of myocardial infarction in women. *ESC Hotline 2013.*

Thomas GS, Haraszti RA. A new frontier in atherosclerotic coronary imaging. Lancet. 2014;383:674-5.

Thompson RC, Allam AH, Lombardi GP, Wann LS, Sutherland ML, Sutherland JD, Soliman MA, Frohlich B, Mininberg DT, Monge JM, Vallodolid CM, Cox SL, Abd el-Maksoud G, Badr I, Miyamoto MI, el-Halim Nur el-Din A, Narula J, Finch CE, Thomas GS. Atherosclerosis across 4000 years of human history: the Horus study of four ancient populations. Lancet. 2013;381:1211-22.

FIGURE 1. Focal 18F-Fluoride Uptake in Patients with Myocardial Infarction and Stable Angina

Patient with acute ST-segment elevation myocardial infarction with (A) proximal occlusion (red arrow) of the left anterior descending artery on invasive coronary angiography and (B) intense focal 18F-fluoride uptake (yellow-red) at the site of the culprit plaque (red arrow) on the combined positron emission and computed tomogram.

Patient with anterior non-ST-segment elevation myocardial infarction with (C) culprit (red arrow; left anterior descending artery) and bystander non-culprit (white arrow; circumflex artery) lesions on invasive coronary angiography that were both stented during the index admission. Only the culprit lesion had increased 18F-fluoride uptake on combined positron emission and computed tomography (D) following percutaneous coronary intervention.

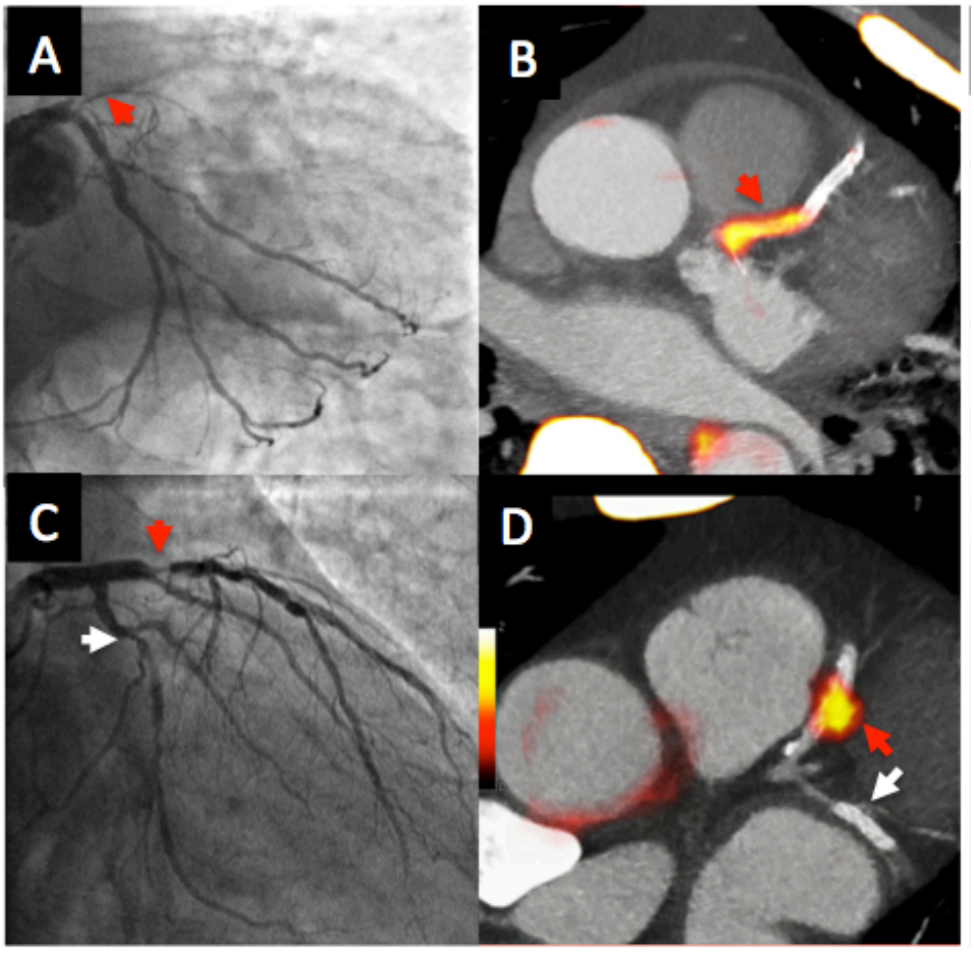

FIGURE 2. Patients with Stable Angina and 18F-Fluoride Uptake

Representative examples for 18F-fluoride uptake in patients with stable angina. Panels A-D, computed tomography coronary angiograms; panels E-H, 18F-fluoride positron emission tomograms; and panels I-L, fused positron emission tomograms and computed tomography coronary angiograms.

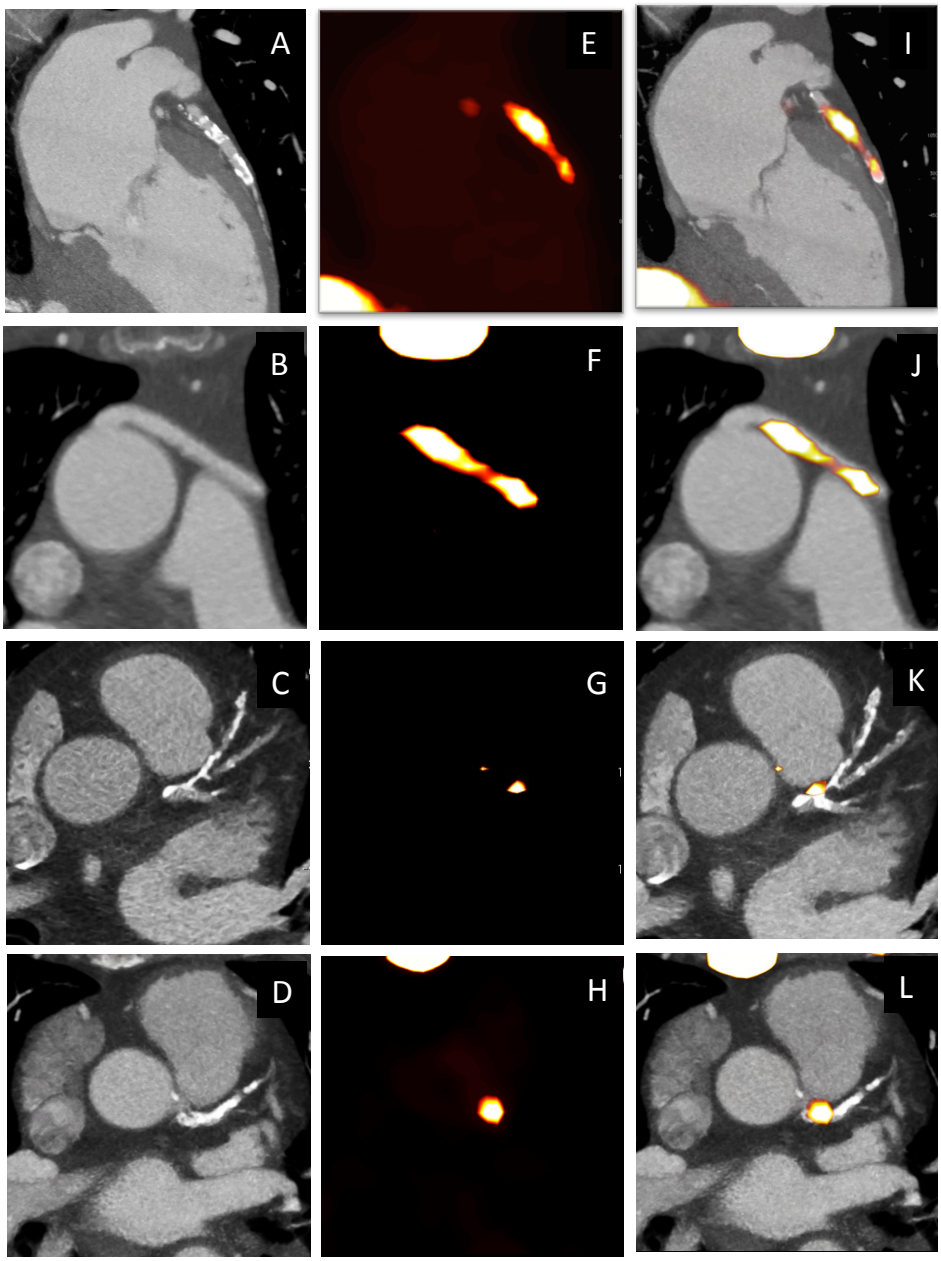

FIGURE 3. Patient Flow Chart

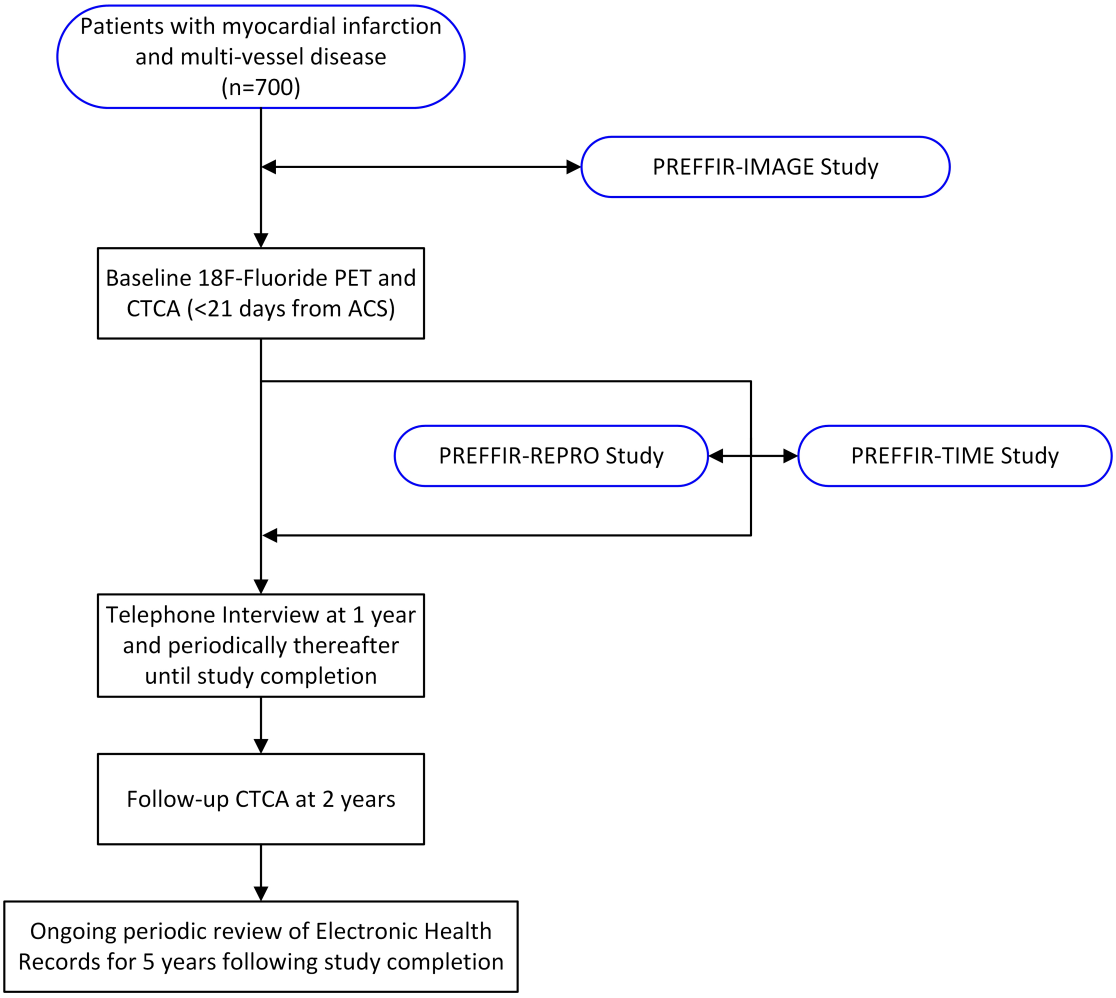

Academic and Clinical Central Office for Research and Development

Study Protocol

Dual antiplatelet therapy to Inhibit coronary Atherosclerosis and MyOcardial injury in patients with Necrotic high-risk coronary plaque Disease

Co-sponsors	University of Edinburgh & NHS Lothian ACCORD The Queen's Medical Research Institute 47 Little France Crescent Edinburgh EH16 4TJ
Funder	Wellcome Trust and AstraZeneca
Funding Reference Number	WT103782AIA - Senior Investigator Award
AstraZeneca Reference Number	ISSBRIL0250
Chief Investigator	Professor David Newby
EudraCT Number	2014-000952-26
REC Number	14/SS/0089
ClinicalTrials.gov ID number	NCT02110303
Version Number and Date	2.2, 5th June 2015

COORDINATING CENTRE

Chief Investigator Professor David E Newby Centre of Cardiovascular Science Chancellor's Building 51 Little France Crescent Edinburgh EH16 4SB Tel: 0131 242 6515 Fax: 0131 242 6379 Email: d.e.newby@ed.ac.uk	**Co-sponsor Representative** Elizabeth Craig University of Edinburgh Queen's Medical Research Institute 47 Little France Crescent Edinburgh EH16 4SB Tel: 0131 242 3325 Email: elizabeth.craig@ed.ac.uk
Trial Statistician Steff Lewis Centre for Population Health Sciences University of Edinburgh Teviot Place Edinburgh EH8 9AG Tel: 0131 650 3198 Email: steff.lewis@ed.ac.uk	**PARTICIPATING SITES** **Edinburgh Royal Infirmary** **Principal Investigator** Philip Adamson Centre of Cardiovascular Science Chancellor's Building 51 Little France Crescent Edinburgh EH16 4SB Tel: 0745 345 8084 Email: philadamson.nz@gmail.com

CONTENTS

PROTOCOL APPROVAL

DIAMOND

EudraCT number 2014-000952-26

Signatures

Professor David Newby	_____	_____
Chief Investigator	Signature	Date
Steff Lewis	_____	_____
Trial Statistician	Signature	Date
Elizabeth Craig	_____	_____
Sponsor(s) Representative	Signature	Date
Philip Adamson	_____	_____
Principal Investigator	Signature	Date

LIST OF ABBREVIATIONS

ACCORD	Academic and Clinical Central Office for Research & Development - Joint office for University of Edinburgh and NHS Lothian
AE	Adverse Event
AR	Adverse Reaction
CI	Chief Investigator
CT	Computer Tomography
CTA	Clinical Trial Authorisation
CTCA	Computer Tomography Coronary Angiography
CTIMP	Clinical Trial of an Investigational Medicinal Product
CRF	Case Report Form
DNA	Deoxyribose Nucleic Acid
eGRF	Estimated Glomerular Filtration Rate
GCP	Good Clinical Practice
ICH	International Conference on Harmonisation
IMP	Investigational Medicinal Product
ISF	Investigator Site File
MHRA	Medicines and Healthcare products Regulatory Authority
NIMP	Non Investigational Medicinal Product
PET	Positron Emission Tomography
PLATO	PLATelet Inhibition and Patient Outcomes
R&D	Research & Development
REC	Research Ethics Committee
SAE	Serious Adverse Event
SAR	Serious Adverse Reaction
SmPC	Summary of Product Characteristics
SOP	Standard Operating Procedure
SUSAR	Suspected Unexpected Serious Adverse Reaction
TMF	Trial Master File
UAR	Unexpected Adverse Reaction

1 INTRODUCTION

1.1 BACKGROUND

1.1.1 Pathogenesis of Coronary Artery Disease

Coronary plaque rupture of mildly stenotic coronary atherosclerosis is the commonest cause of acute coronary thrombosis and myocardial infarction [Davies, 2000]. This is the dominant type of plaque event causing an acute coronary syndrome, especially in men. It is closely linked to hypercholesterolaemia and has a dominant inflammatory phenotype. Classical histological features include a lipid-rich pool, thin fibrous cap, paucity of vascular smooth muscle cells and an intense inflammatory cell infiltrate [Davies, 2000].

Plaque rupture does not invariably lead to thrombotic occlusion of the coronary artery. Coronary plaque events are very common and the majority of such events do not cause coronary occlusion [Mann & Davies, 1999; Davies, 2000]. Here, plaque rupture and thrombosis is organised, remodelled and incorporated into the atherosclerotic plaque itself. Indeed, 80% of plaques that cause over 50% diameter stenosis have evidence of old healed plaque rupture with incorporation of thrombus into the atheroma [Mann & Davies, 1999]. This process contributes to the progression of coronary atherosclerosis and explains the first appearance, or step change in severity, of angina pectoris.

Coronary plaque events are often not isolated. Plaque rupture can occur throughout the body and is not confined to a single vascular bed. Moreover, in patients with acute coronary syndromes, it is common for multiple plaque events to occur simultaneously and beyond the culprit lesion itself. Post-mortem studies indicate that, on average, 2.4 coronary thrombotic events occur in each patient who presents with fatal coronary heart disease [Mann & Davies, 1999; Davies, 2000]. This suggests that systemic and generalised mechanisms and mediators play an important role in addition to local factors within the coronary artery wall.

In summary, coronary atherosclerosis is characterised by multiple and recurrent plaque rupture events that are often sub-clinical and cause step-wise growth of the plaque as it heals and remodels. Patients undergoing repeated plaque rupture events are likely to be at increased risk of myocardial infarction, especially if such an event coincides with a period of increased blood thrombogenicity. If these patients can be identified then there would be a clear rationale for using powerful anti-platelet agents, such as ticagrelor, to dampen down their thrombotic potential and the risk of adverse cardiovascular events.

1.1.2 Ticagrelor

Ticagrelor (AZD6140) is a reversible and direct-acting oral antagonist of the adenosine diphosphate $P2Y_{12}$ receptor. It provides faster, greater, and more consistent $P2Y_{12}$ inhibition than clopidogrel [Gurbel *et al*, 2009]. In the PLATelet inhibition and patient Outcomes (PLATO) trial of 18,624 patients presenting with an acute coronary syndrome, ticagrelor was superior to clopidogrel for the prevention of cardiovascular events and death [Wallentin *et al*, 2009]. It is unknown whether these anti-platelet and anti-thrombotic benefits extend to patients with coronary artery disease in the absence of an acute coronary syndrome.

1.1.3 Non-invasive Imaging of the Vulnerable Plaque

In the study of coronary artery disease, many researchers have searched for a non-invasive imaging biomarker of plaque vulnerability and rupture. For the first time, we have demonstrated that 18F-fluoride positron emission tomography can detect high-risk coronary plaque in patients with stable coronary artery disease [Joshi *et al*, 2013].

In the vasculature, 18F-fluoride acts as a marker of novel calcification activity [Dweck *et al*, 2012a; Dweck *et al*, 2013]. Similar to other conditions, calcification in coronary atheroma occurs as a healing response to intense necrotic inflammation, making 18F- fluoride a useful marker of high-risk atherosclerotic plaque. We have previously demonstrated increased uptake of this tracer in the coronary vasculature localizing to individual coronary lesions and identifying patients with increased cardiovascular risk factor profiles [Dweck *et al*, 2012b].

More recently we have conducted a prospective study of 40 patients with myocardial infarction in whom 18F-fluoride localised to the culprit plaque (Figure 1) in over 90% of patients [Joshi *et al*, 2013]. This finding was confirmed in 12 patients with a recent stroke undergoing carotid endartectomy where 18F-fluoride uptake was observed at the site of plaque rupture in 100% of patients and this uptake correlated with increased calcification activity and areas of necrosis on histology. Finally we studied 40 patients with stable coronary artery disease. Increased uptake was observed in 45% of these patients and this again localized to individual coronary plaques (Figure 2). Interestingly these lesions were associated with multiple high-risk markers on radiofrequency and gray-scale intravascular ultrasound (necrotic core, positive remodeling and microcalcification). Importantly, plasma high-sensitivity troponin concentrations were much higher in patients with 18F-fluoride positive plaques compared with patients without evidence of uptake (7.89±9.34 *versus* 3.10±1.89 ng/L, P=0·047; Figure 3). The latter observation is of particular interest as it supports the hypothesis that 18F-fluoride is detecting subclinical plaque rupture in those with stable disease, similar to its mechanism of activity following myocardial infarction. Moreover plasma troponin concentrations measured by a high-sensitivity assay also predict an adverse outcome amongst patients with stable coronary artery disease [Omland *et al*, 2013] and provide a useful surrogate biomarker of therapeutic efficacy.

1.1.4 High-Sensitivity Cardiac Troponin I

Cardiac troponins are regulatory muscle proteins that are released into the circulation following acute myocardial injury. Assays that quantify cardiac isoforms of troponin have greater specificity and sensitivity for the diagnosis of myocardial infarction than traditional cardiac enzymes. Indeed, we have demonstrated that this improved precision can lead to improved outcomes in patients with suspected acute coronary syndromes [Mills *et al*, 2011; Mills *et al*, 2012].

Recent advances have led to greatly improved assay sensitivity permitting quantification of extremely low concentrations of troponin with excellent precision. High-sensitivity cardiac troponin assays have limits of detection 10- to 100-fold lower than contemporary assays and are able to detect troponin in the circulation of the majority of healthy persons. Indeed, we have recently demonstrated important sex-specific thresholds for cardiac troponin when assessing patients with suspected acute coronary syndromes [Shah *et al*, 2013]. However, it is becoming increasingly recognized that plasma high-sensitivity troponin concentrations are powerful markers of future risk even when within the normal reference range. As previously indicated, plasma high-sensitivity troponin concentrations are increased in patients with high-risk 18F-fluoride positive coronary artery plaque [Joshi *et al*, 2013] and appear to predict an adverse outcome amongst patients with stable coronary artery disease [Omland *et al*, 2013].

1.2 RESEARCH HYPOTHESIS

Ticagrelor will reduce biomarkers of myocardial injury and inhibit disease progression in patients with stable coronary heart disease and evidence of high-risk coronary plaque defined by 18F-fluoride uptake on positron emission tomography.

1.3 RATIONALE FOR STUDY

The rationale for this study is based on two main observations relevant to the pathogenesis of coronary artery disease.

1. The majority of episodes of plaque rupture are subclinical because thrombus formation is non-occlusive and microembolism causes covert myocardial micro-injury that is insufficient to cause overt symptoms.
2. Cycles of rupture and non-occlusive thrombus formation lead to plaque expansion and coronary artery disease progression.

These two features can now be tracked using a high-sensitivity cardiac troponin I assay and computer tomography coronary angiography respectively.

Given this central role of thrombosis in atherogenesis, anti-thrombotic interventions have major potential to impact on the consequences and progression of atherosclerotic disease [Williams *et al*, 1997; Rioufol *et al*, 2004; Kwon *et al*, 2005]. With the advent of more potent platelet inhibition with ticagrelor, there is now the opportunity to assess whether dual anti-platelet therapy can improve markers of myocardial injury and disease progression.

To enhance the opportunity to detect such effects, we propose a stratified medicine approach where we will specifically select patients who have evidence of high-risk or subclinical ruptured coronary artery plaque identified by coronary 18F-fluoride uptake. We will then compare outcomes between those with and those without uptake, anticipating that only patients with high-risk plaque will demonstrate evidence of reduced injury and disease progression.

2 STUDY OBJECTIVES

2.1 OBJECTIVES

2.1.1 Primary Objective

To determine whether ticagrelor will reduce plasma high-sensitivity troponin concentrations compared with placebo in patients with stable coronary heart disease and high-risk coronary atheroma.

2.1.2 Secondary Objectives

a) To assess whether ticagrelor will reduce plasma high-sensitivity troponin concentrations in patients without increased coronary 18F-fluoride uptake.

b) To assess whether ticagrelor will reduce plasma high-sensitivity troponin concentrations over a 1-year time frame.

c) To assess whether ticagrelor will reduce coronary plaque volume or calcium score at the site of 18F-fluoride uptake.

d) To confirm the reproducibility of 18F-fluoride PET positivity

e) To assess the natural history of 18F-fluoride PET positive coronary plaque

2.1.3 Safety Objective

To determine whether the addition of ticagrelor to standard optimal medical therapy is safe and well tolerated in patients with stable coronary heart disease on optimal medical therapy. All bleeding events will be categorised according to the previous PLATO criteria [Wallentin *et al*, 2009] and recorded on the CRF.

2.1.4 Exploratory Objectives

The study design will also allow us to establish the effect of ticagrelor on disease progression. Using the baseline and repeat computed tomography coronary angiograms, we will be able to investigate changes in plaque burden, calcium score and lesion severity alongside the end points described above. This will be assessed throughout the coronary circulation as well as specifically at the site of 18F-fluoride uptake. As a measurement of treatment compliance and efficacy, we will also assess platelet-monocyte aggregates before and after *in vitro* stimulation with 20 μm adenosine diphosphate [Frelinger *et al*, 2011].

2.2 ENDPOINTS

2.2.1 Primary Endpoint

Plasma high sensitivity cardiac troponin I (hsTnI) concentration at 30 days in patients with coronary 18F-fluoride uptake.

2.2.2 Secondary Endpoints

a) Plasma hsTnI concentrations at 30 days in patients without coronary 18F-fluoride uptake.

b) High sensitivity cardiac troponin I (hsTnI) concentration at 30 days in total study population.

c) Plasma hsTnI concentrations at 1 year

d) Total calcium score at 1 year

e) Plaque volume at 1 year at the site of baseline coronary 18F-fluoride uptake

f) Reproducibility of 18F-fluoride uptake detected on PET imaging at 1 week

g) Natural history of 18F-fluoride uptake over 1 year

3 STUDY DESIGN

3.1 RATIONALE FOR STUDY DESIGN, DOSES AND CONTROL GROUPS

The study will be a randomised double blind placebo-controlled trial to ensure a rigorous study design and the avoidance of systematic biases of outcome measures. All recruited patients will undergo computed tomography coronary angiography and 18F-fluoride positron emission tomography (PET) scanning at baseline. Patients will then be randomized to ticagrelor 90 mg or matched placebo twice daily [Wallentin *et al*, 2009]. The dose has been selected on the basis of the PLATO trial [Wallentin *et al*, 2009]. The control groups will be two-fold. First there will be the active and inactive comparators of ticagrelor and placebo. Second we will examine for the presence and magnitude of an effect in the groups of patients with or without coronary 18F-fluoride uptake.

The primary outcome will be the comparison between ticagrelor and matched placebo on the change in plasma troponin concentration from baseline to one month in patients with coronary 18F-fluoride uptake. Secondary analyses will undertake the same assessment in patients without coronary 18F-fluoride uptake to determine whether this is particular to patients with high-risk coronary plaque or is seen in all patients with multivessel coronary artery disease.

Further longitudinal comparisons of these groups will determine whether the dominant effect on plasma troponin concentrations is seen only in the early phase or whether potential benefits are seen throughout the study period. Finally, we will assess whether in comparison to placebo, ticagrelor will inhibit progression of coronary atheroma (calcium score and plaque volume) at the site of high-risk coronary plaque.

An additional exploratory component to the study will be to assess the reproducibility and natural history of 18F-fluoride uptake within coronary plaques. This will be investigated with repeat PET scanning within a subgroup of the total population.

4 STUDY POPULATION

4.1 Number Of Participants

We will recruit 250 patients with stable coronary heart disease from the Edinburgh Heart Centre.

4.2 Inclusion Criteria

For inclusion in the study subjects should fulfill the following criteria:

1. Patients aged ≥40 years with angiographically proven multivessel coronary artery disease defined as at least two major epicardial vessels with any combination of either (a) >50% luminal stenosis, or (b) previous revascularization (percutaneous coronary intervention or coronary artery bypass graft surgery).
2. Provision of informed consent prior to any study specific procedures
3. Receiving aspirin

4.3 Exclusion Criteria

Subjects should not enter the study if any of the following exclusion criteria are fulfilled:

1. An acute coronary syndrome within the last 12 months
2. An indication for dual anti-platelet therapy, such as drug eluting stent
3. Receiving thienopyridine therapy such as clopidogrel or prasugrel
4. Percutaneous coronary intervention or coronary artery bypass graft surgery within the last 3 months
5. Inability or unwilling to give informed consent
6. Women who are pregnant, breastfeeding or of child-bearing potential (women who have experienced menarche, are pre-menopausal and have not been sterilised) will not be enrolled into the trial
7. Known hypersensitivity to ticagrelor or one of its excipients
8. Active pathological bleeding or bleeding diathesis
9. Significant thrombocytopenia: platelets <100 x 10^9 /L
10. History of intracranial haemorrhage
11. Moderate to severe liver impairment (Child's Grade B or C)
12. Maintenance therapy with strong CYP3A4 inhibitors, such as ketoconazole, nefazodone, ritonavir, indinavir, atazanavir, or clarithromycin
13. Major intercurrent illness or life expectancy <1 year
14. Renal dysfunction (eGFR ≤30 mL/min/1.73 m^2)
15. Contraindication to iodinated contrast agents
16. Planned coronary revascularization or major non-cardiac surgery in the next 12 months
17. Maintenance therapy with simvastatin or lovastatin at doses greater than 40mg daily
18. Receiving oral anticoagulants including warfarin, rivaroxaban, dabigatran or apixaban.

4.4 Co-Enrolment

Co-enrolment with another clinical trial of an investigational medical product or of a trial involving the use of an additional anticoagulant (e.g. warfarin, dabigatran, rivaroxaban or apixaban) or antiplatelet (e.g. clopidogrel, prasugrel) will not be allowed with this study. A minimum of 4 months must elapse between studies of this nature prior to patient being eligible.

Co-enrolment involving trials not excluded above will be allowed provided this is not expected to place undue burden upon participants and their families. Consideration will also be given to the total exposure to ionising radiation should additional studies require further exposure.

5 PARTICIPANT SELECTION AND ENROLMENT

5.1 IDENTIFYING PARTICIPANTS

Patients will be identified by their usual care team from outpatient clinics and existing clinical databases (the Tomcat and TrakCare databases). They will initially be approached (either verbally or in writing) for study recruitment by their usual care team who are based at the Edinburgh Heart Centre. Patients will be provided with a Patient Information Sheet and given an opportunity to ask questions about participation in the trial.

5.2 CONSENTING PARTICIPANTS

After 2 days, patients willing to participate in the trial will be asked to attend a consent and screening visit at the Clinical Research Facility, Edinburgh. Written informed consent will be obtained by a suitably qualified member of the research team before any study related procedures are performed. Patients will be advised to inform their physicians and dentists that they are enrolled on the study before any surgery is scheduled and before any new medicinal product is taken.

5.3 SCREENING FOR ELIGIBILITY

Screening of clinical records for eligibility will be performed after written consent is obtained. If eligibility cannot be confirmed based on pre-existing clinical investigations (i.e. standard clinical biochemical and haematological variables have not been assessed within the past 6 months) then blood tests will be obtained to assess these variables. Once a patient has agreed to participate and is deemed eligible they will be invited to attend the baseline visit.

Baseline assessments will include clinical history and examination, review of patient records to confirm study eligibility and record clinical profile, standard clinical biochemical and haematological variables, plasma high sensitivity cardiac troponin I measurement, 12-lead electrocardiogram, 18F-fluoride positron emission tomography, computed tomography coronary calcium score and angiography, and storage of plasma, serum and DNA for future analysis.

5.4 INELIGIBLE AND NON-RECRUITED PARTICIPANTS

Ineligible and non-recruited patients will receive standard medical care. An anonymised log will be kept of patients who were screened for the study and subsequently found to be ineligible or not recruited.

5.5 PROCEDURES FOR HANDLING SUBJECTS INCORRECTLY ENROLLED, RANDOMISED OR INITIATED ON INVESTIGATIONAL MEDICINAL PRODUCT

Patients incorrectly randomized to the wrong treatment group will be maintained on allocated therapy unless blinding has been compromised. Given that this is a mechanistic study and not a clinical endpoint trial, they will be assigned to the treatment they actually received as part of the statistical analysis. Records will be kept of the treatment they were originally assigned to, and the treatment they received.

After the first 30 and 90 patients have been randomized into the trial, ECTU will check to ensure that minimization has achieved matching of the two treatment groups.

5.6 RANDOMISATION

5.6.1 Randomisation Procedures

Eligible patients will be randomized using a web-based randomization service to ensure allocation concealment. Given the modest sample size, we will minimise treatment allocation according to age, sex, baseline plasma troponin concentration and the presence of coronary 18F-fluoride uptake.

5.6.2 Treatment Allocation

The placebo and active medication will be presented in numbered packages in collaboration with the Investigational Supplies Group (University of Edinburgh).

5.6.3 Methods to Ensure Blinding

The inactive placebo comparator will be presented and packaged in a form that will be indistinguishable from the active medication, ticagrelor. Therefore the treating clinical staff and patient will be blind to the allocated treatment. An indication of treatment allocation will potentially be apparent with platelet-monocyte aggregate testing. This will be undertaken by a dedicated technician distinct from the clinical investigational team. Samples will be presented to the technician using anonymised sample codes. Results will be stored in the database but not released to the study investigators until the end of the trial.

5.6.4 Emergency Unblinding Procedures

Web-based computer randomisation software will generate a randomisation list based on the values used for minimisation. This list will then be provided to the Investigational Supplies Group (ISG) for drug labelling purposes. The randomisation software will also contain unblinding codes which can only be accessed using a username and password. A username and password will only be provided to the Sponsor and Pharmacy department and can be used if emergency unblinding is required. Requests for unblinding will either go through the Chief or Principal Investigator and unblinding will be performed as required by the duty Pharmacist.

5.6.5 Discontinuation of Investigational Medicinal Product

The investigational product will be discontinued under the following circumstances:

1. At the request of the patient or if the patient withdraws from the study.
2. By the investigator or the responsible clinician if this was felt to be in the best interests of the patient.
3. On completion of the study.

Brief interruptions of therapy will be permitted (<14 days) where there is a clinical need, such as unavoidable surgical intervention. In such circumstances, the IMP will be withdrawn 5 days prior to surgery and recommenced as appropriate by the clinical team.

5.6.6 Withdrawal of Study Participants

Participants are free to withdraw from the study at any point or a participant can be withdrawn by the investigator. If withdrawal occurs, the primary reason for withdrawal will be documented in the participant's case record form. The patient will have the option of withdrawal from (i) the repeat PET and CT sub-study only (ii) study medication with continued study procedures and collection of clinical and safety data (iii) all aspects of the trial but continued use of data collected up to that point, (iv) all aspects of the trial with removal of all previously collected data.

Randomised patients who wish to be withdrawn from the study before they have provided a blood sample for the assessment of plasma troponin concentration at one month of the trial,

will be withdrawn from the study and another participant will be recruited to replace them. Data on the original participant will be kept on the database.

6 INVESTIGATIONAL MEDICINAL PRODUCT AND PLACEBO

6.1 STUDY DRUG

Investigational product	Dosage form and strength	Manufacturer
Ticagrelor (AZD6410)	90 mg tablet	Astrazeneca

6.1.1 Study Drug Identification

Ticagrelor is presented as a round biconvex film-coated yellow tablet marked with Œ90¹ above ŒT¹ on one side.

6.1.2 Study Drug Manufacturer

AstraZeneca AB
Gärtunavägen
SE-151 85 Södertälje

SWEDEN

6.1.3 Marketing Authorisation Holder

AstraZeneca AB
S-151 85
Södertälje
Sweden

MA number EU/1/10/655/001-006

6.1.4 Labelling and Packaging

Astra Zeneca will supply study medication and placebo in prefilled HDPE bottles with Child resistant caps. The HDPE bottles will be clearly labelled for the purpose of this trial including the study title, trial subject number and study contact by the Investigational Supplies Group, Edinburgh (ISG).

A Qualified Person from ISG will then release the study drug to the Pharmacy Department at the Royal Infirmary of Edinburgh.

6.1.5 Storage

All study medication will be kept in a secure place under appropriate storage conditions in the Pharmacy Department at the Royal Infirmary of Edinburgh.

6.1.6 Summary of Product Characteristics or Investigators Brochure

The Summary of Product Characteristics (SmPC) is given in Appendix 1.

6.2 PLACEBO

Astra Zeneca will supply a matched placebo in prefilled HDPE bottles with Child resistant caps. The placebo will then be labelled by ISG and released to the Pharmacy Department at the Royal Infirmary of Edinburgh.

6.3 DOSING REGIME

One tablet twice daily for 12 months.

6.4 DOSE CHANGES

No alteration in the planned dosing regime will be allowed.

6.5 PARTICIPANT COMPLIANCE AND ACCOUNTABILITY

Members of the research team will assess treatment compliance at attendance of each of the study visits by interview and pill count. Any unused study medication will be returned to the Pharmacy Department at the Royal Infirmary for destruction.

6.6 OVERDOSE

Ticagrelor is well tolerated in single doses up to 900 mg. Gastrointestinal toxicity was dose-limiting in a single ascending dose study. Other clinically meaningful adverse reactions which may occur with overdose include dyspnoea and ventricular pauses.

In the event of overdose, we will observe for these potential adverse reactions and consider ECG monitoring. There is currently no known antidote to reverse the effects of ticagrelor and it is not expected to be dialysable. Treatment of overdose will follow local standard medical practice. The expected effect of excessive ticagrelor dosing is prolonged bleeding risk associated with platelet inhibition. If bleeding occurs appropriate supportive measures will be taken.

If an overdose occurs in the course of the study, the investigators or other site personnel will inform appropriate AstraZeneca representatives **within one day**, ie, immediately but no later than **the end of the next business day** of when he or she becomes aware of it.

The designated AstraZeneca representative will work with the investigator to ensure that all relevant information is provided to the AstraZeneca Patient Safety data entry site.

6.7 OTHER MEDICATIONS

6.7.1 Non-Investigational Medicinal Products

18F-Sodium Fluoride (18F-NaF)

At the time of positron emission tomography and computed tomography coronary angiography, patients may receive oral and/or intravenous beta-blockade, such as metoprolol 5-100 mg, to slow the heart rate to below 65 beats per minute to maximise image quality and reduce radiation exposure. Glyceryl trintrate spray or tablet will be administered sublingually (200-400 µg) to induce coronary vasodilatation to enhance image quality of the coronary angiogram.

6.7.2 Permitted Medications

All patients will be maintained on aspirin 75 mg once daily and maximally tolerated dose of statin. Patients will be encouraged to be maintained on maximally tolerated doses of angiotensin-converting enzyme inhibition and beta-blocker therapy as clinically indicated and

in accordance with local guidelines. Following completion of the study, the trial medications will be discontinued.

6.7.3 Prohibited Medications

- Strong CYP3A4 inhibitors, such as ketoconazole, clarithromycin, nefazodone, ritonavir, atazanavir.Thienopyridines such as prasugrel, clopidogrel and ticlopidine
- Coumarin anticoagulants such as warfarin
- Direct thrombin inhibitors such as dabigatran
- Factor Xa inhibitors such as rivaroxaban and apixaban
- Ergot alkaloids
- Cisapride
- Simvastatin or lovastatin when taken at doses >40 mg daily

7 STUDY ASSESSMENTS

Trial participants will undergo 8 study visits: screening visit, baseline, randomisation and after 1, 3, 6, 9 and 12 months.

7.1 SAFETY ASSESSMENTS

The study does not have any pre-specified safety outcome measures. However, all bleeding events will be categorized according to the previous PLATO criteria [Wallentin *et al*, 2009]. These will be reported through adverse event reporting mechanisms (see Section 10).

7.2 STUDY ASSESSMENTS

This is a prospective single-centre randomized double blind matched placebo controlled trial of ticagrelor 90 mg twice daily in patients with stable coronary artery disease for 1 year. Subjects will attend for clinical assessments at 30 days, 3, 6, 9 and 12 months with a final computed tomography coronary angiogram at the end of the study. The randomisation visit must be conducted within 25 days of the baseline visit.

	Screening -183 days	Baseline (-15 days ±10 days)	Randomisation (Day 0)	30 days (±5 days)	3 months (±14 days)	6 months (± 14 days)	9 months (± 14 days)	1 year (± 14 days)
Eligibility Criteria and PIS	X							
Continuing eligibility confirmed			X	X	X	X	X	
Consent	X							
Concomitant medications		X		X	X	X	X	X
Clinical History		X		X	X	X	X	X
Physical Examination		X						
Clinical Biochemistry and haematology	X (if not checked in past 6 months)	X					X	
Blood sampling for hsTnI		X		X	X	X	X	X
Blood sampling for PMA		X		X				
12-lead ECG		X		X	X	X	X	X
AE/SAE Reporting		X		X	X	X	X	X
Treatment allocation/Medication dispensed			X		X	X	X	
Compliance check				X	X	X	X	X
18F-Fluoride PET		X	X		X	X		X
			Additional 18F-Fluoride PET scans will be performed in a subgroup only					
CT attenuation correction								
			CT attenuation correction is required prior to each PET scan for the subgroups who undergo this					
CT Calcium Score		X						X
CT Coronary Angiogram		X	Repeat CTCA scans will be performed at the time of each PET scan for those who are in the reproducibility and natural history sub-studies					X

7.2.1 Baseline Assessments

Baseline assessments will include clinical history and examination, review of patient records to confirm study eligibility and record clinical profile, standard clinical biochemical and haematological variables, plasma high sensitivity cardiac troponin I measurement, platelet-monocyte aggregates, 12-lead electrocardiogram, 18F-fluoride positron emission tomography, computed tomography coronary calcium score and angiography, and storage of plasma, serum and DNA for future analysis.

7.2.2 Follow Up Assessments

At 1, 3, 6, 9 and 12 months, participants will undergo repeat clinical assessment, blood sampling, and 12-lead electrocardiogram. Compliance will be recorded by patient history and tablet count by a delegated member of the research team. At the final study visit (12 months), subjects will also undergo a repeat computed tomography coronary calcium score and angiography.

7.2.3 High Sensitivity Cardiac Troponin I

Plasma cardiac troponin I concentrations will be measured by the accredited Clinical Biochemistry Department of the Royal Infirmary of Edinburgh using the ARCHITECT$_{STAT}$ high-sensitive troponin I assay (Abbott Laboratories, Abbott Park, IL). This is the first commercially available high-sensitivity troponin I assay that has greater precision at very low concentrations compared with the contemporary assay. The limit of detection is 1.2 ng/L and the inter-assay coefficient of variation <10% at 4.7 ng/L. The upper reference limit (99th percentile) based on 4,590 samples from healthy men and women is 34 ng/L for men and 16 ng/L for women.

7.2.4 Positron Emission and Computed Tomography Coronary Angiography

Study scans will be performed in the Clinical Research Imaging Centre.

Patients with a heart rate exceeding 65 beats/min may receive intravenous or oral beta-blockade (e.g. 5 to 100 mg metoprolol) 1 h before computed tomography. All patients will receive sublingual glyceryl trinitrate (200-400 µg) just prior to the computed tomography coronary angiography.

All patients will undergo dual cardiac and respiratory-gated positron emission and computed tomography imaging of the coronary arteries with a hybrid scanner (64-multidetector Biograph mCT, Siemens Medical Systems, Erlangen, Germany). Study subjects will be administered a target dose of 250 MBq 18F-fluoride intravenously and subsequently rested in a quiet environment for 60 min. An attenuation correction computed tomography scan (non-enhanced 120 kV and 50 mA) will then be performed, followed by positron emission tomography imaging of the thorax in list-mode for 30 min.

Computed tomography coronary calcium score and angiography will be undertaken in the same visit as the 18F-floride scan and again at 1 year. With the patient lying still on the scanner after acquisition of the positron emission tomography scan, an electrocardiogram-gated breath-hold computed tomography scan (non-contrast-enhanced, 40 mAs/rotation, 120 kV; CareDose, Siemens Medical Systems) of the coronary arteries will be performed at the following settings: 330 ms rotation time, 100 (body mass index [BMI] <25 kg/m^2) or 120 (body mass index >25 kg/m^2) kV tube voltage, 160-245 mAs tube current, 3·8 mm/rotation table feed, prospective (heart rate regular and <60/min), or retrospective (heart rate >60 /min) electrocardiogram-gated. Depending on the BMI, a bolus of 80-100 mL of contrast (400 mgI/mL; Iomeron, Bracco, Milan, Italy) will be injected intravenously at 5 mL/s, after determining the appropriate trigger delay with a test bolus of 20 mL contrast material.

The positron emission tomography scans will be reconstructed in multiple phases of the cardiac cycle, with the diastolic phase (50-75%) used for analysis. The computed tomography coronary angiography scans will be reconstructed at 0·75 x 0·7 mm and 0·6 x 0·3 mm for retrospective and prospective acquisitions respectively at 60%, 65% and 70% of the cardiac cycle. Additional reconstructions will be undertaken as necessary. Positron emission tomography scans will correct for cardiac motion correction using electrocardiogram-gated images.

18F-F PET Natural History Sub-study

Using the same scan process as outlined above a sub-group of patients will be selected for 1 additional PET scan. In total this will involve 80 patients out of the total cohort. The first 20 participants to be scanned will be to assess the reproducibility of 18F-fluoride uptake and will undergo a second PET scan at the randomisation visit (1 week after the baseline scan). This group will comprise 10 patients from both of the PET positive and PET negative samples. Following this we will investigate the natural history of 18F-fluoride uptake by performing

repeat PET scans on 60 patients in total from the initial PET positive sample with 20 patients scanned at the 3 month, 6 month and 12 month follow up visits. No individual patient will undergo more than 2 PET scans during the course of the study. In order to allow accurate co-registration of images, repeat CT coronary angiograms will be performed at the time of the repeat PET scans. The additional PET scan for those in the sub-study will be performed at the 1 week, 3 month, 6 month or 12 month visit but the additional CTCA scan will only be performed at 1 week, 3 month or 6 month visits as the CTCA scan at 12 months will be performed on all participants irrespective of whether they are taking part in the sub-study

7.2.5 Platelet-Monocyte Aggregates

The effect of ticagrelor on platelet activation will be assessed before and after *in vitro* stimulation with 20μm adenosine diphosphate to assess inhibition of the $P2Y_{12}$ receptor [Harding *et al*, 2007; Burdess *et al*, 2010; Frehling *et al* 2011]. This will be performed at the baseline visit (before study medication ingestion) and at the 30 day visit [Gurbel et al 2009; Frehling et al 2011]. Platelet-monocyte aggregate measurements will be performed by a trained technician independent to the study team to ensure blinding of treatment allocation is not compromised.

Blood will be anticoagulated with D-phenylalanyl-L-prolyl-L-arginine chloromethylketone (PPACK; Cambridge Biosciences, UK). Five minutes after sample collection, samples will be stained with the following conjugated monoclonal antibodies: APC-conjugated CD14 (Becton-Dickinson, UK);, PE-conjugated CD62P (Becton-Dickinson, UK); PE-Cy7-conjugated CD11b(Becton-Dickinson, UK); FITC-conjugated CD42a(Becton-Dickinson, UK); and appropriate control samples prepared. Once stained, samples will be incubated for 20 min at room temperature and fixed with FACS-Lyse (PMA analysis) or paraformaldehyde (platelet analysis). Samples will be analyzed using a FACScalibur flow cytometer (Becton-Dickinson, UK). Platelet–monocyte aggregates will be defined as monocytes staining positive for CD42a, as described previously [Harding *et al*, 2007]. Analysis will be performed using FlowJo (Treestar, USA).

7.2.6 Biological Samples

Blood samples will be collected and tested at baseline, 30 days and 3, 6, 9 and 12 months. At baseline, blood samples will be taken for routine clinical biochemistry and haematology (including full blood count, urea, creatinine and electrolytes, liver function tests, total cholesterol and glucose).

Approximately 20 mL of blood will be obtained on each visit except that an additional 20 mL will be taken at baseline for the clinical biochemistry and haematology assessments. Blood will also be stored for DNA extraction for subsequent analysis as appropriate.

Blood samples will be processed and stored in the Clinical Research Facility. Blood sample will be processed (plasma and serum) and stored at -80°C for later analysis of potential extracellular matrix and inflammatory biomarkers. Blood will also undergo DNA extraction and flow cytometric assessment for platelet monocyte aggregates [Burdess *et al*, 2010].

All samples will be stored in locked secure freezers and in compliance with the sponsor's tissue governance policies.

All samples will be retained unless consent is withdrawn by the participant who specifically requests that their samples are destroyed.

8 DATA COLLECTION

All trial data will be recorded onto written case record forms (CRF) by a member of the research team and then entered into electronic CRFs designed and developed by the Edinburgh Clinical Trials Unit.

9 STATISTICS AND DATA ANALYSIS

9.1 SAMPLE SIZE CALCULATION

Patients with increased 18F-fluoride activity had plasma high-sensitivity troponin concentrations that were more than double those patients without increased 18F-fluoride uptake (7.89±9.34 versus 3.10±1.89 ng/L; P=0·047) in our recent trail [Joshi et al, 2013]. Based upon the assumption that ticagrelor will reduce plasma high sensitivity troponin concentrations by one half (i.e from 7.89 to 3.95 ng/L, with standard deviations of 9.34 and 1.89 respectively), we will require 48 patients per treatment arm at 80% power and two-sided P<0.05. Allowance for missing data brings this to 55 per group. We have previously demonstrated that 45% of patients with advanced but stable coronary artery disease demonstrate increased 18F-fluoride uptake so that in total we will need to recruit 250 patients with positron emission tomography to identify these 110 patients with coronary uptake of 18F-fluoride.

The Edinburgh Heart Centre performs more than 5,000 diagnostic angiograms and 2,500 angioplasty procedures per year. This should allow an adequate pool of potentially suitable patients with angiographically proven stable coronary artery disease from which to recruit.

9.2 PROPOSED ANALYSES

9.2.1 Description of Analysis Sets

The primary analysis will be to determine whether ticagrelor will reduce plasma high-sensitivity troponin concentrations compared with placebo in patients with stable coronary heart disease and increased coronary 18F-fluoride uptake. For this primary analysis, we will exclude any patient who does not have a blood sample for estimation of the one-month plasma troponin concentration or whose compliance is deemed inadequate (as estimated from pill counts). The required level of medication compliance will be described in the statistical analysis plan.

9.2.2 Methods of Statistical Analysis

For the primary analysis, the change in plasma high-sensitivity troponin concentration from baseline to 30 days will be compared between the two treatment groups (ticagrelor and placebo) using linear regression, adjusting for the minimisation variables, in patients with coronary 18F-fluoride uptake. Prior to analysis, tests for normality will be undertaken and, where data are skewed, logarithmic transformation will be considered prior to analysis. Effect sizes and 95% confidence intervals will be calculated. Similar analyses will be performed for the assessment of troponin at 30 days in patients without coronary 18F-fluoride uptake, and in the study population as a whole; for troponin at 1 year; and for calcium score and plaque volume at 1 year at the site of baseline coronary 18F-fluoride uptake.

Statistical analysis will be performed using SAS. A two-sided P<0·05 will be taken as statistically significant. A full statistical analysis plan will be documented prior to data base lock. This will be overseen by the trial statistician in the Edinburgh Clinical Trials Unit.

10 ADVERSE EVENTS

The Investigator is responsible for the detection and documentation of events meeting the criteria and definitions detailed below.

Full details of contraindications and side effects that have been reported following administration of the IMP can be found in the relevant Summary of Product Characteristics (SmPC).

Participants will be instructed to contact their Investigator at any time after consenting to join the trial if any symptoms develop. All adverse events (AE) that occur after joining the trial

must be reported in detail in the Case Report Form (CRF) or AE form. In the case of an AE, the Investigator should initiate the appropriate treatment according to their medical judgment. After initially recording an AE, the Investigator should follow each AE until resolution of the event or until no longer medically indicated.

10.1 DEFINITIONS

An **adverse event** (AE) is any untoward medical occurrence in a clinical trial participant which does not necessarily have a causal relationship with an investigational medicinal product (IMP).

An **adverse reaction** (AR) is any untoward and unintended response to an IMP which is related to any dose administered to that participant.

A **serious adverse event** (SAE), **serious adverse reaction** (SAR). Any AE or AR that at any dose:

- results in death of the clinical trial participant;
- is life threatening*;
- requires in-patient hospitalisation^ or prolongation of existing hospitalisation;
- results in persistent or significant disability or incapacity;
- consists of a congenital anomaly or birth defect;
- results in any other significant medical event not meeting the criteria above.

*Life-threatening in the definition of an SAE or SAR refers to an event where the participant was at risk of death at the time of the event. It does not refer to an event which hypothetically might have caused death if it were more severe.

^Any hospitalisation that was planned prior to randomisation will not meet SAE criteria. Any hospitalisation that is planned post randomisation will meet the SAE criteria.

A suspected unexpected serious adverse reaction (SUSAR) is any AR that is classified as serious and is suspected to be caused by the IMP, that it is not consistent with the information about the IMP in the Summary of Product Characteristics (SmPC) or Investigators Brochure.

10.2 IDENTIFYING AEs AND SAEs

All AEs and SAEs will be recorded from the time a participant signs the consent form to take part in the study until the last study visit.

Participants will be asked about the occurrence of AEs/SAEs at every visit during the study. Open-ended and non-leading verbal questioning of the participant will be used to enquire about AE/SAE occurrence. Participants will also be asked if they have been admitted to hospital, had any accidents, used any new medicines or changed concomitant medication regimens. If there is any doubt as to whether a clinical observation is an AE, the event will be recorded.

AEs and SAEs may also be identified via information from support departments e.g. laboratories.

10.3 RECORDING AEs AND SAEs

When an AE/SAE occurs, it is the responsibility of the Investigator to review all documentation (e.g. hospital notes, laboratory and diagnostic reports) related to the event. The Investigator will then record all relevant information in the CRF and on the SAE form (if the AE meets the criteria of serious).

Information to be collected includes dose, type of event, onset date, Investigator assessment of severity and causality, date of resolution as well as treatment required, investigations needed and outcome.

10.4 ASSESSMENT OF AEs AND SAEs

Seriousness, causality, severity and expectedness will be assessed by the Principal Investigator. For randomised double blind studies, AEs will be assessed as though the participant is taking active IMP. Cases that are considered serious, possibly, probably or definitely related to IMP and unexpected (i.e. SUSARs) will be unblinded.

The Investigator is responsible for assessing each AE.

The Chief Investigator (CI) may not downgrade an event that has been assessed by an Investigator as an SAE or SUSAR, but can upgrade an AE to an SAE, SAR or SUSAR if appropriate.

10.4.1 Assessment of Seriousness

The Investigator will make an assessment of seriousness as defined in Section 10.1.

10.4.2 Assessment of Causality

The Investigator will make an assessment of whether the AE/SAE is likely to be related to the IMP according to the definitions below.

- Unrelated: where an event is not considered to be related to the IMP.
- Possibly Related: The nature of the event, the underlying medical condition, concomitant medication or temporal relationship make it possible that the AE has a causal relationship to the study drug. The assessment of causality will be made against the reference safety information found in the Summary of Product Characteristics.

Where non Investigational Medicinal Products (NIMPs) e.g. rescue/escape drugs are given: if the AE is considered to be related to an interaction between the IMP and the NIMP, or where the AE might be linked to either the IMP or the NIMP but cannot be clearly attributed to either one of these, the event will be considered as an AR. Alternative causes such as natural history of the underlying disease, other risk factors and the temporal relationship of the event to the treatment should be considered and investigated. The blind should not be broken for the purpose of making this assessment.

10.4.3 Assessment of Expectedness

If an event is judged to be an AR, the evaluation of expectedness will be made based on knowledge of the reaction and the relevant product information documented in the SmPC/IB.

The event may be classed as either:

Expected: the AR is consistent with the toxicity of the IMP listed in the SmPC/IB.

Unexpected: the AR is not consistent with the toxicity in the SmPC/IB.

10.4.4 Assessment of Severity

The Investigator will make an assessment of severity for each AE/SAE and record this on the CRF or SAE form according to one of the following categories:

Mild: an event that is easily tolerated by the participant, causing minimal discomfort and not interfering with every day activities.

Moderate: an event that is sufficiently discomforting to interfere with normal everyday activities.

Severe: an event that prevents normal everyday activities.

Note: the term 'severe', used to describe the intensity, should not be confused with 'serious' which is a regulatory definition based on participant/event outcome or action criteria. For example, a headache may be severe but not serious, while a minor stroke is serious but may not be severe.

10.5 REPORTING OF SAEs/SARs/SUSARs

Once the Investigator becomes aware that an SAE has occurred in a study participant, the information will be reported to the ACCORD Research Governance & QA Office **immediately or within 24 hours**. If the Investigator does not have all information regarding an SAE, they should not wait for this additional information before notifying ACCORD. The SAE report form can be updated when the additional information is received.

The SAE report will provide an assessment of causality and expectedness at the time of the initial report to ACCORD according to Sections 10.4.2, Assessment of Causality and 10.4.3, Assessment of Expectedness.

The SAE form will be transmitted by fax to ACCORD on **+44 (0)131 242 9447** or may be transmitted by hand to the office or submitted via email to Safety.Accord@ed.ac.uk. Only forms in a pdf format will be accepted by ACCORD via email.

Where missing information has not been sent to ACCORD after an initial report, ACCORD will contact the investigator and request the missing information.

All reports faxed to ACCORD and any follow up information will be retained by the Investigator in the Investigator Site File (ISF).

10.6 REGULATORY REPORTING REQUIREMENTS

The ACCORD Research Governance & QA Office is responsible for pharmacovigilance reporting on behalf of the co-sponsors (Edinburgh University and NHS Lothian).

The ACCORD Research Governance & QA Office has a legal responsibility to notify the regulatory competent authority and relevant ethics committee (Research Ethics Committee (REC) that approved the trial). Fatal or life threatening SUSARs will be reported no later than 7 calendar days and all other SUSARs will be reported no later than 15 calendar days after ACCORD is first aware of the reaction.

ACCORD will inform Investigators at participating sites of all SUSARs and any other arising safety information.

An Annual Safety Report/Development Safety Update Report will be submitted, by ACCORD, to the regulatory authorities and RECs listing all SARs and SUSARs.

10.7 ASTRA ZENECA REPORTING REQUIREMENTS

All SAEs will be reported to AstraZeneca within 7 days, whether or not considered causally related to the investigational product.

The report will indicate, either in the SAE report or the cover page, the causality of events in relation to all study medications and if the SAE is related to disease progression, as determined by the principal investigator.

A cover page/the SAE report will detail the following:

- Investigator Sponsored Study (ISS)

- The Investigator IND number assigned by the FDA
- The Investigator's name and address
- The trial name/title and AstraZeneca ISS reference number

The SAE report will be sent [with the accompanying cover page] by fax to AstraZeneca's designated fax line: 01582 838 010 or by email to: CRGSAERportingGlobalStudies@astrazeneca.com

10.8 FOLLOW UP PROCEDURES

After recording and reporting an SAE, the Investigator will follow each participant until resolution or death of the participant. Follow up information on an SAE will be reported to the ACCORD office.

After initially recording an AE, the Investigator should follow each AE until resolution of the event or until no longer medically indicated.

11 PREGNANCY

Woman of child-bearing potential will not be enrolled into the trial (woman who have experienced menarche, are pre-menopausal, have not been sterilised or who are currently pregnant).

Pregnancy is not considered an AE or SAE; however, the Investigator will collect pregnancy information for any female participants or female partners of male participants who become pregnant while participating in the study. The Investigator will record the information on a Pregnancy Notification Form and submit this to the ACCORD office within 14 days of being made aware of the pregnancy.

All pregnant female participants and partners of male participants will be followed up until following the outcome of the pregnancy.

All outcomes of pregnancy will be reported to AstraZeneca.

12 TRIAL MANAGEMENT AND OVERSIGHT ARRANGEMENTS

12.1 TRIAL MANAGEMENT GROUP

The trial will be coordinated by a Project Management Group, consisting of the grant holders (Chief Investigator and Principal Investigator in Edinburgh) and a coordinating Clinical Research Facility nurse.

The Principal Investigator will oversee the study and will be accountable to the Chief Investigator. The Principal Investigator will be responsible for checking the CRFs for completeness, plausibility and consistency. Any queries will be resolved by the Investigator or delegated member of the trial team.

A Delegation Log will be prepared for each site, detailing the responsibilities of each member of staff working on the trial.

12.2 TRIAL STEERING COMMITTEE

A Trial Steering Committee (TSC) will be established to oversee the conduct and progress of the trial. The review of SAEs will be added to the TSC agenda to ensure that appropriate action is taken if any safety issues arise.

12.3 DATA MONITORING COMMITTEE

In the PLATelet inhibition and patient Outcomes (PLATO) trial of 18,624 patients presenting with an acute coronary syndrome, ticagrelor was superior to clopidogrel for the prevention of cardiovascular events and death [Wallentin *et al*, 2009]. There were modest increases in the risks of bleeding and low rates of other side effects, such as dyspnoea. It is extremely unlikely that we will observe any substantial increased risk in our trial population given the small sample size of 250 patients and the very similar disease population in the PLATO trial that had a 100-fold larger trial population size. For this reason, an independent Data Monitoring Committee (DMC) will not be convened for this study and all study adverse events will be reported to the sponsors and AstraZeneca and will be discussed by the TSC.

12.4 INSPECTION OF RECORDS

Investigators and institutions involved in the study will permit trial related monitoring and audits on behalf of the sponsor, REC review, and regulatory inspection(s). In the event of an audit or monitoring, the Investigator agrees to allow the representatives of the sponsor direct access to all study records and source documentation. In the event of regulatory inspection, the Investigator agrees to allow inspectors direct access to all study records and source documentation.

12.5 RISK ASSESSMENT

An independent risk assessment will be performed by an ACCORD Clinical Trials Monitor to determine if monitoring is required and if so, at what level. An independent risk assessment will also be carried out by the ACCORD Quality Assurance Group to determine if an audit should be performed before/during/after the study and if so, at what locations and at what frequency.

12.6 BENEFIT/RISK BALANCE

12.6.1 Benefits

Patients may benefit from the treatment intervention. The benefits of ticagrelor in addition to standard medical therapy may include a reduction in the consequences and progression of coronary artery disease. In the PLATO trial [Wallentin *et al*, 2009], there appeared to be an ongoing and continuous improvement in outcomes beyond three months of an acute coronary syndrome. Ticagrelor may therefore have important ongoing secondary preventative benefits even in patients with apparently stable coronary artery disease. This is the rationale for the ongoing trial of the prevention of cardiovascular events in patients with prior myocardial infarction using ticagrelor compared with placebo on a background of aspirin: the PEGASUS trial (NCT01225562).

Patients may also benefit from additional procedures and investigations that they will undergo as part of the study. This will include closer medical supervision and non-invasive imaging investigations that may identify important incidental findings.

12.6.2 Risks

The risks of ticagrelor principally relate to bleeding, transient bradyarrhythmias and dyspnoea. As with most anti-thrombotic treatments, there is a risk of excess bleeding. The incidence of excess major bleeding was modest and we will ensure robust exclusion criteria to prevent inclusion of patients at risk of bleeding. Bradyarrhythmias have been described but are generally transient and do not require intervention. We will record 12-lead electrocardiograms at subject visits and question patients regarding symptoms of dizziness and syncope. For dyspnea, there is a 14% rate of breathlessness associated with ticagrelor in the PLATO trial [Wallentin *et al*, 2009]. However, again this is usually mild and self-limiting, and discontinuation of study medication was necessary in only 1% of patients.

There are some potential hazards of the non-invasive investigations that we will perform as part of the trial. The main issues relate to exposure to ionising radiation and contrast agent administration. We have a well-developed protocol for cardiac positron emission and computed tomography imaging that minimizes radiation exposure and has clear procedures for managing adverse contrast reactions. We anticipate that the total research protocol dose (TPRD) radiation exposure will be 30 mSv. The TRPD includes radiation exposure from both the PET and CT scans combined. The estimated associated risk of developing fatal cancer is proportional to dose. Using a risk of 5% per Sv [ARSAC Notes] in a healthy population in this age group the estimated associated risk of developing fatal cancer as a result of this exposure is in the region 1 in 650. This risk can be classified as moderate. It is likely that in a population of any patients in the age group 40-50 years the cancer risk is approximately 5% per Sv (and correspondingly less than 5% per Sv as age increases above 50 years). For comparison the average annual background radiation dose arising from natural sources of ionising radiation in the environment in the UK is 2.2 mSv. The TRPD of 30 mSv incurred in this study is approximately 13-14 times annual background radiation from natural sources. An objective of this study is to assess reproducibility of NaF PET/CT. A subgroup of 80 subjects will receive a second PET/CT and additional CT coronary angiogram. This increases the TRPD to 46 mSv in those subjects that have their repeat scan at the randomisation visit, 3 months or 6 months and to 38mSv in those that undergo their repeat scan at 12 months. The associated risk of developing cancer as a result of this exposure is in the region of 1 in 450. This risk can be classified as moderate. A TRPD of 46 mSv is approximately 21 times annual background radiation from natural sources in the UK. All subjects will have two CT coronary angiograms and those in the sub-studies returning at the randomisation visit, 3 months or 6 months will have 3 CT coronary angiograms. We note that in occasional individual cases the effective dose from CT coronary angiography may increase to approximately 20 mSv, if the subject's heart rate cannot be kept sufficiently low, requiring an alternative retrospective gating technique to be used. This will add approximately 12 mSv to the total research protocol dose for all subjects having CTCA.

This can be compared with other commonly used cardiovascular imaging techniques, such as nucleotide myocardial perfusion imaging (15-20 mSv) and diagnostic coronary angiography (7 mSv) [Einstein *et al*, 2007]. The risks of exposure to the contrast medium include allergic reactions and impairment of kidney function. Amongst patients with moderate-to-severe chronic kidney disease, there is a 2-4% risk of kidney impairment after computed tomography angiography [Barrett *et al*, 2006]. The risk of contrast exposure in this study will be minimised by exclusion of high-risk patients who have significant kidney disease (estimated glomerular filtration rate <30 mL/min/1.73m^2).

12.7 STUDY MONITORING AND AUDIT

An ACCORD Clinical Trials Monitor or an appointed monitor will visit the Investigator site prior to the start of the study and during the course of the study if required, in accordance with the monitoring plan if required. Risk assessment will determine if audit, by the ACCORD QA group, is required. Details will be captured in an audit plan. Audit of Investigator sites, study management activities and study collaborative units, facilities and 3rd parties may be performed.

13 GOOD CLINICAL PRACTICE

13.1 ETHICAL CONDUCT

The study will be conducted in accordance with the principles of the International Conference on Harmonisation Tripartite Guideline for Good Clinical Practice (ICH GCP).

A favorable ethical opinion will be obtained from the appropriate REC and local R&D approval will be obtained prior to commencement of the study.

13.2 REGULATORY COMPLIANCE

The study will not commence until a Clinical Trial Authorisation (CTA) is obtained from the appropriate Regulatory Authority. The protocol and study conduct will comply with the Medicines for Human Use (Clinical Trials) Regulations 2004, as amended.

13.3 INVESTIGATOR RESPONSIBILITIES

The Investigator is responsible for the overall conduct of the study at the site and compliance with the protocol and any protocol amendments. In accordance with the principles of ICH GCP, the following areas listed in this section are also the responsibility of the Investigator. Responsibilities may be delegated to an appropriate member of study site staff.

13.3.1 Informed Consent

The Investigator is responsible for ensuring informed consent is obtained before any protocol specific procedures are carried out. The decision of a participant to participate in clinical research is voluntary and should be based on a clear understanding of what is involved.

Participants must receive adequate oral and written information – appropriate Participant Information and Informed Consent Forms will be provided. The oral explanation to the participant will be performed by the Investigator or qualified delegated person, and must cover all the elements specified in the Participant Information Sheet and Consent Form.

The participant must be given every opportunity to clarify any points they do not understand and, if necessary, ask for more information. The participant must be given sufficient time to consider the information provided. It should be emphasised that the participant may withdraw their consent to participate at any time without loss of benefits to which they otherwise would be entitled.

The participant will be informed and agree to their medical records being inspected by regulatory authorities and representatives of the sponsor(s) but understand that their name will not be disclosed outside the hospital.

The Investigator or delegated member of the trial team and the participant will sign and date the Informed Consent Form(s) to confirm that consent has been obtained. The participant will receive a copy of this document and a copy filed in the Investigator Site File (ISF) and participant's medical notes.

13.3.2 Study Site Staff

The Investigator must be familiar with the IMP, protocol and the study requirements. It is the Investigator's responsibility to ensure that all staff assisting with the study are adequately informed about the IMP, protocol and their trial related duties.

13.3.3 Data Recording

The Principle Investigator is responsible for the quality of the data recorded in the CRF at each Investigator Site. The source data plan identifies which source data correspond to CRF data and states which data are recorded directly into the CRF.

13.3.4 Investigator Documentation

Prior to beginning the study, each Investigator will be asked to provide particular essential documents to the ACCORD Research Governance & QA Office, including but not limited to:

- An original signed Investigator's Declaration (as part of the Clinical Trial Agreement documents);
- Curriculum vitae (CV) signed and dated by the Investigator indicating that it is accurate and current.

The ACCORD Research Governance & QA Office will ensure all other documents required by ICH GCP are retained in a Trial Master File (TMF), where required, and that appropriate documentation is available in local ISFs.

13.3.5 GCP Training

All study staff must hold evidence of appropriate GCP training.

13.3.6 Confidentiality

All laboratory specimens, evaluation forms, reports, and other records must be identified in a manner designed to maintain participant confidentiality. All records must be kept in a secure storage area with limited access. Clinical information will not be released without the written permission of the participant. The Investigator and study site staff involved with this study may not disclose or use for any purpose other than performance of the study, any data, record, or other unpublished, confidential information disclosed to those individuals for the purpose of the study. Prior written agreement from the sponsor or its designee must be obtained for the disclosure of any said confidential information to other parties.

13.3.7 Data Protection

All Investigators and study site staff involved with this study must comply with the requirements of the Data Protection Act 1998 with regard to the collection, storage, processing and disclosure of personal information and will uphold the Act's core principles. Access to collated participant data will be restricted to those clinicians treating the participants, representatives of the sponsor(s) and representatives of regulatory authorities.

Computers used to collate the data will have limited access measures via user names and passwords.

Published results will not contain any personal data that could allow identification of individual participants.

14 STUDY CONDUCT RESPONSIBILITIES

14.1 PROTOCOL AMENDMENTS

Any changes in research activity, except those necessary to remove an apparent, immediate hazard to the participant in the case of a urgent safety measure, must be reviewed and approved by the Chief Investigator.

Amendments to the protocol must be submitted in writing to the appropriate REC, Regulatory Authority and local R&D for approval prior to participants being enrolled into an amended protocol.

14.2 PROTOCOL VIOLATIONS AND DEVIATIONS

Prospective protocol deviations, i.e. protocol waivers, will not be approved by the sponsors and therefore will not be implemented, except where necessary to eliminate an immediate hazard to study participants. If this necessitates a subsequent protocol amendment, this should be submitted to the REC, Regulatory Authority and local R&D for review and approval if appropriate.

Protocol deviations will be recorded in a protocol deviation log and logs will be submitted to the sponsors every 3 months. Each protocol violation will be reported to the sponsor within 3 days of becoming aware of the violation.

14.3 SERIOUS BREACH REQUIREMENTS

A serious breach is a breach which is likely to effect to a significant degree:

(a) the safety or physical or mental integrity of the participants of the trial; or

(b) the scientific value of the trial.

If a potential serious breach is identified by the Chief investigator, Principal Investigator or delegates, the co-sponsors (accord.seriousbreach@ed.ac.uk) must be notified within 24 hours. It is the responsibility of the co-sponsors to assess the impact of the breach on the scientific value of the trial, to determine whether the incident constitutes a serious breach and report to regulatory authorities and research ethics committees as necessary.

14.4 STUDY RECORD RETENTION

All study documentation will be kept for a minimum of 5 years from the protocol defined end of study point. When the minimum retention period has elapsed, study documentation will not be destroyed without permission from the sponsor.

14.5 END OF STUDY

It is anticipated that the study will last 2 years: one year for recruitment and one year of follow-up. The end of study is defined as the last participant's last visit.

The Investigators and/or the trial steering committee and/or the co-sponsor(s) have the right at any time to terminate the study for clinical or administrative reasons.

The end of the study will be reported to the REC and Regulatory Authority within 90 days, or 15 days if the study is terminated prematurely. The Investigators will inform participants of the premature study closure and ensure that the appropriate follow up is arranged for all participants involved.

A summary report of the study will be provided to the REC and Regulatory Authority within 1 year of the end of the study.

14.6 CONTINUATION OF DRUG FOLLOWING THE END OF STUDY

The study medication will not be continued at the trial conclusion as it is not currently licensed for use in stable coronary artery disease. Patients will remain eligible to use ticagrelor for any approved indication however (i.e. for 12 months following an acute coronary syndrome).

14.7 INSURANCE AND INDEMNITY

The co-sponsors are responsible for ensuring proper provision has been made for insurance or indemnity to cover their liability and the liability of the Chief Investigator and staff.

The following arrangements are in place to fulfil the co-sponsors' responsibilities:

- The Protocol has been designed by the Chief Investigator and researchers employed by the University and collaborators. The University has insurance in place (which includes no-fault compensation) for negligent harm caused by poor protocol design by the Chief Investigator and researchers employed by the University.
- Sites participating in the study will be liable for clinical negligence and other negligent harm to individuals taking part in the study and covered by the duty of care owed to them by the sites concerned. The co-sponsors require individual sites participating in the study to arrange for their own insurance or indemnity in respect of these liabilities.
- Sites which are part of the United Kingdom's Nation Health Service will have the benefit of NHS Indemnity.
- Sites out with the United Kingdom will be responsible for arranging their own indemnity or insurance for their participation in the study, as well as for compliance with local law applicable to their participation in the study.

- The manufacturer supplying IMP has accepted limited liability related to the manufacturing and original packaging of the study drug and to the losses, damages, claims or liabilities incurred by study participants based on known or unknown Adverse Events which arise out of the manufacturing and original packaging of the study drug, but not where there is any modification to the study drug (including without limitation re-packaging and blinding).

15 REPORTING, PUBLICATIONS AND NOTIFICATION OF RESULTS

15.1 AUTHORSHIP POLICY

Ownership of the data arising from this study resides with the study team. On completion of the study, the study data will be analysed and tabulated, and a clinical study report will be prepared in accordance with ICH guidelines.

15.2 PUBLICATION

The clinical study report will be used for publication and presentation at scientific meetings. Investigators have the right to publish orally or in writing the results of the study.

Summaries of results will also be made available to Investigators for dissemination within their clinics (where appropriate and according to their discretion).

15.3 PEER REVIEW

The study protocol and outcomes data have been reviewed by AstraZeneca who have agreed to help support the conduct and part funding of this clinical trial. There is additional peer review from the Trial Steering Committee and the Edinburgh Clinical Trials Unit statistician as well as the Medical Research Council.

16 REFERENCES

ARSAC Notes for Guidance on the Clinical Administration of Radiopharmaceuticals and Use of Sealed Radioactive Sources -March 2006 (updated 2014) Appendix VII

Barrett BJ, Katzberg RW, Thomsen HS, Chen N, Sahani D, Soulez G, Heiken JP, Lepanto L, Ni ZH, Ni ZH, Nelson R. Contrast-induced nephropathy in patients with chronic kidney disease undergoing computed tomography: a double-blind comparison of iodixanol and iopamidol. *Invest Radiol*. 2006;41:815-821.

Burdess A, Nimmo AF, Garden OJ, Murie JA, Dawson ARW, Fox KAA, Newby DE. Randomised controlled trial of dual anti-platelet therapy in patients undergoing surgery for critical limb ischaemia. *Ann Surg*. 2010;252:37-42.

Davies M. The pathophysiology of acute coronary syndromes. Heart. 2000;83:361-6.

Dweck MR, Chow MW, Joshi NV, Williams MC, Jones C, Fletcher AM, Richardson H, White A, McKillop G, van Beek EJ, Boon NA, Rudd JH, Newby DE. Coronary arterial 18f-sodium fluoride uptake: A novel marker of plaque biology. *J Am Coll Cardiol*. 2012b;59:1539-1548

Dweck MR, Jones C, Joshi NV, Fletcher AM, Richardson H, White A, Marsden M, Pessotto R, Clark JC, Wallace WA, Salter DM, McKillop G, van Beek EJ, Boon NA, Rudd JH, Newby DE. Assessment of valvular calcification and inflammation by positron emission tomography in patients with aortic stenosis. *Circulation*. 2012a;125:76-86

Dweck MR, Khaw HJ, Sng GK, Luo EL, Baird A, Williams MC, Makiello P, Mirsadraee S, Joshi NV, van Beek EJ, Boon NA, Rudd JH, Newby DE. Aortic stenosis, atherosclerosis, and

skeletal bone: Is there a common link with calcification and inflammation? *Eur Heart J*. 2013;34:1567-1574.

Einstein AJ, Moser KW, Thompson RC, Cerqueira MD, Henzlova MJ. Radiation dose to patients from cardiac diagnostic imaging. *Circulation*. 2007;116:1290-1305.

Frelinger AL, Michelson AD, Wiviott SD, Trenk D, Neumann FJ, Miller DL, Jakubowski JA, Costigan TM, McCabe CH, Antman EM, Braunwald E.Intrinsic platelet reactivity before P2Y12 blockade contributes to residual platelet reactivity despite high-level P2Y12 blockade by prasugrel or high-dose clopidogrel. Results from PRINCIPLE-TIMI 44. *Thromb Haemost.* 2011;106:219-26.

Gurbel PA, Bliden KP, Butler K, Tantry US, Gesheff T, Wei C, Teng R, Antonino MJ, Patil SB, Karunakaran A, Kereiakes DJ, Parris C, Purdy D, Wilson V, Ledley GS, Storey RF. Randomized double-blind assessment of the ONSET and OFFSET of the antiplatelet effects of ticagrelor versus clopidogrel in patients with stable coronary artery disease: the ONSET/OFFSET study. *Circulation*. 2009;120:2577-85.

Harding SA, Din JN, Sarma J, Jessop A, Weatherall M, Fox KA, Newby DE. Flow cytometric analysis of circulating platelet-monocyte aggregates in whole blood: methodological considerations. *Thromb Haemost* 2007;98:451-6.

Joshi NV, Vesey AT, Williams MC, Shah ASV, Calvert PA, Craighead FHM, Yeoh SE, Wallace W, Salter D, Fletcher AM, van Beek EJR, Flapan AD, Uren NG, Behan MWH, Cruden NLM, Mills NL, Fox KAA, Rudd JHF, Marc R Dweck MR, Newby DE. 18F-Fluoride positron emission tomography identifies ruptured and high-risk coronary atherosclerotic plaques. *Lancet* 2013; in press.

Kwon SU, Cho YJ, Koo JS, Bae HJ, Lee YS, Hong KS, Lee JH, Kim JS. Cilostazol prevents the progression of the symptomatic intracranial arterial stenosis: the multicenter double-blind placebo-controlled trial of cilostazol in symptomatic intracranial arterial stenosis. *Stroke*. 2005;36:782-6.

Mann J, Davies MJ. Mechanisms of progression in native coronary artery disease: role of healed plaque disruption. *Heart*. 1999;82:265-8.

Mills NL, Churchhouse AM, Lee KK, et al. Implementation of a sensitive troponin I assay and risk of recurrent myocardial infarction and death in patients with suspected acute coronary syndrome. *JAMA* 2011;305:1210-16.

Mills NL, Lee KK, McAllister DA, Churchhouse AMD, MacLeod M, Stoddard M, Walker S, Denvir MA, Fox KAA, Newby DE. Implications of lowering the threshold of plasma troponin in the diagnosis of myocardial infarction: a cohort study. *BMJ* 2012;344:e1533.

Omland T, Pfeffer MA, Solomon SD, de Lemos JA, Rosjo H, Saltyte Benth J, Maggioni A, Domanski MJ, Rouleau JL, Sabatine MS, Braunwald E. Prognostic value of cardiac troponin i measured with a highly sensitive assay in patients with stable coronary artery disease. *J Am Coll Cardiol*. 2013;61:1240-1249

Rioufol G, Gilard M, Finet G, Ginon I, Boschat J, André-Fouët X. Evolution of spontaneous atherosclerotic plaque rupture with medical therapy: long-term follow-up with intravascular ultrasound. *Circulation*. 2004;110:2875-80.

Shah ASV, Griffiths M, Lee KK, McAllister, DA, Hunter AL, Cruikshank A, Alan Reid A, Stoddart M, Strachan F, Walker S, Collinson PO,Apple FS, Gray AJ, Fox KAA, Newby DE, Mills NL. High-sensitivity cardiac troponin and the under diagnosis of myocardial infarction in women. *ESC Hotline 2013.*

Wallentin L, Becker RC, Budaj A, Cannon CP, Emanuelsson H, Held C, Horrow J, Husted S, James S, Katus H, Mahaffey KW, Scirica BM, Skene A, Steg PG, Storey RF, Harrington RA for the PLATO Investigators. Ticagrelor versus clopidogrel in patients with acute coronary syndromes. *N Engl J Med.* 2009;361:1045-57.

Williams MJ, Morison IM, Parker JH, Stewart RA. Progression of the culprit lesion in unstable

coronary artery disease with warfarin and aspirin versus aspirin alone: preliminary study. *J Am Coll Cardiol*. 1997;30:364-9.

FIGURE 1 Focal 18f-Fluoride Uptake in Patients with Myocardial Infarction and Stable Angina

Patient with acute ST-segment elevation myocardial infarction with (A) proximal occlusion (red arrow) of the left anterior descending artery on invasive coronary angiography and (B) intense focal 18F-fluoride uptake (yellow-red) at the site of the culprit plaque (red arrow) on the combined positron emission and computed tomogram.

Patient with anterior non-ST-segment elevation myocardial infarction with (C) culprit (red arrow; left anterior descending artery) and bystander non-culprit (white arrow; circumflex artery) lesions on invasive coronary angiography that were both stented during the index admission. Only the culprit lesion had increased 18F-fluoride uptake on combined positron emission and computed tomography (D) following percutaneous coronary intervention.

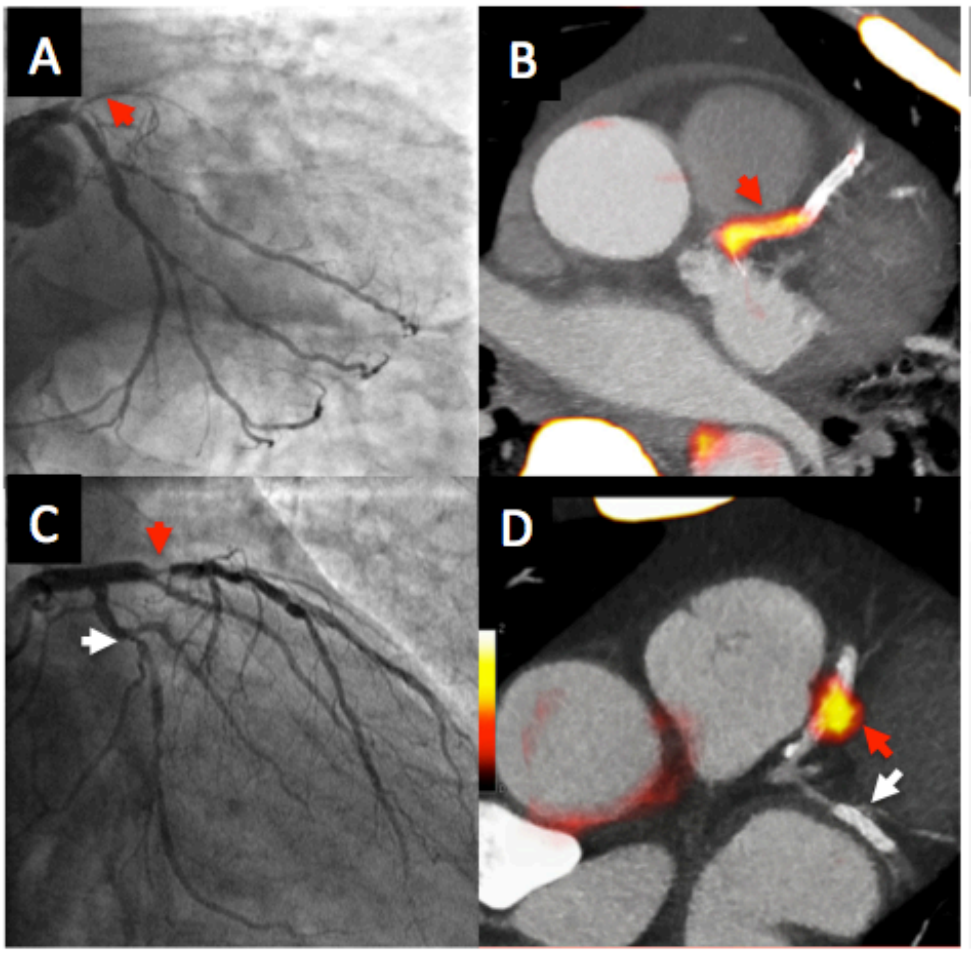

FIGURE 2: Patients with Stable Angina and 18F-Fluoride Uptake

Representative examples for 18F-fluoride uptake in patients with stable angina. Panels A-D, computed tomography coronary angiograms; panels E-H, 18F-fluoride positron emission tomograms; and panels I-L, fused positron emission tomograms and computed tomography coronary angiograms.

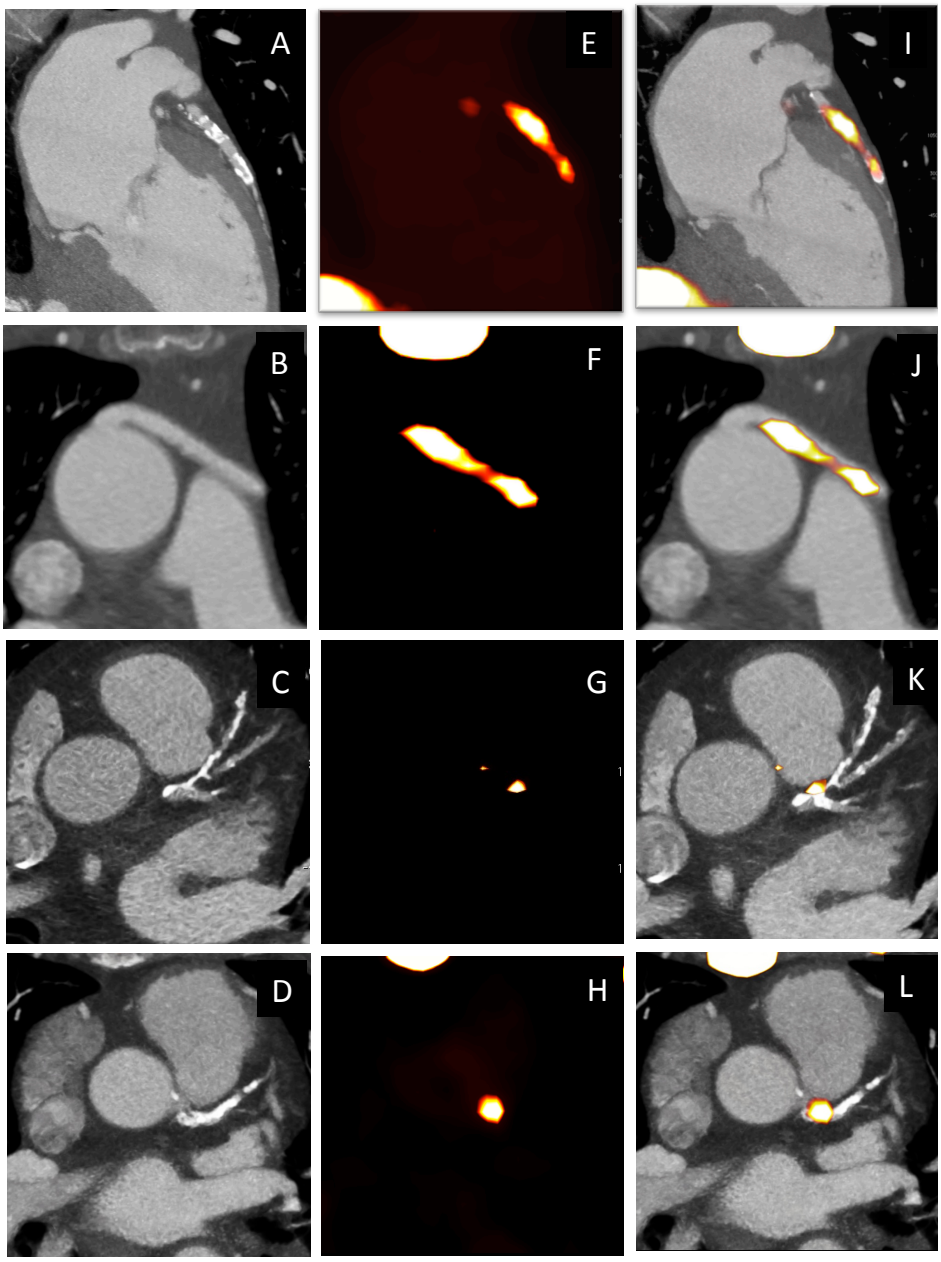

FIGURE 3: High-Sensitivity Troponin I Levels in Patients With Stable Angina Who Have and Do Not Have Increased Coronary 18F-Fluoride Uptake

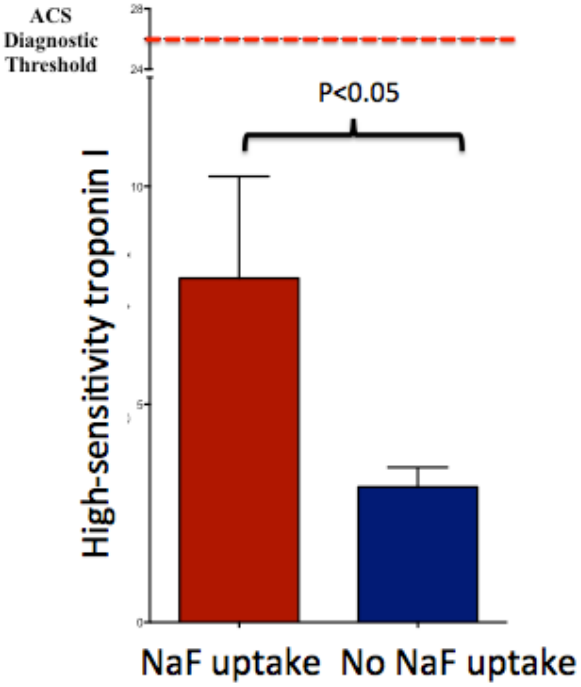

APPENDIX 1: Summary of Product Characteristics

http://www.medicines.org.uk/emc/medicine/23935/SPC/Brilique+90+mg+film+coated+tablets/

APPENDIX 2: Trial Investigators

Chief Investigator:	Professor David Newby
Principal Investigator:	Dr Philip Adamson
Co-Investigators:	Dr Marc Dweck
	Dr Nicholas Mills
	Dr Anoop Shah
	Dr James Rudd
	Professor Edwin van Beek
	Dr Alison Fletcher
	Dr Christopher Lucatelli
	Dr Tom MacGillivray

Study Protocol

Magnetic Resonance Imaging Using Ultrasmall Superparamagnetic Particles of Iron Oxide in Patients Under Surveillance for Abdominal Aortic Aneurysms to Predict Rupture or Surgical Repair

__M__RI for __A__bdominal __A__ortic __A__neurysms to predict __R__upture or __S__urgery: The MA^{3}RS trial

Co-sponsors	University of Edinburgh & NHS Lothian ACCORD The Queen's Medical Research Institute 47 Little France Crescent Edinburgh EH16 4TJ
Funder	Medical Research Council
Funding Reference Number	11/20/03
Chief Investigator	Professor David Newby
EudraCT Number	2012-002488-25
REC Number	12/ES/0068
Version Number and Date	V7 5th August 2014

Confidential

COORDINATING CENTRE

Chief Investigator	**Co-sponsor Representative**
Professor David E Newby Centre of Cardiovascular Science Chancellor's Building 51 Little France Crescent Edinburgh EH16 4SB Tel: 0131 242 6515 Fax: 0131 242 6379 Email: d.e.newby@ed.ac.uk	Marise Bucukoglu University of Edinburgh Queen's Medical Research Institute 47 Little France Crescent Edinburgh EH16 4SB Tel: 0131 242 9262 Fax: 0131 242 9447 Email: marise.bucukoglu@ed.ac.uk
Trial Manager	**Trial Statisticians**
Kirsteen Goodman/Kat Oatey Clinical Trials Manager Edinburgh Clinical Trials Unit University of Edinburgh Western General Hospital EH4 2XU Tel: 0131 537 2562/3841 Fax: 0131 537 3851 Email: kirsteen.goodman@ed.ac.uk k.oatey@ed.ac.uk	Gordon Murray Edinburgh MRC Hub for Trials and Research University of Edinburgh Teviot Place Edinburgh EH8 9AG Tel: 0131 650 3233 Fax: 0131 650 3224 Email: Gordon.murray@ed.ac.uk
Research Fellow Rachael Forsythe Research Fellow Centre of Cardiovascular Science Chancellor's Building 51 Little France Crescent Edinburgh, EH16 4SB Email: rachael.forsythe@ed.ac.uk	

PARTICIPATING SITES

Glasgow	**Fife and Forth Valley**
Principal Investigator Mr Wesley Stuart Consultant Vascular Surgeon Western Infirmary Glasgow G11 6NT Email: Wesley.stuart@ggc.scot.nhs.uk	**Principal Investigator** Mr Richard Holdsworth Consultant Vascular Surgeon Forth Valley Royal Hospital Stirling Road, Larbert FK5 4WR Tel: 01324 566830 Email: Richard.holdsworth@nhs.net

CONTENTS

PROTOCOL APPROVAL

Magnetic Resonance Imaging Using Ultrasmall Superparamagnetic Particles of Iron Oxide to Predict Clinical Outcome in Patients Under Surveillance for Abdominal Aortic Aneurysms

EudraCT number 2012-002448-25

Signatures

Chief Investigator	Signature	Date
Trial Statistician	Signature	Date
Sponsor(s) Representative	Signature	Date
Principal Investigator	Signature	Date

LIST OF ABBREVIATIONS

GCP	Good Clinical Practice
ICH	International Conference on Harmonisation
IMP	Investigational Medicinal Product
ISF	Investigator Site File
TMF	Trial Master File
SOP	Standard Operating Procedure
CRF	Case Report Form
AE	Adverse Event
SAE	Serious Adverse Event
AR	Adverse Reaction
SAR	Serious Adverse Reaction
UAR	Unexpected Adverse Reaction
SUSAR	Suspected Unexpected Serious Adverse Reaction
ACCORD	Academic and Clinical Central Office for Research & Development - Joint office for University of Edinburgh and NHS Lothian
WTCRF	Wellcome Trust Clinical Research Facility
MRI	Magnetic Resonance Imaging
CT	Computed Tomography
US	Ultrasound
AAA	Abdominal Aortic Aneurysm
Fe	Iron

SUMMARY

Abdominal aortic aneurysms have a prevalence of 5% in 65-74 year-old men and when ruptured, are associated with a mortality of up to 90%. Ruptured aortic aneurysms are a common cause of death in the United Kingdom, being the thirteenth commonest cause of death and accounting for 6,800 deaths each year in England and Wales.[1] Open surgical or endovascular intervention to prevent rupture is considered when the aortic aneurysm diameter exceeds 55 mm or expansion rates are greater than 10 mm/year.

Population screening halves the mortality associated with abdominal aortic aneurysms[1] and has led to the establishment of a national screening and surveillance programme. Currently, abdominal aortic aneurysm surveillance is complex because of the non-linearity and unpredictability of expansion rates, although the best predictor of aneurysm expansion is the baseline aneurysm diameter. However, up to one fifth of ruptured abdominal aortic aneurysm are less than 55 mm in diameter[2] and many patients present with diameters considerably greater than 55 mm without prior symptoms or rupture. Taken together, these data highlight the need for a more accurate method of rupture prediction that would better inform decisions to undertake preventative and potentially life-saving surgery.

We have developed a novel magnetic resonance imaging method that is based upon the known biological processes underlying aneurysm expansion and rupture. For the first time, the MA^{3}RS study proposes to assess this novel approach to identify aneurysms that are likely to expand more rapidly and potentially rupture. This technique would provide potentially important additional information to the current simplistic gold-standard of ultrasound measurement of aneurysm diameter.

1 INTRODUCTION

1.1 BACKGROUND

Aortic aneurysms frequently occur in patients with atherosclerosis and the two disease processes share several common risk factors. However, there are distinct differences. Atherosclerotic lesions are pre-dominantly located in the intima, whereas the media and adventitia are primarily involved in aneurysms. Aneurysm disease is also much more closely associated with smoking and hypertension, and has a particular predilection for the abdominal aorta.

The formation, growth and rupture of aneurysms are now recognised to be the result of a complex interplay between biological and mechanical factors. Aneurysm tissue is characterised by excessive medial neovascularisation, infiltration of inflammatory cells (principally macrophages) and irreversible remodeling of the extracellular matrix. These pathological processes do not affect the aorta uniformly but are focal in nature. Shear wall stress varies spatially within the aneurysm[3] and tensile strength varies in different parts of the aneurysm sac.[4] Focal neovascularisation occurs at the site of rupture and its presence corresponds to the degree of inflammation. These biological 'hotspots' represent sites of potential rupture and are putative targets for novel imaging strategies aiming to predict aneurysm expansion and assess the risk of rupture. In addition, tissue and wall stresses vary spatially within the aneurysm and tensile strength varies in different parts of the aneurysm sac. Synergy between these biological 'hotspots' and areas of intense biomechanical stress may be the focal point precipitating aneurysm rupture. Indeed, there is strong evidence that aneurysm rupture is seen in those patients with more rapid aneurysm expansion rates.[5, 6]

1.1.1 Magnetic Resonance Imaging

Magnetic resonance imaging is emerging as a useful investigative tool for cardiovascular disease that can distinguish the different atherosclerotic plaque components, such as the lipid-rich core and areas of calcification.[7] Standard gadolinium-based magnetic resonance imaging identifies areas of thrombus formation and fibrosis in abdominal aortic aneurysms.[8] Newer contrast agents containing superparamagnetic particles of iron oxide (SPIO) have been developed that provide additional biological and functional information through the detection of cellular inflammation within tissues. Ultrasmall SPIO (USPIO), with particle sizes in the range 10-30 nm, escape immediate recognition by the reticulo-endothelial system and persist for longer in the bloodstream allowing them to be used to assess the accumulation of macrophages within vascular and lymphatic tissues.[9, 10, 11, 12, 13] Current preparations are biodegradable and safe for clinical administration.[14, 15, 16]

USPIO accumulate in the aortae of hypercholesterolaemic rabbits[17] and in murine models of abdominal aortic aneurysms.[18] In humans, USPIO accumulate in ruptured or rupture- prone carotid plaques rather than stable plaques,[11, 12] and treatment with atorvastatin reduces both inflammation and USPIO uptake in carotid plaques.[13]

We have recently conducted a series of magnetic resonance imaging studies in patients with abdominal aortic aneurysms and shown that uptake of USPIO in the aortic wall correlates with macrophage activity and identifies cellular inflammation.[19, 20] Using a 3T magnetic resonance scanner, patients with asymptomatic abdominal aortic aneurysms (n=29; aneurysm diameter 4.0- 6.6 cm) attending our surveillance programme were imaged before and 24-36 hours after intravenous administration of USPIO. Histological examination of aneurysm tissue confirmed co-localization and uptake of USPIO in areas of macrophage infiltration (Figure 1).[19]

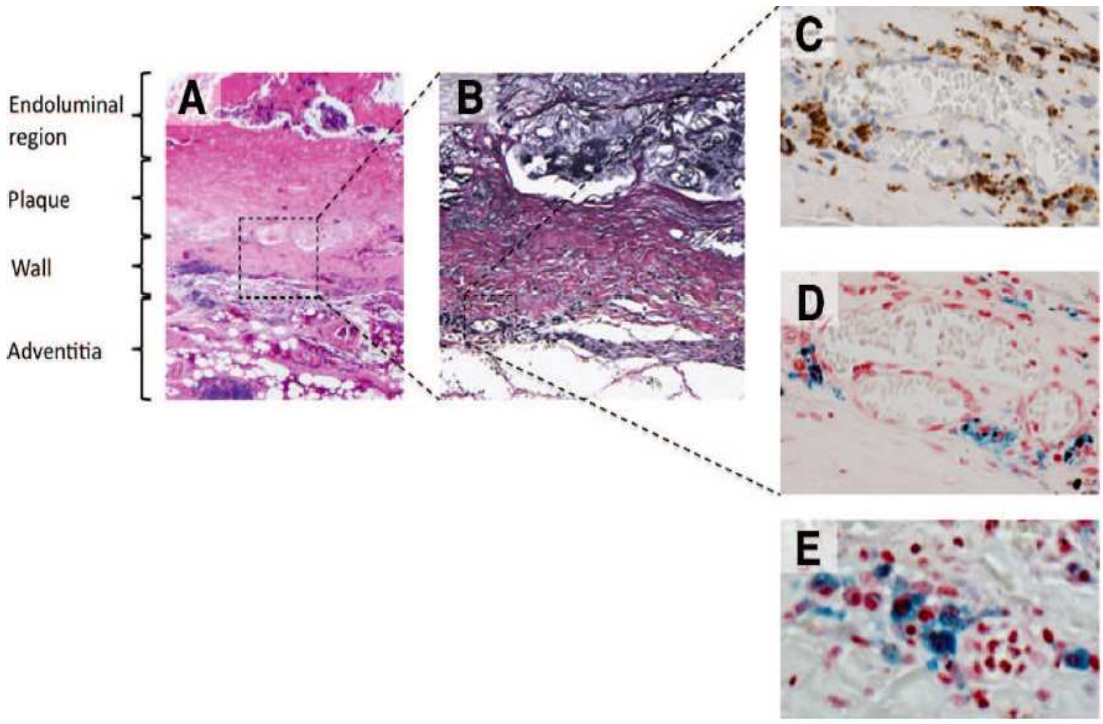

Figure 1. Representative histological sections of the aortic wall. **A**, Haematoxoylin and eosin (x20) of the full thickness of the aortic wall including atherosclerotic plaque, adherent thrombus and periadventitial fatty tissue. **B,** Elastin-van Gieson stain (x100) of the aortic wall showing complete destruction of the normal wall structure, including fibrosis (collagen, pink) of the media and adventitia and virtual absence of intact medial elastic fibers (black). **C,** Prussian blue staining for iron demonstrating co-localisation of CD68-positive macrophages (x400; brown) with **D,** Ultrasmall super-paramagnetic particles of iron oxide particles (x400; blue), **E,** High power (x1000) Prussian blue staining shows intracytoplasmic accumulation of USPIO within macrophages.

Furthermore, aortic aneurysms with mural USPIO uptake had a three-fold higher expansion rate when compared to abdominal aortic aneurysms with no or non-specific USPIO uptake despite similar baseline anteroposterior diameters (Figure 2).[19] Indeed, one patient with substantial mural USPIO uptake died suddenly 2 months after scanning from presumed aneurysm rupture. We have therefore shown that this technique holds major promise as a new method of risk-stratification of patients with abdominal aortic aneurysm that extends beyond simple anatomical measurements of aneurysm diameter.

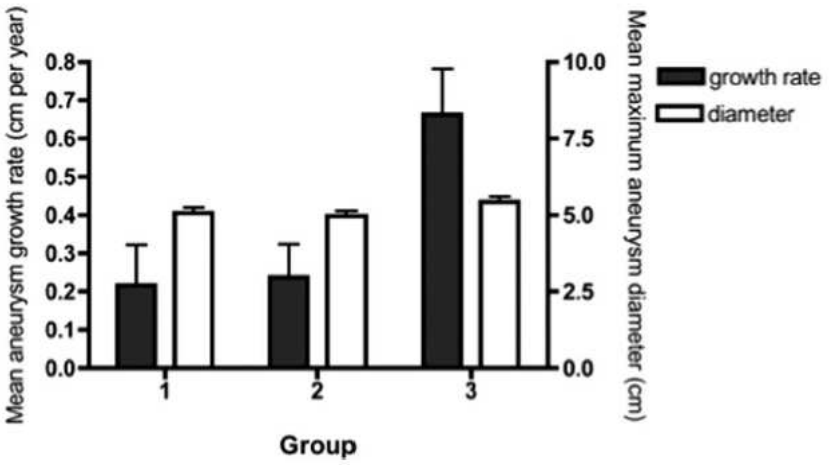

Figure 2. USPIO uptake in the aortic wall (group 3; 45% of total population) predicted a 3-fold increase in aneurysm expansion rate despite similar aortic diameters.

To date, the assessment of USPIO uptake has been qualitative or based on relative changes in signal intensity within regions of interest defined by vessel quadrants.[12, 13] However, this change in signal intensity can be caused by other factors including imaging artifacts. During the process of our studies, we have developed a more robust semi-quantitative image acquisition methodology for the detection of iron nanoparticle accumulation in humans using 3T magnetic resonance imaging.[19, 20] Here we apply a multi-echo gradient sequence to define the T2* value of the tissue. Images before and after USPIO administration are then co-registered and the difference in T2* value quantified. Following repeatability measurements in patients with abdominal aortic aneurysms, we have identified a threshold of change in signal intensity (59%) that defines USPIO accumulation in tissues (Figure 3).[20]

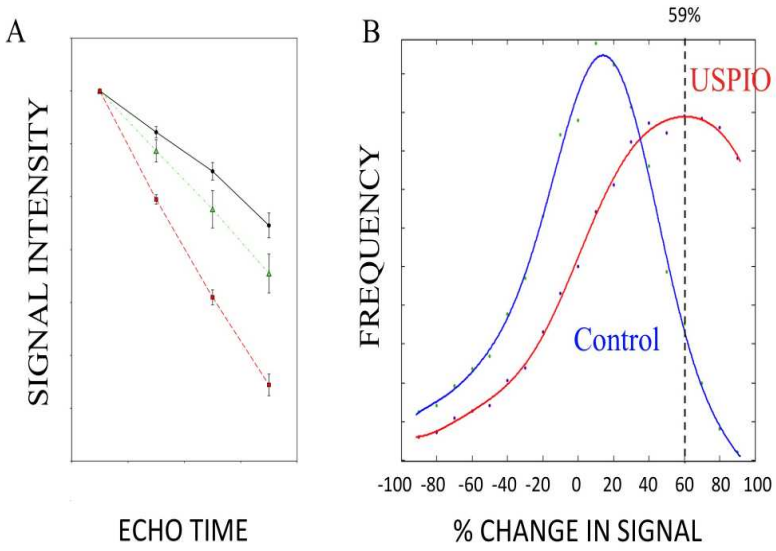

Figure 3. A. Signal intensity as percentage of first echo time (4.9 ms) within the multi-echo sequence of pre-contrast and post- contrast images in areas of no (black circles), low (green triangles) and high (red squares) USPIO uptake. **B.** Frequency of voxels with per cent change in T2* for patients who did (red) or did not (blue) receive USPIO. The upper 95% threshold of per cent change in T2* in the absence of USPIO was 59%.

1.1.2 Biomechanical Stress

Another potential predictive marker of aneurysm rupture is wall tissue stress. Information on aneurysm geometry is provided by computed tomography and magnetic resonance imaging, and this can be combined with finite element analysis to enable prediction of tissue stresses within the aneurysm wall.[3, 21] Peak wall tissue stress is higher in patients with symptomatic aneurysms[22] and co-localises with regions of inflammation identified by 18F-fluorodeoxyglucose positron emission tomography.[23] This suggests combining stress analysis with imaging of inflammation may provide added predictive value in the assessment of aneurysm expansion and potential rupture.

1.2 RATIONALE FOR STUDY

Ruptured AAA is the thirteenth commonest cause of death in the United Kingdom and accounts for 6,800 deaths each year in England and Wales. Population screening halves the mortality associated with AAA, and has led to the establishment of national screening and surveillance programmes. However, AAA surveillance is complex because of the non-linearity and unpredictability of expansion rates. Although the best predictor of aneurysm expansion is the aneurysm diameter, up to one fifth of ruptured AAA are less than 55 mm in diameter, and many patients present with diameters

considerably greater than 55 mm without prior symptoms or rupture. There is therefore a major unmet clinical need to predict aneurysm growth and rupture more accurately so that surgeons can better target preventative potentially life-saving surgery. We have developed a novel magnetic resonance imaging method that is based upon the known biological processes underlying aneurysm expansion and rupture. For the first time, this study proposes to assess this novel approach to identify aneurysms that are likely to expand more rapidly and potentially rupture. This technique would provide potentially important additional information to the current simplistic gold-standard of ultrasound measurement of aneurysm diameter.

2 STUDY OBJECTIVES

2.1 OBJECTIVES

2.1.1 Primary Objective

To determine whether mural uptake of USPIO provides incremental risk prediction in addition to standard risk markers such as aneurysm diameter, smoking and blood pressure.

2.1.2 Secondary Objectives

In patients under surveillance for abdominal aortic aneurysms, to determine whether mural uptake of USPIO:

i. Correlates with the rate of aneurysm expansion

ii. Occurs more commonly in patients who progress to surgery or whose aneurysm subsequently ruptures

iii. Co-localises with, or relates to, areas of biomechanical stress

iv. Occurs in a reproducible manner

We will investigate other inter-related mechanisms associated with aneurysm growth. We will specifically explore the added value of biomechanical stress modeling as we suspect co-localisation of both USPIO uptake and areas of high mechanical stress could act synergistically and cause more marked aneurysm growth. We will also examine correlates with other blood biomarkers including regulators of extracellular matrix turnover (such as matrix metalloproteinases and tissue inhibitors of metalloproteinases) and vascular inflammation (such as C-reactive protein and interleukin-6).

2.2 ENDPOINTS

2.2.1 Primary Endpoint

The primary end-point of the study will be the composite of aneurysm rupture or aortic aneurysm repair.

2.2.2 Secondary Endpoints

Secondary end-points will include:

i. the rate of aneurysm rupture
ii. the rate of surgical repair of the aneurysm
iii. the aneurysm growth rate
iv. all-cause and aneurysm-related mortality

We will conduct exploratory analyses examining the interactions between mural USPIO uptake, biomechanical stress, clinical risk factors and serum biomarkers of extracellular matrix turnover and inflammation.

Clinicians involved directly with patient surveillance and care will be blinded to the magnetic resonance imaging findings of mural USPIO uptake.

3 STUDY DESIGN

The study will be a prospective observational cohort study of patients participating in abdominal aortic aneurysm surveillance programmes with blinded assessments of USPIO uptake. The study aims to recruit 350 participants in three study centres, with participants being followed up at six monthly intervals for 2 years.

We aim to validate the findings of our previous proof-of-concept study,[19] focusing on the relationship between baseline USPIO uptake and the subsequent clinical outcome and aneurysmal expansion rates. We will also look at the interplay between various risk factors affecting the growth rates and aneurysm-related adverse clinical events such as rupture, surgical repair, and death. This will lay the foundation for a large multicentre randomised controlled trial targeted at applying this technique to determine clinical management and surgical intervention. This will be particularly important given that screening programmes for the detection of abdominal aortic aneurysms are being rolled out across the United Kingdom and this is likely to increase substantially the number of patients being entered into surveillance programmes.

Reproducibility of the technique will be assessed in a subgroup of study participants (from the Edinburgh study centre) who will undergo repeat magnetic resonance scanning and USPIO administration at 1 month and 1 year (n=20) and at 1 year only (n=60). Short-term (1 month) reproducibility is likely to reflect the variability in USPIO uptake whereas long-term (1 year) reproducibility is likely to represent the variation in biology of the aortic aneurysm with time. Patients recruited in Edinburgh who undergo elective surgery will also have AAA wall tissue collected and stored for the assessment of tissue resident macrophages and matrix metalloproteinases. Figure 4 shows the study flow chart.

Patients with abdominal aortic aneurysms (identified in surveillance program and other study site clinics)

350 patients with abdominal aortic aneurysm > 40mm who meet inclusion and exclusion criteria AND who agree to take part

Baseline Assessment (2 days)

Day 1:

- Consent
- Clinical Assessment
- Ultrasound scan (occurs as standard care and can occur up to 1 month prior to baseline assessment)
- 3T Magnetic resonance scan
- i.v. ferumoxytol
- Computed Tomography scan with contrast (can be done on day 2)
- Blood sample collection (can be done on day 2)
- Pulse wave analysis (can be done on day 2)

Day 2 (24-36 hours after Day 1):

- 3T Magnetic resonance scan (post ferumoxytol) *

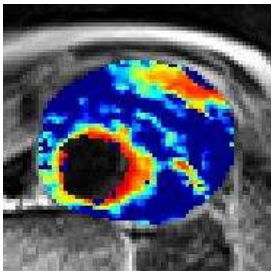

6 Monthly assessments (6, 12 and 18 months)

- Clinical assessment
- Ultrasound scan
- Blood sample collection (**Edinburgh site only**)
- Pulse wave analysis (**Edinburgh site only**)

Final 2 year assessments

- Clinical assessment
- Ultrasound scan
- Computed Tomography scan
- Blood sample collection
- Pulse wave analysis

317 Patients with 2 year follow up (allowing for drop-outs)

* 20 patients will undergo MRI reproducibility assessments at 1 month and 1 year and 60 will have the assessment at 1 year only.

Figure 4: Study Flow Chart

4 STUDY POPULATION

Participants will be identified from the clinical surveillance program and given a patient information leaflet about the study. Eligible participants who are interested in the study will attend a baseline visit where they will provide written informed consent. All other study assessments for this baseline visit and the visits though-out the study are detailed in section 7.2

4.1 NUMBER OF PARTICIPANTS

We will recruit 350 patients with abdominal aortic aneurysms from the clinical surveillance program. Patients will be recruited from three centres; Royal Infirmary of Edinburgh, Western Infirmary in Glasgow and Forth Valley Royal Hospital. Patients recruited from Edinburgh will undergo limited additional procedures. Full details are in section 7.2.

4.2 INCLUSION CRITERIA

1. Abdominal aortic aneurysms measuring ≥40 mm in anteroposterior diameter on ultrasound scanning.
2. Age ≥40 years. Patients with abdominal aortic aneurysms less than 40 years may have a connective tissue disorder and a different aetiology to their disease.

4.3 EXCLUSION CRITERIA

1. Patients expected to, or already received, imminent elective or emergency surgical or endovascular repair.
2. Contraindication to magnetic resonance imaging scanning identified from magnetic resonance imaging safety questionnaire
3. Patients refusing or unable to give informed consent
4. Woman with child-bearing potential and who are breastfeeding will not be enrolled into the trial (woman who have experienced menarche, are pre-menopausal, have not been sterilised or who are currently pregnant).
5. Intercurrent illness including patients with a systemic inflammatory disorder or underlying malignancy (life expectancy < 2 years)
6. Renal dysfunction (eGFR ≤30 mL/min/1.73m^2)
7. Polycythemia
8. Contraindication to ferumoxytol (evidence of known iron overload, hemochromatosis, known hypersensitivity to ferumoxytol or its components or anaemia not caused by iron deficiency)9. Contraindication to Iodine.
10. Patients with any known history of drug allergy (including hypersensitivity) to other parenteral iron products.

5 PARTICIPANT SELECTION AND ENROLMENT

5.1 IDENTIFYING PARTICIPANTS

Patients will be identified from the clinical surveillance programmes and databases in Edinburgh, Glasgow and Forth Valley.

5.2 CONSENTING PARTICIPANTS

Written informed consent will be obtained by a suitably qualified member of the research team at study entry.

5.3 SCREENING FOR ELIGIBILITY

Once patients have been identified from the surveillance service database, they will be seen at their surveillance ultrasound appointment (standard clinical care) and eligibility will be assessed. Eligibility will be confirmed prior to consent. If patients are not seen in the ultrasound appointment, the study will be discussed with the patient over the phone and study information sent to them in the post. An appointment will be made for a baseline visit (where consent takes place) for all patients who are eligible and are interested in taking part.

5.4 INELIGIBLE AND NON-RECRUITED PARTICIPANTS

Ineligible and non-recruited patients will receive standard medical care. An anonymised log will be kept for patients who were screened for the study and subsequently found to be ineligible or not recruited.

5.5 CO-ENROLMENT

Co-enrolment is permitted into the 18F-Sodium Fluoride Imaging of Abdominal Aortic Aneurysms (SoFIA^3) substudy. Study participants at the Edinburgh site may be invited to take part in this sub-study, which is detailed in a separate protocol.

Co-enrolment should not be considered with other interventional studies without prior discussion and agreement from the Sponsors and the Chief Investigators of both studies.

5.6 PREMATURE WITHDRAWAL

Participants are free to withdraw from the study at any point or a participant can be withdrawn by the investigator. If withdrawal occurs, the primary reason for withdrawal will be documented in the participant's Case Report Form (CRF).

If a patient who has consented for the study states that they wish to be withdrawn from the study before they have been administered ferumoxytol, they will be withdrawn from the study and another participant will be recruited in their place.

Clinicians should not withdraw participants who have received ferumoxytol but have not undergone the baseline MRI scanning protocol. These participants should continue to be followed up.

5.7 RANDOMISATION

There is no randomisation in this study.

6 INVESTIGATIONAL MEDICINAL PRODUCT AND PLACEBO

6.1 STUDY DRUG

6.1.1 Study Drug Identification

Rienso® (ferumoxytol) is composed of ultrasmall superparamagnetic particles of iron oxide (USPIOs) coated with polyglucose sorbitol carboxymethylether. It is supplied as an aqueous colloidal product that is formulated with mannitol and presented in single use vials

6.1.2 Study Drug Manufacturer

AMAG Pharmaceuticals Inc.Lexington, MA 02421, USA

Takeda Italia Farmaceutici S.p.A. Via Crosa, 86, 28065 Cerano (NO), Italy are responsible for batch release.

6.1.3 Marketing Authorisation Holder

Takeda Pharma A/S, Langebjerg 1, DK-4000 Roskilde, Denmark

6.1.4 Labelling and Packaging

Rienso® is supplied in a labelled vial containing 510 mg of elemental iron in a volume of 17mL of mannitol. Each mL of the sterile colloidal solution contains 30 mg of elemental iron and 44 mg of mannitol.

6.1.5 Storage

Consistent with the Summary of Product Characteristics (November 2012), Rienso® will be stored in the original package in order to protect from light and will not be frozen.

6.1.6 Summary of Product Characteristics or Investigators Brochure

A copy of the latest version of the Summary of Product Characteristics (SmPC) is available in the Investigator Site File.

6.2 PLACEBO

No placebo will be used in this study.

6.3 DOSING REGIME

The single use vials are diluted and administered as an intravenous infusion over 15-30 minutes. The ferumoxytol dose (4.0 mg/kg) is diluted in sterile 0.9% sodium chloride up to a final concentration of 2-8 mg iron per mL.

Patients should be reclined or in a semi-reclining position during infusion and for 30 minutes thereafter. Blood pressure (systolic and diastolic) will be recorded before ferumoxytol infusion and 30 minutes after the infusion to monitor for hypotension as detailed in the Summary of Product Characteristics.

The single dose is given 24-36 hours before magnetic resonance imaging.

In a subset of patients (n=20), repeated magnetic resonance imaging scans will be performed at 1 month and 1 year. These patients will receive a further dose (4.0 mg/kg) of ferumoxytol 24 (± 6) - 36 hours before each magnetic resonance imaging (total of 3 doses of ferumoxytol in one year).

A further subset of patients (n=60), repeated magnetic resonance imaging scans will be performed at 1 year only. These patients will receive a further dose (4.0 mg/kg) of ferumoxytol 24 (± 6) - 36 hours before each magnetic resonance imaging (total of 2 doses of ferumoxytol in one year).

6.4 DOSE CHANGES

All patients will receive the same dose (4.0 mg/kg) 24-36 hours before magnetic resonance imaging.

In a subset of patients (n=20), magnetic resonance imaging will be repeated at 1 month (± 1 week) and 1 year (± 1 month) to determine short and long-term reproducibility respectively. These patients will receive a further dose (4.0 mg/kg) of ferumoxytol 24 (±6h) -36 hours before each magnetic resonance imaging (total of 3 doses of ferumoxytol in one year).

Another subset of patients (n=60), repeated magnetic resonance imaging scans will be performed at 1 year (± 1 month) only. These patients will receive a further dose (4.0 mg/kg) of ferumoxytol 24 (± 6) - 36 hours before each magnetic resonance imaging (total of 2 doses of ferumoxytol in one year).

All study participants who agree to be part of the reproducibility sub-study will consent for the extra scans. Consecutive patients imaged in the Edinburgh centre will be approached until 20 patients have undergone repeated scanning at 1 month and 1 year and 60 patients have undergone repeated scanning at 1 year.

6.5 PARTICIPANT COMPLIANCE

Responsibility for the infusion of ferumoxytol will be with the research team. Timing and volume of administration will be noted in the CRF. Any reason for non-administration of the ferumoxytol will be noted.

If intolerable side effects are experienced during the infusion of Ferumoxytol, the infusion will be abandoned and appropriate medical care will be delivered to the participant.

6.6 OVERDOSE

Overdose is unlikely as ferumoxytol will be prescribed and administered in the hospital. If accidental overdose is suspected, the patient will be followed up for signs of iron excess and will be referred for specialist assessment if appropriate.

For 270 patients, a single dose of ferumoxytol will be administered. In a random subset of patients (n=20) magnetic resonance imaging will be repeated at 1 month (± 1 week) and 1 year (± 1 month) to determine short and long-term reproducibility respectively. These patients will receive a further dose (4.0 mg/kg) of ferumoxytol 24 (±6h) -36 hours before each magnetic resonance imaging (a total of 3 doses of ferumoxytol in one year and a total of 6 MRI scans). In a further subset of patients (n=60), magnetic resonance imaging will be repeated at 1 year (± 1 month) only. These patients will receive a further dose (4.0 mg/kg) of ferumoxytol 24 (±6h) -36 hours before each magnetic resonance imaging (a total of 2 doses of ferumoxytol in one year and a total of 4 MRI scans). The manufacturers have good evidence of repeated dosing of Ferumoxytol in more than 200 patients, where repeat dosing occurred as short as 22 days, without adverse effect on the patient. In addition, serial data from patients undergoing multiple MRIs over a 2-week period, following a single dose of ferumoxytol show no residual ferumoxytol in the brain by 5-7 days.

Each dose of ferumoxytol equates to approximately 7% of total body iron.

6.7 OTHER MEDICATIONS

6.7.1 Buscopan

20mg of intravenous Buscopan (hyoscine butylbromide) will be given before each MRI scan. If patients have a contraindication (allergic reaction, narrow angle glaucoma, paralytic ileus, myasthenia gravis, obstructive prostatic hypertrophy) to this drug they will not receive it but will proceed with MRI scanning.

6.7.2 Permitted Medications

Any other medication necessary for clinical care can be taken.

For patients taking Metformin refer to section 7.1.

6.7.3 Prohibited Medications

Any other medication necessary for clinical care can be taken.

For patients taking Metformin refer to section 7.1.

7 STUDY ASSESSMENTS

7.1 SAFETY ASSESSMENTS

In patients with no history of renal disease, hypertension or diabetes, a normal eGFR within the last six months will be considered to be acceptable. For patients with risk factors for renal dysfunction or no blood tests within the last 6 months, clinical biochemical analysis of a blood sample will be performed prior to receiving contrast agent.

All patients are advised to drink water prior to their scan for adequate hydration.

For patients with a normal eGFR (60 mL/min/1.73m^2) and taking Metformin they should continue taking the medication up until the scan. After the scan they should withhold Metformin for 48 hours and then have a blood test to check renal function. They will be informed when they are to restart the Metformin following the result of this.

For patients with an eGFR 30 – 60 mL/min/1.73m^2 and taking Metformin they will be advised to stop the medication for 48 hours before and 48 hours after the scan. They will then have a blood test to check renal function and informed when they are to restart the Metformin following the result of this.

These safety assessments are part of standard clinical care with regards to CT scanning with an intravenous contrast agent.

The magnetic resonance imaging safety questionnaire will be applied to identify patients with a contraindication to scanning.

Blood pressure (systolic and diastolic) will be recorded before ferumoxytol infusion and 30 minutes after the infusion to monitor for hypotension as detailed in the Summary of Product Characteristics. Patients should be reclined or in a semi-reclining position during infusion and for 30 minutes thereafter.

7.2 STUDY ASSESSMENTS

A preliminary assessment of eligibility will be conducted by a suitably qualified member of the research team. See tables 1.0 and 2.0 for the assessments performed at each study visit.

Additional assessments:

In patients that are to undergo elective repair of their aneurysms during the course of their follow-up, a repeat computed tomography scan may be performed immediately prior to surgery.

Patients recruited in Edinburgh who undergo elective surgery will also have AAA wall tissue collected and stored for the assessment of tissue resident macrophages and matrix metalloproteinases.

Table 1.0 Table of study assessments for patients (not taking part in reproducibility study).

Assessments	Visits						
	SV	BV (a)	BV (b)	6 Mo	12 Mo	18 Mo	24 Mo
Screening/Eligibility	√						
Medical History/Demographics and concomitant medications		√					
Consent		√					
Ultrasound of AAA (**Standard clinical care)**	√			√	√	√	√
Clinical Assessment		√		√	√	√	√
Pulse Wave analysis and velocity		√		√ **	√ **	√ **	√
Blood sampling		√		√ **	√ **	√ **	√
CT scan of AAA *		√					√
MRI scan of AAA (pre-ferumoxytol)		√					
i.v. administration of ferumoxytol		√					
Post ferumoxytol MRI scan of AAA			√				
AE/SAE Reporting		←					→

SV = surveillance clinic; BV(a) = Baseline visit (occurs within 1 month of SV); BV (b) Baseline visit part B; 24-36 hours after part (a);

- * Where patients are to undergo elective repair of their aneurysms during follow up, a repeat CT scan may be performed prior to surgery.
- ** Bloods and pulse wave analysis will only occur every 6 months in Edinburgh only

Table 2.0 Table of study assessments for patients taking part in reproducibility part study

Assessments	Visits									
	SV	BV (a)	BV (b)	RP (a) (1 Mo)	RP (b) (1 Mo)	6 mo	RP (a) 1 yr	RP (b) 1 yr	18 Mo	24 Mo
Screening/Eligibility	√									
Medical History/Demographics and concomitant medications		√								
Consent		√								
Ultrasound of AAA **(Standard clinical care)**	√					√				
Clinical Assessment		√		√	√	√	√	√	√	√
Pulse Wave analysis and velocity		√				√			√	√
Blood sampling		√		√	√	√	√	√	√	√
CT scan of AAA		√								√
MRI scan of AAA (pre-ferumoxytol)		√		√			√		√	√
i.v. administration of ferumoxytol		√		√			√			
Post ferumoxytol MRI scan of AAA			√		√			√		
AE/SAE Reporting		←								→

SV = surveillance clinic; BV (a)= Baseline visit; BV (b) Baseline visit part B; 24-36 hours after part (a); RP = Reproducibility visit where (b) is 24-36 hours after RP (a)

8 DATA COLLECTION

8.1 CLINICAL ASSESSMENT

Patients will have a full formal and standardized clinical assessment at baseline that will include history, examination, documentation of cardiovascular risk factor profile (smoking status, family history, hypertension, hyperlipidaemia, diabetes mellitus) and concomitant medications (anti-hypertensive medication, etc). Concomitant medication will be recorded at baseline and at end of trial.

Brachial artery systolic and diastolic blood pressure, pulse pressure, and mean arterial pressure will be measured after a 30-min supine rest period using an automated oscillometric sphygmomanometer (model 711, Omron Healthcare GmbH, Hamburg, Germany). The mean of three recordings will be taken.

8.2 BLOOD SAMPLING

Blood samples (20 mL on each visit) will be collected at baseline and at 24 months for patients for routine biochemistry and haematology (including full blood count, U&Es, Liver Function Tests, total cholesterol and glucose)

For patients recruited and imaged in the Edinburgh centre a blood sample will be processed (plasma and serum) and stored at -80℃ for later analysis of potential extracellular matrix and inflammatory biomarkers. This will happen at baseline, 6, 12,18 and 24 months. Full details for processing and shipment of serum biomarker samples will be provided in the ISF.

8.3 PULSE WAVE ANALYSIS AND VELOCITY

Pulse wave analysis and velocity will be measured in triplicate using the SphygmoCor^{TM} apparatus (AtCor Medical, Sydney Australia) as previously described [McLeod *et al*, 2004]. This will facilitate the measurement of central aortic pressure to assist in the modelling of biomechanical stress within the aneurysm. This will be measured at baseline and every 6 months (6,12,18 and 24 months) for the patients recruited at the Edinburgh centre. This procedure will be carried out at baseline and at 24 months for patients in other recruiting centres. Pulse wave analysis and velocity measurements should always be done before the MRI scan and CT scans (this can be on day 1 or day 2 of the baseline visit). Patients will be fasted for this procedure.

In some instances, it may not be possible to perform pulse wave analysis and pulse wave velocity on some of the study patients. For example, if they are in atrial fibrillation or a weak pulse. In these instances, we will record that it was not possible to obtain these measurements and no further measurements will be obtained at the relevant follow up timelines.

8.4 ULTRASOUND OF THE ABDOMINAL AORTA

Patients will undergo 6-month ultrasound imaging as part of standard care for the surveillance programme to measure the maximal anteroposterior diameter of the aneurysm (Ultrasound scans should be every 6 months ± 2 months from the last ultrasound scan) A 3.5-MHz linear array transducer will be used to provide standard real time longitudinal B-scan images of the abdominal aortic aneurysm at the point of maximum diameter. Maximum anteroposterior abdominal aortic aneurysm diameter and distensibility (pressure strain elastic modulus and stiffness) will be assessed. Scans will be undertaken by accredited clinical vascular scientists with interobserver coefficient of variation of aortic diameter measurements of 3.5% in our laboratory.[24]

8.5 COMPUTED TOMOGRAPHY OF THE ABDOMINAL AORTA

Contrast enhanced images of the abdominal aorta will be obtained using a 320-multidetector computed tomography scanner (Aquilion ONE; Toshiba) or a 64 slice multi-detector computed tomography detector (Brilliance 64; Philips_at baseline and 2 years at either the Clinical Research Imaging Centre or the Western Infirmary of Glasgow. These data will be reconstructed into three dimensions using volumetric matrices to enable a more comprehensive assessment of the aneurysm geometry and growth than that provided by the ultrasound assessment of the unidimensional aortic anteroposterior diameter. In cases where study participants undergo emergency repair of a ruptured abdominal aortic aneurysm then a CT scan may not be performed. In the event of patients not receiving the CT scan at baseline (due to a CT scanner issue, or other clinical issue), the CT scan will be performed within 1 month of the baseline visit.

8.6 MAGNETIC RESONANCE IMAGING OF THE ABDOMINAL AORTA

Magnetic resonance imaging will be conducted using a 3T Siemens Magnetom Verio scanner (Siemens, Erlangen, Germany) before and 24-36 hours after administration of the USPIO in Edinburgh or Glasgow. Patients will be given intravenous buscopan (hyoscine butylbromide), prior to imaging to minimise bowel motion artifacts. Routine clinical coronal and sagittal breath-held T2-weighted multi-slice HASTE sequences will be used to identify the position and extent of the aneurysm following which a respiratory-gated, electrocardiographically-triggered T2 weighted (T2W) turbo- spin echo sequence will be used to acquire detailed anatomical data (TR/TE 2R-R intervals/72 ms; flip angle 180°; matrix 192 x 256; field of view 400 x 400 mm; slice width 5 mm). A multi-echo, gradient-echo T2*W sequence (TE 4.9, 7.7, 10.5, 13.3 ms; TR 133 ms; flip angle 15°; matrix 192 x 256; field of view 400 x 400 mm; slice width 5 mm) will be used to acquire contiguous axial images of the entire aneurysm (from the neck of the aneurysm down to the iliac bifurcation) with slice positions corresponding to those of the T2W images.

8.7 FOLLOW UP FOR PATIENTS IN CERTAIN CIRCUMSTANCES

If a patient undergoes an open or endovascular repair of their AAA they will not return routinely for US or pulse wave analysis or velocity every 6 months but will be invited to return every 6 months for blood tests and at 2 years for a CT scan.

If a patient is considered not fit for elective surgery then they would normally be discharged from the care of the Vascular Surgeons. However, we will invite these patients to attend for the standard study assessments.

9 STATISTICS AND DATA ANALYSIS

9.1 SAMPLE SIZE CALCULATION

The sample size is determined by the numbers required to build robust prognostic models for rupture and/or surgical repair, and in particular to measure the additional prognostic value of mural USPIO uptake when added to such a prognostic model based only on conventional clinical risk factors. There is a widely accepted 'rule of thumb' that one needs at least 10 and ideally 20 outcome events per covariate to be included in a prognostic model.[25] As described in more detail below, we plan to use the net reclassification index (NRI) as the primary measure of the clinical relevance of the added prognostic value of mural USPIO uptake.[26, 27] Based on two recent papers using the NRI,[28, 29] and also taking account of the Harrell 'rule of thumb, we estimate that we need to observe 130 events (i.e. the composite of rupture or surgical repair) to have adequate sensitivity to answer the primary question. With our estimated event rate of 41% over the mean duration of follow-up of two years,[30] this equates to 317 patients.

There should be very modest losses to follow up for the primary analysis, since all study recruits are already enrolled on a surveillance programme. Moreover we shall seek consent at the time of recruitment to flag the patients so that if any patients are lost to follow up they can be traced to identify any hospital admissions or to identify if they have died. In addition, some patients will drop out due to technical failure of the scan, such as claustrophobia or poor image quality. We have therefore conservatively accounted for a 10% drop-out rate and we will recruit 350 patients to the study.

9.2 PROPOSED ANALYSES

9.2.1 Image analysis of ultrasound

Cursors will be locked onto echoes representing the anterior and posterior aortic walls and the movement of both tracked with each cardiac cycle. The longitudinal image will be used for analysis as experience with the technique and data from formal reproducibility studies indicates that the quality of the data obtained from a longitudinal section is superior to that obtained from a transverse view. Images will be captured digitally for later off-line core laboratory review.

9.2.2 Image analysis of computed tomography

Computed tomography of the abdominal aorta will be performed at baseline and 2 years to assess regional and volumetric growth rates. These two computed tomography scans will be spatially co-registered so that areas of expansion and growth can be more accurately defined and permit correlation with areas of USPIO uptake and fine element analysis modeling.

Three-dimensional computer models will be generated from segmented, contrast-enhanced images allowing geometric indices to be quantified. Semi-automatic segmentation is achievable due to the intensity differences between the aneurysm and surrounding tissues and structures. Intensity thresholding will be used to identify the lumen. To detect the thrombus and complete the segmentation, we will use a 3-D deformable model approach that utilises the level set algorithm as well as modeling the thrombus contour as a radial function starting from the aortic centre line as calculated from the lumen segmentation.

9.2.3 Image analysis of magnetic resonance imaging

A region of interest (ROI) encompassing the aortic wall and thrombus but excluding the lumen will be drawn on each slice of the pre-contrast T2W image. The pre-contrast T2W scan will be used as the base image to which subsequent scans will be co-registered using a semi-automatic rigid three-dimensional voxel registration protocol utilising a normalised mutual information algorithm. To minimise the contribution of bowel and abdominal wall motion in the magnetic resonance imaging datasets, a region for registration will include the aorta, vertebrae and spinal musculature that remain relatively static during the respiratory cycle but exclude the more mobile abdominal wall and bowel.

The four echoes in the multi-echo T2*W sequence will be combined to generate T2* and R2* maps. The T2* value is the decay constant for the exponential decay of signal intensity with time (Figure 3) and its inverse is the R2* value. A 3 x 3 voxel Gaussian filter will be applied to the individual echoes to reduce noise, and the co-efficient of determination will be used to exclude data that do not have an acceptable straight line fit when ln(signal intensity) is plotted against echo time. Images will be co-registered to allow direct comparison of the pre-and post-contrast T2*W magnetic resonance

images. USPIO uptake will be presented visually as a colour map of per cent change in T2* or R2* values between pre- and post-USPIO scans, with our previously validated threshold of significance applied[19, 20] (Figures 3 and 4).

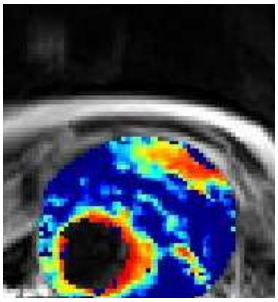

Figure 4. Colour map of magnetic resonance imaging of an abdominal aortic aneurysm. Red and yellow pixels indicate areas of increase T2* value, indicative of USPIO uptake.

The change in T2* or R2* colour maps from the magnetic resonance images will be spatially co-registered to the computed tomography datasets.

9.2.4 Finite element and stress analysis

Using Abaqus, the vessel wall will be modeled as a constant thickness layer of 1.5 mm, with a hyperelastic constitutive model. Thrombus will be modeled as homogenous and isotropic with Young's modulus 0.1 MPa. The model will be inflated from diastolic to systolic pressure using a homogeneous pressure-modeling regime. Peak wall stress and other rupture indices will be calculated and compared against areas of USPIO uptake.

9.2.5 Statistical analysis

The baseline assessment will include the baseline aneurysm diameter, sex, smoking habit and blood pressure. Using these covariates, a prognostic model predicting the time to the composite outcome event of rupture or surgical repair will be developed using Cox proportional hazards regression. The added prognostic value of adding mural USPIO uptake to this model will be assessed using the increase in the area under the receiver operator characteristic (ROC) curve, the Nagelkerke partial R^2, and primarily, the net reclassification index.[26, 27] The NCI is a direct measure of the clinical relevance of adding a covariate to a prognostic model. It is an overall measure of how many patients move from a low predicted risk to a high predicted risk when the covariate is added (and whether these individuals are indeed high risk), and how many move from a high predicted risk to a low predicted risk (and whether these individuals are indeed low risk). For the primary analysis, the USPIO will be taken as a binary covariate (as in Richards *et al*, 2011a), but a sensitivity analysis will explore the potential for including a quantification of the USPIO uptake. Some but not all of the patients will also have a measure of current aneurysm growth rate at baseline, and a further sensitivity analysis will explore using grown rate as a further prognostic factor, using imputation when the estimated growth rate is not available.

A secondary analysis will follow a similar analytical strategy to that set out above, but using prognostic models to predict aneurysm growth rate. This analysis will be far more complex with there being serial measures of aneurysm diameter, and with these measurements being censored on rupture or on surgical repair. Further exploratory analysis will look at the predictive ability of measures of wall stress and how these interact with regional USPIO uptake.

The analysis will be conducted by the study statistician, Catriona Graham (Senior Statistician Wellcome Trust Clinical Research Facility), under the supervision of Gordon Murray (Professor of Medical Statistics).

Reproducibility of the technique will be assessed in a subgroup of study participants who will undergo repeat magnetic resonance scanning and USPIO administration at 1 month and 1 year (n=20) or at 1 year only (n=60). Short-term (1 month) repeatability is likely to reflect the variability in USPIO uptake whereas long-term (1 year) reproducibility is likely to represent the variation in biology of the aortic aneurysm with time. Subjects will be categorised with respect to the presence or absence of USPIO uptake to define the proportionate agreement, with 95% confidence intervals.

10 ADVERSE EVENTS

The Investigator is responsible for the detection and documentation of events meeting the criteria and definitions detailed below.

Full details of contraindications and side effects that have been reported following administration of the IMP can be found in the relevant Summary of Product Characteristics (SmPC).

Participants will be instructed to contact their Investigator at any time after consenting to join the study if any symptoms develop. All adverse events (AE) that require medical attention (for example, visit to a GP, hospital etc) which occur after having received ferumoxytol must be reported in detail in the Case Report Form (CRF) or AE form. In the case of an AE, the Investigator should initiate the appropriate treatment according to their medical judgment. Participants with AEs present at the last visit must be followed up until resolution of the event. For patients that have an aneurysm rupture or repair (elective or emergency), this will be recorded in the AAA case report form and entered into the database (this is one of secondary outcomes). This event will not be recorded as an AE.

10.1 DEFINITIONS

An **adverse event** (AE) is any untoward medical occurrence in a clinical trial participant which does not necessarily have a causal relationship with an investigational medicinal product (IMP).

An **adverse reaction** (AR) is any untoward or unintended response to an IMP which is related to any dose administered to that participant.

An **unexpected adverse reaction** (UAR) is an adverse reaction that is not consistent with the applicable product information for the IMP, e.g. the Investigator Brochure (IB) for a non licensed IMP or the SmPC for a licensed product.

A **serious adverse event** (SAE), **serious adverse reaction** (SAR) or **suspected unexpected serious adverse reaction** (SUSAR) is any AE, AR or UAR that at any dose:

- results in death;
- is life threatening* (i.e. the participant was at risk of death at the time of the event; it does not refer to an event which hypothetically might have caused death if it were more severe);
- requires in-patient hospitalisation or prolongation of existing hospitalisation;
- results in persistent or significant disability or incapacity;
- is a congenital anomaly or birth defect.

10.2 DETECTING AEs AND SAEs

All AEs and SAEs will be recorded from the time a participant signs the consent form to take part in the study until the last study visit.

Participants will be asked about the occurrence of AEs/SAEs at every visit during the study. Open-ended and non-leading verbal questioning of the participant will be used to enquire about AE/SAE occurrence. Participants will also be asked if they have been admitted to hospital or had any accidents. If there is any doubt as to whether a clinical observation is an AE, the event will be recorded.

AEs and SAEs may also be identified by support departments e.g. laboratories.

10.3 RECORDING AEs AND SAEs

When an AE/SAE occurs, it is the responsibility of the Investigator to review all documentation (e.g. hospital notes, laboratory and diagnostic reports) related to the event. The Investigator will then record all relevant information in the CRF and on the SAE form (if the AE meets the criteria of serious).

Information to be collected includes dose, type of event, onset date, Investigator assessment of severity and causality, date of resolution as well as treatment required, investigations needed and outcome.

10.4 ASSESSMENT OF AEs AND SAEs

Seriousness, causality, severity and expectedness will be assessed as though the participant is taking active IMP. The Investigator is responsible for assessing each AE.

The Chief Investigator (CI) may not downgrade an event that has been assessed by an Investigator as an SAE or SUSAR, but can upgrade an AE to an SAE, SAR or SUSAR if appropriate.

10.4.1 Assessment of Seriousness

The Investigator will make an assessment of seriousness as defined in Section 10.1.

10.4.2 Assessment of Causality

The Investigator will make an assessment of whether the AE/SAE is likely to be related to the IMP according to the definitions below.

All AEs/SAEs judged as having a reasonable suspected causal relationship (e.g. possibly related or unrelated) to the IMP will be considered as related to the IMP (ARs/SARs).

Where non Investigational Medicinal Products (NIMPs) e.g. rescue/escape drugs are given: if the AE is considered to be related to an interaction between the IMP and the NIMP, or where the AE might be linked to either the IMP or the NIMP but cannot be clearly attributed to either one of these, the event will be considered as an AR/SAR.

Unrelated: where an event is not considered to be related to the IMP.

Possibly related: The nature of the event, the underlying medical condition, concomitant medication or temporal relationship make it possible that the AE has a causal relationship to the study drug.

Probably related: The temporal relationship and absence of a more likely explanation suggest the event could be related to the study drug.

Definitely related: The known effects of the study drug or its therapeutic class, or based on challenge testing, suggest that study drug is the most likely cause.

Alternative causes such as natural history of the underlying disease, other risk factors and the temporal relationship of the event to the treatment should be considered and investigated.

10.4.3 Assessment of Severity

The Investigator will make an assessment of severity for each AE/SAE and record this on the CRF or AE form according to one of the following categories:

Mild: an event that is easily tolerated by the participant, causing minimal discomfort and not interfering with every day activities.

Moderate: an event that is sufficiently discomforting to interfere with normal everyday activities.

Severe: an event that prevents normal everyday activities.

Note: the term 'severe', used to describe the intensity, should not be confused with 'serious' which is a regulatory definition based on participant/event outcome or action criteria. For example, a headache may be severe but not serious, while a minor stroke is serious but may not be severe.

10.4.4 Assessment of Expectedness

If an event is judged to be an AR/SAR, the evaluation of expectedness will be made based on knowledge of the reaction and the relevant product information documented in the SmPC/IB.

The event may be classed as either:

Expected: the AR is consistent with the toxicity of the IMP listed in the SmPC/IB.

Unexpected: the AR is not consistent with the toxicity in the SmPC/IB.

10.5 REPORTING OF SAEs/SARs/SUSARs

Once the Investigator becomes aware that an SAE has occurred in a study participant, the information will be reported to the ACCORD Research Governance & QA Office **immediately or within 24 hours**. If the Investigator does not have all information regarding an SAE, they should not wait for this additional information before notifying ACCORD. The SAE report form can be updated when the additional information is received.

The SAE report will provide an assessment of causality and expectedness at the time of the initial report to ACCORD according to Sections 10.4.2, Assessment of Causality and 10.4.4, Assessment of Expectedness.

The SAE form will be transmitted by fax to ACCORD on **+44 (0)131 242 9447** or may be transmitted by hand to the office.

All reports faxed to ACCORD and any follow up information will be retained by the Investigator in the Investigator Site File (ISF).

10.6 REGULATORY REPORTING REQUIREMENTS

The ACCORD Research Governance & QA Office is responsible for pharmacovigilance reporting on behalf of the co-sponsors (Edinburgh University and NHS Lothian).

The ACCORD Research Governance & QA Office has a legal responsibility to notify the regulatory competent authority and relevant ethics committee (Research Ethics Committee (REC) that approved the trial). Fatal or life threatening SUSARs will be reported no later than 7 calendar days and all other SUSARs will be reported no later than 15 calendar days after ACCORD is first aware of the reaction.

ACCORD will inform Investigators at participating sites of all SUSARs and any other arising safety information.

An Annual Safety Report will be submitted to the regulatory competent authority and main REC listing all SARs and SUSARs.

10.7 FOLLOW UP PROCEDURES

After initially recording an AE or recording and reporting an SAE, the Investigator will follow each participant until resolution or death of the participant. Follow up information on an SAE will be reported to the ACCORD office.

AEs still present in participants at the last study visit will be monitored until resolution of the event or until no longer medically indicated.

11. PREGNANCY

Woman with child-bearing potential will not be enrolled into the trial (woman who have experienced menarche, are pre-menopausal, have not been sterilised or who are currently pregnant).

12 TRIAL MANAGEMENT AND OVERSIGHT ARRANGEMENTS

12.1 TRIAL MANAGEMENT GROUP

The study will be coordinated by a Project Management Group, consisting of the grant holders (Chief Investigator and Principal Investigator in Edinburgh), Trial Manager and coordinating nurse.

The Trial Manager will oversee the study and will be accountable to the Chief Investigator. The Trial Manager will be responsible for checking the CRFs for completeness, plausibility and consistency. Any queries will be resolved by the Investigator or delegated member of the study team.

A Delegation Log will be prepared for each site, detailing the responsibilities of each member of staff working on the study.

12.2 TRIAL STEERING COMMITTEE

A Trial Steering Committee (TSC) will be established to oversee the conduct and progress of the study, in particular the TSC will monitor the trial event rate. The terms of reference of the Trial Steering Committee, the draft template for reporting and the names and contact details are detailed in the TSC charter.

12.3 DATA MONITORING COMMITTEE

An independent Data Monitoring Committee (DMC) will not be convened for this study. The investigators will report all adverse events to the Sponsor and the Trial Steering Committee. As there is no blinded intervention and the investigational medicinal product will be given to all subjects, there is no risk to the scientific integrity of the study or requirement for a DMC.

12.4 INSPECTION OF RECORDS

Investigators and institutions involved in the study will permit trial related monitoring and audits on behalf of the sponsor, REC review, and regulatory inspection(s). In the event of an audit or monitoring, the Investigator agrees to allow the representatives of the sponsor direct access to all study records and source documentation. In the event of regulatory inspection, the Investigator agrees to allow inspectors direct access to all study records and source documentation.

12.5 RISK ASSESSMENT

An independent risk assessment will be performed by an ACCORD Clinical Trials Monitor to determine if monitoring is required and if so, at what level. An independent risk assessment will also be carried out by the ACCORD Quality Assurance Group to determine if an audit should be performed before/during/after the study and if so, at what locations and at what frequency.

12.5.1 RISKS

The risks to the participants of the study are very modest and are mainly attributable to the magnetic resonance and computed tomography scans and their respective contrast agents.

12.5.1.1 Magnetic resonance imaging

Magnetic resonance imaging is a standard clinical imaging technique that is applied across the world. Contraindications for magnetic resonance imaging are the presence of certain metallic objects, electrical devices and claustrophobia. Patients with implanted electrical devices, such as pacemakers or defibrillators, will be excluded. We have the provision of a wide-bore scanner (diameter, 70 cm) that will minimise the risk of experiencing claustrophobia.

12.5.1.2 Ferumoxytol

Ferumoxytol (Rienso®) was originally developed for the treatment of iron-deficiency anaemia in patients with chronic kidney disease. It consists of a suspension of USPIO with an ultrasmall core (diameter ~7 nm) and a semi-synthetic carbohydrate coating giving an overall particle size of 30 nm. The size of the particle prevents any early redistribution outside the vascular space and therefore can act as a blood-pool imaging agent with a plasma elimination half-life of approximately 10 - 14 hours in humans.

Herborn and colleagues examined the utility of ferumoxytol for imaging atheroma in the aortae of hyperlipidaemic rabbits using a 1.5T magnetic resonance scanner.[31] Susceptibility artifacts were detectable in the aortic wall at day 2 to 3 post administration of contrast. Signal voids were observed as a result of T2/T2* effects and were more homogenous than those seen in similar animals administered ferumoxtran-10. Histology revealed the accumulation of iron particles under the endothelium and into the medial layer of diseased vessels.[31]

Ferumoxytol has been administered safely as a bolus dose of 4 mg/kg for use as a magnetic resonance imaging contrast agent in humans.[32, 33, 34, 35, 36] Most of these studies have examined and confirmed its utility as a blood-pool contrast agent. However, it has also been assessed for its use in lymph node imaging for cancer staging. In a study of patients with prostate cancer, ferumoxytol was administered at 4 mg/kg and imaging performed at baseline, 5, 8 and 24 hours post dose using a 1.5 T scanner. Maximum signal-to-noise ratio was observed in lymph nodes at 24 hours on T2*-weighted MR imaging.[37]

Ferumoxytol is generally very well tolerated. We have administered ferumoxytol to 16 patients with abdominal aortic aneurysms, 28 patients who have undergone coronary artery bypass surgery and 12 patients with a recent acute myocardial infarction. None have experienced any significant major side-effects or serious adverse events. One subject did experience brief muscle cramps; a previously reported mild side effect. Common reported side-effects of ferumoxytol include constipation, diarrhoea, dizziness and nausea. Reported severe reactions include serious hypersensitivity reactions and hypotension, but are rare.

Buscopan is an anticholinergic drug and is generally used to provide relief from spasm of the genito-urinary tract or gastro-intestinal tract. In this study it is used to minimise bowel motion during the imaging protocol of this study to decrease artefacts seen due to digestive movements. Any side effects reported are uncommon or rare and consist of dry mouth and constipation.

12.5.1.3 Computed tomography

As part of the protocol, subjects will receive two extra computed tomography scans with intravenous contrast. This will expose the patient to ionising radiation (~6 mSv per scan for the Glasgow centre and 3mSv in Edinburgh centre) and the potential hazard of allergic reactions and transient renal dysfunction in response to the contrast agent. Thus the maximum total research protocol dose is 12 mSv.

The level of dose is comparable to the average cumulated dose from 5 years of natural background radiation to the UK population. It is equal to 60% of the whole body dose limit for radiation workers.

The associated excess risk of death from radiation induced cancer is approximately 1 in 3000 compared with the cancer mortality rate in the UK of just over 1 in 4.

The risks of exposure to the contrast medium include allergic reactions and impairment of kidney function. Amongst patients with moderate-to-severe chronic kidney disease, there is a 2-4% risk of kidney impairment after computed tomography angiography.[38] The risk of contrast exposure in this study will be minimised by exclusion of high risk patients who have significant kidney disease (estimated glomerular filtration rate ≤30 mL/min/1.73m^2).

12.5.2 Benefits

Patients will benefit from inclusion in a clinical study that includes close clinical supervision. Based on our previous studies and the demographics of the study population, the study may identify other important clinical conditions that require intervention or treatment because of incidental findings on the magnetic resonance or computed tomography scans. This could be viewed as a potential risk but most patients are grateful if covert conditions are detected early and treated more promptly. In addition, patients will benefit from the additional and closer supervision and care that clinical studies deliver.

Society and some of the participants will benefit if the findings of our study demonstrate that USPIO can successfully identify which patients are at risk of more rapid aneurysm expansion and clinical events. This is the main purpose of the study and we hope this will represent an important new method that may become standard of care.

12.5.3 Risk-to-Benefit

The risks associated with the additional scans and the administration of contrast agents are very low and consistent with many routine clinical imaging procedures. Conversely, if this technique is proven to be successful, the major gains in risk stratification and better selection of patients with abdominal aortic aneurysms who should receive surgical intervention, could have major morbidity and mortality benefits. Deferring unnecessary major surgery or bringing forward potentially life-saving surgery will ensure appropriate use of limited health care resources for maximum patient benefit.

12.6 STUDY MONITORING AND AUDIT

An ACCORD Clinical Trials Monitor or an appointed monitor will visit the Investigator site prior to the start of the study and during the course of the study if required, in accordance with the monitoring plan if required. Investigator sites will be risk assessed by the ACCORD QA Manager, or designee, in order to determine if audit by the ACCORD QA group is required.

13 GOOD CLINICAL PRACTICE

13.1 ETHICAL CONDUCT

The study will be conducted in accordance with the principles of the International Conference on Harmonisation Tripartite Guideline for Good Clinical Practice (ICH GCP).

A favorable ethical opinion will be obtained from the appropriate REC and local R&D approval will be obtained prior to commencement of the study.

13.2 REGULATORY COMPLIANCE

The study will not commence until a Clinical Trial Authorisation (CTA) is obtained from the appropriate Regulatory Authority. The protocol and study conduct will comply with the Medicines for Human Use (Clinical Trials) Regulations 2004, and any relevant amendments.

13.3 INVESTIGATOR RESPONSIBILITIES

The Investigator is responsible for the overall conduct of the study at the site and compliance with the protocol and any protocol amendments. In accordance with the principles of ICH GCP, the following areas listed in this section are also the responsibility of the Investigator. Responsibilities may be delegated to an appropriate member of study site staff.

13.3.1 Informed Consent

The Investigator is responsible for ensuring informed consent is obtained before any protocol specific procedures are carried out. The decision of a participant to participate in clinical research is voluntary and should be based on a clear understanding of what is involved.

Participants must receive adequate oral and written information – appropriate Participant Information and Informed Consent Forms will be provided. The oral explanation to the participant will be performed by the Investigator or qualified delegated person, and must cover all the elements specified in the Participant Information Sheet and Consent Form.

The participant must be given every opportunity to clarify any points they do not understand and, if necessary, ask for more information. The participant must be given sufficient time to consider the information provided. It should be emphasised that the participant may withdraw their consent to participate at any time without loss of benefits to which they otherwise would be entitled.

The participant will be informed and agree to their medical records being inspected by regulatory authorities and representatives of the sponsor(s) but understand that their name will not be disclosed outside the research team.

The Investigator or delegated member of the study team and the participant will sign and date the Informed Consent Form(s) to confirm that consent has been obtained. The participant will receive a copy of this document and a copy filed in the Investigator Site File (ISF) and participant's medical notes.

13.3.2 Study Site Staff

The Investigator must be familiar with the IMP, protocol and the study requirements. It is the Investigator's responsibility to ensure that all staff assisting with the study are adequately informed about the IMP, protocol and their study related duties.

13.3.3 Data Recording

The Principal Investigator is responsible for the quality of the data recorded in the CRF at each Investigator Site.

13.3.4 Investigator Documentation

Prior to beginning the study, each Investigator will be asked to provide particular essential documents to the ACCORD Research Governance & QA Office, including but not limited to:

- An original signed Investigator's Declaration (as part of the Clinical Trial Agreement documents);
- Curriculum vitae (CV) signed and dated by the Investigator indicating that it is accurate and current.

The ACCORD Research Governance & QA Office will ensure all other documents required by ICH GCP are retained in a Trial Master File (TMF), where required, and that appropriate documentation is available in local ISFs.

13.3.5 GCP Training

All study staff must hold evidence of appropriate GCP training.

13.3.6 Confidentiality

All laboratory specimens, evaluation forms, reports, and other records must be identified in a manner designed to maintain participant confidentiality. All records must be kept in a secure storage area with limited access. Clinical information will not be released without the written permission of the participant. The Investigator and study site staff involved with this study may not disclose or use for any purpose other than performance of the study, any data, record, or other unpublished, confidential information disclosed to those individuals for the purpose of the study. Prior written agreement from the sponsor or its designee must be obtained for the disclosure of any said confidential information to other parties.

13.3.7 Data Protection

All Investigators and study site staff involved with this study must comply with the requirements of the Data Protection Act 1998 with regard to the collection, storage, processing and disclosure of personal information and will uphold the Act's core principles. Access to collated participant data will be restricted to those clinicians treating the participants.

Computers used to collate the data will have limited access measures via user names and passwords.

Published results will not contain any personal data that could allow identification of individual participants.

13.3.8 Sharing of anonymised data

Toshiba Medical Visualisation Systems (TMVS) have requested permission to use some of the anatomical MA^{3}RS MRI and CT imaging data for the purposes of developing and evaluating registration algorithms. This will enable development of a framework allowing quantitative comparison of various registration algorithms and will only look at the anatomical/structural data that is acquired during the MA3RS imaging protocol. No MA^{3}RS primary outcome data will be included.

The data provided will be fully anonymised (identifiable by MA^{3}RS study ID only). An agreement will be put in place so that only TMVS members that are named on the agreement will be allowed to access the data provided and TMVS will not publish

without explicitly requesting consent. Any further use of the data by TMVS for any purpose will require approval by the University of Edinburgh and the Trial Steering Committee.

14 STUDY CONDUCT RESPONSIBILITIES

14.1 PROTOCOL AMENDMENTS

Any changes in research activity, except those necessary to remove an apparent, immediate hazard to the participant in the case of an urgent safety measure, must be reviewed and approved by the Chief Investigator.

Amendments to the protocol must be submitted in writing to the appropriate REC, Regulatory Authority and local R&D for approval prior to participants being enrolled into an amended protocol.

14.2 PROTOCOL VIOLATIONS AND DEVIATIONS

Investigators will not implement any deviation from the protocol without agreement from the Chief Investigator and appropriate REC, Regulatory Authority and R&D approval except where necessary to eliminate an immediate hazard to study participants.

In the event that an Investigator needs to deviate from the protocol, the nature of and reasons for the deviation will be recorded in the CRF. If this necessitates a subsequent protocol amendment, this should be submitted to the REC, Regulatory Authority and local R&D for review and approval if appropriate.

14.3 SERIOUS BREACH REQUIREMENTS

A serious breach is a breach which is likely to effect to a significant degree:

(a) the safety or physical or mental integrity of the participants of the study; or

b) the scientific value of the study.

If a potential serious breach is identified by the Chief investigator, Principal Investigator or delegates, the co-sponsors (accord.seriousbreach@ed.ac.uk) must be notified within 24 hours. It is the responsibility of the co-sponsors to assess the impact of the breach on the scientific value of the study, to determine whether the incident constitutes a serious breach and take the appropriate action.

Not every violation from the protocol needs to be reported to the regulatory authority as a serious breach. If the sponsor(s) deem the incident to be a violation that does not constitute a serious breach from the protocol when identified, corrective and preventative actions will be taken where appropriate and they will be recorded in file notes, held within the TMF and ISF.

14.4 STUDY RECORD RETENTION

All study documentation will be kept for a minimum of 5 years from the protocol defined end of study point. When the minimum retention period has elapsed, study documentation will not be destroyed without permission from the sponsor.

14.5 END OF STUDY

The end of study is defined as the last participant's last visit.

The Investigators and/or the trial steering committee and/or the co-sponsor(s) have the right at any time to terminate the study for clinical or administrative reasons.

The end of the study will be reported to the REC and Regulatory Authority within 90 days, or 15 days if the study is terminated prematurely. The Investigators will inform participants of the premature study closure and ensure that the appropriate follow up is arranged for all participants involved.

A summary report of the study will be provided to the REC and Regulatory Authority within 1 year of the end of the study.

14.6 CONTINUATION OF DRUG FOLLOWING THE END OF STUDY

Study participants will not receive ferumoxytol once they have completed the study.

14.7 INSURANCE AND INDEMNITY

The co-sponsors are responsible for ensuring proper provision has been made for insurance or indemnity to cover their liability and the liability of the Chief Investigator and staff.

The following arrangements are in place to fulfil the co-sponsors' responsibilities:

- The Protocol has been designed by the Chief Investigator and researchers employed by the University and collaborators. The University has insurance in place (which includes no-fault compensation) for negligent harm caused by poor protocol design by the Chief Investigator and researchers employed by the University.
- Sites participating in the study will be liable for clinical negligence and other negligent harm to individuals taking part in the study and covered by the duty of care owed to them by the sites concerned. The co-sponsors require individual sites participating in the study to arrange for their own insurance or indemnity in respect of these liabilities.
- Sites which are part of the United Kingdom's Nation Health Service will have the benefit of NHS Indemnity.

  Sites out with the United Kingdom will be responsible for arranging their own indemnity or insurance for their participation in the study, as well as for compliance with local law applicable to their participation in the study.

15 REPORTING, PUBLICATIONS AND NOTIFICATION OF RESULTS

15.1 AUTHORSHIP POLICY

Ownership of the data arising from this study resides with the study team. On completion of the study, the study data will be analysed and tabulated, and a clinical study report will be prepared in accordance with ICH guidelines.

15.2 PUBLICATION

The clinical study report will be used for publication and presentation at scientific meetings. Investigators have the right to publish orally or in writing the results of the study.

Summaries of results will also be made available to Investigators for dissemination within their clinics (where appropriate and according to their discretion).

15.3 PEER REVIEW

The protocol has undergone extensive peer review by the funders (Medical Research Council, Efficacy and Mechanism Evaluation programme) and by the Trial Steering Committee of the study.

16 REFERENCES

1. Multicentre Aneurysm Screening Study Group. Multicentre Aneurysm Screening Study (MASS) into the effect of abdominal aortic aneurysm screening on mortality in men: a randomised controlled trial. *Lancet* 2002;360:1531-1539.
2. Darling RC, Messina CR, Brewster DC, Ottinger LW. Autopsy study of unoperated abdominal aortic aneurysms: the case for early resection. *Circulation.* 1977;56:II161–II164.
3. Raghavan ML, Vorp DA. Toward a biomechanical tool to evaluate rupture potential of abdominal aortic aneurysm: identification of a finite strain constitutive model and evaluation of its applicability. *J Biomech* 2000;33:475–482.
4. Vallabhaneni, S.R. et al. Heterogeneity of tensile strength and matrix metalloproteinase activity in the wall of abdominal aortic aneurysms. *J Endovasc Ther* **11**, 494-502 (2004).
5. Brown PM, Zelt DT, Sobolev B. The risk of rupture in untreated aneurysms: the impact of size, gender, and expansion rate. *J Vasc Surg* 2003;37:280-284.
6. Thompson AR, Cooper JA, Ashton HA, Hafez H. Growth rates of small abdominal aortic aneurysms correlate with clinical events. *Br J Surg*. 2010;97:37-44.
7. Cai J, Hatsukami TS, Ferguson MS, Kerwin WS, Saam T, Chu B, Takaya N, Polissar NL, Yuan C. In vivo quantitative measurement of intact fibrous cap and lipid-rich necrotic core size in atherosclerotic carotid plaque: comparison of high-resolution, contrast-enhanced magnetic resonance imaging and histology. *Circulation.* 2005;112:3437-3444.
8. Kramer CM, Cerilli LA, Hagspiel K, DiMaria JM, Epstein FH, Kern JA. Magnetic resonance imaging identifies the fibrous cap in atherosclerotic abdominal aortic aneurysm. *Circulation.* 2004;109:1016-1021.
9. Harisinghani MG, Barentsz J, Hahn PF, Deserno WM, Tabatabaei S, van de Kaa CH, de la Rosette J, Weissleder R. Noninvasive detection of clinically occult lymph-node metastases in prostate cancer. *N Engl J Med.* 2003;348:2491-2499.
10. Heesakkers RA, Hovels AM, Jager GJ, van den Bosch HC, Witjes JA, Raat HP, Severens JL, Adang EM, van der Kaa CH, Futterer JJ, Barentsz J. MRI with a lymph-node-specific contrast agent as an alternative to CT scan and lymph-node dissection in patients with prostate cancer: a prospective multicohort study. *Lancet Oncol.* 2008;9:850-856.
11. Kooi ME, Cappendijk VC, Cleutjens KB, Kessels AG, Kitslaar PJ, Borgers M, Frederik PM, Daemen MJ, van Engelshoven JM. Accumulation of ultrasmall superparamagnetic particles of iron oxide in human atherosclerotic plaques can be detected by in vivo magnetic resonance imaging. *Circulation.* 2003;107:2453-2458.
12. Trivedi RA, Mallawarachi C, JM UK-I, Graves MJ, Horsley J, Goddard MJ, Brown A, Wang L, Kirkpatrick PJ, Brown J, Gillard JH. Identifying inflamed carotid plaques using in vivo USPIO-enhanced MR imaging to label plaque macrophages. *Arterioscler Thromb Vasc Biol.* 2006;26:1601-1606.
13. Tang TY, Howarth SP, Miller SR, Graves MJ, Patterson AJ, JM UK-I, Li ZY, Walsh SR, Brown AP, Kirkpatrick PJ, Warburton EA, Hayes PD, Varty K, Boyle JR, Gaunt ME, Zalewski A, Gillard JH. The ATHEROMA (Atorvastatin Therapy: Effects on Reduction of Macrophage Activity) Study. Evaluation using ultrasmall superparamagnetic iron oxide-enhanced magnetic resonance imaging in carotid disease. *J Am Coll Cardiol.* 2009;53:2039-2050.
14. Bernd H, De Kerviler E, Gaillard S, Bonnemain B. Safety and tolerability of ultrasmall superparamagnetic iron oxide contrast agent: comprehensive analysis of a clinical development program. *Invest Radiol.* 2009;44:336-342.
15. Bourrinet P, Bengele HH, Bonnemain B, Dencausse A, Idee JM, Jacobs PM, Lewis JM. Preclinical safety and pharmacokinetic profile of ferumoxtran-10, an ultrasmall

superparamagnetic iron oxide magnetic resonance contrast agent. *Invest Radiol.* 2006;41:313-324.

16. Muller K, Skepper JN, Posfai M, Trivedi R, Howarth S, Corot C, Lancelot E, Thompson PW, Brown AP, Gillard JH. Effect of ultrasmall superparamagnetic iron oxide nanoparticles (Ferumoxtran-10) on human monocyte-macrophages in vitro. *Biomaterials.* 2007;28:1629-1642.
17. Ruehm SG, Corot C, Vogt P, Kolb S, Debatin JF. Magnetic resonance imaging of atherosclerotic plaque with ultrasmall superparamagnetic particles of iron oxide in hyperlipidemic rabbits. *Circulation.* 2001;103:415-422.
18. Turner GH, Olzinski AR, Bernard RE, Aravindhan K, Boyle RJ, Newman MJ, Gardner SD, Willette RN, Gough PJ, Jucker BM. Assessment of macrophage infiltration in a murine model of abdominal aortic aneurysm. *J Magn Reson Imaging.* 2009;30:455-460.
19. Richards JMJ, Semple SI, MacGillivray TJ, Gray C, Langrish JP, Williams M, Dweck M, Wallace MD, McKillop G, Chalmers RTA, Garden OJ, Newby DE. Abdominal aortic aneurysm growth predicted by uptake of ultrasmall superparamagnetic particles of iron oxide. *Circ Cardiovasc Imaging* 2011a;4:274-81.
20. Richards JMJ, Semple SI, MacGillivray TJ, Gray C, Langrish JP, Williams M, Dweck M, Wallace MD, McKillop G, Chalmers RTA, Garden OJ, Newby DE. Uptake of ultrasmall superparamagnetic particles of iron oxide predicts growth in abdominal aortic aneurysms. *Heart* 2011b;97 Supplement 1: Abstract Young Research Worker's Prize.
21. Doyle BJ, Corbett TC, Callanan A, Walsh MT, Vorp DA, McGloughlin TM. An experimental and numerical comparison of the rupture locations of an abdominal aortic aneurysm. *J Endovasc Ther* 2009;16:322–335
22. Fillinger MF, Raghavan ML, Marra SP, Cronenwett JL, Kennedy FE. In vivo analysis of mechanical wall stress and abdominal aortic aneurysm rupture risk. *J Vasc Surg* 2002;36:589–597.
23. Xu XY, Borghi A, Nchimi A, Leung J, Gomez P, Cheng Z, Defraigne JO, Sakalihasan N. High levels of 18f-fdg uptake in aortic aneurysm wall are associated with high wall stress. Eur J Vasc Endovasc Surg. 2010; 39:295-301.
24. Wilson KA, Hoskins PR, Lee AJ, Fowkes FG, Ruckley CV, Bradbury AW. Ultrasonic measurement of abdominal aortic aneurysm wall compliance: a reproducibility study. *J Vasc Surg.* 2000;31:507-513.
25. Harrell FE, Lee KL, Califf RM, Pryor DB, Rosati RA. Regression modelling strategies for improved prognostic prediction. *Stat. Med*. 1984;3:143-152.
26. Pencina MJ, D'Agostino RB Sr, D'Agostino RB Jr, Vasan RS. Evaluating the added predictive ability of a new marker: from area under the ROC curve to reclassification and beyond. Stat. Med. 2008:27;157-172.
27. Pencina MJ, D'Agostino RB, Steyerberg EW. Extensions of net reclassification improvement calculations to measure usefulness of new biomarkers. *Stat. Med*. 2011:30;11-21
28. Fellahi JL, Le Manach Y, Daccache G, Riou B, Gerard JL, Hanouz JL. Combination of EuroSCORE and cardiac troponin 1 improves the prediction of adverse outcome after cardiac surgery. *Anesthesiology* 2011;114:330-339.
29. Polak JF, Pencina MJ, Pencina KM, o'Donnell CJ, Wolf PA, D'Agostino RB. Carotid-wall intima-media thickness and cardiovascular events. *N. Engl. J. Med*. 2011;365:213-221
30. Wilson KA, Lee AJ, Hoskins PR, Fowkes FG, Ruckley CV, Bradbury AW. The relationship between aortic wall distensibility and rupture of infrarenal abdominal aortic aneurysm. *J Vasc Surg*. 2003;37:112-117.
31. Herborn CU, Vogt FM, Lauenstein TC, Dirsch O, Corot C, Robert P, Ruehm SG. Magnetic resonance imaging of experimental atherosclerotic plaque: comparison of two ultrasmall superparamagnetic particles of iron oxide. *J Magn Reson Imaging.* 2006;24:388-393.
32. Prince MR, Zhang HL, Chabra SG, Jacobs P, Wang Y. A pilot investigation of new superparamagnetic iron oxide as a contrast agent for cardiovascular MRI. *Journal of X-Ray Science and Technology.* 2003;11:231-240.
33. Ersoy H, Jacobs P, Kent CK, Prince MR. Blood pool MR angiography of aortic stent-graft endoleak. *AJR Am J Roentgenol.* 2004;182:1181-1186.
34. Li W, Tutton S, Vu AT, Pierchala L, Li BSY, Lewis JM, Prasad PV, Edelman RR. First-pass contrast-enhanced magnetic resonance angiography in humans using ferumoxytol, a novel ultrasmall superparamagnetic iron oxide (USPIO)-based blood pool agent. *J Magn Reson Imaging.* 2005;21:46-52.

35. Li W, Salanitri J, Tutton S, Dunkle EE, Schneider JR, Caprini JA, Pierchala LN, Jacobs PM, Edelman RR. Lower extremity deep venous thrombosis: evaluation with ferumoxytol-enhanced MR imaging and dual-contrast mechanism--preliminary experience. *Radiology.* 2007;242:873-881.

36. Neuwelt EA, Várallyay CG, Manninger S, Solymosi D, Haluska M, Hunt MA, Nesbit G, Stevens A, Jerosch-Herold M, Jacobs PM, Hoffman JM. The potential of ferumoxytol nanoparticle magnetic resonance imaging, perfusion, and angiography in central nervous system malignancy: a pilot study. *Neurosurgery.* 2007;60:601-611.

37. Harisinghani M, Ross RW, Guimaraes AR, Weissleder R. Utility of a new bolus-injectable nanoparticle for clinical cancer staging. *Neoplasia.* 2007;9:1160-1165.

38. Barrett BJ, Katzberg RW, Thomsen HS, Chen N, Sahani D, Soulez G, Heiken JP, Lepanto L, Ni ZH, Ni ZH, Nelson R. Contrast-induced nephropathy in patients with chronic kidney disease undergoing computed tomography: a double-blind comparison of iodixanol and iopamidol. *Invest Radiol.* 2006;41:815-821.

Curr Cardiol Rep (2014) 16:521
DOI 10.1007/s11886-014-0521-4

NUCLEAR CARDIOLOGY (V DILSIZIAN, SECTION EDITOR)

Will 18F-Sodium Fluoride PET-CT Imaging Be the Magic Bullet for Identifying Vulnerable Coronary Atherosclerotic Plaques?

Nikhil V. Joshi · Alex Vesey · David E. Newby · Marc R. Dweck

© Springer Science+Business Media New York 2014

Abstract Myocardial infarction remains the commonest cause of premature death worldwide with coronary atherosclerotic plaque rupture often initiating the event. Despite an ever-expanding repertoire of cardiovascular imaging techniques, the race is still on to identify atherosclerotic lesions at high-risk of rupture: the so-called vulnerable plaque. Conventional imaging modalities such as stress testing and coronary angiography have consistently failed to identify such plaques, leading to the increasing appreciation that plaque rupture relates to factors other than just the degree of luminal stenosis. Indeed the focus has recently shifted to molecular imaging, in an attempt to directly target the pathological disease processes leading to rupture and thereby localize high-risk lesions. Histological data indicate that inflammation, necrosis and early stage microcalcification are key imaging targets by which to achieve this aim. Here, we discuss how these processes are related, focusing on the rationale and evidence supporting 18F-fluoride positron emission tomography as a novel non-invasive imaging technique for the identification of vulnerable atherosclerotic plaque.

Keywords Positron emission tomography · Computed tomography · 18F-fluoride · PET-CT imaging · Coronary atherosclerosis · Plaques

This article is part of the Topical Collection on *Nuclear Cardiology*

N. V. Joshi · A. Vesey · D. E. Newby · M. R. Dweck
Centre for Cardiovascular Science / Clinical Research Imaging Centre/ Edinburgh Heart Centre, University of Edinburgh, Edinburgh, UK

N. V. Joshi (✉)
University/BHF Centre for Cardiovascular Science, SU 305, Chancellors Building, Little France Crescent, Edinburgh, UK
e-mail: nikhil.joshi@ed.ac.uk

Published online: 08 August 2014

Introduction

Cardiovascular diseases remain the commonest cause of death worldwide. The majority of these deaths are attributed to sudden atherosclerotic plaque rupture resulting in myocardial infarction or stroke [1]. However prediction of cardiovascular events is difficult because most are caused by atherosclerotic plaques that are non-flow limiting and therefore missed by conventional diagnostic modalities such as myocardial stress testing or invasive coronary arteriography. However, these high-risk plaques, the so-called vulnerable plaque, do have certain histopathological characteristics, which potentially can be targeted using modern imaging technology. Indeed the race is now on to identify these high-risk plaques in vivo using both invasive and non-invasive modalities [2, 3••, 4].

The Vulnerable Plaque

The concept of the vulnerable plaque was first introduced by James Muller in 1989 when he described 'hemodynamically insignificant, albeit dangerous lesions' [5], that he believed were at high risk of rupturing and causing myocardial infarction. Since then multiple observational studies have confirmed that most of the plaques causing myocardial infarction are non-flow limiting at the time of antecedent coronary arteriography. However pioneering work over the last two decades has now established that ruptured plaques do have certain key histopathological features including: the presence of a large necrotic core, a thin fibrous cap (<65 μm), a positively remodelled vessel, macrophage infiltration resulting in plaque inflammation, hypoxia leading to neovascularization and finally early stage microcalcification (Fig. 1) [6–11]. Moreover it is widely postulated that intact high-risk plaques are likely to demonstrate the same pathophysiological features immediately before a clinical plaque rupture event, so that identification

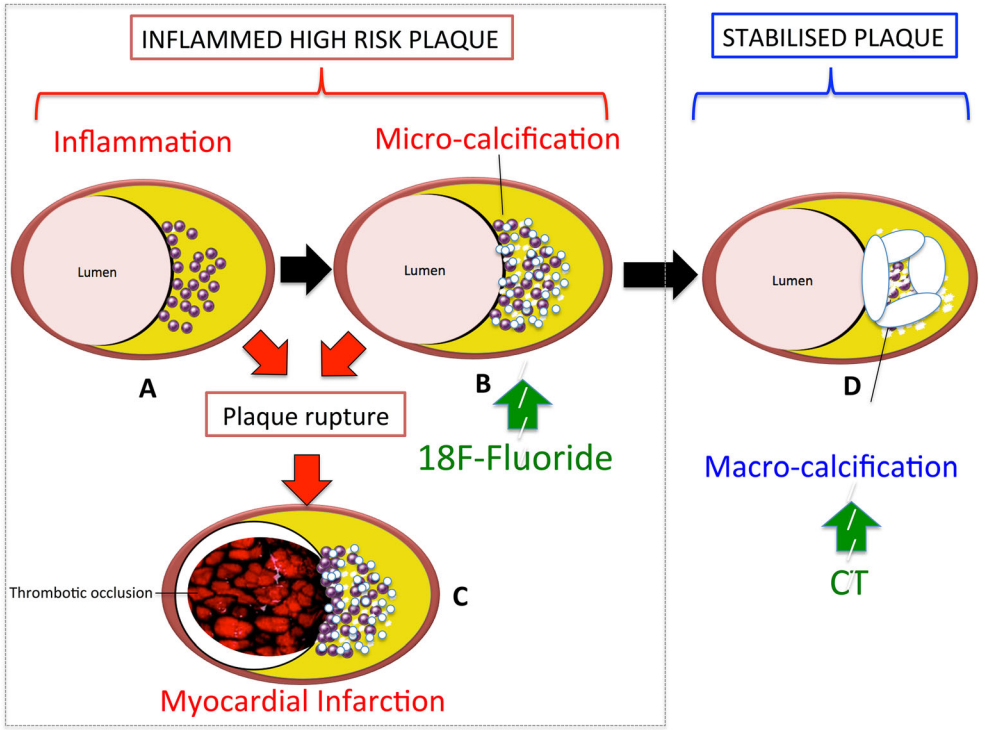

Fig. 1 The relationship between inflammation, biphasic calcific response and adverse cardiovascular events. **a** Typical features of a vulnerable plaque: The initial stages of plaque inflammation and vulnerability are associated with macrophage influx into a large lipid core. By this stage, other features of plaque vulnerability such as positive remodelling, thinning of the fibrous cap, are observed. **b** Microcalcification within the necrotic core: Cell death occurring within the lipid core as a consequence of necrosis and apoptosis triggers microcalcification. This is a high risk plaque type that is ripe to rupture. This can have two consequences: successful plaque calcification by walling off the inflamed area, or initiation of plaque rupture with subsequent thrombotic occlusion. This is the plaque type that is believed to be have avid 18F-fluoride uptake on PET/CT. **c** Plaque rupture with thrombotic occlusion of the lumen resulting in myocardial infarction. **d** Plaque stabilization with successful healing of the necrotic core with obvious macrocalcification that can be detected with conventional imaging modalities such as computed tomography and X-ray angiography

of these characteristics may be of use prospectively. Recent technological advances, coupled with the failure of percutaneous coronary intervention to reduce myocardial infarction in patients with stable angina [12] has renewed interest in detecting these plaques in vivo. Indeed, this has been described by many as the 'holy grail' of clinical cardiology [1, 2, 3••, 13].

The Link Between Inflammation and Calcification

Inflammation plays a critical role in the formation, progression, and rupture of atherosclerotic plaques and is typically characterized by the presence of macrophages within the plaque lipid core (Fig. 1) [6–11]. In an attempt to clear lipid from the vessel intima, these macrophages set up an inflammatory cycle that ultimately proves difficult to contain, leading to progressive matrix degradation and plaque destabilization. Indeed ongoing macrophage infiltration and cell death along with accelerated lipid accumulation contribute to an enlarging necrotic core that becomes progressively more inflamed and hypoxic. Moreover these cells secrete pro-inflammatory cytokines (including interleukin-1, monocyte chemotactic protein-1 and tumour necrosis factor-alpha) and matrix metalloproteinases, which actively weaken the fibrous cap: the only barrier between this highly thrombogenic lipid core and the vessel lumen. Fortunately this is where body defence mechanisms are believed to respond, triggering a calcific healing response that attempts to subdue and wall off this inflamed necrotic environment, thereby reducing the risk of plaque rupture.

Calcification occurs widely in the body and frequently occurring as a healing response to intense necrotic inflammation. This is perhaps best exemplified by tuberculosis where the body attempts to wall off the intense necrotic inflammation associated with caseating granulomata using calcification. Similar mechanisms are believed to occur within coronary atheroma, with calcification occurring as a healing response to intense inflammation within the necrotic core. However in these arteries, calcification appears to have a bi-phasic response, with each stage associated with markedly different plaque characteristics and clinical consequences. The latter phase of macroscopic calcification is readily imaged using standard x-ray angiography and CT, and is widely believed

to impart stability to the plaque. Indeed by this stage the healing process has often successfully subdued inflammation within the vessel wall and separated it from the contents of the vascular lumen. By contrast the earlier phase of micro-calcification is not visible using standard non-invasive imaging techniques and is associated with plaque instability and an increased risk of rupture (Table 1) [14, 15]. The likely explanation is that at this early time-point the healing process has not yet been effective and that the inflamed necrotic environment triggering calcification still exists within the plaque. This risk of plaque rupture related to inflammation therefore persists. However recent data have indicated that in addition micro-calcification might itself increase the propensity to rupture, acting as a focal point that intensifies mechanical stresses on the surface of the cap. Either way a technique capable of directly imaging active ongoing micro-calcification and differentiating it from dormant macroscopic areas would hold real promise as a means of improving our understanding of plaque biology and in identifying high-risk atheroma.

Although there have been significant advances in our understanding as to why atherosclerotic plaques calcify, the exact molecular mechanisms underpinning this observation remain unclear. Multiple potential pathways have been proposed although often these have been established using models of vascular medial calcification. Calcification in the coronary arteries is almost uniquely intimal with medial and adventitial involvement occurring only rarely in conditions such as renal failure. Calcification activity in the intima appears to be closely related to inflammation and cell death within the necrotic core. Several putative pathways have been proposed linking these entities [16–21]. First and most obviously, necrosis of foam cells, vascular smooth muscle cells and other cells in the inflammatory plaque milieu leads to the release of large quantities of phosphate and calcium which may lead to spontaneous dystrophic calcification (as observed in infarctions, haematomas and scars). Second, inflammation may trigger osteogenic metaplasia in a variety of cell types (VSMC, endothelial cells, etc.) which make a phenotypic switch to osteoblast like cells under the influence of RUNX-2 transcription and become capable of roughly recapitulating skeletal osteogenesis in the plaque matrix. Third, circulating osteoprogenitors may be recruited to the plaque before undergoing maturation to classical osteoblasts. Fourth, cells undergoing programmed cell death within the plaque may provide calcifying substrate through the release of apoptotic bodies. Fifth and finally, macrophages themselves may provide the substrate for calcification by directly releasing matrix vesicles (the key and final executors of ordered tissue mineralization) into the extracellular matrix. Aikawa et al. have published the key and highly elegant longitudinal experiments in a mouse model that have conclusively demonstrated the link between inflammation and calcification [14]. They showed that macrophage infiltration is closely associated with osteogenic activity (as assayed by accumulation of OsteoSense; a bisphosphonate-conjugated to a fluorescent reporter). They (and others) have also shown that apoptotic bodies and matrix vesicles that contain calcium orthophosphate nanocrystals execute this early calcific process [20, 22, 23].

Table 1 Key differences between micro and macrocalcification

	Microcalcification	Macrocalcification
Size	<5 μm	>5 μm
Stage of calcification	Early	Late
Inflammation	Persistent	Healed
Surface area	High	Low
Exposed hydroxyapatite	High	Low
Risk of rupture	High risk of rupture	Low risk of rupture
Computed Tomography/ X-ray angiography	Undetectable	Detectable
18F-fluoride binding on positron emission tomography	Avid binding	Low binding

Positron Emission Tomography

Combined positron emission and computed tomography (PET/CT) is a modern non-invasive imaging technique that combines functional information from PET with the fine anatomical detail provided by CT, allowing the activity of specific pathological processes to be studied within even small structures in the body. This technique has been widely used in the clinical assessment of patients with cancer for many years, resulting in the widespread availability of PET/CT scanners [24]. Recent technological advances including ECG-gating, improved PET resolution and fusion with detailed CT angiography of the coronary vessels, has allowed translation of this technology into the heart. Theoretically any pathological process can be studied dependent on a suitable radiotracer being developed, so that potentially each of the established characteristics associated with high-risk plaque may be targeted. However to date the majority of studies investigating coronary atherosclerosis have utilized the tracers 18F-fluorodeoxyglucose (18F-FDG) and 18F-fluoride as markers of inflammation and micro-calcification respectively. Whilst a comprehensive discussion of 18F-FDG activity in the vasculature is beyond the scope of this review, it has become clear that whilst an excellent tracer for imaging vascular inflammation and perhaps hypoxic inflammation in the aorta and carotid arteries, utilization of this tracer in the coronary arteries is problematic. In particular, difficulty has arisen from uptake of this tracer by the adjacent myocardium, which frequently obscures the coronary signal. Whilst ultimately this problem

may be rectified using advanced motion correction algorithms and attempts to switch myocardial metabolism away from glucose, further work is required before 18F-FDG is likely to prove useful in the coronary circulation. By contrast 18F-fluoride demonstrates an excellent signal to noise ratio in the coronary arteries as it is not taken up by adjacent structures and is rapidly cleared from plasma moreover it already appears capable of providing important clinical information with respect to coronary plaque biology.

Mechanism of 18F-Fluoride PET Activity

18F-Fluoride is a PET tracer with favourable pharmacokinetic properties, first introduced by Blau and coworkers in 1962 for the study of bone disease [25–27]. After an intravenous injection, approximately 70 % of 18F-fluoride is plasma based with the remaining 30 % found in erythrocytes. Because of its small size and negligible protein binding, 18F-fluoride demonstrates almost complete clearance from the blood stream on first pass [28–30], resulting in low blood-pool activity. This coupled with its specificity for bone and vascular calcification ensures that it provides excellent signal to noise in these tissues with little contamination from adjacent structures.

The mechanism of 18F-fluoride uptake in bone is well established. First it diffuses via the capillary network into the bone extracellular fluid. Then it exchanges with hydroxyl groups on exposed regions of hydroxyapatite crystal on the bone surface, forming fluoroapatite. The intensity of the signal depends both on the bone blood flow but also upon the surface area of exposed hydroxyapatite, which is increased in regions of new bone formation and remodelling [25–27]. As a consequence 18F-fluoride has been extensively utilized as a marker of bone turnover and used to study various bone related clinical conditions such as Paget's disease [31, 32], osteoporosis [33, 34], renal osteodystrophy [14], fracture healing [35], and osteonecrosis [36]. Moreover, 18F-fluoride PET has become widely established as the most sensitive imaging modality for the detection of malignant bone involvement, leading to its widespread and commercial availability [37–41].

We believe that very similar mechanisms underlie the uptake of 18F-fluoride in the vasculature. Given the nature of the tissue, blood supply is not likely to be a major factor. However like bone, hydroxyapatite is also the key structural component of vascular calcium, so that arterial 18F-fluoride uptake is likely to relate closely to the available surface area of this crystal. Transmission electron microscopy studies have demonstrated that during the early stages of calcification hydroxyapatite crystals are nanosized, very thin and long [42]. This results in a much larger surface area of hydroxyapatite for 18F-fluoride binding in the early stages of microcalcification compared to macroscopic calcification in which much of the hydroxyapatite is internalized and not accessible to the tracer. The hypothesis that 18F-fluoride preferentially binds to vascular micro-calcification activity has been strongly supported by some early yet detailed preclinical work performed by our collaborators at Cambridge University and will no doubt be the subject of intensive future study [43].

Clinical Studies Examining Vascular 18F-Fluoride Activity

Derlin et al. first described the vascular uptake of 18F-fluoride in 2010 in a retrospective analysis of patients with malignancy [44]. The authors noted increased 18F-fluoride uptake in large vessels such as the aorta, carotids and femoral vessels in about three quarters of the patients studied. Interestingly, only a fifth of all calcified plaques on CT demonstrated increased 18F-fluoride uptake, highlighting even at this early stage that 18F-fluoride provides different information to the presence of calcium on CT. Subsequent work by the same group retrospectively compared the distribution of 18F-fluoride and 18F-FDG uptake in oncology patients [45] and suggested that 18F-fluoride signal in the femoral vessels correlated with the calcified plaque burden and cardiovascular risk factors [46]. Beheshti and colleagues first described 18F-fluoride activity localizing to the heart [47] whilst we and other groups have confirmed increased 18F-fluoride activity in the aorta and importantly in the valves of patients with aortic stenosis [48••, 49], where it acts as a marker of calcification activity and predicts disease progression [50].

Coronary 18F-NaF PET Identifies High Risk Patients

We first described 18F-fluoride uptake in the coronary arteries as a novel marker of plaque biology in subjects with and without aortic valve disease [51••]. This demonstrated the feasibility and excellent reproducibility of this tracer in the coronary vasculature. Moreover increased uptake of this tracer localized to individual coronary plaques and importantly identified patients at increased cardiovascular risk, with those subjects having increased Framingham risk scores and prior MACE event rates. This study also confirmed that, as in the aorta, 18F-fluoride provided different information to the presence of coronary calcium on CT. Indeed we observed that >40 % of patients with coronary artery calcium scores >1000 Agatston Units did not have 18F-fluoride uptake, suggesting the ability of 18F- fluoride to distinguish between dormant pacified calcific disease and metabolically active ongoing micro-calcification.

Coronary 18F-Fluoride PET as a Marker of High-Risk Atherosclerotic Plaque

Perhaps the key incidental observation from our initial study came from a patient with aortic stenosis admitted with an inferior non-ST elevation myocardial infarction [51••]. Intense coronary 18F-fluoride uptake was localized to the exact site of the culprit lesion in this patient, despite them having severe three vessel disease and widespread coronary calcium on CT. Based on this observation and the wider results of this preliminary study, we designed a subsequent trial to investigate 18F-fluoride activity in patients with stable and unstable coronary artery disease [52••]. Our hypothesis was that 18F-fluoride would identify high-risk vulnerable plaques in patients with stable angina and ruptured plaques in patients with myocardial infarction.

We examined 40 patients with stable angina referred for invasive angiography, who all underwent 18F-NaF PET/CT imaging alongside CT coronary angiography, invasive coronary angiography and intravascular ultrasound. Increased 18F-fluoride activity localized to individual coronary plaques in ~40 % of patients. These plaques had multiple high-risk features on intravascular ultrasound and CT including microcalcification, positive remodelling and a large necrotic core. It was not possible to undertake histological analysis of the 18F-fluoride signal in these patients. However instead we demonstrated that increased 18F-fluoride activity colocalized with histological evidence of increased macrophage accumulation, cell death and calcification activity in carotid endarterectomy specimens. These data would indicate that 18F-fluoride identifies high-risk atherosclerotic plaque. However the real question is whether these plaques go on to cause myocardial infarction. Ultimately this will require prospective studies but we examined this issue retrospectively, investigating 18F-fluoride uptake in 40 patients who had recently sustained a type 1 myocardial infarction. We observed increased 18F-fluoride uptake at the site of the culprit plaque in 93 % of these patients. Indeed activity was around 30 % higher in the culprit plaque than the maximum activity recorded anywhere else in the coronary vasculature and was independent of coronary artery stenting.

Conclusions and Future Directions

In combination we believe that the clinical studies to date have demonstrated that 18F-fluoride provides complementary information to the presence of calcium on CT and that this technique is able to identify high-risk and ruptured coronary atherosclerotic plaques. It therefore holds major promise as a method of identifying vulnerable plaque and in improving upon current methods for the prediction of myocardial infarction. Indeed if confirmed then this approach may have a significant role to play in our future approach to the treatment of coronary artery disease.

Two major questions still need to be addressed before the potential of 18F-fluoride can be realized. First the mechanism for 18F-fluoride uptake in the vasculatures needs to be confirmed over and above the work we have already performed in the aortic valve and carotid arteries. Second the ability of 18F-fluoride to predict myocardial infarction needs to be addressed in the context of a prospective observational study, ideally in a high-risk population.

We believe that it is improbable that all coronary plaques with increased 18F-fluoride activity will go on to cause a myocardial infarction. Indeed calcification is often likely to prove successful in stabilizing the plaque and even when rupture does occur this will be sub-clinical in the majority of cases (Fig. 1). As a consequence individual plaque-directed treatment strategies are also unlikely to be effective. Instead we believe that the future role of 18F-fluoride will be in identifying the *vulnerable patient*. Those subjects with evidence of metabolically active coronary atheroma who are at an increased risk of myocardial infarction and would therefore benefit from some of the newer medical therapies that appear to have profound effects on coronary plaque biology but do so at great expense.

Compliance with Ethics Guidelines

Conflict of Interest Nikhil V, Joshi, Alex Vesey, David E, Newby, and Marc R. Dweck declare that they have no conflict of interest.

Human and Animal Rights and Informed Consent This article does not contain any studies with human or animal subjects performed by any of the authors.

References

Papers of particular interest, published recently, have been highlighted as:
•• Of major importance

1. Naghavi M, Libby P, Falk E, Casscells SW, Litovsky S, Rumberger J, et al. From vulnerable plaque to vulnerable patient: a call for new definitions and risk assessment strategies: part I. Circulation. 2003;108(14):1664–72.
2. Calvert PA, Obaid DR, O'Sullivan M, Shapiro LM, McNab D, Densem CG, et al. Association between IVUS findings and adverse outcomes in patients with coronary artery disease: the VIVA (VH-IVUS in Vulnerable Atherosclerosis) study. JACC Cardiovasc Imaging. 2011;4(8):894–901.
3.•• Stone GW, Maehara A, Lansky AJ, de Bruyne B, Cristea E, Mintz GS, et al. A prospective natural-history study of coronary atherosclerosis. N Engl J Med. 2011;364(3):226–35. *This landmark study looked at the natural history of coronary atherosclerotic plaques using radiofrequency intravascular ultrasound and provided key pathological insights into our understanding of coronary disease.*

4. Rogers IS, Nasir K, Figueroa AL, Cury RC, Hoffmann U, Vermylen DA, et al. Feasibility of FDG imaging of the coronary arteries: comparison between acute coronary syndrome and stable angina. JACC Cardiovasc Imaging. 2010;3(4):388–97.
5. Muller JE, Tofler GH, Stone PH. Circadian variation and triggers of onset of acute cardiovascular disease. Circulation. 1989;79(4):733–43.
6. Burke AP, Farb A, Malcom GT, Liang Y, Smialek J, Virmani R. Coronary risk factors and plaque morphology in men with coronary disease who died suddenly. N Engl J Med. 1997;336(18):1276.
7. Burke AP, Kolodgie FD, Farb A, Weber DK, Malcom GT, Smialek J, et al. Healed plaque ruptures and sudden coronary death: evidence that subclinical rupture has a role in plaque progression. Circulation. 2001;103(7):934–40.
8. Falk E, Nakano M, Bentzon JF, Finn AV, Virmani R. Update on acute coronary syndromes: the pathologists' view. Eur Heart J. 2013;34(10):719–28.
9. Finn AV, Nakano M, Narula J, Kolodgie FD, Virmani R. Concept of vulnerable/unstable plaque. Arterioscler Thromb Vasc Biol. 2010;30(7):1282–92.
10. Virmani R, Burke AP, Farb A, Kolodgie FD. Pathology of the vulnerable plaque. J Am Coll Cardiol. 2006;47(8 Suppl):C13–8.
11. Virmani R, Kolodgie FD, Burke AP, Farb A, Schwartz SM. Lessons from sudden coronary death: a comprehensive morphological classification scheme for atherosclerotic lesions. Arterioscler Thromb Vasc Biol. 2000;20(5):1262–75.
12. Boden WE, O'Rourke RA, Teo KK, Hartigan PM, Maron DJ, Kostuk WJ, et al. Optimal medical therapy with or without PCI for stable coronary disease. N Engl J Med. 2007;356(15):1503–16.
13. Kato K, Yonetsu T, Kim SJ, Xing L, Lee H, McNulty I, et al. Nonculprit plaques in patients with acute coronary syndromes have more vulnerable features compared with those with non-acute coronary syndromes: a 3-vessel optical coherence tomography study. Circ Cardiovasc Imaging. 2012;5(4):433–40.
14. Aikawa E, Nahrendorf M, Figueiredo JL, Swirski FK, Shtatland T, Kohler RH, et al. Osteogenesis associates with inflammation in early-stage atherosclerosis evaluated by molecular imaging in vivo. Circulation. 2007;116(24):2841–50.
15. Otsuka F, Finn AV, Virmani R. Do vulnerable and ruptured plaques hide in heavily calcified arteries? Atherosclerosis. 2013;229(1):34–7.
16. New SE, Aikawa E. Molecular imaging insights into early inflammatory stages of arterial and aortic valve calcification. Circ Res. 2011;108(11):1381–91.
17. Tintut Y, Patel J, Parhami F, Demer LL. Tumor necrosis factor-alpha promotes in vitro calcification of vascular cells via the cAMP pathway. Circulation. 2000;102(21):2636–42.
18. Radcliff K, Tang TB, Lim J, Zhang Z, Abedin M, Demer LL, et al. Insulin-like growth factor-I regulates proliferation and osteoblastic differentiation of calcifying vascular cells via extracellular signal-regulated protein kinase and phosphatidylinositol 3-kinase pathways. Circ Res. 2005;96(4):398–400.
19. Demer LL, Tintut Y. Vascular calcification: pathobiology of a multifaceted disease. Circulation. 2008;117(22):2938–48.
20. Proudfoot D, Skepper JN, Hegyi L, Bennett MR, Shanahan CM, Weissberg PL. Apoptosis regulates human vascular calcification in vitro: evidence for initiation of vascular calcification by apoptotic bodies. Circ Res. 2000;87(11):1055–62.
21. Shanahan CM. Inflammation ushers in calcification: a cycle of damage and protection? Circulation. 2007;116(24):2782–5.
22. Bobryshev YV, Killingsworth MC, Huynh TG, Lord RS, Grabs AJ, Valenzuela SM. Are calcifying matrix vesicles in atherosclerotic lesions of cellular origin? Basic Res Cardiol. 2007;102(2):133–43.
23. Golub EE. Biomineralization and matrix vesicles in biology and pathology. Semin Immunopathol. 2011;33(5):409–17.
24. Lardinois D, Weder W, Hany TF, Kamel EM, Korom S, Seifert B, et al. Staging of non-small-cell lung cancer with integrated positron-emission tomography and computed tomography. N Engl J Med. 2003;348(25):2500–7.
25. Blau M, Nagler W, Bender MA. Fluorine-18: a new isotope for bone scanning. J Nucl Med. 1962;3:332–4.
26. Blau M, Ganatra R, Bender MA. 18F-fluoride for bone imaging. Semin Nucl Med. 1972;2(1):31–7.
27. Hawkins RA, Choi Y, Huang SC, Hoh CK, Dahlbom M, Schiepers C, et al. Evaluation of the skeletal kinetics of fluorine-18-fluoride ion with PET. J Nucl Med. 1992;33(5):633–42.
28. Blake GM, Park-Holohan SJ, Cook GJ, Fogelman I. Quantitative studies of bone with the use of 18F-fluoride and 99mTc-methylene diphosphonate. Semin Nucl Med. 2001;31(1):28–49.
29. Wootton R, Dore C. The single-passage extraction of 18F in rabbit bone. Clin Phys Physiol Meas. 1986;7(4):333–43.
30. Hoh CK, Hawkins RA, Dahlbom M, Glaspy JA, Seeger LL, Choi Y, et al. Whole body skeletal imaging with [18F]fluoride ion and PET. J Comput Assist Tomogr. 1993;17(1):34–41.
31. Cook GJ, Blake GM, Marsden PK, Cronin B, Fogelman I. Quantification of skeletal kinetic indices in Paget's disease using dynamic 18F-fluoride positron emission tomography. J Bone Miner Res. 2002;17(5):854–9.
32. Installe J, Nzeusseu A, Bol A, Depresseux G, Devogelaer JP, Lonneux M. (18)F-fluoride PET for monitoring therapeutic response in Paget's disease of bone. J Nucl Med. 2005;46(10):1650–8.
33. Frost ML, Fogelman I, Blake GM, Marsden PK, Cook Jr G. Dissociation between global markers of bone formation and direct measurement of spinal bone formation in osteoporosis. J Bone Miner Res. 2004;19(11):1797–804.
34. Messa C, Goodman WG, Hoh CK, Choi Y, Nissenson AR, Salusky IB, et al. Bone metabolic activity measured with positron emission tomography and [18F]fluoride ion in renal osteodystrophy: correlation with bone histomorphometry. J Clin Endocrinol Metab. 1993;77(4):949–55.
35. Hsu WK, Feeley BT, Krenek L, Stout DB, Chatziioannou AF, Lieberman JR. The use of 18F-fluoride and 18F-FDG PET scans to assess fracture healing in a rat femur model. Eur J Nucl Med Mol Imaging. 2007;34(8):1291–301.
36. Schiepers C, Broos P, Miserez M, Bormans G, De Roo M. Measurement of skeletal flow with positron emission tomography and 18F-fluoride in femoral head osteonecrosis. Arch Orthop Trauma Surg. 1998;118(3):131–5.
37. Petren-Mallmin M, Andreasson I, Ljunggren O, Ahlstrom H, Bergh J, Antoni G, et al. Skeletal metastases from breast cancer: uptake of 18F-fluoride measured with positron emission tomography in correlation with CT. Skelet Radiol. 1998;27(2):72–6.
38. Schirrmeister H, Guhlmann A, Kotzerke J, Santjohanser C, Kuhn T, Kreienberg R, et al. Early detection and accurate description of extent of metastatic bone disease in breast cancer with fluoride ion and positron emission tomography. J Clin Oncol. 1999;17(8):2381–9.
39. Hetzel M, Arslandemir C, Konig HH, Buck AK, Nussle K, Glatting G, et al. F-18 NaF PET for detection of bone metastases in lung cancer: accuracy, cost-effectiveness, and impact on patient management. J Bone Miner Res. 2003;18(12):2206–14.
40. Even-Sapir E, Metser U, Mishani E, Lievshitz G, Lerman H, Leibovitch I. The detection of bone metastases in patients with high-risk prostate cancer: 99mTc-MDP Planar bone scintigraphy, single- and multi-field-of-view SPECT, 18F-fluoride PET, and 18F-fluoride PET/CT. J Nucl Med. 2006;47(2):287–97.
41. Beheshti M, Vali R, Waldenberger P, Fitz F, Nader M, Loidl W, et al. Detection of bone metastases in patients with prostate cancer by 18F fluorocholine and 18F fluoride PET-CT: a comparative study. Eur J Nucl Med Mol Imaging. 2008;35(10):1766–74.

42. Rey C, Combes C, Drouet C, Glimcher MJ. Bone mineral: update on chemical composition and structure. Osteoporos Int. 2009;20(6): 1013–21.
43. Agnese Irkle JLB, Skepper JN, Dweck MR, Joshi FR, Vesey AT, Bennett M, et al. 18F-NaF - a Specific Marker for Vascular Calcification in Atherosclerosis. Circulation. 2013;128:A17385.
44. Derlin T, Richter U, Bannas P, Begemann P, Buchert R, Mester J, et al. Feasibility of 18F-sodium fluoride PET/CT for imaging of atherosclerotic plaque. J Nucl Med. 2010;51(6):862–5.
45. Derlin T, Toth Z, Papp L, Wisotzki C, Apostolova I, Habermann CR, et al. Correlation of inflammation assessed by 18F-FDG PET, active mineral deposition assessed by 18F-fluoride PET, and vascular calcification in atherosclerotic plaque: a dual-tracer PET/CT study. J Nucl Med. 2011;52(7):1020–7.
46. Janssen T, Bannas P, Herrmann J, Veldhoen S, Busch JD, Treszl A, et al. Association of linear (18)F-sodium fluoride accumulation in femoral arteries as a measure of diffuse calcification with cardiovascular risk factors: A PET/CT study. J Nucl Cardiol. 2013;20(4): 569–77.
47. Beheshti M, Saboury B, Mehta NN, Torigian DA, Werner T, Mohler E, et al. Detection and global quantification of cardiovascular molecular calcification by fluoro18-fluoride positron emission tomography/computed tomography–a novel concept. Hell J Nucl Med. 2011;14(2):114–20.
48.•• Dweck MR, Jones C, Joshi N, Fletcher AM, Richardson H, White A, et al. Assessment of valvular calcification and inflammation by positron emission tomography in patients with aortic stenosis. Circulation. 2011. doi:10.1161/CIRCULATIONAHA.111.051052. *This important study looks at 18F-fluoride uptake in aortic valve disease.*
49. Dweck MR, Khaw HJ, Sng GK, Luo EL, Baird A, Williams MC, et al. Aortic stenosis, atherosclerosis, and skeletal bone: is there a common link with calcification and inflammation? Eur Heart J. 2013;34(21):1567–74.
50. Dweck MR, Jenkins WS, Vesey AT, Pringle MA, Chin CW, Malley TS, et al. 18F-sodium fluoride uptake is a marker of active calcification and disease progression in patients with aortic stenosis. Circ Cardiovasc Imaging. 2014;7(2):371–8.
51.•• Dweck MR, Chow MW, Joshi NV, Williams MC, Jones C, Fletcher AM, et al. Coronary arterial 18F-sodium fluoride uptake: a novel marker of plaque biology. J Am Coll Cardiol. 2012;59(17):1539–48. *We first described the coronary uptake of 18F-fluoride in patients with or without aortic stenosis in this important paper.*
52.•• Joshi NV, Vesey AT, Williams MC, Shah AS, Calvert PA, Craighead FH, et al. F-fluoride positron emission tomography for identification of ruptured and high-risk coronary atherosclerotic plaques: a prospective clinical trial. Lancet. 2013. doi:10.1016/S0140-6736(13)61754-7. *In this paper, we show that 18F-fluoride can identify ruptured and high risk plaques in patients with myocardial infarction and stable angina. Furthermore, we characterise these plaques with intravascular imaging in patients with stable angina and with histology in patients undergoing carotid endartrectomy.*

Downloaded from jnm.snmjournals.org by on September 15, 2016. For personal use only.

Motion Correction of ^{18}F-NaF PET for Imaging Coronary Atherosclerotic Plaques

Mathieu Rubeaux[1], Nikhil V. Joshi[2], Marc R. Dweck[2], Alison Fletcher[2], Manish Motwani[1], Louise E. Thomson[1], Guido Germano[1], Damini Dey[1], Debiao Li[1], Daniel S. Berman[1], David E. Newby[2], and Piotr J. Slomka[1]

[1]*Cedars-Sinai Medical Center, Los Angeles, California; and* [2]*University of Edinburgh, Edinburgh, United Kingdom*

Ruptured coronary atherosclerotic plaques commonly cause acute myocardial infarction. It has recently been shown that active microcalcification in the coronary arteries, one of the features that characterizes vulnerable plaques at risk of rupture, can be imaged using ^{18}F-NaF PET. We aimed to determine whether a motion correction technique applied to gated ^{18}F-NaF PET images could enhance image quality and improve uptake estimates. **Methods:** Seventeen patients with myocardial infarction ($n = 7$) or stable angina ($n = 10$) underwent ^{18}F-NaF PET and prospective coronary CT angiography. PET data were reconstructed in 4 different ways: the first was 1 gated bin (end-diastolic phase with 25% of the counts), the second was 4 gated bins (consecutive 25% segments), the third was 10 gated bins (consecutive 10% segments), and the fourth was ungated. Subsequently, with data from either 4 or 10 bins, gated PET images were registered using a local, nonlinear motion correction method guided by the extracted coronary arteries from CT angiography. Global noise levels and target-to-background ratios (TBR) defined on manually delineated coronary plaque lesions were compared to assess image quality and uptake estimates. **Results:** Compared with the reference standard of using only 1 bin of PET data, motion correction using 10 bins of PET data reduced image noise by 46% ($P < 0.0001$). TBR in positive lesions for 10-bin motion-corrected data was 11% higher than for 1-bin data (1.98 [interquartile range, 1.70–2.37] vs. 1.78 [1.58–2.16], $P = 0.0027$) and 33% higher than for ungated data (1.98 [1.70–2.37] vs. 1.49 [1.39–1.88], $P < 0.0001$). **Conclusion:** Motion correction of gated ^{18}F-NaF PET/coronary CT angiography is feasible, reduces image noise, and increases TBR. This improvement may allow more reliable identification of vulnerable coronary artery plaques using ^{18}F-NaF PET.

Key Words: motion correction; ^{18}F-sodium fluoride PET; ^{18}F-NaF; coronary atherosclerotic plaques; microcalcification

J Nucl Med 2016; 57:54–59
DOI: 10.2967/jnumed.115.162990

Acute myocardial infarction (MI) is the leading cause of death in the United States, with 735,000 Americans experiencing an acute MI and about 120,000 dying as a consequence each year (*1*). Acute MI most commonly results from coronary atherosclerotic plaque rupture. Despite this cause, current treatment algorithms make no allowance for the presence or absence of vulnerable plaques at risk of rupture, and the current dogma is to treat all patients with any atherosclerosis in the same way. An accurate, noninvasive, a priori method for identifying such rupture-prone plaques would challenge this dogma, allowing high-risk patients to be selectively targeted with patient-specific therapies.

Histopathologic studies of patients who died from acute MI have demonstrated that the plaques that have ruptured and caused acute MI have several common characteristics. Among these, microcalcification is a consistent finding, believed to represent the very early stages of the body's attempt to heal inflamed necrotic plaque. A recent series of studies (*2–4*) demonstrated that ^{18}F-sodium fluoride (^{18}F-NaF)—an inexpensive, Food and Drug Administration–approved, widely available PET tracer—binds preferentially to regions of vascular microcalcification and can be used to identify high-risk plaques and plaque rupture in the coronary arteries. In particular, in a study by Joshi et al. increased ^{18}F-NaF PET activity was found to localize to the exact site of plaque rupture in more than 90% of patients who had recently experienced an acute MI, independent of stenting (*2*).

There are, however, several important limitations still to be addressed. The difference in target-to-background ratio (TBR) between culprit plaques (implicated in acute MI) and nonculprit plaques in ^{18}F-NaF PET is relatively small (~34%) because of blurring of coronary uptake by cardiac, respiratory, and patient motion. The implication is a greater risk of misclassification when this technique is applied to real-world, unselected populations. Unfortunately, recent general-purpose motion correction methods proposed for PET (*5,6*) are not applicable because of lack of clear anatomic landmarks in the heart region on the ^{18}F-NaF scan. To partially address the problem of motion, only a single cardiac phase (representing about 25% of the PET data) was used in the initial study (*2*), at the expense of a significant increase in noise. Although this was a useful exploratory strategy, the combination of an already-narrow diagnostic TBR margin and increased noise is clearly suboptimal.

We previously developed motion correction techniques for cardiac perfusion data from SPECT and PET, which facilitated an increase in image contrast compared with ungated data (*7,8*). In the present study, we aimed to overcome some of the current limitations of ^{18}F-NaF PET by developing a motion correction method for coronary ^{18}F-NaF PET to optimize this promising plaque-imaging technique.

MATERIALS AND METHODS

Patients

Patients were recruited from the Royal Infirmary of Edinburgh between February 2012 and January 2013 in 2 cohorts: 7 patients with acute ST-segment or non–ST-segment elevation acute MI and 10

Received Jun. 30, 2015; revision accepted Oct. 5, 2015.
For correspondence or reprints contact: Piotr J. Slomka, Artificial Intelligence in Medicine Program, 8700 Beverly Blvd., Ste. A047N, Los Angeles, CA 90048.
E-mail: piotr.slomka@cshs.org
Published online Oct. 15, 2015.
COPYRIGHT © 2016 by the Society of Nuclear Medicine and Molecular Imaging, Inc.

Downloaded from jnm.snmjournals.org by on September 15, 2016. For personal use only.

patients with stable angina pectoris undergoing elective invasive coronary angiography. Table 1 shows the demographic and clinical characteristics of these patients. All underwent a comprehensive baseline clinical assessment, including evaluation of their cardiovascular risk factor profile. Studies were done with the approval of the local research ethics committee, in accordance with the Declaration of Helsinki, and with the written informed consent of each participant.

Imaging and Analysis Protocols

All patients underwent ^{18}F-NaF PET/CT imaging of the coronary arteries with cardiac gating on a hybrid scanner (64-detector Biograph mCT; Siemens Medical Systems). The subjects were administered a target dose of 125 MBq of ^{18}F-NaF intravenously and subsequently rested in a quiet environment for 60 min. An attenuation correction CT scan (nonenhanced, 120 kV and 50 mA) was then obtained, followed by PET imaging of the thorax in list-mode for 20 min.

Prospectively gated coronary CT angiography (CCTA) was undertaken during the same visit as the ^{18}F-NaF scan, using a 330-ms rotation time, a 100-kV (body mass index < 25 kg/m^2) or 120-kV (body mass index > 25 kg/m^2) tube voltage, a 160- to 245-mAs tube current, and a 3.8-mm/rotation table feed, with prospective electrocardiography triggering (heart rate regular and < 60 beats/min), or retrospective electrocardiography gating (heart rate > 60 beats/min). Depending on the body mass index, a bolus of 80–100 mL of contrast material (400 mg I/mL, Iomeron; Bracco) was injected intravenously at 5 mL/s, after determining the appropriate trigger delay with a test bolus of 20 mL of contrast material. Electrocardiography-gated PET images were reconstructed using the Siemens Ultra-HD algorithm (time-of-flight plus point spread function) in multiple phases of the cardiac cycle. For this study, 4 different sets of data were reconstructed from list-mode data: 1 bin with 25% of the counts during the end-diastolic phase (the technique used in the original study of Joshi et al. (*2*)), 4 bins, 10 bins, and ungated. The PET pixel size was 2 mm. The CCTA scans were reconstructed at 0.75×0.7 mm and 0.6×0.3 mm for retrospective and prospective acquisitions, respectively, at 70% of the cardiac cycle.

Motion Correction

The goal of the motion correction procedure was to compensate for coronary artery motion in the different phases of the electrocardiography-gated PET data. Gated PET with 4 and 10 time bins were reconstructed from the PET list-mode files. The registration aimed to align all bins to the end-diastolic phase position, synchronizing the registered data to the prospective CCTA and, for comparison purposes, to the 1-bin PET data corresponding to the end-diastolic phase (as used in the original study). The end-diastolic phase, taken as the reference, corresponded to bin 3 in the dataset with 4 bins and to bin 7 in the dataset with 10 bins.

The registration of individual bins of ^{18}F-NaF PET presents a unique challenge because there are no clear anatomic references near the heart, and motion of bones (where there is significant ^{18}F-NaF uptake) does not correlate with motion of the heart. Thus, innovative approaches are required to deal with this problem. The procedure we used is illustrated in Figure 1. To recover the anatomic information that is missing in the PET data, we used the CCTA data that clearly delineate the coronary arteries. The end-expiration position of the CCTA allowed excellent alignment with PET data when the patient remained in the same position. Coronary regions were first extracted from the CCTA by vessel tracking based on Bayesian maximal paths (*9*), as implemented and validated in our Autoplaq CCTA processing software (*10–12*). This algorithm requires as input only proximal and distal points for every coronary artery and automatically finds the vessel centerline. The centerlines of the right, left circumflex, and left anterior descending coronary arteries were extracted for every patient in this manner.

Subsequently, the centerline coordinates were transferred to the PET volumes to automatically extract 3-dimensional tubular volumes of interest surrounding the coronary arteries in the gated PET images, defined by a 20-mm radius around each centerline. This radius was chosen to take into account the maximum displacement that can occur during the cardiac cycle, also allowing for potential remaining misregistration. Techniques that did not constrain the registration by coronary vessel regions were hampered by noise adjacent to the coronary arteries.

Next, a nonlinear level-set algorithm (*13*) was applied to the extracted coronary regions and constrained according to the expected coronary artery motion. Every volume of interest of the PET data from each bin was then registered to the end-diastolic reference artery region. The advantage of this method over other nonlinear registration techniques is the computational efficiency and knowledge-based estimation of the expected arterial motion. After the registration process, all registered volumes of interest were inserted back into their original PET image, using a linear gradient at the border between the registered volume of interest and the nonregistered original PET image to blend both volumes and ensure smooth transition between the regions. Finally, all registered PET images were summed into a single volume. In this manner, we obtained static 4- and 10-bin motion-corrected PET data.

TABLE 1
Patients' Demographic and Clinical Characteristics

Parameter	Stable angina ($n = 10$)	MI ($n = 7$)
Mean age ± SD (y)	67 ± 9	66 ± 7
Men (*n*)	9 (90%)	7 (100%)
Mean BMI ± SD (kg/m^2)	29 ± 5	28 ± 8
Agatston score		
Median	1,010	498
IQR	560–2,175	355–771
History (*n*)		
MI	4 (40%)	0
PCI	5 (50%)	1 (14%)
CABG	5 (50%)	0
Lesions (*n*)	31 (61%)	20 (39%)
Positive	19 (68%)	9 (32%)
Negative	12 (52%)	11 (48%)

BMI = body mass index; MI = myocardial infarction; PCI = percutaneous coronary intervention; CABG = coronary artery bypass graft.

Lesion and TBR

To define the lesions, the PET data were fused with the CCTA data and analyzed on an OsiriX workstation (OsiriX Imaging Software) by experienced observers masked to the clinical diagnosis. Two-dimensional regions of interest were drawn around all major (diameter > 2 mm) epicardial vessels on 3-mm axial slices just beyond the discernible adventitial border. We used a previously established 95% lower reference limit to categorize coronary plaques into ^{18}F-NaF–positive and –negative lesions, on the end-diastolic data as in the original study. Focal uptake with a target-to-background ratio (TBR) more than 25% higher than a proximal reference lesion were categorized as ^{18}F-NaF–positive plaques, whereas plaques were considered ^{18}F-NaF–negative if these criteria were not achieved. This limit was based on our previous study, in which plaques with high ^{18}F-NaF uptake had maximum TBRs that were 44% (95% confidence interval, 26–62) higher than a proximal quiescent reference lesion (*3*).

Downloaded from jnm.snmjournals.org by on September 15, 2016. For personal use only.

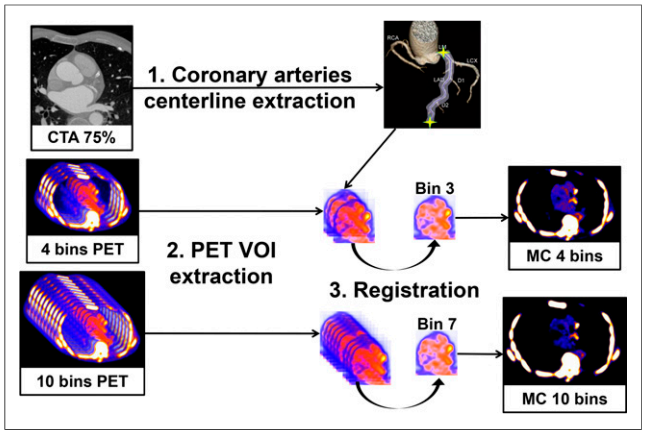

FIGURE 1. Overview of the motion correction method. (1) Coronary artery centerlines are extracted from CCTA in end-diastolic phase using CCTA analysis software. (2) Volumes of interest surrounding coronary arteries are extracted from 4- and 10-bin PET data using previously extracted CCTA centerlines. (3) All bins of data are registered to the common end-diastolic reference bin (bins 3 and 7 for 4- and 10-bin data, respectively) by nonlinear level-set registration restricted to coronary regions. Then, registered VOIs are inserted back into their original PET volumes, and all registered PET images are summed into a single volume to obtain motion-corrected 4- and 10-bin data. MC = motion-corrected; VOI = volume of interest.

TBR was defined as the ratio of the maximum activity values in the manually defined lesion to the mean value of the background, taken to be the blood pool in the middle of the left ventricle. This region was positioned to include the whole blood pool region in a midventricular slice for each patient. The noise was determined as the ratio of the mean to the SD of the background.

Statistical Analysis

Statistical analyses were performed with Analyze-it software. For all continuous variables, the Shapiro–Wilk test was used to assess normality. All continuous variables were described as mean ± SD or median and interquartile range (IQR). Nonparametric results were presented as median and IQR and compared using the Wilcoxon signed-rank test as appropriate. A 2-sided P value of less than 0.05 was taken as statistically significant.

RESULTS

Patients were predominantly middle-aged men and had multiple cardiovascular risk factors (Table 1). Radiation exposure for CCTA and PET is summarized in Table 2. The algorithm successfully registered the gated data for all studies, as assessed visually in the cinematic display. The approximate processing time was about 1 min/study. The results were computed and compared for the 4 sets of reconstructed data: 1 single PET bin corresponding to the end-diastolic phase, as presented in the initial trial (*2*); 4 and 10 bins that were motion-corrected as described above; and ungated data. In total, 51 lesions (28 positive, 23 negative) were delineated in the 17 patients. These lesions were distributed over the major coronary arteries: 17 (33%) in the left anterior descending coronary artery, 21 (41%) in the right coronary artery, and 13 (26%) in the left circumflex coronary artery. The TBR in positive and negative lesions was measured in the 4 sets of data.

Activity

^{18}F-NaF activity (expressed as TBR) in the positive lesions with 10-bin motion-corrected data was 11% higher than with 1-bin data (1.98 [IQR, 1.70–2.37] vs. 1.78 [IQR, 1.58–2.16], $P = 0.0027$) and 33% higher than with ungated data (1.98 [IQR, 1.70–2.37] vs. 1.49 [IQR, 1.39–1.88], $P < 0.0001$). In contrast, no difference was observed when comparing 1- to 4-bin motion-corrected data (1.78 [IQR, 1.58–2.16] vs. 1.75 [IQR, 1.50–2.16], $P = 0.77$) (Fig. 2A).

In ^{18}F-NaF–negative lesions, we observed some differences between 1- and 4-bin motion-corrected data (0.90 [IQR, 0.70–1.05] vs. 0.91 [IQR, 0.76–1.09], $P = 0.006$) as well as between 1- and 10-bin motion-corrected data (0.90 [IQR, 0.70–1.05] vs. 0.93 [IQR, 0.80–1.04], $P = 0.025$) (Fig. 2B), but these absolute differences were much smaller than for the ^{18}F-NaF–positive lesions. Furthermore, the median TBRs in the ^{18}F-NaF–negative lesions were less than 1.0 for all techniques.

Overall, the median TBR difference between ^{18}F-NaF–positive and –negative lesions increased from 0.88 to 1.05 using the 10-bin motion-corrected data, as compared with 1 bin. This technique should therefore allow for better discrimination between positive and negative lesions, as compared with the single end-diastolic bin alone that was presented in the original trial (*2*).

Noise

Noise was significantly reduced by using the 4- or 10-bin motion correction method as compared with the single end-diastolic bin: 0.09 [IQR, 0.08–0.12] vs. 0.18 [IQR, 0.15–0.24], $P < 0.0001$ (Fig. 2C). This is an expected finding since only 25% of the PET counts were used in the 1-bin data. Noise was essentially the same for ungated data and motion-corrected 4- and 10-bin data since all the PET counts were used by these 3 techniques.

Example images illustrating the noise decrease and TBR improvement are shown in Figure 3.

TABLE 2
Patients' Radiation Exposure (mSv) During Study

Parameter	^{18}F-NaF	CCTA dose	AC CT dose	PET/CT + CCTA
Prospective				
Range	2.8–3.1	1.3–5.8	0.5–1.8	4.7–9.9
Mean ± SD	2.9 ± 0.1	3.4 ± 1.2	1.0 ± 0.4	7.3 ± 1.4
Retrospective				
Range	2.8–3.0	7.8–12.7	0.9–1.1	11.6–16.7
Mean ± SD	2.9 ± 0.1	9.7 ± 2.7	1.0 ± 0.1	13.6 ± 2.7

Conversion factors are 0.014 mSv/mGy·cm for CCTA and attenuation-corrected (AC) CT and 0.024 mSv/MBq for ^{18}F-NaF.

Downloaded from jnm.snmjournals.org by on September 15, 2016. For personal use only.

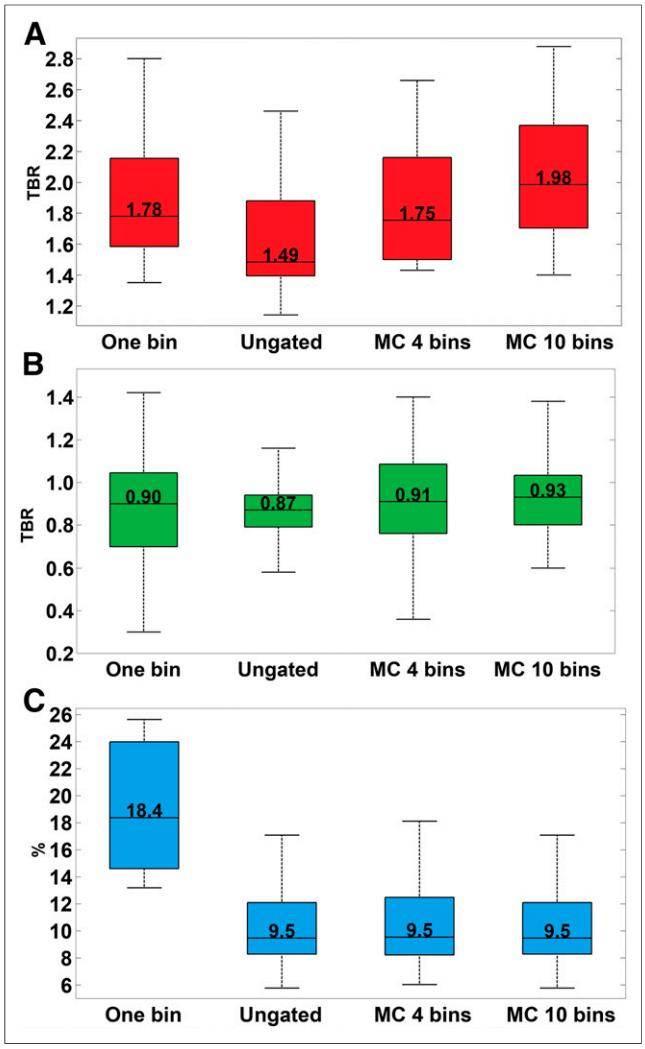

FIGURE 2. TBRs in positive (A) and negative (B) lesions and noise (C) are shown for different PET datasets (1-bin data, ungated data, motion-corrected data created from 4 bins, and motion-corrected data created from 10 bins). (A) TBR in positive lesions increases with motion correction for 10-bin data, as compared with 1-bin data and ungated data. (B) TBR in negative lesions remains below 1 using motion correction. (C) Noise is almost halved using motion correction, as compared with 1-bin data. MC = motion-corrected.

Motion

We also computed the maximal motion of plaques in the different coronary arteries that occurred during the motion correction process. The median end-systolic–to–end-diastolic displacement was 17.2 mm [IQR, 14.6–19.0 mm] in the left anterior descending coronary artery, 17.7 mm [IQR, 16.1–20.7 mm] in the left circumflex coronary artery, and 19.4 mm [IQR, 16.2–22 mm] in the right coronary artery. These results agree with the range of the coronary motion during the cardiac cycle that has been reported in the literature (*14*).

DISCUSSION

We have developed a method to correct coronary motion in ^{18}F-NaF PET imaging data by applying level-set–based nonlinear PET registration of individual PET time-bins to the end-diastolic position. This registration was constrained to the coronary regions extracted from the coregistered CCTA data to avoid registration to spurious noise signals outside the coronary regions. As compared with the original method (*2*), the new method demonstrated increased TBRs while drastically reducing noise (Fig. 3B). The best results were obtained for the 10-bin motion-corrected data since those data provided the best time-resolved motion correction.

Previous studies have addressed cardiac motion correction in PET and SPECT (*7,8*). Dual gating (cardiac/respiratory) (*15,16*) and dual correction have been reported by several groups (*5,6,17,18*). However, all of these methods depend on uptake in anatomic organs (in the case of cardiac imaging, the myocardium) and therefore are not applicable to coronary PET. ^{18}F-NaF PET represents a unique challenge because there are no clear anatomic references near the heart and because bone motion (where there is significant ^{18}F-NaF uptake) does not correlate with coronary motion. To our knowledge, this is the first report of motion-corrected coronary PET by the use of such nonlinear registration methods.

Our technical development study also has several important implications for the future of coronary ^{18}F-NaF PET imaging, which in its infancy has been hampered by cardiac motion, radiation exposure, and cost. The initial approach to motion was to discard all the PET counts when the heart was moving, resulting in high noise in the end-diastolic PET data. This might ultimately limit the accuracy and clinical utility of ^{18}F-NaF PET in distinguishing true uptake in culprit or high-risk sites from noise-related false-positives. The improved separation of positive from negative lesions and reduction of noise enabled by this motion correction method will likely enhance the capability of ^{18}F-NaF PET and lead to better detection of vulnerable plaques. Our technique retains the count statistics from the full PET acquisition and at the same time increases the TBR as compared with the original 1-bin method. This ultimately may facilitate reduced bed times (improving scan efficiency and reducing costs) or reduced tracer dose and radiation exposure.

In this study, CCTA scans were obtained in the original clinical protocol for the purposes of PET uptake localization and plaque characterization. We opted to use these scans as the anatomic framework for PET motion correction since the data were readily available. To our knowledge, all coronary PET studies (with ^{18}F-NaF or ^{18}F-FDG) to date have used contrast CCTA for localization of PET uptake (*2,19,20*). Registration methods that do not use CCTA could be explored in the future, such as with PET/MR systems. Alternatively, ^{18}F-NaF PET testing could be applied in patients who have already undergone anatomic testing with CCTA and present abnormal results with potentially vulnerable plaques. Under such circumstances, the prior CCTA could be reused (after coregistration to the PET scan or CT attenuation scan obtained with ^{18}F-NaF PET) to localize the ^{18}F-NaF PET uptake and guide motion correction without additional radiation or contrast exposure. Furthermore, we have used the method of Vemuri et al. (*13*) for nonlinear registration of the multiple bins of PET data in the selected coronary regions. This method is computationally efficient, which is important since multiple volume registrations are required for each patient. Other registration algorithms, such as the latest optical flow methods, may have additional benefits that warrant further exploration. Given our demonstration of the feasibility of a nonlinear motion correction method for improved coronary PET imaging, these other approaches and refinements warrant further prospective investigation and validation in future studies.

The incorporation of the CCTA anatomic framework as proposed here can also potentially lead to automation and reproducibility of quantitative analysis of PET uptake, allowing less experienced

Downloaded from jnm.snmjournals.org by on September 15, 2016. For personal use only.

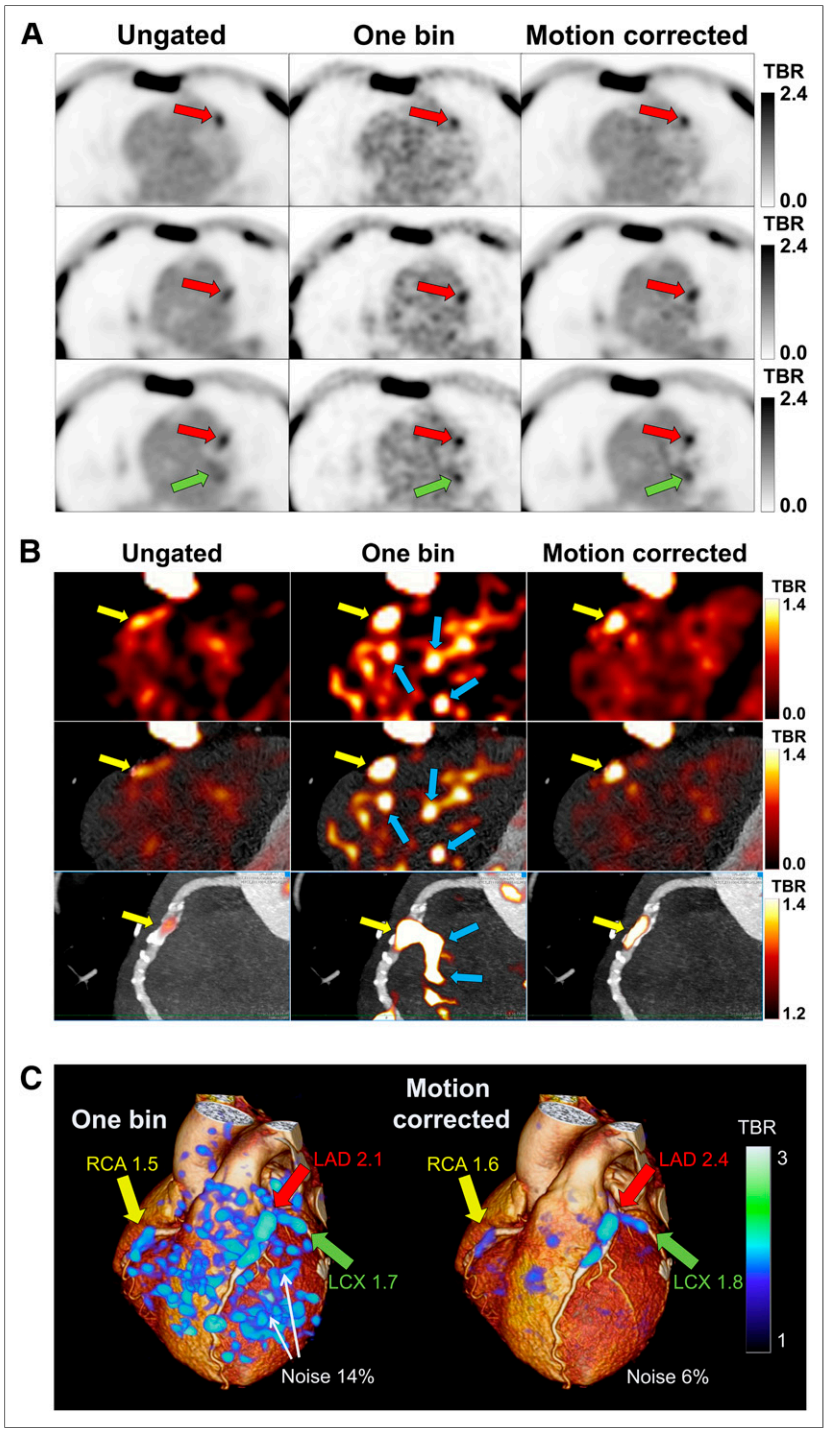

FIGURE 3. Noise decrease and TBR improvement in ^{18}F-NaF PET images of 65-y-old man. (A) On linear grayscale transaxial slices, ^{18}F-NaF plaque uptake is seen in left anterior descending (LAD) (red arrows) and left circumflex (LCX) (green arrows) coronary arteries. The images show blurred lesion signal in ungated images, significant noise in 1-bin images, and high lesion signal with reduced noise in motion-corrected images. (B) On PET (top), PET/CCTA (middle), and multiplanar-reformatted PET/CCTA (bottom) images with exponential color table and same window and level settings, vulnerable plaque is seen in right coronary artery (RCA) (yellow arrows). Low lesion signal is seen in ungated images, significant noise in 1-bin images (blue arrows), and high signal with less noise in motion-corrected images. (C) 3-dimensional rendering of 1-bin image (25% of PET counts) as in study of Joshi et al. (*2*) (left) and motion-corrected image (right) superimposed on rendered CCTA volume. Increased uptake is seen in RCA, LAD, and LCX coronary arteries in high-noise 1-bin image and remains clear in motion-corrected image.

centers to immediately implement this technique and fostering meaningful intercenter comparisons of the data. It is of key importance that this promising PET technique be allowed to reach its full potential by optimizing the image analysis techniques. The CCTA-guided motion correction technique proposed in this work will also be applicable to future PET tracers exploring pathologic processes in the coronary vasculature.

For patients with coronary heart disease, ^{18}F-NaF PET has several applications. First, it may help assess future risk and provide added value to the simple anatomic assessment from CCTA. This may help inform the intensity of medical therapy as well as plan potential coronary revascularization, especially for intermediate lesions or multivessel disease. It may also help determine risk in the context of noncardiac interventions, such as the planning of noncardiac surgery. Finally, it may provide a surrogate biomarker of plaque vulnerability against which novel therapeutic interventions can be assessed.

This study had several limitations. Although it clearly showed significant gains in image quality by the motion correction method applied to ^{18}F-NaF PET imaging, there is room for improvement. Indeed, we are likely to achieve further significant enhancements in TBR by incorporating respiratory and patient motion correction, as well as correction for partial-volume effects. We did not perform these additional corrections in our study because the dual gating and combined correction for these motions is complex. Potentially, PET and CCTA may be misregistered even if CCTA is acquired in end-expiration. Therefore, the CCTA coronary regions may not correspond exactly to the PET regions considered in the motion correction technique. Automatic correction for this alignment may result in further improvements, since our method relies on centerline extraction from the CCTA data, which defines 3-dimensional regions of interest in PET data. Nevertheless, the regions that we used encompassed an approximate coronary artery path neighborhood of 2 cm in diameter, which should allow for some CCTA–PET misregistration. We did not use standardized uptake values (SUVs) in this study, focusing instead on TBR. In our experience, SUV data result in greater variability than TBRs, although this may need to be reevaluated when partial-volume corrections are performed. We acknowledge that the study cohort was small, reflecting the novelty of coronary imaging by ^{18}F-NaF PET. Nevertheless, since there were multiple lesions in each patient, we were able to demonstrate the significant improvements afforded by our technique. We focused on improvement of image quality and discrimination of ^{18}F-NaF PET–positive lesions from ^{18}F-NaF PET–negative lesions, rather than on the clinical utility of coronary ^{18}F-NaF PET. An ongoing prospective

Downloaded from jnm.snmjournals.org by on September 15, 2016. For personal use only.

study (NCT02278211) aims to demonstrate the value of coronary ^{18}F-NaF PET in predicting future myocardial infarction (*21*). When this trial is completed, we plan to apply the techniques to demonstrate improved prediction of myocardial infarction.

CONCLUSION

Motion correction of gated ^{18}F-NaF PET/CT reduces noise and increases TBR as compared with 1-bin imaging and further improves TBR as compared with ungated images without a noise increase. This improvement may allow more reliable identification of vulnerable plaque lesions in the coronary arteries by ^{18}F-NaF PET.

DISCLOSURE

The costs of publication of this article were defrayed in part by the payment of page charges. Therefore, and solely to indicate this fact, this article is hereby marked "advertisement" in accordance with 18 USC section 1734. The study was funded by the Chief Scientist Office, Scotland (ETM/160). David Newby (CH/09/002) and Marc Dweck (FS/14/78) are supported by the British Heart Foundation. David Newby is the recipient of a Wellcome Trust Senior Investigator Award (WT103782AIA). The study was also supported in part by a grant (Cardiac Imaging Research Initiative) from the Adelson Medical Research Foundation at Cedars-Sinai. Piotr Slomka and Daniel Berman receive research grant support from Siemens Medical Systems. No other potential conflict of interest relevant to this article was reported.

REFERENCES

1. Mozaffarian D, Benjamin EJ, Go AS, et al. Heart disease and stroke statistics: 2015 update—a report from the American Heart Association. *Circulation.* 2015; 131:e29–e322.
2. Joshi NV, Vesey AT, Williams MC, et al. ^{18}F-fluoride positron emission tomography for identification of ruptured and high-risk coronary atherosclerotic plaques: a prospective clinical trial. *Lancet.* 2014;383:705–713.
3. Dweck MR, Chow MW, Joshi NV, et al. Coronary arterial ^{18}F-sodium fluoride uptake: a novel marker of plaque biology. *J Am Coll Cardiol.* 2012;59:1539–1548.
4. Irkle A, Vesey A, Lewis D, et al. Identifying active vascular microcalcification by ^{18}F-sodium fluoride positron emission tomography. *Nat Commun.* 2015;6:7495.
5. Gigengack F, Ruthotto L, Burger M, Wolters CH, Jiang X, Schafers KP. Motion correction in dual gated cardiac PET using mass-preserving image registration. *IEEE Trans Med Imaging.* 2012;31:698–712.
6. Lamare F, Le Maitre A, Dawood M, et al. Evaluation of respiratory and cardiac motion correction schemes in dual gated PET/CT cardiac imaging. *Med Phys.* 2014;41:072504.
7. Slomka PJ, Nishina H, Berman DS, et al. "Motion-frozen" display and quantification of myocardial perfusion. *J Nucl Med.* 2004;45:1128–1134.
8. Le Meunier L, Slomka PJ, Dey D, et al. Motion frozen ^{18}F-FDG cardiac PET. *J Nucl Cardiol.* 2011;18:259–266.
9. Lesage D, Angelini ED, Bloch I, Funka-Lea G. Bayesian maximal paths for coronary artery segmentation from 3D CT angiograms. *Med Image Comput Comput Assist Interv.* 2009;12:222–229.
10. Schuhbaeck A, Dey D, Otaki Y, et al. Interscan reproducibility of quantitative coronary plaque volume and composition from CT coronary angiography using an automated method. *Eur Radiol.* 2014;24:2300–2308.
11. Dey D, Achenbach S, Schuhbaeck A, et al. Comparison of quantitative atherosclerotic plaque burden from coronary CT angiography in patients with first acute coronary syndrome and stable coronary artery disease. *J Cardiovasc Comput Tomogr.* 2014;8:368–374.
12. Diaz-Zamudio M, Dey D, Schuhbaeck A, et al. Automated quantitative plaque burden from coronary CT angiography noninvasively predicts hemodynamic significance by using fractional flow reserve in intermediate coronary lesions. *Radiology.* 2015;276:408–415.
13. Vemuri BC, Ye J, Chen Y, Leonard CM. Image registration via level-set motion: applications to atlas-based segmentation. *Med Image Anal.* 2003;7: 1–20.
14. Shechter G, Resar JR, McVeigh ER. Displacement and velocity of the coronary arteries: cardiac and respiratory motion. *IEEE Trans Med Imaging.* 2006;25:369–375.
15. Martinez-Möller A, Souvatzoglou M, Navab N, Schwaiger M, Nekolla SG. Artifacts from misaligned CT in cardiac perfusion PET/CT studies: frequency, effects, and potential solutions. *J Nucl Med.* 2007;48:188–193.
16. Koivumäki T, Nekolla SG, Furst S, et al. An integrated bioimpedance–ECG gating technique for respiratory and cardiac motion compensation in cardiac PET. *Phys Med Biol.* 2014;59:6373–6385.
17. Hong I, Jones J, Casey M. Elastic motion correction for cardiac PET studies. Presented at: Nuclear Science Symposium and Medical Imaging Conference; Seoul, Korea; 2013.
18. Slomka PJ, Rubeaux M, Le Meunier L, et al. Dual-gated motion-frozen cardiac PET with flurpiridaz F18. *J Nucl Med.* September 24, 2015 [Epub ahead of print].
19. Cheng VY, Slomka PJ, Le Meunier L, et al. Coronary arterial ^{18}F-FDG uptake by fusion of PET and coronary CT angiography at sites of percutaneous stenting for acute myocardial infarction and stable coronary artery disease. *J Nucl Med.* 2012;53:575–583.
20. Rogers IS, Nasir K, Figueroa AL, et al. Feasibility of FDG imaging of the coronary arteries: comparison between acute coronary syndrome and stable angina. *JACC Cardiovasc Imaging.* 2010;3:388–397.
21. Newby DE, Dweck M. Prediction of recurrent events with ^{18}F-fluoride (PREFFIR). ClinicalTrial.gov website. https://clinicaltrials.gov/ct2/show/NCT02278211. Received October 14, 2014. Updated May 26, 2015. Accessed October 21, 2015.

^{18}F-fluoride positron emission tomography for identification of ruptured and high-risk coronary atherosclerotic plaques: a prospective clinical trial

Nikhil V Joshi, Alex T Vesey, Michelle C Williams, Anoop S V Shah, Patrick A Calvert, Felicity H M Craighead, Su Ern Yeoh, William Wallace, Donald Salter, Alison M Fletcher, Edwin J R van Beek, Andrew D Flapan, Neal G Uren, Miles W H Behan, Nicholas L M Cruden, Nicholas L Mills, Keith A A Fox, James H F Rudd, Marc R Dweck, David E Newby**

Summary

Background **The use of non-invasive imaging to identify ruptured or high-risk coronary atherosclerotic plaques would represent a major clinical advance for prevention and treatment of coronary artery disease. We used combined PET and CT to identify ruptured and high-risk atherosclerotic plaques using the radioactive tracers ^{18}F-sodium fluoride (^{18}F-NaF) and ^{18}F-fluorodeoxyglucose (^{18}F-FDG).**

Methods **In this prospective clinical trial, patients with myocardial infarction (n=40) and stable angina (n=40) underwent ^{18}F-NaF and ^{18}F-FDG PET-CT, and invasive coronary angiography. ^{18}F-NaF uptake was compared with histology in carotid endarterectomy specimens from patients with symptomatic carotid disease, and with intravascular ultrasound in patients with stable angina. The primary endpoint was the comparison of ^{18}F-fluoride tissue-to-background ratios of culprit and non-culprit coronary plaques of patients with acute myocardial infarction.**

Findings **In 37 (93%) patients with myocardial infarction, the highest coronary ^{18}F-NaF uptake was seen in the culprit plaque (median maximum tissue-to-background ratio: culprit 1·66 [IQR 1·40–2·25] *vs* highest non-culprit 1·24 [1·06–1·38], p<0·0001). By contrast, coronary ^{18}F-FDG uptake was commonly obscured by myocardial uptake and where discernible, there were no differences between culprit and non-culprit plaques (1·71 [1·40–2·13] *vs* 1·58 [1·28–2·01], p=0·34). Marked ^{18}F-NaF uptake occurred at the site of all carotid plaque ruptures and was associated with histological evidence of active calcification, macrophage infiltration, apoptosis, and necrosis. 18 (45%) patients with stable angina had plaques with focal ^{18}F-NaF uptake (maximum tissue-to-background ratio 1·90 [IQR 1·61–2·17]) that were associated with more high-risk features on intravascular ultrasound than those without uptake: positive remodelling (remodelling index 1·12 [1·09–1·19] *vs* 1·01 [0·94–1·06]; p=0·0004), microcalcification (73% *vs* 21%, p=0·002), and necrotic core (25% [21–29] *vs* 18% [14–22], p=0·001).**

Interpretation **^{18}F-NaF PET-CT is the first non-invasive imaging method to identify and localise ruptured and high-risk coronary plaque. Future studies are needed to establish whether this method can improve the management and treatment of patients with coronary artery disease.**

Funding **Chief Scientist Office Scotland and British Heart Foundation.**

Introduction

Coronary atherosclerotic plaque rupture is the principal precipitant of acute myocardial infarction and an important cause of sudden cardiac death. Rupture is challenging to predict because most plaques are non-obstructive and are not identified by stress testing or coronary angiography.[1,2] Atherosclerotic lesions at risk of rupture have certain histopathological characteristics that include positive remodelling, microcalcification, and a large necrotic core.[1–3] The development of modern molecular imaging techniques targeted at these features could lead to the identification of such high-risk plaques in vivo and guide the development of novel treatment strategies.[4–7]

Combined PET and CT is a non-invasive imaging technique that brings functional molecular imaging together with precise anatomical information. We have recently reported preliminary PET-CT data using the tracer ^{18}F-sodium fluoride (^{18}F-NaF) as a marker of valvular and vascular calcification activity in patients with aortic stenosis.[7–9] Other studies have shown the usefulness of ^{18}F-flurodeoxyglucose (^{18}F-FDG) as a surrogate of vascular inflammation and macrophage burden.[6,10–13] We therefore investigated whether, compared with the current non-invasive gold standard of ^{18}F-FDG, ^{18}F-NaF uptake could identify ruptured and high-risk atherosclerotic plaques in patients with symptomatic coronary and carotid artery disease.

Methods

Patients

Patients were recruited from the Royal Infirmary of Edinburgh between February, 2012, and January, 2013, in three cohorts: 40 patients with acute ST-segment or non-ST-segment elevation myocardial infarction,[14] 40 patients with stable angina pectoris undergoing elective invasive coronary angiography, and 12 patients (nine evaluable)

Published **Online** November 11, 2013 http://dx.doi.org/10.1016/S0140-6736(13)61754-7

See **Online/Comment** http://dx.doi.org/10.1016/S0140-6736(13)61911-X

Copyright © Joshi et al. Open Access article distributed under the terms of CC BY

*These authors contributed equally

Centre for Cardiovascular Science, Clinical Research Imaging Centre, and Division of Pathology, University of Edinburgh, Edinburgh, UK (N V Joshi MD, A T Vesey MD, M C Williams MD, A S V Shah MD, F H M Craighead BSc, S E Yeoh, W Wallace MD, D Salter MD, A M Fletcher PhD, E J R van Beek PhD, N L Mills PhD, Prof K A A Fox MD, M R Dweck PhD, Prof D E Newby DSc)**; Edinburgh Heart Centre, Royal Infirmary of Edinburgh, Edinburgh, UK** (A D Flapan MD, N G Uren MD, M W H Behan MD, N L M Cruden PhD)**; and Division of Cardiovascular Medicine, University of Cambridge, Cambridge, UK** (P A Calvert PhD, J H F Rudd PhD)

Correspondence to:
Dr Nikhil Vilas Joshi, SU 305, Chancellors Building, University/BHF Centre for Cardiovascular Science, Little France Crescent, Edinburgh, UK
nikhil.joshi@ed.ac.uk

undergoing carotid endartectomy for symptomatic carotid artery disease.[15]

Exclusion criteria were age younger than 50 years, insulin-dependent diabetes mellitus, women of childbearing age not receiving contraception, severe renal failure (serum creatinine >250 μmol/L), known contrast allergy, and inability to provide informed consent. Only patients older than 50 years were recruited in the study to reduce any long-term risks associated with radiation exposure. Uncontrolled diabetes and high blood glucose concentrations (>11 mmol/L) interfere with the quality of ^{18}F-FDG PET imaging because of the competition between glucose and ^{18}F-FDG for cellular entry. The convention is therefore to exclude such patients from vascular ^{18}F-FDG PET studies.[7,10,12,13]

All patients underwent a comprehensive baseline clinical assessment including evaluation of their cardiovascular risk factor profile. Plasma troponin I concentrations were measured in patients with stable angina using the ARCHITECT STAT high-sensitivity troponin I assay (Abbott Laboratories, Abbott Park, IL, USA; lower limit of detection 1·2 ng/L; 99th percentile diagnostic threshold 26 ng/L). Studies were done with the approval of the local research ethics committee, in accordance with the Declaration of Helsinki, and with the written informed consent of each participant.

Procedures

Patients with myocardial infarction and stable angina underwent ^{18}F-NaF and ^{18}F-FDG PET-CT, CT coronary angiography, and CT calcium scoring (appendix).[7] To minimise myocardial uptake, patients were instructed to adhere to a low-carbohydrate, high-protein, and high-fat diet for at least 24 h before undergoing ^{18}F-FDG PET-CT.

See Online for appendix

Electrocardiograph-gated PET images were reconstructed in diastole (50–75% of the R-R interval, Ultra-HD) using the Siemens Ultra-HD algorithm, fused with the CT coronary angiogram, and analysed by experienced observers blinded to the clinical diagnosis (NJ, MD, FC) using an OsiriX workstation (OsiriX version 5·5·1 64-bit; OsiriX Imaging Software, Geneva, Switzerland). Two-dimensional regions of interest were drawn around all major (diameter >2 mm) epicardial vessels on 3 mm axial slices just beyond the discernible adventitial border. The maximum standard uptake value (the decay corrected tissue concentration of the tracer divided by the injected dose per bodyweight) was measured and corrected for blood pool activity in the superior vena cava to provide tissue-to-background ratio (TBRs) measurements. Using this method, we have previously shown excellent reproducibility for ^{18}F-NaF TBR measurements in the coronary arteries with an intraclass correlation coefficient of 0·99.[7]

We used a previously established 95% lower reference limit to categorise coronary plaques into ^{18}F-NaF positive lesions (focal uptake with a TBR more than 25% higher than a proximal reference lesion) and negative plaques if these criteria were not achieved. This limit was based on our previous study, where plaques with high ^{18}F-NaF uptake had maximum TBRs that were 44% (95% CI 26–62) higher than a proximal quiescent reference lesion.[7] In patients with acute myocardial infarction, ^{18}F-NaF uptake in the culprit plaque was compared with the highest value in any of the non-culprit vessels.

Quantification of ^{18}F-FDG uptake was performed as for ^{18}F-NaF uptake but restricted to the proximal and mid-portions of the coronary arteries, and to regions where myocardial uptake and spillover could be confidently excluded.[7] Again, ^{18}F-FDG positive plaques were defined using the 25% threshold as described for ^{18}F-NaF. Effective myocardial suppression of ^{18}F-FDG was predefined as a standard uptake value of 5·0 or less in the basal ventricular septum (appendix) as per published data.[12]

In patients with stable angina, PET-CT imaging was prospectively used to direct greyscale and radiofrequency intravascular ultrasound (20 MHz Eagle Eye Platinum Catheters [Volcano Corp, San Diago, CA, USA], motorised pull-back 0·5 mm/s) to the ^{18}F-NaF positive and negative plaques. The interventional cardiologist acquiring the intravascular ultrasound data was blinded to the PET-CT status of the plaque.

Intravascular ultrasound analysis was done as described previously[16] using dedicated VIAS software (Volcano Image Analysis Software version 3.0) by operators blinded to the PET data. Regions of interest were drawn around the external elastic membrane and luminal borders, and plaque area and composition (dense calcium, necrotic core, fibro-fatty tissue, and fibrous tissue) calculated.[16–18] The presence of microcalcification (spotty calcification in the absence of acoustic shadowing on three or more consecutive frames) and the maximum frame necrotic core (the highest percentage of necrotic core on a single frame) were recorded.[19] The remodelling index was defined as the ratio between the external elastic membrane cross-sectional area of the lesion and a proximal reference region in the same vessel.[20] Plaques were classified as thin-cap fibroatheroma, thick-cap fibroatheroma, pathological intimal thickening, or fibrocalcific plaque as defined previously.[18,21]

CT analysis was done on a dedicated cardiovascular workstation (Vital Images, Minnetonka, MN, USA). Vessel-specific and total Agatston calcium scores were calculated as described previously.[7] An independent experienced and blinded observer (MW) determined the stenosis severity, plaque composition (calcified, non-calcified, mixed plaque), and presence of high-risk CT features (positive remodelling, microcalcification, necrotic core) according to standard definitions in plaques with and without increased ^{18}F-NaF activity.[22]

Intact atherosclerotic plaques were retrieved at the time of carotid endarterectomy and scanned using ex-vivo PET-CT to allow precise anatomical colocalisation of ^{18}F-NaF activity with pathological evidence of plaque rupture. Plaques were divided into ^{18}F-NaF positive and negative areas, and histological sections were assessed

using Movat's pentachrome and immunohistochemistry to investigate calcification activity (tissue non-specific alkaline phosphatase and osteocalcin), macrophage infiltration (CD68), and cell death (apoptosis, cleaved caspase 3; presence of necrotic core; appendix).

Statistical analysis

The primary endpoint of the study was the comparison of ^{18}F-fluoride tissue-to-background ratios of culprit and non-culprit coronary plaques of patients with acute myocardial infarction. The main secondary endpoints were comparative imaging and histological characterisation of ^{18}F-fluoride positive and negative atherosclerotic plaques in patients with coronary and carotid artery disease. Based on our previous data,[7] we required 36 patients with myocardial infarction to detect a difference of 0·23 in the tissue-to-background ratio between culprit and non-culprit plaques at 90% power and two-sided p<0·05. We recruited 40 patients to account for incomplete data and recruited a similar sized (n=40) comparator group of patients with stable angina.

Continuous data were tested for normality with the D'Agostino-Pearson omnibus test. Continuous parametric variables were expressed as mean (SD) and

	Myocardial infarction			Stable angina All (n=40)
	All (n=40)	STEMI (n=26)	NSTEMI (n=14)	
Age in years, mean (SD)	62 (8)	63 (9)	60 (8)	67 (8)
Men, n (%)	37 (93%)	24 (92%)	13 (93%)	36 (90%)
Body-mass index (kg/m^2), mean (SD)	28 (5)	27 (5)	30 (4)	30 (5)
Antecedent angina (active), n (%)	9 (23%)	5 (19%)	4 (29%)	40 (100%)
Heart rate (per min), mean (SD)*	56 (7)	56 (7)	56 (7)	59 (9)
Systolic blood pressure (mm Hg), mean (SD)	132 (21)	131 (20)	121 (21)	134 (14)
Diastolic blood pressure (mm Hg), mean (SD)	76 (9)	76 (9)	76 (8)	77 (10)
Cardiovascular history, n (%)				
Previous MI	5 (13%)	1 (4%)	4 (29%)	15 (38%)
Previous CVA/TIA	2 (5%)	1 (4%)	1 (7%)	4 (10%)
Previous PCI	5 (13%)	2 (8%)	3 (21%)	19 (48%)
Previous CABG	2 (5%)	2 (8%)	0	11 (28%)
Risk factors, n (%)				
Smoking habit (ex or current)	25 (63%)	19 (73%)	6 (43%)	24 (60%)
Non-insulin dependent diabetes	8 (20%)	7 (27%)	1 (7%)	13 (33%)
Hypertension	17 (43%)	11 (42%)	6 (43%)	36 (90%)
Hypercholesterolaemia	19 (48%)	11 (42%)	8 (57%)	39 (98%)
Medications, n (%)†				
Aspirin	40 (100%)	26 (100%)	14 (100%)	33 (83%)
Clopidogrel	39 (98%)	25 (96%)	14 (100%)	5 (13%)
Statin	39 (98%)	26 (100%)	13 (93%)	36 (90%)
β blocker	32 (80%)	20 (77%)	12 (86%)	28 (70%)
ACEI/ARB	35 (88%)	25 (96%)	10 (71%)	20 (50%)
Calcium channel blockers	2 (5%)	2 (8%)	0	16 (40%)
Other anti-hypertensive	3 (8%)	1 (4%)	2 (14%)	6 (15%)
Oral nitrates	1 (3%)	0	1 (7%)	15 (38%)
Serum biochemistry, mean (SD)				
Cholesterol (mmol/L)	4·7 (1·2)	4·7 (1·3)	4·8 (1·1)	3·9 (0·8)
HDL cholesterol (mmol/L)	1·1 (0·3)	1·1 (0·3)	1·0 (0·3)	1·1 (0·3)
LDL cholesterol (mmol/L)	2·9 (1·1)	2·8 (1·1)	3·1 (1·0)	2·1 (0·7)
Triglycerides (mmol/L)	1·6 (0·8)	1·7 (0·7)	1·5 (0·7)	1·6 (0·7)
Creatinine (μmol/L)	84 (27)	86 (29)	82 (24)	85 (23)
Coronary artery calcium score (Agatston units), median (IQR)	159 (42–456)	176 (45–474)	122 (26–442)	599 (60–1302)
Peak troponin concentration (ng/L), median (IQR)	32 300 (10 200–50 000)	11 200 (3300–50 000)	3800 (1000–9200)	

NSTEMI=non-ST elevation myocardial infarction. MI=myocardial infarction. CVA=cerebrovascular accident. TIA=transient ischaemic attack. PCI=percutaneous coronary intervention. ACEI=angiotensin converting enzyme inhibitor. ARB=angiotensin receptor blocker. CABG=coronary artery bypass graft. HDL=high-density lipoprotein. LDL=low-density lipoprotein. STEMI=ST-elevation myocardial infarction. *Heart rate at the time of CT coronary angiography. †Medications at the time of scan.

Table 1: **Baseline characteristics of patients with coronary artery disease**

compared using Student's *t* tests. Non-parametric data were presented as median (IQR) and compared using Mann-Whitney *U* test or Wilcoxon signed-rank test as appropriate. Fisher's exact test or chi-squared test was used for analysis of categorical variables. Statistical analysis was done with Graph Pad Prism version 5 (GraphPad Software, La Jolla, CA, USA). A two-sided p<0·05 was taken as statistically significant.

The study was registered with ClinicalTrials.gov number NCT01749254.

Role of the funding source

The funding source had no role in the study design (except through its external peer review process), data collection, data analysis, data interpretation, or writing of the report. All authors had access to the primary data and have final responsibility to submit for publication.

Results

Patients were predominantly middle-aged men and had multiple cardiovascular risk factors (table 1). They underwent both ^{18}F-NaF (60 [SD 9] min after 123 [SD 5] MBq) and ^{18}F-FDG (90 [7] min after 192 [11] MBq) PET-CT scanning within a median of 6 (IQR 3–9) days. The median duration between PET-CT scanning and coronary angiography was 7 (IQR 1–12) days. The total effective radiation dose from study participation was 13·7 (SD 3·0) mSv (conversion factor of 0·014 mSv/mGy.cm): ^{18}F-NaF (3·8 [SD 0·3] mSv) and ^{18}F-FDG (4·9 [0·5] mSv) PET-CT, CT coronary angiogram (3·7 [2·1] mSv), and calcium score (1·3 [0·5] mSv).

The culprit vessel was the left anterior descending artery in 17 (42%) patients, the left circumflex artery in seven (18%), and the right coronary artery in 16 (40%). Patients underwent ^{18}F-NaF scans 6 [IQR 3–10] days after hospitalisation for myocardial infarction (symptoms to ^{18}F-NaF scan, 8 [3–10] days). ^{18}F-NaF activity in the culprit plaque was 34% higher than the maximum activity recorded anywhere else in the coronary vasculature (maximum TBR 1·66 [1·40–2·25] *vs* 1·24 [1·06–1·38], p<0·0001; figures 1 and 2). In 37 of the 40 patients (93%), increased ^{18}F-NaF uptake was seen in the culprit plaque (figure 1; appendix). In the three patients without uptake, two were younger smokers (aged 50 and 52 years) and, in the third, the culprit lesion was adjudicated as the right coronary artery although focal increased activity was seen in the left circumflex artery. In five patients, increased ^{18}F-NaF activity was seen at multiple sites within the coronary circulation.

Predefined myocardial suppression of ^{18}F-FDG uptake was achieved in 28 (70%) patients (median myocardial standard uptake value 3·92 [IQR 2·71–5·55]). However, coronary ^{18}F-FDG uptake could not be distinguished from patchy myocardial uptake in 22 patients affecting 52% of vessel territories. Increased uptake of ^{18}F-FDG was observed in the culprit vessels of six (33%) of the remaining 18 patients. Overall, no significant differences could be shown between the maximum TBRs in the culprit plaques and those recorded elsewhere in the coronary vasculature (1·71 [IQR 1·40–2·13] *vs* 1·58 [1·28–2·01], p=0·34: figure 2) with a mean difference of 0·09 (95% CI –0·07 to 0·24).

The median duration between clinical symptoms and carotid endarterectomy was 17 [IQR 10–27] days (appendix). Carotid endarterectomy specimens (figure 3; appendix) were obtained for 12 patients, although three specimens could not be excised intact and were discarded. Ex-vivo ^{18}F-NaF PET-CT was undertaken in nine specimens and uptake was localised to the site of macroscopic plaque rupture in all patients (figure 3). Compared with sections of tissue without uptake (n=15), those with increased ^{18}F-NaF uptake (n=24) had increased calcification activity (tissue non-specific alkaline phosphatase 4·07% [SD 3·42] *vs* 0·76% [0·51], p<0·0001; osteocalcin 1·88% [IQR 0·58–4·10] *vs* 0·25% [0·11–0·58], p<0·0001), macrophage infiltration (CD68, 350 [IQR 172–840] *vs* 145 [24–362] cells/mm², p=0·013), and cell death (apoptosis, cleaved-caspase-3, 1·23% [0·69–1·91] *vs* 0·09% [0·04–1·38], p=0·005; necrotic core, 22/24 *vs* 4/15; p<0·0001; appendix).

Patients with stable angina were older (67 [SD 8] *vs* 62 [8] years, p=0·006) and had more severe coronary artery disease (coronary artery calcium score 599 [IQR 60–1302] *vs* 159 [42–456] Agatston units, p=0·006) than those with myocardial infarction (table 1). Focal ^{18}F-NaF uptake was noted in 18 patients (45%), which did not seem to be related to percutaneous coronary intervention and stent

Figure 1: **Focal ^{18}F-fluoride and ^{18}F-fluorodeoxyglucose uptake in patients with myocardial infarction and stable angina**

Patient with acute ST-segment elevation myocardial infarction with (A) proximal occlusion (red arrow) of the left anterior descending artery on invasive coronary angiography and (B) intense focal ^{18}F-fluoride (^{18}F-NaF, tissue-to-background ratios, culprit 2·27 versus reference segment 1·09 [108% increase]) uptake (yellow-red) at the site of the culprit plaque (red arrow) on the combined positron emission and computed tomogram (PET-CT). Corresponding ^{18}F-fluorodeoxyglucose PET-CT image (C) showing no uptake at the site of the culprit plaque (^{18}F-FDG, tissue-to-background ratios, 1·63 versus reference segment 1·91 [15% decrease]). Note the significant myocardial uptake overlapping with the coronary artery (yellow arrow) and uptake within the oesophagus (blue arrow). Patient with anterior non-ST-segment elevation myocardial infarction with (D) culprit (red arrow; left anterior descending artery) and bystander non-culprit (white arrow; circumflex artery) lesions on invasive coronary angiography that were both stented during the index admission. Only the culprit lesion had increased ^{18}F-NaF uptake (^{18}F-NaF, tissue-to-background ratios, culprit 2·03 versus reference segment 1·08 [88% increase]) on PET-CT (E) after percutaneous coronary intervention. Corresponding ^{18}F-fluorodeoxyglucose PET-CT showing no uptake either at the culprit (^{18}F-FDG, tissue-to-background ratios, culprit 1·62 versus reference segment 1·49 [9% increase]) or the bystander stented lesion. Note intense uptake within the ascending aorta. In a patient with stable angina with previous coronary artery bypass grafting, invasive coronary angiography (G) showed non-obstructive disease in the right coronary artery. Corresponding PET-CT scan (H) showed a region of increased ^{18}F-NaF activity (positive lesion, red line) in the mid-right coronary artery (tissue-to-background ratio, 3·13) and a region without increased uptake in the proximal vessel (negative lesion, yellow line). Radiofrequency intravascular ultrasound shows that the ^{18}F-NaF negative plaque (I) is principally composed of fibrous and fibrofatty tissue (green) with confluent calcium (white with acoustic shadow) but little evidence of necrosis. On the contrary, the ^{18}F-NaF positive plaque (J) shows high-risk features such as a large necrotic core (red) and microcalcification (white).

deployment (appendix). The maximum TBR for ^{18}F-NaF positive plaques was 1·90 [IQR 1·61–2·17] and for ^{18}F-NaF negative plaques was 1·02 [0·82–1·17]. ^{18}F-NaF positive plaques were predominantly (72% of patients) non-obstructive (<70% luminal stenosis) on coronary angiography and showed multiple high-risk features on radiofrequency intravascular ultrasound (positive remodelling [remodelling index 1·12 [IQR 1·09–1·19] *vs*

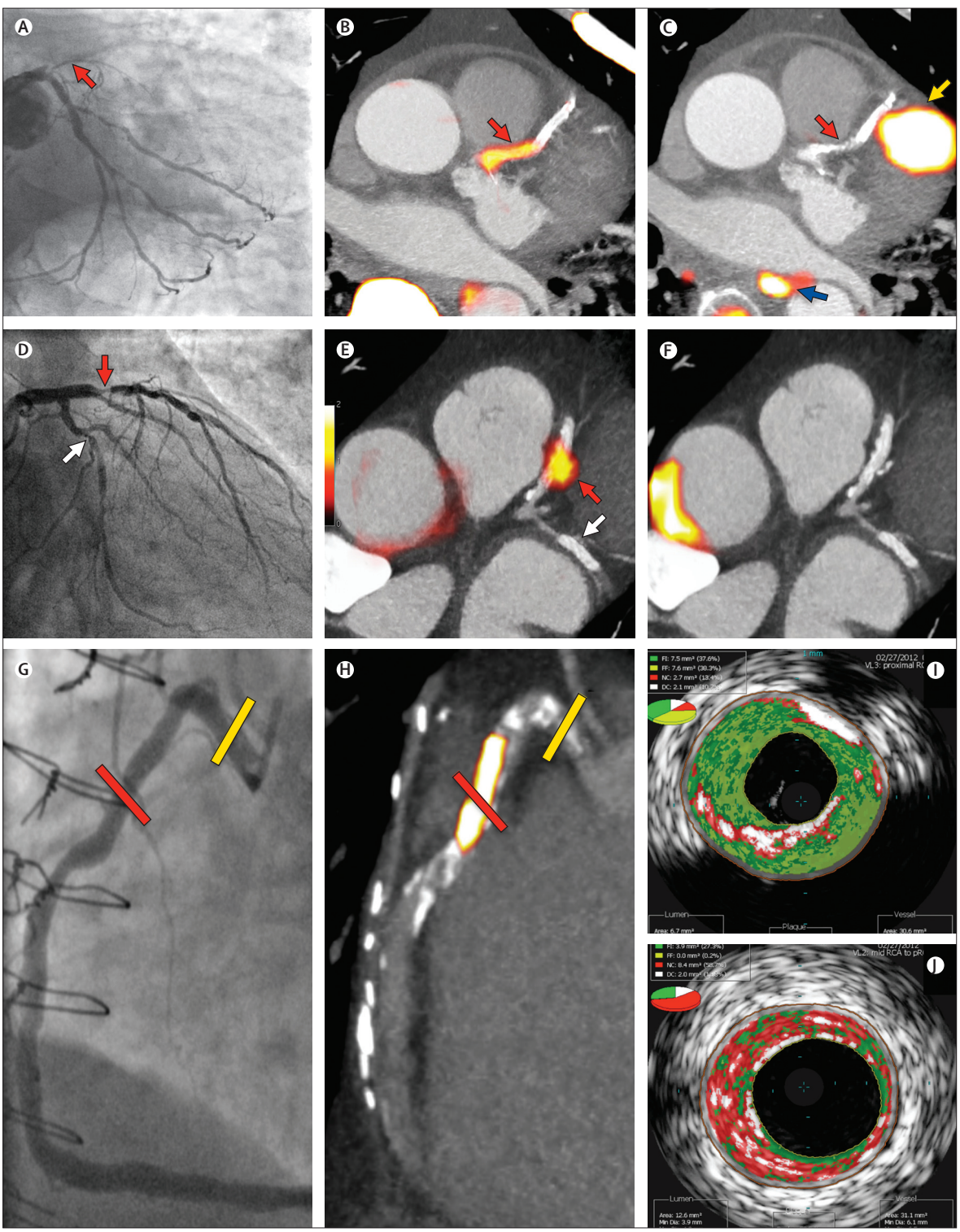

1·01 [0·94–1·06]; p<0·001, microcalcification (73 *vs* 21%, p=0·002) and necrotic core (24·6% [20·5–28·8] *vs* 18·0% [14·0–22·4]), p=0·001), with similar observations for CT (figure 1, table 2; appendix). Multivessel uptake was commonly seen: two-vessel uptake in six (15%) and three-vessel uptake in five (13%) patients. Patients with ^{18}F-NaF positive lesions had higher concentrations of plasma troponin at baseline (3·35 [IQR 2·35–10·20] *vs* 2·45 [1·85–4·02] ng/L; p=0·047), with one individual having a concentration (35 ng/L) above the 99th percentile diagnostic threshold.

Although predefined myocardial suppression of ^{18}F-FDG uptake was achieved in 34 (85%) patients (median myocardial standard uptake value 2·60 [IQR 1·83–3·83]), coronary ^{18}F-FDG uptake could not be confidently interpreted in 45% of vessel territories. Increased focal ^{18}F-FDG uptake was noted in just four patients: three at the site of recent coronary stenting and one at the ostium of a saphenous vein graft.

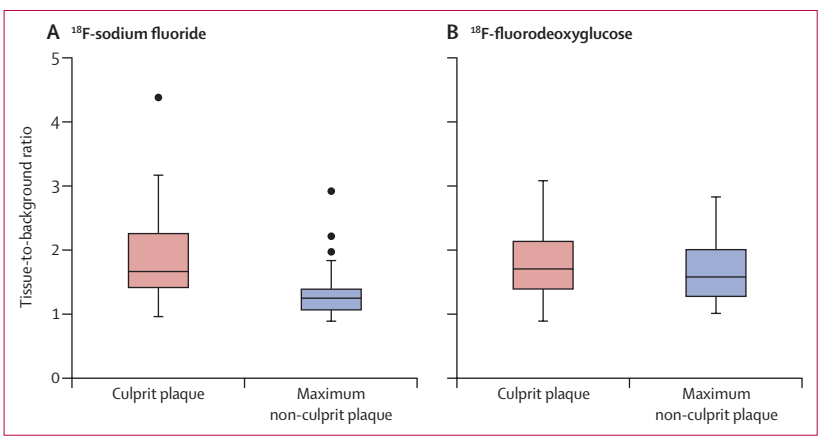

Figure 2: **^{18}F-fluoride and ^{18}F-fluorodeoxyglucose uptake in patients with myocardial infarction**
^{18}F-fluoride activity (maximum tissue-to-background ratio) was increased in the culprit plaque (red) compared with the maximum uptake in any of the non-culprit plaques (blue). By contrast, there was no difference in the activity of ^{18}F-fluorodeoxyglucose between these regions.

Discussion

We have shown that intense ^{18}F-NaF uptake localises to recent plaque rupture in patients with acute myocardial infarction and in those with symptomatic carotid disease. Moreover, in patients with stable coronary artery disease, ^{18}F-NaF uptake seems to identify coronary plaques with high-risk features on intravascular ultrasound. This technique holds major promise as a means of identifying high-risk and ruptured plaque, and potentially informing the future management and treatment of patients with stable and unstable coronary artery disease.

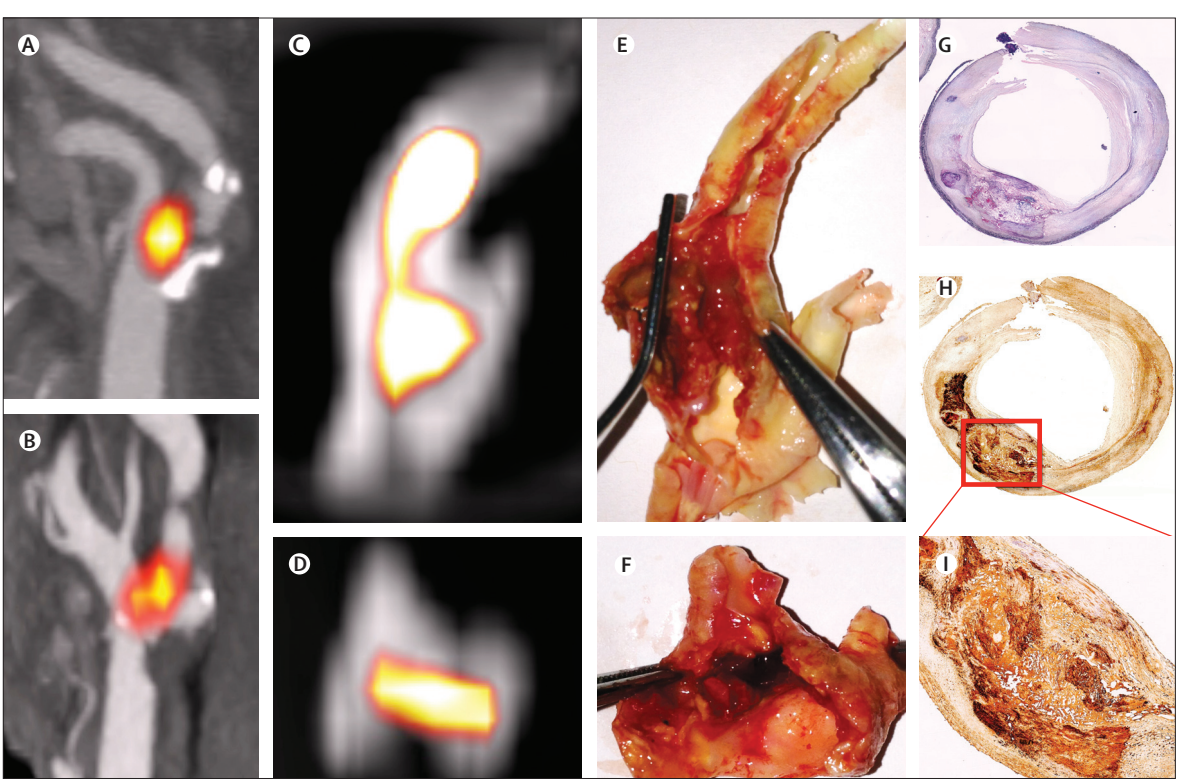

Figure 3: **Carotid ^{18}F-fluoride uptake and carotid plaque rupture**
In-vivo (A and B) and ex-vivo (C and D) positron emission and computed tomograms showing colocalisation of ^{18}F-fluoride (^{18}F-NaF) uptake (yellow-orange) to the site of plaque rupture with adherent thrombus on excised carotid endarterectomy tissue (E and F). Histology of the ^{18}F-NaF-positive region shows a large necrotic core (Movat's pentachrome, magnification 4×, G), within which increased staining for tissue non-specific alkaline phosphatase can be seen as a marker of calcification activity on immunohistochemistry (magnification 4×, H; magnification 10×, I).

Over 90% of our patients with myocardial infarction had increased ^{18}F-NaF uptake at the site of their culprit ruptured plaque, with TBR values that were a third higher than the maximum activity anywhere else in the coronary vasculature. These findings were not unique to the coronary circulation since we also noted increased focal ^{18}F-NaF uptake at the site of plaque rupture in all excised carotid endarterectomy specimens from patients with symptomatic carotid disease. However, we do acknowledge that this was not a universal finding. Of the three patients with myocardial infarction who had no uptake, two were younger smokers with only mild underlying irregularities on coronary angiography, implicating plaque erosion and thrombosis as the mechanism of their infarction rather than plaque rupture.[23] The third patient sustained an inferolateral non-ST segment elevation myocardial infarction and had a lesion stented in the right coronary artery. Increased ^{18}F-NaF activity was seen in the co-dominant circumflex artery that could have equally explained the clinical presentation, raising the intriguing possibility that ^{18}F-NaF might have a clinical role for patients in whom the culprit lesion is not readily apparent.

Focal regions of increased ^{18}F-NaF activity were seen in almost a half of our patients with stable coronary artery disease. To understand the mechanism of uptake in these patients, we sought to compare plaque characteristics of lesions with and without increased ^{18}F-NaF uptake. Because histology of the coronary arteries in this population is not feasible, we undertook greyscale and radiofrequency intravascular ultrasound, a widely used and validated process that provides detailed characterisation of plaque composition.[21] This method showed that lesions with increased ^{18}F-NaF uptake were associated with greater positive remodelling, more microcalcification, and a larger necrotic core. These findings were corroborated by, and consistent with, the findings of plaque analysis done with CT coronary angiography. Plasma troponin concentrations measured by a novel high-sensitivity assay were also higher in those patients with ^{18}F-NaF positive plaques than in patients with ^{18}F-NaF negative plaques, perhaps implicating subclinical plaque rupture with embolisation and microinfarction.

Why does ^{18}F-NaF bind to ruptured or high-risk plaque? Similar to the caseating granulomata of tuberculosis, atherosclerotic vascular calcification is a controlled cellular response to an intense, necrotic, and chronic inflammatory stimulus. Indeed, direct links between inflammatory cells and osteoblastic metaplasia in the vasculature are well described.[24,25] Hydroxyapatite is the central structural component of vascular calcification and is laid down during the earliest and most active stages of mineralisation:[24] hydroxyapatite nanocrystals nucleate, propagate, and mineralise the extracellular matrix. Fluoride ions are incorporated into the hydroxyapatite by ion exchange with hydroxyl groups at the crystal surface. This process is dependent on the crystal surface area that will be greatest in the earliest and most active nanocrystalline stages of mineralisation associated with plaque inflammation and necrosis. We believe that these processes are responsible for the observed ^{18}F-NaF uptake and is consistent with our data showing ^{18}F-NaF uptake in regions of necrosis, macrophage infiltration, apoptosis, microcalcification, and alkaline phosphatase and osteocalcin staining. Moreover, mathematical modelling indicates that microcalcification at the surface of thin-capped atheroma (figure 1) can intensify and double incident stresses.[26] Microcalcification is therefore not only a marker of acute plaque rupture but is implicated in its precipitation.

Coronary arterial calcification is considered pathognomonic of atherosclerosis and is a powerful independent risk predictor for cardiovascular events that can be further refined by the rapidity of its progression.[27,28] Why then not rely on CT coronary calcium scoring alone as a biomarker? Microcalcification cannot be detected on CT and confluent coronary macrocalcification develops slowly, taking many months or years to become apparent on CT, and can become dormant once inflammation in

	^{18}F-fluoride positive plaques (n=15)	^{18}F-fluoride negative plaques (n=24)	p
Lumen			
Area (mm²)	9·0 (5·7–13·5)	6·7 (4·7–9·7)	0·078
Minimal diameter (mm)	2·6 (1·7–3·1)	1·9 (1·7–2·6)	0·165
Maximum diameter (mm)	4·9 (4·1–5·3)	3·6 (3·1–4·6)	0·006
Vessel			
Area (mm²)	24·1 (17·2–27·1)	14·5 (11·9–18·1)	0·002
Minimal diameter (mm)	4·4 (3·4–5·2)	3·6 (3·0–4·1)	0·057
Maximum diameter (mm)	6·5 (6·0–7·1)	5·2 (4·7–5·9)	0·0001
Plaque			
Length (mm)	14·2 (6·2–23·5)	15·2 (6·7–25·0)	0·941
Volume (mm³)	152·9 (99·6–289·7)	91·0 (45·8–158·2)	0·032
Burden (%)*	55·6 (48·6–64·4)	54·2 (46·3–57·3)	0·174
Remodelling index	1·12 (1·09–1·19)	1·01 (0·94–1·06)	0·0004
Plaque composition			
Fibrous tissue (%)	51·0 (46·3–56·6)	58·1 (51·6–65·5)	0·015
Fibro-fatty (%)	10·9 (6·0–13·8)	12·6 (9·3–17·8)	0·092
Necrotic core (%)	24·6 (20·5–28·8)	18·0 (14·0–22·4)	0·001
Maximum frame necrotic core (%)†	35·5 (34·2–40·5)	29·2 (23·9–42·1)	0·009
Dense calcium (%)	12·6 (9·1–18·1)	10·2 (4·0–14·9)	0·092
Microcalcification, n (%)	11 (73%)	5 (21%)	0·002
Plaque classification, n (%)			
Thin-cap fibroatheroma	7 (47%)	4 (16%)	0·068
Thick-cap fibroatheroma	5 (33%)	9 (38%)	1·0
Pathological intimal thickening	0	7 (29%)	0·003
Fibrocalcific plaque	3 (20%)	4 (16%)	1·0

Data are median (IQR) unless otherwise stated. *Plaque burden calculation = (average vessel area – average lumen area) /average vessel area. †Maximum necrotic core in any single frame in the plaque.

Table 2: **Greyscale and radiofrequency intravascular ultrasound characteristics in ^{18}F-fluoride positive and negative plaques of patients with stable angina**

Panel: Research in context

Systematic review

We searched PubMed using variations of the keywords "high-risk plaques", "vulnerable plaques", "ruptured plaques", "^{18}F-fluorodeoxyglucose positron emission tomography", "^{18}F-fluoride positron emission tomography", and "coronary arteries". The search was restricted to human studies. We assessed the quality of the evidence specifically related to cardiovascular disease by reviewing the patient population studied and the methodology for the positron emission and CT imaging.

Non-invasive imaging of carotid plaque inflammation using ^{18}F-fluorodeoxyglucose positron emission tomography was reported by Rudd and colleagues in 2002.[11] Since then, this tracer has been validated and widely used as a surrogate of large vessel inflammation.[8,10] Increased ^{18}F-fluorodeoxyglucose in the coronary arteries has been described in patients with coexisting malignancy.[12,33,34] Since then, three prospective studies have examined the feasibility and reproducibility of assessing uptake of this tracer in the coronary vasculature.[6,7,13] Only two small studies (n=10–20)[6,13] have suggested that ^{18}F-fluorodeoxyglucose might identify some inflamed plaques in patients with recent myocardial infarction, although the largest study showed that in 50% of patients with acute myocardial infarction, there was no uptake of ^{18}F-fluorodeoxyglucose in the culprit plaque.[13]

Four retrospective studies in patients with cancer have recently reported cardiovascular uptake of ^{18}F-fluoride.[29,31,32,35] The aortic uptake of ^{18}F-NaF was first reported by Derlin and colleagues[29] and cardiac ^{18}F-fluoride uptake by Beheshti and colleagues.[31] We reported the coronary uptake of ^{18}F-NaF in a prospective clinical trial involving patients with aortic stenosis,[7,8] and these results were subsequently corroborated by Li and colleagues in their retrospective study of patients with cancer.[30] No study has prospectively assessed this tracer in patients with stable or unstable coronary artery disease or validated its activity against histology or invasive intracoronary imaging, such as intravascular ultrasound. There are no previous reports of ^{18}F-fluoride uptake in relation to plaque vulnerability or rupture.

Interpretation

There are currently no non-invasive imaging techniques that can identify high-risk and ruptured coronary atherosclerotic plaques in vivo in patients with coronary heart disease. For the first time, we have shown that ^{18}F-fluoride positron emission tomography can identify culprit and ruptured plaques in patients with myocardial infarction and symptomatic carotid disease. Moreover, histological characterisation demonstrates that ^{18}F-fluoride activity localises to regions of plaque rupture with evidence of increased inflammation, calcification activity, necrosis, and cell death. In patients with stable angina, ^{18}F-fluoride is associated with coronary plaques that have high-risk features on intravascular ultrasound, including positive remodelling, microcalcification, and necrosis. Given its ability to identify high-risk or ruptured coronary atherosclerotic plaque, this non-invasive imaging technique has the potential to change how we identify, manage, and treat patients with stable and unstable coronary artery disease. Further work is now needed to establish whether ^{18}F-fluoride positron emission tomography will provide a means of improving risk stratification, monitoring disease progression, guiding therapeutic interventions, and assessing novel anti-atherosclerotic therapies.

the plaque has subsided. By identifying areas of nascent and ongoing calcification activity, ^{18}F-NaF uptake allows us to detect regions of metabolically active plaque, thus providing complementary information to CT.[29–32] Indeed, we noted large areas of coronary CT calcium in the absence of increased ^{18}F-NaF uptake (figure 1) whereas other regions with minimal or no CT calcium had intense ^{18}F-NaF uptake (appendix) in keeping with previous observations in the aorta by Derlin and colleagues (panel).[29,32] Moreover, given that ^{18}F-NaF seems more closely aligned with the process of necrotic inflammation and plaque metabolic activity, we believe that it potentially offers major improvements to the prediction of cardiovascular risk compared with calcium scoring.

Our data have already established that ^{18}F-NaF identifies plaque with multiple high-risk features, but prospective studies are now needed in a broad range of patients to assess whether increased coronary ^{18}F-NaF activity will ultimately translate into future adverse events. If the results prove confirmatory then this technique has the potential to fundamentally alter the way we treat coronary artery disease: moving us away from the current framework based on lesion severity and ischaemia to one focused on plaque metabolism and inflammation. It could, for example, permit the identification of the vulnerable patient with single or multiple high-risk or silently ruptured plaques, providing an opportunity to treat and modify their risk to prevent future adverse cardiovascular events.

By contrast with ^{18}F-NaF, ^{18}F-FDG imaging was hampered by problems related to tracer uptake in the myocardium. Our stringent dietary recommendations resulted in suppression of myocardial activity in 70–85% of patients: a rate that compares favourably with previous studies (57–84%).[6,12,13] However, this suppression resulted in a patchy distribution of myocardial uptake that frequently obscured activity in one or more coronary vessels. Increased ^{18}F-FDG uptake might possibly occur in the culprit plaque and we failed to show this because of incomplete data or the delay in scanning. However, given its limitations, we believe that ^{18}F-FDG is unlikely to become sufficiently robust to permit its clinical application to the coronary circulation. Nevertheless, ^{18}F-FDG uptake remains an important measure of general vascular inflammation in the aorta and carotid arteries, providing complementary and distinct metabolic information to that of ^{18}F-NaF uptake.

We acknowledge that there are limitations of our study that include a lack of respiratory gating, potential partial volume artefacts, and the use of surrogate measures for coronary histology.[21] However, we believe that the totality of our comprehensive evidence using multiple approaches and imaging modalities provides a robust and cogent argument to support our contention that ^{18}F-fluoride uptake identifies vulnerable and high-risk plaques in patients with stable and unstable coronary heart disease. Further work is now needed to establish whether ^{18}F-NaF PET-CT will provide a clinically useful technique capable of improving risk stratification, monitoring disease progression, guiding therapeutic interventions, and assessing novel anti-atherosclerotic therapies.

Contributors

NVJ designed the study, undertook experiments, analysed results, and interpreted the data. ATV undertook experiments, analysed and interpreted the data, and prepared the report. MCW, ASVS, PAC, FHMC, SEY, AMF, EJRvB, and KAAF collected, analysed, and interpreted data, and prepared the report. ADF, NGU, MWHB, NLMC, and NLM collected the data and prepared the report. JHFR, MRD, and DEN contributed to the study design, supervision, and interpretation of data. DEN is the chief

investigator for the study and obtained funding for all studies. All authors participated in data interpretation. NVJ drafted the first and subsequent versions of this report with key input from MRD and DEN, and revisions from all authors, who reviewed and approved the final submitted report.

Conflicts of interest

NLM has received honoraria for Abbott Diagnostics and acted as a consultant for Abbott Diagnostics. The other authors declare that they have no conflicts of interest.

Acknowledgments

The study was funded by the Chief Scientist Office, Scotland (ETM/160) and the British Heart Foundation (PG/12/8/29371). MRD, NLM, and DEN are supported by the British Heart Foundation (CH/09/002, FS/10/024, FS/10/026). JHFR and PAC are part-funded by the NIHR Cambridge Biomedical Research Centre and the British Heart Foundation. The Wellcome Trust Clinical Research Facility and the Clinical Research Imaging Centre are supported by NHS Research Scotland (NRS) through NHS Lothian. We acknowledge the support of staff at the Edinburgh Heart Centre at the Royal Infirmary of Edinburgh, the radiography and radiochemistry staff of the Clinical Research Imaging Centre, and the histology staff at the Queens Medical Research Institute.

References

1 Naghavi M, Libby P, Falk E, et al. From vulnerable plaque to vulnerable patient: a call for new definitions and risk assessment strategies: part I. *Circulation* 2003; **108:** 1664–72.

2 Virmani R, Kolodgie FD, Burke AP, Farb A, Schwartz SM. Lessons from sudden coronary death: a comprehensive morphological classification scheme for atherosclerotic lesions. *Arterioscler Thromb Vasc Biol* 2000; **20:** 1262–75.

3 Virmani R, Burke AP, Farb A, Kolodgie FD. Pathology of the vulnerable plaque. *J Am Coll Cardiol* 2006; **47** (suppl)**:** C13–18.

4 Rogers IS, Tawakol A. Imaging of coronary inflammation with FDG-PET: feasibility and clinical hurdles. *Curr Cardiol Rep* 2011; **13:** 138–44.

5 Libby P, DiCarli M, Weissleder R. The vascular biology of atherosclerosis and imaging targets. *J Nucl Med* 2010; **51** (suppl 1)**:** 33S–37S.

6 Rogers IS, Nasir K, Figueroa AL, et al. Feasibility of FDG imaging of the coronary arteries: comparison between acute coronary syndrome and stable angina. *JACC Cardiovasc Imaging* 2010; **3:** 388–97.

7 Dweck MR, Chow MW, Joshi NV, et al. Coronary arterial 18F-sodium fluoride uptake: a novel marker of plaque biology. *J Am Coll Cardiol* 2012; **59:** 1539–48.

8 Dweck MR, Khaw HJ, Sng GK, et al. Aortic stenosis, atherosclerosis, and skeletal bone: is there a common link with calcification and inflammation? *Eur Heart J* 2013; **34:** 1567–74.

9 Dweck MR, Jones C, Joshi NV, et al. Assessment of valvular calcification and inflammation by positron emission tomography in patients with aortic stenosis. *Circulation* 2012; **125:** 76–86.

10 Tawakol A, Migrino RQ, Bashian GG, et al. In vivo 18F-fluorodeoxyglucose positron emission tomography imaging provides a noninvasive measure of carotid plaque inflammation in patients. *J Am Coll Cardiol* 2006; **48:** 1818–24.

11 Rudd JH, Warburton EA, Fryer TD, et al. Imaging atherosclerotic plaque inflammation with [18F]-fluorodeoxyglucose positron emission tomography. *Circulation* 2002; **105:** 2708–11.

12 Wykrzykowska J, Lehman S, Williams G, et al. Imaging of inflamed and vulnerable plaque in coronary arteries with 18F-FDG PET/CT in patients with suppression of myocardial uptake using a low-carbohydrate, high-fat preparation. *J Nucl Med* 2009; **50:** 563–68.

13 Cheng VY, Slomka PJ, Le Meunier L, et al. Coronary arterial ^{18}F-FDG uptake by fusion of PET and coronary CT angiography at sites of percutaneous stenting for acute myocardial infarction and stable coronary artery disease. *J Nucl Med* 2012; **53:** 575–83.

14 Thygesen K, Alpert JS, Jaffe AS, Simoons ML, Chaitman BR, White HD, and the Joint ESC/ACCF/AHA/WHF Task Force for the Universal Definition of Myocardial. Third universal definition of myocardial infarction. *Eur Heart J* 2012; **33:** 2551–67.

15 North American Symptomatic Carotid Endarterectomy Trial Collaborators. Beneficial effect of carotid endarterectomy in symptomatic patients with high-grade carotid stenosis. *N Engl J Med* 1991; **325:** 445–53.

16 Calvert PA, Obaid DR, O'Sullivan M, et al. Association between IVUS findings and adverse outcomes in patients with coronary artery disease: the VIVA (VH-IVUS in Vulnerable Atherosclerosis) Study. *JACC Cardiovasc Imaging* 2011; **4:** 894–901.

17 Murray SW, Stables RH, Hart G, Palmer ND. Defining the magnitude of measurement variability in the virtual histology analysis of acute coronary syndrome plaques. *Eur Heart J Cardiovasc Imaging* 2013; **14:** 167–74.

18 Stone GW, Maehara A, Lansky AJ, et al, and the PROSPECT Investigators. A prospective natural-history study of coronary atherosclerosis. *N Engl J Med* 2011; **364:** 226–35.

19 Ehara S, Kobayashi Y, Yoshiyama M, et al. Spotty calcification typifies the culprit plaque in patients with acute myocardial infarction: an intravascular ultrasound study. *Circulation* 2004; **110:** 3424–29.

20 Mintz GS, Nissen SE, Anderson WD, et al. American College of Cardiology clinical expert consensus document on standards for acquisition, measurement and reporting of intravascular ultrasound studies (IVUS). A report of the American College of Cardiology task force on clinical expert consensus documents. *J Am Coll Cardiol* 2001; **37:** 1478–92.

21 García-García HM, Mintz GS, Lerman A, et al. Tissue characterisation using intravascular radiofrequency data analysis: recommendations for acquisition, analysis, interpretation and reporting. *EuroIntervention* 2009; **5:** 177–89.

22 Motoyama S, Sarai M, Harigaya H, et al. Computed tomographic angiography characteristics of atherosclerotic plaques subsequently resulting in acute coronary syndrome. *J Am Coll Cardiol* 2009; **54:** 49–57.

23 Burke AP, Farb A, Malcom GT, Liang YH, Smialek J, Virmani R. Coronary risk factors and plaque morphology in men with coronary disease who died suddenly. *N Engl J Med* 1997; **336:** 1276–82.

24 Aikawa E, Nahrendorf M, Figueiredo JL, et al. Osteogenesis associates with inflammation in early-stage atherosclerosis evaluated by molecular imaging in vivo. *Circulation* 2007; **116:** 2841–50.

25 New SE, Goettsch C, Aikawa M, et al. Macrophage-derived matrix vesicles: an alternative novel mechanism for microcalcification in atherosclerotic plaques. *Circ Res* 2013; **113:** 72–77.

26 Vengrenyuk Y, Carlier S, Xanthos S, et al. A hypothesis for vulnerable plaque rupture due to stress-induced debonding around cellular microcalcifications in thin fibrous caps. *Proc Natl Acad Sci USA* 2006; **103:** 14678–83.

27 Raggi P, Callister TQ, Shaw LJ. Progression of coronary artery calcium and risk of first myocardial infarction in patients receiving cholesterol-lowering therapy. *Arterioscler Thromb Vasc Biol* 2004; **24:** 1272–77.

28 McEvoy JW, Blaha MJ, Defilippis AP, et al. Coronary artery calcium progression: an important clinical measurement? A review of published reports. *J Am Coll Cardiol* 2010; **56:** 1613–22.

29 Derlin T, Richter U, Bannas P, et al. Feasibility of 18F-sodium fluoride PET/CT for imaging of atherosclerotic plaque. *J Nucl Med* 2010; **51:** 862–65.

30 Li Y, Berenji GR, Shaba WF, Tafti B, Yevdayev E, Dadparvar S. Association of vascular fluoride uptake with vascular calcification and coronary artery disease. *Nucl Med Commun* 2012; **33:** 14–20.

31 Beheshti M, Saboury B, Mehta NN, et al. Detection and global quantification of cardiovascular molecular calcification by fluoro18-fluoride positron emission tomography/computed tomography—a novel concept. *Hell J Nucl Med* 2011; **14:** 114–20.

32 Derlin T, Tóth Z, Papp L, et al. Correlation of inflammation assessed by ^{18}F-FDG PET, active mineral deposition assessed by ^{18}F-fluoride PET, and vascular calcification in atherosclerotic plaque: a dual-tracer PET/CT study. *J Nucl Med* 2011; **52:** 1020–27.

33 Saam T, Rominger A, Wolpers S, et al. Association of inflammation of the left anterior descending coronary artery with cardiovascular risk factors, plaque burden and pericardial fat volume: a PET/CT study. *Eur J Nucl Med Mol Imaging* 2010; **37:** 1203–12.

34 Dunphy MP, Freiman A, Larson SM, Strauss HW. Association of vascular 18F-FDG uptake with vascular calcification. *J Nucl Med* 2005; **46:** 1278–84.

35 Janssen T, Bannas P, Herrmann J, et al. Association of linear (18) F-sodium fluoride accumulation in femoral arteries as a measure of diffuse calcification with cardiovascular risk factors: A PET/CT study. *J Nucl Cardiol* 2013; **20:** 569–77.

A new frontier in atherosclerotic coronary imaging

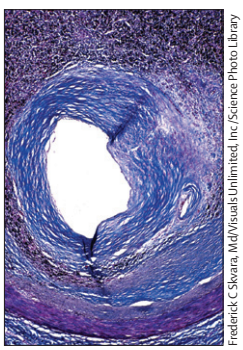

Frederick C Skvara, Md/Visuals Unlimited, Inc./Science Photo Library

Published Online
November 11, 2013
http://dx.doi.org/10.1016/S0140-6736(13)61911-X

See Online/Articles
http://dx.doi.org/10.1016/S0140-6736(13)61754-7

Copyright © Thomas and Haraszti. Open Access article distributed under the terms of CC BY

Ischaemic heart disease resulting from rupture of atherosclerotic plaques is a major cause of death worldwide. Precisely why a plaque ruptures remains a mystery. However, in *The Lancet*, Nikhil Joshi and colleagues' findings[1] suggest that we are close to being able to detect when rupture is about to occur.

The simple and inexpensive ^{18}F-sodium fluoride (^{18}F-NaF) PET radioisotope, used for 30 years to image bone formation, was found to signify metabolically active calcification in the aorta by Derlin and colleagues[2] and in the coronary arteries by Beheshti,[3] Dweck,[4] and Li,[5] and their colleagues. In their landmark article, Joshi and coworkers move this nascent field much farther forward.[1] They prospectively studied 40 patients with recent myocardial infarction (mean 8 days earlier) with invasive coronary angiography, CT coronary angiography, coronary calcium scoring, and cardiac gated PET-CT with ^{18}F-NaF and ^{18}F-fluorodeoxyglucose (^{18}F-FDG). Using invasive coronary angiography as the gold standard for determining the culprit plaque, the area of greatest ^{18}F-NaF uptake in the coronary arteries localised the plaque in 37 of 40 patients (maximum tissue-to-background ratio in the culprit plaque 1·66 [1·40–2·25] *vs* highest non-culprit plaque 1·24 [1·06–1·38]). By contrast, interpretation of ^{18}F-FDG PET-CT images in the same cohort was technically difficult because of the frequent overlap of myocardial ^{18}F-FDG uptake with the adjacent coronary arteries. Of the 55% of vascular territories that were interpretable by ^{18}F-FDG, only a weak correlation was seen with culprit plaque identification.

A second cohort of 40 patients with stable angina underwent the same imaging tests and an intracoronary ultrasound. 18 patients had one or more plaques with high ^{18}F-NaF uptake, defined as at least 25% greater than a proximal reference lesion. Intracoronary ultrasound identified that microcalcification, necrotic core size, and positive remodelling correlated strongly with plaques of high ^{18}F-NaF activity.

Histological correlation was assessed in a third cohort of nine patients who underwent carotid endarterectomy at a mean of 17 days after clinical symptoms. Ex-vivo PET-CT was done on the removed carotid atherosclerotic tissue. Macroscopic plaque rupture was present in each patient, all localised to areas of high ^{18}F-NaF uptake. Plaques with increased ^{18}F-NaF uptake had substantially larger necrotic cores, more cell death and macrophage infiltration, and, as measured by alkaline phosphatase and osteocalcin staining, more active calcification than those that did not.

With the strong in-vivo correlates of coronary plaque rupture seen on intracoronary ultrasound in patients with stable angina, and histological confirmation of plaque rupture in atherosclerotic carotid tissue with high ^{18}F-NaF activity, the authors can indeed state that of 40 patients with recent myocardial infarction (37 men, three women), plaque rupture can be detected non-invasively.

Now that we can detect plaque rupture, should we? Although the radioisotope ^{18}F-NaF and PET-CT equipment are readily available in the developed world, much research needs to be done before the technique can become a viable clinical option. Just because a plaque at risk for rupture can be identified does not mean that we know what to do with this information. Prospective trials are needed to establish the frequency with which high ^{18}F-NaF plaques rupture, and the timing of rupture. Also, does plaque rupture result in events or simply the rupture and healing cycle believed to result in a stepwise increase in plaque stenosis? If such trials are positive, what will we do with the information? Of Joshi and colleagues' 40 patients with stable angina, nearly all were on antiplatelet agents and 36 were taking statins. Despite this therapy, 18 patients had at least one plaque with high ^{18}F-NaF uptake. However, the ability to assess and potentially quantitatively measure plaque at high risk of rupture as a continuous variable (by maximum standard uptake value) creates a new world of opportunity for the investigation of pharmacological and device therapy.

The technique holds greater promise in populations with myocardial infarction and acute coronary syndrome than in more stable patients. Earlier work by Joshi and colleagues, for example, found a strong correlation between patients with high NaF plaques and those with the more easily and inexpensively obtained total Agatston coronary calcium score.[4]

The technique also creates the opportunity to better assess the commonly accepted belief that most myocardial infarctions are caused by rupture of previously

non-obstructive plaques. The underpinnings of this theory are derived from coronary angiography that is done distant from the index myocardial infarction.[6,7] Narula and colleagues[8] and others have questioned this assumption. The predictive value for increasing non-fatal myocardial infarction and cardiac death consistently seen in studies of increasing ischaemia, as assessed by myocardial perfusion imaging,[9] and worsening obstructive disease by coronary CT[10] and invasive angiography, are also inconsistent with this assumption.

Questions to be answered include: how best to use information derived from an assessment of inflammation by ^{18}F-FDG and active calcification by ^{18}F-NaF. In large vessels without adjacent areas of intense ^{18}F-FDG activity, ^{18}F-FDG assessment is much less handicapped by overlapping structures compared with the coronary arteries. How do Joshi and colleagues' findings apply to women, in whom plaque erosion is a much more common mechanism of myocardial infarction than in men? How do the findings apply to patients with diabetes? Does coronary artery bypass graft biology differ with respect to ^{18}F-NaF activity? Do high ^{18}F-NaF plaques in the carotid and other cerebrovascular vessels predict stroke and transient ischaemic attack? Joshi and colleagues and earlier pioneers have identified a new and hopefully fruitful frontier in nuclear cardiology and atherosclerotic coronary imaging.

*Gregory S Thomas, Reka A Haraszti
Long Beach Memorial Medical Center, Long Beach and University of California, Irvine, CA 90806, USA (GST); and Graduate School of Biomedical Sciences, University of Massachusetts Medical School, Worcester, MA, USA (RAH)
gthomas1@memorialcare.org

We declare that we have no conflicts of interest.

1 Joshi NV, Vesey AT, Williams MC, et al. ^{18}F-fluoride positron emission tomography for identification of ruptured and high-risk coronary atherosclerotic plaques: a prospective clinical trial. *Lancet* 2013; published online Nov 11. http://dx.doi.org/10.1016/S0140-6736(13)61754-7.
2 Derlin T, Richter U, Bannas P, et al. Feasibility of 18F-sodium fluoride PET/CT for imaging of atherosclerotic plaque. *J Nucl Med* 2010; **51:** 862–65.
3 Beheshti M, Saboury B, Mehta NN, et al. Detection and global quantification of cardiovascular molecular calcification by fluoro18-fluoride positron emission tomography/computed tomography—a novel concept. *Hell J Nucl Med* 2011; **14:** 114–20.
4 Dweck MR, Chow MW, Joshi NV, et al. Coronary arterial ^{18}F-sodium fluoride uptake: a novel marker of plaque biology. *J Am Coll Cardiol* 2012; **59:** 1539–48.
5 Li Y, Berenji GR, Shaba WF, Tafti B, Yevdayev E, Dadparvar S. Association of vascular fluoride uptake with vascular calcification and coronary artery disease. *Nucl Med Commun* 2012; **33:** 14–20.
6 Ambrose JA, Tannenbaum MA, Alexopoulos D, et al. Angiographic progression of coronary disease and the development of myocardial infarction. *J Am Coll Cardiol* 1988; **12:** 56–62.
7 Little WC, Constantinescu M, Applegate RJ, et al. Can coronary angiography predict the site of a subsequent myocardial infarction in patients with mild-to-moderate coronary artery disease? *Circulation* 1988; **78:** 1157–66.
8 Narula J, Masataka NM, Virmani R, et al. Histopathologic characteristics of atherosclerotic coronary disease and implications of the findings for the invasive and noninvasive detection of vulnerable plaques. *J Am Coll Cardiol* 2013; **61:** 1041–51.
9 Thomas GS, Miyamoto MI, Morello AP, et al. Technetium^{99m} based myocardial perfusion imaging predicts clinical outcome in the community outpatient setting: the Nuclear Utility in the Community (NUC) study. *J Am Coll Cardiol* 2004; **43:** 213–23.
10 Min JK, Dunning A, Lin FY, et al. Age and sex-related differences in all-cause mortality risk based on coronary computerized tomography angiography findings. *J Am Coll Cardiol* 2011; **58:** 849–60.

Neth Heart J (2014) 22:1–2
DOI 10.1007/s12471-013-0500-1

EDITOR'S COMMENT

Molecular imaging of coronary atherosclerosis; predictive of an acute myocardial infarction?

E. E. van der Wall

Published online: 28 November 2013
© The Author(s) 2013. This article is published with open access at Springerlink.com

Coronary atherosclerosis is a leading cause of cardiovascular morbidity and mortality worldwide. Plaque complications occur most commonly from plaque rupture, and also from plaque erosion and calcified nodule formation. Over the past years, advanced structural, metabolic and molecular imaging technologies have emerged and offer new windows into atherosclerosis pathophysiology [1–4]. Molecular imaging complements traditional structural plaque imaging through the use of targeted probes that identify specific molecules and/or biological processes in vivo [5]. Preclinical atherosclerosis molecular imaging has successfully identified nearly all established high-risk plaque characteristics including inflammation, thrombosis, neo-vessel formation, apoptosis, and haemorrhage. However, clinical translation of molecular imaging has been slow compared with the rapid growth within the field.

Currently, clinical atherosclerosis molecular imaging is dominated by non-invasive PET metabolism/inflammation plaque imaging with fluorine 18 (18F)-fluorodeoxyglucose (FDG). For the past two decades, 18F FDG has been the only fluorine-18 radioligand approved by the US Food and Drug Administration (FDA) for PET imaging. Coronary FDG PET is challenging, in part owing to the small size of coronary vessels and cardiac motion artefacts, but also because of the intense FDG uptake of the adjacent highly metabolic myocardium that obscures the coronary FDG signal. However, with dietary myocardial suppression protocols, detection of FDG PET signal in the left main and proximal coronary artery beds is sometimes achievable. Recently, non-invasive coronary FDG PET activity has been investigated in the stented culprit lesions of 20 subjects with acute coronary syndromes (ACS) versus seven non-ACS subjects within 1 week of stent placement [6]. Using a predetermined FDG target to background ratio of 2.0 or greater to identify FDG-positive lesions, the ACS patients correlated positively with elevated stent FDG signal. However, coronary FDG signal was interpretable in only 50 % of ACS patients, implying the need for further improvements in coronary FDG PET.

Apart from 18F FDG coronary imaging, clinically available approaches such as sodium 18F-fluoride (NaF) for PET are emerging. Coronary calcification is a hallmark of advanced atheroma that can be detected with non-invasive NaF PET, which has been used for the past 3 decades to detect cancer bone metastases. As opposed to FDG, background myocardial uptake of NaF is negligible, and therefore NaF can determine coronary osteogenic activity. In a study by Dweck et al. from the University of Edinburgh [7], NaF PET molecular imaging identified sites of active coronary calcification non-invasively by PET and may be a new therapeutic target. The NaF signal was elevated in proportion to coronary CT calcium scores in 119 subjects, except in those with the highest calcium scores that may represent end-stage calcified plaques. From the same research group, Joshi et al. [8] recently (Lancet November 2013) studied coronary plaque imaging using two different radioactive tracers: 18F-NaF and 18F-FDG. The Scottish study included 40 patients with acute myocardial infarction (AMI) and 40 patients with stable angina. All patients underwent PET-CT, invasive coronary angiography, CT coronary angiography, and CT calcium scoring.

Among the 40 patients with AMI, 18F-NaF PET uptake was 34 % higher in the culprit ruptured plaque compared with non-culprit plaques. Nearly all patients (93 %) had increased 18F-NaF uptake in the culprit plaque. With 18F-FDG, however, no differences in uptake between culprit and non-culprit plaques were observed. Among the 40 patients with stable angina, 45 % had plaques with increased 18F-NaF uptake.

E. E. van der Wall (✉)
Interuniversity Cardiology Institute of the Netherlands
(ICIN) - Netherlands Heart Institute (NHI), P.O. Box 19258,
3501 DG Utrecht, the Netherlands
e-mail: ernst.van.der.wall@icin.nl

These plaques were mostly non-obstructive at coronary angiography and contained more high-risk features on intravascular ultrasound compared with plaques without tracer uptake. Consequently, 18F-NaF PET may become an effective tool for predicting an AMI, which would have a great impact for patients with coronary atherosclerosis. Early detection of the atherosclerotic 'danger zones' could include immediate instalment of drugs such as statins or aspirin, drastic changes in lifestyle and even inserting stents into the affected coronary artery.

The use of 18F-NaF PET-CT offers the first non-invasive imaging method to identify and localise ruptured and high-risk coronary plaques. A next step is to show that increased 18F-NaF predicts future adverse clinical events. Further studies are therefore needed to evaluate whether the detection of risky plaques before rather than after an AMI has the potential to save lives. To summarise, the addition of newer molecular imaging tools such as NaF PET-CT will continue to strengthen our understanding of the in vivo biology of high-risk plaques [9, 10]. They are increasingly being translated into clinical use, and in combination with structural imaging they provide more comprehensive information to build risk-prediction tools. Ongoing efforts to improve non-invasive coronary imaging strategies must be pursued. Overall, with continued advances in molecular and structural atherosclerosis imaging, high-risk coronary atherosclerotic plaques will be brightened as never before. The recent study in the Lancet at least suggests that molecular imaging using PET-CT scanning may provide an answer in identifying 'ticking time bomb' patients at risk of an AMI.

Open Access This article is distributed under the terms of the Creative Commons Attribution License which permits any use, distribution, and reproduction in any medium, provided the original author(s) and the source are credited.

References

1. Fleg JL, Stone GW, Fayad ZA, et al. Detection of high-risk atherosclerotic plaque: report of the NHLBI Working Group on current status and future directions. JACC Cardiovasc Imaging. 2012;5:941–55.
2. van der Wall EE, Heidendal GA, den Hollander W, et al. Metabolic myocardial imaging with 123I-labeled heptadecanoic acid in patients with angina pectoris. Eur J Nucl Med. 1981;6:391–6.
3. Knaapen P, de Haan S, Hoekstra OS, et al. Cardiac PET-CT: advanced hybrid imaging for the detection of coronary artery disease. Neth Heart J. 2010;18:90–8.
4. van der Wall EE, den Hollander W, Heidendal GA, et al. Dynamic myocardial scintigraphy with 123I-labeled free fatty acids in patients with myocardial infarction. Eur J Nucl Med. 1981;6:383–9.
5. Thomas G, Haraszti R. A new frontier in atherosclerotic coronary imaging. Lancet. 2013. doi:10.1016/S0140-6736(13)61911-X.
6. Cheng VY, Slomka PJ, Le Meunier L, et al. Coronary arterial 18F-FDG uptake by fusion of PET and coronary CT angiography at sites of percutaneous stenting for acute myocardial infarction and stable coronary artery disease. J Nucl Med. 2012;53:575–83.
7. Dweck MR, Chow MW, Joshi NV, et al. Coronary arterial 18F-sodium fluoride uptake: a novel marker of plaque biology. J Am Coll Cardiol. 2012;59:1539–48.
8. Joshi NV, Vesey AT, Williams MC, et al. 18F-fluoride positron emission tomography for identification of ruptured and high-risk coronary atherosclerotic plaques: a prospective clinical trial. Lancet. 2013. doi:10.1016/S0140-6736(13)61754-7.
9. George RT. 18F-sodium fluoride positron emission tomography: an in vivo window into coronary atherosclerotic plaque biology. J Am Coll Cardiol. 2012;59:1549–50. doi:10.1016/j.jacc.2012.01.029.
10. Chen W, Dilsizian V. Targeted PET/CT imaging of vulnerable atherosclerotic plaques: microcalcification with sodium fluoride and inflammation with fluorodeoxyglucose. Curr Cardiol Rep. 2013;15:364. doi:10.1007/s11886-013-0364-4.

Nature Reviews Cardiology advance online publication 26 November 2013; doi:10.1038/nrcardio.2013.181

CORONARY ARTERY DISEASE

Noninvasive imaging technique can identify high-risk coronary plaques

Atherosclerotic plaque rupture and subsequent acute myocardial infarction are well known to be a major cause of death worldwide. Prediction of plaque rupture, however, has proven challenging. A new noninvasive imaging technique that uses an inexpensive PET radioisotope, ^{18}F-NaF, might prove to be the answer. Indeed, the investigators of a study published in the *Lancet* believe that their technique "holds major promise as a means of identifying high-risk and ruptured plaque, and potentially informing the future management and treatment of patients with stable and unstable coronary artery disease".

When 40 patients who had been hospitalized for myocardial infarction underwent ^{18}F-FDG PET-CT scanning, no significant differences in maximum ^{18}F-FDG uptake were observed between the culprit plaques and plaques located elsewhere in the coronary vasculature. By contrast, increased ^{18}F-NaF uptake was observed in the culprit plaque in 37 of the 40 patients. ^{18}F-NaF activity was found to be 34% higher in the culprit plaque than the maximum activity recorded anywhere else in the coronary vasculature.

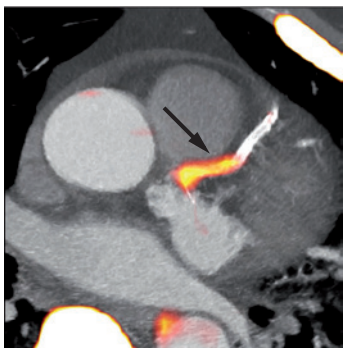

Image reprinted from Joshi, N. V. *et al.* ^{18}F-fluoride positron emission tomography for identification of ruptured and high-risk coronary atherosclerotic plaques: a prospective clinical trial. *Lancet* doi:10.1016/S0140-6736(13)61754-7, Copyright (2013), with permission from Elsevier.

Ex vivo ^{18}F-NaF PET-CT and histological analysis were performed on carotid specimens obtained from nine other patients who had undergone carotid endarterectomy for symptomatic carotid artery disease. Compared with tissue that did not take up ^{18}F-NaF, areas of increased ^{18}F-NaF uptake were found to have increased calcification, macrophage infiltration, and cell death. In their study report, Dr Nikhil Joshi and colleagues describe how they believe ^{18}F-NaF is taken up by high-risk plaques: "Hydroxyapatite is the central structural component of vascular calcification and is laid down during the earliest and most active stages of mineralization ... Fluoride ions are incorporated into the hydroxyapatite by ion exchange with hydroxyl groups at the crystal surface." "By identifying areas of nascent and ongoing calcification activity," they explain, "^{18}F-NaF uptake allows us to detect regions of metabolically active plaque."

Joshi *et al.* also assessed coronary ^{18}F-NaF uptake in 40 patients with stable angina pectoris. Increased ^{18}F-NaF uptake seemed to identify coronary plaques that, although mostly shown to be nonobstructive on coronary angiography, contained high-risk features (increased positive remodelling, microcalcification, and necrotic core) on intravascular imaging.

"Prospective studies are now needed in a broad range of patients to assess whether increased coronary ^{18}F-NaF activity will ultimately translate into future adverse events," say the investigators. "If the results prove confirmatory, then this technique has the potential to fundamentally alter the way we treat coronary artery disease."

Bryony M. Mearns

Original article Joshi, N. V. *et al.* ^{18}F-fluoride positron emission tomography for identification of ruptured and high-risk coronary atherosclerotic plaques: a prospective clinical trial. *Lancet* doi:10.1016/S0140-6736(13)61754-7

© 2013 Macmillan Publishers Limited. All rights reserved

Eur J Vasc Endovasc Surg (2016) 51, 518–526

Positron Emission Tomography and Magnetic Resonance Imaging of Cellular Inflammation in Patients with Abdominal Aortic Aneurysms

O.M.B. McBride [a,b,c,*,e], N.V. Joshi [a,b,c,e], J.M.J. Robson [a,b,c], T.J. MacGillivray [b], C.D. Gray [b], A.M. Fletcher [b], M.R. Dweck [a,b,c], E.J.R. van Beek [a,b], J.H.F. Rudd [d], D.E. Newby [a,b,c], S.I. Semple [b]

[a] Centre for Cardiovascular Science, University of Edinburgh, Edinburgh, UK
[b] Clinical Research Imaging Centre, University of Edinburgh, Edinburgh, UK
[c] Royal Infirmary of Edinburgh, Edinburgh, UK
[d] Division of Cardiovascular Medicine, University of Cambridge, Cambridge, UK

WHAT THIS PAPER ADDS

Comparing these techniques identifies a modest correlation but some key differences related to the spatial distribution of ^{18}F-FDG and USPIO uptake. This may reflect the differing elements of macrophage activity detected by these modalities: glycolysis and phagocytosis. Further studies are needed to assess whether identification of this varying activity will influence aneurysm growth rates and the clinical outcome.

Objectives: Inflammation is critical in the pathogenesis of abdominal aortic aneurysm (AAA) disease. Combined ^{18}F-fludeoxyglucose (^{18}F-FDG) positron emission tomography with computed tomography (PET-CT) and ultrasmall superparamagnetic particles of iron oxide (USPIO)-enhanced magnetic resonance imaging (MRI) are non-invasive methods of assessing tissue inflammation. The aim of this study was to compare these techniques in patients with AAA.

Materials and methods: Fifteen patients with asymptomatic AAA with diameter 46 ± 7 mm underwent PET-CT with ^{18}F-FDG, and T2*-weighted MRI before and 24 hours after administration of USPIO. The PET-CT and MRI data were then co-registered. Standardised uptake values (SUVs) were calculated to measure ^{18}F-FDG activity, and USPIO uptake was determined using the change in R2*. Comparisons between the techniques were made using a quadrant analysis and a voxel-by-voxel evaluation.

Results: When all areas of the aneurysm were evaluated, there was a modest correlation between the SUV on PET-CT and the change in R2* on USPIO-enhanced MRI ($n = 70{,}345$ voxels; $r = .30$; $p < .0001$). Although regions of increased ^{18}F-FDG and USPIO uptake co-localised on occasion, this was infrequent (kappa statistic 0.074; 95% CI 0.026–0.122). ^{18}F-FDG activity was commonly focused in the shoulder region whereas USPIO uptake was more apparent in the main body of the aneurysm. Maximum SUV was lower in patients with mural USPIO uptake.

Conclusions: Both ^{18}F-FDG PET-CT and USPIO-MRI uptake identify vascular inflammation associated with AAA. Although they demonstrate a modest correlation, there are distinct differences in the pattern and distribution of uptake, suggesting a differential detection of macrophage glycolytic and phagocytic activity respectively.

© 2015 The Authors. Published by Elsevier Ltd on behalf of European Society for Vascular Surgery. This is an open access article under the CC BY-NC-ND license (http://creativecommons.org/licenses/by-nc-nd/4.0/).

Article history: Received 11 March 2015, Accepted 12 December 2015, Available online 23 February 2016

Keywords: Abdominal aortic aneurysms, Magnetic resonance imaging, Positron emission tomography, Computed tomography

INTRODUCTION

Recent advances in imaging modalities have generated considerable interest in novel molecular and cellular techniques. In contrast to anatomical and structural approaches, molecular and cellular imaging targets the activity of specific biochemical and cellular processes to provide insight into the aetiology, biology, and pathogenesis of diseased states. Moreover, this has the potential to refine the diagnosis and risk stratification of cardiovascular disease as well as to assess responses to specific therapeutic interventions.[1–5] A combination of morphological imaging with molecular imaging has proven a particularly useful approach.

^{18}F-Fludeoxyglucose (^{18}F-FDG) is used to image metabolically active cells with combined positron emission and computed tomography (PET-CT). ^{18}F-FDG accumulates in all

[e] These authors contributed equally.

* Corresponding author. Centre for Cardiovascular Science, University of Edinburgh, Little France Crescent, Edinburgh EH16 4SB, UK.
E-mail address: olivia.mcbride@ed.ac.uk (O.M.B. McBride).

1078-5884/© 2015 The Authors. Published by Elsevier Ltd on behalf of European Society for Vascular Surgery. This is an open access article under the CC BY-NC-ND license (http://creativecommons.org/licenses/by-nc-nd/4.0/).

http://dx.doi.org/10.1016/j.ejvs.2015.12.018

cells and tissues that metabolise glucose, in direct proportion to their metabolic activity. In atherosclerotic arteries and those affected by vasculitides, ^{18}F-FDG uptake correlates with the degree of arterial inflammation and is reproducible.[6–8] Furthermore, ^{18}F-FDG uptake increases with the number of cardiovascular risk factors present, is predictive of future cardiovascular events,[9–11] and has been used as a biomarker to demonstrate the anti-inflammatory effects of statins and other novel therapies.[12–14] ^{18}F-FDG accumulates in the wall of abdominal aortic aneurysms (AAAs) and several studies have correlated uptake with aortic vessel wall inflammation on histology.[15–17] There is evidence to suggest that ^{18}F-FDG can discriminate between asymptomatic and symptomatic AAA, but its potential use as a marker of aneurysm expansion, progression, and rupture has yet to be established.[15–22]

Magnetic resonance imaging (MRI) with ultrasmall superparamagnetic particles of iron oxide (USPIO) is an alternative approach for detecting cellular inflammation.[23,24] Owing to their small particle size (diameter 10–30 nm), USPIO escape immediate recognition by the reticulo-endothelial system, persist in the bloodstream, and accumulate at sites of vascular inflammation. Here they undergo phagocytosis by tissue-resident macrophages within which they accumulate and are detectable on T2- and T2*-weighted MRI sequences. Within atheromatous plaques, USPIO uptake correlates with macrophage density, distinguishes stable from unstable carotid plaques, and is reduced following high-dose atorvastatin therapy.[25–27] USPIO uptake in the wall of AAAs has previously been demonstrated, where it co-localises with macrophages and is associated with a threefold higher AAA growth rate.[24]

Given that both ^{18}F-FDG PET and USPIO-enhanced MRI have been used to assess vascular inflammation in patients with AAA, the aim of this study was to compare ^{18}F-FDG PET and USPIO-enhanced MRI in patients with AAAs. Specifically, the spatial distribution and intensity of the inflammatory process using both techniques was assessed to determine whether they provided complementary or distinct insights into the pathology of AAAs.

MATERIALS AND METHODS

Subjects

Patients with asymptomatic AAA (diameter 30–55 mm on duplex ultrasound examination) were recruited from the aneurysm surveillance clinic at the Royal Infirmary of Edinburgh. Exclusion criteria were age $<$ 50 years, active systemic inflammatory or malignant disease, renal dysfunction (estimated glomerular filtration rate $<$ 30 mL/min, because of the risks of contrast induced renal dysfunction), hepatic cirrhosis (Child–Pugh score B or C, because of the contrast agent not having been studied in this group of patients), planned AAA surgery within 6 months of screening, any contraindication to MRI and insulin-dependent diabetes mellitus (due to the confounding of ^{18}F-FDG uptake with variable blood glucose concentrations). Studies were performed with the approval of the local research ethics committee, in accordance with the Declaration of Helsinki, and with the written informed consent of each participant.

All patients underwent a comprehensive baseline clinical assessment, including evaluation of their cardiovascular risk factor profile and recording of an abdominal ultrasound scan. ^{18}F-FDG PET-CT and USPIO-MRI data acquisition procedures are detailed in Methods I of the Supplementary Material.

Image analysis

Registration of PET and MRI images. The accuracy of PET-CT to Computed Tomography Aortogram (CTA) registration was confirmed by visual assessment, and minor intra-scan patient movement was corrected using a semi-automatic rigid 3D voxel registration protocol (Analyze 11.0, Mayo Clinic, Rochester, MN, USA). Registration of the MRI data allowed the excellent anatomical detail on the T2W images and the high sensitivity of T2*W images for iron to be utilised. All MR images were registered to the pre-contrast T2W image. The CTA and T2W MRI datasets were also co-registered. At the end of the registration process, the pre-USPIO T2*W MRI, the post-USPIO T2*W MRI, the CTA, and the PET-CT were all co-registered to enable direct comparison. All steps of registration used a semi-automatic rigid 3D voxel registration protocol that has been previously validated and published.[24] All outputs were manually checked and optimised as necessary. Two independent trained observers, who were experienced vascular surgeons who had developed the image analysis techniques, undertook the analyses. There was excellent inter-observer agreement with kappa statistics between 0.84 and 0.89, for all steps.

^{18}F-FDG quantification. The maximum standardised uptake value (SUV_{max}) was used to assess ^{18}F-FDG uptake in the aneurysm. The SUV is the decay-corrected tissue uptake divided by the injected dose per unit body weight and is a semi-quantitative dimensionless unit that has been previously validated and is a commonly used measure of tissue ^{18}F-FDG uptake.[5,28] The SUV in vascular structures can be heavily influenced by variability of ^{18}F-FDG activity in the blood pool. Therefore, the tissue-to-background ratio (TBR) was also calculated by dividing the tissue SUV_{max} by an averaged mean SUV in the blood pool, derived from five circular regions of interest in the centre of the inferior vena cava. An area of ^{18}F-FDG uptake was defined as positive if the SUV_{max} or TBR was $>$ 125% of the value obtained from an averaged SUV_{max} from five randomly selected regions in the non-aneurysmal descending thoracic aorta.[29,30]

USPIO quantification. Using validated in-house software built in the Matlab environment (Mathworks, Natick, MA, USA), all four echoes in the multi-echo T2*W sequence were combined to generate a T2* map in which the magnitude of each voxel represented the T2* value ($S(t) = S(0)\exp - (t/T2^*)$). USPIO uptake was detected using the change in T2* (or R2*; R2* = 1/T2*) following USPIO administration. We applied a validated image analysis

method previously published for ΔT2* thresholding of AAA-USPIO data in order to visually interpret and threshold the UPSIO T2*-weighted data.[24] Increasingly R2* (=1/T2*) are reported to provide a positive correlation between concentration of USPIO and increase in R2* values, facilitating more straightforward data interpretation and visualisation. Detailed USPIO quantification methodology is outlined in Methods II of the Supplementary Material.

The correlation between ^{18}F-FDG uptake and USPIO distribution was analysed using three methods: the signals in different regions of the aneurysm were compared by drawing regions of interest (ROI) around the wall and thrombus, then the co-localisation across the aneurysm as a whole using a voxel-by-voxel analysis was studied. Finally, a previously defined aneurysm classification system based on USPIO uptake on MRI[24] was compared with the mean SUV_{max} and TBR for the positive regions of ^{18}F-FDG uptake in each aneurysm.

Colour maps. Two independent observers, blinded to patient demographics and aneurysm size reviewed the ΔT2* colour maps and the fused PET-CT data. Each axial slice was divided into quadrants and each quadrant was defined as positive if it included at least one region of increased USPIO or ^{18}F-FDG uptake, or negative if it did not. On the ΔT2* colour maps, significant regions of USPIO accumulation were defined as consisting of at least 10 contiguous voxels with ΔT2* above the threshold of 59%.[24] On the PET-CT scans, ROI were drawn around areas of maximum uptake in the wall and thrombus of the aneurysm and defined as positive if the SUV_{max} or TBR was $>$ 125% of the value obtained from an averaged SUV_{max} from five randomly selected regions in the non-aneurysmal descending thoracic aorta.

In order to define the area of the aneurysm where there was increased uptake of USPIO or ^{18}F-FDG, the aneurysm was divided in the axial plane into three distinct regions: on MRI the shoulder region extended one slice (5 mm) above and below the point at which the aorta last measured $\leq$ 30 mm in diameter, whereas on PET-CT, two slices (6 mm) were considered. The bifurcation region was defined in an identical way but from the point where the aneurysm reduced in diameter to $\leq$ 30 mm. The area between these two points was defined as the main body of the aneurysm.

Voxel-by-voxel analysis. The MR images were reconstructed by down-sampling to achieve equivalent voxel sizes with the corresponding PET images. A ROI encompassing the entire aortic wall and thrombus was drawn on each slice of the pre-contrast T2W image. These ROIs were then applied to the PET images and to the calculated ΔR2* colour maps. This enabled a quantitative voxel-by-voxel analysis of USPIO and ^{18}F-FDG uptake.

Aneurysm classification. We have previously shown that mural USPIO uptake predicts expansion; therefore, aneurysms were classified into three predefined groups by two independent blinded observers: Group 1, no mural or thrombus USPIO uptake, except for isolated periluminal enhancement; Group 2, diffuse USPIO uptake, distinct from the periluminal thrombus and aortic wall; and Group 3 focal areas (with at least 10 contiguous voxels) of USPIO uptake within the aortic wall of the aneurysm, distinct from the periluminal area and thrombus.[24] PET activity in regions of increased uptake was then compared across these three groups.

A schematic outlining the image analysis techniques undertaken can be found in Methods III of the Supplementary Material.

Statistical analysis

Normally distributed continuous variables were expressed as mean ± standard deviation. Non-parametric data were presented as median with interquartile ranges. Correlations between normally distributed data were performed using Pearson's correlation. Comparisons were undertaken with paired or unpaired Student's *t*-tests as appropriate. A two-sided $p < .05$ was regarded as statistically significant. Statistical analysis was performed with the use of Graph Pad Prism version 5 (GraphPad Software Inc., La Jolla, CA USA).

RESULTS

Fifteen predominantly elderly men with multiple cardiovascular risk factors and a mean AAA diameter of 46 mm (range 34—55 mm) participated in the study (Table 1). All patients were asymptomatic and had fusiform aneurysms confined to the abdominal aorta. ^{18}F-FDG PET-CT and USPIO-enhanced MRI scans were performed a median of 7 days apart. PET imaging of the abdomen was undertaken a median of 92 (IQR, 89—97) minutes after injection of 237 ± 16 MBq of ^{18}F-FDG. The effective radiation from participation in the study was 10.8 mSv using a conversion

Table 1. Baseline characteristics of patients with abdominal aortic aneurysm ($n = 15$).

Age (years)	73 ± 4
Male:female	13:2
% Male	87%
Maximum anteroposterior diameter of AAA (mm)	46 (range 34—55)
Cardiovascular history	
Coronary artery disease	5 (33%)
Stroke or transient ischemic attack	2 (13%)
Peripheral vascular disease	2 (13%)
Risk factors	
Current smoking habit	6 (40%)
Previous smoking habit	8 (60%)
Diabetes mellitus	1 (7%)
Hypertension	10 (67%)
Hypercholesterolemia	15 (100%)
Medications	
Antiplatelet agent	12 (80%)
Statin	13 (87%)
β-Blocker	6 (40%)
ACE inhibitor/ARB[a]	8 (53%)
Other Anti-hypertensive	2 (13%)

[a] Angiotensin converting enzyme (ACE) inhibitor or angiotensin II receptor blocker (ARB).

factor of 0.014 mSv/mGy cm. The administration of ^{18}F-FDG and USPIO was well tolerated with no adverse events.

^{18}F-FDG uptake

Increased ^{18}F-FDG uptake was observed within the wall of 13 of the 15 AAAs. In total there were 42 regions of increased uptake and all were diffuse and involved the wall. Although it was not possible to resolve whether this uptake localised to the aneurysm wall or the thrombus, the majority were observed in the shoulder region of the aneurysm (25/42, 60%), with a third (14/42) occurring within the main body of the aneurysm and the remainder in close proximity to the bifurcation (3/42). There was increased uptake in the peri-luminal zone of the thrombus in all patients.

USPIO uptake

All AAA demonstrated uptake of USPIO but focal areas of mural USPIO were primarily confined to the main body of the aneurysm (146/271, 54%), with 28% (75/271) located in the shoulder region and 19% (50/271) adjacent to the bifurcation (Table 2). In keeping with our previous study,[24] all patients had USPIO uptake in the periluminal area, representing a movement of particles directly into the thrombus from the blood pool.

Comparison between ^{18}F-FDG and USPIO uptake

When all areas of the aneurysm were considered, there was a modest correlation between the SUV on PET-CT and the absolute change in R2* on MRI ($r = .30$; 95% CI 0.29—0.31, $p < .0001$; Fig. 1).

In general, the main thrombus (excluding the peri-luminal region) did not uptake ^{18}F-FDG or USPIO. In contrast, local inflammation within the wall was readily identifiable but was not reflected by a change in T2* or R2* value in the whole aneurysm because of the associated dilutional effect of the thrombus.

Classification of AAA according to ^{18}F-FDG or USPIO uptake using the quadrant technique was consistent and reproducible with excellent inter-observer agreement and a kappa statistic of 0.87 for ^{18}F-FDG and 0.85 for USPIO. On occasion, areas of increased USPIO and ^{18}F-FDG uptake co-localised to the same quadrant in the aortic wall, although regions of USPIO uptake without corresponding ^{18}F-FDG uptake were also commonly seen (Fig. 2). Overall, co-localisation of areas of increased USPIO and ^{18}F-FDG uptake were poor (kappa statistic 0.074; 95% CI 0.026—0.122) and there were more areas of increased uptake identified on MRI than on PET-CT (Table 3). Focal and discrete uptake of USPIO can be readily discerned on MRI, whereas there was more diffuse and ill-defined uptake of ^{18}F-FDG involving both the wall and the thrombus on PET-CT.

Based on USPIO uptake, four patients were classified into Group 3 and 11 into Groups 1 and 2. SUV_{max} and TBR appeared to be lower in those classified as Group 3 than in those in Groups 1 and 2, but this did not reach statistical significance ($p = .7884$, 95% CI −2.181 to 1.690; Fig. 1). There was no correlation between the grouping classification and the maximum absolute change in R2* ($p = .4123$, 95% CI −86.99 to 37.98).

DISCUSSION

In comparing ^{18}F-FDG PET-CT with USPIO-enhanced MRI in patients with AAA, we have identified a modest correlation between these two imaging modalities but a number of key differences. In particular, activity detected with these two techniques appears to be concentrated in different regions of the aneurysm: largely in the shoulder region with ^{18}F-FDG and in the body of the aneurysm using USPIO. We believe that this reflects the different elements of inflammatory activity detected by these two approaches, with PET-CT providing information related to glycolysis and USPIO information on phagocytosis. Further studies are now required to assess which modality will have the greatest predictive power to determine aneurysm growth and clinical outcome.

Inflammatory cells have a key role in the development and progression of abdominal aortic aneurysms.[17] Histopathologically, the aneurysmal aortic wall is characterised by focal medial neovascularisation, infiltration of inflammatory cells (principally macrophages and lymphocytes), and fragmentation of elastin and collagen fibres within the extracellular matrix. Both ^{18}F-FDG and USPIO imaging aim to detect and quantify the inflammatory cellular component and it is therefore encouraging that a modest correlation between these two measures was observed in this study, confirming that ultimately both identify vascular inflammation, albeit through differing pathways.

Vascular inflammatory cells are metabolically active and take up ^{18}F-FDG in an insulin-insensitive manner. Therefore,

Table 2. Qualitative evaluation of ^{18}F-fludeoxyglucose (FDG) uptake on positron emission tomography and computed tomography (PET-CT) compared to ultrasmall superparamagnetic particles of iron oxide (USPIO) uptake on magnetic resonance imaging (MRI).

	^{18}F-FDG PET-CT	USPIO MRI
Spatial resolution	4—6 mm	2 mm (subject to field of view)
Periluminal enhancement	Present	Present
Region of uptake	Predilection for shoulder region	Predilection for main body of aneurysm
Definition of uptake	> 125% of the averaged SUV_{max} from five randomly selected regions in the non-aneurysmal descending thoracic aorta	10 contiguous voxels with % change in T2* ≥59%
Functional assessment	Glycolytic activity	Phagocytic activity
Ionising radiation	Yes	No

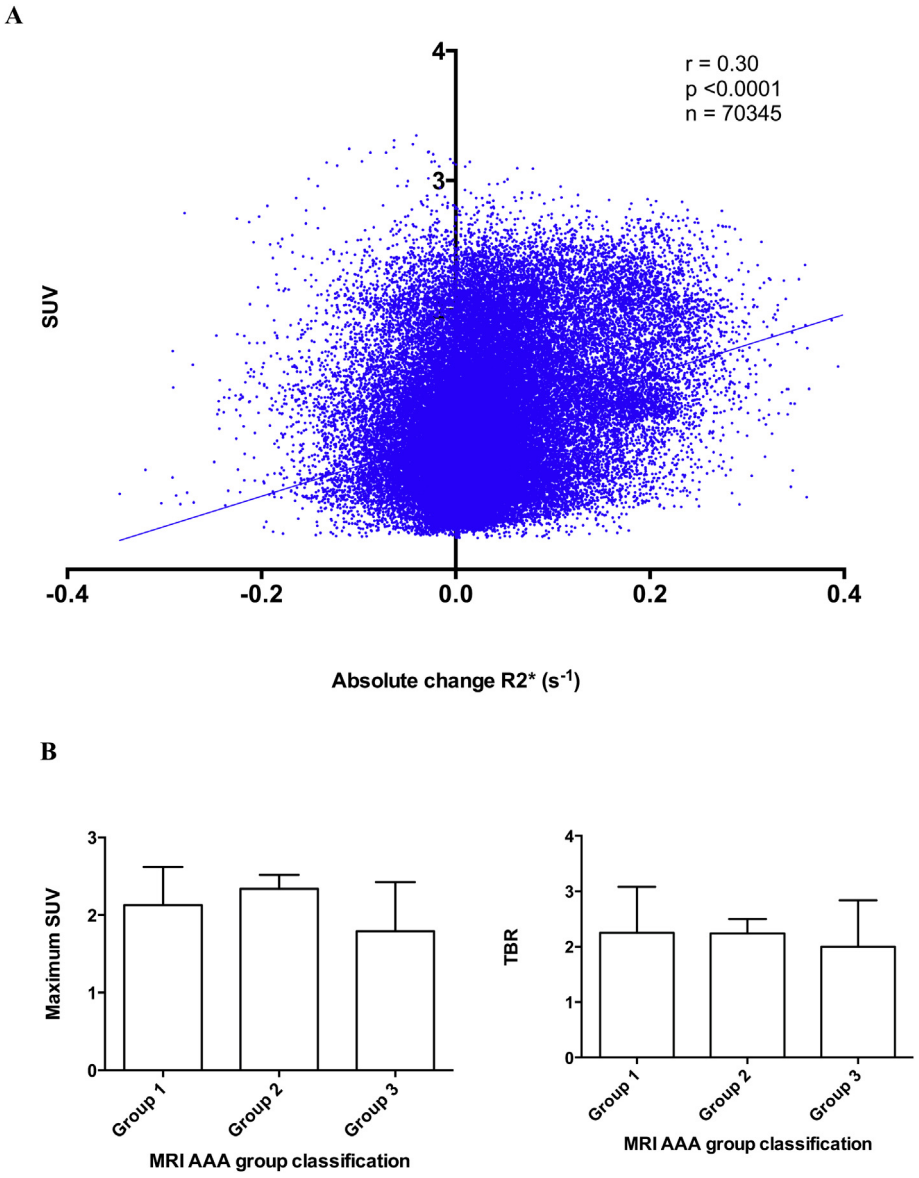

Figure 1. (A.) Comparison of standard uptake value (SUV) and absolute change in R2* in the wall of the abdominal aortic aneurysm (AAA). When the thrombus and wall of the aneurysm are considered there is a modest correlation between the SUV and the absolute change in R2* ($r = 0.30$). (B) MRI group classification compared to maximum SUV (SUV_{max}) and tissue-to-background ratio (TBR) in the wall of the AAA. There was no significant difference between the SUV_{max} ($p = .4696$, 95% CI −1.682 to 0.8194) or TBR ($p = .7884$, 95% CI −2.181 to 1.690) of patients in Groups 1 and 2 and those in Group 3.

^{18}F-FDG uptake in the fasted state has been proposed as a marker of risk for aneurysm progression and rupture with higher uptake associated with inflammation, aortic wall instability, and clinical symptoms.[15,18] However, the role of ^{18}F-FDG PET-CT in AAA disease remains controversial. Recent data have suggested that vascular ^{18}F-FDG activity may relate to more than simply macrophage burden,[31] with several studies identifying high lymphocyte counts and leucocytes[15,17,32] within the aortic wall and implicating hypoxia as an important driver to ^{18}F-FDG uptake.[33] Furthermore, although several small studies have demonstrated the ability of ^{18}F-FDG to discriminate between symptomatic and asymptomatic AAA,[15–18,21] a number of published studies have failed to verify these observations. Palombo et al.[34] showed ^{18}F-FDG uptake was low in asymptomatic AAAs, with a diameter close to surgical indications (mean diameter, 4.9 cm), perhaps reflecting decreased cell density in large AAAs. Tegler et al.[32] found no relationship between ^{18}F-FDG uptake and asymptomatic (small or large) AAAs versus controls and no correlation between histology and uptake. Similarly, Kotze et al.[20] found an inverse relationship between ^{18}F-FDG uptake and future growth rate of AAA.

USPIO-enhanced MRI has been used to explore a number of inflammatory conditions, including atherosclerotic plaques and abdominal aortic aneurysms.[23–25,27] USPIO are taken up by inflammatory phagocytic cells, particularly macrophages, and accumulate at sites of cellular

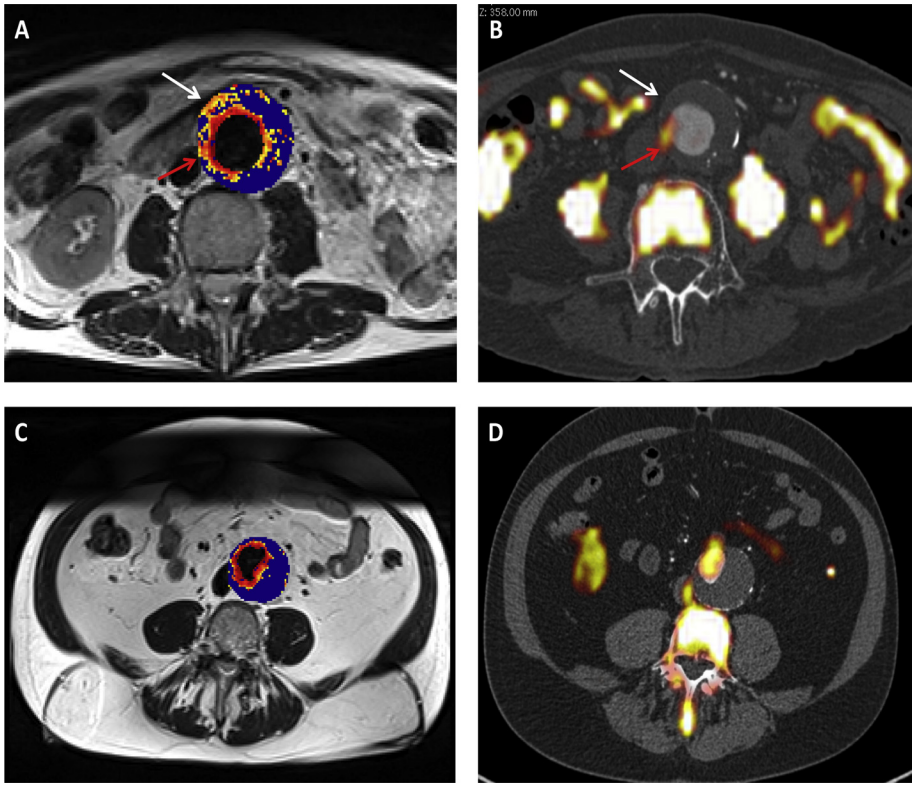

Figure 2. (A,B) Representative magnetic resonance imaging (MRI) (A) and fused positron emission tomography and computed tomography (PET-CT) (B) scans from the same patient with an abdominal aortic aneurysm (AAA). Ultrasmall superparamagnetic particles of iron oxide (USPIO) uptake, defined by percentage change in T2* is demonstrated using a colour scale. Changes in T2* value over the threshold (59%) are presented on a graduated (yellow-red) colour scale and data below the threshold appears blue. Corresponding ^{18}F-fludeoxyglucose (FDG) activity (red arrow) can be seen in B. Differences in the location of regions of uptake between the techniques are apparent, as marked by the white arrow. (C,D) are corresponding MRI and fused PET-CT slices from the same patient who has no USPIO or ^{18}F-FDG uptake in the wall of the AAA, with uptake limited to the peri-luminal area.

inflammation at sufficient concentrations to cause signal changes on MRI. In addition, histological examination of excised tissue, including aneurysm tissue, has confirmed the co-localisation and uptake of USPIO in areas of macrophage infiltration.[24,35–37]

We speculate that USPIO and ^{18}F-FDG uptake represent distinct markers of vascular inflammation that correspond to differing inflammatory and macrophage activities. Clearly, USPIO uptake is a measure of ongoing phagocytic activity of tissue-resident macrophages and potentially neutrophils, whereas ^{18}F-FDG reflects glucose utilisation by cells with high metabolic requirements including the cells implicated in vascular inflammation.[38] Moreover there is evidence that the two techniques target different macrophage subsets. Macrophages exist in varying polarised states and have different roles in vascular tissue. M1 macrophages are considered more destructive, promoting the destabilisation and rupture of atherosclerotic plaques, whereas phagocytosis is more important in the role of M2 macrophages stimulating reparative processes, mediated by the production of anti-inflammatory cytokines and the suppression of pro-inflammatory signalling.[39] It has been suggested that ^{18}F-FDG and USPIO uptake may be able to differentiate these two distinct M1 and M2 macrophage sub-populations respectively.[40] In this study, the majority of ^{18}F-FDG uptake was identified in the shoulder region of the aneurysm, an area of high biomechanical stress,[41,42] with a particular tendency to rupture: perhaps related to a destructive macrophage phenotype in this area.

Even though it has been demonstrated that our USPIO aneurysm classification identifies aneurysms likely to progress and dilate (Group 3; distinct mural USPIO uptake) we found no correlation between this classification and ^{18}F-FDG uptake nor the maximum absolute change in R2*. This supports the suggestion that it is the location of USPIO

Table 3. Quadrant analysis of the aneurysm wall: Regions of uptake identified by magnetic resonance imaging (MRI) and positron emission tomography and computed tomography (PET-CT). kappa statistic = 0.074 (95% C.I. 0.026—0.122), representing a poor strength of agreement.

		PET-CT		
MRI		Regions of uptake	No regions of uptake	Total
	Regions of uptake	70	353	423
	No regions of uptake	69	613	682
	Total	139	966	1015

uptake that is crucial, rather than the degree of USPIO uptake. However, the modest correlation that was demonstrated between maximum absolute change in R2* and SUV on a voxel-by-voxel basis supports the contention that these imaging modalities are both detecting elements of macrophage activity, namely phagocytosis and glucose metabolism.

Study limitations

There are important study limitations and technical considerations when interpreting our findings. We acknowledge that co-registration of the MRI and PET-CT datasets was challenging and cannot exclude partial or incomplete co-registration. Moreover, the limited in-plane resolution of PET-CT makes definition of the aortic wall and thrombus difficult and therefore challenging to locate the exact site of activity. Indeed this may also explain the increased ^{18}F-FDG uptake observed in the shoulder region, which is more prone to partial volume effects due to its angulation through the slice. This may reduce the sensitivity of the study in detecting ^{18}F-FDG or USPIO activity. However, as the thrombus uptakes little contrast agent, if thrombus was inadvertently included in the aortic wall assessment, this would lead to a tendency to under report uptake, thus our findings could be considered conservative. Additionally, there is no consensus or validated definition of quantitative significance values for ^{18}F-FDG or USPIO uptake and despite the excellent inter-observer reproducibility demonstrated in this study, this may contribute to the differences observed.

The contribution of statin therapy to the results of this study also cannot be excluded. To date there is only observational data showing AAA growth reduction with statins and mechanistic data are limited.[43,44] Although statin use has been shown to suppress AAA formation in animal models, this has not been translated to humans.[45,46] The use of statins in vascular patients to reduce cerebrovascular and cardiovascular mortality as well as in patients undergoing AAA surgery is well documented.[47,48] Consequently a clinical trial with and without statin therapy in AAA patients would be ethically challenging. The clinical trial was registered at ClinicalTrials.gov (NCT01749280)

Intra-individual correlation of histologic specimens from areas of minimum and maximum uptake of contrast would provide evidence of co-localisation of inflammatory activity but the practicalities of such are limited with the increase in endovascular abdominal aortic aneurysm repair (EVAR) and the ability to sample only tissue from the anterior portion of the aortic wall. Moreover, ex vivo ^{18}F-FDG uptake is limited by the need for fresh viable tissue, whereas USPIO uptake can only be assessed when undertaken in very close proximity to elective surgery.

This was a small study population that will require prospective evaluation in larger patient cohorts. Furthermore, this study was limited by the exclusion of AAA $\geq$ 55 mm as aneurysm growth and rupture is unpredictable and non-linear. Current guidelines suggest that surveillance with selective repair is the most appropriate management strategy.[49] However, as improvements in device technology for EVAR continues, this may change. Given this limited sample size, we were unable to assess the relationship between uptake of either ^{18}F-FDG or USPIO with AAA growth rates or clinical outcome. A number of small studies have demonstrated the ability of ^{18}F-FDG to differentiate between symptomatic and asymptomatic AAAs[15–18,21] and a recent study has suggested an association between ^{18}F-FDG activity and future clinical events.[41] A pilot study of 29 patients demonstrated that USPIO uptake in the wall of AAA is associated with accelerated expansion rates.[24] Further datasets with long-term follow-up are therefore required to undertake more complete evaluation of these promising imaging approaches.

An observational surveillance trial is currently underway at the centre to assess the relationship between mural USPIO uptake and subsequent clinical outcomes, with the aim of improving risk stratification of patients with AAA: the MA3RS trial (MRI for AAA to predict rupture or surgery; ISRCTN76413758).

In conclusion, the correlation between ^{18}F-FDG PET-CT and USPIO-enhanced MRI to detect vascular inflammation in AAAs is modest and reflects the differing elements of macrophage activity that they detect: glycolysis and phagocytosis respectively. Whether the identification of this varying activity will impact on aneurysm growth rates or risk of aneurysm rupture will require larger longitudinal study.

COMPETING INTERESTS

None.

FUNDING

This research was supported by grants from the National Institutes of Health Research (NIHR) Efficacy and Mechanism Evaluation Programme (11/20/03), the British Heart Foundation (PG/09/083) and the Evelyn Trust (09/22). Dr. McBride is supported by the Academic Department of Military Surgery and Trauma, Royal Centre for Defence Medicine. Dr. Joshi is supported by Chief Scientist Office (ETM/160). Dr. van Beek is supported by the Scottish Imaging Network — a Platform of Scientific Excellence. The work of Dr. Rudd is part-supported by the NIHR Cambridge Biomedical Research Centre, the British Heart Foundation and the Wellcome Trust. Dr. Newby is supported by the British Heart Foundation (CH/09/002). The Wellcome Trust Clinical Research Facility and the Clinical Research Imaging Centre are supported by National Health Service Research Scotland through National Health Service Lothian.

ACKNOWLEDGEMENTS

The authors are grateful to the Wellcome Trust Clinical Research Facility and the Clinical Research Imaging Centre for their help with this study.

APPENDIX A. SUPPLEMENTARY MATERIAL

Supplementary material related to this article can be found at http://dx.doi.org/10.1016/j.ejvs.2015.12.018

REFERENCES

1 Jaffer FA, Libby P, Weissleder R. Molecular imaging of cardiovascular disease. *Circulation* 2007;**116**:1052—61.
2 Jaffer FA, Libby P, Weissleder R. Optical and multimodality molecular imaging: insights into atherosclerosis. *Arterioscler Thromb Vasc Biol* 2009;**29**:1017—24.
3 Choudhury RP, Fisher EA. Molecular imaging in atherosclerosis, thrombosis, and vascular inflammation. *Arterioscler Thromb Vasc Biol* 2009;**29**:983—91.
4 Nahrendorf M, Keliher E, Marinelli B, Leuschner F, Robbins CS, Gerszten RE, et al. Detection of macrophages in aortic aneurysms by nanoparticle positron emission tomography-computed tomography. *Arterioscler Thromb Vasc Biol* 2011;**31**:750—7.
5 Rudd JHF, Warburton EA, Fryer TD, Jones HA, Clark JC, Antoun N, et al. Imaging atherosclerotic plaque inflammation with [^{18}F]-fluorodeoxyglucose positron emission tomography. *Circulation* 2002;**105**:2708—11.
6 Rudd JHF, Myers KS, Bansilal S, Machac J, Rafique A, Farkouh M, et al. (18)Fluorodeoxyglucose positron emission tomography imaging of atherosclerotic plaque inflammation is highly reproducible: implications for atherosclerosis therapy trials. *J Am Coll Cardiol* 2007;**50**:892—6.
7 Tawakol A, Migrino RQ, Hoffman U, Abbara S, Houser S, Gewirtz H, et al. Noninvasive in vivo measurement of vascular inflammation with F-18 fluorodeoxyglucose positron emission tomography. *J Nucl Cardiol* 2005;**12**:294—301.
8 Tawakol A, Migrino RQ, Bashian GG, Bedri S, Vermylen D, Cury RC, et al. In vivo 18F-fluorodeoxyglucose positron emission tomography imaging provides a noninvasive measurement of carotid plaque inflammation in patients. *J Am Coll Cardiol* 2006;**48**:1818—24.
9 Rominger A, Saam T, Wolpers S, Cyran CC, Schmidt M, Foerster S, et al. ^{18}F-FDG PET/CT identifies patients at risk for future vascular events in an otherwise asymptomatic cohort with neoplastic disease. *J Nucl Med* 2009;**50**:1611—20.
10 Rudd JHF, Myers KS, Bansilal S, Machac J, Woodward M, Fuster V, et al. Relationships among regional arterial inflammation, calcification, risk factors, and biomarkers: a prospective fluorodeoxyglucose positron-emission tomography/computed tomography imaging study. *Circ Cardiovasc Imaging* 2009;**2**:107—15.
11 Tahara N, Kai H, Nakaura H, Mizoguchi M, Ishibashi M, Kaida H, et al. The prevalence of inflammation in carotid atherosclerosis: analysis with fluorodeoxyglucose-positron emission tomography. *Eur Heart J* 2007;**28**:2243—8.
12 Tahara N, Kai H, Ishibashi M, Nakaura H, Kaida H, Baba K, et al. Simvastatin attenuates plaque inflammation: evaluation by fluorodeoxyglucose positron emission tomography. *J Am Coll Cardiol* 2006;**48**:1825—31.
13 Fayad ZA, Mani V, Woodward M, Kallend D, Abt M, Burgess T. dal-PLAQUE Investigators. Safety and efficacy of dalcetrapib on atherosclerotic disease using novel non-invasive multimodality imaging (dal-PLAQUE): a randomised clinical trial. *Lancet* 2011;**378**:1547—59.
14 Tawakol A, Fayad ZA, Mogg R, Alon A, Klimas MT, Dansky H, et al. Intensification of statin therapy results in a rapid reduction in atherosclerotic inflammation: results of a multicenter fluorodeoxyglucose-positron emission tomography/computed tomography feasibility study. *J Am Coll Cardiol* 2013;**62**:909—17.
15 Reeps C, Essler M, Pelisek J, Seidl S, Eckstein H-H, Krause B-J. Increased 18F-fluorodeoxyglucose uptake in abdominal aortic aneurysms in positron emission/computed tomography is associated with inflammation, aortic wall instability, and acute symptoms. *J Vasc Surg* 2008;**48**:417—23.
16 Reeps C, Bundschuh RA, Pellisek J, Herz M, Marwick S, Schwaiger M, et al. Quantitative assessment of glucose metabolism in the vessel wall of abdominal aortic aneurysms: correlation with histology and role of partial volume correction. *Int J Cardiovasc Imaging* 2012;**29**:505—12.
17 Courtois A, Nusgens BV, Hustinx R, Namur G, Gomez P, Somja J, et al. 18F-FDG uptake assessed by PET/CT in abdominal aortic aneurysms is associated with cellular and molecular alterations prefacing wall deterioration and rupture. *J Nucl Med* 2013;**54**:1740—7.
18 Sakalihasan N, Hustinx R, Limet R. Contribution of PET scanning to the evaluation of abdominal aortic aneurysm. *Semin Vasc Surg* 2004;**17**:144—53.
19 Kotze CW, Menezes LJ, Endozo R, Groves AM, Ell PJ, Yusuf SW. Increased metabolic activity in abdominal aortic aneurysm detected by 18F-fluorodeoxyglucose. *Eur J Vasc Endovasc Surg* 2009;**38**:93—9.
20 Kotze CW, Groves AM, Menezes LJ, Harvey R, Endozo R, Kayani IA, et al. What is the relationship between ^{18}F-FDG aortic aneurysm uptake on PET/CT and future growth rate? *Eur J Nucl Med Mol Imaging* 2011;**38**:1493—9.
21 Truijers M, Kurvers HA, Bredie SJ, Oyen WJ, Blankensteijn JD. In vivo imaging of abdominal aortic aneurysms: increased FDG uptake suggests inflammation in the aneurysm wall. *J Endovasc Ther* 2008;**15**:462—7.
22 Nchimi A, Defawe O, Brisbois D, Broussaud TK, Defraigne J-O, Magotteaux P, et al. MR Imaging of iron phagocytosis in intraluminal thrombi of abdominal aortic aneurysms in humans. *Radiology* 2010;**254**:973—81.
23 Sadat U, Taviani V, Patterson AJ, Young VE, Graves MJ, Teng Z, et al. Ultrasmall superparamagnetic iron oxide-enhanced magnetic resonance imaging of abdominal aortic aneurysms-a feasibility study. *Eur J Vasc Endovasc Surg* 2011;**41**:167—74.
24 Richards JMJ, Semple SI, MacGillivray TJ, Gray C, Langrish JP, Williams M, et al. Abdominal aortic aneurysm growth predicted by uptake of ultrasmall superparamagnetic particles of iron oxide: a pilot study. *Circ Cardiovasc Imaging* 2011;**4**:274—81.
25 Trivedi RA, Mallawarachi C, U-King-Im J-M, Graves MJ, Horsley J, Goddard MJ, et al. Identifying inflamed carotid plaques using in vivo USPIO-enhanced MR Imaging to label plaque macrophages. *Arterioscler Thromb Vasc Biol* 2006;**26**:1601—6.
26 Tang TY, Muller KH, Graves MJ, Li ZY, Walsh SR, Young V, et al. Iron oxide particles for atheroma imaging. *Arterioscler Thromb Vasc Biol* 2009;**29**:1001—8.
27 Morishige K, Kacher DF, Libby P, Josephson L, Ganz P, Weissleder R, et al. High-resolution magnetic resonance imaging enhanced with superparamagnetic nanoparticles measures macrophage burden in atherosclerosis. *Circulation* 2010;**122**:1707—15.
28 Dweck MR, Jones C, Joshi NV, Fletcher AM, Richardson H, White A, et al. Assessment of valvular calcification and inflammation by positron emission tomography in patients with aortic stenosis. *Circulation* 2012;**125**:76—86.
29 Dweck MR, Chow M, Joshi NV, Williams MC, Jones C, Fletcher AM, et al. Coronary arterial ^{18}F-sodium fluoride uptake: a novel marker of plaque biology. *J Am Coll Cardiol* 2012;**59**:1539—48.
30 Joshi NV, Vesey AT, Williams MC, Shah AS, Calvert PA, Craighead FH, et al. 18F-fluroide positron emission tomography for identification of ruptured and high-risk coronary

atherosclerotic plaques: a prospective clinical trial. *Lancet* 2014;**383**:705—13.
31 Defawe OD, Hustinx R, Defraigne JO, Limet R, Sakalihasan N. Distribution of F-18 fluorodeoxyglucose (F-18 FDG) in abdominal aortic aneurysm: high accumulation in macrophages seen on PET imaging and immunohistochemistry. *Clin Nucl Med* 2005;**30**:340—1.
32 Tegler G, Ericson K, Sörensen J, Björck M, Wanhainen A. Inflammation in the walls of asymptomatic abdominal aortic aneurysms is not associated with increased metabolic activity detectable by 18-flurodeoxyglucose positron-emission tomography. *J Vasc Surg* 2012;**56**:802—7.
33 Folco EJ, Sheikine Y, Rocha VZ, Christen T, Shvartz E, Sukhova GK, et al. Hypoxia but not inflammation augments glucose uptake in human macrophages: implications for imaging atherosclerosis with 18fluorine-labeled 2-deoxy-D-glucose positron emission tomography. *J Am Coll Cardiol* 2011;**58**:603—14.
34 Palombo D, Morbelli S, Spinella G, Pane B, Marini C, Rousas N, et al. A positron emission tomography/computed tomography (PET/CT) evaluation of asymptomatic abdominal aortic aneurysms: another point of view. *Ann Vasc Surg* 2012;**26**:491—9.
35 Ruehm SG, Corot C, Vogt P, Kolb S, Debatin JF. Magnetic resonance imaging of atherosclerotic plaque with ultrasmall superparamagnetic particles of iron oxide in hyperlipidemic rabbits. *Circulation* 2001;**103**:415—22.
36 Kooi ME, Cappendijk VC, Cleutjens KBJM, Kessels AGH, Kitslaar PJEHM, Borgers M, et al. Accumulation of ultrasmall superparamagnetic particles of iron oxide in human atherosclerotic plaques can be detected by in vivo magnetic resonance imaging. *Circulation* 2003;**107**:2453—8.
37 Schmitz SA, Taupitz M, Wagner S, Wolf KJ, Beyersdorff D, Hamm B. Magnetic resonance imaging of atherosclerotic plaques using superparamagnetic iron oxide particles. *J Magn Reson Imaging* 2001;**14**:355—61.
38 Choke E, Cockerill G, Wilson WRW, Sayed S, Dawson J, Loftus I, et al. A review of biological factors implicated in abdominal aortic aneurysm rupture. *Eur J Vasc Endovasc Surg* 2005;**30**:227—44.
39 Shaikh S, Brittenden J, Lahiri R, Brown PAJ, Thies F, Wilson HM. Macrophage subtypes in symptomatic carotid artery and femoral artery plaques. *Eur J Vasc Endovasc Surg* 2012;**44**:491—7.
40 Satomi T, Ogawa M, Mori I, Ishino S, Kubo K, Magata Y, et al. Comparison of contrast agents for atherosclerosis imaging using cultured macrophages: FDG versus ultrasmall superparamagnetic iron oxide. *J Nuc Med* 2013;**54**:999—1004.
41 Nchimi A, Cheramy-Bien JP, Gasser TC, Namur G, Gomez P, Seidel L, et al. Multifactorial relationship between 18F-fluorodeoxy-glucose positron emission tomography signaling and biomechanical properties in unruptured aortic aneurysms. *Circ Cardiovasc Imaging* 2014;**7**:82—91.
42 Xu XY, Borghi A, Nchimi A, Leung J, Gomez P, Cheng Z, et al. High levels of 18F-FDG uptake in aortic aneurysm wall are associated with high wall stress. *Eur J Vasc Endovasc Surg* 2010;**39**:295—301.
43 Schlosser FJV, Tangelder MJD, Verhagen HJM, van der Heijden GJMG, Muhs BE, van der Graaf Y, et al. Growth predictors and prognosis of small abdominal aortic aneurysms. *J Vasc Surg* 2008;**47**:1127—33.
44 Karrowni W, Dughman S, Hajj GP, Miller FJ. Statin therapy reduces growth of abdominal aortic aneurysms. *J Investig Med* 2011;**59**:1239—43.
45 Kalyanasundaram A, Elmore JR, Manazer JR, Golden A, Franklin DP, Galt SW. Simvastatin suppresses experimental aortic aneurysm expansion. *J Vasc Surg* 2006;**43**:117—24.
46 Shiraya S, Miyake T, Aoki M, Yoshikazu F, Ohgi S, Nishimura M, et al. Inhibition of development of experimental aortic abdominal aneurysm in rat model by atorvastatin through inhibition of macrophage migration. *Atherosclerosis* 2009;**202**:34—40.
47 Kertai MD, Boersma E, Westerhout C, van Domburg R, Klein J, Bax JJ, et al. Association between long-term statin use and mortality after successful aortic aneurysm surgery. *Am J Med* 2004;**116**:96—103.
48 Schoulten O, Hoeks SE, Welten GM, Davignon J, Kastelein JJ, Vidakovic R. Effect of statin withdrawal on frequency of cardiac events after vascular surgery. *Am J Cardiol* 2007;**100**:316—20.
49 Chaikof EL, Brewster DC, Dalman RL, Makaroun MS, Illig KA, Sicard GA, et al. The care of patients with an abdominal aortic aneurysm: the Society for Vascular Surgery practice guidelines. *J Vasc Surg* 2009;**50**(Suppl. 4):S8—49.